Fibrillation atriale : des mécanismes physiopathologiques à la prise en charge thérapeutique

Pedro Raphaël Martins

THÈSE / UNIVERSITÉ DE RENNES 1
sous le sceau de l'Université Européenne de Bretagne

pour le grade de

DOCTEUR DE L'UNIVERSITÉ DE RENNES 1

Mention : Biologie et Sciences de la Santé

Vie Agro Santé

présentée par

Raphaël P. MARTINS

Préparée à l'unité de recherche INSERM U 1099
Laboratoire du Traitement du Signal et de l'Image

Fibrillation atriale : des mécanismes physiopathologiques à la prise en charge thérapeutique

Thèse soutenue à l'Université de Rennes 1
le 17 Juin 2014

devant le jury composé de :

Stéphane HATEM
Directeur de Recherche à l'INSERM
Université Pierre et Marie Curie / *rapporteur*

Dominique BABUTY
PU-PH, Université de Tours / *rapporteur*

Christian DE CHILLOU
PU-PH, Université de Nancy / *examinateur*

José JALIFE
Directeur du Center for Arrhythmia Research,
Ann Arbor, Michigan, USA/*examinateur*

Alfredo HERNANDEZ
Directeur de Recherche à l'INSERM
Université de Rennes 1/*examinateur*

Philippe MABO
PU-PH, Université de Rennes /
Directeur de Thèse

Remerciements

« Je sais que lire un manuscrit de thèse peut être intéressant mais aussi relativement indigeste. Je comprends donc ceux, qui ne liront pas complètement le présent manuscrit. Néanmoins et de façon assez remarquable, tout le monde s'attarde sur le chapitre des remerciements. J'imagine donc que ce préambule sera la partie la plus lue de ma thèse! C'est une raison suffisante je pense pour que je m'applique à y être la plus juste possible. »

C.S.

En 2009, l'idée de réaliser une Thèse de Sciences a commencé à germer dans mon esprit, et celui de mes chers patrons…Une année aux USA se profilait, à faire de la recherche fondamentale dans un laboratoire d'électrophysiologie de renom, mais dans un lieu cependant peu glamour à première vue…en effet, les gens à Ann Arbor ne vous demandent pas combien d'années vous êtes censés rester mais plutôt « combien d'hivers »…Venant d'un pays méditerranéen et n'étant par conséquent pas très fan de la neige et du froid, vous pouvez comprendre mon désarroi... Mais finalement, à mesure que le projet prenait forme, j'y ai pris cœur de plus en plus.

Quelques mois avant le départ, on m'annonçait qu'il ne fallait pas partir une mais deux années. Je n'y étais absolument pas favorable à première vue, puisque l'idée de passer « deux hivers » à Ann Arbor et de si longs mois loin d'un service hospitalier et d'une salle d'électrophysiologie m'effrayaient. Les Professeurs Mabo et Sadoul m'ont finalement convaincu du bien fondé de ce retournement de situation…et je m'y suis résolu. Bien m'en a pris…

Ces deux années ont été riches sur tous les plans.
Sur le plan professionnel, elles m'ont permis d'appréhender un monde qui m'était totalement inconnu, peuplé de rotors, de points de singularité et de fréquences dominantes…mais également de côtoyer d'excellents scientifiques, parmi lesquels le Dr José Jalife. Ce projet ne serait pas ce qu'il est sans son aide précieuse, sans ses qualités de leadership et ses valeurs humaines.
Sur le plan personnel, ces deux années m'ont permis de rencontrer des gens exceptionnels, venant de presque tous les continents…j'en ai tiré, outre un carnet d'adresses bien fourni pour mes vacances futures, une richesse culturelle unique et des amitiés sincères.
Revenir n'a pas été chose simple, mais (presque) toutes les bonnes choses ont une fin.
J'en suis revenu la mémoire pleine de souvenirs personnels inoubliables et de connaissances scientifiques qui me serviront dans mon exercice futur.

Merci à tous ceux qui ont contribué à faire aboutir ce projet…

Je remercie le **Professeur Dominique Babuty** qui me fait l'honneur de juger d'être rapporteur de cette thèse. Vous avez été le premier à me faire aimer la cardiologie, lorsque je n'étais qu'externe dans votre service, et vos conseils (« Va à Rennes !! ») ont guidé mon devenir. Je vous en suis profondément reconnaissant.

Je remercie le **Professeur Stéphane Hatem** qui me fait l'honneur de juger et d'être le rapporteur de cette thèse. Je vous remercie de m'avoir ouvert les portes de votre laboratoire, il y a 4 ans, pour mon Master 2 et de m'avoir initié au monde de la recherche.

Je remercie le **Professeur Christian De Chillou** qui me fait l'honneur de juger mon travail. Travailler avec vous lors de mon passage à Nancy a été un plaisir, et j'en ai tiré de nombreuses connaissances en électrophysiologie qui me servent au quotidien.

Je remercie le **Docteur Alfredo Hernandez** qui me fait l'honneur de juger mon travail. Que ce travail soit l'expression de ma plus grande reconnaissance et de ma gratitude.

I would like to thank the **Doctor José Jalife**, for all he taught me during these two years.
When I joined your lab, I was relatively new to the field of basic research. You were very careful in guiding me through every step and taught me various lab techniques. This has helped me to gain experience in a whole new arena of working with large animal models.
All this work would not exist without our daily interactions, your invaluable help and your remarkable leadership.
Your guidance, positive vision, and the interaction with the other lab colleagues helped me to be confident both scientifically and personally, thus enabling me to shape my career towards a successful path.

Enfin, je remercie tout particulièrement le **Professeur Philippe Mabo**, sans qui ce travail n'aurait jamais vu le jour.
Vous avez veillé sur ma formation médicale au cours de mes années d'internat, et su me conseiller dans chacune des étapes importantes de ma formation. J'apprécie encore plus notre collaboration depuis mon retour à Rennes, et espère que celle-ci s'épanouira au fil des années.
Merci pour votre confiance, votre aide et vos précieux conseils scientifiques et humains.

Je remercie le **Professeur Jean-Claude Daubert**, dont la rigueur et l'étendue des connaissances sont pour moi un exemple. Merci de la confiance et du soutien que vous m'avez apporté au long de ces années. Que ce travail soit l'expression de mon admiration et de mon estime la plus sincère.

Je remercie le **Professeur Christophe Leclercq**, c'est un plaisir d'avoir rejoint votre équipe. Travailler à vos cotés et bénéficier quotidiennement de votre savoir-faire est une richesse. Merci pour votre écoute et votre disponibilité.

Je remercie le **Docteur Dominique Pavin**, qui m'a permis, grace à son expertise sur l'ablation de la FA, de réaliser une partie de cette Thèse. J'espère que celle-ci sera le fruit de nombreuses idées de recherche qui nous permettront encore de travailler ensemble sur ce domaine qui nous passionne. Merci pour tout ce que tu m'apprends en salle d'électrophysiologie et pour ta disponibilité au quotidien.

I'd like to thank all the people from the **Center for Arrhythmia Research** who helped me to complete this crazy study. You taught me so many things! It was great fun to work on this project. The huge amount of effort and commitment everyone involved spent toward the completion of the AF project was invaluable.

Special thanks to **Steve R. Ennis**, the funniest American guy I met! We spent so many hours at the farm, running after the sheep, freezing at 0°F or melting at 100°F (pour les français: courir après les moutons à -20°C l'hiver et +40°C l'été...vous imaginez???). It was nice to spend this time with you, speaking about science, comparing American and French culture/politics/religion…, learning new swear words. I consider you as a Friend, and look forward to see you again.

To **Cicero B. Willis**, **Rafael J. Ramirez**, **Yoshio Takemoto**, excellent scientists and even more excellent golfers! I'm waiting for you guys in 2018 in Paris as we promised!

To **Uma M. Avula**, my very good Friend, you were always there during this couple of years. Thanks for all you did! Working with you was a pleasure.

To **Vedran Velagic**, having you for the last months was fun! I'm looking forward to see you in France.

To **David Filgueiras-Rama**, thanks for teaching me "the job", from handling the sheep to the pacemaker implantations.

A **Jérôme Kalifa**, j'ai rencontré en toi un chercheur d'exception. Tu as été un moteur pendant mes 2 années américaines, me donnant sans cesse de nouvelles idées, me faisant réfléchir sur mes résultats, m'aidant à progresser au quotidien, le tout dans la bonne humeur. Merci à toi!

To **Guadalupe Guerrero-Serna** and **Kuljeet Kaur**, thanks for your help, for your leadership, your comments and advises regarding the project.

More than colleagues, I met Friends in USA. From all over the world.

I'm waiting for you guys now, in France!

A **Olivier Cesari**, qui m'a suivi depuis mon arrivée à Rennes. Notre amitié est pour moi unique. Merci pour ton soutien, pour tes conseils toujours très pertinents, pour tout le savoir que tu me transmets à chacune de nos longues discussions. Tu es une source de motivation perpétuelle pour moi, et je n'en serais sûrement pas là sans toi. Merci !

A mes 2 Amis de salle de rythmologie… A **David Hamon**, passer ces 6 mois à tes côtés a été un plaisir quotidien, merci pour ces fous rires, pour tout ce que tu m'as appris (les patients en sont ravis !), et pour ton aide dans notre travail commun…j'espère que ce n'est que le début d'une longue collaboration ! Et à **Albin Behaghel**, merci pour ton soutien sans faille, pour ton écoute attentionnée, et pour tes conseils tant professionnels que personnels. Reviens vite !

Je souhaitais également remercier les internes qui m'ont accompagné pendant ces quelques mois d'écriture: **Aurélie**, **Clémence** et **Damien** ; **Solène**, **Frank** et **Alexandre** ; **Nelly**, **Guillaume** et **Yvan**. Merci pour votre patience au quotidien, pour votre soutien dans mes moments de découragement, pour les débriefings de fin de journée dans mon bureau et dehors ;), et pour les cadeaux inattendus…

A **Alban Baruteau** et **Christophe Thébault**, pour notre amitié sincère résistante à la distance et au temps. Et à toutes les personnes qui m'ont soutenu pendant ces 2 années et qui ne sont pas dans ces remerciements ! A mon Amie **Catherine Szymanski**, pour la phrase d'introduction de mes remerciements, que j'ai en fait volée à sa Thèse de Sciences !

Merci également à tout le **personnel de salle d'électrophysiologie** qui ont supporté mon indisponibilité ces dernières semaines d'écriture...

A ma **famille** qui n'est pas présente aujourd'hui mais qui m'accompagne par les pensées, y compris mon principal fan depuis la première heure (mon grand-père !), à mes **parents** et ma **sœur** pour leur soutien sans failles. A la meilleure **belle famille** du monde ! Merci pour vos pensées et prières, et pour vos excellents conseils de vie (ndlr, surtout les tiens Maëlle) !

A **Marie**, qui a toujours été présente pendant ces longs mois de travail. Merci pour ta patience et ta compréhension, car je sais que je n'ai pas été vraiment présent pendant ces dernières semaines de rédaction. Merci de m'avoir soutenu au quotidien malgré la distance qui nous sépare. La Providence a permis que nos chemins se croisent. Qu'elle nous permette de marcher ensemble encore longtemps, main dans la main, dans la même direction…Il me tarde de voir ce qu'elle nous réserve !!!

Enfin, nombreux sont ceux qui ont œuvré pour que ce projet aboutisse. Chacun à donné un peu de sa personne ou de son temps, mais personne, vraiment personne, n'a donné autant que ceux que je vais remercier en dernier, à savoir…les **moutons**, qui ont donné de leur vie pour que nos connaissances sur la FA avancent…
Combien sont-ils à avoir participé… ? Probablement une centaine…
Espérons que leur sacrifice n'ait pas été vain.

Mon héros est l'homme qui découvre.
Car le monde tel que nous le percevons aujourd'hui en Occident
-le Temps dans sa perspective, les terres et les océans, les corps célestes, et notre propre corps, la flore et la faune, l'histoire et la vie des sociétés humaines, passées et présentes-,
ce monde là, il a fallu, pour nous en ouvrir les portes, d'innombrables Christophe Colomb.
Ceux-ci, lorsqu'ils se perdent dans la nuit des temps, sont bien sûr anonymes.
Mais d'autres, plus près de nous, surgissent dans la lumière de l'Histoire,
galerie de personnages aussi divers que l'est la nature humaine.
Les découvertes, alors, deviennent épisodes de biographies,
imprévisibles comme les nouveaux mondes que ces découvreurs nous ont révélés.

Daniel Boorstein
« Les découvreurs », 1983

Sommaire

Abréviations

α-SMA : α-smooth muscle actin
AMS : automatic mode switching
APD70 : durée du potentiel d'action à 70% de la repolarisation
APD90 : durée du potentiel d'action à 90% de la repolarisation
ARC-Adv-CB : cryoballon Artic Front Advance
ARC-CB : cryoballon Artic Front
CaMKII : protéine kinase II dépendante de la calmoduline/ Ca^{2+}
CB: cryoballon
CFAE : complex fractionnated atrial electrogram
Cx : connexine
DAD : delayed after-depolarisations (post-dépolarisations tardives)
DF : dominant frequency (fréquence dominante)
EAD : early after-depolarisations (post-dépolarisations précoces)
ECG : électrocardiogramme
EGM : électrogramme
FA : fibrillation atriale
FEVG : fraction d'éjection ventriculaire gauche
FIRM : Focal Impulses and Rotor Modulation
FFT : fast Fourrier transform
FV : fibrillation ventriculaire
LA : left atrium (oreillette gauche)
LS-PAF : long standing persistent atrial fibrillation (fibrillation atriale persistante de longue durée)
NFAT : nuclear factor of activated T-cells
NCX : échangeur Na^{+}-Ca^{2+}
OD : oreillette droite
OG : oreillette gauche
PIIINP : Procollagen III N-terminal propetide
PA : potentiel d'action
PLA : posterior left atrium (paroi postérieure de l'oreillette gauche)
PP : paralysie phrénique
PVP : potentiel veineux pulmonaire
RA : right atrium (oreillette droite)
RF : radiofréquence
RyR2 : récepteur à la ryanodine de type 2
SERCA : Ca^{2+} ATPase du réticulum sarcoplasmique
SR : sinus rhythm (rythme sinusal)
TA : tachycardie atriale
TV : tachycardie ventriculaire
VCS : veine cave supérieure
VP : veine pulmonaire

VPID : veine pulmonaire inférieure droite
VPIG : veine pulmonaire inférieure gauche
VPSD : veine pulmonaire supérieure droite
VPSG : veine pulmonaire supérieure gauche

Introduction

La fibrillation atriale (FA) est l'arythmie soutenue la plus fréquente. Elle est responsable d'une augmentation de la morbidité et de la mortalité. En plus des symptômes éventuels, palpitations, dyspnée ou lipothymies, la FA augmente de façon significative le risque d'insuffisance cardiaque, de troubles cognitifs et d'accident embolique[1]. La FA affecte environ 1 à 2% de la population. La prévalence augmente avec l'âge, allant de 0.5% avant 40-50 ans jusqu'à 10% chez les patients octogénaires.[2] Une augmentation significative du nombre de sujets atteints est attendue dans les années à venir compte tenu du vieillissement de la population.[3] L'analyse la cohorte de Framingham, après ajustement pour les principales comorbidités associées, a mis en évidence une majoration du risque de mortalité de 50% chez l'homme et de 90% chez la femme.[4]

Différentes cardiopathies ou comorbidités cardio-vasculaires augmentent le risque de FA, telles que l'hypertension artérielle, la coronaropathie, la dysfonction ventriculaire gauche (quelle qu'en soit l'étiologie), les valvulopathies, les cardiopathies congénitales, ou la chirurgie cardiaque. La dilatation atriale, l'étirement (« stretch ») et/ou l'ischémie ont été décrits comme de potentiels mécanismes impliqués. La FA peut également survenir en l'absence de toute cardiopathie sous-jacente et est alors appelée « Lone AF » ou FA sur cœur sain. Par ailleurs, de nombreux facteurs extra-cardiaques prédisposent à la FA tels que la consommation d'alcool, l'hyperthyroïdie, le syndrome d'apnées-hypopnées du sommeil ou l'obésité.

L'histoire naturelle de la FA débute habituellement par des épisodes paroxystiques, définis par des épisodes de courte durée cédant spontanément dans les 7 jours (habituellement dans les premières 48 heures). Certains patients vont présenter des épisodes de FA paroxystique indéfiniment, mais une grande partie d'entre eux va évoluer vers la forme persistante, définie comme des épisodes de FA durant plus de 7 jours et nécessitant une intervention médicale (cardioversion électrique ou médicamenteuse) pour restaurer le rythme sinusal. Si la stratégie de contrôle du rythme échoue ou n'est pas ou plus souhaitée par le patient et/ou le médecin, la FA est définie comme permanente. L'inexorable progression de la FA paroxystique vers la FA persistante puis permanente reflète le remodelage électrophysiologique et structurel progressif survenant au niveau du tissu atrial, rendant les sources de l'arythmie plus stables, facilitant ainsi son caractère soutenu.

Malgré plus de 100 ans de recherche clinique et fondamentale, les mécanismes impliqués dans l'initiation et le maintien de la FA et ceux impliqués dans la transition de la forme paroxystique à la forme persistante sont mal connus. Par ailleurs, les thérapies aujourd'hui utilisées ne sont pas optimales. De nombreux traitements anti-arythmiques ont été testés et ont montré un succès limité dans les cas de FA persistante. A l'opposé, la démonstration par Haissaguerre et al.[5] en 1998 de la responsabilité des foyers veineux pulmonaires dans le déclenchement de la FA a significativement amélioré la prise en charge de la maladie, et aujourd'hui l'isolation veineuse pulmonaire est curative dans près de 70 à 80% des cas de FA paroxystique.[6] Cependant, le succès de l'ablation de la FA persistante et ce d'autant qu'elle est de longue-durée reste limité. Incontestablement, seule une meilleure compréhension des mécanismes impliqués dans le maintien de cette arythmie nous permettrait de concevoir des traitements curatifs et/ou préventifs plus efficaces et spécifiques.

Le présent travail a pour but de présenter différents travaux effectués afin de progresser dans la connaissance sur la FA et sa prise en charge thérapeutique. Dans une

première partie, nous exposerons les études effectuées dans le but d'améliorer la compréhension des mécanismes physiopathologiques impliqués dans la genèse et le maintien de l'arythmie (*Circ Arrhythm Electrophysiol. 2012 ;5 :1160-1167*), les techniques utilisées pour l'étude de la dynamique des ondes fibrillatoires (*J Vis Exp, 2011 ;53*) ainsi que des travaux de revue sur la physiopathologie de cette arythmie (*Circ Arrhythm Electrophysiol. 2012 ;5 :1207-1215*).

Ensuite, nous exposerons un travail de recherche portant sur l'analyse de la transition de la FA paroxystique à la FA persistante (*Circulation, under review*) et le modèle animal utilisé (*Manual of Research Techniques in Cardiovascular Medicine, Chapter 3: Generating a large animal model of persistent atrial fibrillation*).

Enfin, nous aborderons la prise en charge thérapeutique de l'arythmie, en exposant des travaux portant sur les anti-arythmiques (*Circ Arrhythm Electrophysiol .2012 ;5 :561-570*) et l'ablation par cryothérapie (*Heart Rhythm, under review*).

.

Première partie

Eléments généraux de physiopathologie

A. Généralités

En 1924, Walter Garrey publiait une revue de la littérature de 36 pages sur la FA dans *Physiological Reviews*,[7] contenant plus de 150 références. En 2011, le même journal publiait à nouveau une revue sur le même thème, signée par Ulrich Schotten, de 61 pages et contenant 656 références.[8] En près d'un siècle de recherche clinique et fondamentale, nos connaissances sur les mécanismes gouvernant la FA ont considérablement avancé. Les travaux cliniques ainsi que les modèles animaux de FA créés au cours des 20 dernières années,[9] parmi lesquels les modèles de stimulation atriale à haute fréquence,[10, 11] ont permis de mieux appréhender la physiopathologie de cette arythmie.

D'une façon générale, l'initiation et l'entretien d'une arythmie dépendent de la conjonction de trois facteurs : une gâchette (« triggers »), un substrat propice, et l'action du système nerveux autonome, ensemble connu sous le nom de « Triangle de Coumel ». Comme nous le verrons, les triggers déclenchant la FA proviennent préférentiellement des veines pulmonaires (VP),[5] structures qui sont également impliquées dans le maintien de l'arythmie. Plusieurs théories ont successivement été émises pour expliquer l'initiation et l'entretien de la FA, telles que les ectopies atriales focales, les « leading circles », les rotors ou la théorie des vaguelettes multiples (« multiple wavelets theory »). Nous allons exposer brièvement ces différentes hypothèses avant d'expliquer le rôle majeur des VP dans la FA.

1. L'hypothèse focale

Les ectopies atriales focales peuvent résulter d'une hyperautomaticité (dépolarisation diastolique spontanée) ou d'activités déclenchées (post-dépolarisations).

Les post-dépolarisations tardives (« Delayed after-depolarizations » = DAD) sont une importante source d'ectopies. Elles sont la conséquence d'une anomalie de l'homéostasie calcique, principalement secondaire à une fuite de calcium (Ca^{2+}) à travers les récepteurs à la ryanodine de type 2 (RyR2).[12] Cette fuite peut résulter d'une augmentation de la concentration en Ca^{2+} dans le réticulum sarcoplasmique, d'une diminution de la chélation calcique dans le réticulum sarcoplasmique par la calsequestrine ou d'une hyperphosphorylation du RyR2 augmentant alors sa sensibilité à la concentration sarcoplasmique intra-luminale en Ca^{2+}.[13] La fuite calcique sarcoplasmique aboutit à un excès diastolique en ions Ca^{2+} qui vont être pris en charge par l'échangeur sodium-calcium (NCX). Le NCX transporte 3 ions sodium (Na^{+}) à l'intérieur du cardiomyocyte en échange de l'extrusion d'un ion Ca^{2+}. Cet échange d'ions est électrogène et crée un courant net dépolarisant appelé « courant entrant transitoire » (transient inward current, I_{ti}) capable d'initier un potentiel d'action si la dépolarisation atteint le potentiel seuil. Voigt et al. ont récemment démontré ce mécanisme chez l'homme sur des échantillons d'oreillette droite (OD), mécanisme faisant intervenir l'hyperphosphorylation de RyR2 mediée par la Calmoduline Kinase de type II (CaMKII) et l'hyperactivation du NCX.[14]

Les post-dépolarisations précoces (« Early after-depolarizations » = EAD) surviennent quand le potentiel d'action (PA) est excessivement prolongé, permettant aux canaux calciques de sortir de leur état d'inactivation et d'initier un nouveau PA.[15]

Des EAD particulières, dénommées « EAD tardives en phase 3 » (« late phase 3 EADs »), survenant lorsque deux situations concomitantes sont présentes, à savoir un raccourcissement du PA et une augmentation de la concentration en calcium intra-cellulaire, ont été décrites comme étant responsables de récurrences précoces de FA après retour à un rythme sinusal.[16] Ce phénomène, décrit initialement chez le chien, n'a pour le moment pas encore été démontré chez l'homme.

2. L'hypothèse réentrante

a. La « multiple wavelets theory » et le « leading circle »

Très tôt, des constatations expérimentales ont mis en évidence que des phénomènes réentrants étaient impliqués dans l'initiation et le maintien de la FA. La responsabilité de tels phénomènes comme sources de la FA a été décrite initialement par Mines en 1913[17] et implémentée plus tard par Lewis qui a décrit le « circus movement hypothesis of reentry ».[18] Lewis a émis l'hypothèse que des phénomènes de réentrée pouvaient expliquer le flutter atrial et la FA, selon la taille du circuit et la période réfractaire du tissu. Cette hypothèse est par la suite devenue controversée quand l'école prônant l'hypothèse d'une origine focale à la FA a regagné de l'intérêt.[19] A l'inverse, Gordon Moe proposait une théorie décrivant la FA comme étant le résultat de « multiples fronts d'activation, changeant constamment en nombre et en direction ».[20] D'après cette théorie, de multiples fronts d'activation se propagent dans les oreillettes, avec pour conséquence de multiples interactions entre fronts et queues d'activation (« wavefront-wavetail interactions »), des collisions d'ondes et des blocs de conduction.[21] Des modélisations informatiques[22] et des études expérimentales chez l'animal[23] confirmant cette hypothèse ont par la suite été publiées, appuyées également par le succès de la procédure chirurgicale d'ablation de la FA (Cox-Maze) dans laquelle la compartimentalisation des oreillettes empêche les vaguelettes de s'auto-entretenir.[24]

En 1973, Allessie et al. firent une découverte essentielle en démontrant qu'une réentrée pouvait s'auto-entretenir en l'absence d'obstacle anatomique.[25] D'après ce concept, dénommé le « leading circle », la taille du circuit de réentrée adopte la taille minimale possible déterminée par la longueur d'onde du circuit (défini comme le produit de la vitesse de conduction et de la période réfractaire du tissu). Le centre de rotation est maintenu réfractaire par l'activation électrotonique continue provenant du front de dépolarisation, engendrant une réentrée fonctionnelle. La principale caractéristique du « leading circle » est la présence d'un gap excitable minime, rendant l'arrêt de la réentrée par stimulation prématurée improbable. Par ailleurs, de minimes changements dans les propriétés électrophysiologiques du tissu auront des conséquences importantes dans la dynamique de la réentrée, favorisant alors son arrêt spontané. Le nombre de « leading circles » pouvant coexister dans un même tissu dépend de la taille de celui-ci et de la longueur d'onde des circuits. Ainsi, la dilatation atriale et le raccourcissement de la longueur d'onde augmentent le nombre de « leading circles » pouvant exister au sein de l'oreillette.

Cette théorie a prévalu pendant une vingtaine d'années jusqu'à ce qu'on démontre qu'elle ne pouvait pleinement expliquer le maintien de la FA.[26] Les principaux points allant à

l'encontre de cette théorie étaient : 1) le fait que le centre de rotation est constamment dépolarisé, empêchant le front d'activation de l'envahir et à la réentrée de se déplacer ; or, le déplacement constant des réentrées a été démontré dans les oreillettes en FA mais également dans les ventricules en fibrillation ventriculaire (FV)[27, 28] ; 2) les bloqueurs des canaux sodiques (i.e. la flécaïnide) sont très efficaces pour restaurer le rythme sinusal, particulièrement en cas de FA paroxystique ; or ils diminuent la vitesse de conduction et selon le concept du « leading circle » devraient réduire la longueur d'onde des circuits de réentrée et favoriser l'entretien de l'arythmie. L'allongement des périodes réfractaires contrecarre en pratique cet effet, et explique l'efficacité de la flécaïnide.

b. Les rotors

A l'époque où le concept de « leading circle » émergeait, une nouvelle forme de réentrée était théorisée, à savoir les rotors.[29] Un rotor est défini comme une réentrée fonctionnelle organisée autour d'un core central (Figure 1). L'onde bidimensionnelle résultant de cette réentrée est appelée une « onde spirale » (« spiral wave »). Son équivalent tridimensionnel est une « scroll wave » (ou « onde rouleau »).

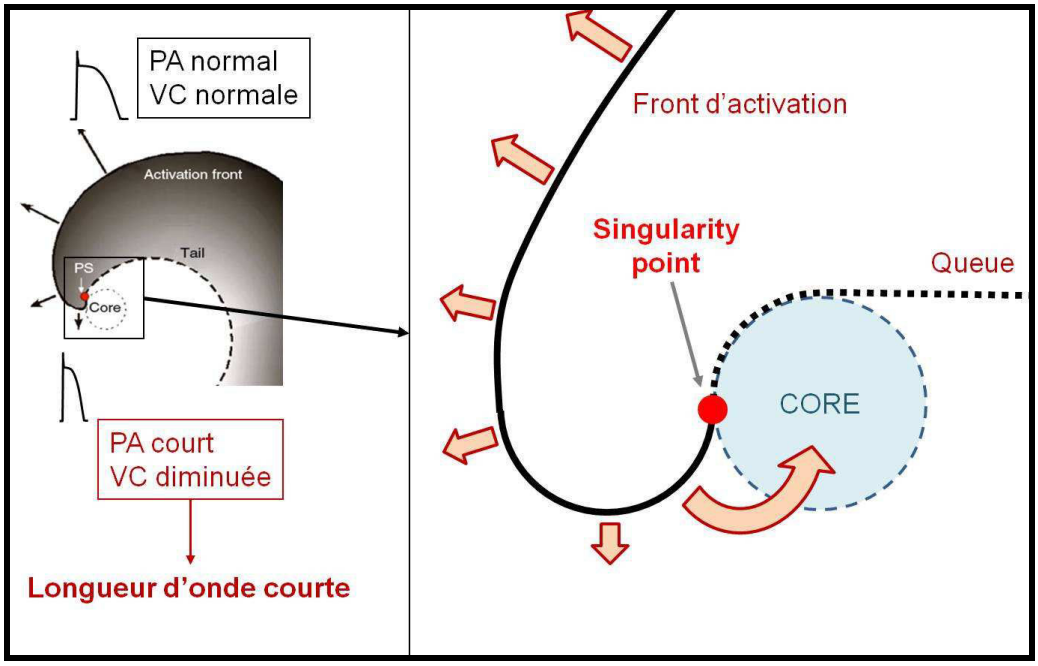

Figure 1 : Schéma d'un rotor. A gauche : Schématisation du front d'activation convexe, avec, à mesure qu'on se rapproche du centre de rotation, un raccourcissement de la durée du potentiel d'action et une diminution de la vitesse de conduction. A droite : La courbure du front d'activation augmente à mesure que l'on se rapproche du centre de rotation jusqu'au point de singularité, zone où la courbure atteint une valeur critique, séparant alors le front de la queue d'activation.

L'existence des rotors a été initialement prouvée sur des modélisations informatiques[30] puis dans des études expérimentales.[31] Leurs propriétés fondamentales sont les suivantes :[32] 1) ils peuvent être fixes ou mobiles ; 2) le core est une zone excitable mais non excitée; 3) la

courbure du front de dépolarisation est de plus en plus convexe à mesure que l'on se rapproche du centre de rotation, résultant en une diminution progressive de la vitesse de conduction et de la durée du PA ; par conséquent, la longueur d'onde est plus courte près du core central ; 4) le front d'activation et sa queue se rencontrent au niveau du point de singularité, i.e. le point de pivot central de la réentrée fonctionnelle ; 5) dans une structure tridimensionnelle (comme le tissu atrial), les rotors peuvent traverser l'épaisseur du myocarde, avec présence d'un point de singularité sur l'épi- et l'endocarde, prenant alors un forme dite en I. Des formes non linéaires (en L, en U, en O,…) peuvent être générées.

Quelques différences fondamentales existent entre les théories des rotors et celle des « leading circles ». Tout d'abord, la théorie du « leading circle » ne prend pas en compte la courbure du front d'activation comme facteur modulant la vitesse de propagation de l'influx et la dynamique de l'activité réentrante.[33] Au contraire, la théorie des rotors donne à ce paramètre une importance majeure. En effet, une onde concave se propage plus rapidement qu'une onde plane, elle-même se propageant plus rapidement qu'une onde convexe. Ce phénomène est lié à un mécanisme dénommé « sink-source mismatch » : dans le cas d'une onde convexe, chaque cellule du front d'activation doit dépolariser un nombre plus important de cellules en aval, ce qui ralentit la conduction, alors que dans le cas contraire, chaque cellule d'aval est dépolarisée par plusieurs cellules en amont et la vitesse de conduction résultante est élevée. En ce qui concerne les rotors, l'onde de propagation est courbe et convexe, convexité qui se majore de plus en plus à mesure que l'on se rapproche du core central. Au niveau du point de singularité, la courbure est telle qu'elle atteint une valeur critique qui empêche l'activité d'envahir le core et explique que ce point sépare le front de la queue d'activation.

Cette propriété explique la seconde différence majeure entre les 2 théories : dans la théorie du « leading circle », le centre de rotation est entièrement réfractaire, compte tenu de sa perpétuelle invasion par les ondes centripètes provenant de l'activité rotatoire. Ceci l'empêche en théorie de se déplacer au sein d'un tissu et l'activité rotatoire est supposée être fixe. A l'opposé, le core central autour duquel tourne un rotor est excitable mais non excité et perpétuellement envahi par le front d'activation, ce qui le rend mobile est lui permet de se déplacer à mesure que la rotation s'effectue.

Troisième différence majeure, la longueur d'onde du tissu n'est pas fixe comme cela est théorisé dans le « leading circle » mais se raccourcit à mesure que l'on se rapproche du point de singularité (comme conséquence du raccourcissement de la durée du potentiel d'action et du ralentissement de la vitesse de conduction, Figure 1).

Enfin, la théorie des rotors implique la présence d'un gap excitable de grande taille, prenant lui aussi une forme de spirale, puisque suivant constamment la queue d'activation.[34]

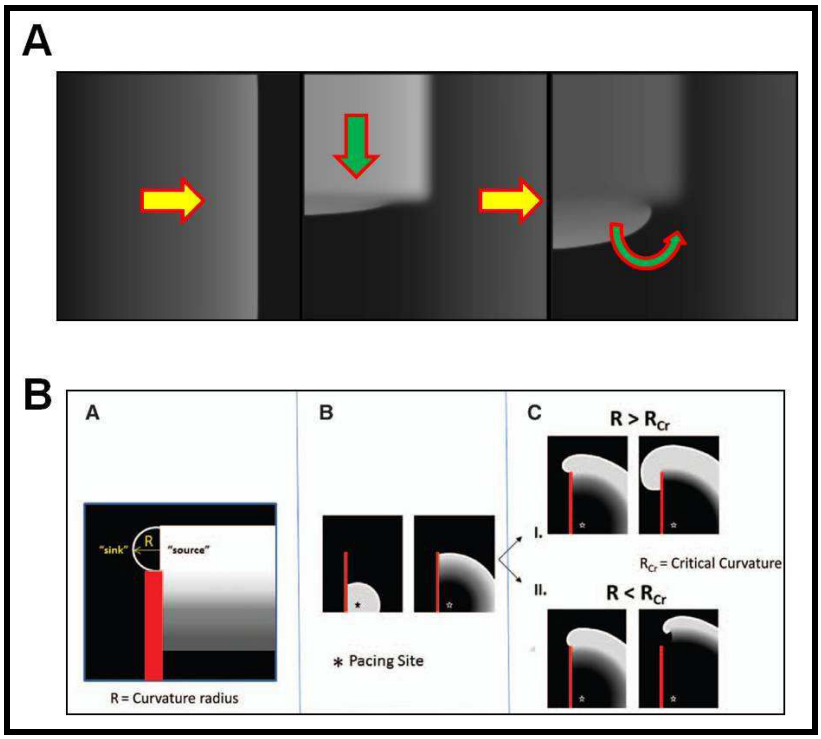

Figure 2 : Initiation d'un rotor. A. Collision entre un front d'activation (vert) avec une queue d'activation (jaune). B. Collision d'un front d'activation avec un obstacle anatomique (représenté en rouge). En fonction du rayon de courbure du front d'activation, celui-ci se propage autour de l'obstacle (c. en haut) ou se détache (c. en bas), créant ainsi un rotor. Modifié d'après Pandit et al.[35]

L'étape initiale dans l'initiation d'un rotor est la rupture d'un front d'activation (« wavebreak ») résultant de sa collision avec une queue d'activation (« wavefront-wavetail interaction », Figure 2A). L'autre mécanisme d'initiation est une collision avec un obstacle fonctionnel ou anatomique, par un phénomène de « vortex shedding » (détachement tourbillonnaire, Figure 2B).[36] Ce phénomène particulier explique par exemple les turbulences créées quand un flux d'eau ou d'air rencontre un obstacle étroit (pylône d'un pont ou aile d'avion). En fonction du rayon de courbure du front d'activation, celui-ci contourne l'obstacle ou se détache pour initier un rotor. Différentes conditions physiopathologiques, telles que l'ischémie ou le remodelage atrial (par une diminution de la densité du courant I_{Na} réduisant l'excitabilité et l'apparition de fibrose créant des obstacles à la propagation de l'influx), créent le lit de l'initiation et du maintien de la FA.

L'existence des rotors a été prouvée *ex-vivo* dans de nombreuses espèces, de la souris à l'homme. Une loi universelle déterminant la fréquence des rotors en FV a été retrouvée par Noujaim et al, mettant en relation la masse corporelle et la fréquence de rotation.[37] En regroupant 40 études sur 11 espèces différentes (de la souris au cheval), les auteurs ont mis en évidence que la fréquence des rotors en FV était d'environ 18.9 x Masse Corporelle$^{-1/4}$ (de 38.0Hz chez la souris à 6.8Hz chez l'homme). Ce phénomène doit probablement être en relation avec la durée des PA et la masse ventriculaire. La fréquence en FA doit vraisemblablement suivre un tel type de relation, bien que ceci n'ait pour le moment pas été démontré.

Les progrès concernant la cartographie optique (« optical mapping ») ont permis d'étudier la dynamique des rotors via la réalisation de cartes de phase (« phase mapping »). Cette technique permet d'identifier les points de singularité et les différentes phases de dépolarisation/repolarisation des ondes fibrillatoires. Les rotors peuvent ainsi être visualisés et leur dynamique étudiée (Figure 3).

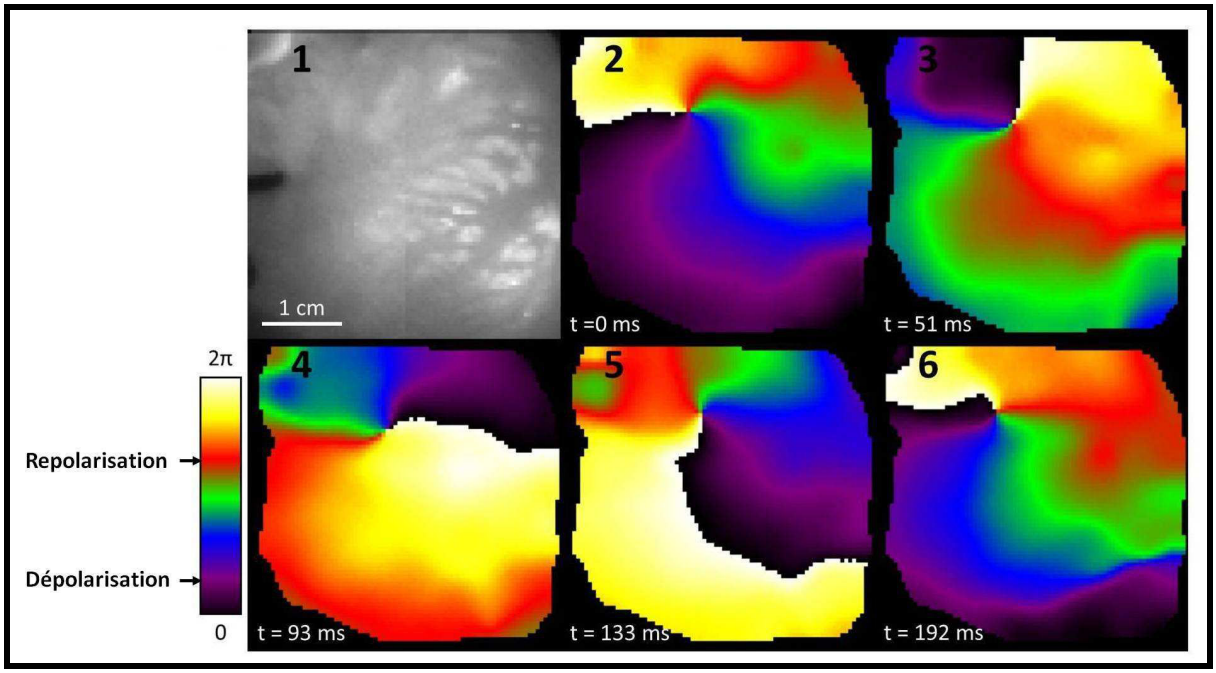

Figure 3. Rotor visualisé lors d'une expérience d'optical mapping, avec cartographie de phase. Image 1. Visualisation de la paroi latérale de l'oreillette gauche (OG) qui est cartographiée pendant l'expérience; une sonde de stimulation visible à gauche de l'image permet de stimuler à haute fréquence et déclencher la FA. Images 2 à 6 : Visualisation d'un rotor stable tournant dans le sens horaire.

Par ailleurs, l'analyse spatio-temporelle de l'activité peut être associée à une analyse fréquentielle du signal. Ainsi, en appliquant une transformée de Fourrier rapide (Fast Fourier Transform = FFT) sur les signaux optiques, on obtient une carte de fréquence d'activation de l'aire cartographiée, qui permet d'apprécier la distribution spatiale des fréquences et de connaitre la fréquence dominante (dominant frequency = DF) de la surface étudiée, appelée DF maximale (DF_{max}). Un exemple d'analyse fréquentielle réalisée lors d'une expérience de cartographie optique est montré dans la Figure 4.

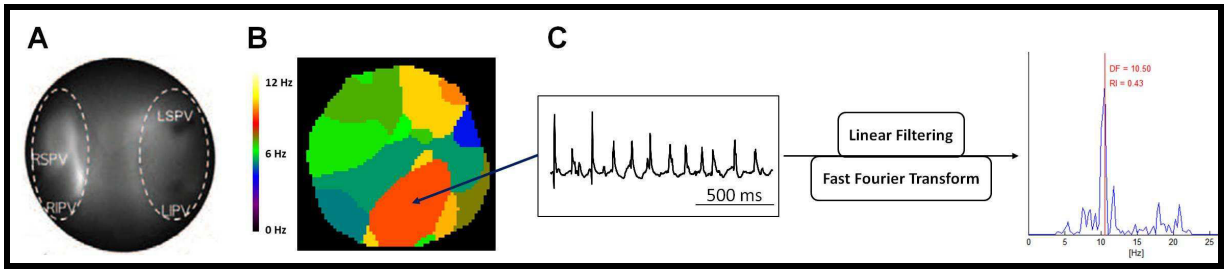

Figure 4. Analyse fréquentielle de l'activité atriale en FA. A. Dans cette expérience, la surface cartographiée est l'endocarde de la paroi postérieure de l'OG. B. Une carte de fréquence d'activation de l'aire cartographiée peut alors être obtenue par application d'une FFT sur les signaux optiques. C. La DF_{max} dans cet exemple est de 10.5Hz.

Ainsi, une très grande organisation spatio-temporelle des rotors a été démontrée, et leur responsabilité dans le maintien de la FA confirmée.[27] L'hétérogénéité tissulaire (périodes réfractaires effectives et « sink-source » mismatch), la fibrose[38] et les obstacles anatomiques (orifices veineux et valvulaires) rendent la conduction en 1:1 à partir d'un rotor impossible et résultent en une cassure du front de dépolarisation et en une conduction fibrillatoire dans l'ensemble de l'oreillette.[39]

Un ou plusieurs rotors peuvent maintenir une oreillette en FA, chacun ayant une fréquence de rotation différente, dont l'un, ayant une fréquence plus élevée, entretien le maintien des autres. Au cours d'un épisode, certains rotors s'éteignant et d'autres réapparaissant à la faveur de nouvelles collisions des fronts d'activation. Dans la plupart de cas, la fin d'un épisode de FA s'explique par la collision du point de singularité du rotor principal avec un obstacle anatomique, entrainant l'extinction de l'ensemble des ondes spirales.

La démonstration récente de l'existence de rotors chez l'homme a confirmé leur importance dans le maintien de la FA,[40] et devrait mener au développement de nouveaux outils thérapeutiques permettant probablement d'améliorer l'efficacité des procédures d'ablation endocavitaire.

L'ensemble de ces mécanismes (hyperautomaticité, activités déclenchées, vaguelettes multiples, rotors) est probablement associé à un degré variable selon le type de FA (paroxystique, persistante ou permanent) et selon l'existence ou non d'une cardiopathie sous-jacente.

3. La FA en pratique clinique

a. L'importance des veines pulmonaires

L'initiation d'un épisode de FA nécessite une gâchette (« trigger ») qui engendre l'arythmie et un substrat prédisposé pour maintenir l'arythmie. Chez l'homme, des nombreux travaux ont démontré l'importance des VP dans l'initiation de la FA.

Le rôle essentiel des VP a été originellement décrit par Haissaguerre et al. en 1998.[5] Dans cette étude, les auteurs ont démontré que les VP étaient une source majeure d'ectopies initiant des épisodes de FA paroxystique, et pouvant être la cible des thérapies ablatives. Cette découverte a mis en évidence l'importance des VP dans le déclenchement de la FA et particulièrement celle des manchons de tissu musculaire pénétrant les VP (Figure 5). Ces extensions ont été initialement décrites chez l'homme plus de 40 ans auparavant[41] mais le travail d'Haissaguerre et al. a suscité la publication de nombreux travaux décrivant plus précisément l'anatomie et les propriétés électrophysiologiques des VP.

Dans une étude autopsique, Hassink et al. ont retrouvé ces extensions myocardiques chez 100% des patients aux antécédents de FA, mais également chez 85% des patients n'en ayant jamais présenté.[42] Les patients avec un antécédent de FA présentaient cependant plus d'hétérogénéité dans l'architecture des manchons myocytaires, plus de myocytes hypertrophiques et plus de fibrose. Ces extensions myocardiques s'organisent en un réseau complexe à la surface externe des VP, séparées de la couche de cellules musculaires lisses

veineuses par un tissus fibro-adipeux. Les caractéristiques anatomiques des manchons (étendue en longueur et en circonférence) sont différentes à l'échelon inter-individuel mais également entre chacune des VP d'un même patient. Ainsi, des extensions variant entre 0.4 et 4.8 cm de longueur, le plus souvent entre 1 et 1.3 cm, ont été décrites.[42-45] Leur épaisseur est plus importante dans la région inter-veineuse (carène, partie inférieure des VP supérieures et supérieure des VP inférieures) et est corrélée avec la présence de potentiels veineux pulmonaires (PVP) pouvant être enregistrés par des cathéters dédiés. Ces PVP peuvent être enregistrés chez des patients n'ayant jamais présenté de FA, mais présentent alors des caractéristiques différentes, en termes d'amplitude, de durée et de couplage par rapport au potentiel atrial.[46]

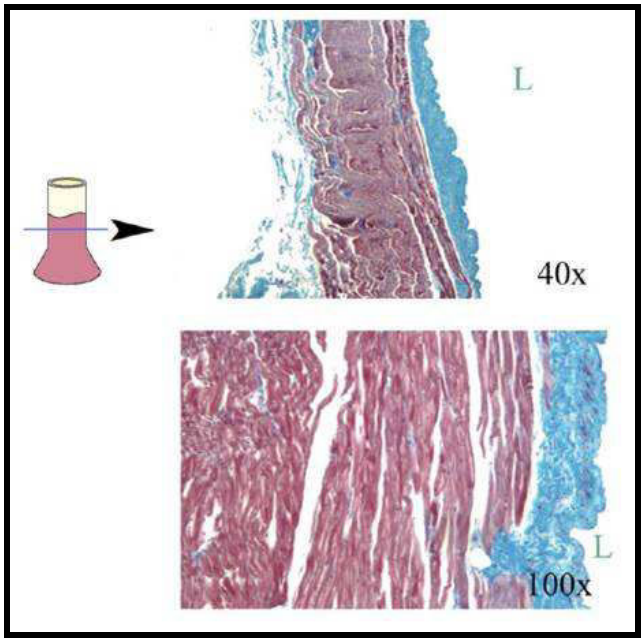

Figure 5 : Manchons myocytaires veineux pulmonaires. Section d'une VP de chien (coloration au trichrome de Masson). Une organisation hétérogène des fibres musculaires est visible. La face endoluminale de la VP est marquée par un « L ». Modifié d'après Verheule et al[47] et Schotten et al.[8]

Les myocytes des VP ont des propriétés électrophysiologiques distinctes : leur potentiel transmembranaire de repos est moins négatif que celui du tissu atrial environnant (#-70mV), la densité des courants I_{CaL}[48] et I_{K1}[49] réduite, alors que celle d'I_{Kr}[48] et d'I_{Ks}[48] est augmentée. D'autre part, la densité en connexine-40 est diminuée.[47, 50] Une hétérogénéité dans le potentiel trans-membranaire de repos, la durée du PA (qui est plus courte que celle du tissu atrial) et la période réfractaire effective cellulaire entre la partie proximale et distale des manchons mycoytaires a également été décrite, expliquant le rôle essentiel de cette région dans l'initiation et le maintien de la FA.[51]

Le mécanisme exact du caractère pro-arythmique des VP est inconnu. Les différents mécanismes décrits précédemment (hyperautomaticité, micro-réentrées et activités déclenchées) sont probablement en cause. Les caractéristiques propres des myocytes veineux pulmonaires en association avec l'architecture chaotique des manchons myocytaires expliquent très certainement le fait qu'elles soient le siège d'ectopies initiant la FA ; l'anisotropie et l'hétérogénéité de conduction locales permettant quant-à-elles de perpétuer l'arythmie par un mécanisme de « sink-source mismatch ».[52, 53] Le stretch atrial a été démontré comme étant responsable d'une organisation des ondes de dépolarisation provenant de la jonction entre la partie supérieure des VP et de l'OG, mécanisme physiopathologique

expliquant probablement pourquoi les patients ayant une dilatation atriale et une augmentation de la pression atriale ont un risque plus élevé de développer des arythmies.[54]

Hormis les VP, d'autres structures ont été décrites comme étant responsables de l'initiation et du maintien de la FA.[55] La veine cave supérieure (VCS) est probablement la plus fréquente, responsable chez 37% des patients présentant des triggers extra-veineux pulmonaires.[55] Les autres sources d'ectopies sont le ligament de Marshall (reliquat de la VCS gauche), le sinus coronaire, la crista terminalis, et la veine cave inférieure. L'ensemble de ces foyers peut être traité par les méthodes d'ablation.

b. Les électrogrammes complexes fractionnés atriaux

Les électrogrammes complexes atriaux fractionnés (complex fractionnated atrial electrograms = CFAE) sont des électrogrammes endocavitaires enregistrés dans l'oreillette au cours d'un épisode de FA présentant 1) un fractionnement important, 2) des cycles courts (<120ms) et/ou 3) un bas-voltage (0.06 à 0.25 mV) et 4) des potentiels multiples.[56] Nademanee et al. ont été les premiers à cibler ces potentiels via l'ablation par radiofréquence (RF) chez les patients présentant une FA réfractaire au traitement anti-arythmique, démontrant alors un taux d'arrêt per-procédure de la FA élevé et un faible taux de récidive au cours du suivi.[57] Une récente méta-analyse des principales études ayant évalué l'efficacité de l'ablation des CFAE en complément d'une isolation veineuse pulmonaire standard a démontré une augmentation du taux de persistance du rythme sinusal chez les patients présentant une FA non-paroxystique, après une seule procédure sans adjonction d'anti-arythmiques.[58] A l'opposé, les patients présentant une FA paroxystique ne semblent pas tirer bénéfice de cette stratégie.

Bien que ces résultats soient prometteurs, une approche plus mécanistique est nécessaire afin d'appréhender au mieux ces potentiels, mais à ce jour, malgré de nombreux travaux, leur réel implication dans le maintien de la FA est inconnu. Deux hypothèses sont possibles. D'une part, ils pourraient représenter des marqueurs de zones critiques dans l'entretien de l'arythmie, telles que des zones de fibrose, ou des zones hétérogènes où peuvent s'ancrer les rotors. Cette hypothèse est vérifiée par l'efficacité de l'ablation des CFAE dans certaines situations cliniques, mais également par leur stabilité temporelle et spatiale sur différents épisodes de FA chez un patient donné.[59] A l'opposé, ces zones de CFAE pourraient en fait ne représenter que des territoires passifs de ralentissement/blocs de conduction ou de collisions/cassures de fronts d'activation situés plus ou moins loin d'un rotor,[60, 61] expliquant alors pourquoi ils peuvent être enregistrés sur des oreillettes saines[62, 63] et l'inefficacité relative de l'ablation ciblée sur ces régions.

La localisation des plexi ganglionnaires dans l'OG concorde avec celle où sont enregistrés des CFAE,[64] et il a été proposé que ces derniers pouvaient en fait refléter l'activation du système nerveux autonome. Cependant, tout comme l'ablation des CFAE, l'ablation des plexi ganglionnaire est controversée et n'a pas démontré de réel bénéfice sur le maintien du rythme sinusal à long terme.[65-67]

La limite majeure concernant la cartographie et l'ablation des CFAE est liée à leur définition même. En effet, la définition de la Heart Rhythm Society, de l'European Heart

Rhythm Association et de l'European Cardiac Arrhythmias Society (HRS/EHRA/ECAS)[56] inclus différents paramètres objectifs difficiles à utiliser au quotidien dans un laboratoire d'électrophysiologie, et la plupart des médecins utilisent une appréciation visuelle totalement subjective afin de définir ce qui est ou non un potentiel fragmenté. Il a ainsi été récemment démontré que le pourcentage de sites considérés comme des CFAE variait selon les critères choisis pour les définir.[61] L'utilisation d'algorithmes de détection automatique intégrés dans les systèmes de cartographie tridimensionnelle a permis de faciliter l'identification de ces potentiels,[68] mais de nouveaux travaux de recherche seront nécessaires afin de savoir si ces sites sont ou non des régions actives dans le maintien de la FA et donc de potentielles cibles de l'ablation.

4. Remodelage atrial secondaire à la FA

Des épisodes courts de FA peuvent survenir sur des oreillettes saines. Cependant, une modification significative des propriétés électrophysiologiques et structurelles des oreillettes est nécessaire afin de soutenir des épisodes sur une durée prolongée. Ce mécanisme, appelé « remodelage atrial » est une conséquence directe de l'arythmie et favorise son entretien. Depuis le milieu des années 1990, de nombreuses équipes ont étudié les différents éléments impliqués dans le remodelage atrial en utilisant des modèles animaux.[10, 11]

a. Remodelage électrophysiologique

L'activation rapide des myocytes atriaux en FA va provoquer une augmentation de la concentration intra-cellulaire en Ca^{2+}. Afin de limiter la surcharge calcique, les cardiomyocytes atriaux vont déclencher des mécanismes protecteurs d'action rapide et retardée en activant la chaine calcineurine/calmoduline Ca^{2+} dépendante. La translocation nucléaire de NFAT (*nuclear factor of activated T cells*) médiée par la calcineurine va entrainer une régulation négative de la transcription de la sous-unité α du gène codant I_{CaL}, Cav1.2.[69] Le microARN miR-328, surexprimé chez les patients et les chiens en FA, a été démontré comme favorisant la dégradation du transcrit de Cav1.2 et contribue au remodelage électrique au cours de l'arythmie,[70] et de nombreux autres mécanismes ont été impliqués dans la diminution du courant I_{CaL}. Ces altérations du métabolisme calcique intra-cellulaire sont également responsables de la dysfonction contractile observée après récupération du rythme sinusal.

La conséquence immédiate de la diminution de I_{CaL} est la réduction de la durée du PA et de la période réfractaire effective de l'oreillette, diminuant alors la longueur d'onde et facilitant la présence de multiples circuits de réentrée. L'augmentation du courant potassique à rectification entrante (I_{K1}) due en partie à une augmentation de sa sous-unité Kir2.1 est également impliquée dans le raccourcissement de la durée du PA.[71] Cette augmentation est probablement la conséquence d'une réduction des micro-ARN inhibiteurs miR-1 et miR-26.[72] L'augmentation de la densité d'I_{K1} va accélérer la fréquence de rotation des rotors et accroitre leur stabilité, ainsi que favoriser l'hyperexcitabilité cellulaire par l'hyperpolarisation membranaire et la majoration de la disponibilité du courant sodique.[34] Un gradient d'I_{K1}

gauche-droit a récemment été décrit et explique sans doute en partie la présence de DF_{max} plus élevées dans l'OG.[73] La densité du courant potassique à rectification entrante constitutivement actif et dépendant de l'acétylcholine (I_{KAch}) est également augmentée et contribue au raccourcissement du PA.[74] Les mécanismes impliqués dans les modifications de densité d' I_{KAch} sont une augmentation de l'activité de la protéine kinase activatrice PKCε et une dimuntion de l'activité inhibitrice de la PKCα.[75] De façon similaire à I_{K1}, un gradient gauche-droite d'I_{KAch} et des niveaux élevés d'ARNm de Kir3.4 ont été mis en évidence chez les moutons[76] comme chez l'homme.[77] Ceci explique également l'effet plus prononcé de l'acétylcholine sur l'OG comparé à l'OD.[76] En résumé, au-delà du rôle des obstacles anatomiques (tels que le faisceau de Bachmann) dans la fragmentation des ondes de fibrillation et dans la diminution de la fréquence d'activation de l'OG vers l'OD, des propriétés éléctrophysiologiques distinctes concernant les canaux potassiques expliquent le gradient de DF observé chez l'animal comme chez l'homme.[73, 76, 78]

Différents modèles animaux ont mis en évidence une diminution du courant sodique entrant I_{Na},[79, 80] mais les résultats publiés chez l'homme sont discordants, retrouvant tantôt une diminution[71] ou aucune modification[81] de la densité de ce courant. Comme décrit précédemment, l'augmentation du courant I_{K1} va entrainer une cinétique de récupération de l'inactivation plus rapide ainsi qu'une augmentation de la disponibilité des canaux sodiques.

Les autres modifications ioniques induites par la FA incluent : une diminution du courant potassique sortant transitoire et à rectification retardée (I_{to} et I_{Kur})[82, 83] et une augmentation du courant I_{NCX} (échangeur sodium potassium).[84] Les données concernant I_{Kr} et I_{Ks} sont rares et controversées, mettant en évidence soit une diminution, soit aucun changement, selon le modèle animal étudié (stimulation atriale rapide ou FA associée à de l'insuffisance cardiaque).[84-86]

b. Remodelage structurel

La seconde forme de remodelage survenant après le passage en FA est d'ordre structurel, s'exprimant principalement par l'apparition de fibrose et d'un remodelage génique/protéique des cardiomyocytes. En 1997, Ausma et al ont décrit en détail ces modifications incluant l'hypertrophie myocytaire, la myolyse, l'accumulation de glycogène, le changement de forme et de taille des mitochondries, et la fragmentation du réticulum sarcoplasmique de chèvres en FA induite par stimulation rapide.[87] De telles modifications ont été confirmées sur des biopsies atriales chez l'homme.[88]

La fibrose atriale est une des principales conséquences structurelles de la FA. Les fibroblastes cardiaques, en se transformant en myofibroblastes sont à l'origine du remodelage du tissu conjonctif,[89] puisque produisant les protéines de la matrice extra-cellulaire ainsi que des cytokines affectant les propriétés des cardiomyocytes.[90] De nombreuses voies profibrotiques ont été décrites. Ainsi, l'angiotensine II, via ses récepteurs de type 1 est impliquée dans l'apparition de fibrose liée à la FA. D'autres voies de signalisation (telles que ERK/MAPK, JAK/STAT, Phospholipase C,…)[91] et de nombreuses cytokines (telles que le TGF-β,[92] le PDGF-β[93] et le CTGF[94]) ont été décrites comme d'importants facteurs de fibrose atriale.

Les myofibroblastes peuvent se connecter aux cardiomyocytes et affecter leurs propriétés électrophysiologiques.[95, 96] En effet, les myofibroblastes ont un potentiel trans-membranaire de repos moins négatif (environ -30mV) qui va modifier celui des cardiomyocytes vers des valeurs plus positives. En conséquence, la réactivation des canaux sodiques est ralentie et la pente de dépolarisation du PA (dV/dt) ainsi que la vitesse de conduction diminuées. La durée des PA des cardiomyocytes, dépendante de leur intensité de couplage aux myofibroblastes, va elle aussi être modifiée, pouvant se retrouver diminuée ou au contraire augmentée.

Le couplage et la vitesse de conduction myocyte-myocyte dépendent fortement des connexines (Cx). Une altération de l'expression et de la localisation des Cx40 et Cx43 apparait au cours de la FA.[97-99] Ces observations expliquent les formes familiales et monogéniques de FA chez les patients présentant une mutation de la Cx40.[100] Par ailleurs, Igarashi et al ont récemment démontré dans un modèle porcin de FA induite par stimulation rapide que le transfert atrial des gènes codant pour la Cx40 ou la Cx43 améliorait la conduction dans l'oreillette et prévenait l'apparition de formes plus soutenues de l'arythmie.[101]

En résumé, les modifications de couplage cardiomyocytes-myofibroblastes, associées à la présence d'obstacles anatomiques représentés par la fibrose entrainent une anisotropie de conduction, favorisant le maintien des réentrées et la perpétuation de la FA. Ce remodelage est une cible pour de potentielles interventions thérapeutiques.

c. Remodelage du système nerveux autonome

Des terminaisons nerveuses adrénergiques et cholinergiques sont présentes à forte densité autour des VP et de l'OG, principalement dans les 5mm autour de la jonction VP-OG.[102] Le système nerveux autonome cardiaque intrinsèque est un important acteur dans la FA.[103] Les systèmes sympathiques et parasympathiques favorisent l'initiation et le maintien de l'arythmie, respectivement par la genèse de DAD liées à l'activation des récepteurs β-adrénergiques et à une fuite diastolique de Ca^{2+} à travers récepteur à RyR2;[13] et par l'activation d'I_{KAch} menant à un raccourcissement de la durée du PA et à une stabilisation des rotors.[104] Un remodelage concernant ces 2 systèmes survient au cours de la FA, matérialisé par l'augmentation du nombre de terminaisons nerveuses sur la paroi postérieure de l'OG et au pourtour des VP.[104, 105]

Les interventions modulant l'activité du système nerveux autonome, qu'elles soient pharmacologiques ou non, pourraient constituer d'importantes stratégies thérapeutiques pour prévenir l'initiation de l'arythmie ou en empêcher le maintien. Le blocage sélectif d'I_{KAch} a une action anti-arythmique sur les modèles animaux via l'augmentation de la durée du PA.[106] Les modifications des périodes réfractaires atriales induites par la stimulation rapide peuvent être prévenues sur des modèles animaux par l'ablation des 4 principaux plexi ganglionnaires atriaux gauches et du ligament de Marshall,[107] ou par stimulation vagale.[108] L'ablation par RF des plexi ganglionnaires a été évaluée chez l'homme mais les résultats pour le moment publiés ont un faible niveau d'évidence.[109] Chez un groupe de patients présentant des épisodes de FA déclenchés par un mécanisme vagal, l'ablation des plexi ganglionnaires atriaux droits

seule (sans isolation des VP) a permis d'obtenir un taux de maintien du rythme sinusal de 70% à 18 mois.[110] De nouvelles études seront nécessaires afin de connaître l'exacte localisation des plexi ganglionnaire atriaux impliqués dans la FA et de déterminer le type de patients/d'arythmie qui pourrait tirer bénéfice d'une ablation ciblée.

5. Formes génétiques de FA

Des causes génétiques[111] et développementales[112] ont récemment été décrites comme étant à l'origine de certains types de FA. Une prédisposition génétique a été mise en évidence dans l'étude de Framingham mettant en évidence une augmentation de 85% du risque d'apparition de FA chez les patients dont au moins un des parents était atteint.[113]

Des études développementales ont démontré que le myocarde des VP exprimait le facteur de transcription Nkx2-5 et sa cible le gène *Cx40*. La sous-expression de Nkx2-5 modifie le phénotype de ces cellules en les transformant en cellules de type « pacemaker » Cx40-négative, Hcn4-positives.[112] Ainsi, une réduction de l'expression de ce facteur de transcription pourrait donner aux myocytes des VP un phénotype plus nodal augmentant leur propension à l'automaticité. Cette observation a par la suite été confirmée par la découverte de mutations de Nkx2-5 chez des patients en FA.[114]

A l'heure actuelle, de très rares mutations monogéniques responsables de formes familiales de FA ont été décrites, affectant des gènes modifiant les propriétés électrophysiologiques ou structurelles des oreillettes.

La majorité des mutations affectant des sous-unités des canaux ioniques reproduisent les conséquences du remodelage électrophysiologique des formes non-familiales de FA, à savoir le raccourcissement du PA et des périodes réfractaires effectives des cardiomyocytes atriaux. Différentes mutations responsables d'un gain de fonction du courant potassique I_{Ks} ont été décrites. Ces mutations affectent soit la sous-unité α formant le pore du canal ionique (*KCNQ1*[115-117]) ou sa sous-unité β (*KCNE2*[118], *KCNE5*[119]) et provoquent une augmentation du courant sortant repolarisant. Une mutation du gène codant pour Kir2.1 responsable du courant potassique à rectification entrante I_{K1} (*KCNJ2*) a été décrite.[120] Cette mutation résulte en un gain de fonction d'I_{K1}, situation connue pour augmenter la stabilité et la fréquence de rotation des rotors lors en FA et en FV.[121] Un gain de fonction du canal hERG codé par le gène *KCNH2* a été décrit comme étant responsable de phénotypes mixtes associant syndrome du QT court et FA.[122] Récemment, 2 mutations dans le gène *KCNA5* codant pour le canal potassique ultra-rapide à rectification retardée I_{Kur} et responsables d'une perte de fonction ont été décrites.[123, 124] Les analyses fonctionnelles de ces mutants ont mis en évidence une prolongation du PA et la présence d'activités déclenchées potentiellement responsables de l'initiation d'épisodes de FA. Des mutations du canal sodique ont été retrouvées chez des patients présentatnt une histoire familiale de FA avec des phénotypes le plus souvent mixtes (associés à des cardiomyopathies dilatées, des troubles conductifs ou un syndrome de Brugada), bien que les mécanismes reliant la mutation à l'apparition de FA sont obscurs. Deux mutations de type perte de fonction[125, 126] et une de type gain de fonction[127] dans la sous-unité α du canal sodique ont été décrites. Enfin, deux mutations de type perte de fonction sur les gènes encodant la sous-unité β de ce canal ont été reportées.[128]

De très rares mutations ne codant pas pour des protéines composant des canaux ioniques ont été décrites, à savoir les gènes de la nucléoporine (*NUP155*[129]), de la Cx40 (*GJA5*[100]) et du peptide natriurétique atrial (*NPPA*[130]). Les mécanismes reliant ces mutations au déclenchement de la FA ne sont pour pas le moment complètement élucidés. Enfin, des études sur le génome entier (« genome wide association studies ») ont récemment identifié des polymorphismes géniques (« single nucleotide peptide ») augmentant de façon significative la susceptibilité à la FA. Trois loci ont été identifiés sur les chromosomes 4q25, 16q22 et 1q21.[131]

En conclusion, de nombreuses mutations monogéniques ainsi que des polymorphismes favorisent la survenue de la FA. Cependant, dans la grande majorité des cas de FA familiale, aucune mutation causale n'est mise en évidence, ce qui sous-entend que d'autres gènes sont impliqués.

Circulation
Arrhythmia and Electrophysiology

American Heart Association

Translational Research in Atrial Fibrillation: A Quest for Mechanistically Based Diagnosis and Therapy

Felipe Atienza, Raphael P. Martins and José Jalife

Circ Arrhythm Electrophysiol. 2012;5:1207-1215; originally published online September 27, 2012;
doi: 10.1161/CIRCEP.111.970335
Circulation: Arrhythmia and Electrophysiology is published by the American Heart Association, 7272 Greenville Avenue, Dallas, TX 75231

Print ISSN: 1941-3149. Online ISSN: 1941-3084

Translational Research in Atrial Fibrillation

A Quest for Mechanistically Based Diagnosis and Therapy

Felipe Atienza, MD, PhD; Raphael P. Martins, MD; José Jalife, MD

Atrial fibrillation (AF) is the most common arrhythmia seen in clinical practice and is associated with increased risk of stroke, heart failure, and death.[1] However, currently available treatments for AF are less than satisfactory. Many drugs have been tried with limited success.[2] However, the demonstration of AF triggers in the atrial sleeves of the pulmonary veins (PVs)[3] has led to a significant improvement in therapy. Today, PV isolation by means of radiofrequency (RF) ablation is a gold standard treatment for paroxysmal AF.[4] However, the success rate of RF ablation in the more prevalent and highly heterogeneous persistent and long-term persistent AF populations has been disappointing.[5] The reasons are probably multifactorial, but undoubtedly incomplete understanding of the mechanism(s) underlying this complex arrhythmia has contributed substantially to such a poor outcome.

Increased knowledge of cardiac arrhythmias in general has come from studies aimed at elucidating cardiac impulse formation and propagation at several levels of integration, from computer modeling, through electrophysiological experiments in cells, tissues and the whole animal, and the human patient.[6] In clinical electrophysiology (EP), progress has been driven, to a large extent, by available technology designed for the detection of electrical signals on the endocardial and epicardial surfaces of the heart. Although the surface ECG is the obvious first and compulsory starting point in the clinical diagnostic ladder, programmed cardiac stimulation, combined with intracardiac activation mapping, enables electrophysiological characterization and is the cornerstone for successful diagnosis and treatment of most types of arrhythmias.[7]

In contrast to what happens in most other arrhythmic problems, electrical impulses during AF often are highly irregular, changing in number, direction, and width on a beat-to-beat basis, with significant temporal variations in the timing and morphology of the intracardiac atrial electrograms. Consequently, time-domain analysis of the signals recorded by electrodes positioned concurrently at different locations in the atria reveals extremely complex spatiotemporal activation patterns that preclude meaningful interpretation. It is, therefore, fair to state that understanding the mechanisms of AF maintenance has been hampered in part by the inability to reproducibly quantify activation patterns during ongoing AF. Consequently, the demonstration in the late 1990s that the PVs are the most common site of triggers for AF led the clinical EP community to adopt an anatomic approach to the RF treatment of AF, involving the creation of circumferential lesions around the right and the left PV ostia,[8] which probably impacts not only the triggers, but also the substrate of AF. This was in great part responsible for reducing the interest in performing extensive mapping of the atria or immersing into the study of AF mechanisms.

Perhaps more important, the relatively poor outcomes of pharmacological AF therapy, together with the apparently greater effectiveness of RF ablation in controlling the arrhythmia, has contributed to significantly reduce the interest of clinical EPs for mechanistically based approaches to AF therapy. However, basic EPs have focused on scientific and technological innovations in biology, which have provided unprecedented opportunities for the discovery of genetic and molecular bases of both acquired and inheritable arrhythmogenic diseases, with the idea of searching for novel therapeutic targets.[9] Unfortunately, the unintended consequence of the above success stories was that clinical and basic EPs stopped speaking the same language. Probably, with few exceptions, basic and clinical EPs seem to be lost in translation and appear unaware of each other's work. In other words, the reduced communication between the 2 groups during the past 20 years has engendered a void separating on one side the world of the clinical electrophysiologist, whose primary immediate interest is the health and quality of life of his/her patient, and on the other, the world of the basic electrophysiologist whose novel scientific discoveries may take years to reach that patient.

During the past 20 years, and until recently, mechanistically oriented EP studies in the clinic have been relatively scarce.[10-13] Much of the insight into EP mechanisms and complex dynamics of wave propagation in AF have come from detailed investigation using numerical and animal models of AF,[14] where there is substantially greater flexibility to explore the AF process from the molecule to the organism

Received May 1, 2012; accepted August 6, 2012.

From the Hospital General Universitario Gregorio Marañón, Madrid, Spain (F.A.); Service de Cardiologie, Centre Cardio-Pneumologique, CHU de Rennes, Rennes, France (R.P.M.); and Center for Arrhythmia Research, University of Michigan, Ann Arbor, MI (R.P.M., J.J.).

The online-only Data Supplement is available at http://circep.ahajournals.org/lookup/suppl/doi:10.1161/CIRCEP.111.970335/-/DC1.

Correspondence to José Jalife, MD, Center for Arrhythmia Research, North Campus Research Complex, University of Michigan 2800 Plymouth Rd, Ann Arbor, MI 48109. E-mail jjalife@umich.edu

(*Circ Arrhythm Electrophysiol.* 2012;5:1207-1215.)

and where high spatiotemporal resolution of the fibrillatory dynamics can be achieved.[15]

Excellent reviews have appeared in the recent literature on the consensus among clinicians for treatment,[1] the epidemiology, and the genetic, molecular, and pathophysiological bases of AF and atrial remodeling[9,16-20] Therefore, our aim here is not to present an exhaustive discussion on fundamental AF mechanisms. Instead, this article focuses on attempts by clinicians and basic scientists to find potential AF diagnostic tools and treatments based on the pathophysiological mechanisms responsible for AF initiation and maintenance. By discussing the evidence, we hope to promote reflection and to encourage both clinical and basic EP communities to reacquaint with each other's work, find common ground, and collaborate toward improving knowledge and advance therapy of AF.

Finding Our Way in Translation

Translation of knowledge derived from the experimental setting to clinical practice plays a critical role in scientific advancement,[21,22] and the importance of building clinical research on the solid foundations provided by scientifically rigorous basic research has been long recognized. Basic research can advance clinical research and practice in several ways[22]: (1) it informs clinical research by building the foundation of biological knowledge; (2) it guides clinicians in their practice by indicating not only what direction to pursue but also what directions are possible; and (3) it contributes to the development and testing of medical devices, surgical procedures, and candidate drugs. In fact, most medical diagnostic tests and therapies in use today were initially developed and tried in animals. For example, the development, testing, and clinical application of angiotensin-converting enzyme inhibitors constitute a paradigmatic example of successful translational research from bench to bedside.[23] However, many results of animal experiments often never undergo clinical testing or eventually fail to be replicated when tested in rigorous human trials.[21,24] Francis Collins, Director of the National Institutes of Health, has commented that despite a dizzying rate of basic science discoveries, far too often promising diagnostic devices and treatments are not making it to market. In a systematic review of highly cited animal studies, only 37% were replicated in human randomized trials, and 45% remained untested.[21] According to an article published recently in *Nature*,[24] "…translational research is seen by many as a solution to this disparity that could ensure that many fundamental discoveries are effectively translated into benefits in medicine."

Diagnosis and treatment of AF is at a point at which it would greatly benefit from translational research. Despite many years of basic and clinical research, fundamental mechanisms governing AF initiation and maintenance, and the transition from paroxysmal to permanent forms of AF are far from being understood,[15] and we have not learned how to treat AF effectively. The inexorable progression from paroxysmal to persistent and permanent AF reflects the progressive electrophysiological and structural remodeling occurring in both atria,[25-28] making the sources of the arrhythmia more stable and long-lasting. A long-term follow-up study reported a 30-year cumulative probability risk of progression from paroxysmal/persistent to permanent AF of 29%, with most of the transitions occurring within the first 15 years after diagnosis.[29] Yet, it is unknown which factors contribute to that progression, let alone whether or not we have the appropriate tools to prevent it.

Fortunately, the demonstration of AF triggers in the atrial sleeves of the PVs has led to a significant improvement in therapy.[3] Today, PV isolation by means of RF ablation is curative in ≈70% to 80% of patients with paroxysmal AF who are treated in the EP laboratory.[4] However, PV isolation is a relatively new procedure, and the very long-term outcomes are not known. In addition, AF ablation is reserved for the subset of patients with symptoms of paroxysmal or persistent AF. Furthermore, the financial burden of AF ablation therapy may be significant and is unlikely to be cost-effective for patients who have preserved quality of life despite their AF or for patients whose quality of life is not expected to improve substantially despite elimination of AF.[30] Therefore, there is much room for improvement, despite the great success. As will be further discussed later, here we and others see opportunities for translation toward the discovery of novel and effective therapies.[31] Interestingly, research into the fundamental understanding of some of the potential targets for therapy began ≈40 years ago, with the discovery of the cellular mechanisms of delayed afterdepolarization–induced triggered activity[32-34] and the mechanisms of rotor initiation and maintenance.[35]

Unfortunately, the success rate of RF ablation in the more prevalent and highly heterogeneous persistent and long-term persistent AF populations is ≈30% or less.[36] Furthermore, a slow but steady decline in arrhythmia-free survival after 5 years is noted, despite successful ablation treatment, especially among patients with persistent AF.[37] Perhaps our current incomplete understanding of the mechanisms involved in the maintenance and perpetuation of AF has prevented us from being able to generate more specific prevention and treatment of this dangerous and debilitating disease. It may be argued, however, that one important reason for such disappointing outcomes is the paucity of communication that has existed, and continues to exist, between the basic scientists and the clinicians during the past 20 years. But there is a glimmer of hope. Academic investigators on both sides of the aisle now have access to scientific resources and technology that should enable them to participate in translational research and collaborate in unprecedented ways. Advances have occurred in the basic understanding of the molecular mechanisms of AF-induced remodeling, including both electric and structural remodeling, on the one hand, and in the development of highly sophisticated magnetic resonance imaging and high-resolution electrode mapping technologies capable of identifying AF sources in the clinical EP laboratory, on the other hand. Such advances should help place basic and clinical investigators in a new position to partner together with industry and play a more powerful part in therapeutic development in both paroxysmal and persistent AF. In the following lines, we review the evolution of the principal ideas that have attempted to explain AF maintenance mechanisms, from the perspective of how translation of the results of experimental studies might influence future clinical practice.

AF Maintenance Mechanisms

The principal competing hypotheses attempting to explain AF mechanisms have been around >100 years, and their historical evolution has been recently reviewed.[15] From the beginning of the past century, 2 such hypotheses were proposed to explain AF maintenance mechanisms: single-source focus and circus movement reentry. According to these hypotheses, AF may be caused either by a rapidly discharging, spontaneously active atrial ectopic focus or by a single functional reentrant circuit. In either case, the activation wave fronts spawned at high frequency were thought to interact with the heterogeneous atrial muscle to give rise to what we know now as fibrillatory conduction. Although investigators at the time saw these 2 hypotheses as mutually exclusive, common to both hypotheses was the idea that AF was maintained by a localized source of atrial activity and required the continuous presence of the ectopic focus or, alternatively, the reentrant circuit. A third hypothesis, proposed subsequently by Moe et al,[38,39] postulated that AF depended on the sustained, but random propagation of multiple wavelets and that maintenance of the arrhythmia was self-sustaining and independent of the initiating event.

To our knowledge, not a single one of the above competing hypotheses has reached consensus among basic or clinical scientists. Over the years, arguments for or against each of the above schools of thought have been forcefully advanced by one or the other group, and the debate continues even today. Undoubtedly, the debate will continue for years to come. Below, we briefly review the pathophysiological nature of each of these mechanisms and their respective implications for potential therapy, as well as the treatment strategies that have been devised according to each conceptual hypothesis.

The Multiple Wavelet Hypothesis

The multiple wavelet hypothesis was the dominant mechanistic model of AF during the second half of the 20th century. In 1962, Moe postulated that AF was the result of randomly propagating multiple electrical wavelets, ever changing in number and direction, with local excitation limited by the heterogeneous distribution of refractory periods throughout the atria.[38,39] In Moe's model, the number of wavelets was a function of the mass of the tissue and inversely related to the product of the duration of refractory period and the conduction velocity (ie, the wavelength). The model predicted that a critical number of 23 to 40 wavelets was necessary for the maintenance of AF.[39] Any factor that increased the total number of wavelets (eg, wavelength shortening) would serve to perpetuate the arrhythmia, whereas, conversely, any factor that decreased the total number of wavelets would favor termination.[38] This hypothesis was later reinforced by high-resolution electrode mapping experiments in dogs.[40] In support of Moe's model,[39] Allessie et al[40] suggested that AF was maintained by 6 to 7 wavelets that propagated through relatively refractory tissue in which there was no fully excitable gap, enabling the coexistence of multiple simultaneous wavelets in a minimum amount of tissue (ie, critical mass). However, translation of the multiple wavelet hypothesis into human persistent AF diagnosis and therapy has been difficult and has not yet resulted in widely accepted strategies to effectively terminate AF. Nevertheless, the idea is widespread in the literature, although both experimental and clinical studies have raised important questions and argue against the applicability of the multiple wavelet hypothesis to explain sustained AF. Examples follow.

First, the surgical Maze procedure is able to successfully treat some cases of chronic AF, which has been attributed to a reduction in the tissue mass and thus the number of wavelets that the atria can sustain.[41] However, other factors may explain the success of this intervention, including PV isolation,[3] cardiac denervation,[42] and empirical elimination of sites responsible for AF maintenance.[43] Furthermore, several studies challenged the critical mass hypothesis by demonstrating that fibrillation can be sustained by tissues of very small size. Chen et al[44] showed that the minimal length that allows for the sustenance of reentry in the left atrium (LA) of the sheep heart is ≈4 mm. Gray et al[45] demonstrated theoretically that rodent hearts can accommodate 1 or 2 reentrant sources (rotors), whereas in larger hearts (eg, sheep, dogs, and humans), a greater number of rotors may coexist. Such a theoretical prediction has been borne out by the demonstration that in mammalian hearts from mouse to horse, the ventricular fibrillation cycle length scales with the fourth power of the body mass.[46] Finally, clinical studies have shown that AF can also be sustained by small portions of tissue, such as remnants of receptor atrial tissue after orthotopic heart transplantation (online-only Data Supplement Figure I),[47] which also argues against the idea of a critical mass for AF. Second, wavelength shortening would be expected to increase the number and instability of randomly propagating wavelets as a means to perpetuate the arrhythmia and increase its complexity. Instead, Schuessler et al[48] found in a canine model of acute AF that, with increasing concentrations of acetylcholine and below a critical level of refractory period (<95 ms), the rapid repetitive responses initially characterized by multiple reentrant circuits stabilized to a single circuit that became stable and dominated activation.[48]

Third, the absence of a fully excitable gap should make the arrhythmia amenable for termination by pharmacological interventions that increase the refractory period (and thereby the wavelength). It should also limit the number of wavelets that may coexist simultaneously. Thus, several drugs capable of prolonging the atrial effective refractory period (ERP), which also increases the wavelength and the size of the reentry circuit during AF, have been used in the clinic with variable success.[49,50] However, the above prediction is incompatible with the antiarrhythmic effect of Na^+ channel blockade, which, by decreasing conduction velocity and thereby wavelength, should promote AF instead of terminating it, such as occurs in clinical practice.[51] Finally, because there is no anatomically determined circuit, there should be no theoretical possibility of interrupting the arrhythmia by disrupting the circuit through the application of localized lesions. However, several experimental and clinical studies have demonstrated that AF can terminate by limited RF applications directed to localized sources in the atria.[52–54]

In what appears to be a new variant of the multiple wavelet hypothesis, Allessie et al[55] recently put forth the idea that the electric dissociation of neighboring atrial muscle bundles is a key element in the electropathological substrate of

long-standing persistent AF in patients with structural heart disease. In addition, from experiments in the goat heart, the same investigators have suggested that, during AF, pronounced dissociation of electrical activity occurs between the epicardial layer and the endocardial bundle network, which they attributed to progressive uncoupling between the epicardial layer and the endocardial bundles.[56] This interesting idea might lead to identification of novel molecular targets for therapeutic agents and the design of more effective antifibrillatory drugs. However, it is unclear why such dissociation would occur in the absence of dissociation within any of the 2 layers. Furthermore, even if longitudinal dissociation occurs, unless otherwise demonstrated, the phenomena described by the Allessie group[55,56] are fully compatible with fibrillatory conduction maintained by a single high-frequency source, either focal or reentrant, generating waves from a remote location.

Single-Source Hypothesis

Experimental evidence showing that AF may be the result of a single localized electrical source, acting as a rapidly discharging ectopic focus, dates back to the beginning of the 20th century.[57] However, this observation fell largely in disfavor as a result of the convincing evidence provided at that time by the circus movement defenders, particularly Sir Thomas Lewis.[58] Nevertheless, Lewis recognized that "[atrial] fibrillation, like flutter, may also on occasion be terminated in the auricle by cold or pressure very locally applied".[58] In 1949, Scherf and Terranova[59] induced atrial tachycardia or fibrillation by applying aconitine crystals on the epicardial surface of the right atrial appendage of the dog. The arrhythmia could be terminated by cooling the area of injection, suggesting that the mechanism of AF was compatible with an ectopic focus.[59] More recently, Yamazaki et al[60] provided direct demonstration that reentrant ventricular tachycardia and ventricular fibrillation may be terminated by local cooling at or near the center of rotation. This argues against being able to distinguish between arrhythmogenic mechanisms based on changes in temperature alone.

Nevertheless, there is no question that although focalized atrial ectopy can result from microreentry, enhanced atrial automaticity (spontaneous diastolic depolarization) or triggered activity (afterdepolarizations) is an important mechanism involved in AF initiation.[61] The vast majority (≈90%) of ectopic discharges that trigger AF localize in the PVs[3] and are thought to result from either early or delayed afterdepolarizations. Early afterdepolarizations occur when action potential duration is excessively prolonged, allowing Ca^{2+} channels to recover from inactivation. Ca^{2+} enters into the cell and initiates a new action potential upstroke.[62] Delayed afterdepolarizations may be the consequence of intracellular Ca^{2+} handling dysfunction, secondary to abnormal Ca^{2+} leak from the sarcoplasmic reticulum through the type-2 ryanodine receptors channels.[63] Clinical observation indicates that autonomic blockade with propranolol suppresses bursts of AF.[64] However, isoproterenol infusion, which facilitates calcium release from the sarcoplasmic reticulum and promotes delayed afterdepolarizations and triggered activity, has a high sensitivity and specificity for induction of AF in patients with persistent atrial fibrillation.[65] Figure SII (online-only Data Supplement) shows a possible mechanism of induction of triggered activity at the PV by the intravenous infusion of isoproterenol, as routinely done in the clinical EP laboratory in combination with rapid pacing.

Rotors and Fibrillatory Conduction

A significant deviation from the prevailing concepts used to explain AF maintenance was derived several years ago from the theory of wave propagation in excitable media[35] and from studies using voltage-sensitive probes and high-resolution video imaging. The increased understanding through mathematical modeling of the manner in which waves propagate in a wide variety of physical, chemical, and biological excitable media, together with the ability to record electrical wave propagation on the surface of isolated hearts with an unprecedented spatial and temporal resolution, lead to a better understanding of the dynamics of AF and of its nature.[44,45,66] Such an advanced technology has confirmed that the turbulent electrical activity seen in the electrogram recordings of the atria may in some cases be explained by a single or a small number of rapidly spinning rotors.[67,68] Rotor formation or its maintenance does not require a permanent anatomic obstacle; a transient functional heterogeneity that is able to generate a wavebreak suffices to generate a singularity around which the newly formed wave front with extreme curvature rotates (Figure 1).[69] These studies demonstrated that the self-organized functional reentrant sources (ie, the rotors) that maintain AF adopt the appearance of a pinwheel, which rotates rhythmically at high rates and sheds large numbers of spiral waves (online-only Data Supplement Figure IIIA). A rotor resembles a hurricane or a tornado, and its vortex-like activity is organized by a phase singularity near its center at which all phases (colors) of the excitation–recovery cycle converge (online-only Data Supplement Figure IIIB).[35,45] Accordingly, the spiral waves emitted by the rotor propagate through the heterogeneous cardiac muscle and interact with anatomic and functional obstacles, leading to wave front fragmentation and fibrillatory conduction.[70]

Wave Fractionation and CFAEs

Just as the advancement of clinical medicine requires insights from basic research (ie, forward translational research), clinical work also helps clarify unresolved biological behaviors. This notion is known as backward translational research.[71,72] In fact, several proposals for basic research stemming from the AF Guidelines have been recently proposed.[72] Although these proposals are yet to be resolved, in the following lines we describe several examples of backward translational research that provided significant insights into the mechanisms of AF.

In 2004, Nademanee et al[43] proposed that areas with complex fractionated atrial electrograms (CFAEs) were critical sites for perpetuation of AF, and their elimination with RF ablation was associated with a high probability of sinus rhythm maintenance. Recent studies have targeted CFAEs at a range of atrial sites as a means to increase AF ablation success after circumferential PV isolation.[1,53] However, clinical results have been controversial at best, calling into question the role of CFAEs in AF maintenance, especially in patients with paroxysmal AF.

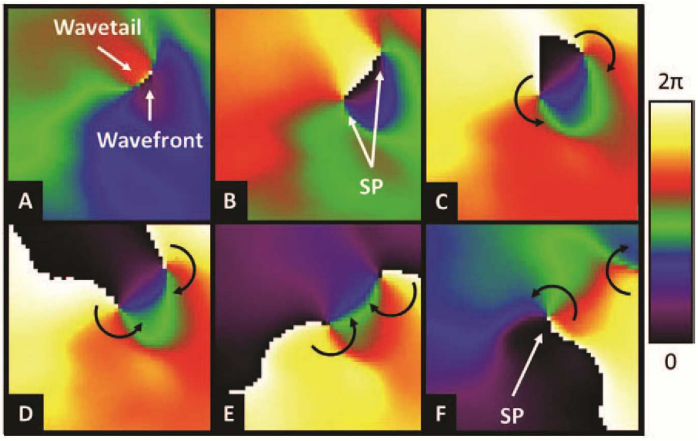

Figure 1. Wavebreak and singularity point (SP) formation. **A**, The front of a wave (green) moves rapidly to the neighborhood of the refractory tail of a slowly dissipating wave tail of a preceding wave. **B**, When the wave front reaches the wave tail, it attaches to it and divides into 2 daughter waves that propagate forward as they encounter excitable tissue. **C** to **F**, Under appropriate conditions of reduced excitability, the 2 wave fronts detach from the wave tail forming an SP at their respective broken tips. At each SP, the curvature of the wave front is extreme, which forces the rest of the wave front to curl around it and spin. In this case, 2 counter revolving rotors would be formed.

Although some fractionated signals might represent critical zones related to AF maintenance (ie, high-frequency sources driving AF), others might be passive and unrelated to the primary arrhythmia mechanism (ie, wave front collision or overlapping).[1,10,73] Still others appear to be located in areas surrounding the autonomic ganglionated plexi.[74,75] In fact, the pathophysiological relationship between high-frequency PV discharges and CFAEs on the posterior left atrial wall is far from being understood. Experimental and clinical studies have shown that fractionated signals need not be critical for AF maintenance. Kalifa et al[76] found that the periphery of high-frequency AF drivers is the area at which most fractionation occurs. That is the area where the phenomenon of fibrillatory conduction is most manifest. Rotor meandering might also underlie, at least in part, the electrogram fractionation at close proximity of the source.[73] This might explain the success of some CFAE ablation procedures that by chance produce an anatomic obstacle around the highest dominant frequency (DF) site. However, other studies suggest that CFAEs might be unrelated to the primary arrhythmia mechanism and simply represent transient pivoting, wave front collision, or wave fractionation.[10,13,77] The latter has been confirmed by a recent study with typical bench-to-bedside design showing that, in paroxysmal AF, electrogram fractionation at the posterior left atrial wall is a reflection of fibrillatory conduction and a consequence of the dynamic interaction between high-frequency reentrant sources and the atrial anatomy (online-only Data Supplement Figure IV).[78,79]

Validation of Experiments Using Optical Mapping

Not surprisingly, most experimentally derived information on mechanisms of cardiac fibrillation has come from large animal models.[14] In general, fibrillation in small animals such as mice or rats is difficult to initiate or maintain for relatively long periods of time. Nevertheless, as discussed above, there might be a strong similarity in the underlying mechanisms of fibrillation in most, if not all, mammalian species,[46] which may be of considerable fundamental and practical significance and provides some validation for the transition of data derived from experimental studies to arrhythmias in humans, including AF. We summarize some of these results in the next section.

Left-to-Right Atrial Frequency Gradients

Several methods have been used to analyze and compare AF signals. On the one hand, time-domain analysis is routinely used in the clinical EP laboratory to record the electrical signals of the atria during AF. However, a few catheter-based electrodes positioned at different locations in the atria commonly reveal extremely complex spatiotemporal activation patterns that often preclude straightforward interpretation. On the other hand, analyses in the frequency domain, while imperfect,[66] enable reliable quantification of the local frequency of activation, which reveals a high degree of spatiotemporal organization.[80] Using these signal processing methods, experimental studies in the isolated sheep heart have demonstrated that the highest frequency rotors that maintain acute cholinergic AF are usually localized in the LA. Propagation of the waves that emanate from such rotors undergo spatially distributed intermittent block processes that give rise to fibrillatory conduction and result in a left-to-right gradient of excitation frequencies.[71,73,79,80] More recently, a significant number of studies have characterized the spatial distribution of DFs during AF in patients, confirming the existence of a similar hierarchical organization in the rate of atrial activation in both patients with paroxysmal and chronic AF.[52,54,81,82] Simultaneous time- and frequency-domain analyses have demonstrated a high correlation between the location of maximal DF areas and the origin of incoming waves, which led investigators to infer that during organized AF episodes the posterior wall of the LA is passively activated from high-frequency sources located at the PV–LA junction.[7,79] As a natural consequence of these studies, real-time spectral mapping techniques have been used to identify and ablate high-frequency sites in patients with AF,[54] and recent work has demonstrated that an unequal distribution of inward rectifier[28] and other K^+ currents[27] underlies this

spatial distribution of frequencies, which may represent new therapeutic targets.

An important limitation of using DF mapping in human patients is the low number of intracardiac electrodes that can be used simultaneously in the clinical EP laboratory, which makes it hard to localize the highest DF sources.[81] Optical mapping techniques, on the other hand, enable high-resolution mapping and relatively easy localization of the highest frequency sources, as well as the determination of the frequency gradients and their quantification. In fact, cardiac optical mapping has evolved to become a powerful tool that can provide new mechanistic insights into the most complex atrial and ventricular arrhythmias.[83] In the ventricles, its submillimeter spatial resolution enabled the demonstration that ventricular fibrillation in isolated human hearts is associated with wavebreaks and singularity point formation and is maintained by high-frequency rotors and fibrillatory conduction.[84] With the development of new infrared voltage-sensitive dyes,[85] optical mapping based on sophisticated catheter-based endoscopic mapping protocols (online-only Data Supplement Figure V) may someday be used in the clinical EP laboratory to localize AF sources in the human heart.[86] However, until that day comes, catheter electrode mapping will have to suffice. As discussed below, important advances in this area have created new enthusiasm for the possibility of using mechanistic approaches to effectively terminate AF based on novel RF ablation strategies.

Role of High-Frequency Sites in Human AF Maintenance

Using a canine chronic AF model, Morillo et al[87] demonstrated that AF cycle lengths were consistently shorter in the LA than in the right atrium (RA). The shortest cycle lengths were measured in the area of the posterior left atrial wall near the PV–LA junctions. This suggested that AF in that model was maintained by high-frequency drivers in the posterior LA that gave rise to consistent left-to-right frequency gradient.[69] Furthermore, cryoablation of this area significantly prolonged atrial cycle length and successfully restored sinus rhythm in most dogs, confirming the crucial role of localized sites with high activation frequency. The observations of Morillo et al[87] were amply confirmed and expanded upon by large numbers of experiments in the sheep heart.[67,70] Confirmation of a hierarchical organization of AF frequencies in humans, however, came later, with seminal work of Haïssaguerre et al[5] demonstrating that ectopic foci in the PVs were the most common triggers, that they were capable of initiating and even maintaining AF, and that they could be eliminated by treatment with RF ablation.

Recently, we used a combination of real-time DF mapping and RF ablation to determine the safety and long-term outcome of targeting maximal DF sites in patients.[54] We demonstrated that real-time spectral analysis of AF was safe and that it enabled identification and elimination of sources responsible for AF maintenance (Figure 2). Most important, we showed that targeting such sources followed by circumferential PV isolation resulted in long-term sinus rhythm maintenance in 75% of paroxysmal and 50% of persistent AF patients.[54]

As discussed above, most experimentally derived information on the existence of rotors or drivers as a mechanism of cardiac fibrillation has come from large animal models using high-resolution video imaging.[14] This is not surprising and not only caused by conceptual differences but also by substantial differences of mapping techniques used in the clinic as well as in various experimental laboratories. Not only is the number of electrodes highly variable, but the electrodes may be unipolar or bipolar, the mapped area may be too small, and while some investigators use high-resolution cameras others use photodiode arrays.[83] The type of voltage-sensitive dyes and the software specifically designed to look for AF sources also vary. Undoubtedly, all of the above have contributed to the inconsistent detection of rotors in both animal models and humans. Therefore, perhaps the most remarkable development in the field of AF therapy since the discovery of the PV triggers has been the recent direct demonstration by Narayan et al[88] that AF in humans may result of long-standing rotors with fibrillatory conduction to the surrounding atrium. They used a novel computational mapping approach via 2 basket catheters, one in the RA and the other in the LA, each with 64 electrodes, to reveal AF rotors in the left or right atrium. Most important, brief RF ablation at or near the center of rotation alone acutely terminated AF,[88] which supported the conclusion that rotors are the primary drivers of AF, at least in some patients. The results further suggest that heterogeneity in the atrium in the form of spatially distributed refractory period gradients constitutes a likely arrhythmogenic substrate in which rotors remain relatively stable as a result of such gradients, and that waves emanating at high frequency result in the turbulent electrical activation which manifests as fibrillatory conduction. Although the results of Narayan et al[88] need to be confirmed by other laboratories, they are nevertheless an exciting mechanistically-based approach to AF therapy, which derives from translation of basic science knowledge into clinical practice.

Conclusions

There is an urgent need for enhanced communication between basic scientists and clinical electrophysiologists. Clearly, both communities are interested in preventing the expansion of the AF epidemic by improving outcomes in AF therapy. Together, both communities, in collaboration with industry, should endeavor to identify strategies to pursue the translation of their discoveries into clinical practice. Although RF ablation has been relatively successful in improving the quality of life of some patients with AF, it is clear that current ablation strategies are insufficient for controlling the arrhythmia in the majority of patients. Mechanistically based approaches to AF therapy offer a potentially exciting alternative, but this requires greater communication and collaboration. We submit that generating insights into AF mechanisms through novel theory and experimentation will require the use of relevant numerical and biological models, where translation of basic science concepts into clinical practice should be the critical final step. Translational EP will be essential in our future

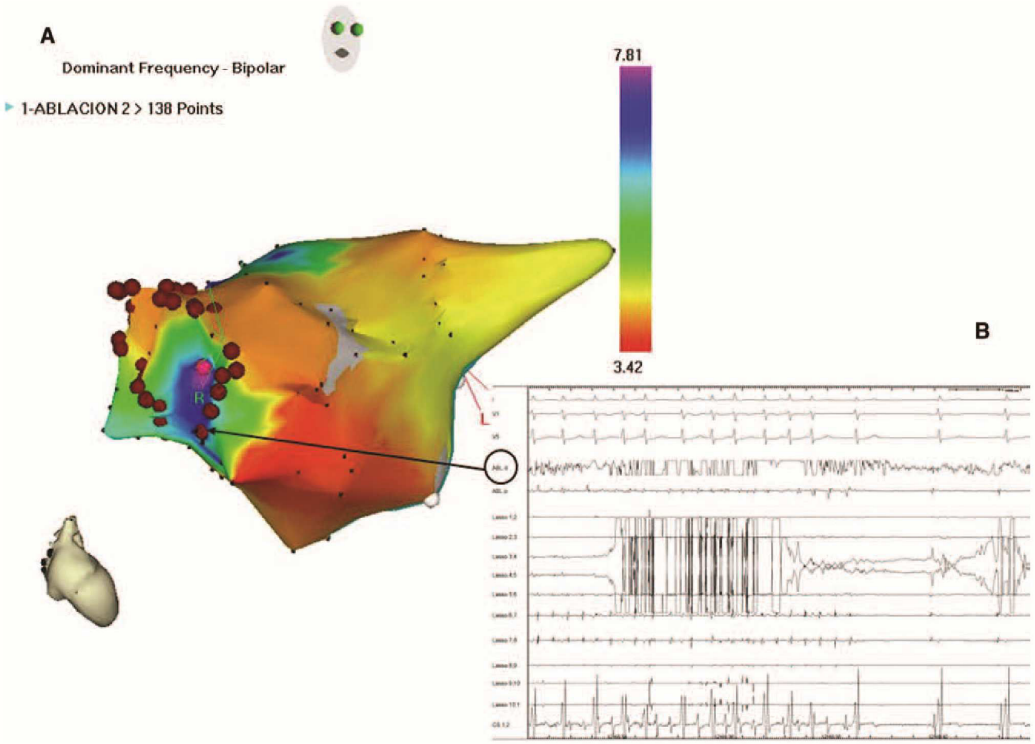

Figure 2. **A**, Real-time atrial dominant frequency (DF) map (right anterior view; CARTO system) in a paroxysmal atrial fibrillation (AF) patient. Purple, High DF site on right superior pulmonary vein (PV) antrum. Red dots, Circumferential ablation line. **B**, Surface ECG leads and intracardiac lasso catheter electrograms within the right superior pulmonary vein (RSPV); coronary sinus and ablation catheter (**black arrow**) during radiofrequency delivery, with sinus rhythm conversion, before isolation of the RSPV, confirming the reentrant nature of AF, incompatible with the multiple wavelet theory (unpublished).

attempts to improve patient care and develop new, safe, and more successful therapies.

Sources of Funding

This work was supported by the Spanish Society of Cardiology (to F.A.); National Heart, Lung, and Blood Institute grants P01-HL039707 and P01-HL87226 (to J.J.); the Leducq Foundation (to J.J.); the Fédération Francaise de Cardiologie (to R.P.M.); and Centro Nacional de Investigaciones Cardiovasculares (proyecto CNIC-13; to F.A., J.J.).

Disclosures

Dr Atienza, received a research grants from St Jude Medical and is on the Advisory Board of Medtronic, Inc. Dr Jalife receives a research grant from Gilead, Inc; he is on the Scientific Advisory Board of Topera, Inc (stock options) and the Scientific Advisory Board of Rhythm Solutions, Inc (stock options). R.P.M has no conflicts to report.

References

1. Calkins H, Kuck KH, Cappato R, Brugada J, Camm AJ, Chen SA, Crijns HJ, Damiano RJ Jr, Davies DW, DiMarco J, Edgerton J, Ellenbogen K, Ezekowitz MD, Haines DE, Haissaguerre M, Hindricks G, Iesaka Y, Jackman W, Jalife J, Jais P, Kalman J, Keane D, Kim YH, Kirchhof P, Klein G, Kottkamp H, Kumagai K, Lindsay BD, Mansour M, Marchlinski FE, McCarthy PM, Mont JL, Morady F, Nademanee K, Nakagawa H, Natale A, Nattel S, Packer DL, Pappone C, Prystowsky E, Raviele A, Reddy V, Ruskin JN, Shemin RJ, Tsao HM, Wilber D. 2012 HRS/EHRA/ECAS Expert Consensus Statement on Catheter and Surgical Ablation of Atrial Fibrillation: recommendations for patient selection, procedural techniques, patient management and follow-up, definitions, endpoints, and research trial design. *Europace*. 2012;14:528–606.
2. Dobrev D, Nattel S. New antiarrhythmic drugs for treatment of atrial fibrillation. *Lancet*. 2010;375:1212–1223.
3. Haïssaguerre M, Jaïs P, Shah DC, Takahashi A, Hocini M, Quiniou G, Garrigue S, Le Mouroux A, Le Métayer P, Clémenty J. Spontaneous initiation of atrial fibrillation by ectopic beats originating in the pulmonary veins. *N Engl J Med*. 1998;339:659–666.
4. Cappato R, Calkins H, Chen SA, Davies W, Iesaka Y, Kalman J, Kim YH, Klein G, Natale A, Packer D, Skanes A, Ambrogi F, Biganzoli E. Updated worldwide survey on the methods, efficacy, and safety of catheter ablation for human atrial fibrillation. *Circ Arrhythm Electrophysiol*. 2010;3:32–38.
5. Weerasooriya R, Khairy P, Litalien J, Macle L, Hocini M, Sacher F, Lellouche N, Knecht S, Wright M, Nault I, Miyazaki S, Scavee C, Clementy J, Haissaguerre M, Jais P. Catheter ablation for atrial fibrillation: are results maintained at 5 years of follow-up? *J Am Coll Cardiol*. 2011;57:160–166.
6. Packer DL. Evolution of mapping and anatomic imaging of cardiac arrhythmias. *J Cardiovasc Electrophysiol*. 2004;15:839–854.
7. Wellens HJ. Forty years of invasive clinical electrophysiology: 1967-2007. *Circ Arrhythm Electrophysiol*. 2008;1:49–53.
8. Pappone C, Oreto G, Rosanio S, Vicedomini G, Tocchi M, Gugliotta F, Salvati A, Dicandia C, Calabrò MP, Mazzone P, Ficarra E, Di Gioia C, Gulletta S, Nardi S, Santinelli V, Benussi S, Alfieri O. Atrial electroanatomic remodeling after circumferential radiofrequency pulmonary vein ablation: efficacy of an anatomic approach in a large cohort of patients with atrial fibrillation. *Circulation*. 2001;104:2539–2544.

9. Iwasaki YK, Nishida K, Kato T, Nattel S. Atrial fibrillation pathophysiology: implications for management. *Circulation*. 2011;124:2264–2274.
10. Konings KT, Kirchhof CJ, Smeets JR, Wellens HJ, Penn OC, Allessie MA. High-density mapping of electrically induced atrial fibrillation in humans. *Circulation*. 1994;89:1665–1680.
11. Konings KT, Smeets JL, Penn OC, Wellens HJ, Allessie MA. Configuration of unipolar atrial electrograms during electrically induced atrial fibrillation in humans. *Circulation*. 1997;95:1231–1241.
12. Kumagai K, Khrestian C, Waldo AL. Simultaneous multisite mapping studies during induced atrial fibrillation in the sterile pericarditis model. Insights into the mechanism of its maintenance. *Circulation*. 1997;95:511–521.
13. Ortiz J, Niwano S, Abe H, Rudy Y, Johnson NJ, Waldo AL. Mapping the conversion of atrial flutter to atrial fibrillation and atrial fibrillation to atrial flutter. Insights into mechanisms. *Circ Res*. 1994;74:882–894.
14. Nishida K, Michael G, Dobrev D, Nattel S. Animal models for atrial fibrillation: Clinical insights and scientific opportunities. *Europace*. 2010;12:160–172.
15. Jalife J. Déjà vu in the theories of atrial fibrillation dynamics. *Cardiovasc Res*. 2011;89:766–775.
16. Sinner MF, Ellinor PT, Meitinger T, Benjamin EJ, Kääb S. Genome-wide association studies of atrial fibrillation: past, present, and future. *Cardiovasc Res*. 2011;89:701–709.
17. Dobrev D, Nattel S. New insights into the molecular basis of atrial fibrillation: mechanistic and therapeutic implications. *Cardiovasc Res*. 2011;89:689–691.
18. Wakili R, Voigt N, Kääb S, Dobrev D, Nattel S. Recent advances in the molecular pathophysiology of atrial fibrillation. *J Clin Invest*. 2011;121:2955–2968.
19. Van Wagoner DR, Pond AL, McCarthy PM, Trimmer JS, Nerbonne JM. Outward K+ current densities and Kv1.5 expression are reduced in chronic human atrial fibrillation. *Circ Res*. 1997;80:772–781.
20. Dun W, Boyden PA. Aged atria: electrical remodeling conducive to atrial fibrillation. *J Interv Card Electrophysiol*. 2009;25:9–18.
21. Hackam DG, Redelmeier DA. Translation of research evidence from animals to humans. *JAMA*. 2006;296:1731–1732.
22. Musch TI, Carroll RG, Just A, Lane PH, Talman WT. A broader view of animal research. *BMJ*. 2007;334:274.
23. Moyé LA, Pfeffer MA, Braunwald E. Rationale, design and baseline characteristics of the survival and ventricular enlargement trial. SAVE Investigators. *Am J Cardiol*. 1991;68:70D–79D.
24. Wadman N. The bridge between lab and clinic. *Nature*. 2010;468:877.
25. Voigt N, Maguy A, Yeh YH, Qi X, Ravens U, Dobrev D, Nattel S. Changes in I K, ACh single-channel activity with atrial tachycardia remodelling in canine atrial cardiomyocytes. *Cardiovasc Res*. 2008;77:35–43.
26. Bosch RF, Zeng X, Grammer JB, Popovic K, Mewis C, Kühlkamp V. Ionic mechanisms of electrical remodeling in human atrial fibrillation. *Cardiovasc Res*. 1999;44:121–131.
27. Caballero R, de la Fuente MG, Gómez R, Barana A, Amorós I, Dolz-Gaitón P, Osuna L, Almendral J, Atienza F, Fernández-Avilés F, Pita A, Rodríguez-Roda J, Pinto A, Tamargo J, Delpón E. In humans, chronic atrial fibrillation decreases the transient outward current and ultrarapid component of the delayed rectifier current differentially on each atria and increases the slow component of the delayed rectifier current in both. *J Am Coll Cardiol*. 2010;55:2346–2354.
28. Voigt N, Trausch A, Knaut M, Matschke K, Varró A, Van Wagoner DR, Nattel S, Ravens U, Dobrev D. Left-to-right atrial inward rectifier potassium current gradients in patients with paroxysmal versus chronic atrial fibrillation. *Circ Arrhythm Electrophysiol*. 2010;3:472–480.
29. Jahangir A, Lee V, Friedman PA, Trusty JM, Hodge DO, Kopecky SL, Packer DL, Hammill SC, Shen WK, Gersh BJ. Long-term progression and outcomes with aging in patients with lone atrial fibrillation: a 30-year follow-up study. *Circulation*. 2007;115:3050–3056.
30. Kautzner J, Bulkova V, Hindricks G, Maniadakis N, Della Bella P, Jais P, Kuck KH. Atrial fibrillation ablation: a cost or an investment? *Europace*. 2011;13:ii39–ii43.
31. Dobrev D, Carlsson L, Nattel S. Novel molecular targets for atrial fibrillation therapy. *Nat Rev Drug Discov*. 2012;11:275–291.
32. Rosen MR, Gelband H, Merker C, Hoffman BF. Mechanisms of digitalis toxicity. Effects of ouabain on phase four of canine Purkinje fiber transmembrane potentials. *Circulation*. 1973;47:681–689.
33. Hashimoto K, Moe GK. Transient depolarizations induced by acetylstrophanthidin in specialized tissue of dog atrium and ventricle. *Circ Res*. 1973;32:618–624.
34. Ferrier GR, Moe GK. Effect of calcium on acetylstrophanthidin-induced transient depolarizations in canine Purkinje tissue. *Circ Res*. 1973;33:508–515.
35. Winfree AT. Spiral waves of chemical activity. *Science*. 1972;175:634–636.
36. Chao TF, Tsao HM, Lin YJ, Tsai CF, Lin WS, Chang SL, Lo LW, Hu YF, Tuan TC, Suenari K, Li CH, Hartono B, Chang HY, Ambrose K, Wu TJ, Chen SA. Clinical outcome of catheter ablation in patients with nonparoxysmal atrial fibrillation: results of 3-year follow-up. *Circ Arrhythm Electrophysiol*. 2012;5:514–520.
37. Tzou WS, Marchlinski FE, Zado ES, Lin D, Dixit S, Callans DJ, Cooper JM, Bala R, Garcia F, Hutchinson MD, Riley MP, Verdino R, Gerstenfeld EP. Long-term outcome after successful catheter ablation of atrial fibrillation. *Circ Arrhythm Electrophysiol*. 2010;3:237–242.
38. Moe G. On the multiple wavelet hypothesis of atrial fibrillation. *Arch Int Pharmacodyn Ther*. 1962;140:183–188.
39. Moe GK, Rheinboldt WC, Abildskov JA. A computer model of atrial fibrillation. *Am Heart J*. 1964;67:200–220.
40. Allessie MA, Lammers WJEP, Bonke FIM, Hollen J. Experimental evaluation of moe's multiple wavelet hypothesis of atrial fibrillation. In: Zipes DP, jalife, J, eds. *Cardiac Electrophysiology and Arrhythmias*. Orlando, FL: Grune & Straton; 1985;265–275.
41. Cox JL, Boineau JP, Schuessler RB, Ferguson TB Jr, Cain ME, Lindsay BD, Corr PB, Kater KM, Lappas DG. Successful surgical treatment of atrial fibrillation. Review and clinical update. *JAMA*. 1991;266:1976–1980.
42. Sheng X, Scherlag BJ, Yu L, Li S, Ali R, Zhang Y, Fu G, Nakagawa H, Jackman WM, Lazzara R, Po SS. Prevention and reversal of atrial fibrillation inducibility and autonomic remodeling by low-level vagosympathetic nerve stimulation. *J Am Coll Cardiol*. 2011;57:563–571.
43. Nademanee K, McKenzie J, Kosar E, Schwab M, Sunsaneewitayakul B, Vasavakul T, Khunnawat C, Ngarmukos T. A new approach for catheter ablation of atrial fibrillation: mapping of the electrophysiologic substrate. *J Am Coll Cardiol*. 2004;43:2044–2053.
44. Chen J, Mandapati R, Berenfeld O, Skanes AC, Gray RA, Jalife J. Dynamics of wavelets and their role in atrial fibrillation in the isolated sheep heart. *Cardiovasc Res*. 2000;48:220–232.
45. Gray RA, Pertsov AM, Jalife J. Spatial and temporal organization during cardiac fibrillation. *Nature*. 1998;392:75–78.
46. Noujaim SF, Berenfeld O, Kalifa J, Cerrone M, Nanthakumar K, Atienza F, Moreno J, Mironov S, Jalife J. Universal scaling law of electrical turbulence in the mammalian heart. *Proc Natl Acad Sci USA*. 2007;104:20985–20989.
47. Waldo A, Atienza F. Atrial flutter. In: Zipes DP, Jalife J, eds. *Cardiac Electrophysiology: From Cell to Bedside*. Philadelphia, PA: Saunders Elsevier; 2009:567–576.
48. Schuessler RB, Grayson TM, Bromberg BI, Cox JL, Boineau JP. Cholinergically mediated tachyarrhythmias induced by a single extrastimulus in the isolated canine right atrium. *Circ Res*. 1992;71:1254–1267.
49. Wijffels MC, Dorland R, Mast F, Allessie MA. Widening of the excitable gap during pharmacological cardioversion of atrial fibrillation in the goat: effects of cibenzoline, hydroquinidine, flecainide, and d-sotalol. *Circulation*. 2000;102:260–267.
50. Hayashi H, Fujiki A, Tani M, Usui M, Inoue H. Different effects of class Ic and III antiarrhythmic drugs on vagotonic atrial fibrillation in the canine heart. *J Cardiovasc Pharmacol*. 1998;31:101–107.
51. Nattel S, Khairy P, Roy D, Thibault B, Guerra P, Talajic M, Dubuc M. New approaches to atrial fibrillation management: a critical review of a rapidly evolving field. *Drugs*. 2002;62:2377–2397.
52. Sanders P, Berenfeld O, Hocini M, Jais P, Vaidyanathan R, Hsu LF, Garrigue S, Takahashi Y, Rotter M, Sacher F, Scavée C, Ploutz-Snyder R, Jalife J, Haïssaguerre M. Spectral analysis identifies sites of high-frequency activity maintaining atrial fibrillation in humans. *Circulation*. 2005;112:789–797.
53. Oral H, Chugh A, Good E, Sankaran S, Reich SS, Igic P, Elmouchi D, Tschopp D, Crawford T, Dey S, Wimmer A, Lemola K, Jongnarangsin K, Bogun F, Pelosi F Jr, Morady F. A tailored approach to catheter ablation of paroxysmal atrial fibrillation. *Circulation*. 2006;113:1824–1831.
54. Atienza F, Almendral J, Jalife J, Zlochiver S, Ploutz-Snyder R, Torrecilla EG, Arenal A, Kalifa J, Fernández-Avilés F, Berenfeld O. Real-time dominant frequency mapping and ablation of dominant frequency sites in atrial fibrillation with left-to-right frequency gradients predicts long-term maintenance of sinus rhythm. *Heart Rhythm*. 2009;6:33–40.
55. Allessie MA, de Groot NM, Houben RP, Schotten U, Boersma E, Smeets JL, Crijns HJ. Electropathological substrate of long-standing persistent atrial fibrillation in patients with structural heart disease: longitudinal dissociation. *Circ Arrhythm Electrophysiol*. 2010;3:606–615.
56. Eckstein J, Maesen B, Linz D, Zeemering S, van Hunnik A, Verheule S, Allessie M, Schotten U. Time course and mechanisms of endo-epicardial electrical dissociation during atrial fibrillation in the goat. *Cardiovasc Res*. 2011;89:816–824.

57. Rothberger C, Winterberg H. Vorhofflimmern und arhythmia perpetua. *Wien Klin Wochenschr.* 1909;22:839–844.
58. Lewis T. Oliver-Sharpey Lectures on the nature of flutter and fibrillation of the auricle. *Br Med J.* 1921;1:590–593.
59. Scherf D, Terranova R. Mechanism of auricular flutter and fibrillation. *Am J Physiol.* 1949;159:137–142.
60. Yamazaki M, Honjo H, Ashihara T, Harada M, Sakuma I, Nakazawa K, Trayanova N, Horie M, Kalifa J, Jalife J, Kamiya K, Kodama I. Regional cooling facilitates termination of spiral-wave reentry through unpinning of rotors in rabbit hearts. *Heart Rhythm.* 2012;9:107–114.
61. Hoffman BF, Dangman KH. Mechanisms for cardiac arrhythmias. *Experientia.* 1987;43:1049–1056.
62. Ming Z, Nordin C, Aronson RS. Role of L-type calcium channel window current in generating current-induced early afterdepolarizations. *J Cardiovasc Electrophysiol.* 1994;5:323–334.
63. Hove-Madsen L, Llach A, Bayes-Genis A, Roura S, Rodríguez Font E, Aris A, Cinca J. Atrial fibrillation is associated with increased spontaneous calcium release from the sarcoplasmic reticulum in human atrial myocytes. *Circulation.* 2004;110:1358–1363.
64. Dixit S, Gerstenfeld EP, Callans DJ, Marchlinski FE. Mechanisms underlying sustained firing from pulmonary veins: evidence from pacing maneuvers and pharmacological manipulation. *Pacing Clin Electrophysiol.* 2004;27:1120–1129.
65. Oral H, Crawford T, Frederick M, Gadeela N, Wimmer A, Dey S, Sarrazin JF, Kuhne M, Chalfoun N, Wells D, Good E, Jongnarangsin K, Chugh A, Bogun F, Pelosi F Jr, Morady F. Inducibility of paroxysmal atrial fibrillation by isoproterenol and its relation to the mode of onset of atrial fibrillation. *J Cardiovasc Electrophysiol.* 2008;19:466–470.
66. Berenfeld O, Ennis S, Hwang E, Hooven B, Grzeda K, Mironov S, Yamazaki M, Kalifa J, Jalife J. Time- and frequency-domain analyses of atrial fibrillation activation rate: the optical mapping reference. *Heart Rhythm.* 2011;8:1758–1765.
67. Mandapati R, Skanes A, Chen J, Berenfeld O, Jalife J. Stable microreentrant sources as a mechanism of atrial fibrillation in the isolated sheep heart. *Circulation.* 2000;101:194–199.
68. Mansour M, Mandapati R, Berenfeld O, Chen J, Samie FH, Jalife J. Left-to-right gradient of atrial frequencies during acute atrial fibrillation in the isolated sheep heart. *Circulation.* 2001;103:2631–2636.
69. Jalife J, Berenfeld O, Mansour M. Mother rotors and fibrillatory conduction: a mechanism of atrial fibrillation. *Cardiovasc Res.* 2002;54:204–216.
70. Berenfeld O, Mandapati R, Dixit S, Skanes AC, Chen J, Mansour M, Jalife J. Spatially distributed dominant excitation frequencies reveal hidden organization in atrial fibrillation in the Langendorff-perfused sheep heart. *J Cardiovasc Electrophysiol.* 2000;11:869–879.
71. Mankoff SP, Brander C, Ferrone S, Marincola FM. Lost in Translation: Obstacles to Translational Medicine. *J Transl Med.* 2004;2:14.
72. Nattel S. From guidelines to bench: implications of unresolved clinical issues for basic investigations of atrial fibrillation mechanisms. *Can J Cardiol.* 2011;27:19–26.
73. Zlochiver S, Yamazaki M, Kalifa J, Berenfeld O. Rotor meandering contributes to irregularity in electrograms during atrial fibrillation. *Heart Rhythm.* 2008;5:846–854.
74. Lin J, Scherlag BJ, Zhou J, Lu Z, Patterson E, Jackman WM, Lazzara R, Po SS. Autonomic mechanism to explain complex fractionated atrial electrograms (CFAE). *J Cardiovasc Electrophysiol.* 2007;18:1197–1205.
75. Jackman WM, Scherlag BJ. Nature of electrogram fractionation during atrial fibrillation. *Circ Arrhythm Electrophysiol.* 2012;5:5–7.
76. Kalifa J, Tanaka K, Zaitsev AV, Warren M, Vaidyanathan R, Auerbach D, Pandit S, Vikstrom KL, Ploutz-Snyder R, Talkachou A, Atienza F, Guiraudon G, Jalife J, Berenfeld O. Mechanisms of wave fractionation at boundaries of high-frequency excitation in the posterior left atrium of the isolated sheep heart during atrial fibrillation. *Circulation.* 2006;113:626–633.
77. Berenfeld O, Zaitsev AV, Mironov SF, Pertsov AM, Jalife J. Frequency-dependent breakdown of wave propagation into fibrillatory conduction across the pectinate muscle network in the isolated sheep right atrium. *Circ Res.* 2002;90:1173–1180.
78. Klos M, Calvo D, Yamazaki M, Zlochiver S, Mironov S, Cabrera JA, Sanchez-Quintana D, Jalife J, Berenfeld O, Kalifa J. Atrial septopulmonary bundle of the posterior left atrium provides a substrate for atrial fibrillation initiation in a model of vagally mediated pulmonary vein tachycardia of the structurally normal heart. *Circ Arrhythm Electrophysiol.* 2008;1:175–183.
79. Atienza F, Calvo D, Almendral J, Zlochiver S, Grzeda KR, Martínez-Alzamora N, González-Torrecilla E, Arenal A, Fernández-Avilés F, Berenfeld O. Mechanisms of fractionated electrograms formation in the posterior left atrium during paroxysmal atrial fibrillation in humans. *J Am Coll Cardiol.* 2011;57:1081–1092.
80. Dibs SR, Ng J, Arora R, Passman RS, Kadish AH, Goldberger JJ. Spatiotemporal characterization of atrial activation in persistent human atrial fibrillation: multisite electrogram analysis and surface electrocardiographic correlations–a pilot study. *Heart Rhythm.* 2008;5:686–693.
81. Atienza F, Almendral J, Moreno J, Vaidyanathan R, Talkachou A, Kalifa J, Arenal A, Villacastín JP, Torrecilla EG, Sánchez A, Ploutz-Snyder R, Jalife J, Berenfeld O. Activation of inward rectifier potassium channels accelerates atrial fibrillation in humans: evidence for a reentrant mechanism. *Circulation.* 2006;114:2434–2442.
82. Sahadevan J, Ryu K, Peltz L, Khrestian CM, Stewart RW, Markowitz AH, Waldo AL. Epicardial mapping of chronic atrial fibrillation in patients: preliminary observations. *Circulation.* 2004;110:3293–3299.
83. Herron TJ, Lee P, Jalife J. Optical imaging of voltage and calcium in cardiac cells & tissues. *Circ Res.* 2012;110:609–623.
84. Nanthakumar K, Jalife J, Massé S, Downar E, Pop M, Asta J, Ross H, Rao V, Mironov S, Sevaptsidis E, Rogers J, Wright G, Dhopeshwarkar R. Optical mapping of Langendorff-perfused human hearts: establishing a model for the study of ventricular fibrillation in humans. *Am J Physiol Heart Circ Physiol.* 2007;293:H875–H880.
85. Matiukas A, Mitrea BG, Qin M, Pertsov AM, Shvedko AG, Warren MD, Zaitsev AV, Wuskell JP, Wei MD, Watras J, Loew LM. Near-infrared voltage-sensitive fluorescent dyes optimized for optical mapping in blood-perfused myocardium. *Heart Rhythm.* 2007;4:1441–1451.
86. Kalifa J, Klos M, Zlochiver S, Mironov S, Tanaka K, Ulahannan N, Yamazaki M, Jalife J, Berenfeld O. Endoscopic fluorescence mapping of the left atrium: a novel experimental approach for high resolution endocardial mapping in the intact heart. *Heart Rhythm.* 2007;4:916–924.
87. Morillo CA, Klein GJ, Jones DL, Guiraudon CM. Chronic rapid atrial pacing. Structural, functional, and electrophysiological characteristics of a new model of sustained atrial fibrillation. *Circulation.* 1995;91:1588–1595.
88. Narayan SM, Krummen DE, Rappel WJ. Clinical mapping approach to diagnose electrical rotors and focal impulse sources for human atrial fibrillation. *J Cardiovasc Electrophysiol.* 2012;23:447–454.

KEY WORDS: ablation ■ arrhythmia (mechanisms) ■ atrial fibrillation ■ electrophysiology mapping ■ imaging

SUPPLEMENTAL MATERIAL

Online Supplement

Translational Research in Atrial Fibrillation:

A Quest for Mechanistically Based Diagnosis and Therapy

Felipe Atienza, M.D.[1] Raphael P. Martins, M.D. [2,3] and José Jalife, M.D.[3*]

[1]Hospital General Universitario Gregorio Marañón, Madrid, Spain; [2]Service de Cardiologie, Centre Cardio-Pneumologique, CHU de Rennes, Rennes, France; [3]Center for Arrhythmia Research, University of Michigan, Ann Arbor, Michigan, USA.

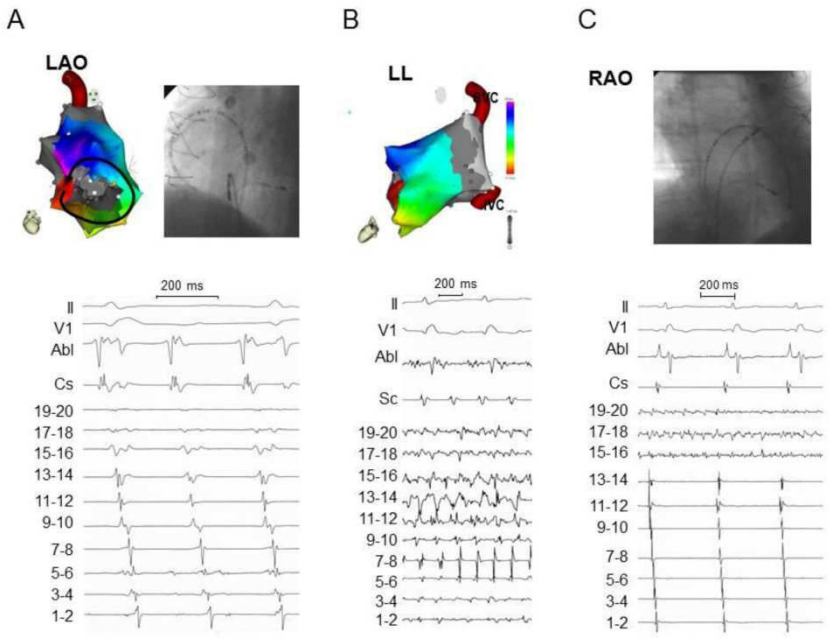

Figure S1. Typical atrial flutter in a transplanted heart, with atrial fibrillation in the remnant atrial tissue of the recipient atrium. Panel A. Surface electrocardiogram shows typical atrial flutter in leads II and V1, and the sequence of intracardiac electrograms recorded along the tricuspid annulus of the right donor atrium (corresponding to the LAO fluoroscopic view above). The LAO electroanatomic activation map shows counterclock wavefront propagation around a reentrant circuit bounded anteriorly by the tricuspid annulus and posteriorly by extensive areas of scar in the connection with the recipient atrium. Dark gray represents zones of low voltage (<0.1 mV) that correspond to the connecting orifice scar and light gray area corresponds to the recipient atrium. Panel B shows typical atrial flutter recordings in surface electrocardiogram and CS and ablation catheter positioned at the cavotricuspid isthmus, while intracardiac electrograms recorded from the multipolar catheter positioned at the recipient atrium (light gray area in LL projection) is recording atrial fibrillation. Panel C, RAO fluoroscopic projection after sinus rhythm conversion at the donor atrium following cavo-tricuspid isthmus ablation, with sinus rhythm activation recorded in bipoles located at the donor´s atrium, while the recipient atrium remained in atrial fibrillation (15-20). LAO: left anterior oblique; LL: left lateral; RAO: right anterior oblique. (Modified from ref. [1] with permission).

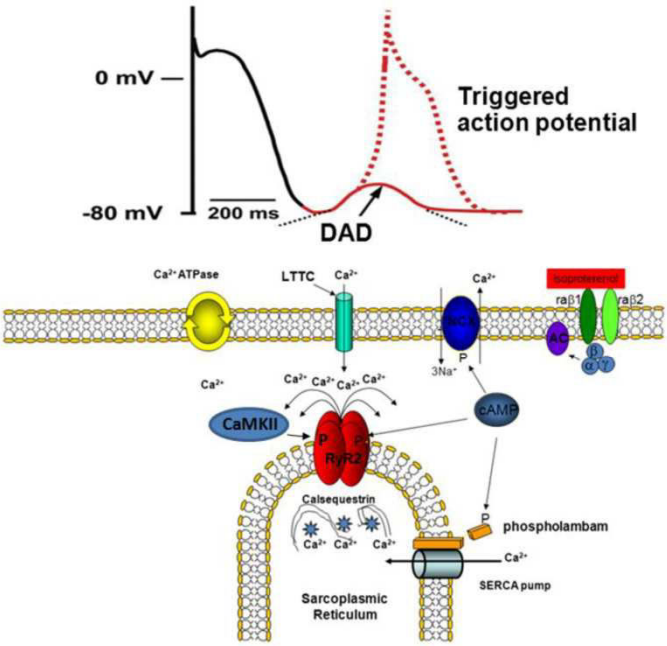

Figure S2. Hypothetical mechanism of induction of triggered activity at the PV induced by intravenous infusion of isoproterenol in the clinical EP lab. Beta-adrenergic stimulation induces cAMP mediated phosphorylation of RyR2 and other calcium regulatory proteins. This, together with rapid pacing promotes the leakage of calcium from the SR, but the precise mechanism is still under debate.[2] Ca^{2+} leak might be a consequence of an increase in luminal SR Ca^{2+} concentration, a reduced SR Ca^{2+} binding to calsequestrin or hyperphosphorylation of RyR2, which would increase its sensitivity to cytosolic Ca^{2+},[3] thus reducing the threshold SR Ca^{2+} content at which SR Ca^{2+} leak occurs. Ca^{2+} leak results in calcium overload during diastole and also activates CaMKII leading in return to RyR2 phosporylation.[4] The calcium is recycled to the SR by the SERCA pump or extruded from the cell by the sodium-calcium exchanger (NCX). NCX transports three Na^{+} ions into the cardiomyocyte in exchange for a single Ca^{2+} ion moving out. Therefore, the exchange across the membrane is electrogenic, which creates a net depolarizing current called 'transient inward current' or I_{ti} leading to a DAD, which if of sufficient amplitude may generate triggered activity and premature impulse propagation, ultimately leading to wavebreak, reentry and sustained AF. Voigt et al recently demonstrated that this mechanisms in human right-atrial myocytes was mediated by hyperphosphorylation of RyR2 induced by the Ca-calmodulin dependent kynase-II (CaMKII).[4] Therefore, while not universally accepted, the general consensus appears to be that CaMKII, and not protein kinase A (PKA), increases calcium leak.[2] Consequently, it is likely that the proarrhythmic activity of CaMKII mediates DAD initiation. As discussed very recently by Dobrev et al this and other recent discoveries provide a robust mechanistic rationale for the development of new anti-AF drugs[5]

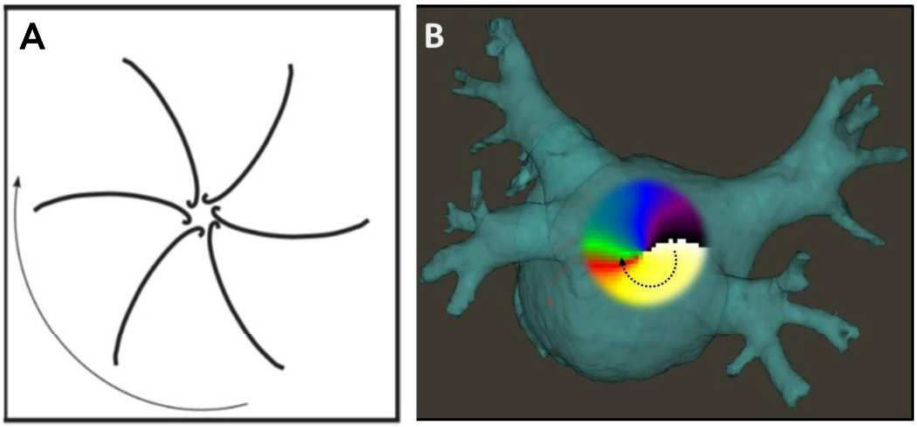

Figure S3. The behavior of a rotor. A. Once formed, the rotor adopts the shape of a pinwheel that spins at high speed and sheds multiple spiraling wavelets in its periphery. B. Montage indicating how a clockwise spinning rotor on the posterior left atrial wall of a human heart would be seen when recorded optically at high spatio-temporal resolution.

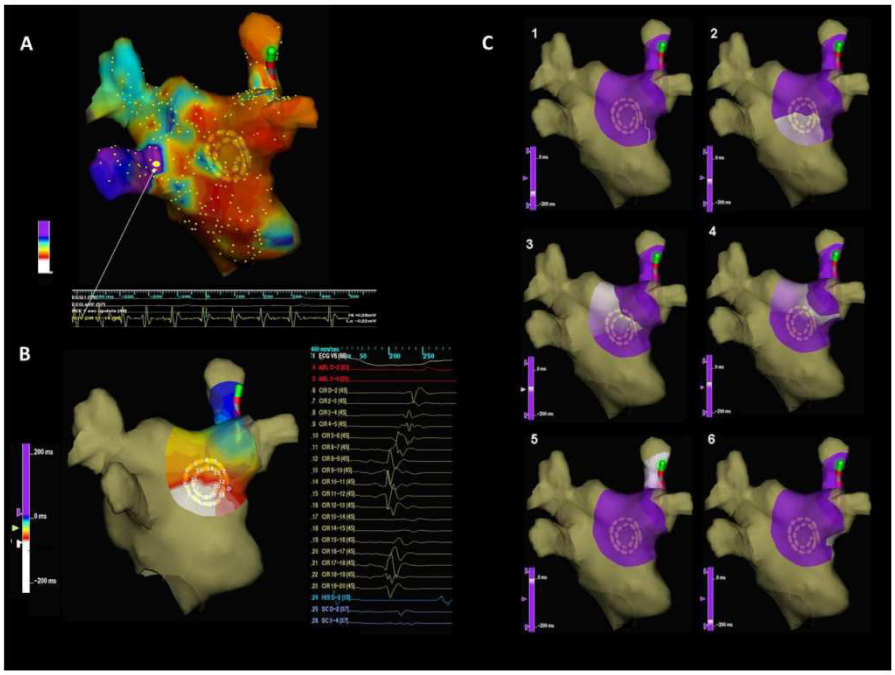

Figure S4. A: Left atrial dominant frequency (DF) map (posterior view) with highest DF site (10.8 Hz) at the left inferior pulmonary vein antrum (white arrow). B: Posterior left atrial wall (PLAW) activation map and corresponding intracardiac recordings during organized phase before fragmentation shows an incoming wave pattern of activation progressing from closest to the highest DF site at the left inferior pulmonary vein (left, white) to the right (purple-blue). C: Snapshots of wave propagation at the PLAW during transitions to fragmentation. Sequence 1 to 6: purple, unactivated regions; white, advancing activation. Re-entrant circuit with a clockwise propagation around a pivoting point located to the right edge of the septo-pulmonary bundle. (Modifed from Ref. 82 by permission of the publisher).

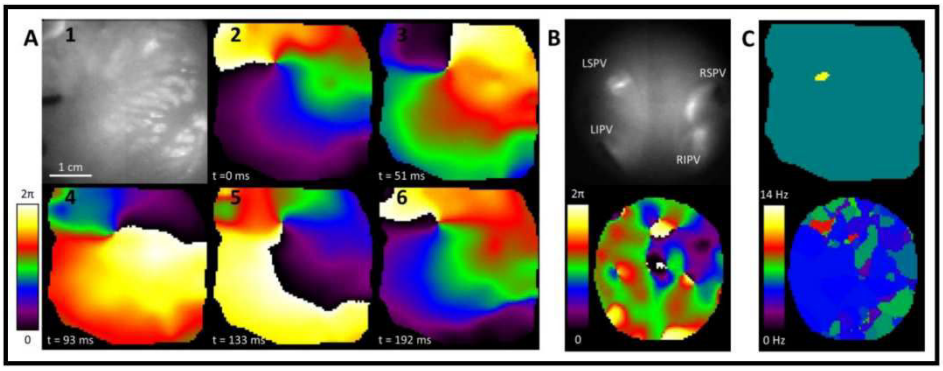

Figure S5. A. Spiral wave on the left atrial free wall of an isolated sheep heart during sustained AF induced by burst pacing in the presence of stretch (11 cm H_20); A1: Snapshot of the area visualized by the CCD camera. The tip of the pacing lead is visualized on the left side of the image. A2 through A6: Snapshots of a phase movie revealing the presence of a stable spiral wave rotating clockwise. B. The posterior left atrium mapped simultaneously using a rigid borescope (upper panel) demonstrates fibrillatory conduction in the posterior wall of the left atrium (lower panel). C: Dominant frequency (DF) maps of the left atrial free wall (upper panel) and the posterior left atrium (lower panel) showing the presence of a high DF area at the center of the core (upper panel, DF = 11.9 Hz) and lower DFs at the periphery of the spiral wave (5.5 Hz). The DF in posterior left atrium (lower panel) is heterogeneous, with a maximum of 9 Hz and resulting of the fibrillatory conduction.

References

1. Waldo AL, Feld GK. Inter-relationships of atrial fibrillation and atrial flutter mechanisms and clinical implications. *J Am Coll Cardiol*. 2008;51:779-786.
2. Valdivia HH. Ryanodine receptor phosphorylation and heart failure: Phasing out s2808 and “criminalizing” s2814 *Circulation Research*. 2012;110:1398-1402.
3. Dobrev D, Voigt N, Wehrens XH. The ryanodine receptor channel as a molecular motif in atrial fibrillation: Pathophysiological and therapeutic implications. *Cardiovasc Res*. 2011;89:734-743.
4. Voigt N, Li N, Wang Q, Wang W, Trafford AW, Abu-Taha I, Sun Q, Wieland T, Ravens U, Nattel S, Wehrens XH, Dobrev D. Enhanced sarcoplasmic reticulum ca2+ leak and increased na+-ca2+ exchanger function underlie delayed afterdepolarizations in patients with chronic atrial fibrillation. *Circulation*. 2012;125:2059-2070.
5. Dobrev D, Carlsson L, Nattel S. Novel molecular targets for atrial fibrillation therapy. *Nat Rev Drug Discov*. 2012;11:275-291.

6. Cartographier les sources de la FA

Comprendre les mécanismes en jeu dans la FA requiert la visualisation de l'activité électrique avec des résolutions spatiale et temporelle suffisantes. Alors qu'une bonne résolution temporelle peut être atteinte via l'utilisation de cathéters diagnostics standards utilisés régulièrement dans les laboratoires d'électrophysiologie, le faible nombre d'électrodes pouvant être utilisé simultanément en limite la résolution spatiale. Ceci empêche l'analyse détaillée des rotors et des ondes de fibrillation.

L'utilisation de la cartographie optique dès le début des années 1990 a permis de mieux caractériser l'activité fibrillatoire en FA sur des modèles animaux, et ce avec une résolution spatiale infra-millimétrique. Cette technique a permis de mettre en évidence l'existence des rotors, antérieurement proposée et modélisée. Par ailleurs, l'association de l'optical mapping avec l'analyse spectrale des signaux (FFT) a permis de démontrer l'existence d'une hétérogénéité dans la fréquence de l'activité en FA, ainsi que des gradients intra- et inter-atriaux.

Nous avons utilisé cette technique de façon régulière sur un modèle de FA induite par le stretch chez le cœur de mouton explanté et perfusé par la méthode de Langendorff. En plus de la cartographie épicardique usuelle, nous avons associé une cartographie endocardique de la paroi postérieure de l'OG en utilisant un endoscope couplé à une caméra haute résolution.

La technique utilisée était la suivante (Figure 6):

- Des moutons pesant 30-40 kg étaient anesthésiés en utilisant 4-6 mg/kg de propofol et 60-100 mg/kg de pentobarbital sodique. Les cœurs étaient explantés après thoracotomie et les différentes structures veineuses et artérielles isolées du tissu conjonctif et pulmonaire.
- Les cœurs étaient alors connectés à un système de perfusion de type Langendorff avec une solution de perfusion oxygénée (95%O_2, 5% CO_2) à un flux constant de 240-270 ml/min de type Tyrode contenant (en mM) : NaCL 130, KCl 4, $MgCL_2$ 1, $CaCl_2$ 1.8, $NaHCO_3$ 24, NaH_2PO_4 1.2, Glucose 5.6 et albumine 0.04 g/l, à un pH de 7.4 et une température entre 35.5 et 37.5°C. De la blebbistatine (10 µM, bloqueur de la myosine II) était utilisée afin d'éliminer l'activité contractile, source d'artefacts dans l'analyse des signaux optiques.
- Une ponction trans-septale était effectuée afin de permettre une égalisation de la pression atriale gauche et droite.
- Tous les orifices veineux étaient ligaturés, à l'exception de la veine cave inférieure qui était canulée et connectée à un senseur digital (Biopac Systems tranducer-TSD104A ; Biopac Systems, Inc., Goleta, CA, USA) et à un système permettant de contrôler la pression intra-atriale.
- Des cathéters quadripolaires (Torq®, Medtronic Inc./Minneapolis/MN/USA) étaient placés dans les veines pulmonaires avant leur ligature afin d'enregistrer des signaux bipolaires à partir du dipôle distal (fréquence d'échantillonnage 1.0Hz). Enfin, deux électrodes bipolaires étaient placées sur les auricules droit et gauche.

- La pression était alors augmentée à 12 cmH_2O, menant à une augmentation de près de 30% du volume atrial par rapport à une pression de 6 cm H_2O. La pression était alors maintenue stable pendant toute la durée de l'expérimentation.
- Après mise en place des caméras, 5 à 10 ml d'un produit fluorescent sensible au voltage (Di-4-ANEPPS ; 10mg/ml ; Sigma-Aldrich, St Louis, MO, USA) étaient injectés dans la solution de perfusion. Après 10 min d'incubation, la fluorescence apparaissait à la surface du myocarde après excitation laser (532nm). La fluorescence émise était filtrée (filtre passe-haut 600 nm) et acquise par une caméra CCD (80x80 pixels, SciMeasure Analytical Systems, Inc. Decatur, GA, USA) à la vitesse de 800 images par seconde.
- La première caméra, épicardique, était dirigée vers la paroi latérale de l'OG, avec une surface de cartographie d'environ 14 cm². Parallèlement, une seconde caméra permettait de cartographier l'endocarde de la paroi postérieure de l'OG. Celle-ci était connectée à un endoscope rigide de 10mm de diamètre (Everest VIT, Inc. Flanders, NJ, USA) avec un champ de vision de 90°, introduit à travers la paroi antérieure du ventricule gauche et la valve mitrale. La surface de l'endocarde cartographié était d'environ 4 cm², permettant de visualiser les quatre VP et l'endocarde postérieur de l'OG après excitation laser (532 nm). Les 2 caméras (endo- et épicardiques) étaient synchronisées afin de comparer l'activation des différentes structures atriales à un instant donné.

Une fois l'ensemble du système mis en place, des acquisitions de 5 secondes en rythme sinusal étaient réalisées. La FA était déclenchée par stimulation atriale à haute fréquence via l'électrode placée sur l'auricule gauche (12Hz, durée du pulse 5 ms, à une énergie double du seuil de stimulation) à l'état basal ou sous certaines conditions (le plus fréquemment stretch intra-atrial, ou alors par perfusion d'acétylcholine avec une pression intra-atriale normale) et des acquisitions de 5 secondes effectuées toutes les 2 minutes.

Les signaux optiques lors des acquisitions étaient synchronisés entre eux mais également aux enregistrements bipolaires (VP, auricules droit et gauche).

Afin d'étudier la dynamique de propagation en rythme sinusal et en FA, des cartes de phase étaient générées. Brièvement, la phase du potentiel d'action enregistré à un instant donné à chaque pixel était déterminée en transformant les composantes spectrales du signal original. Par la suite, la phase instantanée du signal était obtenue à partir de l'inverse de la tangente du ratio [signal transformé/signal original]. L'angle de phase, dont la valeur varie entre les radians - π et π, était représenté dans une échelle colorimétrique continue afin de construire une carte de phase, dans laquelle les changements spatiaux de phase reflètent le processus d'excitation et de repolarisation. Différents types de propagation peuvent alors être visualisés (Figure 7), dont :

- Les rotors, identifiés comme une zone où toutes les phases convergent au niveau du « point de singularité », se maintenant pendant plus d'une rotation ;
- Les décharges focales (« breakthroughs »), défini comme un front de dépolarisation apparaissant au niveau de la zone cartographiée et se propageant aux alentours de manière centripète ;

- Les ondes périodiques organisées sur le plan spatio-temporel, définies comme un minimum de 4 ondes périodiques séquentielles provenant d'une même localisation du champ d'observation, se dirigeant dans la même direction, à cycle constant.

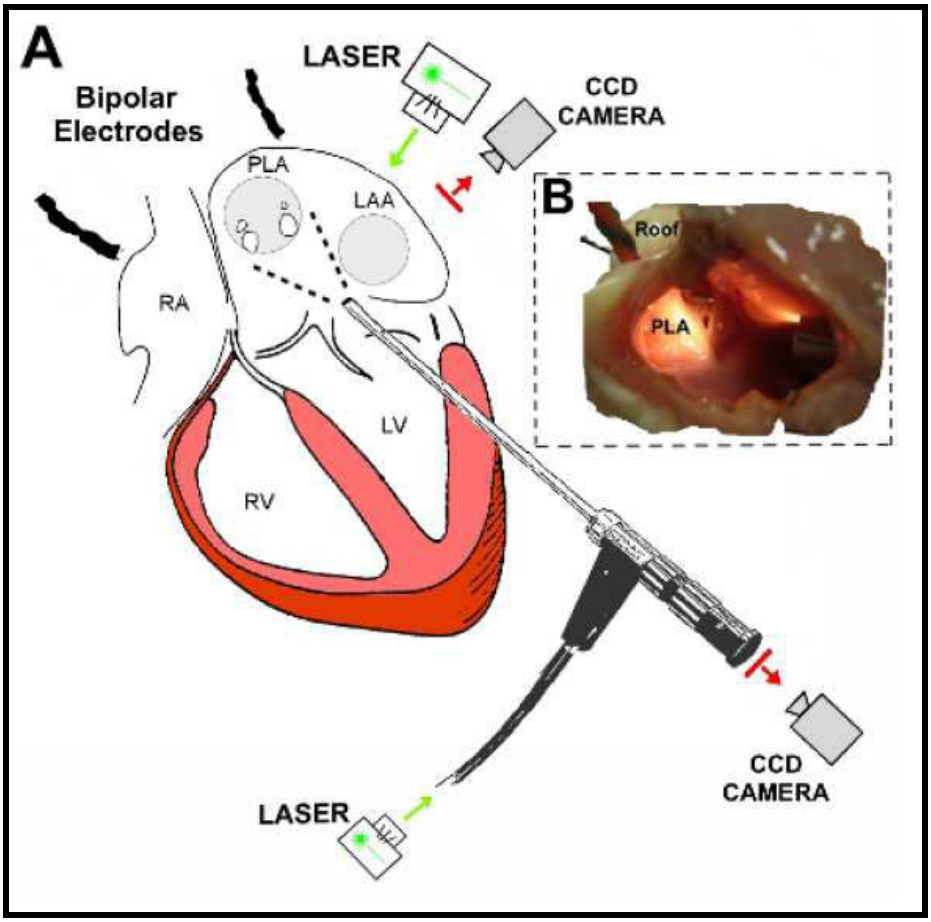

Figure 6 : Représentation schématique du montage utilisé lors des expériences de cartographie optique. A. Un endoscope rigide est introduit à travers la paroi antérieure du ventricule gauche et de l'orifice mitral et dirigé vers le mur postérieur de l'OG. Une caméra CCD est couplée à l'endoscope et l'illumination laser apportée par la partie inférieure de l'endoscope. Une cartographie optique conventionnelle épicardique de la paroi latérale de l'OG est effectuée dans le même temps. Des électrodes bipolaires sont placées sur les auricules droit et gauche, sur le toit de l'OG ainsi que dans chacune des VP. **B.** Vue latérale de l'OG après ouverture de la paroi latérale.

.

Par ailleurs, une analyse fréquentielle était effectuée afin d'identifier les régions présentant une fréquence d'activation élevée et de rechercher des gradients de fréquence. Des cartes de fréquences dominantes DF étaient alors générées pour chaque acquisition en appliquant une FFT aux signaux enregistrés à chaque pixel de l'image. Parallèlement, une FFT était appliquée aux électrogrammes bipolaires obtenus de façon synchrone aux enregistrements vidéo (filtre passe-haut à 3 Hz et filtre passe-bas à 35 Hz).

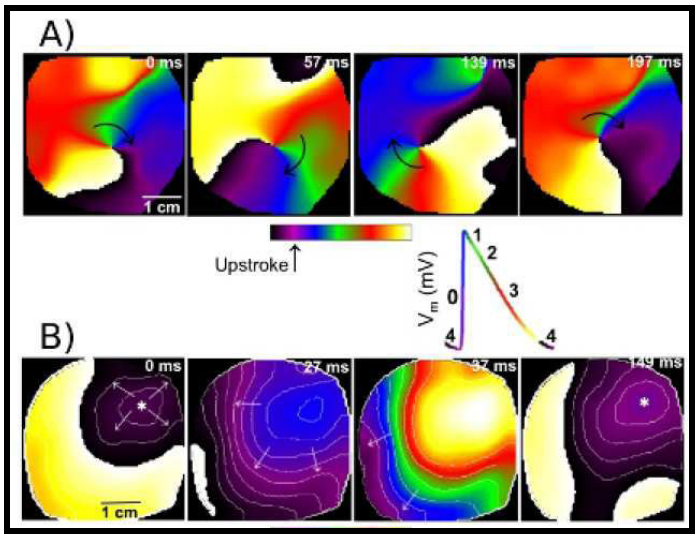

Figure 7 : Types d'activation enregistrés par optical mapping lors d'un épisode de FA. A. Clichés séquentiels de la paroi latérale de l'OG mettant en évidence un rotor pivotant autour d'un point de singularité ; une rotation complète est montrée de gauche à droite. **B.** Décharge focale (« breakthrough ») où l'onde de dépolarisation apparait dans l'angle supérieur droit du champ et se propage de façon centripète.

Cette technique a permis d'améliorer les connaissances sur la dynamique de la FA. Nous l'avons récemment décrite dans le *Journal of Visualized Experiments.*[132]

Cette technique a permis d'étudier les gradients de DF entre l'OD et l'OG, mais également au sein d'une même oreillette, pendant des épisodes de FA induite par le stretch ou par l'acétylcholine. Un épisode de FA représentatif est illustré dans la Figure 8.

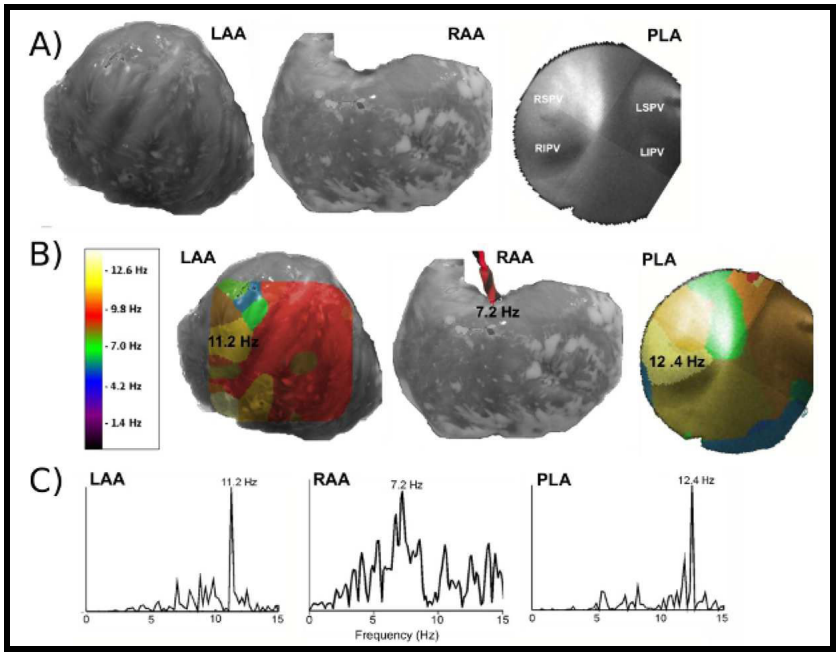

Figure 8 : Identification des régions avec les fréquences d'activation les plus élevées lors d'un épisode de FA induit par le stretch sur un cœur de mouton isolé et perfusé par la méthode de Langendorff. A. Vue anatomique du mur latéral de l'OG (LAA) et de l'OD (RAA) ainsi que de la vue de la paroi postérieure de l'OG (PLA). On distingue au pourtour de l'endocarde postérieur les 4 VP. **B.** Cartes de DF obtenues par optical mapping de l'OG endo- et épicardique. La fréquence d'activation la plus rapide (DF_{max}) est retrouvée au niveau du mur postérieur de l'OG. **C.** Spectres de puissance représentatifs d'un épisode de FA induit par le stretch : la DF_{max} est retrouvée au niveau du mur postérieur, et un gradient gauche-droit est mis en évidence (7.2 Hz dans l'OD, 11.2 Hz dans l'OG et 12.4 Hz dans l'endocarde postérieur de l'OG).

Video Article

High-Resolution Endocardial and Epicardial Optical Mapping in a Sheep Model of Stretch-Induced Atrial Fibrillation

David Filgueiras-Rama, Raphael Pedro Martins, Steven R. Ennis, Sergey Mironov, Jiang Jiang, Masatoshi Yamazaki, Jérôme Kalifa, Josè Jalife, Omer Berenfeld

Center for Arrhythmia Research. Internal Medicine, University of Michigan

Correspondence to: Omer Berenfeld at oberen@med.umich.edu

URL: http://www.jove.com/details.php?id=3103

DOI: 10.3791/3103

Keywords: Medicine, Issue 53, atrial fibrillation, endocardial mapping, patterns of activation, posterior left atrium,

Date Published: 29/7/2011

Citation: Filgueiras-Rama, D., Martins, R.P., Ennis, S.R., Mironov, S., Jiang, J., Yamazaki, M., Kalifa, J., Jalife, J., Berenfeld, O. High-Resolution Endocardial and Epicardial Optical Mapping in a Sheep Model of Stretch-Induced Atrial Fibrillation. J. Vis. Exp. (53), e3103, DOI : 10.3791/3103 (2011).

Abstract

Atrial fibrillation (AF) is a complex cardiac arrhythmia with high morbidity and mortality.[1,2] It is the most common sustained cardiac rhythm disturbance seen in clinical practice and its prevalence is expected to increase in the coming years.[3] Increased intra-atrial pressure and dilatation have been long recognized to lead to AF,[1,4] which highlights the relevance of using animal models and stretch to study AF dynamics. Understanding the mechanisms underlying AF requires visualization of the cardiac electrical waves with high spatial and temporal resolution. While high-temporal resolution can be achieved by conventional electrical mapping traditionally used in human electrophysiological studies, the small number of intra-atrial electrodes that can be used simultaneously limits the spatial resolution and precludes any detailed tracking of the electrical waves during the arrhythmia. The introduction of optical mapping in the early 90's enabled wide-field characterization of fibrillatory activity together with sub-millimeter spatial resolution in animal models[5,6] and led to the identification of rapidly spinning electrical wave patterns (rotors) as the sources of the fibrillatory activity that may occur in the ventricles or the atria.[7-9] Using combined time- and frequency-domain analyses of optical mapping it is possible to demonstrate discrete sites of high frequency periodic activity during AF, along with frequency gradients between left and right atrium. The region with fastest rotors activates at the highest frequency and drives the overall arrhythmia.[10,11] The waves emanating from such rotor interact with either functional or anatomic obstacles in their path, resulting in the phenomenon of fibrillatory conduction.[12] Mapping the endocardial surface of the posterior left atrium (PLA) allows the tracking of AF wave dynamics in the region with the highest rotor frequency. Importantly, the PLA is the region where intracavitary catheter-based ablative procedures are most successful terminating AF in patients,[13] which underscores the relevance of studying AF dynamics from the interior of the left atrium. Here we describe a sheep model of acute stretch-induced AF, which resembles some of the characteristics of human paroxysmal AF. Epicardial mapping on the left atrium is complemented with endocardial mapping of the PLA using a dual-channel rigid borescope c-mounted to a CCD camera, which represents the most direct approach to visualize the patterns of activation in the most relevant region for AF maintenance.

Video Link

The video component of this article can be found at http://www.jove.com/details.php?id=3103

Protocol

1. Heart removal and Langendorff perfusion

Sheep weighing 35-40 Kg are anesthetized using 4-6 mg/Kg propofol and 60-100 mg/Kg of sodium pentobarbital. Hearts are removed via thoracotomy and connected to a Langendorff-perfusion system with circulating oxygenated (95% O2, 5% CO2) Tyrode's solution at a constant flow rate of 240-270 ml/min, pH 7.4 and 35.5-37.5 °C. The Tyrode's composition (in mM) is: NaCl 130, KCl 4.0, MgCl2 1, CaCl2 1.8, NaHCO3 24, NaH2PO4 1.2, Glucose 5.6, and Albumin 0.04 g /L. Blebbistatin 10 μM (Enzo Life Science International, INC. Plymouth Meeting, PA, USA) is used to reduce the contractile force.

2. Stretch-induced atrial fibrillation in the Langendorff-perfused sheep heart

The isolated, coronary perfused heart undergoes an atrial trans-septal puncture to enable equalized intracavitary pressure in both atria. All vein orifices are then sealed, except the inferior vena cava, which is cannulated and connected to a digital sensor (Biopac Systems transducer-TSD104A; Biopac Systems, Inc., Goleta, CA, USA) and to an outflow cannula whose open-ended height above the atria controls the intra-atrial pressure. The pressure is then increased to 12 cm H_2O, which leads to a ~30% increase in atrial volume relative to the volume at 6 cm H_2O. The pressure is maintained stable throughout the experiment. Prior to sealing the veins tetrapolar electrode catheters (Torq, Medtronic Inc./Minneapolis/MN/USA) are placed in each of the pulmonary veins to record bipolar signals from the two distal electrodes (sampling rate, 1.0 kHz) using a Biopac Systems amplifier (DA100C; Biopac Systems, Inc., Goleta, CA, USA). Two additional custum-made bipolar electrodes are placed on the roof of left atrial appendage (LAA) and the top of right atrial appendage.

3. Optical mapping set up

1. Epicardial mapping of the left atrial appendage. A bolus injection of 5 to 10 ml Di-4-ANEPPS (10 mg/mL) (Sigma-Aldrich, St. Louis, MO, USA) and a loading period of 10 min are needed to obtained voltage-sensitive fluorescence upon laser excitation (532 nm) of the epicardial surface. The emitted fluorescence is then transmitted through a 600 nm long pass filter and projected onto LittleJoe CCD video camera (80x80 pixels, SciMeasure Analytical Systems, Inc. Decatur, GA, USA) and acquired at a rate of 800 frames per second (See schematic representation on Figure 1A). Five-second movies are obtained at 2 min intervals during AF. The area of the mapped epicardial surface is ~14 cm^2.
2. Endocardial optical mapping of the PLA of the intact heart. A second LittleJoe CCD camera (80x80 pixels) is synchronized with the epicardial camera. A 10 mm diameter dual-channel rigid borescope (Everest VIT, Inc. Flanders, NJ, USA) with a 90-degree field of view is introduced through the anterior wall of the left ventricle, across the mitral valve and focused on the endocardial surface of the PLA. The optically mapped area on the PLA is ~4 cm^2, which allows visualizing the four pulmonary veins and the atrial septo-pulmonary bundle (Figure 1A, B). The borescope is c-mounted to the CCD camera through a custom-made eyepiece adapter. Laser 532 nm light is then delivered to the excitation channel of the borescope through a liquid light-guide (0.2 in core).

4. Atrial fibrillation protocol

Under continuous atrial stretch AF is induced via burst pacing (12 Hz, 5 ms pulses, 2x diastolic threshold) by a pacing electrode located on top of the LAA. AF is allowed to continue for 50 minutes and 5-sec optical movies are acquired at two min intervals. Bipolar recordings are collected continuously. Acquisition of the optical movies triggers simultaneous acquisition of 5-sec segments of the bipolar recordings.

5. Frequency analysis

Frequency analysis allows identification of regions with high activation rate during AF, along with frequency gradients between left and right atrium. Dominant frequency (DF) maps are obtained from each optical movie after applying a fast Fourier transform algorithm (FFT) to the time-series fluorescence signal recorded at each pixel.[7] FFT is also applied to the 5 second bipolar signals (High-pass filtered at 3 Hz and low-pass filtered at 35 Hz) synchronized with the optical movies.

6. Atrial fibrillation dynamics

1. Generation of phase maps. Analysis of AF dynamics takes advantage of phase movies generated via Hilbert transformation.[14] Briefly, the instantaneous phase of the action potential recorded at each pixel is determined by transforming the original time-series signals such that every spectral component is shifted by its corresponding quarter cycle.[15] Afterwards, the instantaneous phase of the signal is obtained from the inverse tangent of the ratio of the transformed signal to the original signal. The phase angle, with values between $-\pi$ and π radians is represented as a continuous color scheme to construct a phase map, in which the continuous spatial phase change reflects the process of excitation, repolarization and recovery.[14]
2. Characterization of activation patterns. Various classes of activation patterns can be identified using phase movies (Figure 2), including the following:
    - A rotor is identified by the presence of all phases converging on a singularity point lasting more than one rotation (Figure 2A).
    - A breakthrough is defined as a wavefront appearing in the field of view and propagating outward (Figure 2B) in a target-like pattern.
    - Spatiotemporally organized periodic waves are defined as a minimum of four sequential periodic waves emerging from the same location in the field of view, with similar direction and inter-wave interval (Figure 2C).

Further quantification allows spatial correlation of highest frequency domains with the most common pattern of activation obtained from that particular region. The latter highlights the crucial role of mapping the endocardial surface of the PLA, since it commonly represents the region where the highest frequency domains are located during acute AF.

7. Representative Results:

Dominant frequency (DF) gradients from PLA to LAA and RAA are present during acute stretch-induced AF. The highest DF region is localized either at or near one of the pulmonary veins or somewhere in the PLA.[11] A representative AF episode is shown in Figure 3, in which the highest DF is localized on the PLA (Right inferior pulmonary vein). The results support the presence of high frequency sources in the PLA driving AF consistent with the left to right DF gradients observed during ablative procedures in paroxysmal human AF.[16]

Quantification of patterns of activation using phase map movies shows that the highest number of rotors is found at the PLA and the junction between the PLA and the LAA.[8] Occasionally it is possible to identify long-lasting rotors whose center of rotation (Singularity point) localizes with the highest frequency domain.[10] Since atrial tissue represents a three-dimensional structure, identifying rotors on the mapped endocardial surface of the PLA suggests that the center of rotation of those rotors (filament) is eventually perpendicular to the surface of the mapping area. Figure 4 shows such a rotor recorded from the endocardium of the PLA with simultaneous fibrillatory conduction toward the LAA, which also correlates with a frequency gradient between the PLA and the LAA (9 and 6.4 Hz respectively). The number of rotors is consistently higher at the PLA than the LAA, which suggests an essential role of reentry on the PLA to maintain the arrhythmia in this model.

Overall, the results support the theory that stable and fast rotors in the left atrium may drive acute stretch-induced AF and emanating waves undergo complex, spatially distributed conduction block patterns as they head toward the right atrium, manifesting as fibrillatory conduction and progressively decreasing dominant frequency.

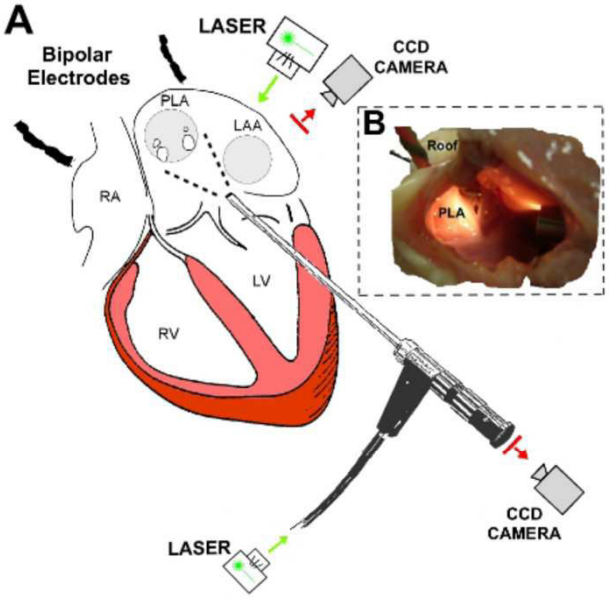

Figure 1. Diagrammatic representation of the experimental set up. A: A rigid borescope is introduced through the anterior wall of the left ventricle and the mitral valve orifice and focused on the endocardial surface of the posterior left atrium (PLA). A CCD camera is coupled to the borescope and laser illumination is provided through a laser liquid guide connected to the inferior part of the borescope. Epicardial mapping is performed on the LAA. Bipolar electrodes are placed on right atrium and roof of the left atrium. Additional bipolar signals are obtained from the pulmonary veins. B: Lateral view of the left atrium following opening the lateral wall for illustration purposes. The tip of the borescope illuminates the endocardial surface of the PLA. A bipolar electrode is located on the roof of the left atrium. LAA: left atrial appendage. LV: left ventricle. RA: right atrium. RV: right ventricle.

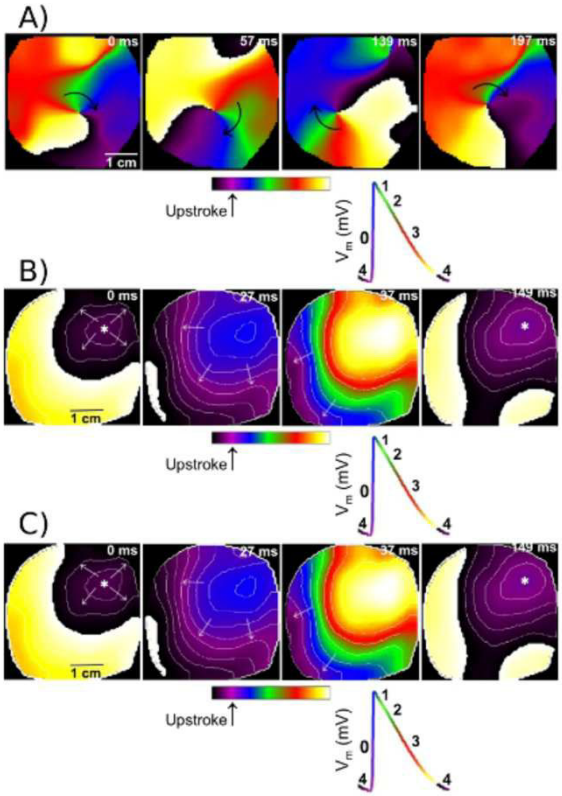

Figure 2. Different patterns of activation identified after the generation of phase movies. A: Sequential snap shots of the left atrial appendage (LAA) show the pivoting of a rotor around its center of rotation (Singularity point). From left to right, one full rotation is completed. B: A sample breakthrough activation pattern on the LAA. The wave appears on the upper right corner of the field of view and propagates outward. C: Four spatiotemporally organized periodic waves (At 0, 182, 352 and 512 ms, respectively) coming from the PLA region toward the LAA. Isochrones are plotted at 10 ms intervals. Bottom, key for the different phases of the action potential is color-coded.

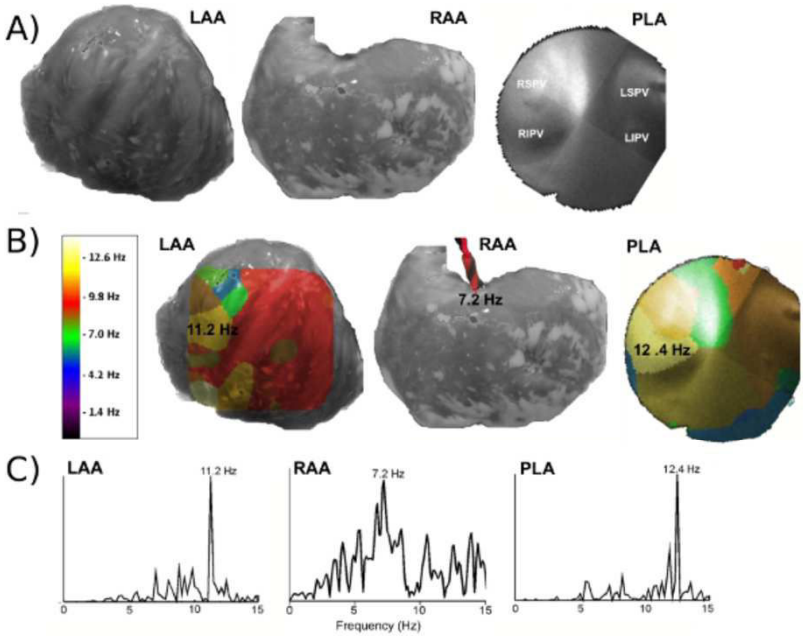

Figure 3. Identification of the regions with the highest frequency activity during acute stretch-induced AF in a Langendorff-perfused isolated sheep heart. A: Anatomical view of the left atrial appendage (LAA), right atrial appendage (RAA) and posterior left atrium (PLA). PLA image is an endoscopic view of the mapped region with the four pulmonary veins (PVs). B: DF maps obtained by optical mapping on the LAA and PLA. Frequency value in the RAA was obtained from bipolar electrograms. The highest frequency region is located in the PLA. C: Representative power spectra, in which the maximum DF corresponds to 12.4 Hz at the PLA region of the right PVs. LSPV: left superior pulmonary vein. LIPV: left inferior pulmonary vein. RSPV: right superior pulmonary vein. RIPV: right inferior pulmonary vein. Reproduced from reference 11 (David Filgueiras Rama & José Jalife. Mechanisms Underlying Atrial Fibrillation. in *Basic Science for Clinical Electrophysiologist*, Vol. 3 (ed. Charles Antzelevitch) 141-156 (SAUNDERS, 2011).

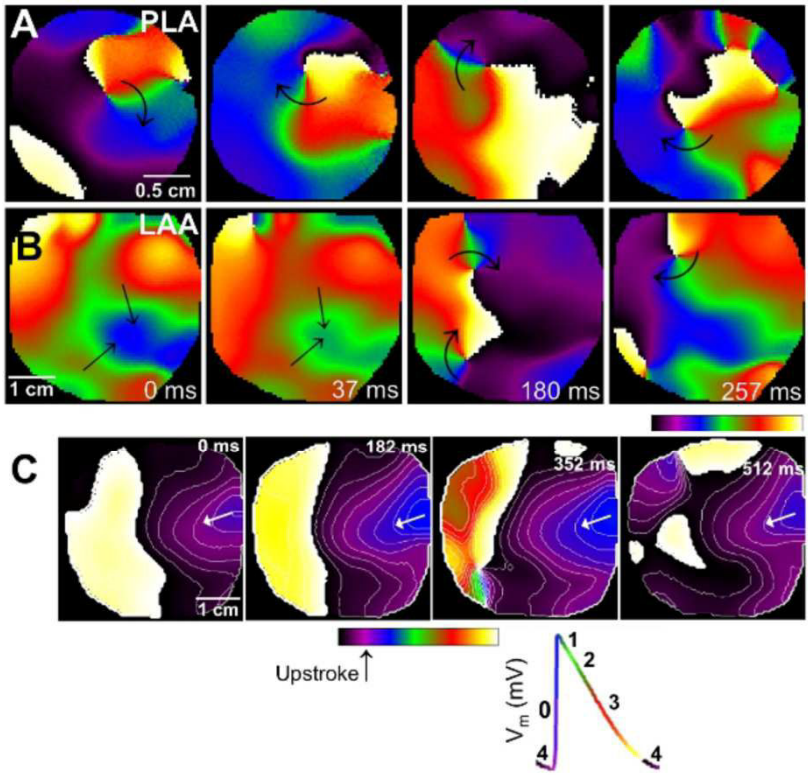

Figure 4. Simultaneousphase maps (A, B) and dominant frequency maps (C) from posterior left atrium (PLA) and left atrial appendage (LAA). A: Sequential snap shots from the PLA showing a rotor and the drifting of its singularity point. B: Simultaneous phase snap shots from the LAA. Patterns of activation show propagation waves compatible with fibrillatory conduction. Singularity points are also present in correlation with wavebreaks in the fibrillatory conduction region. (See also video 4) C: Simultaneous dominant frequency maps from the PLA and the LAA. The fastest region is located at the PLA (9 Hz), which correlates with the presence of a rotor in the phase map analysis. The highest frequency at the LAA is 6 Hz, which correlates with fibrillatory conduction. On the right side of panel C, single pixel optical activations from PLA and LAA are shown.

Discussion

The characteristics of acute stretch-induced AF in the isolated sheep heart resemble some of the properties of human paroxysmal AF. An acute increase in intra-atrial pressure in the sheep heart allows the maintenance of AF for long periods of time, similar to a higher risk of AF observed in patients with atrial dilatation.[1] The presence of left-to-right DF gradients in the sheep atria is also similar to those registered in human electrophysiological studies.[16] Therefore, understanding the mechanism sustaining AF in this acute model may improve the therapeutic strategies currently used in human paroxysmal AF. Some of the limitations of the current approach are: first, the difficulty of reproducing the effect of the autonomic nervous system on the fibrillation in isolated hearts, which precludes extrapolation of the results to *in vivo* situations. And second, the model focuses on acute stretch-induced AF, and therefore conclusions should not be extended to structurally remodeled hearts, in which fibrosis and alterations in electrical properties might affect patterns of activation on the PLA and LAA. Lastly, it should be noted that due to optical constraints as well as toxicity of voltage-sensitive dyes and motion-uncoupling compounds, optical mapping techniques are currently not feasible in living subjects.

Notwithstanding, the use of optical mapping and specifically the endocardial mapping of the PLA as demonstrated in this protocol advances our mechanistic understanding of AF by identifying the highest number of rotors in the fastest frequency domains. The latter suggest that reentry may be essential to sustain the arrhythmia. Thus, different pharmacological strategies focus on terminating reentry can be studied using this model, which makes it suitable for relevant translational studies.

Technological improvements in the optical mapping approach are continually being sought after. Although the wide-field view and high spatial and temporal resolution obtained with optical mapping allows the identification of long lasting rotors on the 2D mapped surface, very often those rotors drift away from the field of view. Thus, a more panoramic optical mapping approach would enable better tracking of drifting rotors and the arrhythmia in general. New dyes that provide deeper-penetrating signals and new mathematical analyses might also allow tracking rotors and their filaments inside the 3D structure of the PLA wall. The latter would also allow a better understanding of patterns of activations previously described as surface breakthroughs, which might represent intramural reentrant activity. Additional improvements being pursued include: reduced toxicity of the voltage-sensitive dyes; optical probes for further physiological parameters, such as intracellular calcium concentration; improved compounds and techniques for motion reduction.

Disclosures

No conflicts of interest declared.

Acknowledgements

Supported in part by NHLBI Grants P01-HL039707 and P01-HL087226 and the Leducq Foundation (J.J. and O.B.), by a Spanish Society of Cardiology Fellowship, Fundación Pedro Barrié de la Maza and Fundación Alfonso Martín Escudero (D.F.R.), by Fédération Française de Cardiologie (R.P.M.), by a Heart Rhythm Society fellowship Award, The Fellowship of Japan Heart Foundation/The Japanese Society of Electrocardiology (M.Y.).

References

1. Kannel, W.B., Wolf, P.A., Benjamin, E.J., & Levy, D. Prevalence, incidence, prognosis, and predisposing conditions for atrial fibrillation: population-based estimates. *Am J Cardiol*. **82**, 2N-9N (1998).
2. Wolf, P.A., Abbott, R.D. & Kannel, W.B. Atrial fibrillation as an independent risk factor for stroke: the Framingham Study. *Stroke*. **22**, 983-988 (1991).
3. Miyasaka, Y., *et al*. Secular trends in incidence of atrial fibrillation in Olmsted County, Minnesota, 1980 to 2000, and implications on the projections for future prevalence. *Circulation*. **114**, 119-125 (2006).
4. Ravelli, F. & Allessie, M. Effects of atrial dilatation on refractory period and vulnerability to atrial fibrillation in the isolated Langendorff-perfused rabbit heart. *Circulation*. **96**, 1686-1695 (1997).
5. Gray, R.A., Pertsov, A.M. & Jalife, J. Spatial and temporal organization during cardiac fibrillation. *Nature*. **392**, 75-78 (1998).
6. Gray, R.A., *et al*. Mechanisms of cardiac fibrillation. *Science*. **270**, 1222-1223; author reply 1224-1225 (1995).
7. Samie, F.H., *et al*. Rectification of the background potassium current: a determinant of rotor dynamics in ventricular fibrillation. *Circ Res*. **89**, 1216-1223 (2001).
8. Kalifa, J., *et al*. Intra-atrial pressure increases rate and organization of waves emanating from the superior pulmonary veins during atrial fibrillation. *Circulation*. **108**, 668-671 (2003).
9. Mandapati, R., Skanes, A., Chen, J., Berenfeld, O. & Jalife, J. Stable microreentrant sources as a mechanism of atrial fibrillation in the isolated sheep heart. *Circulation*. **101**, 194-199 (2000).
10. Yamazaki, M., *et al*. Mechanisms of stretch-induced atrial fibrillation in the presence and the absence of adrenocholinergic stimulation: interplay between rotors and focal discharges. *Heart Rhythm*. **6**, 1009-1017 (2009).
11. David Filgueiras Rama & José Jalife. Mechanisms Underlying Atrial Fibrillation. in *Basic Science for Clinical Electrophysiologist*, Vol. 3 (ed. Charles Antzelevitch) 141-156 (SAUNDERS, 2011).
12. Berenfeld, O., Zaitsev, A.V., Mironov, S.F., Pertsov, A.M., & Jalife, J. Frequency-dependent breakdown of wave propagation into fibrillatory conduction across the pectinate muscle network in the isolated sheep right atrium. *Circ Res*. **90**, 1173-1180 (2002).
13. Haissaguerre, M., *et al*. Spontaneous initiation of atrial fibrillation by ectopic beats originating in the pulmonary veins. *N Engl J Med*. **339**, 659-666 (1998).
14. Warren, M., *et al*. Blockade of the inward rectifying potassium current terminates ventricular fibrillation in the guinea pig heart. *J Cardiovasc Electrophysiol*. **14**, 621-631 (2003).
15. Claerbout, J.F. *Fundamentals of Geophysical Data Processing*, (McGraw-Hill, New York, 1976).
16. Atienza, F., *et al*. Real-time dominant frequency mapping and ablation of dominant frequency sites in atrial fibrillation with left-to-right frequency gradients predicts long-term maintenance of sinus rhythm. *Heart Rhythm*. **6**, 33-40 (2009).

B. Etude de l'évolution de la DF en FA

L'analyse de la distribution spatiale des DF dans les modèles animaux a apporté de nombreuses connaissances sur les mécanismes de la FA. Les travaux d'analyse spectrale de l'oreillette en FA paroxystique chez l'animal[133] et chez l'homme[134] ont démontré que la DF_{max} se situait au niveau ou près des VP avec un gradient de fréquence gauche-droite. Ce gradient a été retrouvé dans les cœurs de moutons explantés et perfusés par la technique de Langendorff, supportant l'hypothèse que la FA est la conséquence de sources rapides situées dans l'OG.[28] Les zones de bloc anatomiques (tels que le faisceau de Bachmann) et/ou fonctionnels conduisent à une fragmentation des fronts de dépolarisation, à la formation de nouveaux rotors, et à une diminution de la fréquence d'activation. Des gradients gauche-droite ont été retrouvés chez l'homme en cas de FA paroxystique, mais pas toujours en FA persistante.[135]

Différentes études ont analysé l'efficacité de l'ablation ciblée sur ces zones de DF élevée. Sanders et al ont combiné les systèmes de cartographie électroanatomiques avec l'analyse spectrale des signaux en utilisant un transformée rapide de Fourier afin de recréer des cartes tridimensionnelles de DF de l'oreillette humaine en FA.[136] Les patients en FA paroxystique et persistante présentaient des gradients OG-OD-sinus coronaire. Les patients en FA paroxystique avaient une DF moyenne plus lente et leurs sites de DF les plus élevées se situaient au pourtour des VP. A l'opposé, les patients en FA persistante présentaient une DF moyenne plus rapide, avec des zones de DF élevées situées le plus souvent dans le tissu atrial hors des VP. L'ablation au niveau des sites de DF les plus élevées résultait en un ralentissement du cycle moyen de la FA ou au retour en rythme sinusal, confirmant leur importance dans le maintien de l'arythmie.

Lin et al ont démontré que la zone de DF élevée n'était pas obligatoirement située près des VP chez les patients en FA paroxystique, mais près de la veine thoracique la plus arythmogène, générant alors respectivement un gradient gauche-droite ou droite-gauche si les VP ou la VCS étaient les plus arythmogènes.[137] La relation entre DF et cycle moyen en FA a récemment été analysé par Elvan et al. qui ont rapporté une corrélation faible entre les deux analyses d'un même électrogramme.[138] Ainsi, les sites avec le plus court cycle d'activation et la DF la plus élevée n'étaient concordants que dans moins d'un tiers des cas. Cependant, Berenfeld et al ont analysé la même corrélation en comparant cette fois-ci le cycle moyen et la DF des électrogrammes en FA avec la DF obtenue par optical mapping sur des cœurs de mouton.[139] Les auteurs ont ainsi démontré que les DF des signaux uni- ou bipolaires étaient bien plus corrélés aux DF enregistrées par optical mapping qu'au cycle moyen d'activation des électrogrammes (EGM). Ainsi, les zones de DF élevées semblent être de meilleures cibles pour l'ablation que celles avec un cycle moyen court.

1. Hypothèse de travail

Les études sur la FA persistante chez l'animal[140] et chez l'homme[73] ont attribué l'accélération de l'activation atriale au remodelage électrophysiologique et structurel. Cependant, ces travaux étaient limités par le fait qu'ils n'ont étudié que des périodes de FA de durée relativement courte[140] ou inconnue[141, 142] de FA persistante. De plus, aucune

information n'était apportée quant à la distribution spatiale de la fréquence d'activation atriale. Afin de répondre à ces questions, nous avons étudié l'évolution de la DF et du gradient gauche-droite en FA chez des moutons implantés d'un stimulateur cardiaque permettant de générer une FA induite par stimulation atriale à haute fréquence.[143]

2. Méthodes

Huit moutons âgés de 6 à 8 mois ont utilisés dans cette étude. L'anesthésie était induite par du propofol (4-6 mg/kg IV) et maintenue par de l'isoflurane. Un stimulateur cardiaque simple chambre était implanté en sous-cutané dans la région cervicale, relié à une sonde introduite par la veine jugulaire externe, et vissée dans l'auricule droit. Par ailleurs, un enregistreur d'évènements (Reveal ®, Medtronic) était implanté en latero-sternal gauche afin de monitorer l'apparition des épisodes de FA. Dix jours après l'implantation, le protocole de stimulation était débuté, consistant en une alternance entre 30 secondes de stimulation à 20Hz suivi d'une période de 10 secondes de blanking.

Trois signaux étaient enregistrés de façon hebdomadaire: 1) EGM endocavitaire unipolaire (boitier-dipôle distal) atrial droit ; 2) EGM sous-cutané obtenu via l'enregistreur d'évènements, positionné en regard de l'OG et permettant d'obtenir un enregistrement far-field du signal atrial gauche, exporté sous forme d'un fichier PDF ; 3) dérivation I de l'électrocardiogramme (ECG) de surface.

Les signaux étaient analysés via Matlab (MathWorks, Natick, MA) afin d'en déterminer la DF_{max}. L'EGM extrait de l'enregistreur d'évènements était composé de l'activité ventriculaire (complexe QRS) sur un fond de FA. Afin d'extraire et d'analyser l'activité atriale en elle-même, les complexes QRS étaient soustraits en utilisant une technique d'analyse en composantes principales.

Afin de générer un modèle de FA similaire à ce qui est constaté chez l'homme, la stimulation était interrompue après une période comprise entre 9 et 24 semaines. La FA était définie comme persistante si l'absence de retour en rythme sinusal était constatée après 7 jours sans stimulation. Si la FA s'interrompait spontanément moins de 7 jours après l'arrêt définitif du protocole de stimulation, elle était considérée comme étant paroxystique.

Parmi les huit animaux, cinq ont été suivis pendant 20-24 semaines, période après laquelle ils étaient sacrifiés et leur cœurs explantés afin d'analyser la dynamique des ondes fibrillatoires par cartographie optique comme décrit précédemment.[132]

Par ailleurs, une analyse de la fibrose atriale était effectuée par coloration au trichrome de Masson et au Rouge Sirius.

3. Résultats

La détection du 1er épisode de FA après l'initiation du protocole de stimulation variait considérablement selon les animaux, entre 5 et 60 jours (médiane 14 jours, Figure 9).

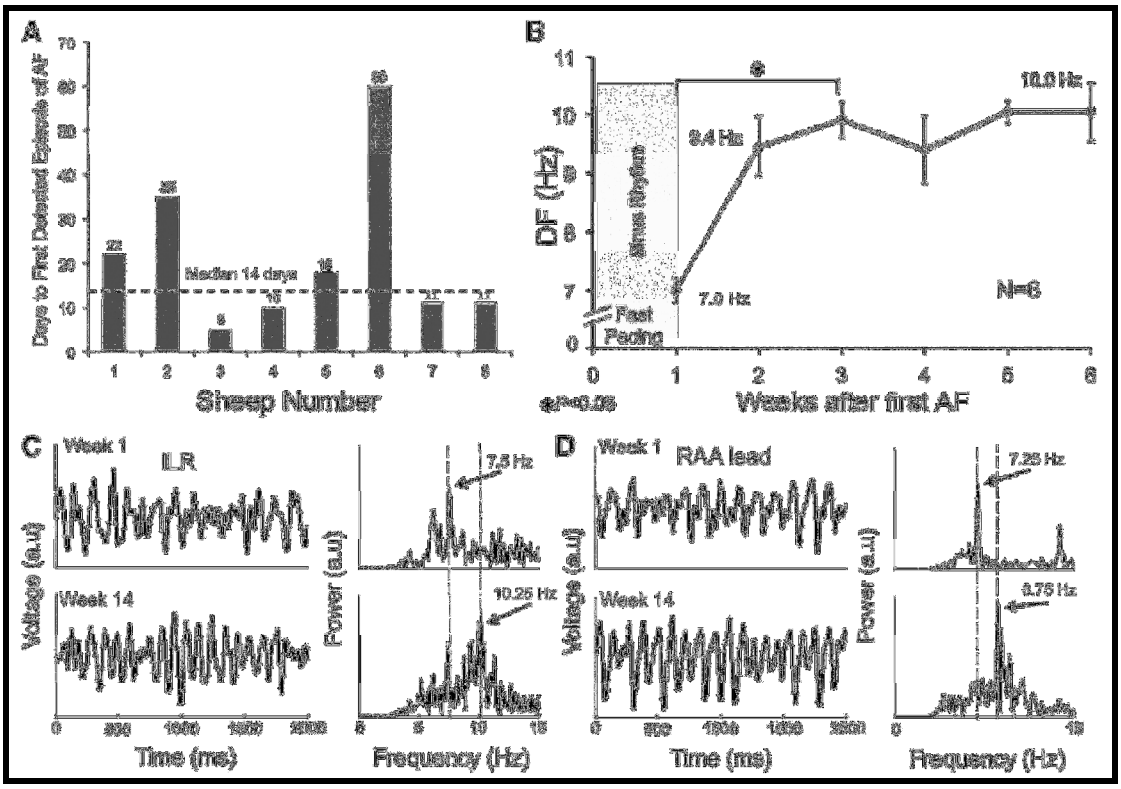

Figure 9 : Initiation de la FA et accélération de la DF. A. Nombre de jours nécessaires à l'apparition du 1er épisode de FA après initiation du protocole de stimulation. B. Evolution de la DF obtenue à partir des tracés du Reveal® démontrant une augmentation de la DF_{max} pendant les 2 premières semaines de stimulation. C. Tracés représentatifs obtenus à partir du Reveal® après soustraction du QRS et filtration du signal. La DF_{max} augmente de 7.5 à 10.25Hz de la 1ère à la 14éme semaine. D. Tracés représentatifs obtenus à partir du stimulateur cardiaque (auricule droit) après filtration du signal pendant la même période. La DF_{max} augmente de 7.25 à 8.75Hz de la 1ère à la 14éme semaine.

Sur les 8 animaux implantés, le 1er épisode a pu être enregistré chez 6 d'entre eux. L'analyse de la DF obtenue par le Reveal® a démontré une augmentation significative de la DF pendant les 2 premières semaines d'évolution de la FA de 7.0±0.2 à 9.9±0.3 Hz ($p<0.05$), période après laquelle la DF restait stable tout au long du suivi. Des tracés représentatifs des signaux obtenus via l'enregistreur d'évènements et la sonde atriale droite après 1 et 14 semaines de FA sont montrés sur la Figure XC et XD.

Une fois la FA initiée, les DF obtenues via l'enregistreur d'évènements et la sonde atriale droite étaient extraites et analysées de façon hebdomadaire. De façon constante, un gradient de DF gauche-droite était retrouvé tout au long du suivi (10.6±0.08 *vs.* 9.3±0.1 Hz ; $p<0.0001$; figure 10).

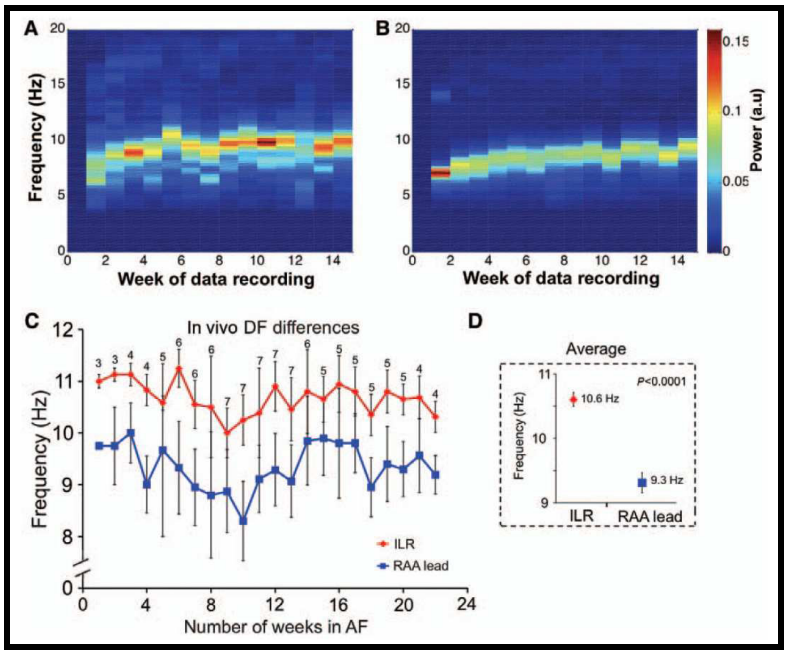

Figure 10 : Gradients de DF gauche-droite *in-vivo*. A et B. Spectrogrammes générés chez l'un des animaux en FA d'après les signaux de l'enregistreur d'évènements (panel A) et la sonde atriale droite (panel B). Le spectre de puissance moyen augmente progressivement au cours de l'évolution de l'arythmie. C et D. Les DF obtenues via l'enregistreur d'évènements, correspondant au signal atrial gauche (rouge) sont supérieures à celles obtenues via la sonde atriale droite (bleu).

Cinq moutons ont été suivis pendant 20-24 semaines de stimulation atriale à haute fréquence. A la fin de ce suivi, les cœurs étaient explantés et connectés à un système de perfusion de type Langendorff. Après mise en place d'une pression intra-atriale physiologique (# 5cm H_20), une cartographie optique de l'épicarde de la paroi latérale (LAA) et de l'endocarde de la paroi postérieure de l'OG (PLA) a été effectuée, comme précédemment décrit.[132] Des acquisitions de 5 secondes toutes les 2 minutes pendant 50 minutes ont été réalisées. L'évolution de la DF_{max} de la paroi latérale de l'OG (PLA) et de l'OD (RAA) est présentée sur la Figure 11A. Des fréquences élevées ont constamment été retrouvées dans le PLA, significativement supérieures à celles de la paroi latérale de l'OG et de l'OD (Figure 11B). Par ailleurs, un gradient *in-vivo* - *in-vitro* dans les fréquences de l'OG était mis en évidence (10.6±0.1 à 9.1±0.2 Hz ; $p<0.0001$), probablement secondaire à la dénervation autonomique post-explantation.

Afin de mieux caractériser l'activation de la paroi postérieure de l'OG, nous avons étudié les acquisitions de phase afin de comparer le nombre d'ondes entrant/sortant de la région cartographiée. La Figure 12A montre que le nombre d'ondes émanant de l'endocarde postérieur de l'OG dépasse de façon significative celles qui y pénètrent (6.6±0.2 *vs.* 2.9±0.2, $p<0.05$).

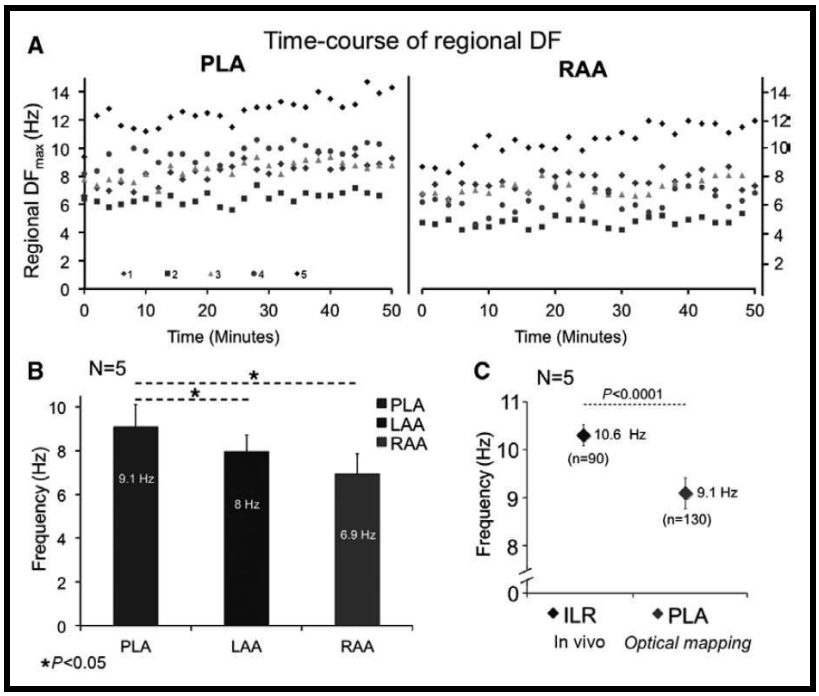

Figure 11 : Analyse des DF *in-vitro*. A Evolution de la DF au cours des 50 min d'optical mapping chez 5 animaux. De façon consistante, la DF_{max} était enregistrée dans la paroi postérieure de l'oreillette gauche (PLA). B. Un gradient significatif PLA>LAA>RAA était retrouvé. C. Différence de DF_{max} atrial gauche enregistrée *in-vivo* et *in-vitro*.

Deux images représentatives sont présentées dans la figure 12B. Par ailleurs, le type d'activation a été analysé en dénombrant le nombre total de rotations et de décharges focales par cm² : un nombre significativement supérieur d'activations focales a été retrouvé dans l'endocarde postérieur de l'OG (Figure 12C). L'étude précise de l'activation des parois de l'OG cartographiées (épicarde latéral et endocarde postérieur) a par ailleurs mis en évidence que la DF_{max} était localisée là où les rotors se situaient, tantôt sur l'épicarde ou l'endocarde (figure 12D).

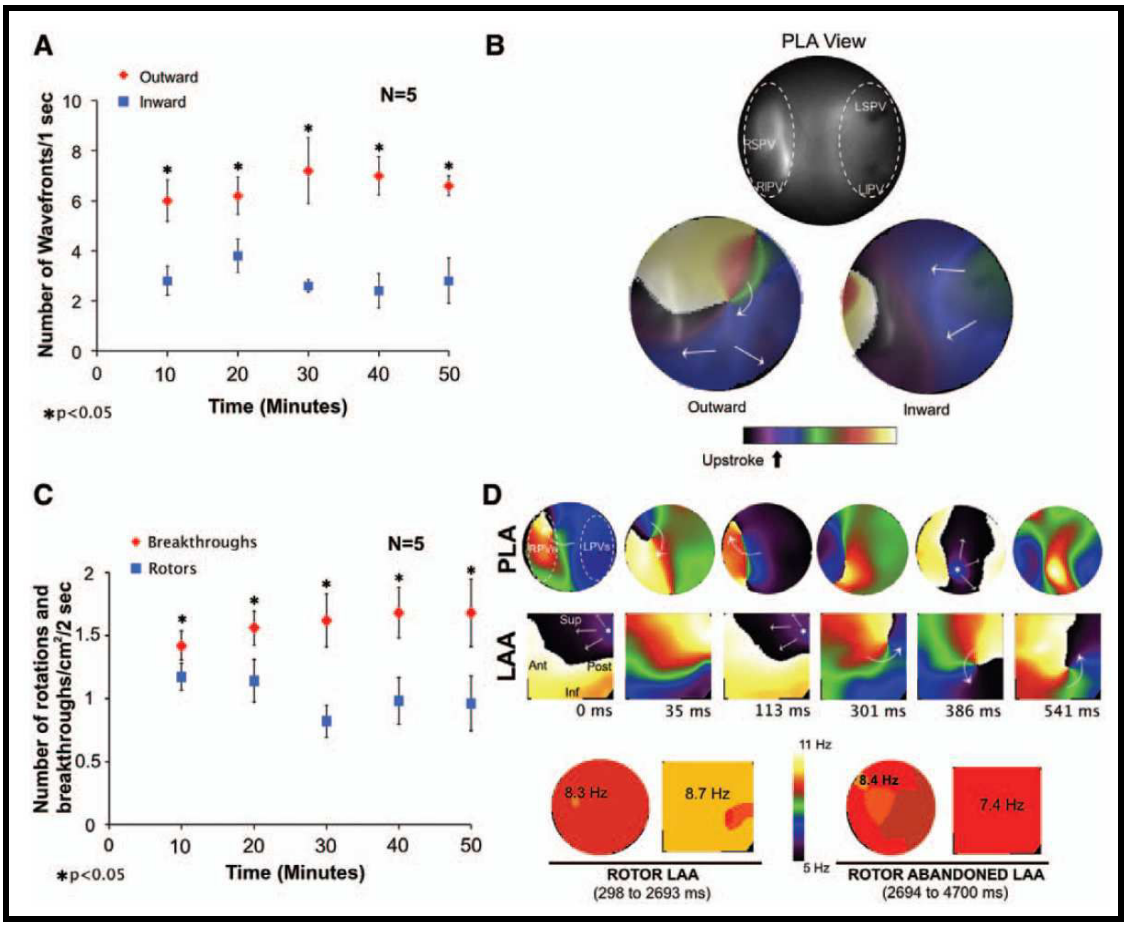

Figure 12 : Activation de l'endocarde postérieur en FA dans les cœurs de moutons isolés. A. Graphique démontrant que le nombre d'ondes émanant de la paroi postérieur de l'OG excède celui des ondes entrantes. B. Haut : Endocarde de la paroi postérieur de l'OG visualisé lors des expériences de cartographie optique ; bas : arrêts sur images des acquisitions de phase montrant des ondes émanant (à gauche) et entrant (à droite) vers la paroi postérieure de l'OG. C. Le nombre de décharges focales excède le nombre de rotations/cm². D. Haut : arrêts sur images d'acquisitions de phase montrant un rotor apparaissant dans le champ d'enregistrement de la paroi latérale de l'OG. Le type d'activation initialement de type focale (0-113ms) se transforme en un rotor mobile (301-541ms). Bas : La DF_{max} est située dans la paroi latérale de l'OG lorsque le rotor s'y trouve, puis dans l'endocarde postérieur lorsque le rotor quitte l'épicarde latéral.

Dans ce modèle, une alternance de 30 secondes de stimulation à haute fréquence et de 10 secondes de blanking a été utilisée pour générer de la FA chez le mouton. Le protocole de stimulation était stoppé une semaine avant le sacrifice des animaux afin de s'assurer du caractère persistant de la FA (par définition : persistance de la FA pendant 7 jours sans retour en rythme sinusal, et sans intervention extérieure). De façon étonnante, sur les 7 animaux menés au terme de l'expérimentation, 2 sont revenus spontanément en rythme sinusal (Figure 13). La DF_{max} en FA avant arrêt du protocole de stimulation était similaire chez les animaux restant en FA et ceux étant retourné en rythme sinusal (respectivement 10.0±0.8 *vs* 10.0±2.1, p=0.67). Ceci sous-entend qu'une DF élevée (probable reflet du remodelage électrophysiologique) ne permet pas isolément de maintenir la FA et que d'autres paramètres entrent en compte dans le maintien de l'arythmie. Par ailleurs, chez les 2 animaux étant

revenus en rythme sinusal, nous avons relancé le protocole de stimulation et observé que la DF_{max} du nouvel épisode induit était identique à celle du 1er épisode de FA enregistré 6 mois auparavant (Figure 12C), phénomène probablement en rapport avec la perte du remodelage électrophysiologique secondaire à l'arythmie (remodelage inverse).

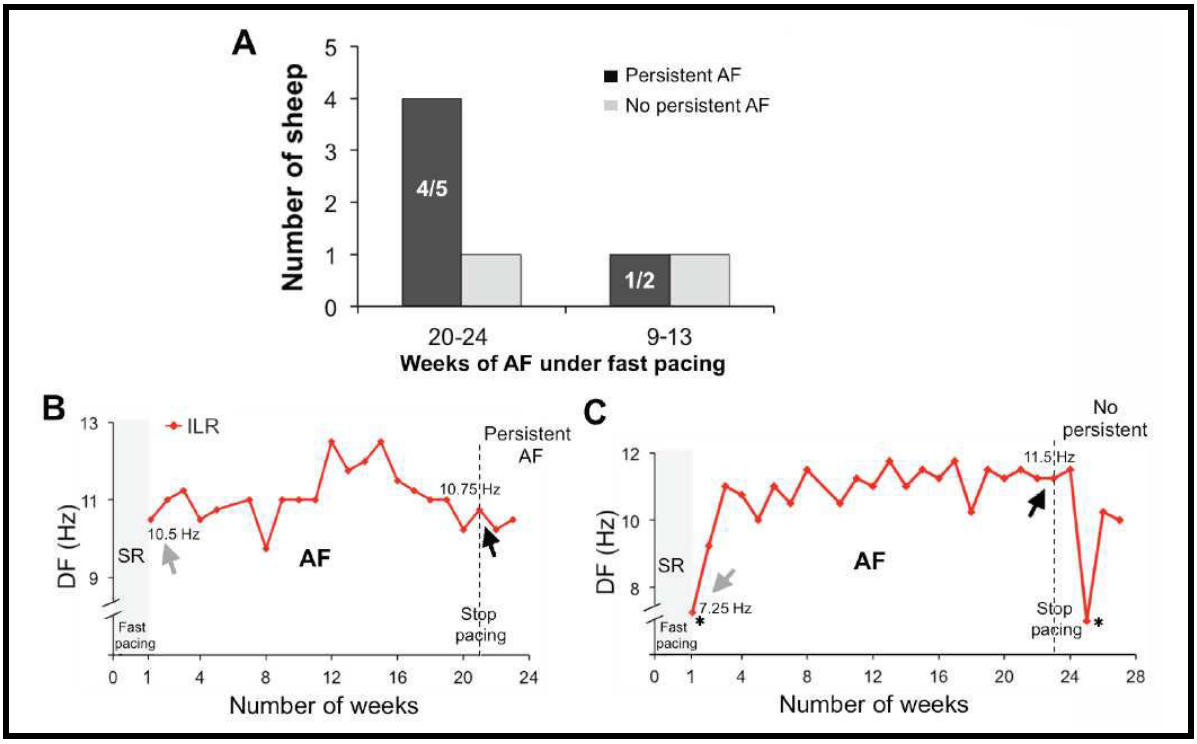

Figure 12 : Persistance de la FA après l'arrêt de la stimulation à haute fréquence. A. Sur l'ensemble des animaux, 2 sont revenus en rythme sinusal dans la semaine suivant l'arrêt du protocole de stimulation. B et C. Evolution de la DF_{max} chez 2 animaux représentatifs. En B, la FA s'est maintenue malgré l'arrêt de la stimulation (=FA persistante), alors qu'en C, on observe un retour en rythme sinusal après 3 jours d'arrêt de la stimulation. Après réinduction de la FA, on observe que la DF_{max} est similaire à celle du 1er épisode (astérisque). Les flèches grises et noires indiquent respectivement la DF_{max} du 1er épisode de FA enregistré et de celui avant l'arrêt du protocole de stimulation.

Afin de connaitre l'effet de l'arythmie en termes de remodelage structurel, nous avons analysé l'aire de la paroi postérieure de l'OG et le pourcentage de fibrose chez les animaux en FA et les animaux contrôles. Comme le montre la Figure 13A et B, une dilatation atriale significative était mise en évidence chez les moutons en FA (7.48±0.25 *vs.* 5.96±0.29 cm², p=0.006). Par ailleurs, aucune augmentation significative du pourcentage de fibrose n'était retrouvée dans l'OD, l'OG ou la paroi postérieure. Ceci s'explique probablement par le fait qu'il s'agit d'un modèle de « FA sur cœur sain », aucun phénomène de tachycardiomyopathie n'étant mis en évidence (fonction ventriculaire gauche normale chez l'ensemble des animaux en FA).

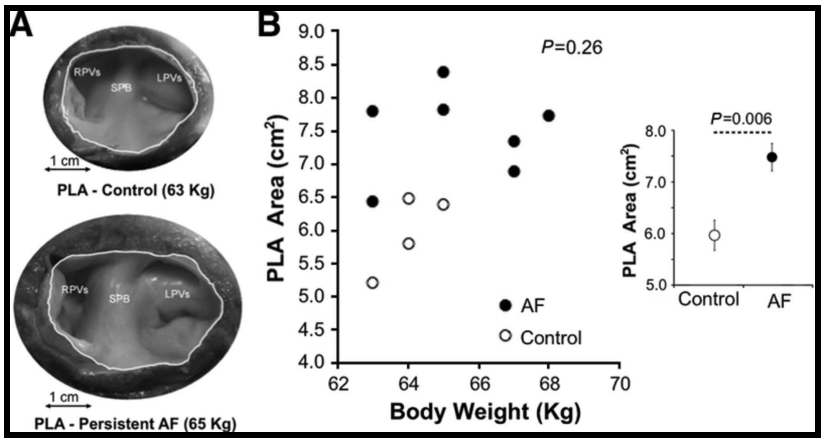

Figure 13 : Dilatation atriale secondaire à la FA. A. Images macroscopiques de l'endocarde de la paroi postérieure de l'OG des moutons en FA (bas) et d'animaux contrôles appareillés au poids (haut). B. Une dilatation atriale significative était retrouvée chez les moutons en FA, comparée au groupe contrôle.

4. Discussion

Ce modèle de FA induit par stimulation atriale à haute fréquence nous a permis de démontrer que la DF augmente pendant les 2 premières semaines de FA, probablement en conséquence du remodelage électrophysiologique (modifications des courants ioniques menant au raccourcissement du PA). De plus, nous avons retrouvé un gradient OG-OD tout au long du suivi des animaux, gradient également retrouvé *ex-vivo* et mis sur le compte de la présence de rotors et d'une propagation émanent préférentiellement de la paroi postérieure de l'OG. Atienza et al ont démontré qu'un gradient de DF entre l'OG et l'OD existe chez 84% des patients en FA persistante.[144] Dans cette étude, les auteurs ont également mis en évidence un taux élevé de maintien en rythme sinusal chez les patients en FA persistante lorsque l'ablation diminuait la DF_{max} dans l'OG et l'OD et abolissait le gradient OG-OD. Dans une population plus large de patients en FA persistante de longue durée, Hocini et al ont suivi l'évolution du cycle de la FA dans les 2 oreillettes lors d'une ablation par étapes (« stepwise approach », isolation veineuse pulmonaire puis en cas de persistance de la FA : ablation des CFAE, ligne du toit de l'OG, isthme mitral ; en cas de persistance de la FA avec cycle d'activation OD>OG : ablation dans l'OD).[145] Chez la plupart des patients, une augmentation progressive du cycle de la FA était observée parallèlement dans l'OG et l'OD, jusqu'au retour en rythme sinusal. Au contraire, chez près de 20% des patients, le cycle de la FA enregistré dans l'OD ne montrait pas de prolongation lors de l'ablation dans l'OG, créant alors un gradient de fréquence droit-gauche. Ce sous-groupe de patient avait une histoire de FA plus longue et des oreillettes droites plus dilatées. L'ablation ciblée de potentiels fractionnés dans l'OD a permis un retour en rythme sinusal chez près de la moitié d'entre eux.

Le modèle ovin que nous avons crée peut probablement être mis en parallèle avec la FA persistante clinique, à ses débuts, où un gradient de fréquence OG-OD est toujours présent et l'activité fibrillatoire maintenant la FA située dans l'endocarde postérieur de l'OG. A ce stade de l'arythmie, le remodelage électrophysiologique est survenu, alors que le remodelage strucurel n'est pas encore maximal, comme en témoigne l'absence d'augmentation significative du pourcentage de fibrose chez les moutons. Cependant, bien qu'aucune fibrose significative n'ait été retrouvée, nous avons mis en évidence une dilatation atriale pouvant expliquer que les rotors aient une propension moindre à rencontrer un obstacle anatomique et

à disparaitre, rendant alors l'arythmie stable dans le temps. Ceci n'explique cependant pas pourquoi nous avons observé un retour en rythme sinusal chez 2 animaux après arrêt du protocole de stimulation.

Les réels déterminants ioniques et cellulaires à l'origine du maintien de la FA et de sa progression vers des formes plus soutenues sont pour le moment inconnus. Leur étude permettrait de comprendre pourquoi certains animaux n'ont pas progressé vers la FA persistante et sont revenus en rythme sinusal malgré la persistance de la stimulation atriale pendant 6 mois. C'est pour répondre à cette question que nous avons envisagé un nouveau travail permettant d'étudier spécifiquement la période de transition de la FA de sa forme paroxystique à sa forme persistante.

C. Conclusion

La FA résulte d'une interaction entre une gâchette (« triggers » souvent en lien avec les VP), le substrat et le système nerveux autonome, associés à des degrés différents selon l'ancienneté de l'arythmie et l'existence d'une éventuelle cardiopathie sous-jacente. Notre compréhension des mécanismes physiopathologiques de la FA s'est grandement améliorée lors des 20 dernières années, les études animales et celles menées chez l'homme ayant permis de reconnaitre les sources de l'arythmie et d'en comprendre le remodelage atrial associé.

Des études complémentaires seront nécessaires afin d'avoir une approche translationnelle, à savoir comment générer des approches thérapeutiques effectives (anti-arythmiques, « upstream therapies », thérapies génique ou cellulaire, nouvelles cibles d'ablation) à partir des connaissances mécanistiques apportées par la recherche fondamentale.

Circulation
Arrhythmia and Electrophysiology

American Heart Association.

Long-Term Frequency Gradients During Persistent Atrial Fibrillation in Sheep Are Associated With Stable Sources in the Left Atrium

David Filgueiras-Rama, Nicholas F. Price, Raphael P. Martins, Masatoshi Yamazaki, Uma Mahesh R. Avula, Kuljeet Kaur, Jérôme Kalifa, Steven R. Ennis, Elliot Hwang, Vijay Devabhaktuni, Jose Jalife and Omer Berenfeld

Circ Arrhythm Electrophysiol. 2012;5:1160-1167; originally published online October 10, 2012;
doi: 10.1161/CIRCEP.111.969519
Circulation: Arrhythmia and Electrophysiology is published by the American Heart Association, 7272 Greenville Avenue, Dallas, TX 75231

Print ISSN: 1941-3149. Online ISSN: 1941-3084

Long-Term Frequency Gradients During Persistent Atrial Fibrillation in Sheep Are Associated With Stable Sources in the Left Atrium

David Filgueiras-Rama, MD*; Nicholas F. Price, MSc*; Raphael P. Martins, MD; Masatoshi Yamazaki, MD; Uma Mahesh R. Avula, MD; Kuljeet Kaur, PhD; Jérôme Kalifa, MD; Steven R. Ennis, PhD; Elliot Hwang, BSE; Vijay Devabhaktuni, PhD; Jose Jalife, MD; Omer Berenfeld, PhD

Background—Dominant frequencies (DFs) of activation are higher in the atria of patients with persistent than paroxysmal atrial fibrillation (AF), and left atrial (LA)-to-right atrial (RA) DF gradients have been identified in both. However, whether such gradients are maintained as long-term persistent AF is established remains unexplored. We aimed at determining in vivo the time course in atrial DF values from paroxysmal to persistent AF in sheep and testing the hypothesis that an LA-to-RA DF difference is associated with LA drivers in persistent AF.

Methods and Results—AF was induced using RA tachypacing (n=8). Electrograms were obtained weekly from an RA lead and an implantable loop recorder implanted near the LA. DFs were determined for 5-second-long electrograms (QRST subtracted) during AF in vivo and in ex vivo optical mapping. Underlying structural changes were compared with weight-matched controls (n=4). After the first AF episode, DF increased gradually during a 2-week period (7±0.21 to 9.92±0.31 Hz; n=6; $P<0.05$). During 9 to 24 weeks of AF, the DF values on the implantable loop recorder were higher than the RA (10.6±0.08 versus 9.3±0.1 Hz, respectively; n=7; $P<0.0001$). Subsequent optical mapping confirmed a DF gradient from posterior LA-to-RA (9.1±1.0 to 6.9±0.9 Hz; $P<0.05$) and demonstrated patterns of activation compatible with drifting rotors in the posterior LA. Persistent AF sheep showed significant enlargement of the posterior LA compared with controls.

Conclusions—In the sheep, transition from paroxysmal to persistent AF shows continuous LA-to-RA DF gradients in vivo together with enlargement of the posterior LA, which harbors the highest frequency domains and patterns of activation compatible with drifting rotors. (***Circ Arrhythm Electrophysiol.* 2012;5:1160-1167.**)

Key Words: atrial fibrillation ■ electrophysiology mapping ■ remodeling ■ dominant frequency ■ rotors

Atrial fibrillation (AF) is the most common sustained arrhythmia in clinical practice.[1] When the arrhythmia lasts continuously for >7 days, it is designated as persistent. Spontaneous, pharmacological, or ablative resumption of sinus rhythm becomes infrequent as the arrhythmia lasts >1 year, termed permanent AF.[2]

Clinical Perspective on p 1167

Experimental studies using high-resolution optical mapping have shown that acute AF often depends on discrete drivers or rotors generating relatively periodic and organized activity in the form of spiral waves that spin at high frequency around a functional core.[3] The waves emanating from such rotors interact with anatomic and functional obstacles in their path, giving rise to fibrillatory conduction and establishing a spatially distributed hierarchical organization in the local dominant frequencies (DFs) of atria.[4] Thus, spectral analysis in animal[5] and human[5] paroxysmal AF, demonstrating maximal DF (DF_{max}) at or near the pulmonary veins and gradients toward the left and right atria (LA and RA), also demonstrated a colocalization of sources and DF_{max} sites. The DF_{max} has been suggested to provide both mechanistic and ablative guidance; the presence of an LA-to-RA DF_{max} gradient and its eradication by radiofrequency ablation predict long-term freedom from both paroxysmal and persistent AF.[6]

The atria of persistent AF patients have a more widespread distribution of DF_{max}, mainly outside the pulmonary veins region, and higher DF_{max} values than paroxysmal AF patients.[6,7] Studies on persistent AF have attributed the acceleration of the atrial activation rate to atrial remodeling in both animals[8] and humans.[9]

Received December 1, 2011; accepted September 3, 2012.

From the Center for Arrhythmia Research, Department of Internal Medicine (D.F.-R., N.F.P., R.P.M., M.Y., U.M.R.A., K.K., J.K., S.R.E., E.H., J.J., O.B.), Department of Molecular and Integrative Physiology (J.J.), and Department of Biomedical Engineering (O.B.), University of Michigan, Ann Arbor, MI; and Department of Electrical Engineering and Computer Science, College of Engineering, University of Toledo, Toledo, OH (N.F.P., V.D.).

*These authors contributed equally to this work.

The online-only Data Supplement is available at http://circep.ahajournals.org/lookup/suppl/doi:10.1161/CIRCEP.111.969519/-/DC1.

Correspondence to Omer Berenfeld, PhD, Center for Arrhythmia Research, University of Michigan, 2800 Plymouth Rd, Ann Arbor, MI 48109. E-mail oberen@med.umich.edu

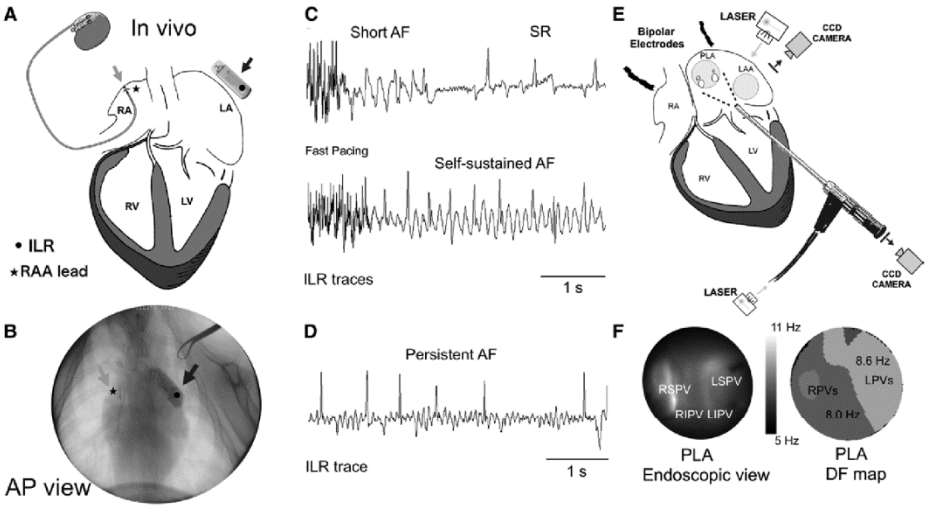

Figure 1. In vivo and ex vivo model, protocols, and mapping experiments. **A**, A diagram of a pacemaker with the lead in the right atrial appendage (RAA; **light gray arrow**) and implantable loop recorder (ILR; **dark gray arrow**) close to the left atrium (LA). **B**, Fluoroscopic view of the lead in the RAA (**light gray arrow**) and the ILR next to the LA (**dark gray arrow**). **C**, ILR traces at different stages of the persistent atrial fibrillation (AF) protocol. Rapid pacing appears at the beginning of the trace. **D**, A 6-second-long AF episode during AF that persisted for >7 days after turning off the fast pacing. **E**, Ex vivo epicardial and endocardial mapping setup includes synchronized dual charge-coupled device (CCD) cameras, as well as bipolar electrodes placed in the right atrium and the roof of the LA. Bipolar signals are also obtained from the pulmonary veins. **F**, Endoscopic view of the posterior LA (PLA; **left**) and dominant frequency (DF) map during AF. AP indicates anteroposterior.

However, those studies were somehow limited by the fact that they addressed persistent AF of relatively short[8] or unconfirmed duration.[10,11] In addition, no information was provided on the spatial distribution of the atrial activation rates. Here, we aimed at filling those gaps by studying in vivo the time course of the changes in DF values and the evolution of the left-to-right DF dispersion during the transition from paroxysmal to persistent AF.

Using a chronic RA tachypacing model of persistent AF in the sheep, along with continuous cardiac rhythm monitoring by dual implantable devices, we tested the hypothesis that in vivo DF values during AF progressively increase while preserving in the long-term a DF difference between LA and RA. Mapping of the atria and subsequent structural analyses ex vivo confirmed the presence of DF gradients from posterior LA (PLA) to RA, together with patterns of activation consistent with the contention that drifting rotors in an enlarged PLA may underlie AF dynamics in this model.

Methods

Induction of Persistent AF

All procedures were approved by the University of Michigan Committee on Use and Care of Animals and complied with National Institutes of Health guidelines. Eight 6- to 8- month-old sheep (≈40 kg) were used for implantation. Anesthesia was induced using propofol (4–6 mg/kg IV) and maintained by isoflurane inhalation. A bipolar lead was inserted into the RA appendage (RAA) through the left external jugular vein. The proximal end of the lead was screwed to the sterile pacemaker (Victory XLDR; St Jude Medical. Sylmar, CA), which was sheltered in a subcutaneous pouch. Thereafter, an implantable loop recorder (ILR, Reveal XT; Medtronic, Inc, Minneapolis, MN) was placed subcutaneously on the left side of the sternum in close proximity to LA (Figure 1A and 1B). Based on fluoroscopy images, a distance of ≈2 cm between the ILR and the LA free wall was confirmed, and it was guaranteed that it was opposing the RAA lead location and recorded primarily LA activity. We obtained left ventricular ejection fraction measurements at implantation and before euthanasia by transthoracic echocardiography (Sonos 5500; Hewlett-Packard, Palo Alto, CA) using a long-axis parasternal view (online-only Data Supplement Figure V).

After 10 days of recovery, the pacemaker was programmed to induce AF by fast atrial pacing with an algorithm consisting of 30-second pacing at 20 Hz followed by 10-second sensing. The ILR was programmed to identify AF episodes lasting >6 seconds during the 10-second sensing. The pacemaker and ILR were interrogated weekly during the study period, including automatic registration of detected AF events by the ILR when available. The duration in weeks until the first self-sustained AF episode (>6 seconds in duration; Figure 1C) was quantified for each animal, after which weekly monitoring confirmed the maintenance of AF.

To generate a clinically relevant persistent AF model, we stopped the pacing algorithm at the end of the follow-up period between 9 and 24 weeks. Persistent AF was defined based on the criteria used for human AF as those episodes lasting >7 days upon switching off the fast pacing program (Figure 1D). Episodes lasting ≤7 days were considered paroxysmal AF.[2]

In Vivo Determination of DF

Data Acquisition

Two electrograms were simultaneously obtained during the in vivo protocol: (1) RAA lead tip electrograms with a case reference were exported at a sampling rate of 512 Hz, and (2) ILR-recorded single-lead electrograms were exported as a vector PDF file, which was magnified 1200% and then digitized in the Matlab (MathWorks, Natick MA) environment. The digitized signal was then superimposed on the original electrogram image for visual inspection to ensure quality data. The time scale (effective sample rate acquisition) was calculated

for each trace individually based on the average distance between gridline centers in the vector PDF file.

Data Processing

Recordings obtained by the ILR, whose canister was external to the LA, contained a mixture of atrial and ventricular activity. To analyze the atrial activity, the ventricular activity (dubbed QRST) was subtracted from the original recordings. To enhance confidence in the QRST removal, 2 single-lead QRST removal algorithms were used: (1) a principal component analysis–based AF estimation[12] and (2) an adaptive singular value QRST cancellation.[13] After QRST removal, a bias-free bidirectional Butterworth band-pass filter (4–35 Hz) was applied to each trace. The fast Fourier transform was then used to obtain the DF in 5-second-long signals from the ILR and RAA electrograms. Finally, DF values from RAA and ILR electrograms were compared to identify in vivo differences between the 2 regions (see online-only Data Supplement Methods and online-only Data Supplement Figures I–IV for details).

Evaluation of Ventricular Activity Removal

To further validate the methods for QRST removal, performance was evaluated against a set of synthesized time-series test cases constructed with a known reference atrial and ventricular activity that was obtained from the animals studied. Each test case was constructed by adding a selected set of QRST complexes to a 5-second-long episode of atrial-only activity extracted and spliced manually from the original electrograms. The effective heart rate was set for the average heart rate of the sheep during the study (≈100 beats per minute). Test cases were grouped according to the morphological variability between QRST complexes as measured by the Pearson correlation index.

Mapping of Isolated Hearts

Five sheep (≈66 kg) underwent 20 to 24 weeks of continuous tachypacing-induced AF. Hearts were removed via thoracotomy and connected to a Langendorff-perfusion system with recirculating oxygenated (95% O_2, 5% CO_2) Tyrode solution.

The experiments were performed under constant intra-atrial pressure to subthreshold AF-inducing level of 5 cm H_2O, resembling the diastolic LA pressure.[14] Tetrapolar electrode catheters were placed in each of the pulmonary veins. Two additional custom-made bipolar electrodes were placed on the top of the RAA and LA appendage (LAA; Figure 1E). Epicardial and endocardial optical mapping (Di-4-ANEPPS 5–10 mg/mL) of the LAA and PLA, respectively, were performed simultaneously as described elsewhere (see Figure 1E and 1F and online-only Data Supplement Methods).[15]

AF and DF Analysis in Isolated Hearts

Spontaneous AF in the Langendorff-perfused hearts was allowed to continue uninterruptedly for 50 minutes. Five-second-long optical movies were acquired at 2-minute intervals. Acquisition of the optical movies triggered simultaneous acquisition of the bipolar recordings.

DF maps were obtained from each optical movie after applying a fast Fourier transform to the fluorescence signal time series recorded at each pixel (Figure 1F). Fast Fourier transform was also applied to the 5-second bipolar signals after 4- to 35-Hz band-pass filters. In the PLA, waves were tracked for outward and inward directionality at 10-minutes intervals using phase movies constructed by means of Hilbert transformation.[16] Patterns of activation were classified as rotors and breakthroughs as described elsewhere.[15]

Structural Changes in Persistent AF

Hearts preserved in 10% neutral buffered formalin from AF animals (n=7) and body weight–matched controls (n=4) were used to quantify the area of the PLA and to determine changes in interstitial fibrosis as described in the online-only Data Supplement Methods.

Statistical Analyses

Data are reported as mean±SEM except where noted. Normal distribution of variables was assessed with Shapiro-Wilk test. A mixed regression model has been applied to multiple group analyses and

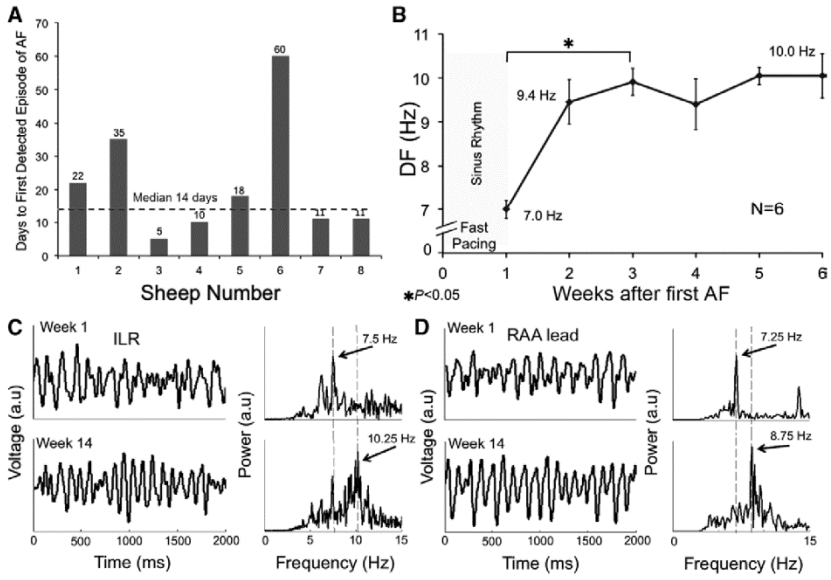

Figure 2. Heterogeneous onset of atrial fibrillation (AF) and its acceleration. **A**, Number of weeks of tachypacing before any AF episode is detected in sheep sorted by sequential implantation order. **B**, Dominant frequency (DF) values from the implantable loop recorder (ILR) traces show an increase in DF during a 2-week period after the first tachypacing-induced AF episode. **C**, AF traces and corresponding power spectra obtained from the ILR after QRST removal and filtering. DF increases from 7.5 to 10.25 Hz from week 1 to week 14, respectively. **D**, Right atrial appendage (RAA) lead traces and corresponding power spectra. DF increases from 7.25 to 8.75 Hz during the same period.

repeated measurements data. The Mann-Whitney *U* test was used to compare the PLA area in AF animals with weight-matched controls and to assess differences in the degree of atrial fibrosis. Post hoc comparisons were corrected by Bonferroni test when appropriate. $P<0.05$ was considered statistically significant.

Results

DF Increases After the First AF Episode

Traces stored in the memory of the ILR were carefully analyzed during weekly interrogations to search for the presence of AF and its DF. As shown in Figure 2A, the time for detection of the first AF episode varied considerably between 5 and 60 days (median 14; normality by Shapiro-Wilk test; $P=0.05$) of tachypacing. Using the ILR AF detection ability, we identified first-time self-sustained AF in 6 episodes. In Figure 2B, we show a progressive increase in DF values from 7±0.21 to 9.9±0.31 Hz (n=6; $P<0.05$) during the first 2 weeks, after which the DF remained stable for the duration of the follow-up period. The first AF episode was considered as the zero reference point. Sample data from the ILR and RAA lead at week 1 and week 14 are shown in panels C and D. The principal component analysis method was used for QRST removal in the ILR signal based on best performance analysis over larger range of QRST variability (see Methods and online-only Data Supplement Figures VI and VII). After 14 weeks under tachypacing-induced AF, the power spectra showed an increase in DF in both ILR (7.5–10.25 Hz) and RAA lead traces (7.25–8.75 Hz).

In Vivo Long-Term Left-to-Right DF Differences

Once AF was detected for the first time, DF values obtained from the ILR and the RAA lead were determined weekly and analyzed. One sheep with a 9-week follow-up was excluded, because only traces from the ILR were available. The DF value for each week and animal was determined as the mode DF (the most commonly occurring) in a median of 5 ILR (range 2–8) and 34 RAA lead (range 3–327) episodes of 5-second-long signal each. In Figure 3A and 3B, the spectrograms obtained from a sample animal show a progressive increase in the DF of the average power spectra (Welch method) of the traces for a given week, across the 14-week period. The ILR consistently recorded significantly higher overall average DFs compared with the RAA lead (9.4±0.21 versus 8.4±0.22 Hz, respectively; $P=0.002$). In Figure 3C, the cumulative plot for all the animals shows that the DF values in the ILR (red) remain 1.3±0.1 Hz higher than the RAA values (blue) for up to 22 weeks. Time and again, the ILR detected higher DF values than those detected by the RAA lead (10.6±0.08 versus 9.3±0.1 Hz, respectively; $P<0.0001$; Figure 3D) during the entire period of recording. The results suggest the presence of long-term persistent high-frequency sources in the LA.

Optically Mapped Isolated Hearts

Spontaneous AF was present in each of the explanted hearts (n=5) upon Langendorff perfusion. The time course of the DF_{max} on the PLA and RAA of each heart is shown in Figure 4A during a 50-minute period of spontaneous AF. Visual examination of the DF_{max} data reveals variations between hearts and between the PLA and RAA, with temporal fluctuations, but without a trend. In Figure 4B, we present the mean regional DF_{max} values during the entire 50 minutes of self-sustained AF for the PLA, LAA, and RAA, either optically mapped or electrically recorded. The global DF_{max} was consistently localized at the PLA with a statistically significant DF gradient from PLA to LAA and RAA (9.1±1.0 versus 7.9±0.7 and 6.9±0.9 Hz, respectively; $P<0.05$).

In addition, in vivo DF values from the ILR were compared with DF_{max} in the Langendorff-perfused hearts. Figure 4C shows

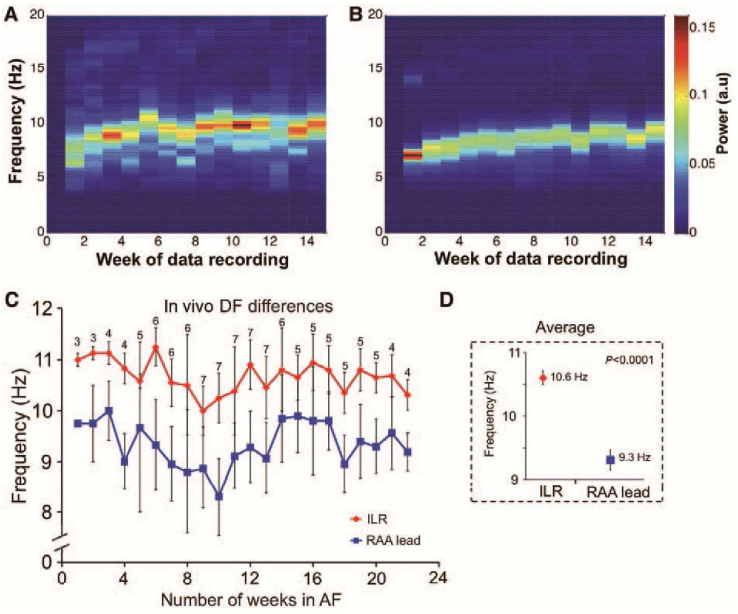

Figure 3. Left-to-right dominant frequency (DF) differences in vivo. **A** and **B**, Spectrograms generated from the implantable loop recorder (ILR) and right atrial appendage (RAA) lead signals, respectively, in a sample animal. The average power spectra (Welch method) of the traces for a given week show a progressive increase in DF (14 weeks are shown). **C** and **D**, DF values obtained from the ILR (red symbols) are significantly higher than those obtained from the RAA lead; 22 weeks of follow-up are shown.

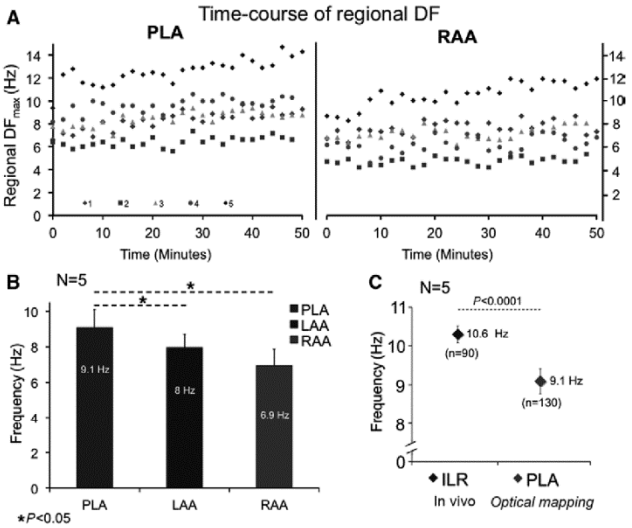

Figure 4. **A**, Time course of dominant frequency (DF) in 5 isolated hearts during a 50-minute period (each color represents 1 heart). The maximal DF (DF_{max}) was consistently localized in the posterior left atrium (PLA). **B**, Statistically significant DF gradient from PLA to left atrial appendage (LAA)-right atrial appendage (RAA). **C**, In vivo mean DF_{max} from the implantable loop recorder (ILR) was significantly different from mean DF_{max} at the PLA (10.6±0.1 vs 9.1±0.2 Hz; $P<0.0001$). N represents the number of animals and n the total number of measurements.

lower DF_{max} in the isolated hearts (9.1±0.2 versus 10.6±0.1 Hz; $P<0.0001$), which might be explained by autonomic denervation.

To further establish the patterns of activation underlying the DF_{max} values in the PLA, we used phase movies to compare the number of waves leaving versus entering the mapped PLA region (1-second-long segments). In Figure 5A, data from 5 hearts at 10-minute intervals demonstrate that the number of waves propagating outward consistently exceeded those propagating inward (6.6±0.2 versus 2.9±0.2, respectively; $P<0.05$). Panel B shows examples of outward (bottom left)/inward (bottom right) propagation from/toward the field of view on the PLA (top). In addition, rotors and breakthroughs in the PLA were analyzed by counting the total number of rotations/cm^2 (regardless of lifespan of rotors) and breakthroughs/cm^2 in 2-second-long segments. Figure 5C shows at 10-minute intervals a significantly higher number of breakthroughs/cm^2 compared with rotations/cm^2 in the mapped PLA.

Whether those breakthroughs are the surface expression of intramural reentrant activity or focal activity can be assessed by movies such as online-only Data Supplement Movie I and the snapshots of Figure 5D, in which a rotor with its filament perpendicular to the field of view drifts from the PLA toward the LAA. As soon as the rotor enters in the LAA field of view, the patterns of activation switch from breakthroughs to reentry and the drifting rotor becomes the main source driving the AF. Concomitant transition in the DF_{max} values from the PLA to the LAA when the rotor appears in the field of view of the LAA further confirms the essential role of rotors in this persistent AF model.

Structural Changes and the Persistence of AF

Using the clinical classification of persistent AF would require episodes to last >7 days without artificial intervention by the pacemaker.[2] However, the transition into such condition may vary considerably from one animal to another as was shown for AF induction (Figure 2A). Although all animals developed self-sustained AF during intermittent fast atrial pacing, 2 of 7 did not develop persistent AF after stopping the pacing protocol (online-only Data Supplement Figure VIIIA). Two representative examples are shown in online-only Data Supplement Figure VIII; whereas in one animal the AF lasted >7 days after the pacing program was switched off (panel B), in the other one spontaneous AF termination was observed 3 days after the pacing program was stopped (panel C).

DF values measured on the ILR (n=7) during the last week before the offset of tachypacing were not significantly different when comparing persistent AF versus nonpersistent AF animals (10.0±0.8 versus 10.0±2.1, respectively; $P=0.67$). Therefore, additional factors other than the increase in DF values must be involved in the progressive development of the arrhythmia. As shown in Figure 6, sectioning of the LA and quantification of the endocardial side of the PLA area (panel A) demonstrate that long-term tachypacing-induced AF animals (n=7) have a significantly enlarged PLA area compared with body weight–matched controls (n=4; 7.48±0.25 versus 5.96±0.29 cm^2; $P=0.006$; Figure 6B). However, as presented in online-only Data Supplement Figure IXA, fibrosis quantification on images obtained from slices stained with Picrosirius red did not show significant increase in fibrosis in any of the sectioned areas compared with weight-matched controls. Additional sectioning in the LA areas and staining using Masson trichrome further confirmed those results (online-only Data Supplement Figure IXB).

Development of atrial fibrosis is well established in AF models associated with congestive heart failure.[17] Conversely, predominant electric remodeling with minimal or no changes in atrial fibrosis is present in tachypacing-induced AF models even after long periods of fast pacing, as long as tachycardiomyopathy is not present.[18] Echocardiographic data at baseline and before euthanasia showed that the left ventricular ejection fraction was preserved (57±1.4% to 55±0.7%, respectively) in all animals studied (online-only Data Supplement Table I). In addition, the average heart rate during the follow-up remained

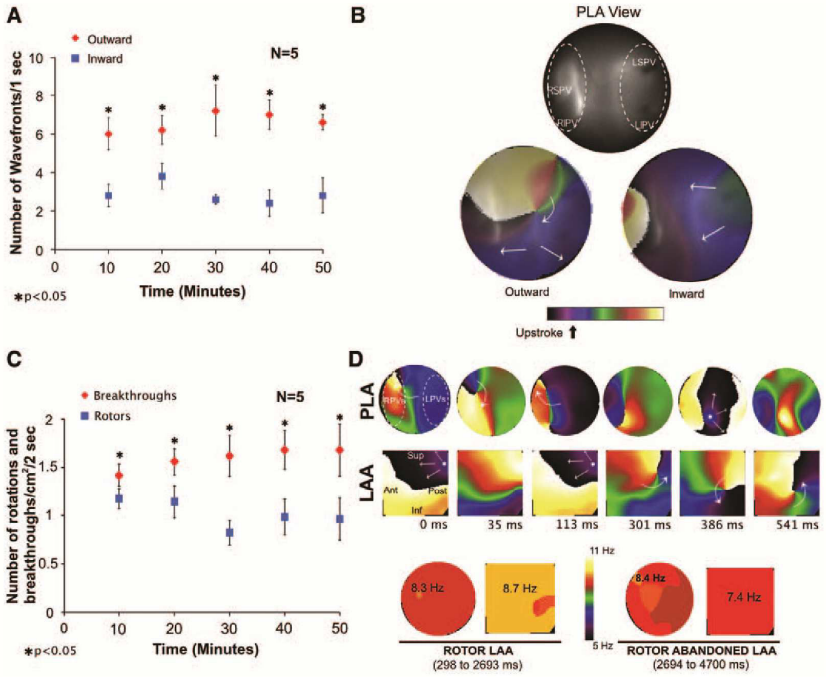

Figure 5. Patterns of activation in the posterior left atrium (PLA) of isolated hearts during atrial fibrillation (AF). **A**, The graph shows that the number of outwardly propagating wave fronts/second was significantly larger than the number of inwardly propagating wave fronts/second. **B**, **Top**, Optical field on the endocardium of the PLA; **bottom**, snapshots of phase movies showing a rotor generating outwardly propagating waves (**left**). An inwardly propagating wave is shown on the **right**. **C**, The number of breakthroughs/cm^2 per 2 seconds is higher than the number of rotations/cm^2 per 2 seconds. **D**, **Top**, Snapshots from a phase movie show a rotor appearing in the field of view of the left atrial appendage (LAA). The patterns of activation switch from breakthroughs (0–113 ms) to a meandering rotor (301–541 ms). **Bottom**, Maximal DF (DF_{max}) is in the LAA when the rotor stays in the field of view and goes back to PLA when the rotor drifts outside the LAA.

within the upper normal limit in sheep (99 beats per minute; online-only Data Supplement Table I), which makes the development of tachycardiomyopathy very unlikely.

Discussion

We have used a sheep model of persistent AF induced by intermittent atrial tachypacing, in which we monitored on a weekly basis the time course of the DF in the ILR (in close proximity to LA) and the RA. The results show a progressive spontaneous increase in DF during a 2-week period after the first detected AF episode, suggesting electric remodeling secondary to AF. Most important, a consistent LA-versus-RA DF difference lasting >22 weeks in most animals correlated with the presence of rotors, DF gradients, and outward propagation from the PLA during sustained AF in the explanted, Langendorff-perfused hearts. Although in this model interstitial fibrosis does not significantly increase, atrial structural changes leading to PLA enlargement may make rotors less likely to collide with anatomic boundaries, thus contributing to the persistence of the arrhythmia. However, changes in subcellular structures, such as the ryanodine receptor, may have led to sarcoplasmic reticulum Ca^{2+} leak and contributed to AF persistence by increasing triggered activity, dispersion of refractoriness, or promoting reentry initiation.[19] Altogether, our data support the contention that drifting transmural and intramural rotors may drive the highest frequency activity detected in the PLA.

Temporal criteria for persistent AF are well defined in the clinical setting.[2] However, persistent AF in animal models has not been rigorously defined, which may have led to inconsistencies in the results reported for models versus patients with persistent AF.[8,10] Fast atrial pacing is a common approach to

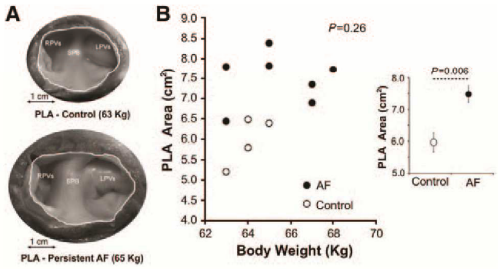

Figure 6. Enlargement of the posterior left atrium (PLA) area in sheep with atrial fibrillation (AF). **A**, Macroscopic images of the endocardial side of the PLA area in a persistent AF sheep (**bottom**) and weight-matched control (**top**). **B**, No significant correlation between body weight and PLA area was observed (Spearman test). Inset: On average, AF sheep show a significantly larger PLA area compared with weight-matched controls (Mann-Whitney *U* test).

induce AF in animal models. Yet, some studies use the term persistent AF for those episodes in which the arrhythmia sustains in the short term (<7 days) in the absence of pacing,[8,10] either for cardioversion attempts or for electrophysiological measurements.[11,20] Although spontaneous termination has been observed after 4 weeks of tachypacing-induced AF in chronically instrumented goats,[21] cases of AF have also been defined as long-lasting when they sustain for few days after rapid atrial pacing.[21] In the current study, most of the animals developed persistent AF lasting >1 week; thus, the time course of the DF and its left-to-right gradient we quantify are highly relevant to the progression of a clinical-like persistent AF.

Implications of Left-to-Right DF Gradients in Persistent AF

Although few data clearly demonstrate the presence of left-to-right DF gradients in patients with persistent and permanent AF, Sahadevan et al,[22] using epicardial mapping during cardiac surgery, have demonstrated the presence of rapid and regular rhythms mainly located at the LA in 7 of 9 patients with persistent/permanent AF. The cycle length of the rapid and regular rhythm areas was shorter than that of the areas with irregular activation. Atienza et al[6] have shown that left-to-right DF gradients were present in 84% of patients with persistent AF. Furthermore, persistent AF patients remained AF-free on follow-up when ablation significantly reduced DF_{max} in the LA and RA, abolishing the LA-to-RA DF gradient. Similarly, in a larger population of patients with long-lasting persistent AF, Hocini et al[23] have observed that in some cases of AF ablation a right-to-left frequency gradient appeared after prolongation of the AF LA cycle length. RA ablation terminated AF in 55% of those patients. Interestingly, those patients had longer AF duration and larger RA diameter. Somehow, our model resembles early stages of clinical persistent AF, in which the LA-to-RA gradient is still present and organized period activity is identified in the PLA, giving raise to fibrillatory conduction toward the rest of the atria. Longer periods in AF might eventually increase the fibrosis quantification and make other areas of the atria suitable for harboring reentrant sources.

Mechanism Underlying the DF_{max} in Persistent AF

Atrial electrical remodeling and functional changes in subcellular structures lead to both abbreviation of atrial action potential duration and refractory period[11] and increase in susceptibility to Ca^{+2}-dependent triggered activity,[19] altogether promoting reentry. However, whether random fibrillatory waves, triggered activity, or highly organized 3-dimensional reentrant sources are the underlying mechanism of persistent AF is controversial. Data from patients with persistent AF who underwent cardiac surgery and electric epicardial mapping in LA, RA, and PLA show the presence of nonrepetitive epicardial breakthroughs more frequently occurring in the pulmonary veins area compared with RA and LA.[24] Although those results might suggest the presence of fibrillation waves propagating in deeper layers of the atrial wall, important limitations, such as sequential and exclusive epicardial mapping, preclude ruling out the presence of endocardial/intramural reentrant sources giving raise to epicardial breakthroughs. In addition, the lack of simultaneous recording of Ca^{+2} transients prevents us from ruling out the possibility that the epicardial breakthroughs were caused by triggered activity.[19] Similarly, our study also identifies higher number of breakthroughs compared with rotors in the PLA. However, direct visualization of the endocardial side of the PLA, simultaneous mapping of PLA-LAA, and much higher mapping resolution (≈0.23 mm^2/pixel) than the conventional multielectrode arrays allowed the demonstration of a rotor drifting toward the LAA with its center of rotation oriented perpendicular to the field of view; an apparent breakthrough pattern before the rotor enters turns to a rotor pattern when the rotor is visible. Concomitant changes in the DF_{max} values from PLA to LAA upon entering the rotor further support the essential role of rotors in maintaining persistent AF. The latter also makes Ca^{+2}-dependent triggered activity more likely to be related to reentry initiation rather than maintenance of the arrhythmia.

Limitations

In vivo LA-to-RA DF differences were obtained from only 2 single-lead traces, which limit the ability to characterize the spatial distribution of the DF values across the atria. In addition, the lack of synchronization of in vivo recordings prevented an in vivo directionality analysis. Atrial activity obtained from the ILR may be considered more global than that recorded by the intracardial lead. However, as shown in Figure 1B, the close proximity of the ILR to the LA of the sheep and the confirmation of the DF_{max} at the PLA in optically mapped hearts support the results obtained from the ILR traces.

Fibrosis quantification was performed in preserved hearts after optical mapping, and is not clear whether or not this affects Picrosirius red staining. Additional sectioning and staining using Masson trichrome reproduced similar results, which reduces likelihood for biased estimation of the fibrosis.

Finally, cellular and ionic remodeling underlying AF initiation, rotor activity, and DF gradients have not been investigated in this study because of incompatibility with the optical mapping of the entire heart. Importantly, the DF gradients observed in this persistent AF model cannot be extrapolated to longer periods of AF, such as permanent AF, in which stronger structural remodeling may be involved and left-to-right gradients may decrease.[6]

Conclusions

Time-course analysis of in vivo AF in sheep shows an initial 2-week period of progressive increase in DF followed by DF stabilization for up to 24 weeks thereafter. The different long-term DFs in the ILR and the RA recorded in vivo, together with DF gradients and patterns of activation in the optically mapped explanted hearts, strongly suggest the presence of long-lasting AF reentrant drivers located at the PLA in this model of persistent AF.

Acknowledgments

We thank Andreu Climent and María Guillém for assistance in signal processing. We also thank Gail Rising and Krishna Bandaru for technical assistance and Rosario Madero for assistance in statistical analyses. We thank St Jude Medical and Medtronic for assistance with implantable devices.

Sources of Funding

This work was supported, in part, by National Heart, Lung, and Blood Institute Grants (P01-HL039707 and P01-HL087226 to J.J. and O.B.), the Leducq Foundation and Centro Nacional de Investigaciones Cardiovasculares (Spain) (to J.J. and O.B.), the University of Michigan Gelman/Innovation and Coulter Awards (to

O.B.), St. Jude Medical Grant (to J.J., O.B., J.K.), a Spanish Society of Cardiology Fellowship, the Alfonso Martín Escudero Foundation (to D.F.R.), and the Fédération Française de Cardiologie (R.P.M.).

Disclosures

None.

References

1. Kannel WB, Wolf PA, Benjamin EJ, Levy D. Prevalence, incidence, prognosis, and predisposing conditions for atrial fibrillation: population-based estimates. *Am J Cardiol*. 1998;82:2N–9N.
2. Camm AJ, Kirchhof P, Lip GY, Schotten U, Savelieva I, Ernst S, Van Gelder IC, Al-Attar N, Hindricks G, Prendergast B, Heidbuchel H, Alfieri O, Angelini A, Atar D, Colonna P, De Caterina R, De Sutter J, Goette A, Gorenek B, Heldal M, Hohloser SH, Kolh P, Le Heuzey JY, Ponikowski P, Rutten FH; European Heart Rhythm Association; European Association for Cardio-Thoracic Surgery; ESC Committee for Practice Guidelines. Guidelines for the management of atrial fibrillation: the Task Force for the Management of Atrial Fibrillation of the European Society of Cardiology (ESC). *Europace*. 2010;12:1360–1420.
3. Mandapati R, Skanes A, Chen J, Berenfeld O, Jalife J. Stable microreentrant sources as a mechanism of atrial fibrillation in the isolated sheep heart. *Circulation*. 2000;101:194–199.
4. Mansour M, Mandapati R, Berenfeld O, Chen J, Samie FH, Jalife J. Left-to-right gradient of atrial frequencies during acute atrial fibrillation in the isolated sheep heart. *Circulation*. 2001;103:2631–2636.
5. Atienza F, Almendral J, Moreno J, Vaidyanathan R, Talkachou A, Kalifa J, Arenal A, Villacastín JP, Torrecilla EG, Sánchez A, Ploutz-Snyder R, Jalife J, Berenfeld O. Activation of inward rectifier potassium channels accelerates atrial fibrillation in humans: evidence for a reentrant mechanism. *Circulation*. 2006;114:2434–2442.
6. Atienza F, Almendral J, Jalife J, Zlochiver S, Ploutz-Snyder R, Torrecilla EG, Arenal A, Kalifa J, Fernández-Avilés F, Berenfeld O. Real-time dominant frequency mapping and ablation of dominant frequency sites in atrial fibrillation with left-to-right frequency gradients predicts long-term maintenance of sinus rhythm. *Heart Rhythm*. 2009;6:33–40.
7. Yoshida K, Ulfarsson M, Oral H, Crawford T, Good E, Jongnarangsin K, Bogun F, Pelosi F, Jalife J, Morady F, Chugh A. Left atrial pressure and dominant frequency of atrial fibrillation in humans. *Heart Rhythm*. 2011;8:181–187.
8. Anné W, Willems R, Holemans P, Beckers F, Roskams T, Lenaerts I, Ector H, Heidbüchel H. Self-terminating AF depends on electrical remodeling while persistent AF depends on additional structural changes in a rapid atrially paced sheep model. *J Mol Cell Cardiol*. 2007;43:148–158.
9. Voigt N, Trausch A, Knaut M, Matschke K, Varró A, Van Wagoner DR, Nattel S, Ravens U, Dobrev D. Left-to-right atrial inward rectifier potassium current gradients in patients with paroxysmal versus chronic atrial fibrillation. *Circ Arrhythm Electrophysiol*. 2010;3:472–480.
10. Roka A, Toth E, Szilagyi S, Merkely B. Electrical atrial fibrillation induction affects the characteristics of induced arrhythmia. *J Electrocardiol*. 2008;41:131–137.
11. Yue L, Feng J, Gaspo R, Li GR, Wang Z, Nattel S. Ionic remodeling underlying action potential changes in a canine model of atrial fibrillation. *Circ Res*. 1997;81:512–525.
12. Castells F, Mora C, Rieta JJ, Moratal-Pérez D, Millet J. Estimation of atrial fibrillatory wave from single-lead atrial fibrillation electrocardiograms using principal component analysis concepts. *Med Biol Eng Comput*. 2005;43:557–560.
13. Alcaraz R, Rieta JJ. Adaptive singular value cancelation of ventricular activity in single-lead atrial fibrillation electrocardiograms. *Physiol Meas*. 2008;29:1351–1369.
14. Schotten U, de Haan S, Neuberger HR, Eijsbouts S, Blaauw Y, Tieleman R, Allessie M. Loss of atrial contractility is primary cause of atrial dilatation during first days of atrial fibrillation. *Am J Physiol Heart Circ Physiol*. 2004;287:H2324–H2331.
15. Filgueiras-Rama D, Martins RP, Ennis SR, Mironov S, Jiang J, Yamazaki M, Kalifa J me, Jalife J, Berenfeld O. High-resolution endocardial and epicardial optical mapping in a sheep model of stretch-induced atrial fibrillation. *J Vis Exp*. 2011:e3103.
16. Warren M, Guha PK, Berenfeld O, Zaitsev A, Anumonwo JM, Dhamoon AS, Bagwe S, Taffet SM, Jalife J. Blockade of the inward rectifying potassium current terminates ventricular fibrillation in the guinea pig heart. *J Cardiovasc Electrophysiol*. 2003;14:621–631.
17. Li D, Fareh S, Leung TK, Nattel S. Promotion of atrial fibrillation by heart failure in dogs: atrial remodeling of a different sort. *Circulation*. 1999;100:87–95.
18. Ausma J, Wijffels M, Thoné F, Wouters L, Allessie M, Borgers M. Structural changes of atrial myocardium due to sustained atrial fibrillation in the goat. *Circulation*. 1997;96:3157–3163.
19. Voigt N, Li N, Wang Q, Wang W, Trafford AW, Abu-Taha I, Sun Q, Wieland T, Ravens U, Nattel S, Wehrens XH, Dobrev D. Enhanced sarcoplasmic reticulum Ca2+ leak and increased Na+-Ca2+ exchanger function underlie delayed afterdepolarizations in patients with chronic atrial fibrillation. *Circulation*. 2012;125:2059–2070.
20. Nishida K, Sarrazin JF, Fujiki A, Oral H, Inoue H, Morady F, Nattel S. Roles of the left atrial roof and pulmonary veins in the anatomic substrate for persistent atrial fibrillation and ablation in a canine model. *J Am Coll Cardiol*. 2010;56:1728–1736.
21. Wijffels MC, Kirchhof CJ, Dorland R, Allessie MA. Atrial fibrillation begets atrial fibrillation. A study in awake chronically instrumented goats. *Circulation*. 1995;92:1954–1968.
22. Sahadevan J, Ryu K, Peltz L, Khrestian CM, Stewart RW, Markowitz AH, Waldo AL. Epicardial mapping of chronic atrial fibrillation in patients: preliminary observations. *Circulation*. 2004;110:3293–3299.
23. Hocini M, Nault I, Wright M, Veenhuyzen G, Narayan SM, Jaïs P, Lim KT, Knecht S, Matsuo S, Forclaz A, Miyazaki S, Jadidi A, O'Neill MD, Sacher F, Clémenty J, Haïssaguerre M. Disparate evolution of right and left atrial rate during ablation of long-lasting persistent atrial fibrillation. *J Am Coll Cardiol*. 2010;55:1007–1016.
24. de Groot NM, Houben RP, Smeets JL, Boersma E, Schotten U, Schalij MJ, Crijns H, Allessie MA. Electropathological substrate of longstanding persistent atrial fibrillation in patients with structural heart disease: epicardial breakthrough. *Circulation*. 2010;122:1674–1682.

CLINICAL PERSPECTIVE

The mechanisms underlying persistent atrial fibrillation (AF) are poorly understood. As the presence of the arrhythmia persists, atrial remodeling may become a major reason for the limited efficacy of either antiarrhythmic drugs or catheter-based ablation therapeutic options. In animals, the presence of a left-to-right hierarchical distribution in frequencies of activation during AF has been related to fast reentrant activity (rotors) in the left atrium, which gives rise to fibrillatory conduction toward the rest of the atria. Thus, analysis of human AF in the frequency domain contributes to both a mechanistic insight and ablative guidance. To better understand the development and patterns of activation in persistent AF, we studied in vivo the time course of changes in dominant frequency values in the left and right atria of a sheep subjected to chronically tachypaced right atrium. Continuous cardiac rhythm monitoring by a bipolar lead inserted into the right atrial appendage and an implantable loop recorder in close proximity to left atrium showed a gradual increase in dominant frequency values during AF during a 2-week period followed by a stable left-to-right dominant frequency gradient when the AF becomes persistent for a week or more. Ex vivo mapping confirmed the presence of the in vivo dominant frequency gradients, together with the existence of patterns of activation that are consistent with the contention that meandering rotors in an enlarged posterior left atrium may underlie in vivo AF dynamics in this sheep model. The results might also suggest a long-term fast reentrant source in the left atrium as AF becomes persistent in patients.

SUPPLEMENTAL MATERIAL.

Long-term Frequency Gradients During Persistent Atrial Fibrillation in Sheep are Associated with Stable Sources in the Left Atrium.

David Filgueiras-Rama,[1*] MD, Nicholas F. Price,[1,2*] MSc, Raphael P. Martins,[1] MD, Masatoshi Yamazaki,[1] MD, Uma Mahesh R Avula,[1] MD, Kuljeet Kaur,[1] PhD, Jérôme Kalifa,[1] MD, Steven R. Ennis,[1] PhD, Elliot Hwang,[1] BSE, Vijay Devabhaktuni,[2] PhD, Jose Jalife,[1] MD, Omer Berenfeld,[1] PhD.

Supplemental Methods.

ECG Digitization.

The first step in the analysis of the data from the implantable loop recorder (ILR) is converting the image of the ECG signal into a sequence of time-steps with associated voltage levels. The pixels in the image are treated as discrete time and voltage samples that can be mapped to a one-dimensional digital signal.

Data from the Medtronic Reveal® XT was already collected in the form of PDF file. Only one lead was available in each trace. The ECG waveforms were encoded in the PDF as vector graphics allowing for crisp images to be observed at an arbitrary zoom. Adobe Reader's snapshot tool was first used to select a rectangular section of the ECG signal (5 sec). The image was then magnified to 1200% zoom, then copied and then pasted into Microsoft Paint and saved as a PNG file. In PNG format, the image could be read and

processed by standard Matlab functions from the image-processing library. At 1200% zoom, knowing that the scale indicated on the PDF was 25.0 mm/sec, it was calculated that the effective resolution of the PNG images were approximately 1278 pixels-per-inch – sufficient to expect accurate results.[1]

There were three styles of ECG printouts that were saved from the animal interrogations. All three styles required slightly different approaches to interpret and process, but there were commonalities and overlaps. The main thing that changes between all three is how to determine which pixels belong to the ECG waveform and which are part of the reference gridlines or irrelevant structures. In the first style (Supplemental Figure 1A), the waveform was placed around a baseline, both the waveform and baseline were colored black and the vertical and horizontal gridlines were colored gray. In the second style (Supplemental Figure 1B), there was no baseline and the vertical and horizontal gridlines were encoded as black dots. The third style (Supplemental Figure 1C) had no baseline around the waveform and, as was the case for style 1, gridlines were colored as black and gray respectively. Knowing this information, it was possible to write digitization functions in MATLAB using basic image processing techniques suited for each of the three styles.

Style 1 – Baseline and Gray Gridlines.

The main challenge in digitizing this style was accounting for the baseline, which extended from one end of the ECG trace to the other. In order to identify it, a decision rule algorithm was used to determine which rows of pixels in the PNG file are parts of the baseline. Knowing which pixels were in the baseline was necessary to ensure that they were not

mistaken as part of the waveform during the digitization process. The algorithm used to do this was straightforward, worked well in practice, and proceeded as follows:

1. Determine the maximum number of pixels in any of the rows in the image. This row was labeled as the 'best' row.
2. Identify the rows adjacent to the best row and each other, which have at least 95% of the black pixels as the best row.
3. Identify that cluster of rows as the baseline.

With the knowledge of which rows of pixels are associated with the baseline, a condition can be put in place that prevents pixels in those rows from being interpreted as part of the waveform unless there are no other possible options.

Style 2 – No Baseline and Black Gridlines.

This is the least frequently used style and the most time consuming to process. While there is no baseline that could be confused for the waveform, the gridlines can be. Most of the problems are solved by a few manual modifications to the PNG file and labeling of the image.

Because the gridlines are dotted, labeling the image allows for a way of distinguishing between different regions of black pixels. Image labeling is the process of assigning numerical values to separate contiguous fields of pixels of a particular color (usually in a binary image). By performing this operation, it is easy to determine which black pixels are not parts of the ECG waveform after identifying which label corresponds to the waveform. The waveform could be identified as a region that spans across the length of the image from one end to the other.

Style 3 – No Baseline and Gray Gridlines.

This style is the easiest to digitize. There is no baseline that needs to be separated from the ECG waveform and the gridlines can be identified using thresholding, like in the first style.

Translating into a Signal.

After the pixels associated with the ECG waveform were identified, the translation from image to signal was the same for all styles. At each column of pixels, the median pixel's row coordinate was selected as the voltage level in arbitrary units. This is similar to the method employed by Chebil J. et al.[1] Because the actual magnitude of the signal in units of volts was not relevant for this study, these values were never translated to mV.

After the translation is performed, the original ECG image is displayed with the interpreted signal superimposed on top in red, for visual inspection. There were rarely irregularities, but all digitized ECGs were inspected by the investigators before use to ensure quality data. If irregularities were found, the cause was determined an adjustments made to correct them. Barring that, the trace was eliminated from the data set.

Obtaining the Time Scale.

The time scale along the time-axis was calculated for each trace individually, using the knowledge that every five gridlines delineated one second of time in the image. Determining the distances between the gridlines in pixels was done by counting the number of gridline colored pixels in each column. The columns associated with each gridline are identified as columns in which the number of gridline colored pixels exceed the median number between the column with the maximum number of gridline pixels and the minimum number. The

average distance between gridline centers in pixels was taken to be the normal gridline distance. Simple arithmetic could then determine the amount of time between each column of pixels (or effective samples) and then the effective sampling frequency. In practice, this process consistently calculated that the difference in time between samples was $7.704e^{-4} \pm 6e^{-7}$ sec, which translates to an effective sampling frequency of about 1298±1 Hz.

Reading Data from the Right Atrium Lead.

Custom-made St. Jude Software was used to extract cardiac electrograms (EGMs) from the bipolar lead inserted into the sheep's right atrial appendage. The data could be output in a CSV file format. Knowing that the sampling frequency was 512 Hz, a program can easily be written to parse and interpret the contents of these files.

QRST Complex Removal.

Ventricular activity recorded by the ILR can drastically affect the power spectrum. Because the frequency domain characteristics of QRST complexes overlap those of AF, traditional linear filtering techniques are not adequate to remove them from the signal and minimize interference with analysis of the F-waves.[2] The data collected by the ILR contain only one lead, which is similar to a Holter system.

Two single-lead QRST removal algorithms were used. The first was adaptive singular value QRST cancellation (SVC),[3] the second was principle component analysis based atrial fibrillation estimation (PCA).[4] Both methods are applied to a window around the R-peak of the QRST complex, which extends from the beginning of the Q-wave to the end of the T-wave. The same window size must be used for all the QRST complexes of a trace, so the size of

the longest QRST complex is applied for all of them. Furthermore, both methods involve deriving templates to model the ventricular activity based upon the principle components of the QRST complex samples.

In the SVC method, QRST complexes from the trace are copied into the column vectors of an observation matrix **X**, which undergoes singular value decomposition. This separates the original matrix into the product of the matrices **U**, **S**, and **V**

$$\mathbf{X} = \mathbf{USV}^T$$

Where **U** and **V** are real unitary matrices ($\mathbf{UU}^T=\mathbf{I}$ and $\mathbf{VV}^T=\mathbf{I}$) and **S** is a diagonal matrix. By taking the product of **U** and **S**, such that **C** = **US**, the column vectors of matrix **C** are the non-normalized principle components, in order of significance. For SVC, the first principle component showed on panel **a** of Supplemental Figure 2 is used as a template to be subtracted at each QRST location in the original signal (Supplemental Figure 3). It is scaled by a factor of QR_i/QR_t where QR_i is the difference in amplitude between the Q-peak and the R-peak of the QRST complex being removed and QR_t is the difference in amplitude between the Q-Peak and he R-Peak of the template.

In the PCA method, the QRST complexes from the traces are seen as samples from random variables, for which a covariance matrix is derived. The eigenvectors and eigenvalues of the covariance matrix are then calculated with the eigenvectors placed in one matrix **E** and the eigenvalues placed in a diagonal matrix **D**. From these two matrices, a whitening matrix (a matrix that transforms the original observation matrix X into a matrix of whitened principle components) and a dewhitening matrix (a matrix which undoes the whitening process) is derived as such:

$$\mathbf{W} = \mathbf{D}^{-1/2}\mathbf{E}^{T} \text{ (Whitening Matrix)}$$

$$\mathbf{W}^{-1}=\mathbf{E}\mathbf{D}^{1/2} \text{ (Dewhitening Matrix)}$$

$$\mathbf{P}=\mathbf{W}\mathbf{X} \text{ (Principle Components)}$$

The principle components can then be derived from the observation matrix and whitening matrix by multiplication. These principle components were combined using their associated weights in the dewhitening matrix to create an individualized template for each QRST complex in the trace. The first principal components showed in panels **a** and **b** of Supplemental Figure 2 are assumed to express the ventricular activity because they express the highest amount of variance from the original observations.[4] Templates were created by combining the first 2 principle components, using their associated mixing variables from the dewhitening matrix $\mathbf{W}^{-1}$. These templates were then subtracted from the row vectors of the original matrix, which were then copied back into their place in the trace (Supplemental Figure 3).

As we show in Supplemental Figure 3, in most cases the SVC and the PCA methods produced results that were the same or very similar. However, in cases in which there were significant differences in the dominant frequency (DF) calculated when the two methods were used, the investigators inspected the trace and usually preferred the PCA method. The adjustability in the template morphology of the PCA method usually made it more effective when cancelling traces that had more variable QRST morphologies than was the SVC method.

Filtering.

After QRST removal, a bidirectional Butterworth band-pass filter was applied to each trace (Supplemental Figure 4). The pass-band was set between 4 Hz and 35 Hz.

Spectral Analysis.

The fast Fourier transform (FFT) was used to convert the trace into the frequency domain. The DF was determined to be the frequency where the highest peak in the spectrum was located. This value was then rounded to the nearest 0.25 Hz for determining the mode.

Mapping of Isolated Hearts.

Hearts were removed via thoracotomy and connected to a Langendorff-perfusion system with re-circulating oxygenated (95% O_2, 5% CO_2) Tyrode's solution at a constant flow rate of 340 ml/min (pH, 7.4; temperature, 35.5-37.5 °C). The Tyrode's solution composition (in mM) was: NaCl 130, KCl 4.0, $MgCl_2$ 1, $CaCl_2$ 1.8, $NaHCO_3$ 24, NaH_2PO_4 1.2, Glucose 5.6 and Albumin 0.04 g /L. Blebbistatin 10 μM (Enzo Life Science International, INC. Plymouth Meeting, PA, USA) was used to reduce motion.

After an atrial trans-septal puncture all the vein orifices were sealed, except the inferior vena cava, which was connected to a digital sensor and to an open-end cannula to control the intra-atrial pressure. The pressure was then increased to a subthreshold AF-inducing level of 5 cm H_2O, resembling the diastolic LA pressure and maintained throughout the experiment. Prior to sealing the veins, tetrapolar electrode catheters were placed in each of the PVs. Two additional custom-made bipolar electrodes were placed on the top of the RAA

and LA appendage (LAA). All recordings were bipolar signals obtained with a sampling rate of 1.0 kHz (DA100C; Biopac Systems, Inc., Goleta, CA, USA).

Epicardial and endocardial optical mapping (Di-4-ANEPPS 5-10 mg/mL) of the LAA and PLA, respectively, were performed simultaneously. Excitation (532 nm) was obtained by synchronized lasers. The emitted fluorescence (645 nm) on the epicardial surface of the LAA was projected onto a CCD camera (80x80 pixels, 600 fr/sec; LittleJoe, SciMeasure Analytical Systems, Inc. Decatur, GA, USA). A second CCD camera was coupled to a rigid borescope for direct visualization of the endocardial surface of the PLA.

Creating Spectrograms.

Spectrograms are used to demonstrate how the power spectrum of a signal varies across some independent variables, such as time. The spectrograms showed the average power spectrum of the traces for a given week, across several weeks of data recording.

To calculate them, the power spectra for each week were normalized, such that the area under the spectra summed to 1 between 0 and 20 Hz. The power spectra between 0 and 20 Hz were then summed, and again scaled by a factor of 1/n, where n is the number of traces used for that week. This ensured that the same weight was given to every trace within a week in producing an average power spectrum and each average power spectrum had the same weight in the overall spectrogram.

Echocardiographic Studies.

Data from transthoracic echocardiography (Sonos 5500, Hewlett-Packard, Palo Alto, CA) obtained at baseline and before euthanasia were reviewed off-line to assess the left

ventricular ejection fraction (LVEF). The measurements and calculations are based on parasternal views (Supplemental Figure 5), on account that the ovine thorax morphology (similar to pectus carinatum) provokes apical foreshortening, makes it difficult to obtain adequate apical, 4-chamber and 2-chamber views.

Structural Changes in Persistent AF.

Hearts preserved in 10% neutral buffered formalin from AF animals (N=7) and body weight-matched controls (N=4) were used to first section the LA and then obtain macroscopic images of the endocardial side of the PLA. The area of the PLA was quantified by manually delineating the boundaries outside the PVs. Then, tissue samples were obtained from the LA and RA free walls (longitudinal), and septum pulmonary bundle (longitudinal and transversal). The myocardial tissue, fixed in a 10% formalin solution, was embedded in paraffin and sectioned (4 μm-thick sections). Slides were blinded for the type of sheep and tissue location.

Quantitative evaluations of fibrosis were performed on images obtained from slides after staining with Picrosirius red. Slides were blinded for the type of sheep and tissue location. Images were photographed using 10x objective, with either a digital 3-chip color CCD camera (DC-330, DAGE-MTI) installed on a Zeiss Axioplan2e microscope or a 12 bits color CCD camera (Qicam, Qimaging) installed on a Zeiss ACIO imager A1 microscope. On average, five images were photographed from each slide. These digital images were processed using ImageJ software (NIH), with additional threshold color plug-ins to process jpeg images. Pixels corresponding to the area stained in red were normalized to the total pixel area of the tissue image and the results were expressed as percentage of collagen. Determining the total tissue areas occupied by cardiomyocytes and collagen and excluding the lumen assessed this

percentage. Perivascular, endocardial and epicardial fibrosis were excluded from the analysis by setting regions of interest. Similar analysis was performed after additional sectioning in the LA areas and Masson´s trichrome staining to confirm the Picrosirius red results.

Supplemental Results

Accuracy of In-vivo ILR-based DF Results.

In the main manuscript we investigated the DF evolution and inter-atrial heterogeneity during *in-vivo* AF. The *in-vivo* DF corresponding to the LA was calculated from the ILR signal following a QRST subtraction. In Supplemental Figure 6 we demonstrate the possible inaccuracies presented in our processing. The digitized ILR-based ECG signal (Supplemental Figure 6A) is composed of a mixture of atrial and ventricular activity. To enhance confidence in the QRST removal 2 single-lead QRST removal algorithms were used: (i) PCA (Supplemental Figure 6B) (ii) SVC (Suppplemental Figure 6C). However the insets in panels B and C show how changes in QRST morphology may result in different QRST removal properties by SVC (asterisk, panel C) compared to PCA (asterisk, panel B).

Accordingly, here we assess the performance of the SVC and PCA methods enabling unmasking the atrial activity during AF. Initially we compare the performance of the two methods against a known reference atrial activity that was manually created by splicing atria-only segments of recorded activity from the ECG data of the animals, excluding any ventricular activity. The ventricular activity (i.e., the QRST), extracted from the ECG data during periods of sinus rhythm, was then added to the atrial-only signal to generate a recording containing a mixture of atrio-ventricular activity. Each test case was constructed by

adding a selected set of QRST complexes to a 5 sec snippet of the atrial activity signal. Similarity between signals was measured by the Pearson correlation index (P):

$$P = \frac{1}{n\sigma_1\sigma_2}\sum_{t=1}^{n} s_1(t)s_2(t)$$

where s1 and s2 are the two zero-mean digital signals being compared, n is the number of samples and σ1 and σ2 are the standard deviations of the corresponding signals. The index is scaled such that if *P* is equal to one, the two signals are identical while if *P* is equal to zero the two signals are completely uncorrelated.

Five groups of sequences of QRST complexes were added: Each group was characterized by a different average value of the variability index (V), defined as $V = 1 - |P|$, measured between each pair of QRST complexes. One hundred test cases were generated for each group by shuffling randomly the sequence of the atrial segments and QRST complexes. Both the SVC and PCA algorithms were then applied to each test case and their resulting estimates of the time-series were compared against the known reference atrial activity signal using the Pearson index, which provided a quality of estimation coefficient.

In Supplemental Figure 7 we show sample results of our performance evaluation. In panel A, a relatively uniform set of QRST complexes (average QRST variability index, V_{AVG}=0.05) was added to the atrial activity and both methods demonstrate almost equal quality of estimation.

In panel B, a sample case with higher QRST variability (V_{AVG}=0.25) is shown to yield a higher estimation quality for PCA in comparison with SVC. Cumulative results in panel C show that the PCA method was significantly superior to SVC for test cases with average

QRST variability index ≥0.25 ($p<0.05$). The QRST removal by the two methods for a sample digitized ILR trace with $V_{AVG}=0.28$ is shown in Supplemental Figure 6 above; Variability in QRST morphology yield a difference of the estimated atrial activity. While no quantification of the error is possible here, visual inspection reveals that the SVC method results in an obvious ventricular residual signal (panel C) that is absent when the PCA method is used (panel B).

To further quantify the certainty in the DF results from the ILR, percent difference between the resulting DFs with PCA and SCV methods was obtained for individual traces, considering as reference the mean DF of the values of both methods as shown is the following formula.

$$\Delta DF(\%) = \frac{|DF_{PCA} - DF_{SVC}|}{\frac{1}{2}(DF_{PCA} + DF_{SVC})} \times 100$$

Considering all 690 ILR traces analyzed in the study, the average of these percent difference in DFs values was 5.77%. When the formula was applied to the selected mode value for each week, there was an average 5.82% difference. Overall, it is demonstrated that differentiation in DFs detected between RAA and ILR, and between AF onset and prolonged timing, is feasible.

Optimal Method for QRST Removal.

Digitized traces obtained from the ILR require QRST removal before calculating the DF. Although numerous approaches to remove QRST complexes have been developed, none of them have been established as the gold standard. As discussed in detail throughout the online supplement, we selected two single-lead QRST removal algorithms, SVC[3] and PCA,[4] to obtain the atrial activity. Since, our DF analysis relies on the accuracy of those results we compared both methods to estimate the average percent difference on the DF values

obtained from 690 ILR traces. Although the average percent difference result is 5.77%, further analysis, with synthesized AF traces and different QRST variability index, showed that PCA has significantly higher accuracy over larger range of QRST variability index (Supplemental Figure 7C). Since QRST complex can vary during experimental data as shown in Supplemental Figures 3 and 6, our analysis suggests that PCA is a better method for QRST removal in single lead recordings.

References

1. Jalel Chebil, Jamal Al-Nabulsi, Al-Maitah M. A novel method for digitizing standard ecg papers. *Proceedings of the International Conference on Computer and Communication Engineering*. 2008:1308-1312.

2. Rieta JJ, Castells F, Sanchez C, Zarzoso V, Millet J. Atrial activity extraction for atrial fibrillation analysis using blind source separation. *IEEE Trans Biomed Eng*. 2004;51:1176-1186.

3. Alcaraz R, Rieta JJ. Adaptive singular value cancelation of ventricular activity in single-lead atrial fibrillation electrocardiograms. *Physiol Meas*. 2008;29:1351-1369.

4. Castells F, Mora C, Rieta JJ, Moratal-Perez D, Millet J. Estimation of atrial fibrillatory wave from single-lead atrial fibrillation electrocardiograms using principal component analysis concepts. *Med Biol Eng Comput*. 2005;43:557-560.

Supplemental Figure legends.

Supplemental Figure 1. Three styles of ECG printouts obtained from the implantable loop recorder (ILR). A) Style 1, baseline and gray gridlines. B) Style 2, no baseline and black gridlines (dots). C) No baseline and gray gridlines.

Supplemental Figure 2. Both methods, adaptive singular value QRST cancellation (SVC) and principle component analysis based atrial fibrillation estimation (PCA) are applied to a window around the R-peak of the QRST complex, which extends from the beginning of the Q-wave to the end of the T-wave. For SVC, the first principle component showed on panel **a** is used as a template to be subtracted at each QRST location in the original signal. For PCA, templates were created by combining the first 2 principle components showed in panels **a** and **b**, using their associated mixing variables from the dewhitening matrix $\mathbf{W}^{-1}$. These templates were then subtracted from the row vectors of the original matrix, which were then copied back into their place in the trace.

Supplemental Figure 3. QRST complex removal in a sample case (top) by PCA (center) and SVC (bottom). In this case both methods produced very similar results.

Supplemental Figure 4. A) A sample digitized ILR-based ECG after QRST removal. B) Same trace after applying a bidirectional Butterworth band-pass filter (4 Hz and 35 Hz).

Supplemental Figure 5. Top, the long-axis parasternal echocardiographic view of the left ventricle was used to assess the LVEF. Bottom, sample case showing the M-Mode to quantify the LVEF.

Supplemental Figure 6. A sample digitized ILR-based ECG and QRST removal. **A)** Digital translation of the original ILR image displayed in red. **B)** and **C)** QRST removal by PCA and

SVC is shown, respectively. Changes in QRST morphology may result in incomplete QRST removal by SVC (asterisk, **C**) compared to proper elimination by PCA (asterisk, **B**).

Supplemental Figure 7. Performance of QRST removal by SVC and PCA methods. A) Synthesized AF trace with V_{AVG}=0.05 and appropriate QRST removal with both methods. B) Trace with V_{AVG}=0.25 and incomplete QRST removal using SCV (asterisk). C) Graph shows significantly better QRST removal profile for PCA than for SCV for V_{AVG}≥0.25.

Supplemental Figure 8. Persistence of AF after tacypacing induced AF. A) Bars show that persistent AF was achieved in most of animals under tachypacing induced AF (5 out of 7). B) and C) Time-course of DF in 2 representative AF cases. In B, AF was persistent and lasted >7 days after stopping the fast pacing. Conversely in C, AF was not persistent and lasted only for 3 days after stopping the fast pacing. DF values after AF re-induction were similar to the first AF episode (Asterisks). Grey arrows in each plot show the beginning and DF_{max} of self-sustained (>6 sec) tachypacing induced AF. Black arrows show self-sustained AF and DF_{max} before stopping the fast pacing.

Supplemental Figure 9. Fibrosis quantification. Bars show no significant differences in percentage of fibrosis between long-term tachypacing induced AF animals and weight-matched controls in all regions studied, either using Picrosirius red (A) or Masson´s trichrome staining (B). Results depicted as Mean±STD). SPB-T/L: septum-pulmonary bundle transversal/longitudinal.

Supplemental Movie legends.

Supplemental Movie 1. The phase movie shows a rotor with its center of rotation (a phase singularity point representing the surface end point of a filament perpendicular to the field of view) drifting towards the LAA (right). As soon as the rotor enters in the field of view of the LAA, the patterns of activation switch from breakthroughs to reentry and the meandering rotor becomes the main source driving the AF (DF_{max}). Similarly, once the rotor travels outside of the field of view, the pattern of activation in the LAA switches back to breakthroughs.

Supplemental Table 1. LVEF and heart rate at baseline and in atrial fibrillation.

	Number of weeks in AF						
	Baseline	Week 4	Week 8	Week 12	Week 16	Week 20	Week 22
Heart rate (bpm)	82±6.5 (n=7)	101.4±5.2 (n=7)	108.5±6.1 (n=7)	103.4±8.5 (n=6)	91.6±5.9 (n=5)	94.2±3.7 (n=5)	94±6.4 (n=4)
LVEF (%) (n=7)	57.5±1.4						55.6±0.7 (Before euthanasia)

Data are presented as mean±SEM. LVEF indicates left ventricular ejection fraction.

Supplemental Figure 1.

Supplemental Figure 2.

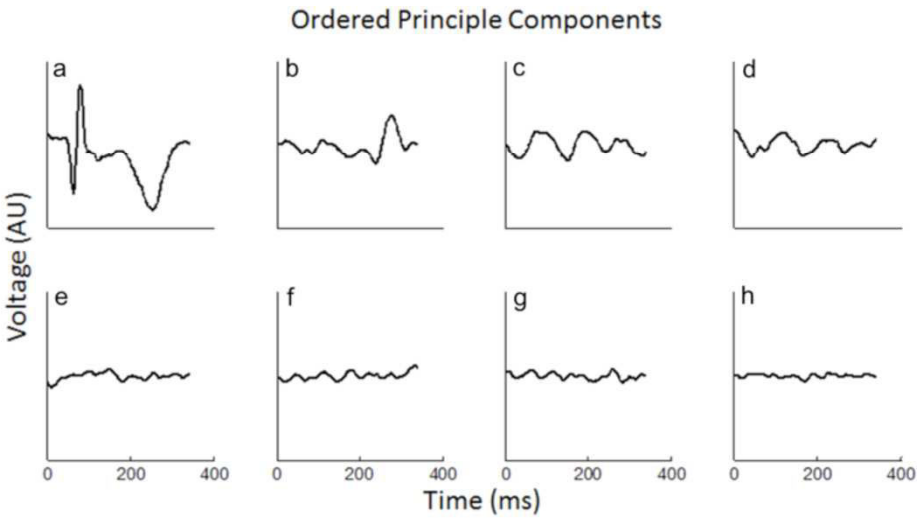

Supplemental Figure 3.

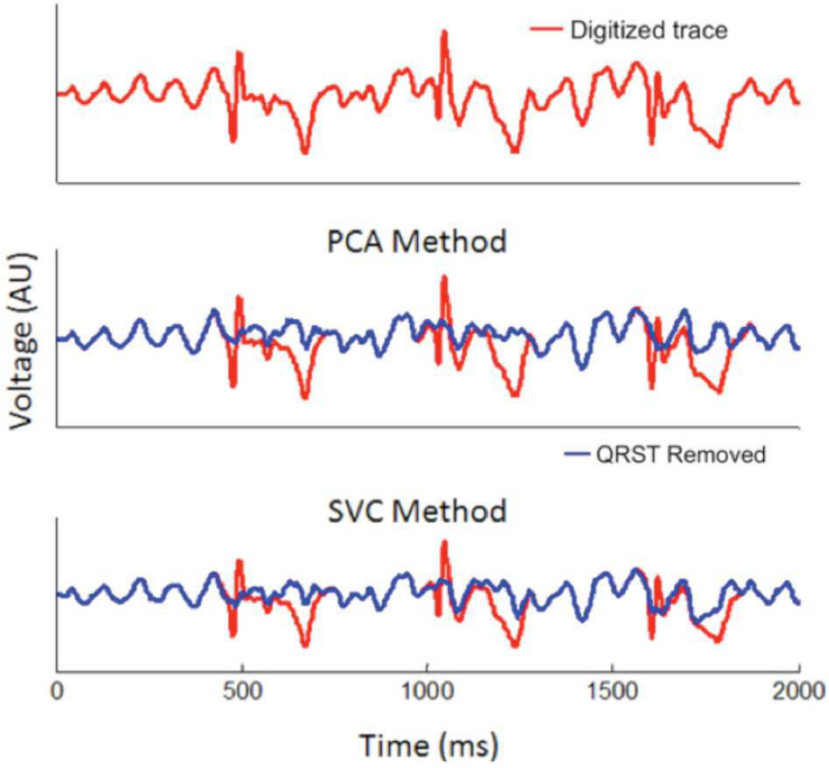

Supplemental Figure 4.

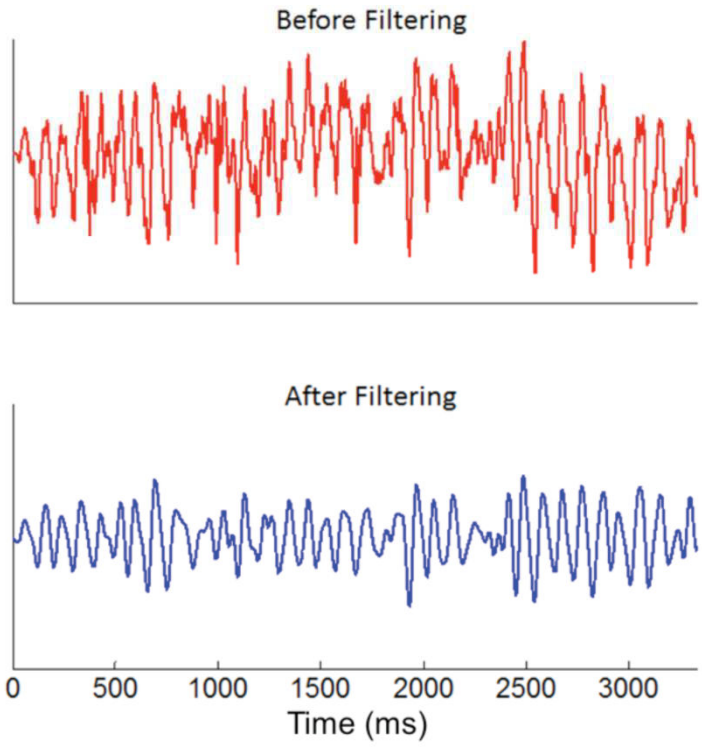

Supplemental Figure 5.

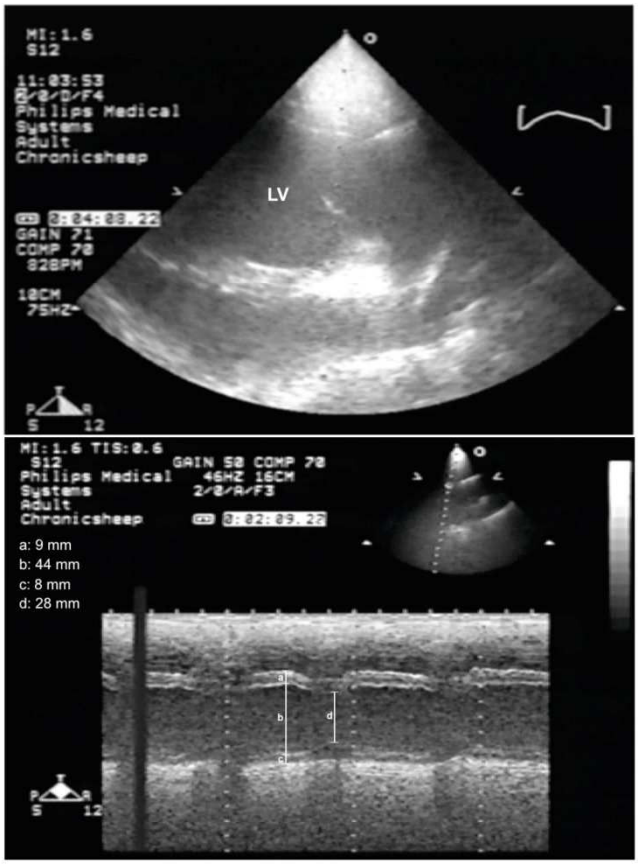

Supplemental Figure 6.

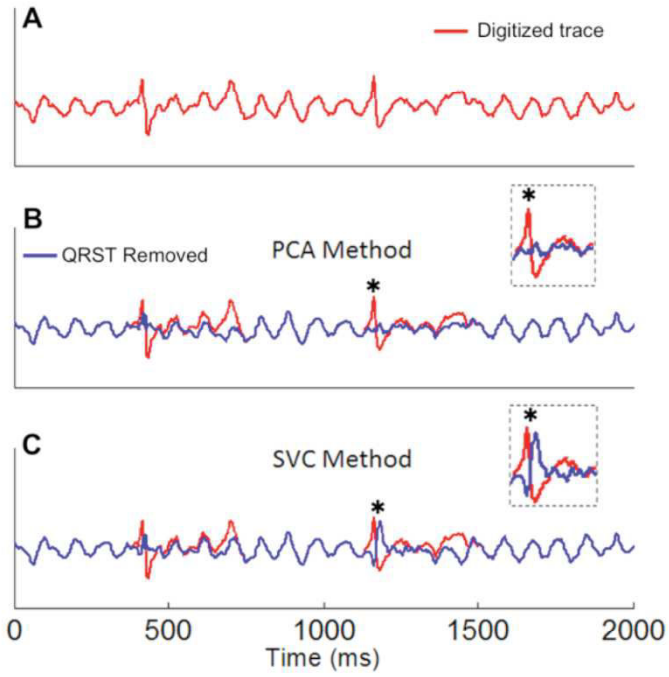

Supplemental Figure 7.

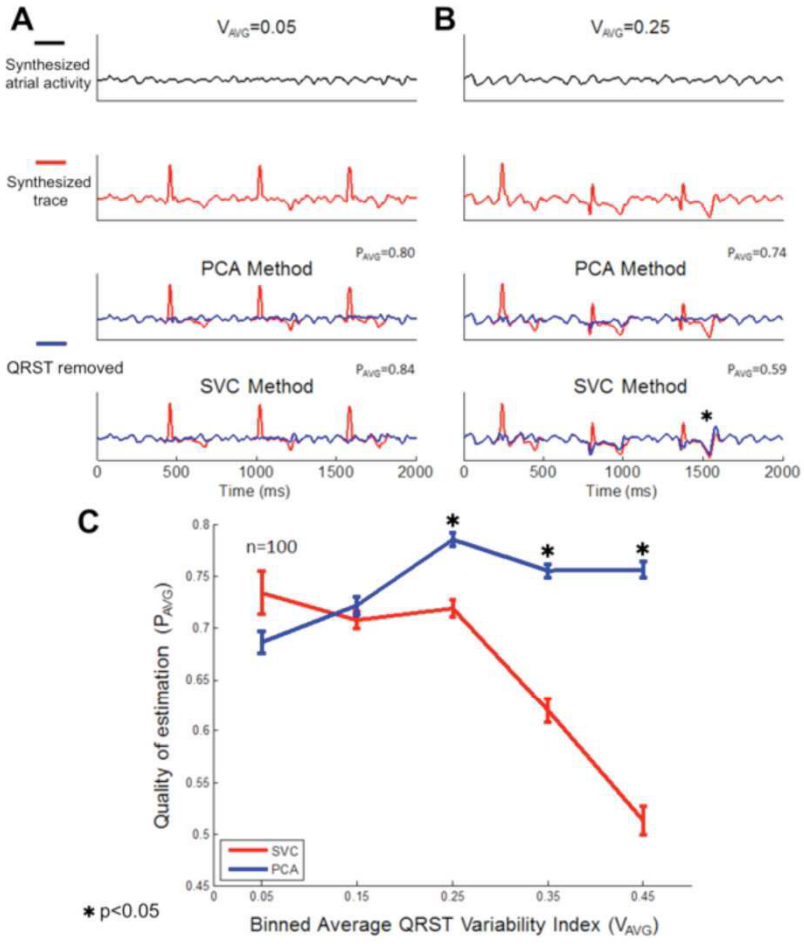

Supplemental Figure 8.

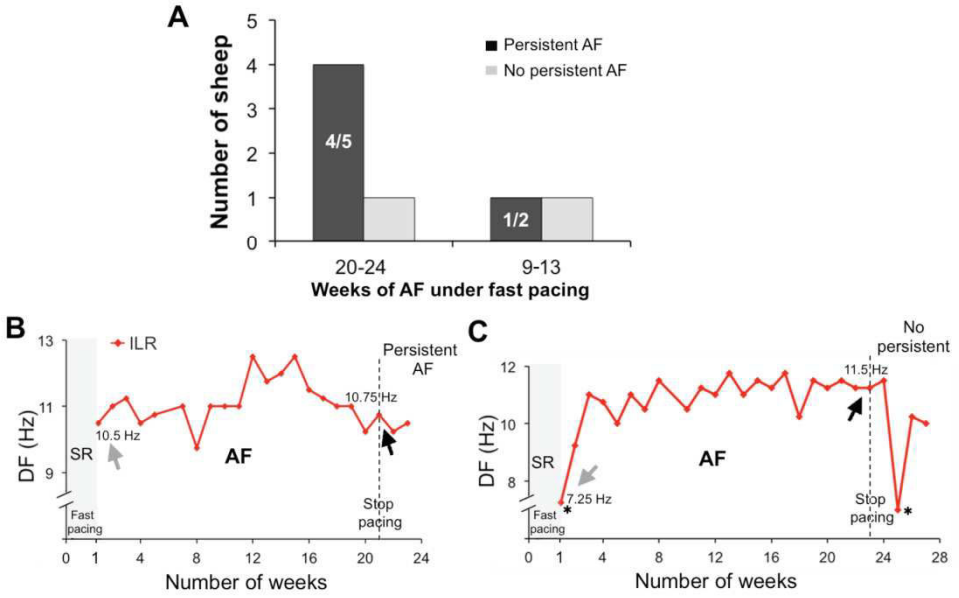

Supplemental Figure 9.

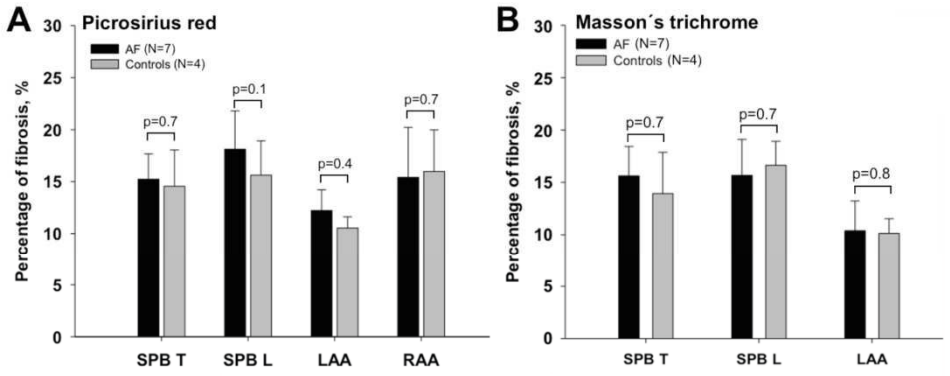

Deuxième partie

De la FA paroxystique à la FA persistante

A. Généralités

La FA peut se présenter sous différentes formes définies selon un critère temporel (durée de l'arythmie) : 1) La FA paroxystique : les épisodes sont spontanément résolutifs, durant moins de 7 jours, et typiquement moins de 48h ; au-delà de 48h, la probabilité de cardioversion spontanée est faible, et une anticoagulation curative doit être envisagée avant réduction ; 2) La FA persistante : les épisodes durent plus de 7 jours, et nécessitent une intervention médicale afin de rétablir le rythme sinusal, qu'elle soit médicamenteuse (médicaments anti-arythmiques) ou non (cardioversion électrique) ; 3) La FA persistante de longue durée (« long-lasting persistant AF ») lorsque la FA persistante dure depuis plus d'un an sans retour en rythme sinusal spontané ou après cardioversion ; 4) La FA permanente, lorsque le retour en rythme sinusal n'est plus possible ou non envisagé, que ce soit par le choix du patient ou du soignant. De nombreux épisodes de FA sont totalement asymptomatiques,[146] étant alors découverts lors d'un ECG systématique ou lors de la survenue d'une complication.

L'histoire de la FA évolue le plus souvent sur de nombreuses années, débutant volontiers par de brefs épisodes paroxystiques devenant plus fréquents et plus longs au fil du temps jusqu'à ce que des formes soutenues apparaissent. Le registre allemand AFNET (Registry of the German competence NETwork on Atrial Fibrillation) a inclus 9852 patients entre 2004 et 2006 en les différenciant selon le type de FA présentée (1er épisode, FA paroxystique, persistante ou permanente).[147] La présence de comorbidités, définies par l'âge ≥ 75 ans, l'hypertension artérielle, le diabète, la présence d'une cardiomyopathie, l'insuffisance cardiaque et les valvulopathies (ou antécédents de remplacements valvulaires) étaient notées. La Figure 14 montre que la proportion de patients en FA permanente augmente linéairement en fonction de la présence de comorbidités, alors que parallèlement la proportion de patients en FA paroxystique décroit. De façon surprenante, la proportion de patients en FA persistante reste stable, aux alentours de 15 à 20%, donnée suggérant que cette forme ne représente probablement qu'un « état de transition » entre la FA paroxystique et la FA permanente.

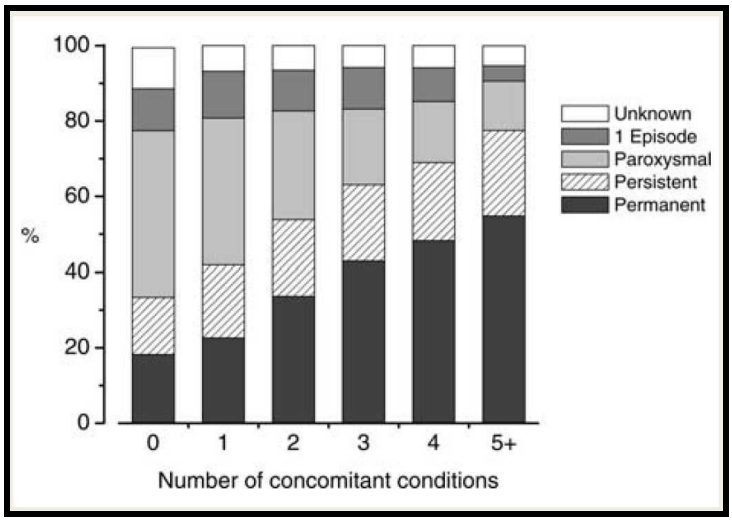

Figure 14 : Evolution de la proportion du type de FA en fonction du nombre de comorbidités concomitantes, parmi lesquelles l'âge ≥ 75 ans, l'hypertension artérielle, le diabète, la présence d'une cardiomyopathie, l'insuffisance cardiaque et les valvulopathies ou antécédents de remplacements valvulaires. D'après Nabauer et al, Europace, 2009.[147]

L'Euro Heart Survey sur la FA a inclus 5333 patients entre 2003 et 2004, pour lesquels un suivi à 1 an était prévu afin de déterminer leur statut clinique et d'analyser le taux de récidive et de progression de la FA.[148] Dans cette intéressante sous-étude, les auteurs ont montré que 46% des patients ayant présenté un premier épisode de FA n'ont jamais eu de récidive au cours de l'année de suivi (Figure 15). Après 1 an de suivi, environ 20% présentaient une réelle histoire de FA paroxystique, 10% une FA persistante et 20% étaient en FA permanente.

Les patients présentant quant-à-eux à l'inclusion une FA paroxystique n'ont pour la majorité (80%) pas progressé vers des formes plus soutenues ; 30% des patients en FA persistante ont progressé vers la forme permanente alors que, logiquement, ceux en FA permanente sont globalement (96%) restés dans cette forme de la maladie.

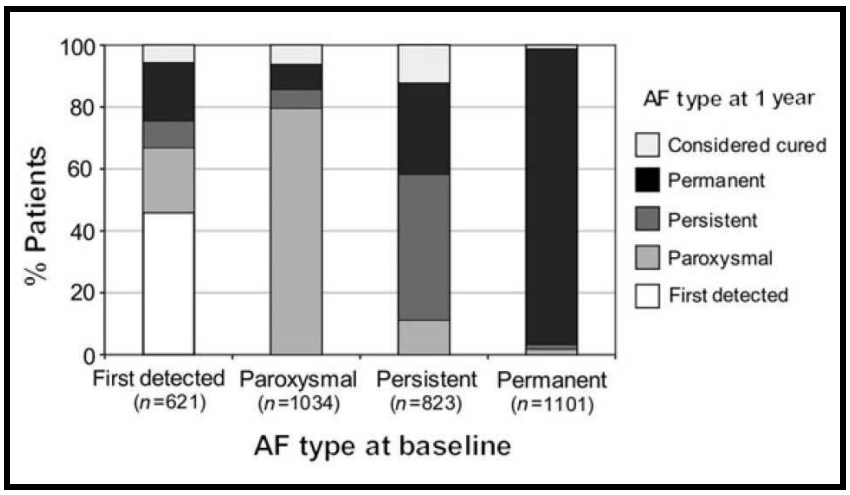

Figure 15 : Evolution du type de FA après 1 an de suivi, selon le type de FA à l'inclusion, chez les patients inclus dans l'Euro Heart Survey on Atrial Fibrillation. D'après Nieuwlaat et al, Eur Heart J, 2008.[148]

Ainsi, parmi les patients présentant un premier accès de FA sans cause aiguë réversible, près de la moitié ne récidiverons jamais alors que l'autre moitié s'inscrira dans une réelle histoire de FA.

De nombreuses autres études, résumées dans le Tableau 1, ont analysé le risque de progression de la FA au fil du temps[148-158] : celui-ci apparait extrêmement variable, dépendant principalement de la méthode diagnostique utilisée lors du suivi (ECG de repos, Holter ECG, enregistreur d'évènements, …), allant de 8.6 à 24% à 1 an[148-151, 153, 157, 158] et atteignant près de 30% dans les études avec un suivi prolongé.[152, 156] Saskena et al, en utilisant une méthode plus sensible (interrogation des mémoires de stimulateurs cardiaques chez des patients implantés pour une indication anti-bradycardique standard) ont retrouvé un pourcentage de progression de la FA paroxystique vers la FA persistante élevé de 24%, survenant à un intervalle moyen de 147±149 jours.[157] De façon intéressante, les auteurs retrouvaient une augmentation significative de la charge et de la durée des épisodes chez les patients progressant vers des formes plus soutenues de l'arythmie par rapport à ceux demeurant en FA paroxystique (pente d'augmentation 14s/jour *vs.* 0s/jour, $p<0.001$). La raison pour laquelle certains patients voient leur charge en arythmie augmenter au fil du temps et d'autres non est pour le moment inconnue.

Auteur	Revue	Année	Ref	N	Progression	Suivi	% progression
Kerr	Am Heart J	2005	[153]	757	Px → Pm	1 an	8.6%
De Vos	Am Heart J	2012	[150]	2137	Px → Ps/Pm	1 an	15%
De Vos	JACC	2010	[151]	1219	Px → Ps/Pm	1 an	15%
Zhang	Am J Cardiol	2013	[158]	955	Px→ Ps/Pm Ps → Pm	1 an	18.6%
Barrett	Am J Em Med	2013	[149]	253	Px → Ps/Pm	1 an	24%
Nieuwlaat	Eur Heart J	2008	[148]	4192	Px → Ps/Pm Ps → Pm	379 jours	#15% 30%
Saksena	Am Heart J	2007	[157]	330	Px → Ps	400 jours	24%
Ruigomez	BMC Cardiovasc	2005	[159]	418	Px → Ps/Pm	2.7 ans	18.6%
Kerr	Am Heart J	2005	[153]	757	Px → Pm	5 ans	24.7%
Koide	Clin Cardiol	2002	[155]	102	Px → Ps	61±13 mois	35.3%
Koide	Am J Cardiol	2008	[154]	204	Px → Ps	66±8 mois	35.3%
Potpara	Chest	2012	[156]	346	Px → Pm	12±7 ans	26.9%
Kato	Circ J	2004	[160]	171	Px → Ps/Pm	14.1 ans	77.2%
Jahangir	Circulation	2007	[152]	71	Px/ Ps → Pm	25.2±9.5 ans	30.9%

Tableau 1 : prévalence de la progression de la FA vers des formes soutenues.
Px = FA paroxystique ; Ps = FA persistante ; Pm = FA permanente.

De nombreux facteurs prédictifs de progression vers des formes soutenues de FA ont été mis en évidence, qu'ils soient :

- Cliniques : âge,[151-153, 155, 156, 158] hypertension artérielle,[150, 151] antécédent d'accident vasculaire ischémique transitoire ou constitué,[151, 158] broncho-pneumopathie chronique obstructive (BPCO),[151] stratégie de contrôle de la fréquence chez les patients en FA paroxystique,[150, 158] cardiomyopathie/insuffisance cardiaque,[150, 151, 153, 156] consommation d'alcool modérée[159],
- Structurels : dilatation atriale,[153, 154, 161] valvulopathies mitrales ou aortiques[153, 159],
- Electrocardiographiques : durée et dispersion de l'onde P[154, 155].

Un score permettant d'identifier les patients à haut risque de transition de la forme paroxystique aux formes persistante/permanente a récemment été décrit.[151] Ce score, dénommé « HATCH score », n'inclut que des paramètres cliniques qui se voient pondérés d'1 ou 2 points (score total allant de 0 à 7 pts) : l'hypertension artérielle (1 pt), l'âge ≥ 75 ans (1 pt), un antécédent d'accident vasculaire ischémique transitoire ou constitué (2 pts), la BPCO (1pt) et la présence d'une insuffisance cardiaque (2 pts). Dans cette étude, le pourcentage de progression moyen de 15% à 1 an variait notablement en fonction du score, puisque avoisinant respectivement 6%, 10%, 24% et 37% pour les patients à risques très faible (score à 0), faible (score à 1), modéré (score de 2 à 4) et élevé (score de 5 à 7). Ce score, très récemment introduit, n'a pas encore pu être évalué dans des études de suivi à long-terme,

mais uniquement dans 2 études rétrospectives qui ne lui ont retrouvé cependant qu'une valeur prédictive limitée sur le risque de transition.[149, 162]

Certains patients présentant une réelle histoire de FA paroxystique sur cœur sain (« lone atrial fibrillation ») sans aucun des facteurs cliniques composant le HATCH score et sans aucun des facteurs échocardiographiques ou électrocardiographiques cités précédemment ont tout de même un risque de voir leur arythmie évoluer spontanément ou malgré la mise en place d'un traitement anti-arythmique, ce qui sous-entend que le remodelage électrophysiologique et structurel à l'origine de la transition est un processus complexe faisant intervenir d'autres paramètres. Il est tout de même important de noter que la FA peut avoir une histoire naturelle différente, avec des formes paroxystiques fréquentes n'évoluant jamais vers des formes plus soutenues[157] ou des formes d'emblée permanente.

Sur le plan physiopathologique, l'évolution de la forme paroxystique vers la forme persistante puis permanente de la FA reflète la progression du remodelage électrophysiologique et structural atrial consécutif à l'arythmie et parfois aggravé par des facteurs associés (cardiopathie sous-jacente, comorbidités, …). En 1995, Carlos Morillo[10] et Maurits Wijffels[11] ont développé des modèles animaux de FA, respectivement chez le chien et la chèvre, qui ont permis d'innombrables avancées dans la compréhension de la physiopathologie de cette arythmie. Dans l'étude de Wijffels et al,[11] les auteurs ont implanté des chèvres avec des stimulateurs cardiaques leur permettant de stimuler l'oreillette à haute fréquence (50 Hz) et d'induire des épisodes de FA. Ces épisodes, initialement de courte durée (6±3 secondes) devenaient progressivement de plus en plus longs jusqu'à dépasser une semaine (7.1±4.8 jours). Le cycle moyen de la FA quant-à-lui décroissait au cours des 24 premières heures de l'arythmie de 145±18 à 108±8 ms parallèlement au raccourcissement de la période réfractaire atriale effective et à une perte de son adaptation à l'augmentation de fréquence. L'ensemble de ces modifications électrophysiolgiques était complètement réversibles après 1 semaine passée en rythme sinusal. Du titre de cette étude est né le concept de « atrial fibrillation begets atrial fibrillation » (la FA engendre la FA), illustrant l'inexorable progression de l'arythmie vers des formes soutenues.

Sur le plan thérapeutique, la progression de la FA de la forme paroxystique à la forme persistante puis persistante de longue durée a des conséquences importantes. En effet, au stade le plus précoce, lorsque la FA est paroxystique, celle-ci dépend principalement des « triggers » représentés par les extrasystoles atriales provenant des VP, alors qu'à mesure que la charge en arythmie augmente, le remodelage structurel atrial prend de l'importance. Ceci correspond à la transformation d'une maladie dépendant du « trigger » à une maladie dépendant du substrat. Cela complexifie la stratégie thérapeutique médicamenteuse, mais également les procédures d'ablation endocavitaires. En cas de FA paroxystique, l'isolation veineuse pulmonaire seule permet de prévenir les récidives chez près de 80% des patients.[6] Au contraire, en cas de FA persistante, la procédure est plus complexe, et doit associer à l'isolation veineuse pulmonaire des lignes complémentaires (toit, isthme mitral, …), l'isolation de foyers extra-veineux (VCS, sinus coronaire, auricule gauche) ou l'ablation d'autres cibles potentielles. Ces procédures, complexes et fastidieuses, ont une efficacité limitée comme en témoigne le faible pourcentage de patients en rythme sinusal après un suivi à moyen-terme.[163]

Pour le moment, nous ne disposons que de peu de données sur les facteurs permettant de ralentir la progression de la FA. Alors que l'étude AFFIRM a démontré que la stratégie de contrôle pharmacologique du rythme ne diminuait pas la mortalité des patients en FA,[164] quelques études ont établi qu'elle réduisait le risque de transition vers des formes plus soutenues de l'arythmie à 1 an de suivi par rapport à une stratégie de contrôle de la fréquence (5.8% *vs.* 27.6%, p<0.001 dans l'étude de Zhang et al[158] et 11 *vs.* 26% dans l'étude de De Vos et al[150]). Deux études récentes ont également confirmé de façon rétrospective qu'une stratégie de contrôle du rythme par ablation diminuait le risque de progression de la FA paroxystique vers des formes soutenues.[162, 165] L'étude prospective multicentrique et contrôlée ATTEST (Atrial Fibrillation Progression Trial, numéro Clinicaltrials.gov NCT01570361) débutée en février 2012 a pour but de valider cette stratégie, à savoir si l'ablation par RF de la FA paroxystique retarde la progression vers des formes soutenues, par rapport à une stratégie purement médicale de contrôle du rythme ou de la fréquence. Un total de 330 patients seront inclus et les résultats attendus en fin d'année 2016.

Pouvoir éviter la transition de la FA vers des formes plus soutenues ou à défaut, prédire dans quel délai les patients en FA paroxystique vont évoluer vers des formes persistantes ou permanentes permettrait d'améliorer la prise en charge de ces patients, diminuant ainsi la morbidité (qualité de vie, symptômes, complications) et la mortalité associées à l'arythmie.

B. Apport d'un modèle ovin de FA dans la compréhension des mécanismes impliqués dans la transition de la FA paroxystique à persistante

1. Hypothèse de travail

Bien que de nombreux facteurs prédictifs cliniques, échocardiographiques ou électrocardiographiques de transition de la forme paroxystique à la forme persistante aient été décrits, [150-156, 158, 159, 161] les réels mécanismes physiopathologiques à l'origine de cette transition sont actuellement inconnus. Wijffels et al, dans leur étude, statuaient[11] : *« As soon as the fibrillation interval passes a critical threshold of 120 ms, obviously atrial fibrillation becomes more stable and the duration of AF starts to increase. This in turn will further shorten the fibrillation interval which will prolong the duration of AF again, etc. »* (Dès que le cycle de fibrillation se raccourcit en deçà de 120 ms, la FA devenait à l'évidence plus stable et les épisodes plus prolongés. Ceci a pour conséquence un raccourcissement encore plus prononcé du cycle de fibrillation, qui va augmenter d'autant plus la durée de la FA, etc). Ceci sous-entendait qu'un intervalle critique du cycle de fibrillation était probablement nécessaire pour que la FA s'auto-entretienne sans retour possible en rythme sinusal.

Par ailleurs, si les caractéristiques électrophysiologiequs et structurelles du myocarde atrial normal et en FA sont connues, celles correspondant au moment de la transition de la forme paroxystique vers la forme persistante n'ont jamais été explorées en détails.

2. Méthodes

Afin de répondre à ces questions, nous avons amélioré notre modèle ovin de FA induite par stimulation atriale. Alors que dans notre précédent modèle, les 30 secondes de stimulation étaient suivies de 10 secondes de « blanking », [143] nous avons remplacées ces dernières par 10 secondes de « sensing » pendant lesquelles le stimulateur cardiaque était capable de détecter l'activité atriale, rythme sinusal ou FA. Pour ce faire, l'algorithme d' « Automatic Mode Switching » (AMS) a été activé, permettant à la fin de chaque cycle de stimulation d'analyser le rythme atrial. En cas de présence de rythme sinusal, un nouveau cycle de 30 secondes de stimulation était initié. Au contraire, si de la FA était détectée, la stimulation n'était plus relancée jusqu'à détection d'un éventuel retour en rythme sinusal (Figure 16). Ceci nous a permis de créer un modèle de FA, certes induite par la stimulation haute fréquence, mais auto-entretenue et par conséquent plus pertinente sur le plan clinique.

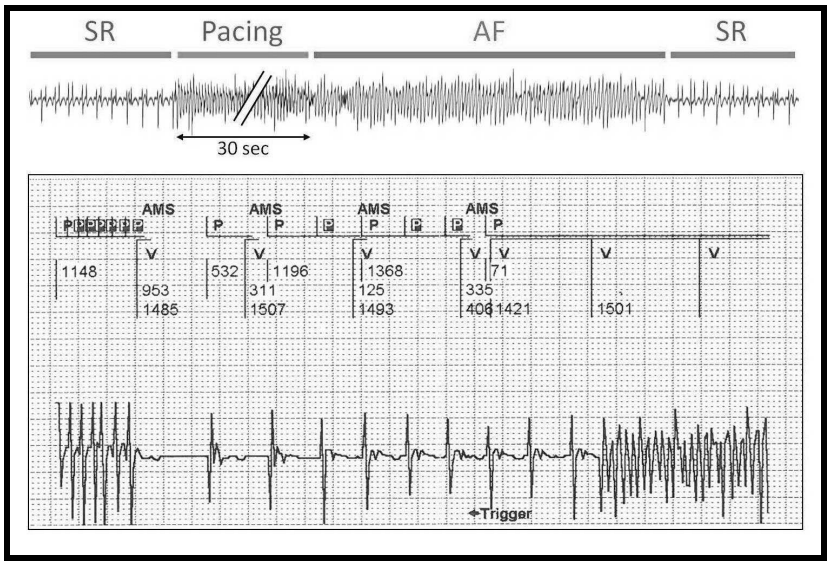

Figure 16 : Haut : Initiation de la stimulation à haute fréquence (20Hz) induisant un épisode court de FA. Bas : Electrogramme endocavitaire obtenu via l'électrode atriale droite montrant un retour spontané en rythme sinusal (gauche) détecté par l'algorithme du pacemaker qui initie alors un cycle de stimulation.

Par ailleurs, les mémoires des stimulateurs cardiaques nous fournissaient, de façon hebdomadaire, le nombre et la durée des épisodes de FA survenus depuis la précédente interrogation (exemple représenté dans la Figure 17), ce qui nous permettait de suivre précisément, semaine après semaine, l'évolution de l'arythmie, et de savoir si les épisodes étaient paroxystiques ou persistants.

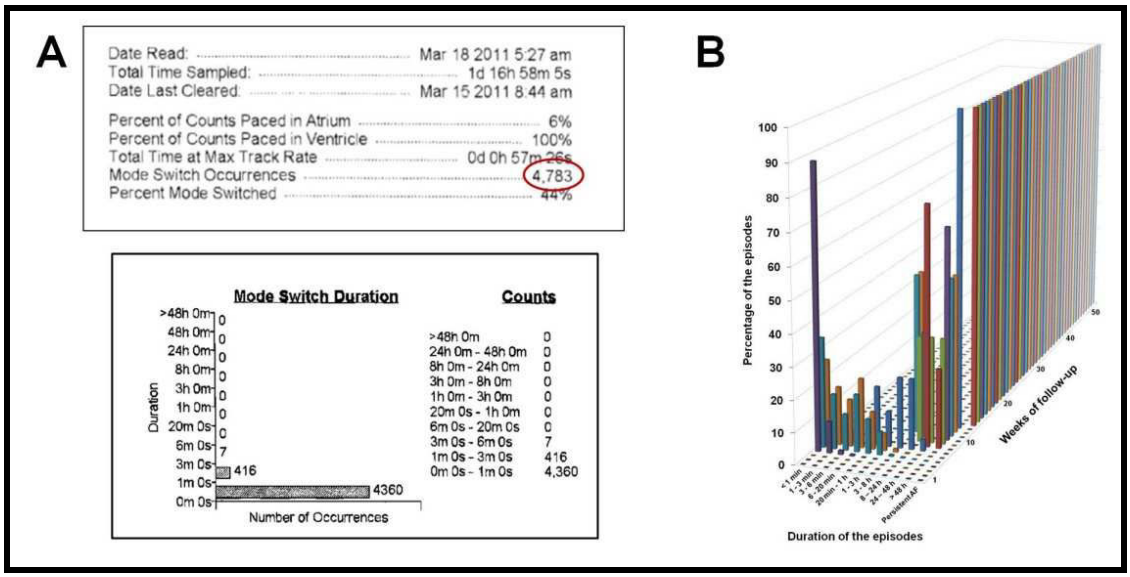

Figure 17 : A. Informations obtenues par les mémoires embarquées des stimulateurs cardiaques permettant de savoir le nombre (haut) et la durée (bas) des différents épisodes de FA survenus entre 2 interrogations. B. Représentation tridimensionnelle de l'évolution de la FA chez un des moutons au cours d'un an de suivi. La durée (X), le pourcentage des épisodes (Y) ainsi que les semaines de suivi (Z) sont représentées. Dans cet exemple, le 1er épisode survenait après 3 semaines de suivi, et la FA persistante apparaissait après 12 semaines.

Une approche similaire à celle mise en œuvre dans notre précédent travail a été réalisée,[143] à savoir l'enregistrement de trois EGM de façon hebdomadaire: 1) EGM endocavitaire unipolaire (boitier-dipôle distal) atrial droit ; 2) EGM sous-cutané obtenu via l'enregistreur d'évènements (Reveal®), positionné en regard de l'oreillette gauche et permettant d'obtenir un far-field du signal atrial gauche ; 3) dérivation I de l'ECG de surface.

Vingt-et-un moutons ont été implantés, divisés en trois groupes de sept animaux :

- <u>un groupe contrôle</u>, implanté d'un stimulateur cardiaque réglé en mode OAO, et par conséquent en rythme sinusal permanent, que nous avons suivi pendant 1 an ;
- <u>un groupe Transition</u>, sacrifié après plus de 7 jours sans retour en rythme sinusal ;
- <u>un groupe FA persistante de longue durée</u> (« Long-standing persistent AF » = LS-PAF), sacrifié après 1 an de FA persistante auto-entretenue (soit 1 an après le dernier retour en rythme sinusal)

3. Résultats

a. Evolution de la DF au cours de l'évolution de la FA

Grace aux mémoires de l'appareil, l'histoire de la FA pour chaque animal a été analysée. Tout comme chez l'homme, nous avons retrouvé une très grande variabilité dans

l'apparition et l'évolution de la FA, représentée dans la Figure 18. Ainsi, le premier épisode de FA apparaissait après une médiane de 2 jours (moyenne = 11.3±5.3, de 0 à 62 jours). Les épisodes étaient alors paroxystiques (< 7 jours) pendant une durée médiane de 43.5 jours (moyenne = 73.2±23.0 jours, extrêmes de 19 à 346 jours) avant que la FA persistante (épisode > 7 jours sans retour spontané en rythme sinusal) n'apparaisse après une médiane de 55 jours (moyenne = 88.2±27.6 jours, extrêmes de 23 à 406 jours).

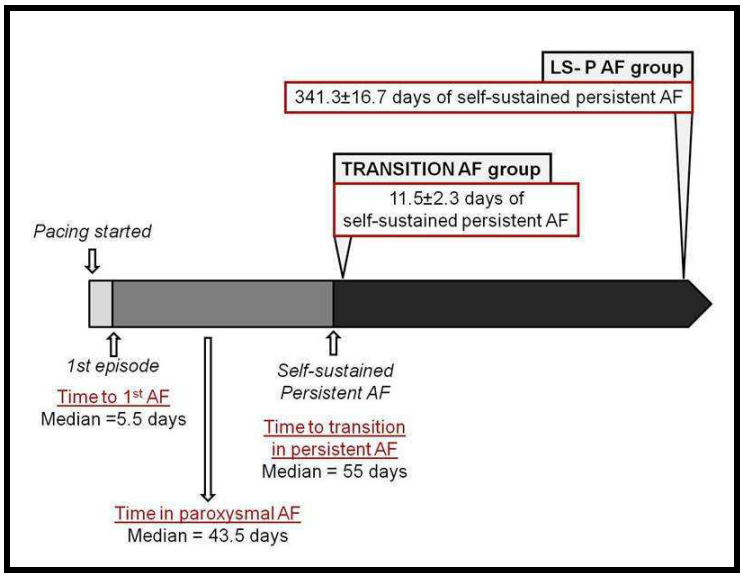

Figure 18 : Schéma représentant le temps nécessaire au développement de la FA, de l'apparition d'épisodes paroxystiques à la transition vers la FA persistante.

Les fréquences dominantes du 1er épisode de FA détecté étaient respectivement de 7.5±0.1 Hz (de 6.5 à 8.25 Hz), 9.0±0.1 Hz (de 8.9 à 9.4 Hz) et 7.7±0.2 Hz (de 6.5 à 9.25 Hz) pour l'OD, l'OG et l'ECG de surface (Figure 19). Comme nous l'avions décrit précédemment,[143] une augmentation significative (p<0.001) de la DF était retrouvée au cours de l'évolution de la FA chez tous les animaux. A la transition de la FA paroxystique à la FA persistante, la DF était ainsi de 10.1±0.4 Hz, 10.7±0.2 Hz et de 10.4±0.4 Hz pour l'OD, l'OG, et l'ECG de surface. Le gradient OG-OD initialement retrouvé au premier épisode (p<0.001) n'était presque plus présent à la transition (p=0.06). Chez le groupe LS-PAF, la DF après 1 an de FA n'augmentait que très discrètement, et de façon non significative (10.9±0.3 Hz, 11.5±0.2 Hz, et 10.9±0.3 Hz ; p=0.1).

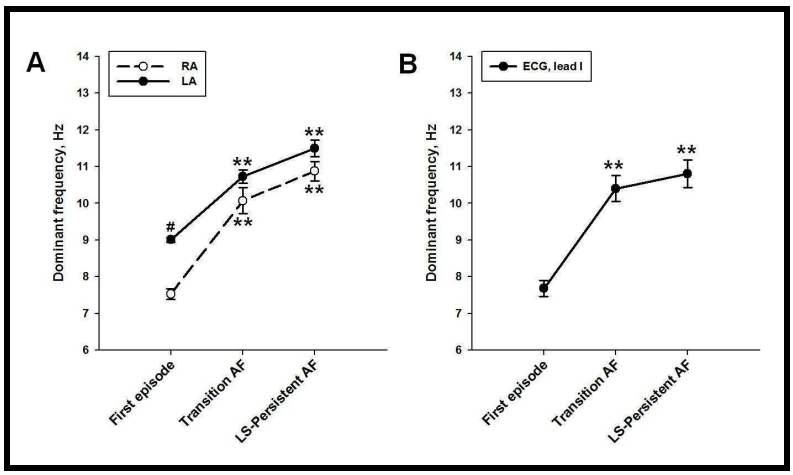

Figure 19 : Evolution des fréquences dominantes des oreillettes droite et gauche, ainsi que de l'ECG de surface (dérivation I) au cours de la progression de la FA.
N=14 for RA, N=8 for LA. #p< 0.001 for RA *vs.* LA, **p< 0.001 *vs.* sham.
LA: left atria; RA: right atria.

Par conséquent nous avons démontré que l'augmentation significative de la DF observée au cours du développement de la FA ne s'effectuait que lors de la période en FA paroxystique, et que celle-ci se stabilisait dès lors que la FA devenait persistante.

b. Prédire la transition vers la FA persistante

La première hypothèse que nous avons émise afin de tenter de prédire le moment de survenue de la transition était qu'il fallait atteindre une DF_{max} « seuil » pour permettre à la FA de s'auto-entretenir et de devenir persistante, comme cela avait été suggéré par Wijffels et al.[11] De façon surprenante, nous n'avons pas observé de telle valeur, la DF à la transition variant grandement selon les animaux de 8 à 12.25 Hz dans l'OD et de 10.1 à 11.4 Hz dans l'OG (Figure 20). Par conséquent, il ne semble pas nécessaire d'atteindre une DF_{max} critique pour passer d'un stade paroxystique à un stade persistant de FA.

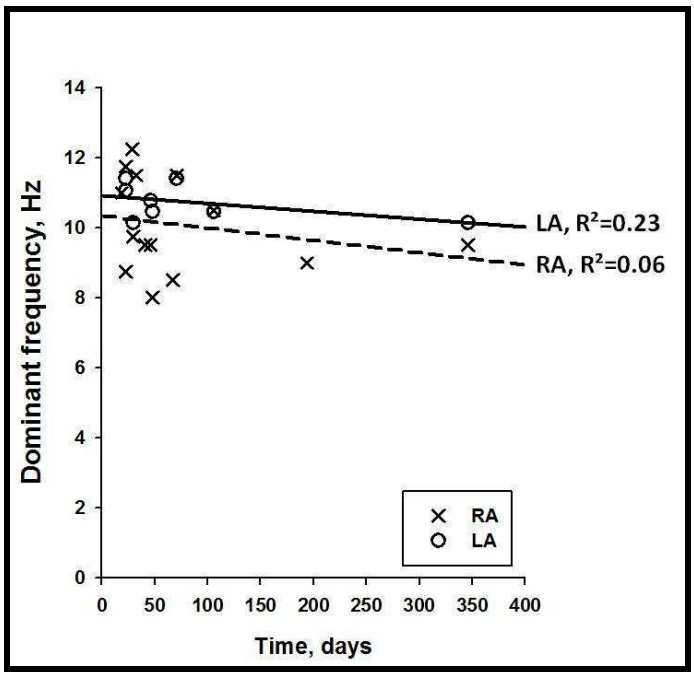

Figure 20 : Relation entre la DF_{max} à la transition et le temps en FA paroxystique. Aucune corrélation n'était mise en évidence entre la DF_{max} à la transition et le temps entre le 1er épisode de FA et la transition vers la FA persistante. LA = left atrium (OG), RA = right atrium (OD).

Cependant, nous avons observé que la pente d'augmentation de la DF_{max} (dDF/dt) était différente pour chaque animal (de 0.003 à 0.15 Hz/jour pour l'OD et de 0.001 à 0.12 Hz/jour pour l'OG), et que celle-ci semblait être corrélée à la vitesse d'apparition d'une forme persistante de FA, puisque ceux ayant une dDF/dt élevée présentaient une transition plus rapide (Figure 21A).

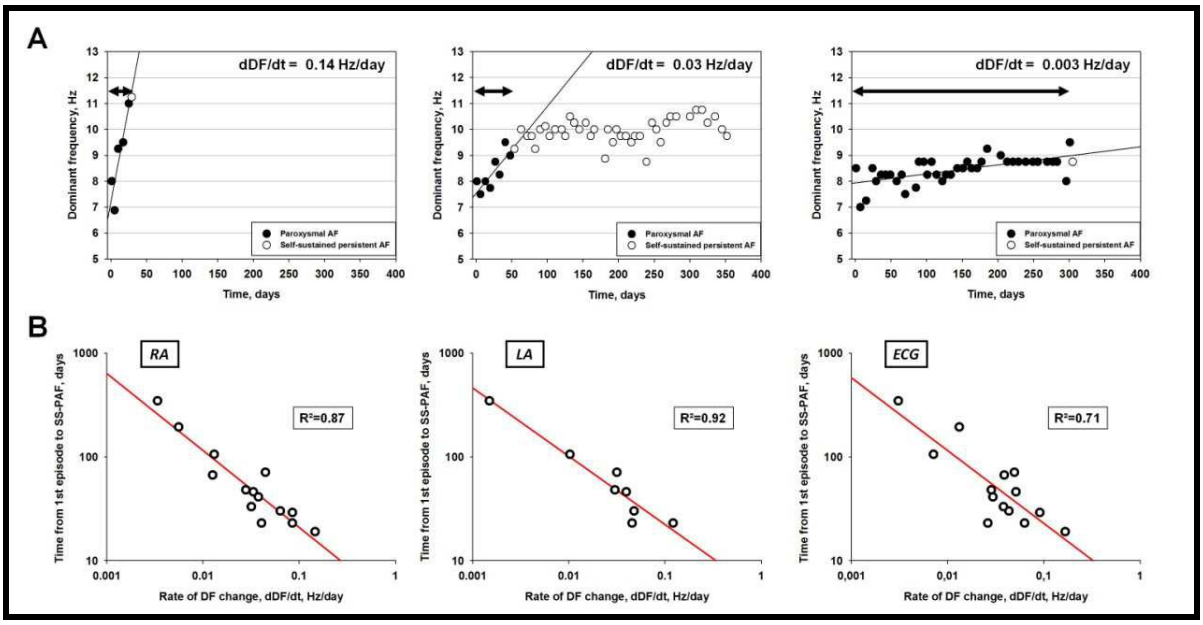

Figure 21 : Augmentation de la fréquence dominante au cours de l'évolution de la FA. A. Graphiques montrant l'évolution de la DF chez 3 moutons au cours de l'histoire de la FA ; les animaux de gauche, du milieu et de droite avaient respectivement une dDF/dt élevée, moyenne et faible. B. Représentation logarithmique de la dDF/dt en fonction du temps en FA paroxystique (entre le 1er épisode et la transition vers la FA persistante). LA = left atrium (OG), RA = right atrium (OD).

La dDF/dt a donc été reportée sur un graphique en fonction de la durée en FA paroxystique (du 1er épisode à la transition) nous permettant de mettre en évidence une forte relation significative entre ces 2 valeurs (Figure 21B). Ainsi, plus la dDF/dt était élevée, plus la FA persistante survenait rapidement. Par ailleurs, une corrélation significative entre les dDF/dt observées sur l'EGM de l'OD, de l'OG et de l'ECG de surface était retrouvée (Figure 22).

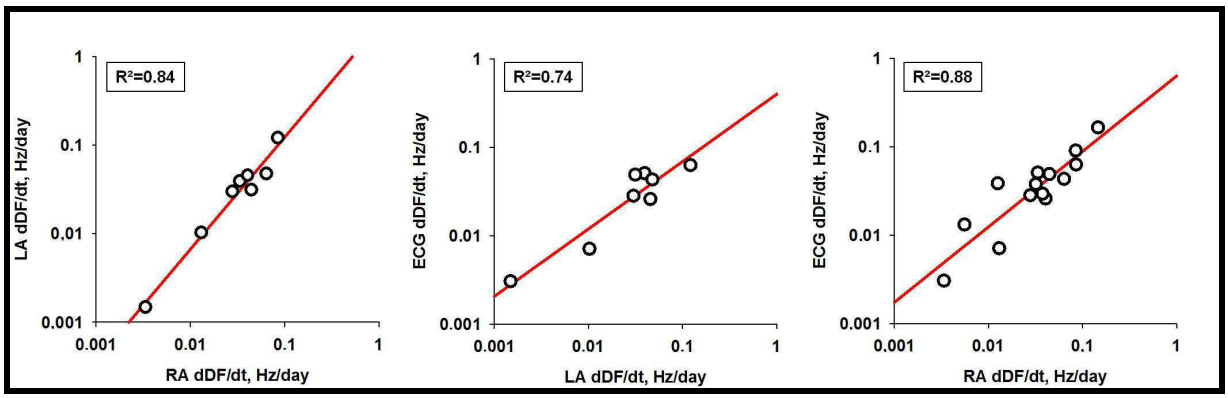

Figure 22 : Corrélations entre les dDF/dt mesurés via la sonde atriale droite, l'enregistreur d'évènements et l'ECG de surface. Une corrélation significative était retrouvée entre les dDF/dt de l'OG et de l'OD (gauche), de l'OG et de l'ECG de surface (centre) et de l'OD et de l'ECG de surface (droite). LA = left atrium (OG), RA = right atrium (OD).

Nous avons donc réussi à démontrer qu'il était possible de prédire la survenue de la transition de la FA paroxystique à la FA permanente en analysant l'augmentation de la DF_{max} au moyen d'un EGM endocavitaire ou d'un ECG de surface.

Si de tels résultats étaient reproduits chez l'homme, ils permettraient de différencier les patients selon leur risque à évoluer précocement ou non vers des formes soutenues de l'arythmie, et de renforcer ainsi le traitement anti-arythmique ou d'envisager précocement une ablation chez ceux ayant une dDF/dt élevée.

c. Remodelage cellulaire et électrophysiologique

Afin de comprendre si l'accélération progressive de la DF pouvait être expliquée par des modifications ioniques et/ou structurelles, nous avons explanté le cœur des moutons après anesthésie au pentobarbital sodique, et prélevé la partie antérieur de l'OD et de l'OG que nous avons séparé en trois fragments (Figure 23) :

- Partie antérieure : pour dissociation cellulaire et analyse électrophysiologique (patch clamp),
- Partie médiane : pour analyse histologique (fibrose),
- Partie postérieure: pour analyse biochimique.

Par ailleurs, la paroi postérieure de l'OG était également prélevée pour analyse histologique et biochimique (pas d'étude électrophysiologique effectuée sur cette partie de l'OG).

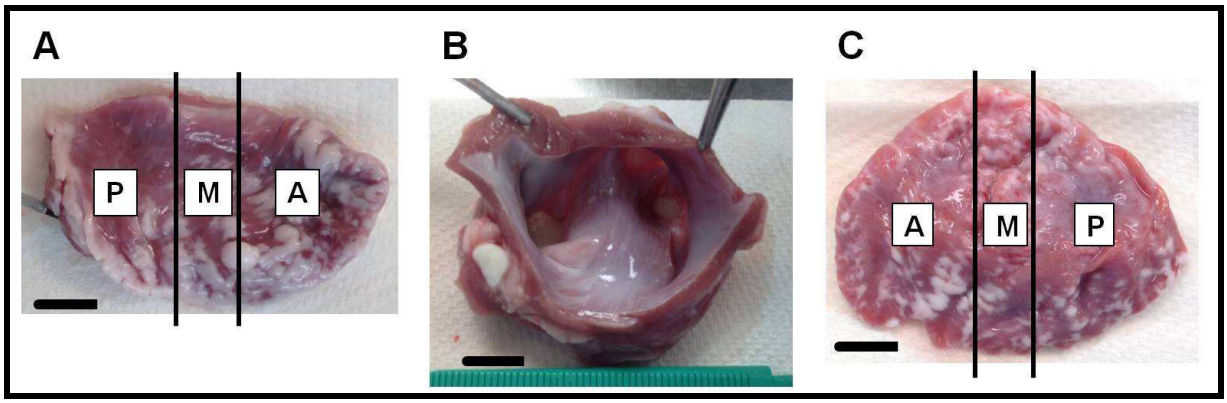

Figure 23 : Photos des parois antérieure de l'OD (A), postérieure (B) et antérieure de l'OG (C) telles qu'elles étaient prélevées chez les moutons dans notre étude. L'OG et l'OD étaient séparées en 3 fragments (P = postérieur, M = médian, A = antérieur) pour analyse ultérieure. Barre d'échelle = 1cm.

La première étape à l'analyse électrophysiologique était l'isolation cellulaire effectuée par digestion enzymatique à la collagénase et à la protéase. Une fois les cellules dissociées, elles étaient resuspendues dans une solution de KB avant utilisation (pour analyse du PA et des courants sodique, calcique et potassique).

L'analyse des PA a démontré que ceux-ci étaient déjà significativement plus courts dans les deux oreillettes au stade de la transition, et que plus aucun raccourcissement significatif n'était observé au cours de l'année de suivi en FA persistante (Figure 24). Les

animaux en FA, quelque soit son stade évolutif, montraient une tendance à une légère dépolarisation du potentiel transmembranaire de repos, pour l'OD (respectivement -69.8±2.8 mV, -60.2±3.4 mV and -57.6±4.6 mV) comme pour l'OG (respectivement -72.1±4.1 mV, -66.6±3.6 mV and -63.5±2.3 mV).

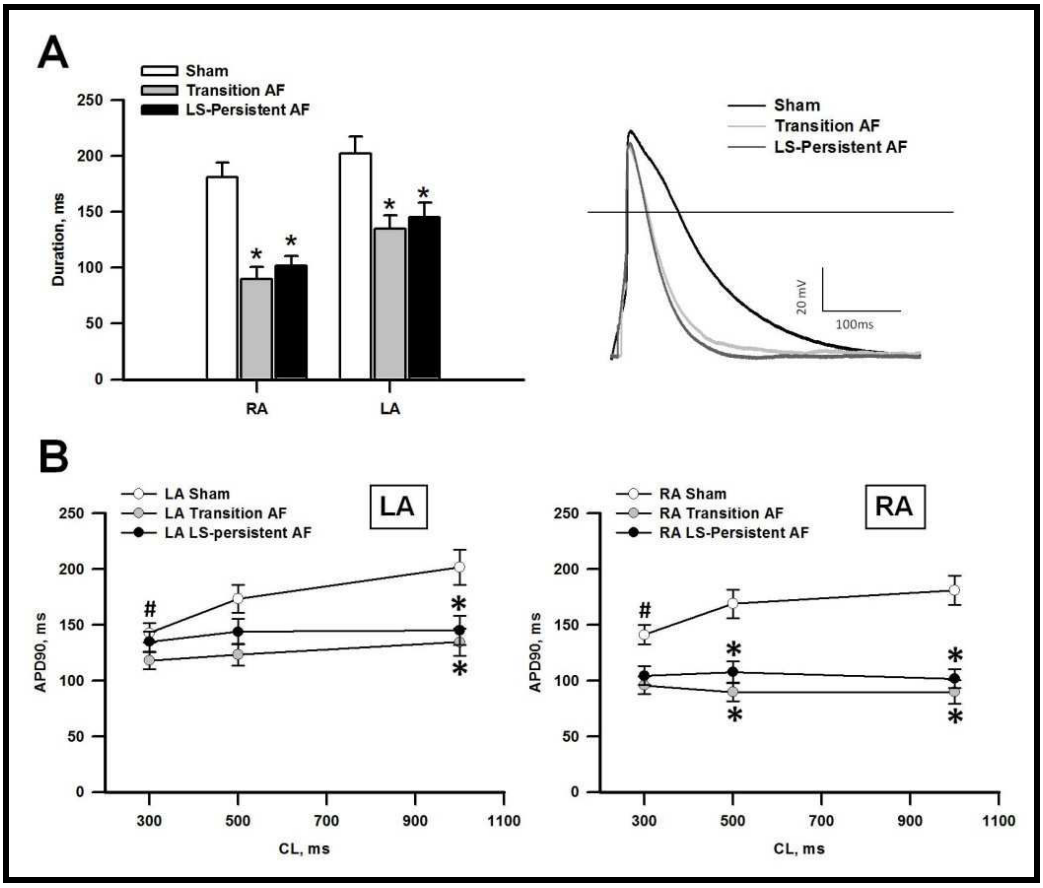

Figure 24 : Analyse des PA et de leur caractère fréquence-dépendant. A. Durée des PA à une fréquence de stimulation de 1Hz (durée à 90% de la durée totale du potentiel d'action APD_{90}). Pour l'OD : N=3/n=13 (contrôles), N=3/n=13 (transition), N=3/n=14 (LS-PAF) ; pour l'OG : N=3/n=18 (controles), N=3/n=14 (transition), N=3/n=18 (LS-PAF). *p<0.05. A droite: potentiels d'action gauches représentatifs. B. Fréquence-dépendance de l'APD_{90}. Pour l'OD : N=3/n=13 (contrôles), N=3/n=13 (transition), N=3/n=14 (LS-PAF) ; pour l'OG : N=3/n=18 (contrôles), N=3/n=14 (transition), N=3/n=18 (LS-PAF). *p<0.05 *vs.* contrôles pour la même fréquence de stimulation. #p<0.05 *vs.* fréquence de stimulation à un cycle de 1000ms.

Afin de comprendre ces modifications de durée du PA, nous avons étudié les densités des principaux courants dépolarisants (I_{Na}, I_{CaL}) et repolarisants (I_{K1}, I_{to}) des cardiomyocytes.

Le pic du courant entrant sodique (I_{Na}, Figure 24) était significativement réduit d'environ 50% à la transition pour les myocytes gauches, et d'environ 30% pour les myocytes droits, responsables à ce stade d'un gradient gauche-droit. Après 1 an en FA persistante, une réduction similaire dans les 2 oreillettes de 50% d'I_{Na} était retrouvée (p<0.001 vs. groupe contrôle). De façon semblable, le pic du courant calcique lent (I_{CaL}, Figure 24) était réduit à la transition et après 1 ans en FA persistante (p<0.05). Ces modifications d'I_{Na} et d'I_{CaL} résultaient d'une diminution de l'expression des canaux Nav1.5

et Cav1.2, eux-mêmes secondaires à une diminution des taux d'ARNm de SCN5A et CACNA1C mRNA.

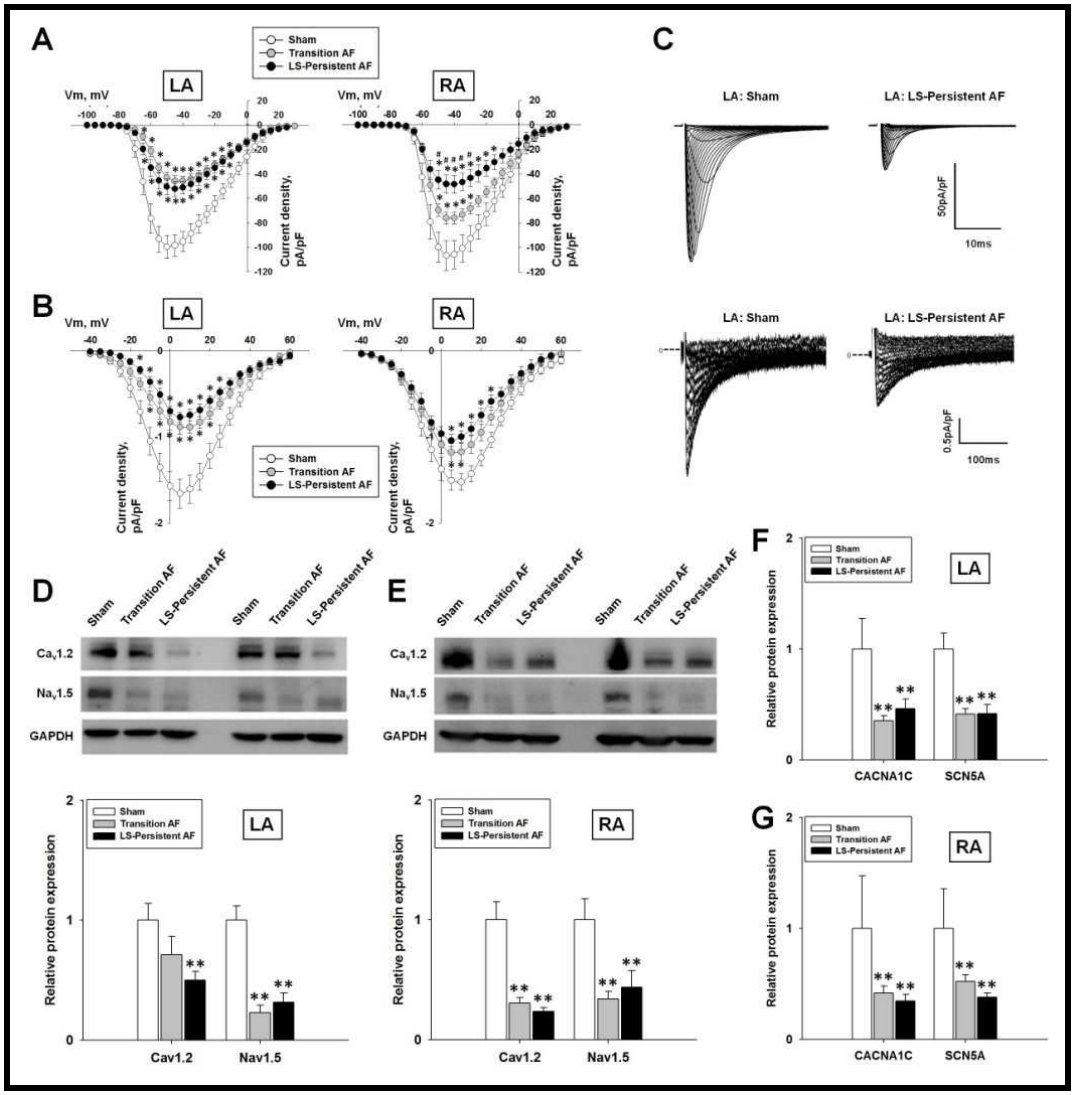

Figure 24 : La FA entraîne une diminution de la densité des courants I_{Na} et I_{CaL}. A. Courbes courant-voltage pour I_{Na} pour les cardiomyocytes de l'OG (gauche) et de l'OD (droite). Pour l'OG : N=3/n=12 (contrôles), N=4/n=21 (transition), N=5/n=21 (LS-PAF) ; pour l'OD : N=3/n=10 (contrôles), N=4/n=18 (transition), N=5/n=18 (LS-PAF). *p<0.05 *vs.* contrôles, #p<0.05 *vs.* transition. B. Courbes courant-voltage pour I_{CaL} pour les cardiomyocytes de l'OG (gauche) et de l'OD (droite). Pour l'OG : N=3/n=13 (contrôles), N=4/n=17 (transition), N=4/n=11 (LS-PAF) ; pour l'OD : N=3/n=12 (contrôles), N=4/n=16 (transition), N=4/n=14 (LS-PAF). *p<0.05 *vs.* contrôles. C. Tracés représentatifs d'I_{Na} et d'I_{CaL} de cardiomyocytes de l'OG d'un animal contrôle en en LS-PAF. D-E. Quantification protéique de Na$_v$1.5 et Ca$_v$1.2 par western blot sur les tissus atriaux gauche (D) et droit (E), (quantification par rapport à l'expression de la GAPDH, N=6, **p<0.01 *vs.* contrôles). F-G : Analyse de l'expression génique par RT-PCR de *SCN5A* et de *CACNA1C* sur les tissus atriaux gauche (F) et droit (G), (quantification par rapport à l'expression de la GAPDH, N=6, **p<0.01 *vs.* contrôles).

A l'opposé, la densité du courant potassique à rectification entrante (I_{K1}, Figure 25) était multipliée par 2 à 3 à la transition au niveau des 2 oreillettes, et augmentait encore en densité après 1 an de FA (p<0.05 vs. groupe contrôle). Cette augmentation résultait d'une surexpression du canal Kir2.3.

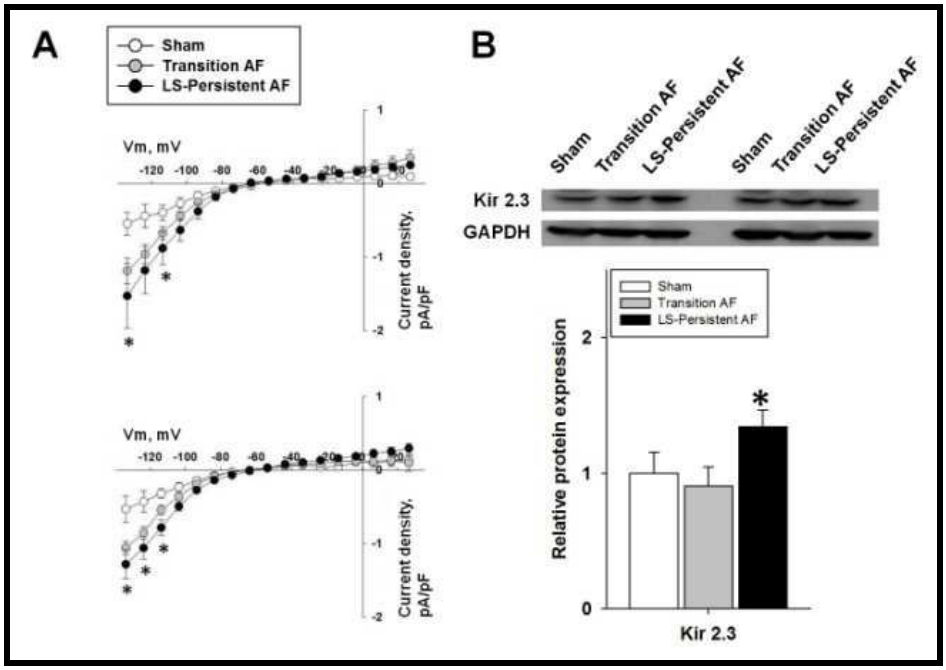

Figure 25 : La FA entraîne une augmentation de l'expression de Kir2.3. A. Courbes courant-voltage pour I_{K1} pour les cardiomyocytes de l'OG (haut) et de l'OD (bas). Pour l'OG : N=3/n=7 (contrôles), N=5/n=10 (transition), N=2/n=4 (LS-PAF) ; pour l'OD : N=3/n=6 (contrôles), N=3/n=10 (transition), N=3/n=9 (LS-PAF). *p<0.05 *vs.* contrôles. B. Quantification protéique de Kir2.3 par western blot sur le tissu atrial gauche (quantification par rapport à l'expression de la GAPDH, N=6, **p<0.05 *vs.* contrôles).

Le courant potassique transitoire sortant (I_{to}) était réduit de près de 85% à la transition et après 1 an de FA (p<0.001). L'expression de Kv11.1 (HERG) était quant-à elle inchangée (Figure 26).

d. La FA persistante entraine une dilatation atriale et une hypertrophie myocytaire

Alors qu'aucune modification de la fraction d'éjection du ventricule gauche (FEVG) n'était mise en évidence au cours du suivi (éliminant tout processus de « tachycardiomyopathie »), une dilatation biatriale progressive était observée, débutant une fois la transition survenue, mais n'étant significativement différent qu'après un an de suivi en FA persistante (p<0.05, Figure 27).

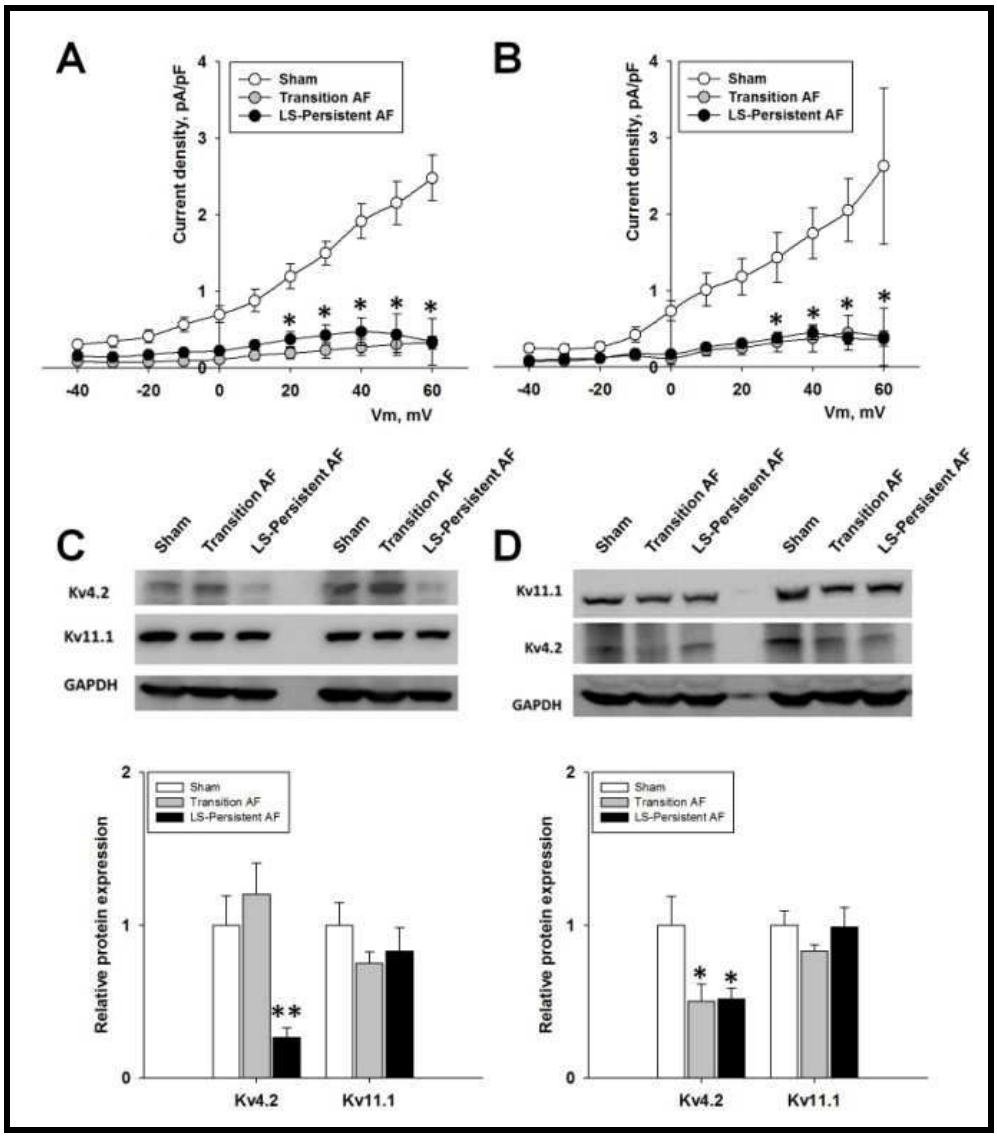

Figure 26 : La FA réduit l'expression du courant potassique sortant transitoire (I_{to}) sans entraîner de modification de hERG. A-B Courbes courant-voltage pour I_{to} pour les cardiomyocytes de l'OG (A) et de l'OD (B). Pour l'OG : N=2/n=6 (contrôles), N=3/n=510 (transition), N=6/n=10 (LS-PAF) ; pour l'OD : N=2/n=6 (contrôles), N=3/n=5 (transition), N=3/n=5 (LS-PAF). *p<0.05 *vs.* contrôles pour les groupes transition et LS-PAF. C-D : Quantification protéique de K_v4.2 et de K_v11.1 par western blot sur les tissus atriaux gauche (C) et droit (D) (quantification par rapport à l'expression de la GAPDH, N=6, **p<0.05 et **p<0.01 *vs.* contrôles).

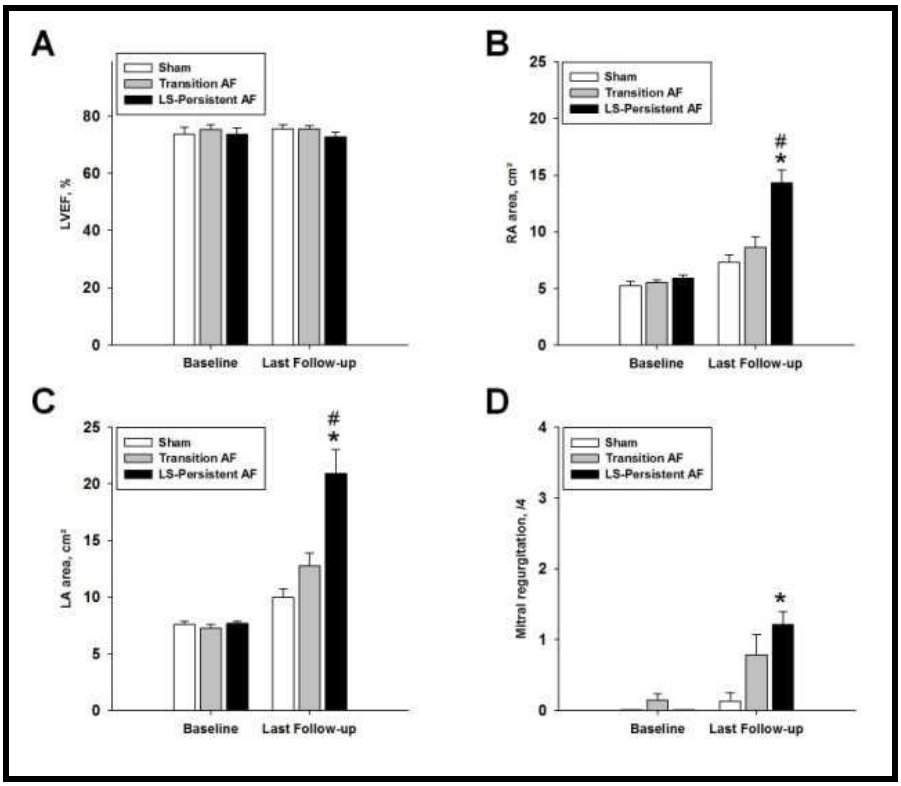

Figure 27 : Modifications échocardiographiques objectivées au cours du suivi. A : La FEVG ne s'altérait pas au cours du suivi des animaux en FA. B-C : Une dilatation atriale droite (B) et gauche (C) était mise en évidence dans le groupe LS-PAF uniquement. D : Une insuffisance mitrale significative était mise en évidence au stade de LS-PAF. *p<0.05 *vs.* contrôles, p<0.05 *vs.* transition, avec respectivement N=6, N=7 et N=7 pour les groupes contrôle, transition et LS-PAF.

A l'échelon cellulaire, comme le montre la Figure 28, les longueurs et largeurs des myocytes atriaux droits et gauches étaient similaires pour les animaux du groupe contrôle. A la transition, les myocytes atriaux gauches étaient significativement plus longs et plus larges qu'à l'état de base (respectivement p<0.001 and p<0.01) ; aucune modification significative n'était observée pour les droits, et par conséquent, à la transition, une différence significative en terme de longueur était observée entre les myocytes atriaux gauches et droits (p<0.001). Après un an en FA persistante, aucune nouvelle modification n'était survenue pour les myocytes gauches, alors que les droits s'étaient significativement élargis (p<0.001). Par conséquent, au stade de FA persistante de longue durée, les myocytes atriaux gauches étaient significativement plus longs (p=0.002) et plus fins (p=0.001) que les droits.

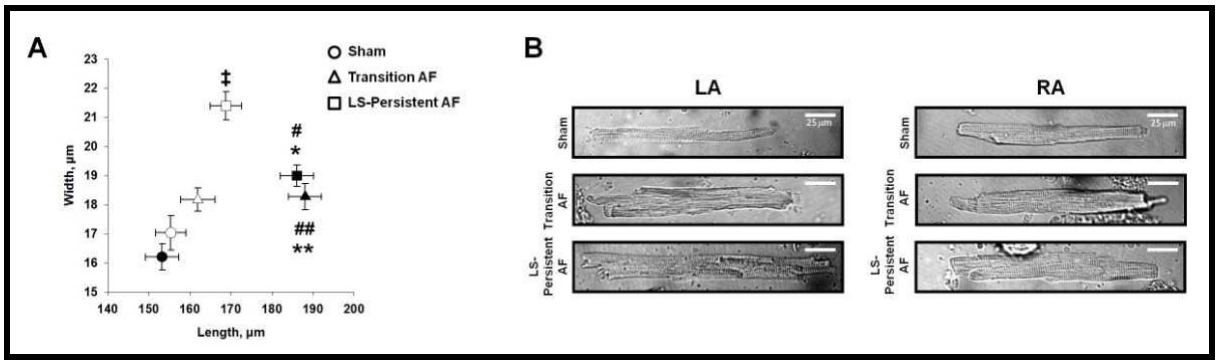

Figure 28 : La FA entraine une hypertrophie myocytaire. A : Longueurs et largeurs moyennes des cardiomyocytes droits (blanc) et gauches (noir). N=3/n=60 (contrôles), N=4/n=70 (transition) et N=5/n=90 (LS-PAF). B : Photographies représentatives pour chacun des stades évolutifs de la FA. Pour l'OD : ‡p=0.01 *vs.* contrôles pour la largeur. Pour l'OG au stade de transition et LS-PAF : *p=0.01 et **p<0.001 *vs.* contrôles respectivement pour la largeur et la longueur des cardiomyocytes, #p<0.001 et ##p=0.002 *vs.* LS-PAF respectivement pour la largeur et la longueur des cardiomyocytes.

Sur le plan de la matrice extra-cellulaire, une augmentation significative de la fibrose interstitielle était observée dans l'oreillette gauche (de 5.5±1.2 à 10.7±1.5%, p<0.05) et la paroi postérieure (de 4.1±0.6 à 14.6±1.4%, p<0.001), particulièrement au stade de FA persistante (Figure 29, A et B). Ces données étaient corrélées aux taux sériques de PIIINP (Procollagen III N-terminal propetide, un marqueur sanguin de la dégradation du collagène) et au niveau tissulaire de collagène III et d'α-SMA (actine des cellules musculaires lisses, Figure 29C et D).

e. Remodelage calcique

Une analyse biochimique par Western blot de 5 protéines impliquées dans l'homéostasie calcique (RyR2, Ca^{2+} ATPase du réticulum sarcoplasmique = SERCA, phospholamban = PLN, échangeur Na^{+}-Ca^{2+} = NCX et la protéine kinase II dépendante de la calmoduline/ Ca^{2+} = CaMKII) a été effectuée dans les OD et les OG, dans chacun des trois groupes. Comme illustré dans la figure X, SERCA, le PLN, et la CaMKII étaient soit diminués, soit inchangés, alors que le NCX était augmenté dans l'OG uniquement. De plus, la phosphorylation de RyR2 n'était pas affectée, et le ratio RyR2 phosphorylé/ RyR2 total était inchangé. L'ensemble de ces résultats suggèrent que dans ce modèle de FA, un mécanisme de fuite calcique et d'activités déclenchées (post-dépolarisations tardives) n'est pas impliqué dans la transition de la FA paroxystique à persistante.

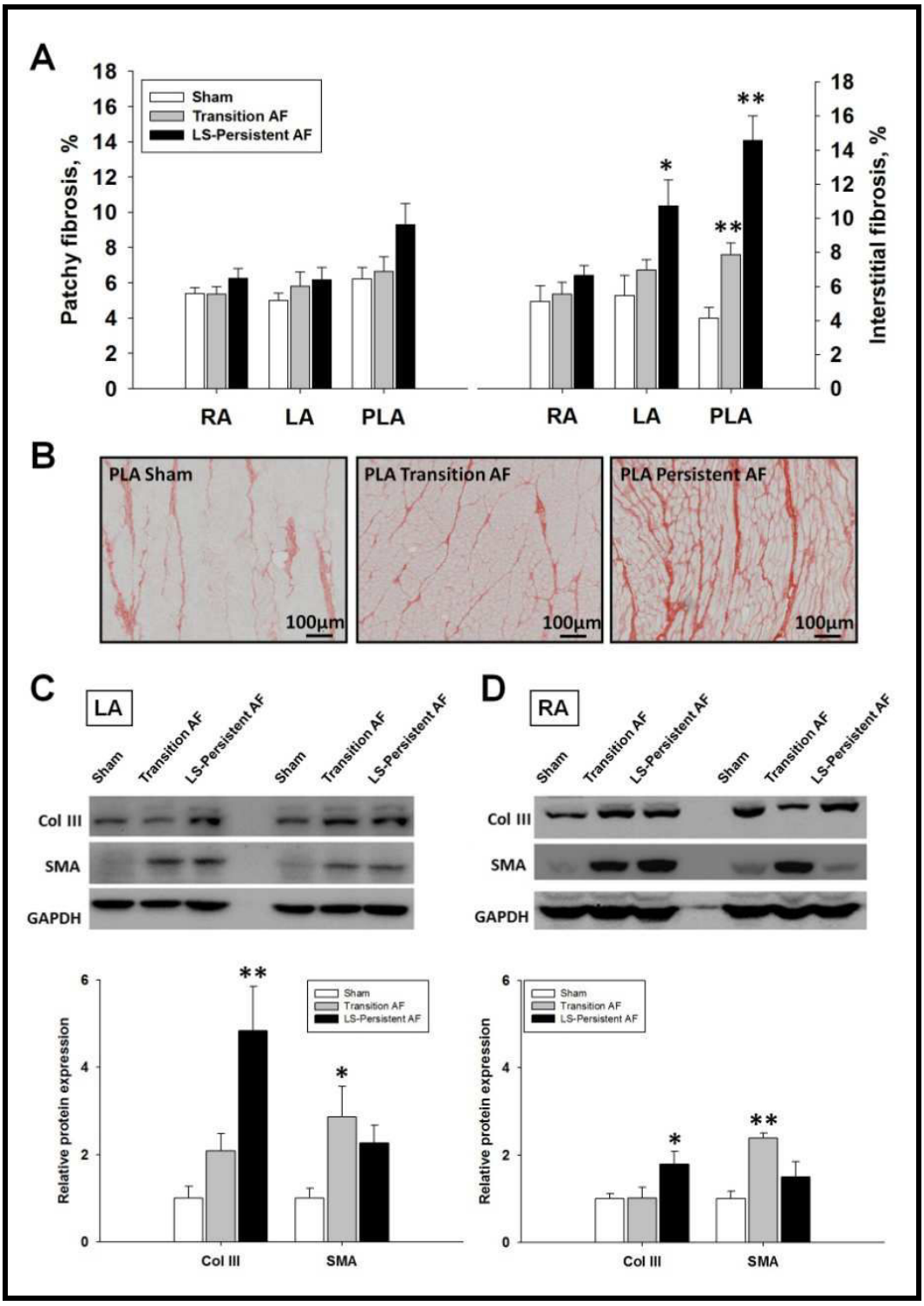

Figure 29 : Remodelage structurel induit par la FA.

A. Fibrose en patch (gauche) et fibrose interstitielle (droite) dans l'OD (RA), l'OG (LA) et la paroi postérieure de l'OG (PLA) dasn le groupe contrôle (Sham, N=6), Transition (N=7) et LS-PAF (N=7) ; *p<0.05, **p<0.001 *vs.* Sham. B : Images représentatives de la paroi postérieure (rouge sirius). C et D : Expression tissulaire de l'actine musculaire lisse (α-smooth muscle actin = SMA) et du collagène III (Col III) dans l'OG et l'OD analysées par Western blots. N=6 dans chaque groupe. *p<0.05, **p<0.01 *vs.* Sham.

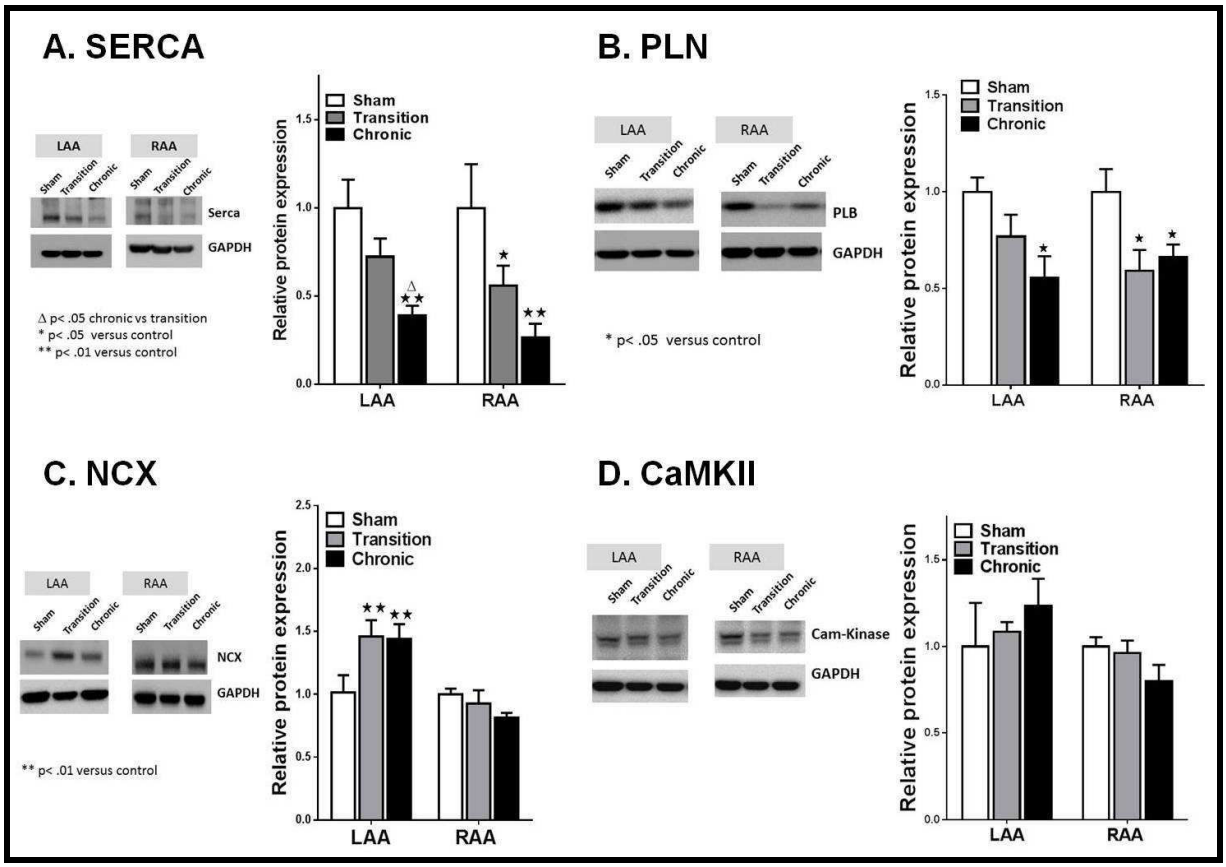

Figure 30 : Modifications des protéines impliquées dans l'homéostasie calcique. Analyse par Western Blot de SERCA (A), du phospholamban (B), du l'échangeur Na^{+}-Ca^{2+} (C) et de la CaMKII (D).

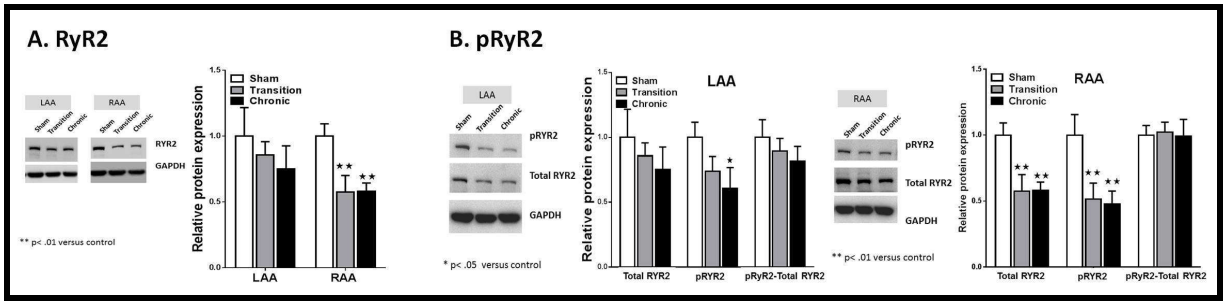

Figure 31 : Modifications de RyR2. Analyse du RyR2 total et sa fraction phosphorylée.

f. Les modifications ioniques peuvent-elles expliquer l'accélération de fréquence ?

Comme nous l'avons vu, les modifications électrophysiologiques apparaissent pendant la période de FA paroxystique, alors que le remodelage structurel ne se met en place qu'une fois survenue la transition vers la FA persistante. Afin de vérifier si l'ensemble des modifications observées pouvaient expliquer l'accélération de DF constatée in-vivo chez les animaux, nous avons mené une série de modélisations informatiques en utilisant le modèle de potentiel d'action atrial humain de Grandi-Pandit récemment publié dans Circulation

Research.[166] Trois situations ont été modélisées : 1) une situation « contrôle » ; 2) un modèle de « transition FA paroxystique – FA persistante » intégrant l'ensemble des modifications électrophysiologiques observées dans les moutons du groupe Transition ; et 3) un modèle de « FA paroxystique » généré de façon empirique en créant une situation intermédiaire entre le groupe contrôle et le groupe Transition.

A la transition, l'APD90 était significativement réduit (-62%) par rapport à ceux de la FA paroxystique (-18%). Parallèlement, une hyperpolarisation de -2mV était observée à la transition, responsable d'une augmentation de la disponibilité des canaux sodiques et d'une hyperexcitabilité tissulaire (Figure 32A).

Un modèle bidimensionnel de réentrée a été utilisé afin de générer des rotors et d'étudier leurs propriétés (Figure 32B). Lors de la FA paroxystique, ces derniers étaient non soutenus, montraient une fréquence de rotation lente (5.0Hz), étaient peu stables et disparaissaient par collision sur un des bords du modèle 2D (Figure 32C). À l'inverse, dans le modèle de transition, les rotors étaient plus stables dans le temps et l'espace et avaient une fréquence de rotation significativement plus élevée (7.67Hz). Lorsque la réduction d'I_{Na} n'était pas incorporée au modèle, la nouvelle augmentation de DF_{max} n'était que discrète (8.67Hz) et les rotors générés étaient instables et disparaissaient après quelques rotations.

Chacune des modifications ioniques objectivées par nos expériences de patch clamp a été modélisée séparément afin d'en comprendre l'impact dans la réduction de la durée du potentiel d'action :

- ainsi, nous retrouvé qu'une augmentation de 100% d'I_{K1} hyperpolarisait les cardiomyocytes de -2mV, réduisait la durée du PA de 23% et permettait de générer des rotors ayant une fréquence de rotation lente de 4.7Hz ;
- une diminution d'I_{CaL} de 30% (comme cela est supposé lors des premiers épisodes de FA paroxystique) réduisait l'APD_{90} de 37% et engendrait des rotors de 4.7Hz (Figure 33A); lorsqu'I_{CaL} était réduit de 65%, tel que nous l'avons observé au stade de transition, l'APD_{90} était drastiquement réduit (environ 64%), permettant alors d'atteindre une fréquence de rotation des rotors de 8.0Hz (Figure 33B);
- la diminution d'I_{to} de 75% telle qu'observée au stade de transition n'avait quant-à-elle qu'un effet négligeable sur la durée du potentiel d'action et s'accompagnait de rotors lents (3.38Hz) et instables ;
- enfin, une diminution de 50% d'I_{Na} résultait également en des rotors lents (3.8Hz) et instables.

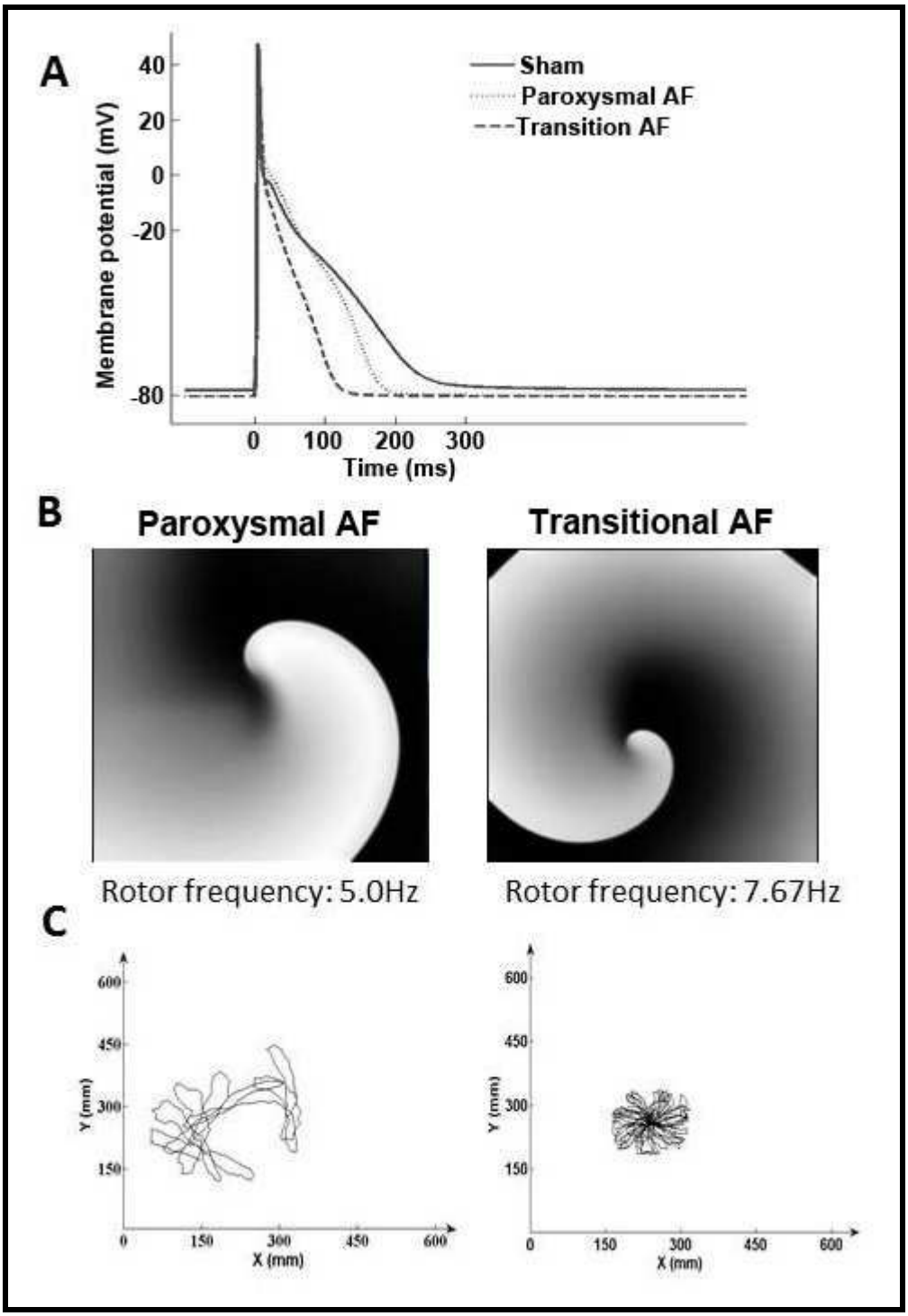

Figure 32 : Prédiction de l'effet du remodelage électrophysiologique sur la fréquence des rotors en FA. A. Potentiels d'action dans une situation contrôle (Sham), à la transition et en FA paroxystique en modifiant expérimentalement les courant ioniques du modèle d'après les enregistrements effectués en patch-clamp. Un raccourcissement du PA associé à une hyperpolarisation de 2 mV est retrouvé uniquement à la transition, et très peu au stade paroxystique. B-C : Rotors générés dans une situation de FA paroxystique (B) et à la transition vers la FA persistante (C). En FA paroxystique, la fréquence de rotation est faible et les cores très mobiles, rendant la probabilité de collision avec obstacle, et par conséquent l'extinction du rotor, élevés. A l'opposé, à la transition, les rotors apparaissent plus stables, sont plus rapides et persistent tout au long de la simulation.

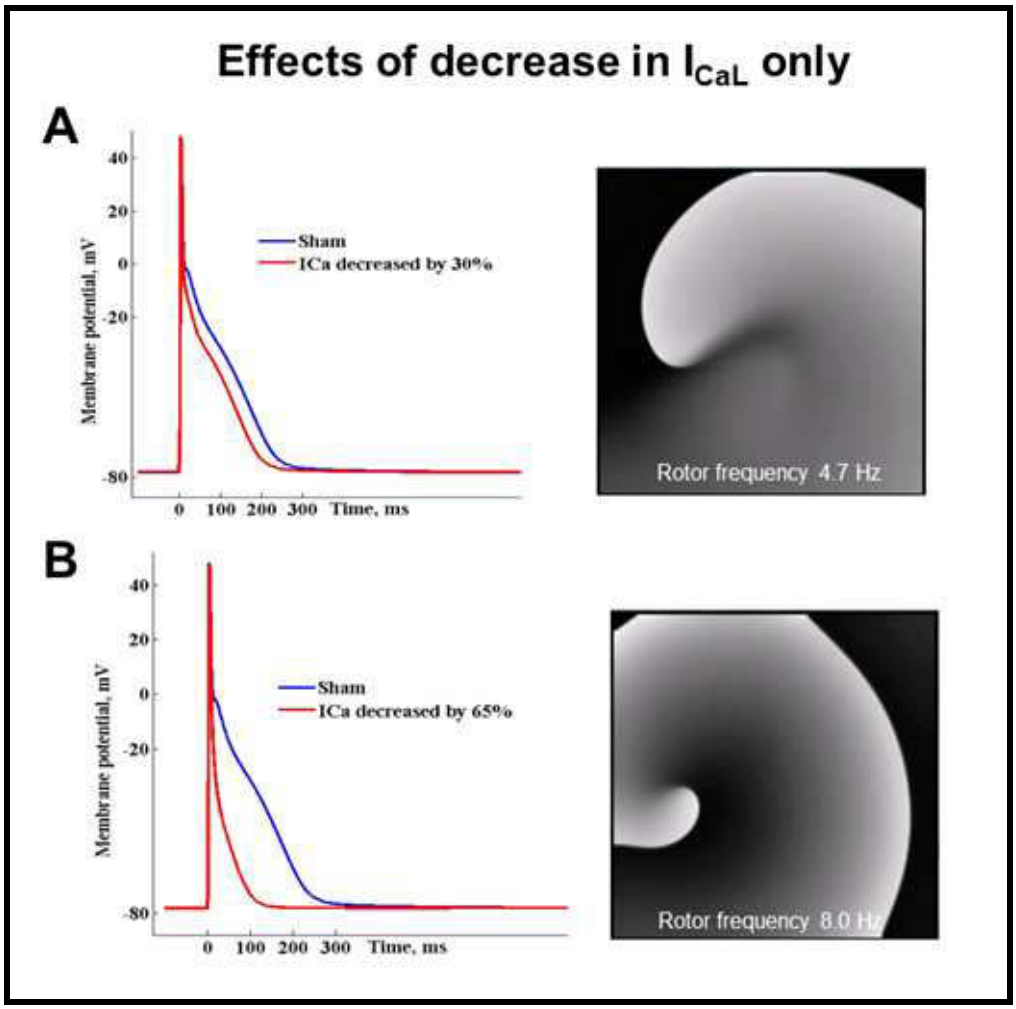

Figure 33. Effet de la réduction isolée d'I_{CaL} sur la durée du PA et sur la fréquence de rotation des rotors. A. Lorsque qu'I_{CaL} est réduit de 30%, le PA n'est que très peu raccourcit (37%) et les rotors générés sont lents et instables. B. Lorsque qu'I_{CaL} est réduit de 65%, telle que nous l'avons observé chez nos animaux au stade de transition, la fréquence de rotation est élevée (8.0Hz) et les rotors sont stables.

Par conséquent, nos simulations ont démontré qu'à la transition FA paroxystique - FA persistante, le raccourcissement du PA secondaire majoritairement à la diminution d'I_{CaL} et à une moindre mesure d'I_{K1}, associé à l'hyperpolarisation membranaire étaient responsables d'une hyperexcitabilité tissulaire rendant les rotors plus stables et plus rapide.

g. Mécanismes expliquant la variabilité interindividuelle dans la transition de la FA

Afin de comprendre pourquoi certains animaux transitaient lentement et d'autres rapidement vers la FA persistante, nous avons comparé les caractéristiques électrophysiologiques et structurelles de leurs oreillettes en les séparant selon le temps nécessaire à la transition (< 45 jours : 4 moutons, et > 45 jours : 3 animaux, nombre de jours correspondant au temps médian de transition).

Comme cela est démontré dans les Figures 34 et 35, la dDF/dt était significativement plus élevée chez les animaux progressant rapidement vers la FA persistante (p=0.005 pour l'OG), sous-groupe qui par ailleurs montraient des PA significativement plus courts, probablement en rapport avec une tendance à la diminution d'I_{CaL}. La densité d'I_{K1}, tout comme la dilatation atriale (124% *vs.* 45% d'augmentation de l'aire atriale gauche, p=0.014) était plus importantes chez les animaux progressant lentement vers la FA persistante. Le pourcentage de fibrose, la taille des cardiomyocytes et le poids des oreillettes après explantation étaient par ailleurs similaires entre les 2 groupes.

En conclusion, le principal facteur permettant de différencier les animaux en termes de rapidité de progression vers la FA persistante est le raccourcissement du PA lié à la diminution de la densité d'I_{CaL}. A l'opposé, les animaux progressant lentement n'ont probablement pas un remodelage électrophysiologique suffisant pour permettre la transition et nécessitent une augmentation supplémentaire d'I_{K1} ainsi qu'un remodelage structurel plus important pour permettre aux épisodes de FA de devenir soutenus.

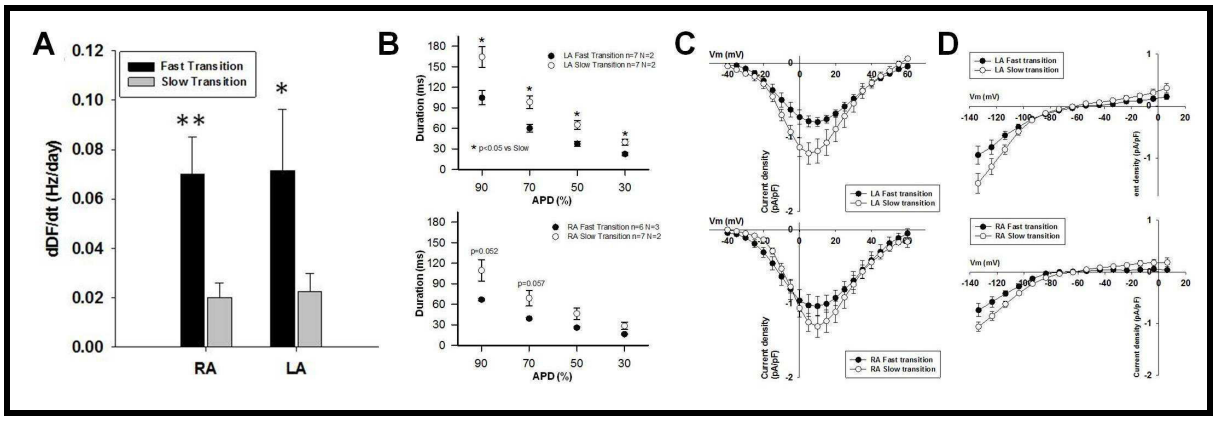

Figure 34. Différences de remodelage électrophysiologique entre les animaux passant rapidement (Fast transition) ou lentement (Slow transition) en FA persistante. Comme attendu, la dDF/dt était retrouvée plus élevée chez animaux transitant rapidement en FA persistante (A). Sur le plan électrophysiologique, un raccourcissement significativement plus important de la durée du PA (B), lié à une diminution plus importante d'I_{CaL} était mise en évidence (C). A l'opposé, une augmentation plus importante d'I_{K1} (D) était retrouvée chez les animaux progressant lentement en FA persistante.

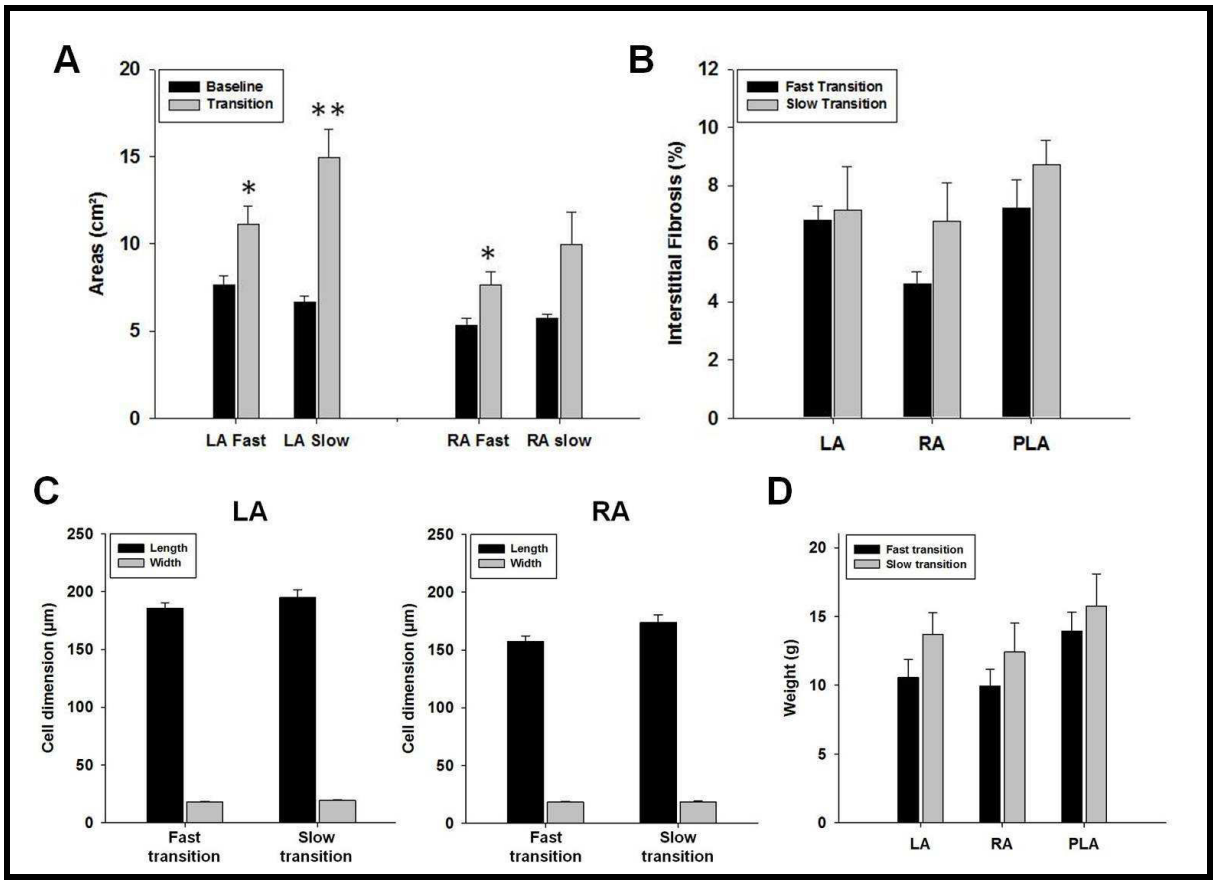

Figure 35. Différences de remodelage structurel entre les animaux passant rapidement (Fast transition) ou lentement (Slow transition) en FA persistante. Une dilatation atriale significativement plus marqué était retrouvée chez les animaux transitant lentement en FA persistante (A). Aucune différence significative n'était retrouvée en termes de fibrose (B), de dimensions cellulaires (C) et de poids des oreillettes (D).

4. Discussion

Les principaux résultats de cette étude sont : 1) la stimulation atriale rapide chez le mouton résulte en un FA dont les épisodes deviennent de plus en plus soutenus jusqu'à ce que l'arythmie devienne persistante ; 2) la DF_{max} augmente progressivement pendant le temps en FA paroxystique et se stabilise au moment où l'arythmie devient persistante ; 3) l'accélération de la DF_{max} (dDF/dt) est corrélée au temps passé en FA paroxystique avant la transition ; 4) un raccourcissement du PA, secondaire à des modifications ioniques (par diminution de l'expression génique de $Na_v1.5$, de $Ca_v1.2$ et de Kv4.2 ; augmentation de l'expression génique de Kir2.3) est déjà présent à la transition et explique l'accélération de la DF_{max} ; 5) une dilatation atriale progressive, une régurgitation mitrale, une hypertrophie myocytaire et une fibrose atriale apparaissent secondairement, en l'absence de toute dysfonction ventriculaire gauche, une fois que la DF_{max} s'est stabilisée. L'ensemble de ces résultats démontre donc que l'accélération de la DF_{max} reflète les modifications du PA et des densités d'I_{Cal}, I_{K1}, I_{Na} et I_{to}. Par ailleurs, il s'agit de la première caractérisation détaillée du remodelage

électrophysiologique et structurel impliqué dans la transition de la FA paroxystique à persistante et au stade de FA persistante de longue durée.

a. Modifications de la DF en FA

Différentes études animales ont démontré la présence d'une distribution spatiale de la DF en FA. Des gradients de fréquence gauche-droite ont été retrouvés sur des cœurs de moutons isolés, étayant l'hypothèse que la FA résulte de la présence de sources rapides localisées dans l'OG.[28] Ces gradients ont également été confirmés chez l'homme,[135, 136] principalement lors d'épisodes de FA paroxystique, mais moins fréquemment chez des patients présentant des formes soutenues de l'arythmie, puisque celle-ci entraine un remodelage atrial substantiel permettant aux sources de la FA (rotor, vaguelettes multiples, …) de se localiser dans les deux oreillettes.[134-136] Par ailleurs, les patients en FA persistante ont des DF habituellement plus élevées que ceux en FA paroxystique.[136]

Dans notre précédente étude, nous avons démontré sur un modèle ovin de FA qu'une augmentation progressive de la DF survenait au cours des 2 premières semaines de l'arythmie.[143] Or, nous avons utilisé un algorithme de stimulation alternant 30 secondes de stimulation suivies de 10 secondes de blanking, alternance maintenue pendant une durée de 20-24 semaines, que l'oreillette soit en FA ou non. Par conséquent, l'augmentation de DF observée lors des 15 premiers jours, très similaire d'un animal à l'autre, était probablement « accélérée » par la persistance de la stimulation atriale rapide malgré l'apparition de la FA.
Par conséquent, nous avons souhaité réaliser un modèle de FA plus proche de ce qui est observé en clinique, et transformé la période de 10 secondes de blanking en une période de détection de l'activité atriale. Dans ce modèle, la stimulation atriale n'est réinitiée qu'en l'absence de détection de FA. En utilisant cet algorithme, nous avons observé une augmentation de la DF_{max} différente pour chaque animal, se mettant en place progressivement sur une durée de 4 à 50 semaines. Le premier épisode était lent, et la DF s'accélérait progressivement pendant le temps en FA paroxystique, atteignant sa valeur maximale à la transition vers la FA persistante. Une fois survenue la FA persistante, plus aucune augmentation de DF_{max} n'était observée pendant l'année de suivi.

L'augmentation progressive de la DF_{max} en FA paroxystique est une conséquence du remodelage électrophysiologique. La FA va entrainer un raccourcissement du PA et de la période réfractaire atriale, diminuant la longueur des ondes de fibrillation et facilitant l'accélération et la stabilisation des réentrées. Les principaux déterminants du raccourcissement du PA sont la diminution de la densité d'I_{CaL} et l'augmentation de celle d'I_{K1}.[167, 168] Sur un modèle canin de stimulation atriale rapide continue, le raccourcissement du PA était retrouvé dès le 1er jour, et atteignait son maximum au bout de 7 jours.[142] Sur le plan électrophysiologique, une diminution des densités d'I_{CaL} et d'I_{to} étaient mises en évidence, sans modifications d'I_{K1} toutefois. Cependant, le remodelage atrial survenant chez l'homme en conséquence de la FA est autrement plus complexe et provoque une diminution d'I_{to1}[169] et d'I_{Kur}[169] et une augmentation d'$I_{Ks,}$[169] d'I_{K1} et d'I_{KAch}.[73] La contribution de ces différentes modifications ioniques dans le raccourcissement du PA chez l'homme ont été analysées sur des simulations informatiques suggérant que l'augmentation d'I_{K1} en était le mécanisme prédominant.[170]

Nos résultats confirment les résultats des modélisations informatiques réalisées chez l'animal et chez l'homme. La diminution de densité d'I_{Na} et d'I_{CaL} secondaires à la réduction d'expression de Nav1.5 et de Cav1.2, et l'augmentation de densité de d'I_{K1} liée à l'augmentation d'expression de Kir2.1 étaient les principales modifications observées à la transition, remodelage ionique survenant par conséquent pendant le temps en FA paroxystique. Ces modifications n'évoluaient majoritairement plus lors de l'année de suivi en FA persistante.

La régulation positive d'I_{K1} augmente l'excitabilité cardiaque via l'hyperpolarisation de la membrane cellulaire et l'augmentation de la disponibilité des canaux sodiques, et de part l'augmentation de fréquence de rotation des rotors en FA et en FV.[35] Nos simulations confirment ces résultats puisque les rotors générés en implémentant les modifications ioniques observées lors de la transition (et principalement I_{CaL} et I_{K1}) étaient plus stables et persistaient tout au long des simulations, contrairement à ceux générés dans les conditions de FA paroxystique. De façon similaire, la diminution d'I_{Na}, malgré la faible réduction d'excitabilité qu'elle entraine, contribue à la stabilisation des rotors, puisque ceux générés en l'absence de diminution d'I_{Na} étaient instables et s'éteignaient spontanément par collision avec un des bords de la simulation.

b. Relation entre remodelage structurel et électrophysiologique

Un remodelage structurel progressif était observé dans ce modèle de FA, marqué principalement par une hypertrophie myocytaire, une dilatation atriale, et une fibrose interstitielle. Ces modifications avaient déjà débuté au stade de la transition et devenaient significatives au stade de LS-PAF. Le niveau de PIIINP, un marqueur sérique de dégradation du collagène et de fibrose tissulaire augmentait progressivement au cours de l'évolution de la FA, augmentation devenant également significative après 1 an en FA persistante. L'augmentation du niveau tissulaire d'α-SMA, une protéine marqueur de l'activation myofibroblastique,[171] était observée dans les deux oreillettes au stade de transition, et avait tendance à diminuer au stade de LS-PAF (phénomène probablement semblable à ce qui est observé après la survenue d'un infarctus du myocarde, où une phase de prolifération myofibroblastique laisse place à une phase de maturation pendant laquelle la cellularité tissulaire décroit et la matrice extracellulaire locale remplacée par une cicatrice fibreuse[172]). Ainsi, l'augmentation de l'α-SMA reflète l'activation myofibroblastique atriale possiblement liée à la libération de cytokines (tels que le PDGF, cytokine réduisant la duré du PA atrial et la densité d'I_{CaL}[173]) ou à l'activation de canaux perméables au Ca^{2+} (transient receptor potential canonical-3=TRPC3).[174]

Cependant, aucune régulation négative des protéines impliquées dans l'homéostasie calcique et aucun changement dans le ratio RyR2 phosphorylé/RyR2 total n'étaient retrouvés, ce qui sous-entend l'absence d'implication des phénomènes d'activités déclenchées dans la transition vers la FA persistante.

c. Prédire la transition vers la FA persistante

Dans notre étude, nous avons observé une très grande hétérogénéité dans le temps nécessaire à la transition vers la FA persistante. Contrairement à la DF_{max} du premier épisode et à celle observée à la transition, nous avons retrouvé que la dDF/dt, correspondant au taux

d'accélération de la DF_{max}, était corrélée au temps passé en FA paroxystique avant la survenue de la transition. Ce paramètre est probablement un marqueur de la rapidité de survenue du remodelage électrophysiologique dans les oreillettes droite et gauche, c'est-à-dire la rapidité à laquelle les modifications d'I_{CaL} et d'I_{K1} sont suffisantes pour assurer un raccourcissement du PA tel que les rotors deviennent stables et persistants.

d. Limites du travail

Nous avons utilisé un modèle de FA induite par stimulation atriale rapide (30 secondes à 20Hz) alternant avec une courte période de détection, et d'autres études seront nécessaires pour savoir si les résultats observés sont confirmés dans d'autres modèles animaux de FA, mais également chez l'homme. De plus, notre modèle reproduit ce qui est observé chez l'homme en l'absence de cardiopathie (FA sur cœur sain), et l'évolution de la DF_{max} en cas d'association de la FA à d'autres comorbidités (insuffisance cardiaque, hypertension artérielle, valvulopathies,…) est inconnue. Par ailleurs, nous avons choisi d'étudier uniquement les principaux courants impliqués dans la genèse du PA, n'examinant par exemple pas les modifications d'I_{KAch}, courant dont la densité augmente après le passage en FA.[73, 175] De même, nous avons analysé certaines protéines impliquées dans l'homéostasie calcique, nous permettant de conclure qu'une fuite de Ca^{2+} ou des DAD n'étaient pas responsables de la transition de la FA ; cependant, une étude spécifique et plus approfondie devra être réalisée afin de confirmer ces résultats. Enfin, lors de la réalisation des simulations informatiques, nous n'avons pas modélisé le stade de LS-PAF car plus aucune modification ionique significative n'était mise en évidence après 1 an de suivi. Cependant, l'apparition du remodelage structurel une fois la FA devenue persistante (dilatation atriale, fibrose, hypertrophie myocytaire) peut sans doute modifier la dynamique des ondes de fibrillation mais n'ont pas été incorporées dans les simulations.

C. Conclusion

Nous avons donc démontré que prédire la transition de la FA paroxystique à persistante était réalisable sur un modèle ovin de FA. Si des résultats similaires étaient retrouvés chez l'homme, ils permettraient de stratifier les patients selon leur risque de progression vers des formes soutenues de l'arythmie. Les patients en FA paroxystique ayant une dDF/dt élevée pourraient rapidement être dirigés vers un centre d'ablation avant qu'une forme persistante n'apparaisse, celle-ci étant plus complexe à traiter.[176] A l'opposé, les patients ayant une dDF/dt basse pourraient être considérés à faible risque de progression, et bénéficier plus longtemps d'un traitement médical anti-arythmique avant de bénéficier d'une ablation endocavitaire. Par ailleurs, nous avons démontré que la dDF/dt analysée sur l'ECG de surface après soustraction des QRS était corrélée à celles enregistrées dans l'OG et l'OD. Une analyse purement non-invasive pourrait ainsi permettre de guider les médecins en charge de patients présentant une FA et d'envisager une thérapie individualisée selon leur risque à présenter un remodelage atrial précoce et une transition rapide vers des formes soutenues de l'arythmie.

3 Generating a large animal model of persistent atrial fibrillation

Raphaël P. Martins[1,2] and José Jalife[1]

[1] University of Michigan, Ann Arbor, MI, USA

[2] University Hospital of Rennes, Rennes, France

Introduction

Atrial fibrillation (AF) is the most common, sustained cardiac arrhythmia seen in clinical practice [1]. Yet despite more than 100 years of basic and clinical research in AF, we still do not fully understand its fundamental mechanisms and we have not learned how to treat it effectively. Many drugs have been tried in persistent, long-lasting persistent, and permanent AF with very limited success [2]. On the other hand, the demonstration of AF triggers in the atrial sleeves of the pulmonary veins (PVs) has led to a significant improvement in therapy and today PV isolation using radiofrequency ablation (RF) is curative in about ~80% of paroxysmal AF patients. However, the success rate of RF ablation in the more prevalent and highly heterogeneous persistent and long-term persistent AF populations has, thus far, been a disappointing 30–50% [3–5]. Arguably, only a profound and complete understanding of the mechanisms involved in the maintenance and perpetuation of AF would allow us to generate more specific prevention and/or treatment of this dangerous and debilitating disease. Therefore, animal models have played, and will likely continue to play, an important role in the study of the pathophysiology of AF, including its molecular basis, its ion-current determinants, its anatomical features, and its macroscopic mechanisms, as well as in the development of new therapeutic approaches, whether drug-based, molecular therapeutics, or device-related [6]. In this chapter we focus our attention on the description step-by-step of how to develop an ovine model of long-term persistent AF in which atrial tachypacing for ~9 weeks leads to stable, self-sustaining AF persisting for over 6 months. This novel, clinically relevant model is likely to open new paths toward the understanding of the mechanisms of persistent AF, as well as the development of more effective preventative approaches. We then switch gears to briefly review some of the animal models that have been used over the last 18 years to study the consequences of atrial tachycardia-induced electrical and structural remodeling that characterizes sustained AF.

Insights from tachypacing-induced AF models

When AF lasts continuously for more than 7 days it is designated as persistent AF. Spontaneous, pharmacological, or ablative resumption of sinus rhythm is infrequent in persistent AF, with prompt recurrences or commonly failed cardioversions in episodes lasting for more than 1 year, termed long-term persistent AF [2]. It is reasonable to speculate that continuous, high frequency, and heterogeneous bombardment of the atrial cells and tissues with fibrillatory waves during long-lasting AF leads to a modification of the molecular substrate on which waves propagate, with consequent electrical and structural remodeling, substantial enough to

Manual of Research Techniques in Cardiovascular Medicine, First Edition. Edited by Hossein Ardehali, Roberto Bolli, and Douglas W. Losordo.

E1

increase the likelihood of perpetuation of the electrical sources that maintain the arrhythmia. Therefore, since the mid-1990s investigators have endeavored to examine the mechanisms of remodeling and AF perpetuation using highly sophisticated and labor-intensive large animal models. The use of such models has greatly advanced our understanding of this highly prevalent arrhythmia.

In 1995, Morillo *et al.* [7] developed a novel canine chronic AF model, of right atrial tachypacing. For the first time, they demonstrated that the mean AF cycle length (1/dominant frequency) was significantly shorter in the left atrium compared with the right atrium. Such a consistent left-to-right dominant frequency gradient was similar to what was shown subsequently in optical mapping experiments in the isolated heart [8–10], and later contributed to the "mother rotor hypothesis" of AF [11]. In the experiments of Morillo *et al.* [7], cryoablation of the high-frequency area near the pulmonary veins (PVs) significantly prolonged AF cycle length and successfully restored sinus rhythm in most dogs, confirming the crucial role of localized sites with high activation frequency in the mechanism of AF. Such observations were later confirmed in humans by the seminal work of Haissaguerre *et al.* who demonstrated that ectopic beats originating within the PVs were capable of initiating and even maintaining AF, and that they could be eliminated by treatment with radiofrequency ablation [12].

In a similar model of atrial tachypacing-induced AF, Wijffels *et al.* [13], used goats that were chronically instrumented with electrodes sutured to both atria and connected to a modified external pacemaker that delivered rapid stimuli to the right atrium. These authors demonstrated electrical remodeling manifested as an abbreviation of the atrial effective refractory period (AERP), reversal of AERP rate adaptation, increase in AF rate and inducibility, and progressive increase in episodes duration. This led to the concept of "AF begets AF", which was shown to reverse to sinus rhythm upon switching the pacemaker off. Various groups later have used this model in dogs [14,15], sheep [16], or pigs [17,18].

In addition to electrical remodeling, contractile remodeling also occurs in atrial tachypacing as a consequence of the reduced contractility, and the decreased sarcoplasmic reticulum calcium load [19] and release [20]. The contractile abnormality, also demonstrated in the fibrillating human atria [21], probably exacerbates the thromboembolic risk in AF patients. Moreover, structural remodeling of the atria is also a consequence of AF. The most common abnormalities observed are interstitial fibrosis [22] (although not in all species subjected to chronic atrial pacing), myocyte hypertrophy, accumulation of glycogen, mitochondrial abnormalities [23], and atrial dilation. Therefore, AF results in electrical, contractile, and structural remodeling, all of which leads to more AF and creates a vicious circle able to self-sustain the arrhythmia. This helps to provide a reasonable although unproven explanation for the progression from paroxysmal to persistent and eventually permanent AF that has been observed on occasion in clinical practice.

Protocol

Generating a tachypacing-induced AF model

In this section we provide details of the standard protocol used routinely in our laboratory to generate an ovine model of tachypacing-induced AF. The model derives from those used previously in other species [7,13]. The procedure requires the chronic implantation of a pacemaker and of a transvenous catheter. Yet it is safe, considered minor surgery, and is accompanied by very few complications. In humans, a similar surgical procedure is often performed under conscious sedation and local anesthesia.

Pre-op procedures. We use 6 to 12-month-old male Dorset sheep weighing 30–40 kg. Preprocedural injection of antibiotics is not given routinely. In case of preprocedural signs of infection (fever, cough, diarrhea, shortness of breath, etc.), the procedure is postponed to allow the treatment of the infection; the animal is implanted after full recovery. The length of the surgical fasting period is 12 hours (water restriction is not required).

Sheep are placed in sternal recumbency and safely handled. A 16 to 18-gauge venous catheter is placed for vascular access in a forelimb and secured to allow for the administration of i.v. fluids, induction agents, supplemental parenteral anesthetics, and analgesics. If the animal needs to be calmed before the insertion of the venous catheter, an intramuscular injection of

E1

xylazine (0.2 mg/kg) can be administered. The jugular vein is not catheterized; it is subsequently used for pacemaker lead implantation. Catheter patency is checked using saline solution. Once the catheter is successfully placed, heparin is flushed to avoid coagulation (this procedure is repeated after each drug injection via the catheter). Then, propofol i.v. (4–6 mg/kg) is injected for induction of anesthesia. A slow injection is required to avoid severe bradycardia, which could cause myocardial ischemia, and to minimize the risk of seizures. Buprenorphine (0.01 mg/kg, i.m. or s.c.) is injected at the beginning of the procedure to ensure analgesia.

Next, endotracheal intubation is performed placing the animal in the sternal recumbency or supine position. A laryngoscope is inserted to visualize the larynx and the vocal cords. A 33–37 cm endotracheal tube is then inserted and the cuff inflated; the cuff is checked for leaks before intubation. Ties are used to secure the tube to the lower jaw. The proper position of the tube is checked by auscultation of the chest with a stethoscope to ensure the presence of equal bilateral thoracic sounds and no sounds over the stomach area. In addition, equal bilateral rise and fall of the chest should occur when inflating/ deflating the breathing bag, and there should be vapor in the endotracheal tube. Isoflurane gas is initiated and the animal ventilated at 5–10 mL/kg (respiratory rate 20/min). A rumen tube is placed and ophthalmic ointment is applied to the eyes. Next, the surgical area (right part of the neck and of the upper chest) is clipped and scrubbed with three alternating chlorhexidine/ alcohol scrubs. The animal should be connected to the following monitors: pulse oximetry connected to one of the ears, respiration, body temperature, pulse rate, ECG, and blood pressure. The surgically prepped area is then isolated with sterile towels and sterile drapes.

Pacemaker implantation. The procedure is performed as follows. First, locate the right jugular vein by occluding manually the flow downstream from the future incision site. Then proceed to make an approximately 5-cm long incision on the skin along the jugular vein with a standard scalpel; the incision should be superficial to avoid direct vein incision. An electric scalpel is used to gently cut the skin layers to the subcutaneous tissue through the previous incision. Carefully dissect the subcutaneous tissue using a small artery forceps; small bleeders should be cauterized using an electric cautery. Continue with progressive dissection until the external jugular vein is visualized, carefully avoiding vein damage. Proceed with the dissection to isolate the external jugular vein in its entire circumference all along the skin incision. If the jugular vein receives venous branches, they should be occluded downstream and upstream using non-absorbable silk and then cauterized. Once the jugular vein is perfectly isolated circumferentially from the subcutaneous tissue, it should be occluded upstream at the edge of the incision using non-absorbable silk (for safety reasons, we usually ligate the vein twice); the jugular vein is then totally flat. Thereafter, the canister pocket is molded in the subcutaneous tissue plane by careful blunt dissection using the fingers; the pocket should be filled with gauze pads to perform hemostasis and avoid blood penetration during lead insertion.

The fluoroscopy C-arm is prepared and centered in the chest area. The operator should replace surgical gloves before touching the pacemaker canister and lead.

Lead implantation. The endocardial lead should be a 6 to 8 Fr, 46 to 52 cm bipolar, active fixation and steroid-eluting lead (Figure 3.1). Before implantation, the mechanical function of the helix may be tested by screwing and unscrewing it; the helix should be

Figure 3.1 Pacemaker lead (left) and canister (right). The helix of the lead tip is extended. Shown is a dual-chamber pacemaker (atrial and ventricular ports).

E1

completely retracted before inserting the lead into the vein. To insert the lead start by lifting the vein using a small tissue forceps, and making a small vein incision (2–3 mm) using Potts–Smith scissors to insert the lead (a vein-lifter can be used to facilitate the insertion). Under fluoroscopic guidance (anteroposterior view), push the lead gently and progressively through the jugular vein to the superior vena cava and then the right atrium. Due to the vertical position of the sheep heart, the lead is likely to slide directly from the superior to the inferior vena cava. At this point, insert a J-shaped stylet into the lead; as the stylet approaches the lead tip, retract progressively the lead into the right atrium; the lead tip will spontaneously glide into the right atrial appendage (RAA). Check the correct position of the lead using fluoroscopy. The electrode tip should slightly move from right to left in a windshield wiper-like movement. Then move the fluoroscopy to the lateral view: the J-curve of the lead should appear in profile. Slightly pull the lead/ stylet to give an L-shape to the lead; this movement stabilizes the tip of the lead in the appendage. Using the screw-driver tool, extend the helix to fix the lead to the RAA (clockwise rotation), making sure the helix is extended on the fluoroscopic image. Retract the stylet from the lead with a smooth and steady movement, while keeping the lead tip in position. Then slightly push the lead to give it a correct J-shape assessed in the anteroposterior view.

Intraoperative measurements. Three parameters should be verified during the implantation of the lead: the impedance, the sensitivity, and the stimulation threshold. Such measurements require connecting the pacemaker canister to the lead (or a pacing system analyzer through the programmer).

- Impedance: ideally between 200 and 2000Ω (<200Ω: insulation break, >2000Ω: lead fracture).
- Sensitivity: this reflects the detection ability of the pacemaker in a given position of the lead. Ideally, a high voltage atrial signal (>2 mV) should be detected with a low amplitude ventricular far-field.
- Threshold: this reflects the pacing ability of the pacemaker in a given position of the lead. Ideally, a low stimulation threshold value (<1 V) should be obtained to avoid excessive battery drain during the follow-up and to prevent any loss of capture if the pacing threshold increases after the acute phase.

A good position of the lead is reflected by a high amplitude signal and a low pacing threshold. If the values are not correct, a different position of the lead should be targeted. To secure the lead, the suture sleeve should be firmly tied to the lead and the underlying tissue under fluoroscopic guidance to detect any displacement of the lead tip.

Insertion of the pacemaker canister. First, remove the gauze pads filling the pacemaker pouch. Then check if hemostasis is necessary. Please note that, at this point, the electric cautery should be used very carefully to avoid any damage to the lead. Next, connect the lead to the atrial port of the single chamber pacemaker (if a dual-chamber pacemaker is used and the ventricular port is not used, it should be occluded using specific plugs), and insert the pacemaker canister inside the pouch. Redundant leads should be looped underneath the device. Fluoroscopically examine the lead and the canister to check proper positioning before closure. Proceed with a standard two-layer closure to secure the device and close the pocket: synthetic absorbable suture is used to close the subcutaneous fascia and surgical staples are used to close the skin.

Short-term follow-up. Program the pacemaker for "atrial sensing-only" mode (OAO) and discontinue the anesthesia. The animal should remain intubated until there is evidence of sufficient spontaneous respiration. Daily physical examination should include checking the wound, the animal's weight, breathing and heart rates, and the temperature. Staples should be removed 7 days after pacemaker implantation. The pacemaker is programmed in order to induce AF after a 10-day recovery period.

Pacing protocols

Many different pacing protocols provided by the device industry may be used to induce AF in animals. The pacing protocol most commonly used in published studies is one that includes alternation between burst pacing and waiting periods. The protocol described here is available for St. Jude Medical (St. Paul, Minnesota, USA) pacemaker devices. In this specific pacing algorithm, four parameters can be programmed: (1) **Burst pacing rate**: from 4 to 50 Hz. (2) **Burst pacing period**: 6, 10, 30 s or continuous pacing. (3) **Waiting period**: the

E1

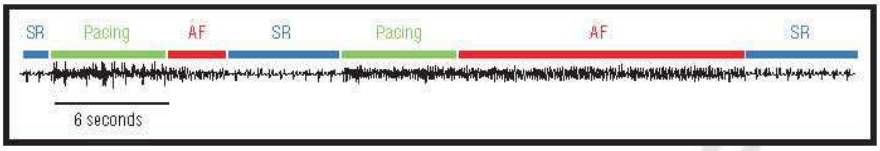

Figure 3.2 Auto mode switch algorithm activated in association with pacing. The pacing period in this example is 6 seconds. After the pacing period, the pacemaker "senses" the atrial activity and only resumes pacing if sinus rhythm (SR) is detected. AF, atrial fibrillation.

time between two burst pacing periods, may last between 2 and 10 s (or absent when in the continuous pacing mode). (4) **Suspension of pacing after the wait period if AF is detected, and resumption of pacing if reversion to sinus rhythm is detected**. This parameter can be activated by switching on the «Auto Mode Switch» (AMS) algorithm of the device, an example of which is presented in Figure 3.2.

The AMS algorithm reliably generates tachypacing-induced self-sustained AF because the pacemaker resumes pacing only if AF stops and sinus rhythm is detected. As such, the algorithm readily reproduces the phenomenon of "AF begets AF" described originally by Wijffels *et al.* [13] Importantly, the approach may be used to predict the evolution of AF that might occur in some human patients, from the initiation of premature atrial beats, to the establishment of paroxysmal and eventually persistent AF [24]. To this aim, the device stores valuable information that may be used to characterize the AF history of the animal, including the number and duration of AF episodes (Figure 3.3A,B), and the precise moment of each episode's occurrence. The device also has Holter capabilities that can be used to record the intracardiac electrogram during initiation and/or termination of a given AF episode. All such features can be used to create histograms and follow the evolution of the arrhythmia (Figure 3.3C).

In our experience, the time to AF stabilization is quite variable. The first AF episode occurs after a median of 5 days from the onset of pacing, sometimes immediately and sometimes up to 2 months after the first pacing burst. The time in paroxysmal AF (episodes <7 days' duration) is around 2 months. Thus, a period of 2.5 months of burst pacing is usually needed before persistent AF is established. A recording of the first AF episode in a sheep is given in Figure 3.4.

Electrical recordings (ECG or intracardiac electrograms) can be used to analyze the characteristics of the arrhythmia. At any time in the AF evolution, animals can be sacrificed to study electrical or structural remodeling from the molecule to the whole organ.

Ventricular rate during AF: to ablate or not to ablate

Conduction of atrial fibrillatory impulses through the atrioventricular (AV) node in animals with AF can be complicated by tachycardiomyopathy and heart failure [25,26]. Heart failure can itself lead to atrial remodeling (electrophysiological and structural), sometimes similar to AF-induced remodeling but sometimes different (see section "congestive heart failure model" later in the chapter) [27], and thus rate control may be necessary in some species. Therefore, some groups have proposed the need to perform His bundle ablation (HBA), together with the implantation of a ventricular lead to control the ventricular rate in the atrial tachypacing model. Radiofrequency energy may be used to perform this ablation [28]. Sequential atrial and ventricular pacing uses a single, or two separate pacemaker canisters. In a sheep model of tachypacing-induced AF, Anné *et al.* did not find any significant difference in terms of AF inducibility although sheep undergoing HBA developed persistent AF later than non-HBA sheep [16]. Furthermore, sheep with normal AV conduction displayed increased LA fibrosis compared to HBA-sheep. Markers of substrate remodeling (e.g. metalloproteinases) were also different in the two groups [28]. However, even though HBA allows investigators to elucidate the substrate and electrical remodeling that depend specifically on atrial tachypacing, it renders the model less clinically relevant.

E1

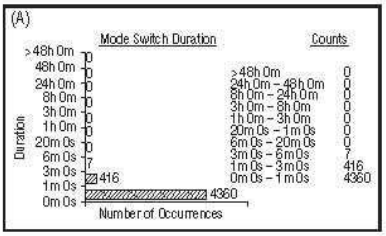

(B)

Date/Time	Duration
Apr 10 2011 4:42 pm	0d 12h 31m 10s
Apr 10 2011 1:57 am	0d 14h 44m 52s
Apr 9 2011 3:25 pm	0d 10h 31m 46s
Apr 9 2011 4:18 am	0d 11h 6m 48s
Apr 7 2011 9:37 pm	1d 6h 41m 24s
Apr 7 2011 9:13 pm	0d 0h 23m 26s
Apr 7 2011 3:15 pm	0d 5h 57m 34s
Apr 7 2011 2:22 pm	0d 0h 53m 22s
Apr 7 2011 1:55 pm	0d 0h 26m 20s
Apr 7 2011 8:33 am	0d 5h 21m 50s
Apr 7 2011 8:04 am	0d 0h 29m 26s
Apr 7 2011 8:04 am	0d 0h 0m 14s
Apr 7 2011 8:02 am	0d 0h 1m 22s
Apr 7 2011 2:59 am	0d 5h 3m 22s
Apr 6 2011 11:26 pm	0d 3h 32m 40s
Apr 6 2011 6:27 pm	0d 4h 58m 16s

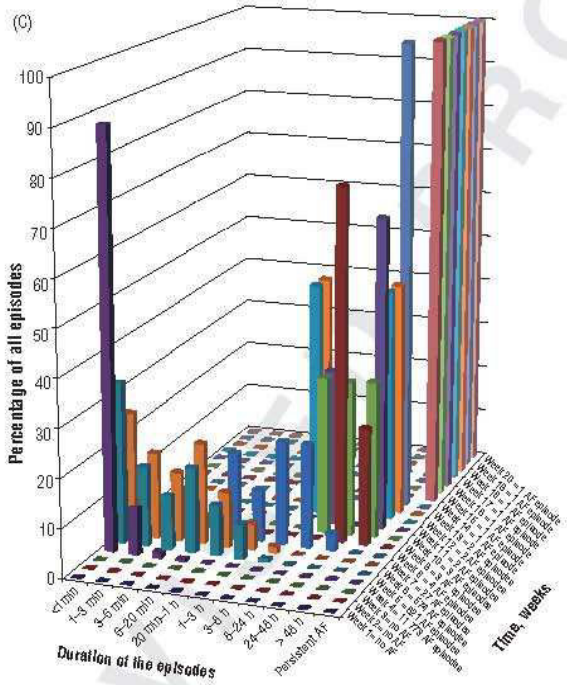

Figure 3.3 Information stored by the device. (A) AF episodes (in this case, 4783 short-lasting episodes in 1 week) are classified according to their duration. (B) The times episodes occur are also stored on the device's memory (two different sheep in A and B). (C) Weekly interrogation can be performed to create a histogram of the evolution of the arrhythmia. In this animal, the first AF episode occurred 4 weeks after the initiation of pacing. Episodes tended to last longer with time until self-sustained persistent AF developed. As this time, the pacemaker is does not resume pacing because sinus rhythm will not be detected.

E1

25

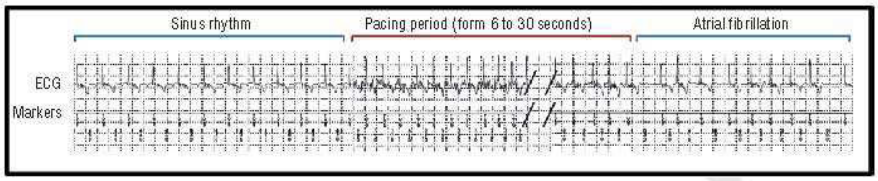

Figure 3.4 First episode of AF detected by an implantable loop recorder. After the wait period in sinus rhythm, pacing resumes for the programmed period (6 to 30 s, in this case 20 Hz during 30 s). At the end of the pacing period, AF is recorded.

Strengths and weaknesses of the model

The greatest strength of the tachypacing-induced AF model is its high reliability in undergoing atrial remodeling and reproducing the changes associated with sustained AF that are often observed in patients. The procedure is well tolerated by the animals and in experienced hands presents very few complications (see section Potential complications) [29]. Moreover, this type of model can provide a vast amount of information on AF, including its evolution, its relation to fibrosis, and when combined with other multidisciplinary approaches, its molecular and cellular mechanisms. Hence, for the last 16 years, atrial burst pacing models have provided important insights into the mechanisms of electrophysiological [13,14] and structural remodeling [23,30] in AF. They have also been used to evaluate the effects of drugs acting on the electrophysiological properties (e.g. antiarrhythmic drugs) or the structural remodeling of the atria (inhibitors of renin–angiotensin system [16], anti-inflammatory drugs [31], statins [32], etc.). However, a major disadvantage of the atrial burst pacing model is its relatively high cost, both in terms of resources and personnel and the need for a long-term commitment to the experiment, particularly when the experimental design calls for a model of long-term persistent AF (>6 months), which can bring the cost of each animal to more than $5000, including the purchase of the animal, surgical procedures, long-term follow up, and ancillary technologies (e.g. biochemistry, patch clamping, optical mapping, etc.).

Another potential disadvantage is that while the atrial burst pacing model nicely reproduces the "lone AF" seen in clinical practice, it does not necessarily apply to other forms of AF. Lone AF is not the same as AF in the context of hypertension or heart failure, or in the patient with ischemic heart disease. Therefore, extreme care must be exerted when attempting to extrapolate its results to the human. In fact, it may be argued that an important requirement for an appropriate animal model of AF is that it closely reproduces the substrate associated with the specific diseased that caused it. On the other hand, one should always keep in mind that this is only a model, which by no means accurately represented the clinical situation and this premise applies to any model. Hence we are convinced that the tachypacing-induced persistent AF model may be used to make predictions about AF mechanisms in general, as long as it is done cautiously and the investigation in question is accompanied by parallel research into the pathophysiological mechanisms associated with the aging process and/or the underlying disease as well as the pathologic processes that generated AF, including, fibrosis, adiposis, and inflammation.

Complications and alternative approaches to study AF

Potential complications

During the last 5 years, we have used this model in 80 sheep. Pacemaker implantation is extremely well tolerated in this species. We have not observed any significant hypotension, syncope, or evidence of device canister intolerance in our experiments, and the overall behavior of the animals is completely normal after the procedure. While persistent AF is induced in most animals, we have not seen any pacemaker infections, strokes, heart failure symptoms, or sudden cardiac deaths. The only complications we have observed are as follows: (1) wound healing: while rare, the major complication at this stage is extrusion of the canister through the

E1

unhealed wound; and (2) acute displacement of the lead: this can be in the form of microdisplacement within the right atrium, revealed by an increase in pacing threshold, a decrease in the amplitude of the detected signal, or a change in impedance. However, should this happen the pacing can still be activated using a higher-energy pacing output. Lead displacement to the right ventricle, revealed by a ventricular morphology when pacing, is tested at the postoperative measurement; fast pacing must not be switched ON since it would immediately induce ventricular fibrillation. A redo procedure is required to reposition the lead. Finally, miscellaneous extracardiac complications may also occur, including cold, pneumonia, parasite infection, etc.

Alternative AF models

Obviously, the choice of any given model should depend on the specific questions being asked. As discussed earlier, the atrial burst pacing model closely reproduces "lone AF" as seen in clinical practice. However, ideally, animal models should attempt to reproduce the conditions that prevail in the pathologies that produce the arrhythmia, including hypertension, heart failure, mitral valve disease, etc. Throughout the years, a number of experimental models have been developed in which AF pathophysiology may be studied in relation to a specific underlying disease. Data derived from all these models have contributed to improve our understanding of AF mechanisms in the clinical setting and have allowed for the development of novel therapeutic approaches. Here we touch on various models, developed over the last 15 years, to mimic the other conditions generating AF.

Congestive heart failure model. In 1999, Li *et al.* developed a canine model of heart failure by pacing the right ventricle at a fast heart rate (>200bpm) [27]. They demonstrated structural and electrophysiological changes in atrial cardiomyocytes. A substantial increase in fibrosis was also noted, but no changes were found in the action potential duration (APD) or AERP [27]. The structural change led to conduction heterogeneity and increased duration of AF episodes, from seconds in the control group to minutes in the congestive heart failure group. Electrophysiological changes supporting the stability of APD were analyzed by the same group [33]: they observed decreases in I_{CaL}, I_{to}, and I_{Ks} current densities and an increase in the transient inward Na^+/Ca^{2+} exchanger. However, they saw no changes in I_{CaT}, I_{Kur}, I_{Kr}, or I_{K1}. Interestingly, complete recovery of ionic remodeling was observed after 4 weeks without pacing, but structural remodeling (fibrosis) did not disappear, which explained in part the persistent vulnerability to AF after stopping the fast ventricular pacing [34]. Substrate remodeling seems to play an important role in maintaining AF in the congestive heart failure model. Remarkably, ionic modifications are different from what is observed in the atrial pacing model: this led Nattel and co-workers to study a model combining atrial and ventricular pacing (atrial tachycardia and congestive heart failure models, respectively), a common association often observed in clinical practice [35]. In this combined model, they demonstrated that the ionic remodeling pattern was different from that of heart failure or atrial pacing alone. They concluded that electrophysiological and substrate remodeling are not unique scenarios in AF but differ depending on the clinical situation.

Structural heart diseases: tricuspid [36] or mitral regurgitation [37–39]. Mitral regurgitation leads to atrial dilation, interstitial fibrosis, and homogeneously increased AERP [39]. In the mitral valve regurgitation model, conduction velocity during normal pacing was comparable between controls and dogs with regurgitation. However, conduction abnormalities were found during pacing at short cycle lengths and during premature extrastimuli, which may have been responsible for the increased AF inducibility in this model [38].

Sterile pericarditis. This model was developed and thoroughly characterized by the Waldo lab [40,41]. It reproduces predominantly atrial flutter, but AF can also occur. The surgical procedure consists of opening the pericardium by way of a right thoracotomy, and to dust the atrial surfaces with talcum powder. This model mimics the postoperative form of AF (occurring in up to 50% of patients after cardiac surgery). It has provided important insight and better understanding of flutter mechanisms and of the flutter–AF inter-relationship [42,43].

Complete AV block. This has been studied mainly in goats [44]. This model leads to progressive left atrial

E1

dilatation. However, there are no changes in AERP or AF cycle length, but the duration of AF episodes increased. Interestingly, histological analysis revealed myocyte hypertrophy but no fibrosis, and no changes in connexin expression were found.

Hypertension. Hypertension carries an important risk in AF patients. Hypertension is a predictor of AF induction and maintenance, and increases the risk of thromboembolic events. The relationship between AF and hypertension has been studied in spontaneously hypertensive rats [45] and in sheep exposed to corticosteroids during the prenatal period [46]. The presence of atrial fibrosis seems to participate in AF inducibility and stability in these models.

Arteriovenous shunts. These are responsible for chronic volume overload and have been studied in rabbits [47], goats [48], and sheep [49]. Although electrophysiological differences were noted in these different species, atrial dilation is a common feature and leads to an increase in AF vulnerability and stability.

Acute atrial injuries. Injuries such as acute stretch [50,51] or atrial ischemia [52] can increase atrial vulnerability to AF, and models of ischemia have been used to investigate experimental AF [53].

Aging. The prevalence of AF is known to increase with age. The atria of older animals display heterogeneous interstitial fibrosis [54,55], which may help to explain a decrease in conduction velocity and increased AF vulnerability. Electrophysiological investigation of right atrial cardiomyocytes from old dogs found no significant differences in resting membrane potential, AP amplitude or upstroke velocity, but the AP plateau was more negative and APD was longer in older animals [54]. Conduction velocity was normal for regular beats but reduced for premature beats.

Vagal nerve stimulation. In clinical practice, many patients present with vagally induced AF episodes; for instance, after vagal syncope, vomiting, or during the postprandial period. Vagal stimulation releases acetylcholine (ACh), which activates muscarinic receptors on the atrial cell and increases I_{KACh}, leading to APD and AERP shortening. Consequently, the wavelength of re-entry (WL = conduction velocity × refractory period) decreases which prevents wavefront–wavetail interactions and increases the stability of the sources that maintain AF [11]. We previously demonstrated the existence of rotors, predominantly located in the left atrium, which is the region having the highest dominant frequency, in acetylcholine-induced AF [10,56]. These observations found in sheep hearts were supported by computer simulations [57], and later confirmed in patients in whom adenosine was used to test for the effects of increasing I_{KACh} [58].

Pharmacologically induced AF. Aconitine crystals impregnated in the atrial muscle have been known to induce focal discharges maintaining AF in open-chest canine models [59,60]. Cesium infusion can also induce AF [61]. Acute asphyxia reproducibly induced AF in rats [62]. In clinical practice, many other drugs are known to induce AF [63].

Transgenic mouse models of AF. Many transgenic mice models have been developed over the last several years. A recent review details the characteristics and use of these different models [64].

Conclusion

Animal models of AF are here to stay. Since the independent publication of atrial tachypacing-induced AF models by two different laboratories more than 15 years ago [7,13], our knowledge of this arrhythmia has increased substantially. Animal models of AF have been an invaluable tool for studying atrial electrical and structural remodeling in AF. These models also offer great opportunities to study mechanisms and to develop novel therapeutic strategies. Knowledge derived from the various AF models will hopefully enable researchers to address important mechanistic questions, such as what processes underlie the transition from paroxysmal to persistent AF, whether there is any relationship between the development of atrial fibrosis and electrophysiological remodeling, and how one can take advantage of that knowledge to prevent AF progression. Animal models of AF are also likely to play crucial roles in the development and testing of new generations of antifibrillatory drugs. Such

E1

progress will be essential in our hope to avert the predicted huge increase in the incidence of this often devastating disease and its consequences [65].

Acknowledgement

Sources of funding: P01-HL087226 (J.J.) and the Leducq Foundation (J.J.). RPM received a grant from the Fédération Francaise de Cardiologie.

References

1 Kannel WB, Wolf PA, Benjamin EJ, Levy D. Prevalence, incidence, prognosis, and predisposing conditions for atrial fibrillation: Population-based estimates. *Am J Cardiol* 1998; **82**: 2N–9N.

2 Camm AJ, Kirchhof P, Lip GY, Schotten U, Savelieva I, Ernst S, *et al.* Guidelines for the management of atrial fibrillation: The task force for the management of atrial fibrillation of the European Society of Cardiology (ESC). *Europace* 2010; **12**: 1360–1420.

3 Matsuo S, Lim KT, Haissaguerre M. Ablation of chronic atrial fibrillation. *Heart Rhythm* 2007; **4**: 1461–1463.

4 Calkins H, Brugada J, Packer DL, Cappato R, Chen SA, Crijns HJ, *et al.* Hrs/ehra/ecas expert consensus statement on catheter and surgical ablation of atrial fibrillation: Recommendations for personnel, policy, procedures and follow-up. A report of the heart rhythm society (hrs) task force on catheter and surgical ablation of atrial fibrillation. *Heart Rhythm* 2007; **4**: 816–861.

5 Cappato R, Calkins H, Chen SA, Davies W, Iesaka Y, Kalman J, *et al.* Worldwide survey on the methods, efficacy, and safety of catheter ablation for human atrial fibrillation. *Circulation* 2005; **111**: 1100–1105.

6 Nishida K, Michael G, Dobrev D, Nattel S. Animal models for atrial fibrillation: Clinical insights and scientific opportunities. *Europace* 2010; **12**: 160–172.

7 Morillo CA, Klein GJ, Jones DL, Guiraudon CM. Chronic rapid atrial pacing. Structural, functional, and electrophysiological characteristics of a new model of sustained atrial fibrillation. *Circulation* 1995; **91**: 1588–1595.

8 Jalife J, Berenfeld O, Skanes A, Mandapati R. Mechanisms of atrial fibrillation: Mother rotors or multiple daughter wavelets, or both? *J Cardiovasc Electrophysiol* 1998; **9**: S2–12.

9 Berenfeld O, Mandapati R, Dixit S, Skanes AC, Chen J, Mansour M, *et al.* Spatially distributed dominant excitation frequencies reveal hidden organization in atrial fibrillation in the langendorff-perfused sheep heart. *J Cardiovasc Electrophysiol* 2000; **11**: 869–879.

10 Mandapati R, Skanes A, Chen J, Berenfeld O, Jalife J. Stable microreentrant sources as a mechanism of atrial fibrillation in the isolated sheep heart. *Circulation* 2000; **101**: 194–199.

11 Jalife J, Berenfeld O, Mansour M. Mother rotors and fibrillatory conduction: A mechanism of atrial fibrillation. *Cardiovasc Res* 2002; **54**: 204–216.

12 Haissaguerre M, Jais P, Shah DC, Takahashi A, Hocini M, Quiniou G, *et al.* Spontaneous initiation of atrial fibrillation by ectopic beats originating in the pulmonary veins. *N Engl J Med* 1998; **339**: 659–666.

13 Wijffels MC, Kirchhof CJ, Dorland R, Allessie MA. Atrial fibrillation begets atrial fibrillation. A study in awake chronically instrumented goats. *Circulation* 1995; **92**: 1954–1968.

14 Gaspo R, Bosch RF, Talajic M, Nattel S. Functional mechanisms underlying tachycardia-induced sustained atrial fibrillation in a chronic dog model. *Circulation* 1997; **96**: 4027–4035.

15 Fareh S, Villemaire C, Nattel S. Importance of refractoriness heterogeneity in the enhanced vulnerability to atrial fibrillation induction caused by tachycardia-induced atrial electrical remodeling. *Circulation* 1998; **98**: 2202–2209.

16 Anné W, Willems R, Holemans P, Beckers F, Roskams T, Lenaerts I, *et al.* Self-terminating af depends on electrical remodeling while persistent af depends on additional structural changes in a rapid atrially paced sheep model. *J Mol Cell Cardiol* 2007; **43**: 148–158.

17 Dudley SC, Jr., Hoch NE, McCann LA, Honeycutt C, Diamandopoulos L, Fukai T, *et al.* Atrial fibrillation increases production of superoxide by the left atrium and left atrial appendage: Role of the nadph and xanthine oxidases. *Circulation* 2005; **112**: 1266–1273.

18 Chen CL, Huang SK, Lin JL, Lai LP, Lai SC, Liu CW, *et al.* Upregulation of matrix metalloproteinase-9 and tissue inhibitors of metalloproteinases in rapid atrial pacing-induced atrial fibrillation. *J Mol Cell Cardiol* 2008; **45**: 742–753.

19 Greiser M, Neuberger HR, Harks E, El-Armouche A, Boknik P, de Haan S, *et al.* Distinct contractile and molecular differences between two goat models of atrial dysfunction: Av block-induced atrial dilatation and atrial fibrillation. *J Mol Cell Cardiol* 2009; **46**: 385–394.

20 Sun H, Gaspo R, Leblanc N, Nattel S. Cellular mechanisms of atrial contractile dysfunction caused by sustained atrial tachycardia. *Circulation* 1998; **98**: 719–727.

21 Schotten U, Greiser M, Benke D, Buerkel K, Ehrenteidt B, Stellbrink C, *et al.* Atrial fibrillation-induced atrial contractile dysfunction: A tachycardiomyopathy of a different sort. *Cardiovasc Res* 2002; **53**: 192–201.

22 Everett THT, Olgin JE. Atrial fibrosis and the mechanisms of atrial fibrillation. *Heart Rhythm* 2007; **4**: S24–27.

23 Ausma J, Wijffels M, Thone F, Wouters L, Allessie M, Borgers M, *et al.* Structural changes of atrial myocardium

E1

due to sustained atrial fibrillation in the goat. *Circulation* 1997; **96**: 3157–3163.
24 Cohen M, Naccarelli GV. Pathophysiology and disease progression of atrial fibrillation: Importance of achieving and maintaining sinus rhythm. *J Cardiovasc Electrophysiol* 2008; **19**: 885–890.
25 Armstrong PW, Stopps TP, Ford SE, de Bold AJ. Rapid ventricular pacing in the dog: Pathophysiologic studies of heart failure. *Circulation* 1986; **74**: 1075–1084.
26 Williams RE, Kass DA, Kawagoe Y, Pak P, Tunin RS, Shah R, *et al.* Endomyocardial gene expression during development of pacing tachycardia-induced heart failure in the dog. *Circ Res* 1994; **75**: 615–623.
27 Li D, Fareh S, Leung TK, Nattel S. Promotion of atrial fibrillation by heart failure in dogs: Atrial remodeling of a different sort. *Circulation* 1999; **100**: 87–95.
28 Anne W, Willems R, Holemans P, Beckers F, Roskams T, Lenaerts I, *et al.* Self-terminating af depends on electrical remodeling while persistent af depends on additional structural changes in a rapid atrially paced sheep model. *J Mol Cell Cardiol* 2007; **43**: 148–158.
29 Nishida K, Michael G, Dobrev D, Nattel S. Animal models for atrial fibrillation: Clinical insights and scientific opportunities. *Europace* 2010; **12**: 160–172.
30 He X, Gao X, Peng L, Wang S, Zhu Y, Ma H, *et al.* Atrial fibrillation induces myocardial fibrosis through angiotensin ii type 1 receptor-specific arkadia-mediated downregulation of smad7. *Circ Res* 2011; **108**: 164–175.
31 Shiroshita-Takeshita A, Brundel BJ, Lavoie J, Nattel S. Prednisone prevents atrial fibrillation promotion by atrial tachycardia remodeling in dogs. *Cardiovasc Res* 2006; **69**: 865–875.
32 Shiroshita-Takeshita A, Schram G, Lavoie J, Nattel S. Effect of simvastatin and antioxidant vitamins on atrial fibrillation promotion by atrial-tachycardia remodeling in dogs. *Circulation* 2004; **110**: 2313–2319.
33 Li D, Melnyk P, Feng J, Wang Z, Petrecca K, Shrier A, *et al.* Effects of experimental heart failure on atrial cellular and ionic electrophysiology. *Circulation* 2000; **101**: 2631–2638.
34 Cha TJ, Ehrlich JR, Zhang L, Shi YF, Tardif JC, Leung TK, *et al.* Dissociation between ionic remodeling and ability to sustain atrial fibrillation during recovery from experimental congestive heart failure. *Circulation* 2004; **109**: 412–418.
35 Cha TJ, Ehrlich JR, Zhang L, Nattel S. Atrial ionic remodeling induced by atrial tachycardia in the presence of congestive heart failure. *Circulation* 2004; **110**: 1520–1526.
36 Boyden PA, Hoffman BF. The effects on atrial electrophysiology and structure of surgically induced right atrial enlargement in dogs. *Circ Res* 1981; **49**: 1319–1331.
37 Guerra JM, Everett THT, Lee KW, Wilson E, Olgin JE. Effects of the gap junction modifier rotigaptide (zp123) on atrial conduction and vulnerability to atrial fibrillation. *Circulation* 2006; **114**: 110–118.
38 Verheule S, Wilson E, Banthia S, Everett THT, Shanbhag S, Sih HJ, *et al.* Direction-dependent conduction abnormalities in a canine model of atrial fibrillation due to chronic atrial dilatation. *Am J Physiol Heart Circ Physiol* 2004; **287**: H634–644.
39 Verheule S, Wilson E, Everett TT, Shanbhag S, Golden C, Olgin J, *et al.* Alterations in atrial electrophysiology and tissue structure in a canine model of chronic atrial dilatation due to mitral regurgitation. *Circulation* 2003; **107**: 2615–2622.
40 Page PL, Plumb VJ, Okumura K, Waldo AL. A new animal model of atrial flutter. *J Am Coll Cardiol* 1986; **8**: 872–879.
41 Kumagai K, Khrestian C, Waldo AL. Simultaneous multisite mapping studies during induced atrial fibrillation in the sterile pericarditis model. Insights into the mechanism of its maintenance. *Circulation* 1997; **95**: 511–521.
42 Roithinger FX, Karch MR, Steiner PR, SippensGroenewegen A, Lesh MD. Relationship between atrial fibrillation and typical atrial flutter in humans: Activation sequence changes during spontaneous conversion. *Circulation* 1997; **96**: 3484–3491.
43 Waldo AL, Feld GK. Inter-relationships of atrial fibrillation and atrial flutter mechanisms and clinical implications. *J Am Coll Cardiol* 2008; **51**: 779–786.
44 Neuberger HR, Schotten U, Verheule S, Eijsbouts S, Blaauw Y, van Hunnik A, *et al.* Development of a substrate of atrial fibrillation during chronic atrioventricular block in the goat. *Circulation* 2005; **111**: 30–37.
45 Choisy SC, Arberry LA, Hancox JC, James AF. Increased susceptibility to atrial tachyarrhythmia in spontaneously hypertensive rat hearts. *Hypertension* 2007; **49**: 498–505.
46 Kistler PM, Sanders P, Dodic M, Spence SJ, Samuel CS, Zhao C, *et al.* Atrial electrical and structural abnormalities in an ovine model of chronic blood pressure elevation after prenatal corticosteroid exposure: Implications for development of atrial fibrillation. *Eur Heart J* 2006; **27**: 3045–3056.
47 Hirose M, Takeishi Y, Miyamoto T, Kubota I, Laurita KR, Chiba S, *et al.* Mechanism for atrial tachyarrhythmia in chronic volume overload-induced dilated atria. *J Cardiovasc Electrophysiol* 2005; **16**: 760–769.
48 Remes J, van Brakel TJ, Bolotin G, Garber C, de Jong MM, van der Veen FH, *et al.* Persistent atrial fibrillation in a goat model of chronic left atrial overload. *J Thorac Cardiovasc Surg* 2008; **136**: 1005–1011.
49 Deroubaix E, Folliguet T, Rucker-Martin C, Dinanian S, Boixel C, Validire P, *et al.* Moderate and chronic

E1

hemodynamic overload of sheep atria induces reversible cellular electrophysiologic abnormalities and atrial vulnerability. *J Am Coll Cardiol* 2004; **44**: 1918–1926.
50 Kalifa J, Jalife J, Zaitsev AV, Bagwe S, Warren M, Moreno J, *et al.* Intra-atrial pressure increases rate and organization of waves emanating from the superior pulmonary veins during atrial fibrillation. *Circulation* 2003; **108**: 668–671.
51 Ravelli F, Allessie M. Effects of atrial dilatation on refractory period and vulnerability to atrial fibrillation in the isolated langendorff-perfused rabbit heart. *Circulation* 1997; **96**: 1686–1695.
52 Sinno H, Derakhchan K, Libersan D, Merhi Y, Leung TK, Nattel S, *et al.* Atrial ischemia promotes atrial fibrillation in dogs. *Circulation* 2003; **107**: 1930–1936.
53 Yamazaki M, Morgenstern S, Klos M, Campbell K, Buerkel D, Kalifa J, *et al.* Left atrial coronary perfusion territories in isolated sheep hearts: Implications for atrial fibrillation maintenance. *Heart Rhythm* 2010; **7**: 1501–1508.
54 Anyukhovsky EP, Sosunov EA, Plotnikov A, Gainullin RZ, Jhang JS, *et al.* Cellular electrophysiologic properties of old canine atria provide a substrate for arrhythmogenesis. *Cardiovasc Res* 2002; **54**: 462–469.
55 Hayashi H, Wang C, Miyauchi Y, Omichi C, Pak HN, Zhou S, Ohara T, *et al.* Aging-related increase to inducible atrial fibrillation in the rat model. *J Cardiovasc Electrophysiol* 2002; **13**: 801–808.
56 Mansour M, Mandapati R, Berenfeld O, Chen J, Samie FH, Jalife J, *et al.* Left-to-right gradient of atrial frequencies during acute atrial fibrillation in the isolated sheep heart. *Circulation* 2001; **103**: 2631–2636.
57 Kneller J, Zou R, Vigmond EJ, Wang Z, Leon LJ, Nattel S, *et al.* Cholinergic atrial fibrillation in a computer model of a two-dimensional sheet of canine atrial cells with realistic ionic properties. *Circ Res* 2002; **90**: E73–87.
58 Atienza F, Almendral J, Moreno J, Vaidyanathan R, Talkachou A, Kalifa J, *et al.* Activation of inward rectifier potassium channels accelerates atrial fibrillation in humans: Evidence for a reentrant mechanism. *Circulation* 2006; **114**: 2434–2442.
59 Scherf D. Studies on auricular tachycardia caused by aconitine administration. *Proc Soc Exp Biol Med* 1947; **64**: 233–239.
60 Hashimoto N, Yamashita T, Tsuruzoe N. Tertiapin, a selective ikach blocker, terminates atrial fibrillation with selective atrial effective refractory period prolongation. *Pharmacol Res* 2006; **54**: 136–141.
61 Satoh T, Zipes DP. Cesium-induced atrial tachycardia degenerating into atrial fibrillation in dogs: Atrial torsades de pointes? *J Cardiovasc Electrophysiol* 1998; **9**: 970–975.
62 Haugan K, Lam HR, Knudsen CB, Petersen JS. Atrial fibrillation in rats induced by rapid transesophageal atrial pacing during brief episodes of asphyxia: A new in vivo model. *J Cardiovasc Pharmacol* 2004; **44**: 125–135.
63 van der Hooft CS, Heeringa J, van Herpen G, Kors JA, Kingma JH, Stricker BH, *et al.* Drug-induced atrial fibrillation. *J Am Coll Cardiol* 2004; **44**: 2117–2124.
64 Nishida K, Michael G, Dobrev D, Nattel S. Animal models for atrial fibrillation: Clinical insights and scientific opportunities. *Europace* 2010; **12**: 160–172.
65 Schmid M, Khattab AA, Gloekler S, Meier B. Future epidemic impact of atrial fibrillation and a new interventional strategy for stroke prophylaxis. *Future Cardiol* 2011; **7**: 219–226.

E1

Circulation

American Heart Association. | American Stroke Association.
Learn and Live.

560 Harrison Avenue
Suite 502
Boston, MA 02118
Phone: 617-542-5100
FAX: 617-542-6539
circ@circulationjournal.org

October 7, 2013

Dr. José Jalife, MD
Center for Arrhythmia Research
University of Michigan
2800 Plymouth Road
Ann Arbor, MI 48109

RE: CIRCULATIONAHA/2013/004742R1
Dominant Frequency Increase Rate Predicts Transition from Paroxysmal to Long-Term Persistent Atrial Fibrillation

Dear Dr. Jalife,

Thank you very much for your submission to *Circulation*. Your manuscript has been evaluated by two reviewers and the editors. We are sorry to report that it is not acceptable for publication in *Circulation* in its present form.

Your revision was discussed with the editors who felt that additional data to address the concerns of the reviewers is needed for the paper to achieve sufficient priority. We would be willing to consider a revised manuscript, if you can address the comments of the reviewers and editors. We are making no commitment to publish your manuscript. Overall, approximately 10% of all submitted manuscripts are ultimately published.

With your response to comments, please provide each comment verbatim in bold followed by your response. If substantive changes have been made to the manuscript, please provide a clear description of what you did and where. If you insert important sentences, paragraphs or sections in response to the comments, please include them in this response. Please also be clear about any deletions. Additionally, a marked up version of the revision with the changes highlighted or tracked should be uploaded as a supplemental file.

Should you choose to resubmit, please comply with our Instructions to Authors. In particular, the following are required upon submission of your revision.

1. The text should not exceed 7,000 words, and the number of figures should not exceed 8. If your manuscript does not comply, it will be returned to you for further revision, prior to review.
2. Conflict of Interest Disclosures Forms must be completed for each author upon submission of the revision; please collect this information prior to returning to the submission site.
3. If an author has been removed from the paper, we require a signed agreement from that author authorizing the removal; otherwise, review of your manuscript will be delayed until we receive the signed agreement.
4. Please provide a short commentary which identifies the potential clinical impact of your paper and puts your research into perspective for the practicing clinician. Your clinical summary should not exceed 250 words and should be limited to one paragraph. Please do not include a reference list.

To submit your revision, please use the following link: <http://circ-submit.aha-journals.org/cgi-bin/main.plex?el=A2Hk5BORN3B1KZy7l6A9HyUsAceSdxKwuwWXFjHQwZ>

Please do not submit your manuscript as a new submission. If you cannot locate the revision link, please contact the editorial office at circ@circulationjournal.org.

Our current guidelines allow you 90 days to complete your revision. If you cannot meet this deadline, please contact the editorial office. All revisions not received within 90 days will be handled as de novo submissions.

We look forward to receiving your revision. Thank you very much.

Sincerely yours,

William G. Stevenson, MD
Associate Editor

Reviewer #1:

I thank the authors for the revised version of their manuscript. In this revised version, the authors have highlighted the issues raised by both reviewers as limitations of their study. This has certainly improved the positioning of this paper. Nonetheless, a few issues remain:

- Adding a short text regarding the putative role of Ca handling abnormalities is insufficient. Also, as discussed, the interpretation appears biased. There is clear evidence for DADs in patients with persistent AF (Voigt et al., Circulation 2012) and these proarrhythmic events could play a prominent role at any of stages studied in the present study. Ca-dependent remodeling as a consequence of Ca handling abnormalities is certainly beyond the scope of the study, but Ca handling abnormalities per se are not. At the very least the authors should perform some studies related to this area in frozen issue and discuss more indepth the importance of Ca handling abnormalities as AF progresses from a paroxysmal to a more persistent form.

- Figure 5A: please specify the CL at which these durations were determined.

- Page 11, first sentence: "Moreover, at persistent AF, resting membrane potential was hyperpolarized -2 mV which increased Na channel availability and improved tissue excitability." In Figure 8, both transition and persistent AF show hyperpolarized RMPs, in line with the increase in IK1 simulated in both groups (Suppl. Table S5). Thus, RMP does not appear to be an important factor for the altered rotor dynamics shown in Figure 8, suggesting that these are purely due to shortened ERP.

Reviewer #2:

Martins et al. present a revised version addressing some points appropriately; however there still remain several important issues, which have to be further addressed and don't seem to be beyond the scope of this study.

1.) Since the authors evaluated fibrosis, and SMA expression, as a marker of myofibroblast activation it seems that this topic is relevant in the context of AF progression; however, despite the data of Harada et al published in Circulation in 2012, which identified TRPC3 channels, miRNA 26 and NFAT as important players in this process promoting AF, the authors did not evaluate these variables. Especially looking at this type of animal model (representing more the state of lone AF than AF in the context of heart failure) it seems very crucial to evaluate potential contributors to AF progression especially in view of potential therapeutic targets preventing AF progression. Hence, the authors should consider determining these factors in there tissue samples of the different animal groups.
2.) Taking the huge amount of data suggesting that calcium handling abnormalities (incl. onset of delayed afterdepolarizations, increased NCX activity, RyR phosphorylation) are involved in initiation and maintenance of AF, which have been presented in the last years, this paradigm has to be addressed in some way. Also taken the fact that NFAT is known to play a crucial role in fibroblast remodeling (see above) and cellular calcium handling (incl. ICa,L remodeling) it remains still unclear why the authors did not evaluate if CaMK-II/Calcineurin/NFAT pathway could play a role at all in the context of AF progression. In the current version it appears that ion channel remodeling (represented by DF) is the major hallmark of AF progression, which is hard to conclude based on the experiments performed in this study.
3.) Based on the potential relevance regarding the transition of AF forms and the underlying or accompanying molecular and electrophysiological changes I still think the focus on factors predicting the transition / time of transition has to be better elaborated. Looking at clinical data, based on pacemaker holters the progression of AF differs a lot within the individual patients (patients can stay in paroxysmal AF for years) and there are recent data in huge discrepancy to previous data (see Sugihara et al. Journal of Interventional Cardiac Electrophysiology, April 2013, Vol13, I1, S1-126). Based on the moderate number of animals studied in the AF group (n=14) it should be possible to separate them into 2 groups of fast transition <43.5 days (median of paroxysmal AF) and one group of slow transition >/= 43.5 days to evaluate if some variables could be identified for differences in progression kinetics (DF of initial AF Episode?), furthermore mean DF acc. rates should for sure be different in these groups. Especially taking the fact that the authors discuss this topic extensively (pages) 15-16, they might try to investigate some other factors besides the dDF/dt in their model.

Response to Reviewers

Reviewer #1:

I thank the authors for the revised version of their manuscript. In this revised version, the authors have highlighted the issues raised by both reviewers as limitations of their study. This has certainly improved the positioning of this paper. Nonetheless, a few issues remain:

We thank the reviewer for his insights and constructive criticisms all of which have contributed to significantly enhance the scientific quality of our manuscript.

- Adding a short text regarding the putative role of Ca handling abnormalities is insufficient. Also, as discussed, the interpretation appears biased. There is clear evidence for DADs in patients with persistent AF (Voigt et al., Circulation 2012) and these proarrhythmic events could play a prominent role at any of stages studied in the present study. Ca-dependent remodeling as a consequence of Ca handling abnormalities is certainly beyond the scope of the study, but Ca handling abnormalities per se are not. At the very least the authors should perform some studies related to this area in frozen issue and discuss more indepth the importance of Ca handling abnormalities as AF progresses from a paroxysmal to a more persistent form.

As requested by the reviewer, we performed western blot analyses to determine whether sustained AF is associated with changes in five different calcium handling proteins (RyR2, SERCA, PLN, NCX and CamKII2) in the left and right atria appendages in each of the three groups of sheep (i.e., sham, transition and persistent AF). We found that RyR2, SERCA, PLN and CaMKII are either down-regulated or unchanged, while NCX is increased only in the left atrial appendage. In addition, the ratio of pRyR2/total RyR2 was unchanged. Altogether, these results suggest that in this model one should not expect an increase in the spontaneous release of Ca^{2+} from the SR or that DADs and triggered activity would be involved. Obviously, more specific analyses should be performed in future studies to more definitely establish whether or not calcium handling abnormalities have a role in the mechanism of AF progression from paroxysmal to more stable forms of the arrhythmia. Data have been added to the supplemental material (Figure S9 and S10) and discussed in the Results and Discussion sections (page 9, top paragraph and page 14, top paragraph; Limitations, Page 15).

- Figure 5A: please specify the CL at which these durations were determined.

The cycle length at which experiments of figure 5A were performed (1Hz) was added to the figure legend.

- Page 11, first sentence: "Moreover, at persistent AF, resting membrane potential was hyperpolarized -2 mV which increased Na channel availability and improved tissue excitability." In Figure 8, both transition and persistent AF show hyperpolarized RMPs, in line with the increase in IK1 simulated in both groups (Suppl. Table S5). Thus, RMP does not appear to be an important factor for the altered rotor dynamics shown in Figure 8, suggesting that these are purely due to shortened ERP.

We regret the incorrect statement. In addition, we found that we had inadvertently labeled our simulation figures incorrectly. As stated in the newly revised version, in Fig. 8 the ionic changes for the transition AF were based on our experimental patch clamp recordings. We did not have ionic current recordings for paroxysmal AF since experiments showed that the DF, APD were not different between transition and persistent AF. We have now corrected this in the revised manuscript. Therefore, to represent paroxysmal AF, we retained the ionic changes made in transition AF, but reduced the magnitude of I_{CaL} by only 30% (Table S5), such that the simulated APD_{90} was shortened significantly by 17% in paroxysmal AF, compared to 51% in transition AF (Table S6). The above revisions have been made in the main manuscript (Page 10, first and second paragraphs) and the Online Supplement.

Reviewer #2:
Martins et al. present a revised version addressing some points appropriately; however there still remain several important issues, which have to be further addressed and don't seem to be beyond the scope of this study.

We thank this reviewer also for his constructive criticisms. We have made a substantial effort to address the reviewer's concerns and hope he will agree that the scientific quality of our manuscript has increased significantly.

-Since the authors evaluated fibrosis, and SMA expression, as a marker of myofibroblast activation it seems that this topic is relevant in the context of AF progression; however, despite the data of Harada et al published in Circulation in 2012, which identified TRPC3 channels, miRNA 26 and NFAT as important players in this process promoting AF, the authors did not evaluate these variables. Especially looking at this type of animal model (representing more the state of lone AF than AF in the context of heart failure) it seems very crucial to evaluate potential contributors to AF progression especially in view of potential therapeutic targets preventing AF progression. Hence, the authors should consider determining these factors in there tissue samples of the different animal groups.
We recognize the enormous importance of understanding the molecular basis of myofibroblast differentiation in the context of lone AF. Thus, we have acknowledged the excellent contribution of Harada et al and also that TRPC3, NFAT and miRNA26 are important players in AF progression (Page 13, bottom paragraph). However, carefully exploring the possible role of such players to match Harada's high quality work using our model would require at least a year's worth of experimental work both in vivo and in vitro that would be impossible to complete in a single study. With all due respect to the reviewer, we submit that it would be unrealistic to attempt to continue adding data to this article, and wish to call his attention to the massive amount of work we have completed to this date. Please note that, after two major revisions, the Online Supplement of our manuscript has already expanded to 17 figures!

-Taking the huge amount of data suggesting that calcium handling abnormalities (incl. onset of delayed afterdepolarizations, increased NCX activity, RyR phosphorylation) are involved in initiation and maintenance of AF, which have been presented in the last years, this paradigm has to be addressed in some way. Also taken the fact that NFAT is known to play a crucial role in fibroblast remodeling (see above) and cellular calcium handling (incl. ICa,L remodeling) it remains still unclear why the authors did not evaluate if CaMK-II/Calcineurin/NFAT pathway could play a role at all in the context

of AF progression. In the current version it appears that ion channel remodeling (represented by DF) is the major hallmark of AF progression, which is hard to conclude based on the experiments performed in this study.

New western blot analyses included in the second revision were conducted to determine whether in this model sustained AF is associated with changes in any of five different calcium handling proteins (RyR2, SERCA, PLN, NCX and CaMKII2) in the left and right atria appendages in each of the three groups of sheep (i.e., sham, transition and persistent AF). The results showed that RyR2, SERCA, PLN and CaMKII2 were either down-regulated or unchanged, while NCX was increased only in the left atrial appendage. In addition, the ratio of pRyR2/total RyR2 was unchanged. Altogether, these results suggest that in this model one should not expect an increase in the spontaneous release of Ca^{2+} from the SR or that DADs and triggered activity would be involved. (These results are presented in Supplemental Figures S9 and S10.) However, as acknowledged in the revised manuscript (Page 14, First Paragraph; Limitations, page 15), it is still possible that Ca^{2+} loading produced by the high AF frequency activated the Ca^{2+}-dependent calmodulin-calcineurin-NFAT system to cause transcriptional downregulation of I_{CaL}.[1] Obviously, additional studies should be conducted.

-Based on the potential relevance regarding the transition of AF forms and the underlying or accompanying molecular and electrophysiological changes I still think the focus on factors predicting the transition / time of transition has to be better elaborated. Looking at clinical data, based on pacemaker holters the progression of AF differs a lot within the individual patients (patients can stay in paroxysmal AF for years) and there are recent data in huge discrepancy to previous data (see Sugihara et al. Journal of Interventional Cardiac Electrophysiology, April 2013, Vol13, I1, S1-126). Based on the moderate number of animals studied in the AF group (n=14) it should be possible to separate them into 2 groups of fast transition <43.5 days (median of paroxysmal AF) and one group of slow transition >/= 43.5 days to evaluate if some variables could be identified for differences in progression kinetics (DF of initial AF Episode?), furthermore mean DF acc. rates should for sure be different in these groups. Especially taking the fact that the authors discuss this topic extensively (pages) 15-16, they might try to investigate some other factors besides the dDF/dt in their model.

We agree with the reviewer. AF progression from paroxysmal to persistent is frequent, but not inevitable. Saksena et al[2] studied patient implanted with pacemakers and used the Holter capabilities of the devices to evaluate the rate and predictors of progression of AF. They observed a 24% rate of progression after 400 days of follow-up. Interestingly, patients developing sustained AF showed increase of AF burden over time, compared with patients remaining in paroxysmal AF who demonstrated no progressive change in AF duration (14 sec/day vs. 0 sec/day, $p<0.001$). Other authors have shown that some patient have a stable AF burden and do not progress to more stable forms of AF.

To answer reviewer's question, we separated slow and fast progressing animals sacrificed at transition depending on the median time to progression (<45 days: 4 animals; >45 days: 3 animals). Unfortunately, because of the small number of animals, most of the data do not reach statistical significance. As expected, dDF/dt was significantly higher for animal progressing quickly to persistent AF (0.07 ± 0.02 *vs.* 0.02 ± 0.007; $p=0.005$ for LA). Interestingly, we found that fast progression animals demonstrate significantly shorter action potential durations in the LA as compared to slow transition animals, and a trend for shorter RA APDs.

A trend for smaller I_{CaL} current densities was found in this subgroup of animals and may explain such differences in APDs. On the other hand, I_{K1} appeared to be increased in slow transition animals (data not significant likely due to low numbers). In addition, animals progressing slowly to persistent AF demonstrated higher levels of structural remodeling, including a significantly more pronounced atrial dilatation (124% *vs.* 45% increase in LA atrial dilatation; p=0.014), and trends for cellular hypertrophy and higher degree of fibrosis. Therefore, the results of the analysis recommended by the reviewer seem to suggest that the major factor contributing to greater APD shortening and dDF/dt increase in the fast transition animals was I_{CaL} downregulation. On the other hand, the slow transition animals appeared to require an additional thrust to achieve AF persistence, brought about by additional I_{K1} increase and greater structural remodeling. The results are presented in the Online Supplement (Figure S16 and S17) and discussed at the end of the Results section of the main manuscript (Page 10, last paragraph to Page 11, first paragraph; Limitations, Page 15).

References

1. Qi XY, Yeh YH, Xiao L, Burstein B, Maguy A, Chartier D, Villeneuve LR, Brundel BJ, Dobrev D, Nattel S. Cellular signaling underlying atrial tachycardia remodeling of l-type calcium current. *Circ Res*. 2008;103:845-854
2. Saksena S, Hettrick DA, Koehler JL, Grammatico A, Padeletti L. Progression of paroxysmal atrial fibrillation to persistent atrial fibrillation in patients with bradyarrhythmias. *Am Heart J*. 2007;154:884-892

University of Michigan
Health System

Center for Arrhythmia Research

William G. Stevenson, MD
Associate Editor
Circulation

RE: CIRCULATIONAHA/2013/004742R1

Dear Dr. Stevenson,
Thank you for giving us a second opportunity to revise our manuscript and to address the reviewers' concerns. We have added a substantial amount of new data and significantly modified the text in both the main manuscript and the Online Supplement to thoroughly address the reviewers concerns. The most important changes include the following:

First, both reviewers were concerned about a possible role of calcium dysfunction in the remodeling demonstrated in our sheep model of lone, persistent atrial fibrillation. We therefore conducted Western blot analyses for five different calcium handling proteins (ryanodine receptor type two-, RyR2; SR Ca2+-ATPase, SERCA, phospholamban, PLN; Na^+-Ca^{2+} exchanger, NCX and Ca^{2+}/calmodulin-dependent protein kinase-II, CaMKII) in the left and right atria appendages in each of the three groups of sheep (i.e., sham, transition and persistent AF). As illustrated in Figures S9 and S10 of the Online Supplement, while NCX was increased in the left atrial appendage, RyR2, SERCA, PLN and CaMKII were either downregulated or unchanged. Most important, the ratio of phosphorylated RyR2/total RyR2 was unaffected either in the transition or the persistent AF animals. Contrary to what was suggested by the reviewers these data do not support the hypothesis that the transition from paroxysmal to persistent AF depends on Ca^{2+} leak or delayed afterdepolarizations. However, it is still possible that Ca^{2+} loading produced by the high AF frequency activated the CaMKII-calcineurin-NFAT system to cause transcriptional downregulation of I_{CaL}. While this is an important question, it is clearly beyond the scope of the present study.

Second, Reviewer #1 identified an inaccurate statement we made in the previous version regarding to the role of membrane hyperpolarization in determining the increase in dominant frequency secondary to electrical remodeling. We have corrected that statement. In addition, we found that we had inadvertently labeled our simulation figures erroneously. As stated in the newly revised version, in Fig. 8 the ionic changes for the transition AF were based on our experimental patch clamp recordings. However, we did not have ionic current recordings for paroxysmal AF since experiments showed that the DF, APD were not different between transition and persistent AF. We have now corrected this in the revised manuscript. Hence, to represent paroxysmal AF, we retained the ionic changes made in transition AF, but reduced the magnitude of I_{CaL} by only 30% (Table S5), such that the simulated APD90 was shortened significantly by 17% in paroxysmal AF, compared to 51% in transition AF (Table S6). These changes did not significantly affect our main conclusion that the rate of DF increase depends primarily on I_{CaL} and subsequently I_{K1} remodeling.

Third, as recommended by Reviewer # 2, we separated slow and fast progressing animals sacrificed at transition depending on the median time to progression (<45 days: 4 animals; >45 days: 3 animals), in an effort to search for determinants of the rate of AF progression. This was a difficult task because by separating the animals the numbers were reduced and therefore the statistical power was also reduced. Nevertheless, presented in this manner the data suggest that the major factor contributing to the larger dDF/dt in the fast transition animals was greater APD shortening secondary to I_{CaL} reduction. On the other hand, the slow transition animals seemed to require an additional thrust to achieve AF persistence, which was brought about by additional I_{K1} increase and greater structural remodeling. These results

are presented in the Online Supplement as Figures S16 and S17, and also discussed in the main manuscript.

It is our hope that you will agree with us that, the massive amounts of data (8 figures in the main manuscript and 17 figures in the Online Supplement) we are now presenting, are of high scientific quality. Altogether, they provide a clear demonstration of the validity of our sheep model to investigate the consequences of sustained AF. In addition, the results provide strong support to the hypothesis that in this model of lone AF, the rate of DF acceleration predicts the time at which AF stabilizes and becomes persistent, reflecting changes in APD and densities of L-type calcium, sodium and inward rectifier currents. Most important, this model represents a novel clinically relevant platform in which to investigate molecular mechanisms of atrial remodeling leading to AF stabilization. Thus, we hope you will agree with us also that this is an important contribution that significantly advances the field and merits publication in *Circulation*.

We have followed your instructions for submission, as follows:

1. The text in the main manuscript is exactly 7,000 words, including title page, abstract, text, references, tables, and figure legends, and the number of figures is 8.

2. Conflict of Interest Disclosures Forms were completed for each author.

3. All authors listed originally remain.

4. We provide a short commentary which identifies the potential clinical impact of our paper and puts our research into perspective for the practicing clinician.

We present our responses to the reviewers' comments in an attached file. With our response we provide each comment verbatim in ***bold Italics*** followed by our response. When substantive changes have been made to the manuscript, we provide a clear description of what we did and where. Important sentences, paragraphs or sections in response to the comments are included in the response. Additionally, a marked up version of the revision with the changes highlighted or tracked has been uploaded as a supplemental file.

Once again, on behalf of my coauthors, I wish to thank you for your kind consideration of our manuscript.

Sincerely,

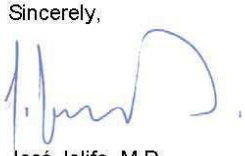

José Jalife, M.D.,
The Cyrus and Jane Professor of Cardiovascular Research and
Professor of Internal Medicine
Professor of Molecular & Integrative Physiology
Co-Director, Center for Arrhythmia Research
University of Michigan
2800 Plymouth Road
Ann Arbor, Michigan 48109

Title: Dominant Frequency Increase Rate Predicts Transition from Paroxysmal to Long-Term Persistent Atrial Fibrillation

Manuscript number: CIRCULATIONAHA/2013/004742R2

Author(s): José Jalife, University of Michigan, Ann Arbor, MI
Raphaël MARTINS, CHU Rennes
Kuljeet Kaur, University of Michigan
Elliot Hwang, University of Michigan
Rafael Ramirez, University of Michigan
Byrd Willis, University of Michigan
David Filgueiras-Rama, Hospital Universitario La Paz
Steven Ennis, University of Michigan
Yoshio Takemoto, University of Michigan
Daniela Ponce-Balbuena, University of Michigan

Manuel Zarzoso, University of Michigan
Ryan O'Connell, University of Michigan
Hassan Musa, University of Michigan
Guadalupe Guerrero-Serna, University of Michigan
Uma Mahesh Avula, University of Michigan
Michael Swartz, University of Rochester
Sandesh Bhushal, Norfolk State University
Makarand Deo, Norfolk State University
Sandeep Pandit, University of Michigan
Omer Berenfeld, Center for Arrhythmia Research, University of Michigan

Dominant Frequency Increase Rate Predicts Transition from Paroxysmal to Long-Term Persistent Atrial Fibrillation

Raphael P. Martins[1], MD, Kuljeet Kaur[1], PhD, Elliot Hwang[1], BS, Rafael J. Ramirez[1], PhD, B. Cicero Willis[1], MD, David Filgueiras-Rama[1], MD, Steven R. Ennis[1], PhD, Yoshio Takemoto[1], MD, PhD, Daniela Ponce-Balbuena[1], PhD, Manuel Zarzoso[1], PhD, Ryan P. O'Connell[1], PhD, Hassan Musa[1], PhD, Guadalupe Guerrero-Serna[1], PhD, Uma Mahesh R. Avula[1], MD, Michael F. Swartz[2], MD, Sandesh Bhushal,[3] BS, Makarand Deo,[3] PhD, Sandeep V. Pandit, PhD[1], Omer Berenfeld[1], PhD, José Jalife[1], MD

[1] Department of Internal Medicine, Center for Arrhythmia Research, University of Michigan, Ann Arbor, MI.
[2] Department of Surgery, University of Rochester, Rochester, NY.
[3] Department of Engineering, Norfolk State University, Norfolk, VA.

Short title: *Transition from Paroxysmal to Persistent AF.*

Correspondence:
José Jalife, M.D.
Center for Arrhythmia Research
University of Michigan
2800 Plymouth Road
Ann Arbor, MI 48109, USA
Email: jjalife@umich.edu

Word count: 7000

Journal subject codes: [5] Arrhythmias, clinical electrophysiology, drugs; [115] Remodeling; [130] Animal models of human disease; [132] Arrhythmias-basic studies

ABSTRACT

Background: Little is known about the mechanisms underlying the transition from paroxysmal to persistent atrial fibrillation (AF). In an ovine model of long-standing persistent AF (LS-PAF) we tested the hypothesis that the rate of electrical and/or structural remodeling, assessed by dominant frequency (DF) changes, determines the time at which AF becomes persistent.

Methods and Results: Self-sustained AF was induced by atrial tachypacing. Seven sheep were sacrificed after 11.5±2.3 days in self-sustained AF without reversal to sinus rhythm (SR); 7 sheep were sacrificed after 341.3±16.7 days of LS-PAF. Seven sham-operated animals were in SR for 1 year. DF was monitored continuously in each group. RT-PCR, western blotting, patch-clamping and histological analyses were used to determine changes in functional ion channel expression and structural remodeling. Atrial dilatation, mitral valve regurgitation, myocyte hypertrophy, and atrial fibrosis occurred progressively and became statistically significant after the transition to persistent AF, with no evidence for left ventricular dysfunction. DF increased progressively during the paroxysmal-to-persistent AF transition and stabilized when AF became persistent. Importantly, the rate of DF increase (dDF/dt) correlated strongly with the time to persistent AF. Significant action potential duration (APD) abbreviation, secondary to functional ion channel protein expression changes ($Ca_V1.2$, $Na_V1.5$ and $K_V4.2$ decrease; Kir2.3 increase), was already present at the transition and persisted for one-year follow up.

Conclusions: In the sheep model of LS-PAF, the rate of DF acceleration predicts the time at which AF stabilizes and becomes persistent, reflecting changes in APD and densities of sodium, L-type calcium and inward rectifier currents.

Keywords: Electrical Remodeling, Structural Remodeling, Fibrosis, Ion Channels, Refractory Period

INTRODUCTION

Atrial fibrillation (AF) is the most common arrhythmia in clinical practice. The natural history of AF usually starts with paroxysmal episodes. Some patients suffer paroxysmal AF indefinitely, mainly under anti-arrhythmic therapy, but a large proportion progress to persistent AF. In these patients, progression from paroxysmal to persistent and permanent AF is likely to reflect progressive electrophysiological and/or structural remodeling in both atria, making the arrhythmia more stable and long-lasting.[1] However, despite more than 100 years of research, fundamental mechanisms governing transition from paroxysmal to persistent and permanent forms are poorly understood, and prevention and treatment remain suboptimal.

Electrical remodeling, reflected by shortening of atrial refractoriness, is known to develop within the first few days of AF.[2] While some ion channel changes associated with electrical remodeling have been described in animal models and humans,[3-5] it is unclear yet how these changes integrate to stabilize AF. Structural remodeling and fibrosis might also contribute to intra-atrial conduction disturbances and increase susceptibility for AF, yet their role in progression from paroxysmal to persistent AF remains to be elucidated. Recently, we developed a clinically relevant ovine model of intermittent right atrial (RA) tachypacing and demonstrated that after the first AF episode, dominant frequency (DF) of both the RA and left atrium (LA) increased gradually during a 2-week period, after which DF remained stable during follow-up.[6] Here we have extended our study to investigate systematically whether gradual DF acceleration can predict when AF becomes persistent. We have modified the model such that pacing stops temporarily when AF is initiated during paroxysmal episodes and permanently once AF is sustained without reverting to sinus rhythm (SR). We compared three groups: Sham-operated, Transition (>7 days of self-sustained AF without reversal to SR) and self-sustained Long-Standing Persistent AF (LS-PAF, > 1 year of AF without reversal to SR). We hypothesized that: 1) DF acceleration rate in paroxysmal AF predicts timing of transition from paroxysmal to persistent AF; and 2) electrophysiological remodeling occurs early in transition, whereas structural remodeling in the form

of interstitial fibrosis appears more gradually and is belatedly manifest once self-sustained persistent AF has stabilized.

METHODS

An expanded methods section is available in the Online Supplement.

Pacemaker implantation: Procedures were approved by the University of Michigan Committee on Use and Care of Animals and complied with National Institutes of Health guidelines. Twenty-one 6-8 month-old sheep (≈40 kg) had a pacemaker implanted subcutaneously, with an atrial lead inserted into the RA appendage. In a subset of thirteen sheep (8 paced and 5 in SR), an implantable loop recorder (ILR) was placed subcutaneously on the left side of the sternum (Figure S1A).

Pacing protocol: After 10 days recovery, sheep were assigned to either Sham-operated or atrial tachypacing groups. Sham-operated animals (N=7) had pacemakers programmed in sensing-only mode (OAO). Automatic mode switch was enabled in atrial-tachypaced animals (Figure S1B). The pacemaker was programmed to induce AF by burst tachypacing (30-sec pacing, 20 Hz, twice diastolic threshold) followed by 10-sec sensing. Pacemakers resumed pacing only if AF stopped and SR was detected. The Holter capabilities of the device were used to record intra-cardiac electrograms (EGMs) to accurately confirm the occurrence of AF, generate histograms, and follow the evolution of AF from the first episode of paroxysmal AF to the eventual establishment of persistent AF. Persistent AF was defined as episodes lasting >7 days without reversal to SR. A subset of tachypaced animals was sacrificed after more than 7 days of self-sustained AF (Transition group, N=7). The remaining animals were sacrificed after one year of self-sustained AF (LS-PAF group, N=7). Pacemakers and ILRs were interrogated weekly.

***Electrogram acquisition and processing*:** Persistence of SR was verified in sham-operated animals and pacemaker memories were checked to detect spontaneous AF episodes. Three recordings were obtained in tachypaced sheep during follow up: 1) RA-lead EGM; 2) ECG Standard lead I; and 3) ILR single lead recording (LA far-field signal).

***Serum measurements*:** Procollagen III N-Terminal Propeptide (PIIINP) levels were measured by enzyme linked immunosorbant assay.

***Echocardiography*:** LA and RA dimensions, severity of mitral regurgitation, left ventricular ejection fraction (LVEF), end-systolic and end-diastolic diameters were evaluated using echocardiography (Figures S2 and S3).[7]

***Heart removal and cell dissociation*:** At termination of follow-up, hearts were removed and atria dissected (Figure S4) for myocyte isolation. patch-clamp recordings, western blotting, real-time PCR and histology (see Online Supplement).

Computer Simulations: We modified the Grandi-Pandit[8] human atrial cell model to simulate action potential and propagation in 2D.

RESULTS

Sheep model of persistent AF: Of 21 implanted sheep one sham-operated animal was excluded and sacrificed prematurely due to severe symptomatic systemic infection. No atrial arrhythmias occurred in any sham-operated animals during follow-up. Also, no tachypaced animals developed signs of heart failure or stroke. Figure 1 summarizes the time-course of AF development. The representative 3D plot (Figure 1A) relates percentage of AF episodes in a given day (Y-axis) to duration of episodes (X-axis) and weeks of follow-up (Z-axis). The first AF episode occurred after a median time of 5.5 days after

initiation of pacing (mean, 15.0±5.9 days; range, 0-62 days, Figure 1B). AF episodes were then paroxysmal (<7 days duration), reaching self-sustained persistent AF (>7 days without reversal to SR) after a median of 43.5 days (mean 73.2±23.0 days; range, 19 to 346 days). Once in persistent, there was no further tachypacing as AF was detected uninterruptedly. Sheep in Transition and LS-PAF were sacrificed 11.5±2.3 days and 341.3±16.7 days, respectively, after occurrence of self-sustained persistent AF (i.e. after the last occurrence of SR).

Persistent AF leads to atrial dilatation: Echocardiographic findings (Table S1, Figures S2 and S3) revealed that LVEF was unchanged whereas RA and LA areas increased significantly in LS-PAF, compared with sham-operated and Transition groups ($p<0.05$, Figure S3). At last follow-up, LS-PAF animals showed significant mitral valve regurgitation (Figure S3B), yet LV end-diastolic volume, LV end-systolic volume or wall thickness were unchanged (data not shown), ruling out tachycardia-induced cardiomyopathy associated with AF. Although, compared to sham-operated animals, the dry weight of isolated atria in the transition group tended to be larger, only the atrial tissues from the LS-PAF group demonstrated a significant increase weight (Table S2).

Persistent AF leads to atrial myocyte hypertrophy: Mean LA and RA myocyte length and width, respectively, were similar for sham-operated animals (Figure S5). At transition, LA myocyte length and width increased significantly ($p<0.001$ and $p<0.01$, respectively); RA myocyte length did not change significantly ($p=0.25$) and a trend for wider cells was observed ($p=0.08$). At transition, LA cells were longer than RA cells ($p<0.001$), and after one year of AF, no further differences were observed for LA myocyte lengths or widths compared to transition. However, RA myocytes that initially did not exhibit significant changes at transition, showed a trend for longer cells and were significantly wider ($p<0.001$). In LS-PAF, LA myocytes were longer ($p=0.002$) and thinner ($p=0.001$) compared to RA.

AF leads to atrial myofibroblast activation and fibrosis in the absence of heart failure: AF-induced changes in the extracellular matrix were analyzed using histology, serum markers and molecular biology. There was a trend towards increased patchy fibrosis in RA, LA and PLA regions during AF

progression, interstitial fibrosis increased in both LA (from 5.5±1.2 to 10.7±1.5%, $p<0.05$) and PLA (from 4.1±0.6 to 14.6±1.4%, $p<0.001$), particularly in LS-PAF (Figure 2A-B, Table S3). These data correlated with measurements of PIIINP, a serum marker for collagen synthesis, which increased progressively, reaching maximal levels in LS-PAF which was increased significantly from Sham-operated animals at a similar time point ($p=0.001$ *vs.* sham, Figure S6). As expected from PIIINP serum levels, tissue protein levels of collagen III, analyzed by western blot, increased significantly in both atria during LS-PAF (Figures 2C and D). A significant increase in atrial α-smooth muscle actin (α-SMA), a marker of myofibroblast activation,[9] was seen in both atria in Transition, but tended to decrease toward control levels in LS-PAF.

Electrophysiological remodeling is reflected by DF changes: During weekly interrogations, we investigated AF occurrence and recorded ongoing episodes. The DF of the first episode recorded from the RA lead was relatively slow at 7.5±0.1 Hz (range 6.5–8.25 Hz). Simultaneous DFs from the surface ECG and ILR after QRST subtraction were 7.7±0.2 Hz (range 6.5 to 9.25 Hz) and 9.0±0.1 Hz (range 8.9 - 9.4 Hz), respectively. Thus, as previously demonstrated,[6] at the outset there was a significant DF difference between RA and LA ($p<0.001$, Figure 3). Thereafter, DF increased progressively in both atria. At both transition and LS-PAF, DFs recorded on the RA, surface ECG and LA were higher than during the first episode ($p<0.001$). However, in the 7 LS-PAF sheep, the last DFs recorded after 1 year of AF were not significantly different from prior corresponding values at transition. Thus, the major increase in DF occurred during paroxysmal AF and not during self-sustained LS-PAF. Additionally, while a significant LA-to-RA frequency gradient was present during the first episode, this gradient diminished at transition ($p=0.06$) and LS-persistent time points ($p=0.1$), likely reflecting remodeling of refractory periods in both atria. In any given animal, once respective maximum DF values were achieved, they remained relatively stable even after one year follow up; there was no significant difference between maximum DF at transition and at ~350 days.

The rate of DF increase predicts the onset of persistent AF: We analyzed several parameters to determine whether or not the time in paroxysmal AF and transition to self-sustained persistent AF could be predicted. We first surmised that a critical DF should be reached before self-sustained persistent AF developed, but the data did not support this hypothesis (Figure S7). Not only did maximal DF vary among animals, but the rate of DF increase during transition was also highly variable, ranging 0.003 to 0.15 Hz/day in the RA and 0.001 to 0.12 Hz/day in the LA. However, sheep that developed self-sustained persistent AF early, also had a steep slope of DF increase with time (dDF/dt), regardless of DF during the first episode, whereas those with a delayed onset of persistent AF had a shallower DF slope (Figure 4A). Thus we hypothesized that dDF/dt could predict when AF became persistent in each animal. Indeed, a strong nonlinear relationship was found between time to persistent AF onset and dDF/dt regardless of whether DF was determined in the RA, LA or surface ECG (R^2= 0.87, 0.92 and 0.71, respectively, Figure 4B). The faster the DF acceleration, the quicker the animal developed self-sustained persistent AF. Furthermore, non-invasive measurement of dDF/dt (surface ECG lead I) correlated strongly with RA and LA dDF/dt (Figure S8).

Cellular and ionic mechanisms of electrical remodeling: We conducted patch-clamp experiments to determine whether the gradual DF increase during transition reflected development of remodeling at the cellular level. Action potential duration at 90 percent repolarization (APD_{90}) was significantly reduced in both RA and LA at transition and LS-PAF groups (Figure 5). Sheep from both groups tended to have more hyperpolarized resting membrane potentials than sham (p=NS, data not shown) for RA (-69.8±2.8 mV, -60.2±3.4 mV and -57.6±4.6 mV, respectively) and LA myocytes (-72.1±4.1 mV, -66.6±3.6 mV and -63.5±2.3 mV, respectively). Action potential (AP) upstroke velocity (dV/dt_{max}) also tended to be lower in myocytes from AF animals, while AP amplitudes did not change significantly (data not shown). Myocytes from animals in AF also showed a loss of rate-adaptation of APD (Figure 5B). Shortest pacing cycle length before AP alternans or failure to capture was significantly longer in sham than transition and LS-PAF groups (data not shown), as a consequence of APD and ERP shortening in both RA (345.7±37.5 ms, 165.7±62.6 ms and 203.3±26.5 ms, respectively, $p<0.05$ vs. sham) and LA (358.3±31.2 ms, 218.1±27.5 ms and 249.4±17.7 ms, respectively, $p<0.05$ vs. sham).

Next, we conducted Western blot analyses in the three groups on animals to test whether remodeling was related to altered intracellular calcium dysfunction. As illustrated in Figures S9 and S10 of the Online Supplement, while the Na^+-Ca^{2+} exchanger was increased in the LA appendage, both total RyR2 and phosphorylated RyR2 proteins were decreased in the AF group, but the ratio of phosphorylated RyR2 to total RyR2 phosphorylation was unaffected. Accordingly, the transition from paroxysmal to persistent AF did not seem to depend on Ca^{2+} leak or delayed afterdepolarizations.[10]

We then focused on possible alterations in sarcolemmal ion channels that might contribute to AF-induced changes in APD and refractoriness. Peak inward sodium current (I_{Na}) was significantly reduced at the transition time-point by about 50% in LA myocytes compared to sham (Figure 6A) and about 30% in RA myocytes. For LS-PAF, peak I_{Na} was decreased in both LA and RA myocytes ($p<0.001$ vs. sham). Similarly, peak L-type calcium current (I_{CaL}) was reduced in LA and RA at transition and LS-PAF ($p<0.05$, Figure 6B). Changes in I_{Na} and I_{CaL} resulted from concomitant decreases in expression of $Na_v1.5$ and $Ca_v1.2$ proteins and *SCN5A* and *CACNA1C* mRNA levels (Figure 6D-G; see Table S4 for primers used in RT-PCR).

In contrast to I_{Na} and I_{CaL}, the density of the inward rectifier potassium current (I_{K1}) increased 2- to 3-fold at negative membrane voltages during the transition in both atria, and continued to increase for LS-PAF ($p<0.05$ *vs.* sham, Figure 7A). Since sheep atria predominantly express Kir2.3 channels,[11] we measured Kir2.3 expression which was increased in LS-PAF animals (Figure 7B). There was no Kir2.3 increase in transition despite the larger current density compared to sham. The transient outward K^+ current (I_{to}) decreased by about 85% by transition (Figure S11) and remained low in LS-PAF ($p<0.001$, Figure S11). For LS-PAF animals, I_{to} reduction could be explained by decreased $K_v4.2$ expression. However, reduced protein was not evidenced in the LA in transition animals, suggesting other mechanisms contributed to I_{to} decrease.[12] Lastly, Kv11.1 protein expression remained unchanged (Figure S11C-D).

Can ionic current changes explain DF acceleration? To address the question of whether differential changes in ion currents demonstrated above could explain DF acceleration during transition from paroxysmal to persistent AF we generated APs for control, paroxysmal, and transition AF conditions using the Grandi-Pandit human atrial AP model (Figure 8A, Table S5). The ionic changes for the transition AF were based on our experimental patch clamp recordings. We did not have ionic current recordings for paroxysmal AF. Therefore, to represent paroxysmal AF, we retained the ionic changes made in transition AF, but reduced the magnitude of I_{CaL} by only 30% (Table S5), such that the simulated APD_{90} was shortened significantly by 17% in paroxysmal AF, compared to 51% in transition AF (Table S6).

We used a 2D sheet model of reentry to investigate whether AP differences between paroxysmal and transition AF simulations would explain the progressive DF acceleration demonstrated in vivo. Sustained functional reentry (rotor) dynamics showed differential properties. The rotor in paroxysmal AF (Figure 8B, left) was short lived, and exhibited low rotation frequency (5.0 Hz) and considerable meandering (Figure 8C, left), eventually self-terminating upon collision with boundary edges. In contrast, in the transition AF model, the rotor was stable and persisted throughout the length of the simulation (Figure 8B, right) with significantly less rotor meander (Figure 8C, right) and higher DF (7.67 Hz) compared to the transition case. When reduction in I_{Na} density was not incorporated, the DF increased only slightly to 8.67 Hz, but the rotor was unstable and eventually stopped.

We also further investigated the roles of individual ionic changes in a subset of simulations. Rotors were simulated in 2D sheets, when individual ionic currents were changed, compared to controls. As discussed in detail in the Online Supplement (Figures S12-S15), the simulation results confirmed that changes in I_{K1} and I_{CaL} are key determinants of rotor acceleration in paroxysmal and transition AF.

Fast versus slow transition. To search for determinants of the rate of AF progression, we separated slow and fast progressing animals sacrificed at transition depending on the median time to progression (<45 days: 4 animals; >45 days: 3 animals). As discussed in detail in the Online Supplement (Figures S16 and

S17), the major factor contributing to the larger dDF/dt in the fast transition animals was greater APD shortening secondary to I_{CaL} reduction. On the other hand, the slow transition animals seemed to require an additional I_{K1} increase and greater structural remodeling.

DISCUSSION

The most important results of this study are: 1) Intermittent rapid tachypacing in a sheep model of long-term, lone persistent AF results in a progressive increase in DF during paroxysmal AF; 2) DF stabilizes when AF becomes persistent; 3) DF acceleration (dDF/dt) correlates strongly with time to persistent AF; 4) APD abbreviation, secondary to ion channel gene expression changes ($Na_V1.5$ $Ca_V1.2$, and $K_V4.2$ decrease; Kir2.3 increase), is already present or occurs rapidly during transition and explains the DF acceleration; 5) In the absence of LV dysfunction, there is a progressive increase in atrial dilatation, mitral valve regurgitation, myocyte hypertrophy, and atrial fibrosis, which became significant after DF had stabilized. Altogether, these results demonstrate that the rate of DF increase during transition predicts the time at which AF stabilizes and becomes persistent, reflecting changes in APD and densities of I_{CaL}, I_{K1}, I_{Na} and I_{to}. Thus, this is the first detailed characterization of the electrophysiological and structural remodeling involved in the transition from paroxysmal to persistent AF and self-sustained LS-PAF.

In-vivo changes in DF during AF. Various animal models and clinical studies have demonstrated the presence of a spatial distribution of DF during AF. Left-to-right frequency gradients were found in isolated sheep hearts, supporting the hypothesis that AF results from rapidly successive wavefronts emanating from fast sources localized in the LA.[13] Similar gradients were confirmed in humans with AF,[14, 15] but were shown to be present mainly during paroxysmal AF, but not always in persistent or permanent AF since longer periods in AF lead to a more complex remodeling making both atria suitable for harboring reentrant sources.[14-16] Patients with persistent AF usually demonstrate higher DFs compared to paroxysmal AF.[15] We recently demonstrated in the ovine model that intermittent

tachypacing results in AF with a progressive increase in DF over a 2-week period after the first detected AF episode.[6] There we used an algorithm of 30-seconds pacing followed by a 10-second blanking period, over a 22-week follow-up, whether or not AF was detected. Thus, continuous pacing likely induced a DF that was similar in all animals studied at that time.[6] To increase the clinical relevance of our AF model, here we modified our pacing algorithm by transforming the 10-second blanking period into a real sensing period, consequently avoiding unnecessary pacing and generating a model of self-sustaining AF. Therefore, in this more realistic model of lone AF, there was a progressive increase in DF that was different for each animal, ranging from 4–50 weeks. The first AF episode was slow followed by a progressive and significant increase in DF during paroxysmal AF, reaching maximal value at the transition to persistent AF. Most important, DF did not increase further even after 1 year of self-sustained persistent AF.

Progressive DF increase during transition is a consequence of electrical remodeling. Sustained AF shortens APD and effective refractory period, decreasing wavelength and facilitating acceleration and stabilization of sustained reentry. The main determinants of APD shortening are the decrease in I_{CaL} and increase I_{K1}.[17,18] In a canine model of constant rapid atrial pacing, appreciable APD shortening occurred after 1 day of pacing, and was near-maximal after 7 days.[19] At the electrophysiological level, reduced I_{CaL} and I_{to} were observed, without significant change in I_{K1}.[19] However, human remodeling as a consequence of AF has been shown to be more complex, involving many changes in potassium currents like decreased of I_{to1}[5] and I_{Kur}[5] and increased I_{Ks}[5], I_{K1} and the constitutively-active I_{KACh}.[4] The contribution of these changes to APD shortening has been analyzed in computer modeling studies suggesting that I_{K1} increase is a predominant mechanism of APD shortening.[20]

Our results support previous numerical predictions. I_{Na} and I_{CaL} decreases secondary to reductions in $Na_V1.5$ and $Ca_V1.5$ expression, and I_{K1} density increases secondary to increased Kir2.3 expression were the major ionic changes observed at transition (remodeling during paroxysmal AF), they evolved parallel with DF increase, and changed negligibly throughout the one-year follow-up in self-sustained persistent AF. Upregulation of I_{K1} is known to enhance cardiac excitability through cell

hyperpolarization and increased sodium channel availability, and to increase frequency and stability of rotors driving AF and VF.[21] Our computer simulations reaffirmed these results since rotors were found to be more stable, less meandering and persistent for transition compared to paroxysmal time-points (7.7 vs. 5.0 Hz, respectively). Similarly, I_{Na} reduction, despite reducing excitability slightly, also contributed to rotor stabilization, as shown by the fact that rotors generated in the absence of I_{Na} reduction exhibited considerable meandering leading to their eventual annihilation. Most important, however, our numerical results predict that downregulation of I_{CaL} and upregulation of I_{K1} to be the most important contributors to the increased DF and rotor stabilization, particularly during transition AF.

Structural remodeling and the link to electrical remodeling: We observed significant structural remodeling in this model of lone, persistent AF. Myocyte hypertrophy and atrial dilatation increased progressively among sham-operated sheep and sheep at transition or LS-PAF, which suggests there might be a connection between atrial enlargement and DF acceleration. Additionally, PIIINP, a serum marker of interstitial fibrosis, increased gradually from the first episode through transition into the last follow-up. Collagen protein levels and interstitial fibrosis also tended to increase during transition and became frankly manifest once self-sustained LS-PAF developed. Notably, a significant increase in atrial α-SMA protein, a marker of myofibroblast activation,[9] was seen in both atria in transition, but this protein tended to decrease toward control levels in LS-PAF animals. These changes might reflect processes similar to those described for myocardial infarction: a myofibroblast proliferative phase gives way to a maturation phase in which the cellularity of tissue decreases and local extracellular matrix is cross-linked forming a collagen-based fibrotic scar.[22] Therefore, the increase in α-SMA protein may reflect increased atrial myofibroblast activation and proliferation induced by atrial tachypacing induced upregulation of transient receptor potential canonical-3 (TRPC3) channels,[23] which may have contributed not only to development of fibrosis, but also to electrical remodeling through release of profibrotic cytokines. One such cytokine is platelet-derived growth factor (PDGF), which, as recently demonstrated, can reduce atrial myocyte APD and I_{CaL} in ways that resemble the effects of persistent

AF as shown in this study.[24] Finally, we found no change or downregulation of most calcium-handling proteins and no change in the phosphorylated RyR2/total RyR2 ratio, which makes it unlikely that, in this animal model of lone AF, the rate of change of AF-induced differential ion channel expression depends on sustained AF-induced intracellular Ca^{2+}-handling remodeling or increased SR Ca^{2+} leak. However, it is still possible that Ca^{2+} loading produced by the high AF frequency activated the Ca^{2+}-dependent calmodulin-calcineurin-NFAT system to cause transcriptional downregulation of I_{CaL}.[25]

Predicting transition from paroxysmal to persistent AF: Mid- to long-term follow-up studies in patients have shown that the rate of progression from paroxysmal to persistent or permanent AF ranges between 14.6% and 35.3% during 1 to 12 years.[26-29] A 30-year follow-up study reported a cumulative probability risk of progression of 29% (95% CI, 16 to 42%) with most transitions occurring within 15 years after diagnosis. Many independent clinical, echocardiographic and electrocardiographic predictors of transition have been described including age,[1, 27-29] hypertension, previous ischemic attack or stroke, chronic obstructive pulmonary disease,[1] presence of cardiomyopathy/heart failure,[1, 26-28] atrial enlargement,[28] valvular diseases[28], filtered P-wave duration ≥150 ms, or P-wave dispersion on ECG.[29] A report using pacemaker memory interrogation found 24% risk of transition at a mean follow-up of 5 months.[26] Interestingly, slope of change in AT/AF burden as a function of time was examined. Patients developing sustained AF showed increase of AF burden over time, compared with patients remaining in paroxysmal AF who demonstrated no progressive change in AF duration (14 sec/day vs. 0 sec/day, $p<0.001$). Similarly, in our study, we observe a very different rate of increase of dDF/dt and episode durations between animals quickly developing persistent AF and those remaining in paroxysmal AF for a long period before transition. Both LA and RA dDF/dt predicted the transition to persistent AF. This is not surprising since DF increased in both atria until AF became persistent (Figure 3). Thus ionic remodeling occurred in both atria, though somewhat more intensely in the LA than RA, particularly for I_{CaL} (Figure 6B) and I_{K1} (Figure 7), both of which contributed to the increased DF and rotor stabilization (Figures S12 and S13). Finally, the possible contribution of cytokines released from ion-channel mediated activation[30] and differentiation of fibroblasts into hypersecretory myofibroblasts as a

common link to structural and electrical remodeling in the fibrillating atria is likely to be important and deserve further exploration.

Limitations: We used a pacing induced self-sustained AF model in which continued periods of SR were not allowed since pacing was resumed as soon as AF terminated (5-10 seconds of SR between spontaneous termination of AF, detection of SR and initiation of the following pacing run). Thus, it is unknown whether the time from paroxysmal to persistent AF would be predictable in other animal models or humans. In addition, while this model enabled us to investigate the consequences of sustained AF in the absence of other co-morbidities, we are well aware that the majority of human AF cases associate with cardiovascular disease. Nevertheless, our results show that the time to AF persistence is predicted by the rate of change of DF and explained primarily by downregulation of I_{CaL} and upregulation of I_{K1}. The results also suggest that the wide range of dDF/dt values and time to persistent AF might be explained by temporal differences in the remodeling of these two channels in animals exhibiting slow-versus-fast progression to LS-PAF, which requires further study. Other currents may be important, including I_{Kl}[18] and I_{KACh}, whose constitutively active isoform is upregulated.[4, 31] Activation of I_{KACh} with adenosine accelerates DF in patients with paroxysmal AF[16]. Therefore studies should be performed to analyze the time-course of I_{KACh} changes during AF progression. In our study I_{to} decrease and I_{K1} increase in transition did not correlate with protein expression, suggesting other genes encoding ion channel alpha- or beta-subunits might be important. Alternatively, open-channel probability in the case of I_{K1}[31] might help explain the changes we have observed. Similarly, while our analysis of Ca^{2+}-handling proteins suggested that the transition from paroxysmal to persistent AF did not depend on Ca^{2+} leak or DADs, more extensive studies involving intracellular Ca^{2+} measurements will be required for definite proof.[25] Lastly, we decided not to model LS-PAF since no major electrophysiological changes occurred during the one-year follow-up. However, additional structural remodeling after the transition (e.g., atrial dilatation, fibrosis, myocyte hypertrophy) are likely to affect DF, but were not incorporated in the simulations.

CLINICAL IMPLICATIONS

We have used a model of intermittent atrial tachypacing that resembles much closer the situation in humans with AF than animal models with atrial tachycardia remodeling in the absence of co-morbidities like left ventricular dysfunction and heart failure. We demonstrate that predicting transition from paroxysmal to persistent AF is feasible. Similar to human AF, we found a very heterogeneous temporal progression to persistent AF among animals, ranging from 4–50 weeks. Similar findings in human AF would help stratify paroxysmal AF patients depending on risk of progression. Patients exhibiting steep dDF/dt increases during follow-up could be rapidly referred to an EP lab for ablation before persistent AF develops, which would reduce ablation time and number of procedures.[32] Conversely, patients with low dDF/dt could be considered at low risk for progression and be treated longer with anti-arrhythmic drugs before being referred to an EP lab. We showed also that dDF/dt analyzed by surface ECG (lead I) correlated well with RA and LA dDF/dt. This would obviate invasive analysis for stratification and be of great help in guiding physicians to individualize therapy.

Acknowledgments: Authors would like to thank Felipe Atienza, Justus M.B. Anumonwo, Mario San Martin-Gomez, and Jérôme Kalifa for their helpful suggestions.

Sources of Support:

This work was supported in part by, the National Heart, Lung, and Blood Institute Grants (P01-HL039707 and P01-HL087226 to JJ and OB), the Leducq Foundation and CNIC (JJ and OB) the Fédération Française de Cardiologie (RPM), Spanish Society of Cardiology Fellowship, and Alfonso Martín Escudero Foundation (DFR).

Conflict of Interest: Dr. Jalife is on the Scientific Advisory Board of avertAF.

REFERENCES

1. de Vos CB, Pisters R, Nieuwlaat R, Prins MH, Tieleman RG, Coelen RJ, van den Heijkant AC, Allessie MA, Crijns HJ. Progression from paroxysmal to persistent atrial fibrillation clinical correlates and prognosis. *J Am Coll Cardiol*. 2010;55:725-731
2. Allessie M, Ausma J, Schotten U. Electrical, contractile and structural remodeling during atrial fibrillation. *Cardiovasc Res*. 2002;54:230-246
3. Van Wagoner DR, Pond AL, Lamorgese M, Rossie SS, McCarthy PM, Nerbonne JM. Atrial l-type ca2+ currents and human atrial fibrillation. *Circ Res*. 1999;85:428-436
4. Voigt N, Trausch A, Knaut M, Matschke K, Varro A, Van Wagoner DR, Nattel S, Ravens U, Dobrev D. Left-to-right atrial inward rectifier potassium current gradients in patients with paroxysmal versus chronic atrial fibrillation. *Circ Arrhythm Electrophysiol*. 2010;3:472-480
5. Caballero R, de la Fuente MG, Gomez R, Barana A, Amoros I, Dolz-Gaiton P, Osuna L, Almendral J, Atienza F, Fernandez-Aviles F, Pita A, Rodriguez-Roda J, Pinto A, Tamargo J, Delpon E. In humans, chronic atrial fibrillation decreases the transient outward current and ultrarapid component of the delayed rectifier current differentially on each atria and increases the slow component of the delayed rectifier current in both. *J Am Coll Cardiol*. 2010;55:2346-2354
6. Filgueiras-Rama D, Price NF, Martins RP, Yamazaki M, Avula UM, Kaur K, Kalifa J, Ennis SR, Hwang E, Devabhaktuni V, Jalife J, Berenfeld O. Long-term frequency gradients during persistent atrial fibrillation in sheep are associated with stable sources in the left atrium. *Circ Arrhythm Electrophysiol*. 2012;5:1160-1167
7. Gottdiener JS, Bednarz J, Devereux R, Gardin J, Klein A, Manning WJ, Morehead A, Kitzman D, Oh J, Quinones M, Schiller NB, Stein JH, Weissman NJ. American society of echocardiography recommendations for use of echocardiography in clinical trials. *J Am Soc Echocardiogr*. 2004;17:1086-1119
8. Grandi E, Pandit SV, Voigt N, Workman AJ, Dobrev D, Jalife J, Bers DM. Human atrial action potential and ca2+ model: Sinus rhythm and chronic atrial fibrillation. *Circ Res*. 2011;109:1055-1066
9. Frangogiannis NG, Michael LH, Entman ML. Myofibroblasts in reperfused myocardial infarcts express the embryonic form of smooth muscle myosin heavy chain (smemb). *Cardiovasc Res*. 2000;48:89-100
10. Voigt N, Li N, Wang Q, Wang W, Trafford AW, Abu-Taha I, Sun Q, Wieland T, Ravens U, Nattel S, Wehrens XH, Dobrev D. Enhanced sarcoplasmic reticulum ca2+-leak and increased na+-ca2+-exchanger function underlie delayed afterdepolarizations in patients with chronic atrial fibrillation. *Circulation*. 2012
11. Dhamoon AS, Pandit SV, Sarmast F, Parisian KR, Guha P, Li Y, Bagwe S, Taffet SM, Anumonwo JM. Unique kir2.X properties determine regional and species differences in the cardiac inward rectifier k+ current. *Circ Res*. 2004;94:1332-1339
12. Tessier S, Karczewski P, Krause EG, Pansard Y, Acar C, Lang-Lazdunski M, Mercadier JJ, Hatem SN. Regulation of the transient outward k(+) current by

ca(2+)/calmodulin-dependent protein kinases ii in human atrial myocytes. *Circ Res*. 1999;85:810-819

13. Mansour M, Mandapati R, Berenfeld O, Chen J, Samie FH, Jalife J. Left-to-right gradient of atrial frequencies during acute atrial fibrillation in the isolated sheep heart. *Circulation*. 2001;103:2631-2636
14. Lazar S, Dixit S, Marchlinski FE, Callans DJ, Gerstenfeld EP. Presence of left-to-right atrial frequency gradient in paroxysmal but not persistent atrial fibrillation in humans. *Circulation*. 2004;110:3181-3186
15. Sanders P, Berenfeld O, Hocini M, Jais P, Vaidyanathan R, Hsu LF, Garrigue S, Takahashi Y, Rotter M, Sacher F, Scavee C, Ploutz-Snyder R, Jalife J, Haissaguerre M. Spectral analysis identifies sites of high-frequency activity maintaining atrial fibrillation in humans. *Circulation*. 2005;112:789-797
16. Atienza F, Almendral J, Moreno J, Vaidyanathan R, Talkachou A, Kalifa J, Arenal A, Villacastin JP, Torrecilla EG, Sanchez A, Ploutz-Snyder R, Jalife J, Berenfeld O. Activation of inward rectifier potassium channels accelerates atrial fibrillation in humans: Evidence for a reentrant mechanism. *Circulation*. 2006;114:2434-2442
17. Bosch RF, Scherer CR, Rub N, Wohrl S, Steinmeyer K, Haase H, Busch AE, Seipel L, Kuhlkamp V. Molecular mechanisms of early electrical remodeling: Transcriptional downregulation of ion channel subunits reduces i(ca,l) and i(to) in rapid atrial pacing in rabbits. *J Am Coll Cardiol*. 2003;41:858-869
18. Dobrev D, Graf E, Wettwer E, Himmel HM, Hala O, Doerfel C, Christ T, Schuler S, Ravens U. Molecular basis of downregulation of g-protein-coupled inward rectifying k(+) current (i(k,ach) in chronic human atrial fibrillation: Decrease in girk4 mrna correlates with reduced i(k,ach) and muscarinic receptor-mediated shortening of action potentials. *Circulation*. 2001;104:2551-2557
19. Yue L, Feng J, Gaspo R, Li GR, Wang Z, Nattel S. Ionic remodeling underlying action potential changes in a canine model of atrial fibrillation. *Circ Res*. 1997;81:512-525
20. Zhang H, Garratt CJ, Zhu J, Holden AV. Role of up-regulation of ik1 in action potential shortening associated with atrial fibrillation in humans. *Cardiovasc Res*. 2005;66:493-502
21. Pandit SV, Jalife J. Rotors and the dynamics of cardiac fibrillation. *Circ Res*. 2013;112:849-862
22. Dobaczewski M, Gonzalez-Quesada C, Frangogiannis NG. The extracellular matrix as a modulator of the inflammatory and reparative response following myocardial infarction. *J Mol Cell Cardiol*. 2010;48:504-511
23. Harada M, Luo X, Qi XY, Tadevosyan A, Maguy A, Ordog B, Ledoux J, Kato T, Naud P, Voigt N, Shi Y, Kamiya K, Murohara T, Kodama I, Tardif JC, Schotten U, Van Wagoner DR, Dobrev D, Nattel S. Transient receptor potential canonical-3 channel-dependent fibroblast regulation in atrial fibrillation. *Circulation*. 2012;126:2051-2064
24. Musa H, Kaur K, O'Connell R, Klos M, Guerrero-Serna G, Avula UM, Herron TJ, Kalifa J, Anumonwo JM, Jalife J. Inhibition of platelet-derived growth factor-ab signaling prevents electromechanical remodeling of adult atrial myocytes that contact myofibroblasts. *Heart Rhythm*. 2013;10:1044-1051
25. Qi XY, Yeh YH, Xiao L, Burstein B, Maguy A, Chartier D, Villeneuve LR, Brundel BJ, Dobrev D, Nattel S. Cellular signaling underlying atrial tachycardia remodeling of l-type calcium current. *Circ Res*. 2008;103:845-854

26. Saksena S, Hettrick DA, Koehler JL, Grammatico A, Padeletti L. Progression of paroxysmal atrial fibrillation to persistent atrial fibrillation in patients with bradyarrhythmias. *Am Heart J*. 2007;154:884-892
27. Potpara TS, Stankovic GR, Beleslin BD, Polovina MM, Marinkovic JM, Ostojic MC, Lip GY. A 12-year follow-up study of patients with newly diagnosed lone atrial fibrillation: Implications of arrhythmia progression on prognosis: The belgrade atrial fibrillation study. *Chest*. 2012;141:339-347
28. Kerr CR, Humphries KH, Talajic M, Klein GJ, Connolly SJ, Green M, Boone J, Sheldon R, Dorian P, Newman D. Progression to chronic atrial fibrillation after the initial diagnosis of paroxysmal atrial fibrillation: Results from the canadian registry of atrial fibrillation. *Am Heart J*. 2005;149:489-496
29. Koide Y, Yotsukura M, Ando H, Aoki S, Suzuki T, Sakata K, Ootomo E, Yoshino H. Usefulness of p-wave dispersion in standard twelve-lead electrocardiography to predict transition from paroxysmal to persistent atrial fibrillation. *Am J Cardiol*. 2008;102:573-577
30. Yue L, Xie J, Nattel S. Molecular determinants of cardiac fibroblast electrical function and therapeutic implications for atrial fibrillation. *Cardiovasc Res*. 2011;89:744-753
31. Dobrev D, Friedrich A, Voigt N, Jost N, Wettwer E, Christ T, Knaut M, Ravens U. The g protein-gated potassium current i(k,ach) is constitutively active in patients with chronic atrial fibrillation. *Circulation*. 2005;112:3697-3706
32. Roten L, Derval N, Pascale P, Scherr D, Komatsu Y, Shah A, Ramoul K, Denis A, Sacher F, Hocini M, Haissaguerre M, Jais P. Current hot potatoes in atrial fibrillation ablation. *Curr Cardiol Rev*. 2012;8:327-346

Figure Legends

Figure 1. Time-course of AF development. A: representative 3D plot of percentage of AF episodes in a given week (Y-axis) vs episode duration (X-axis) and weeks of follow-up after initiation of pacing (Z-axis). The first paroxysmal episode occurred 3 weeks after initiation of pacing. Duration of episodes progressively increased until persistent AF developed (week 12). B: summary of temporal measurements. AF: Atrial fibrillation; LS-PAF: Long-Standing Persistent AF.

Figure 2. AF-induced changes in extracellular matrix. A: Mean±SEM values for patchy fibrosis (left) and interstitial fibrosis (right) in right atrium (RA), left atrium (LA) and posterior left atrium (PLA) of sham-operated (N=6), transition (N=7) and LS-PAF animals (N=7). Twenty pictures per slide were randomly selected and analyzed; *p<0.05; **p<0.001 *vs.* sham. B: Representative picrosirius red staining in PLA of sham-operated, transition and LS-PAF groups. C and D: Western blots of α-smooth muscle actin (SMA) and Collagen III (Col III) in LA and RA tissue homogenates relative to GAPDH. N=6 for each group. *p<0.05, **p<0.01 *vs.* sham.

Figure 3: Dominant frequency increases in RA and LA (A) and surface ECG (B) during progression of AF. N=14 for RA, N=8 for LA. #p<0.001 for RA *vs.* LA, **p<0.001 *vs.* sham.

Figure 4: Rate of increase in DF during paroxysmal AF predicts transition to persistent AF. A: Representative graphs for three animals. The sheep on the left had the highest dDF/dt, middle had intermediate dDF/dt and right had the lowest dDF/dt (left and right from transition group, middle from LS-PAF group). B: log-log plots of time from first episode to onset of self-sustained persistent AF versus dDF/dt for the RA (intracardiac electrode), LA (loop recorder) and ECG (surface Lead 1). Each point represents an animal. The dDF/dt correlated with time to develop self-sustained persistent AF. N=14 for RA and ECG, N=8 for LA.

Figure 5: APD and frequency dependence in myocytes from sham, transition, and persistent AF. A: Action potential duration (APD_{90} at 1Hz) is reduced in both atria at transition from paroxysmal to persistent AF. For RA: N=3/n=13 (sham), N=3/n=13 (transition), N=3/n=14 (LS-PAF); for LA: N=3/n=18 (sham), N=3/n=14 (transition), N=3/n=18 (LS-PAF). *p<0.05. Right: Representative LA APs are superimposed. B: Cycle length (CL) dependence of APD_{90}. For RA: N=3/n=13 (sham), N=3/n=13 (transition), N=3/n=14 (LS-PAF); for LA: N=3/n=18 (sham), N=3/n=14 (transition), N=3/n=18 (LS-PAF). *p<0.05 *vs.* sham at the same CL. #p<0.05 *vs.* 1000ms CL.

Figure 6: Sustained AF reduces functional expression of Na^+ and L-type Ca^{2+} channels. A: Current-voltage relationships for I_{Na} in myocytes from LA (left) and RA (right). For LA: N=3/n=12 (sham), N=4/n=21 (transition), N=5/n=21 (LS-PAF); for RA: N=3/n=10 (sham), N=4/n=18 (transition), N=5/n=18 (LS-PAF). *p<0.05 *vs.* sham, # p<0.05 *vs.* transition. B: Current-voltage relationships for I_{CaL} in myocytes from LA (left) and RA (right). For the LA: N=3/n=13 (sham), N=4/n=17 (transition), N=4/n=11 (LS-PAF); for the RA: N=3/n=12 (sham), N=4/n=16 (transition), N=4/n=14 (LS-PAF). *p<0.05 *vs.* sham. C: Representative traces for I_{Na} (upper) and I_{CaL} (lower) in myocytes from LA of sham-operated and LS-PAF animal. D-E: Western blot analysis of $Na_V1.5$ and $Ca_V1.2$ protein expression in LA tissue homogenates (D) and RA tissue homogenates (E). Top, Representative blots; bottom, Quantification of protein expression relative to GAPDH. N=6. F-G: Real time RT-PCR analysis of *SNC5A* and *CACNA1C* gene expression in tissue homogenates from LA (F) and RA (G); quantification of gene expression relative to GAPDH. N=6. **p< 0.01 *vs.* sham.

Figure 7: Sustained AF increases functional expression of Kir2.3. A: Current-voltage relationships for I_{K1} in myocytes from LA (top) and RA (bottom). For LA: N=3/n=7 (sham), N=5/n=10 (transition), N=2/n=4 (LS-PAF); for RA: N=3/n=6 (sham), N=3/n=10 (transition), N=3/n=9 (LS-PAF). *p<0.05 *vs.* sham. B: Western blots for Kir2.3 in LA tissue homogenates. Top: representative blots of 2 different groups; bottom: quantification of protein expression relative to GAPDH. N=6. *p<0.05 *vs.* sham.

Figure 8: Simulations predict consequences of ion channel remodeling on rotor frequency. A: Action potential traces for sham, paroxysmal and transition AF predicted by experimentally derived ion channel changes (Figures 6-7). APD_{90} was abbreviated in both paroxysmal and transition AF compared

to sham. Resting membrane potential was hyperpolarized -2 mV. B: Rotor in paroxysmal (left) had lower frequency than transition AF. C: Rotors in paroxysmal AF meandered considerably and eventually self-terminated upon collision with boundary. In transition AF, the rotor was stable, had higher frequency and persisted throughout the simulation.

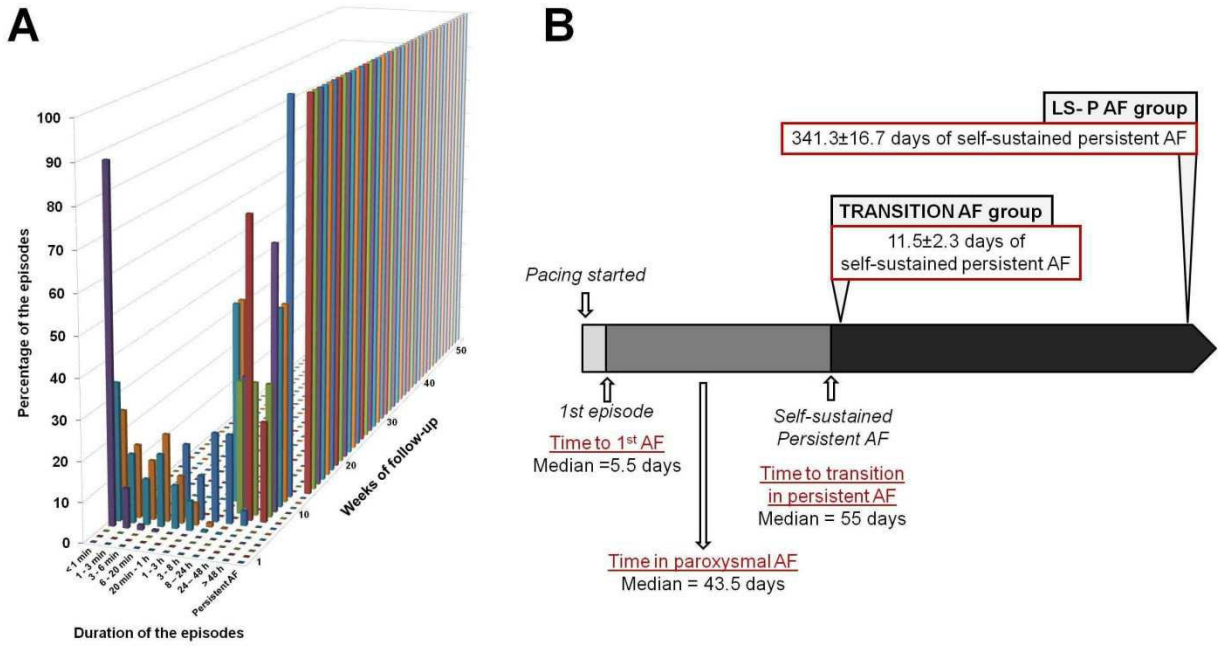
A
Percentage of the episodes
100
90
80
70
60
50
40
30
20
10
0
< 1 min
1 - 3 min
3 - 6 min
6 - 20 min
20 min - 1 h
1 - 3 h
3 - 8 h
8 - 24 h
24 - 48 h
> 48 h
Persistent AF
Duration of the episodes
1
10
20
30
40
50
Weeks of follow-up
B
LS- P AF group
341.3±16.7 days of self-sustained persistent AF
TRANSITION AF group
11.5±2.3 days of
self-sustained persistent AF
Pacing started
1st episode
Time to 1st AF
Median =5.5 days
Self-sustained
Persistent AF
Time to transition
in persistent AF
Median = 55 days
Time in paroxysmal AF
Median = 43.5 days

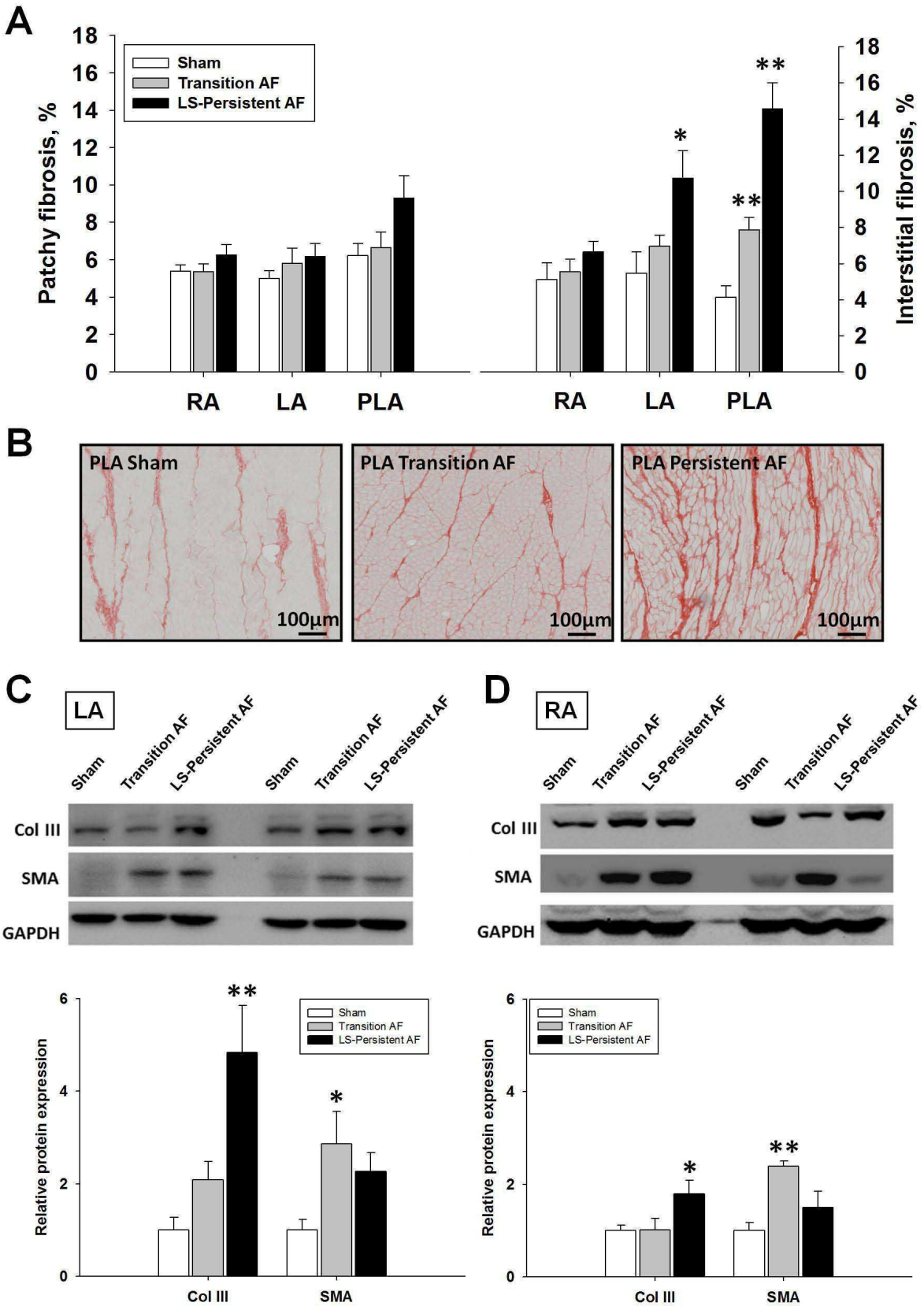
A
Sham
Transition AF
LS-Persistent AF
Patchy fibrosis, %
Interstitial fibrosis, %
RA
LA
PLA
B
PLA Sham
PLA Transition AF
PLA Persistent AF
100μm
C
LA
D
RA
Col III
SMA
GAPDH
Relative protein expression

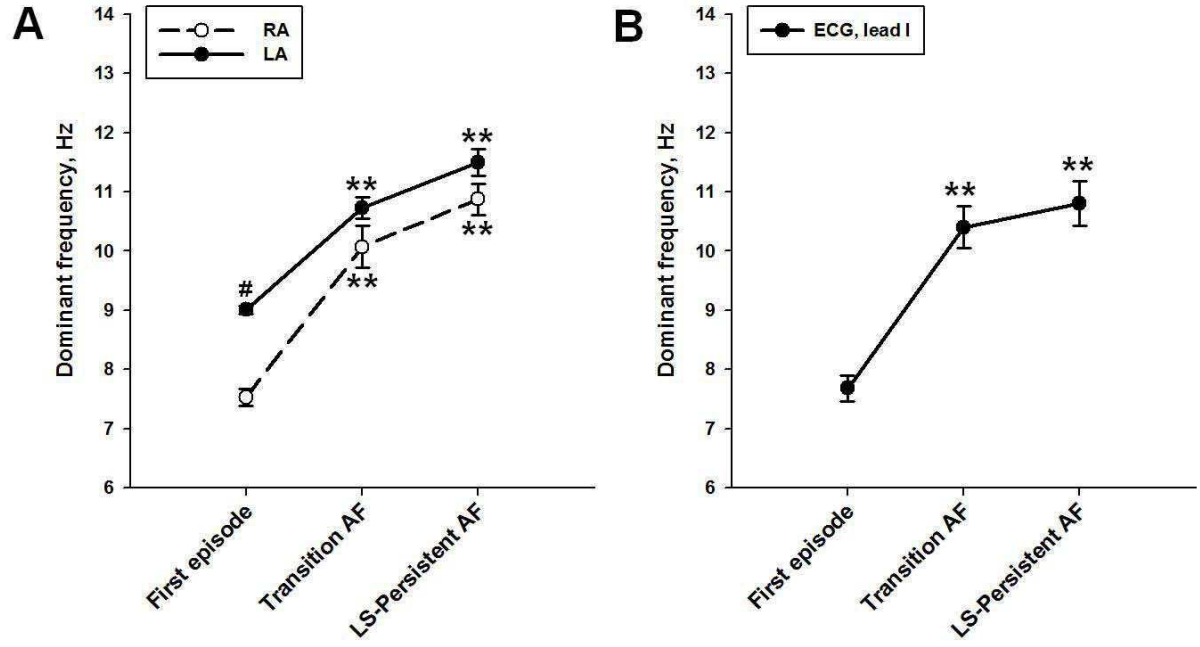
A
RA
LA
Dominant frequency, Hz
First episode
Transition AF
LS-Persistent AF
B
ECG, lead I
Dominant frequency, Hz
First episode
Transition AF
LS-Persistent AF

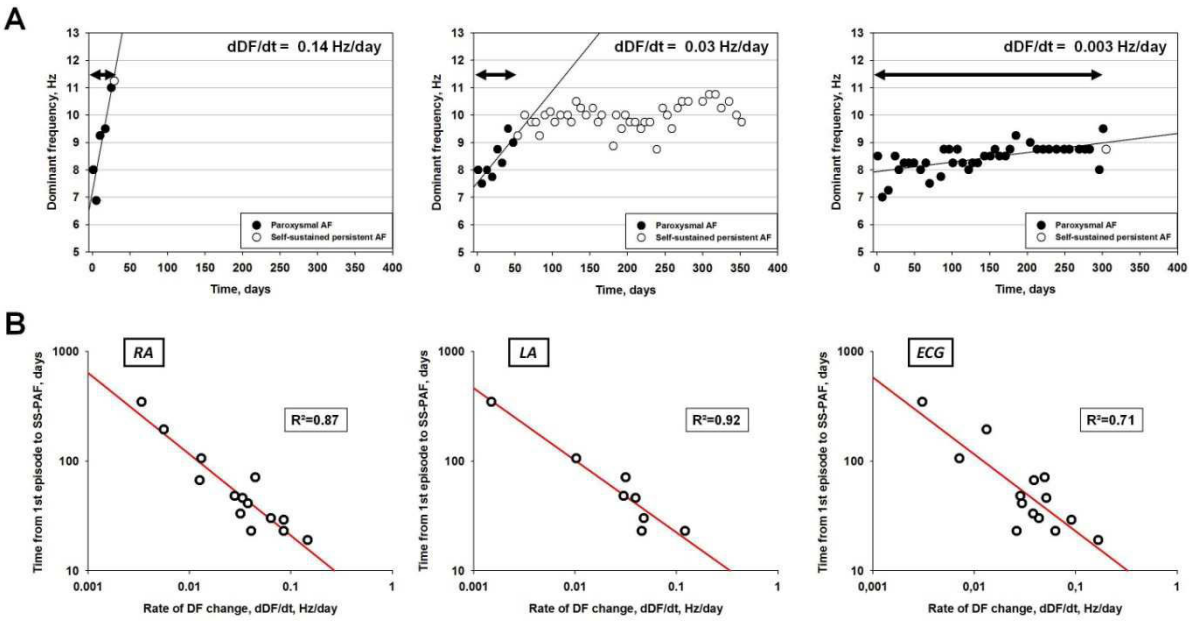
A
dDF/dt = 0.14 Hz/day
dDF/dt = 0.03 Hz/day
dDF/dt = 0.003 Hz/day
Dominant frequency, Hz
Time, days
Paroxysmal AF
Self-sustained persistent AF
B
RA
LA
ECG
R²=0.87
R²=0.92
R²=0.71
Time from 1st episode to SS-PAF, days
Rate of DF change, dDF/dt, Hz/day

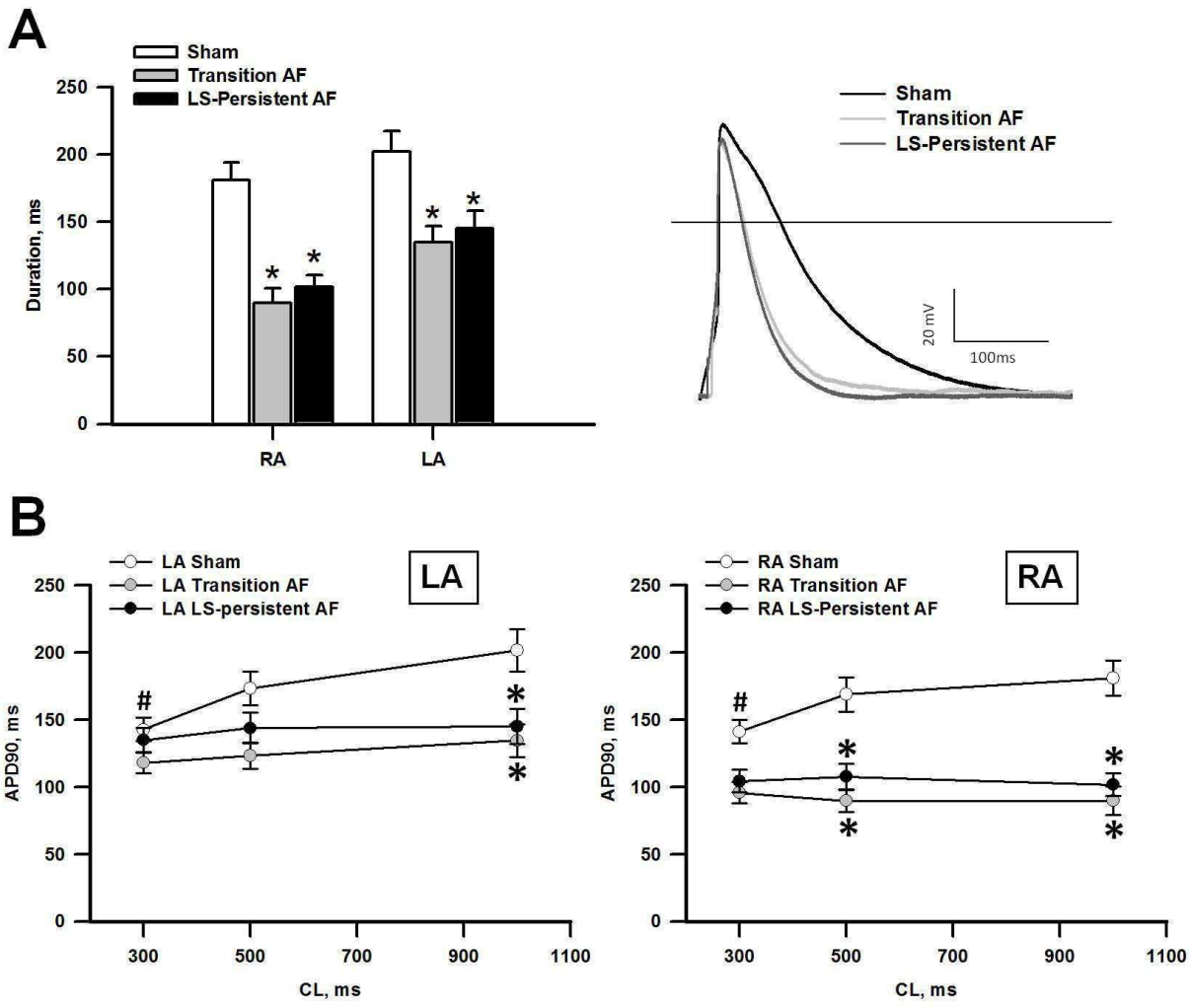
A
Sham
Transition AF
LS-Persistent AF
Duration, ms
250
200
150
100
50
0
RA
LA
Sham
Transition AF
LS-Persistent AF
20 mV
100ms
B
LA Sham
LA Transition AF
LA LS-persistent AF
LA
APD90, ms
CL, ms
300
500
700
900
1100
RA Sham
RA Transition AF
RA LS-Persistent AF
RA

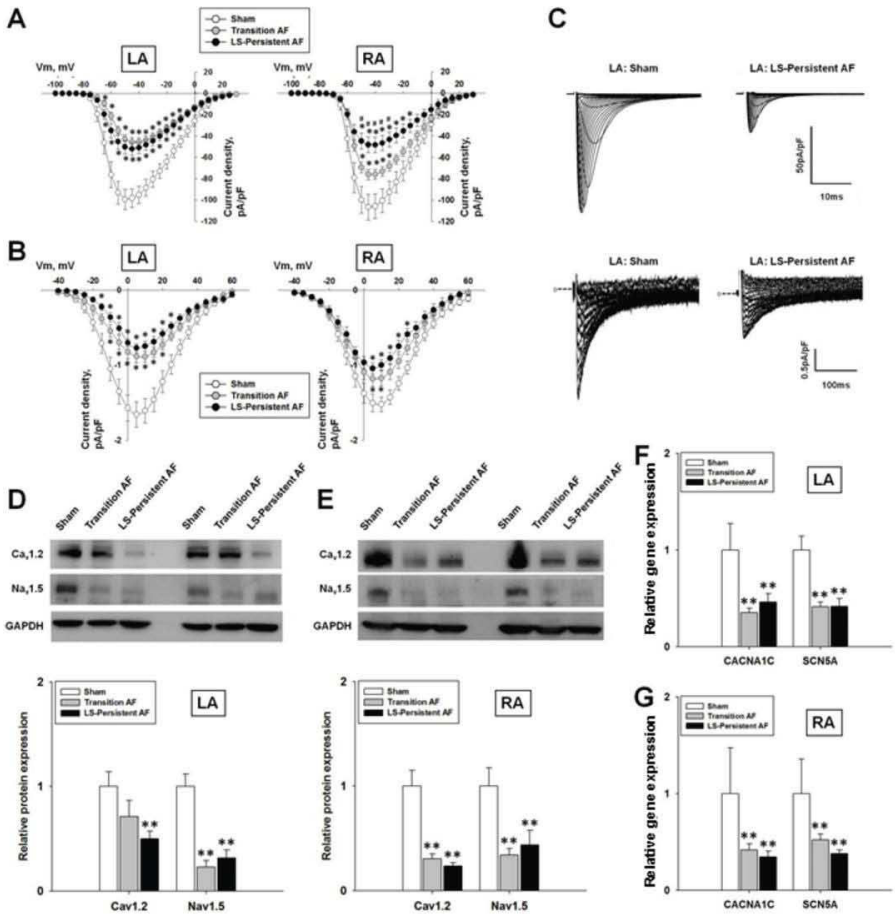
A
Sham
Transition AF
LS-Persistent AF
LA
RA
Vm, mV
Current density, pA/pF
B
C
LA: Sham
LA: LS-Persistent AF
50pA/pF
10ms
0.5pA/pF
100ms
D
E
F
G
Ca$_v$1.2
Na$_v$1.5
GAPDH
Relative protein expression
Relative gene expression
Cav1.2
Nav1.5
CACNA1C
SCN5A

Figure 6

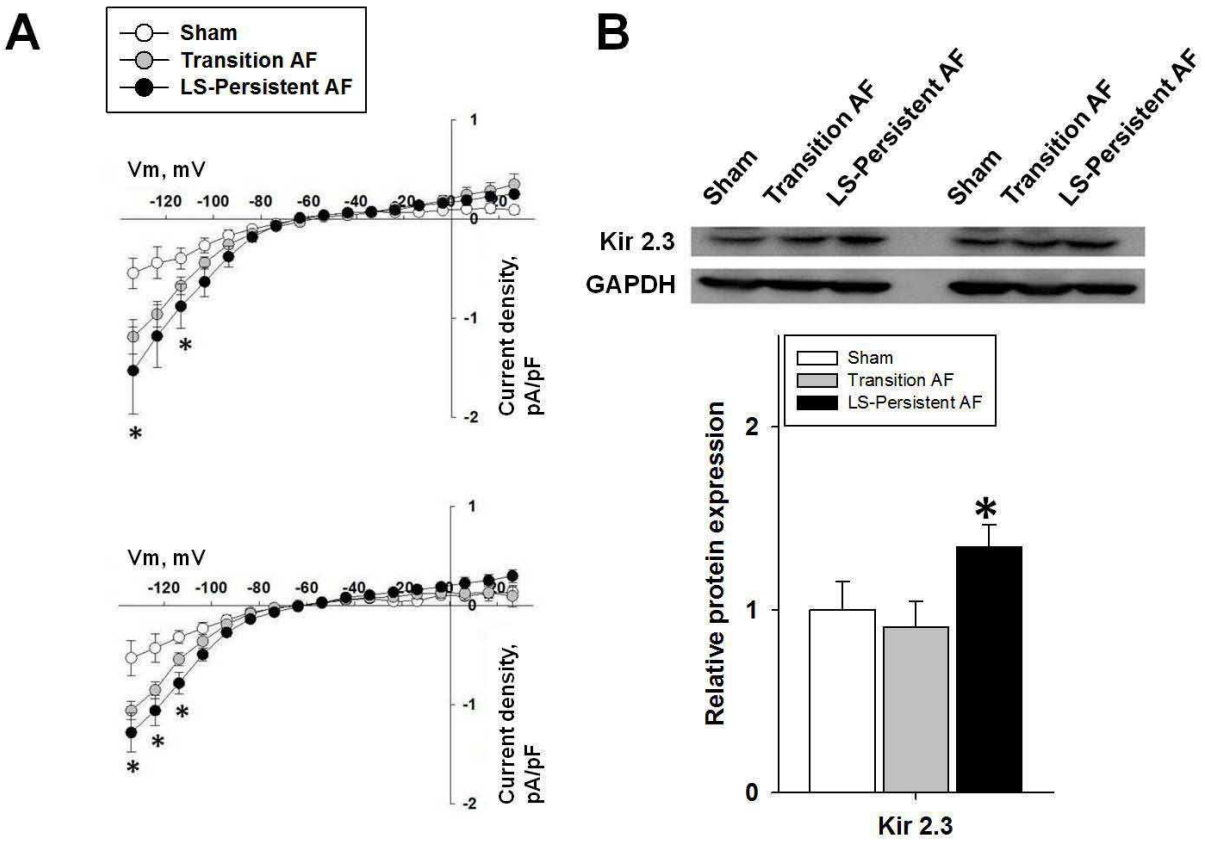
A
Sham
Transition AF
LS-Persistent AF
Vm, mV
Current density, pA/pF
B
Kir 2.3
GAPDH
Relative protein expression

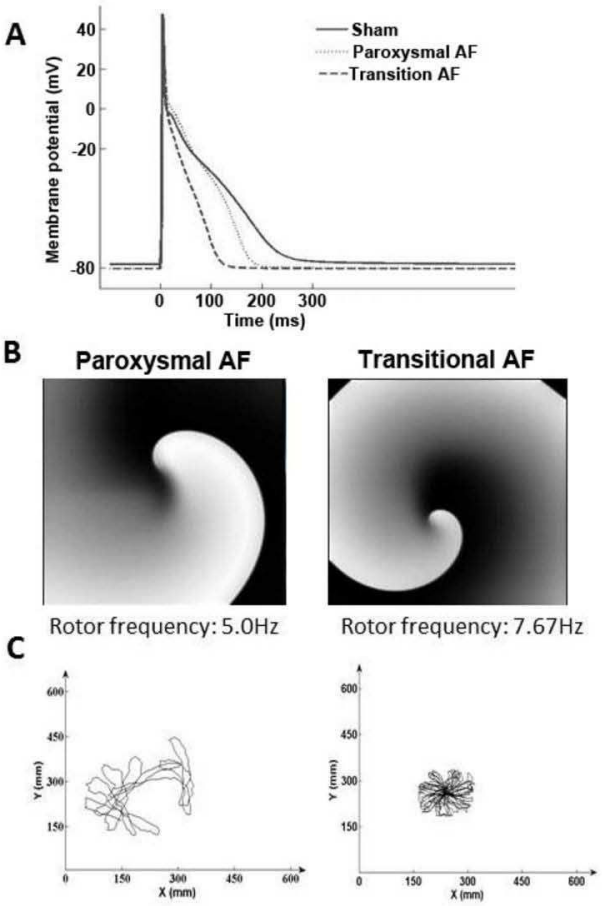
A
Sham
Paroxysmal AF
Transition AF
Membrane potential (mV)
40
20
0
-20
-80
0
100
200
300
Time (ms)
B
Paroxysmal AF
Transitional AF
Rotor frequency: 5.0Hz
Rotor frequency: 7.67Hz
C
Y (mm)
X (mm)
600
450
300
150
0
150
300
450
600

ONLINE SUPPLEMENT

Dominant Frequency Increase Rate Predicts Transition from Paroxysmal to Long-Term Persistent Atrial Fibrillation

Raphael P. Martins[1], MD, Kuljeet Kaur[1], PhD, Elliot Hwang[1], BS, Rafael J. Ramirez[1], PhD, B. Cicero Willis[1], MD, David Filgueiras-Rama[1], MD, Steven R. Ennis[1], PhD, Yoshio Takemoto[1], MD, PhD, Daniela Ponce-Balbuena[1], PhD, Manuel Zarzoso[1], PhD, Ryan P. O'Connell[1], PhD, Hassan Musa[1], PhD, Guadalupe Guerrero-Serna[1], PhD, Uma Mahesh R. Avula[1], MD, Michael F. Swartz[2], MD, Sandesh Bhushal,[3] BS, Makarand Deo,[3] PhD, Sandeep V. Pandit, PhD, Omer Berenfeld[1], PhD, José Jalife[1], MD

[1] Department of Internal Medicine, University of Michigan, Ann Arbor, MI.
[2] Department of Surgery, University of Rochester, Rochester, NY.
[3] Department of Engineering, Norfolk State University, Norfolk, VA.

Table of Contents

Supplemental Methods:

Pacemaker implantation: All procedures were approved by the University of Michigan Committee on Use and Care of Animals and complied with National Institutes of Health guidelines. Twenty-one 6-8 month-old sheep (≈40 Kg) were used for implantation.

Anesthesia was achieved using propofol IV for the induction (4-6 mg/kg) and isoflurane gas at 5-10 ml/kg for maintenance. An endocardial 6 to 8 Fr, bipolar, active fixation and steroid-eluting lead was inserted into the right atrial appendage through the left external jugular vein. Once properly placed, the proximal end was screwed to the atrial port of a sterile dual chamber pacemaker (St. Jude Medical, Inc, St Paul, MN). The ventricular port was occluded using specific plugs. The pacemaker canister was then inserted in a subcutaneous pouch at the base of the neck. In a subset of thirteen sheep (8 paced animals and 5 ones in SR), an implanted loop recorder (ILR, Reveal® XT, Medtronic, Inc. Minneapolis, MN. USA) was placed subcutaneously on the left side of the sternum in close proximity to the LA (Supplemental Figure S1, Panel A).

Pacing protocol: After 10 days of recovery, sheep were assigned to either the Sham-operated group or to one of the atrial tachypacing groups. The sham operated animals had the device programmed in a sensing (OAO) mode only. Pacing voltage output was programmed at least twice the diastolic threshold for 0.4 ms duration to ensure appropriate atrial capture. The automatic mode switch (AMS) mode was enabled in the atrial tachypacing animals in order to avoid unnecessary pacing and allow AF to self-sustain once initiated (Supplemental Figure S1, Panel B). The AMS algorithm reliably generated tachypacing-induced self-sustained AF because the pacemaker resumed pacing only if AF stopped and sinus rhythm was detected. The pacemaker was programmed to induce AF by burst tachypacing; i.e., 30-sec pacing at 20 Hz at twice diastolic threshold followed by 10 sec sensing. The pacemaker resumed pacing only if AF stopped and SR was detected. In addition, devices had the capability of storing information on the history of AF, including the number and duration of AF episodes and the precise moment of each episode's occurrence. The Holter capabilities of the device were used to record intra-cardiac electrograms (EGMs) to accurately confirm the occurrence of AF, generate histograms and follow the evolution of AF. This was an attempt to reproduce the actual evolution of human AF, from the initiation of premature atrial beats, to paroxysmal and eventually persistent AF. Persistent AF was then defined as episodes lasting more than 7 days without reversal to sinus rhythm and necessity for resumption of pacing. Thus, in addition to the Sham-operated group (N=7) a subset of animals assigned to the fast atrial pacing group was sacrificed after 7 days of self-sustained AF (Transition group, N=7). The rest of the animals was sacrificed after one year of self-sustained AF (LS-PAF group, N=7). The ILR was programmed to identify AF episodes lasting >6 sec based on RR irregularity during the 10 sec sensing. Both pacemaker and ILR were interrogated weekly during the study period.

Electrogram acquisition and processing: After group assignment, a weekly interrogation was performed. Persistence of sinus rhythm was verified in sham-operated animals and pacemaker memories were checked to detect if spontaneous episodes of AT/AF occurred. Three recordings were obtained in the tachypaced sheep during the follow-up: 1) RA lead tip EGM with a case reference; 2) Standard Lead I of the resting ECG exported at a 512 Hz sampling rate; and 3) ILR single lead recording (representing a LA far-field signal) exported as a vector PDF file. The EGM waveforms encoded in the PDF files were magnified and then digitized in a custom made Matlab program (MathWorks, Natick MA). The digitized signal was then superimposed on the original EGM image for visual inspection. If a miss-match was found, the cause was determined and adjustments made to correct them and ensure quality data. Recordings obtained by the ILR,

whose canister is external to the LA, contain a mixture of atrial and ventricular activity. To analyze the atrial activity, the ventricular activity (dubbed QRST) was subtracted from the original recordings. A principal component analysis based AF estimation (PCA) was used for QRST removal. After QRST removal, a biased-free bidirectional Butterworth band-pass filter (4-35 Hz) was applied to each trace, as previously described[1]. The fast Fourier transform (FFT) was then used as previously described to extract the dominant frequency (DF) from 5 sec-long signals from the ILR and RAA electrograms. Finally, DF values from RAA and ILR electrograms were compared to identify *in-vivo* differences between the two regions in the left and right atria.

Serum measurements: Serum was obtained from all animals at baseline, after the initiation of paroxsymal AF (i.e. as soon as the first episode was detected), at the transition from paroxysmal to persistent AF and after 1 year of self-sustained LS-PAF maintenance. All samples were obtained from a peripheral vein, the serum extracted, and stored at -20° C. PIIINP (Biotang, Wlatham MA) levels were measured by enzyme linked immunosorbant assay according the manufacturers' specifications. The sensitivity (lower detection limit) for the assay was 12.5 ng/ml. All samples were run in duplicate and measured at 450nm.

Echocardiography: Echocardiograms were obtained in awaked sheep in the sternal recumbency position using a Vivid Q echocardiograph (GE Healthcare, Horten, Norway) at baseline, at the time of transition from paroxysmal to persistent AF and at the last follow-up for the LS-PAF group. LA and RA dimensions and areas, severity of mitral regurgitation, left ventricular ejection fraction (LVEF), end-systolic and end-diastolic diameters, and septal and posterior wall thickness were evaluated using standard criteria of the American Society of Echocardiography.[9]

Heart removal and cell isolation: After the end of the follow-up, hearts were quickly removed via thoracotomy and placed in a cold cardioplegic solution. LA and RA walls were removed, weighted and cut in three different portions. The posterior portion was used for molecular biology, middle portion was used for histology analysis and the anterior portion was used for cell dissociation. The posterior left atrium (PLA) was sectioned longitudinally and stored for subsequent histology and molecular biology analysis.

Cell isolation was performed as previously described[3]. Left and right atrial samples for dissociation were transferred into a stock solution containing (in mM): NaCl (120), KCl (5.4), $MgSO_4$ (5), Pyruvate (5), Glucose (20), Taurine (20), HEPES (20) and nitrilotriacetic acid (5). Tissue was chopped into chunks of about 1 mm^3 with scissors. Chunks were stirred for 12 min in the above-mentioned solution at 37°C oxygenated with 100% O_2. Every 3 min, the tissue was transferred to a fresh solution by filtering solution through gauze. Chunks were then transferred to the calcium free protease digestion solution containing (in mM): NaCl (120), KCl (5.4), $MgSO_4$ (5), Pyruvate (5), Glucose (20), Taurine (20), HEPES (20) and protease type XXIV (Sigma) for 45 min. After the end of the protease digestion, chunks were transferred to the collagenase digestion solution containing (in mM): NaCl (120), KCl (5.4), $MgSO_4$ (5), Pyruvate (5), Glucose (20), Taurine (20), HEPES (20), $CaCl_2$ (0.05) and collagenase type I (Worthington) for 2 digestion time points. At 15 and 30 minutes, the filtrate containing myocytes was decanted and centrifuged for 2 min at 500 rpm. Supernatant was aspirated and pellets resuspended in KB solution containing (in mM): L-Glutamic Acid (50), KOH (70), KCl (30), L-Aspartic Acid-K (10), KH_2PO_4 (10), $MgSO_4$-$7H_2O$ (2), Glucose (20), Taurine (20), Creatine (5), EGTA (0.5) and HEPES (10). Myocytes were centrifuged a second time to aspirate supernatant, and resuspended in KB before use.

Cell dimensions (length and width) were measured in the I_{CaL} extracellular solution before the recordings of the currents at 40x from images recorded using a 40x oil-immersion objective lens (N.A. 1.30) attached to a Nikon Eclipse Ti inverted microscope.

Western Blotting: Sheep LA and RA tissue samples were washed with protease inhibitors (Roche, protease inhibitor tablet) containing PBS and flash frozen in liquid nitrogen. Frozen tissue (50–100mg) was homogenized in 1ml of lysis buffer containing (in mM): Tris•HCl (25), NaCl (150), EDTA (1), NaF (4), Sodium ortho-vanadate (2), Triton X-100 1% and protease inhibitor. The homogenate was centrifuged at 10000 rpm for 5 minutes; the supernatant was used for western blotting. The tissue lysates (20 µg) were then subjected to one-dimensional sodium dodecyl sulfate polyacrylamide gel electrophoresis. The blots were incubated overnight in cold room with one of the following antibodies, mouse monoclonal α-SMA (1:2000); rabbit GAPDH antibody (1:5000) both from Sigma-Aldrich, St. Louis, MO; rabbit $Ca_V1.2$ antibody (1:500); rabbit $Na_V1.5$ antibody (1:500); rabbit KV11.1 antibody (1:1000); rabbit $K_V4.2$ antibody (1:250) all from Alomone Labs, PO Jerusalem, IL; rabbit Col III antibody (1:1000) from Abcam Cambridge, MA; mouse monoclonal Kir2.3 (1:250) from NeuroMab, Davis, CA. The protein bands were visualized using enhanced chemiluminescence (Thermo Scientific, Rockford, IL). For Ca^{2+}-handling proteins , Mouse monoclonal Na^+/Ca^{2+} exchanger (NaCX-1) (1:1000) and mouse monoclonal Phospholamban antibody (1:1000) were purchased from Millipore, CA. Mouse monoclonal ryanodine receptor 2 (RyR2, :4000) and mouse monoclonal SERCA2 ATPase antibody were purchased from Pierce Biotechnology, IL. Rabbit monoclonal RYR2 2814Phospho Serine antibody (1:1000) was purchased from Badrilla Ltd. United Kingdom.

Real-time RT-PCR: Sheep left and right atrial samples were washed in RNase/DNase free ice cold PBS. Clean samples were preserved in RNA stabilizing agent (Ambion, Austin, TX) and stored at -80^{0}C till further use. RNA was isolated from the myocardial tissue using RNAeasy kit from Qiagen (Qiagen, Valencia, CA) according to the manufacturer's instructions. Isolated RNA from these samples was treated with DNase for 15 min at room temperature (Qiagen, Valencia, CA). 2 µg of DNA-free total poly A tail RNA (mRNA) was first subjected to synthesis of cDNA using Oligo dT primers using SuperScript III First-Strand Synthesis System from Invitrogen (Invitrogen, Carlsbad, CA) according to the manufacturer's instructions. cDNA from 20 ng of total RNA was then subjected to RT-PCR using sybergreen real time PCR master mix (Qiagen, Valencia, CA). For real time PCR sheep specific primers were designed using predicted sequences (Table S4). No-template controls and no-RT controls were run during each experiment to detect any RNA and/or genomic DNA contamination.

Patch-clamp recordings: Ion currents and action potentials were recorded in the whole-cell patch-clamp configuration using a MultiClamp 700B amplifier and Digidata 1440A digitizer (Molecular Devices, Sunnyvale, CA). Patch pipettes had resistances of 2 - 6 MΩ when filled with intracellular pipette solution and placed in extracellular solution. After formation of a GΩ seal, the patch membrane was ruptured and cell capacitance (Cm) was determined by integration of capacitive transients elicited by 10-mV hyperpolarizing and depolarizing steps (10 ms duration) from a holding potential of -80 mV. Data acquisition and analysis was performed using pCLAMP software (ver.10.3; Molecular Devices, Sunnyvale, CA). Current amplitudes were divided by Cm and expressed as current densities (pA/pF) to normalize for variable cell sizes.

L-type calcium current (I_{CaL}) was recorded with pipette solution containing (in mM): CsCl (120), TEA-Cl (20), $MgCl_2$ (1), Mg-ATP (5.2), HEPES (10), EGTA (10), adjusted to pH 7.2 with

CsOH; and extracellular solution containing (in mmol/L): TEA-Cl (148), NaH_2PO_4 (0.4), $MgCl_2$ (1), glucose (5.5), CsCl (5.4), $CaCl_2$ (1.8), HEPES (15), adjusted to pH 7.4 with CsOH. Activation of I_{CaL} was elicited by 300-ms voltage steps from a holding potential of -50 mV. Amplitude of I_{CaL} was measured as the difference between peak inward current and current at the end of the voltage step.

Sodium currents (I_{Na}) were recorded at room temperature (20-22 °C) with pipette resistances <2.8 MΩ when filled with pipette filling solution containing (in mM): NaCl (5), CsF (135), EGTA (10), MgATP (5), Hepes (5), pH 7.2. The extracellular bathing solution contained (in mM): NaCl (5), $MgCl_2$ (1), $CaCl_2$ (1.8), $CdCl_2$ (0.1), glucose (11), CsCl (132.5) and Hepes (20); pH was maintained at 7.4 with CsOH at room temperature. Appropriate whole-cell capacitance and series resistance compensation (≥60%) was applied along with leak subtraction. To assess the I_{Na} density, cells were held at -160 mV and stepped to various test potentials from -100 to 30 mV in 5 mV increments, with 200 ms duration pulses and 2800 ms interpulse intervals. Voltage-dependent activation of I_{Na} was assessed by generating conductance voltage relationships (m-infinity curves) and fitting the data with a standard Boltzman function (Origin 8.1, Northampton, MA, USA). Voltage-dependence of inactivation was assessed by holding the cells at -160 mV followed by a 300 ms test pulse from -140 to -40 mV in 5 mV increments; interpulse interval was 2700 ms. Recovery from inactivation was studied by holding cells at -160 mV and applying two 20 ms test pulses (S1, S2) to -45 mv, separated by increasing increments of 1 ms to a maximum S1-S2 interval of 50 ms. The S1-S1 interval was kept constant at 2000 ms.

The conventional whole-cell recording technique was employed to record the transient outward K+ current (I_{to}). Electrophysiological recordings were conducted at room temperature. The bath solution contained (in mM): NaCl (136), KCl (4), $CaCl_2$ (1.8), $MgCl_2$ (2), HEPES (10), tetrodotoxin (0.03), nifedipine (0.005), pH adjusted at 7.4 with NaOH. Recording pipettes contained (mM): KCl (135), $MgCl_2$ (1), EGTA (10), HEPES (10), glucose (5), pH adjusted at 7.2 with KOH. Borosilicate glass electrodes were pulled with a Brown–Flaming puller (model P-97), yielding appropriate tip resistances when filled with pipette solution < 3 MΩ. Appropriate whole-cell capacitance and series resistance compensation (≥70%) was applied. Leakage compensation was not used. Ito was record using a step protocol with a holding potential of -70 mV and stepping from -40 to + 60 mV in 10 mV increments of 5 s at each potential every 20 s. Ito was measured as the difference between the peak current and the current at the end of the 5 s pulse.

Inward rectifier current (I_{K1}) was recorded with pipette solution containing (in mM): KCl (148), $MgCl_2$ (1), EGTA (5), HEPES (5), Creatine (2), ATP (5), Phosphocreatine (5); adjusted to pH 7.2 with KOH and extracellular solution containing (in mM): NaCl (148), NaH_2PO_4 (0.4), $MgCl_2$ (1), Glucose (5.5), KCl (5.4), $CaCl_2$ (1), HEPES (15), pH adjusted at 7.4 with NaOH. Activation of I_{K1} was elicited by a step protocol utilizing 400-msec steps ranging from -120 to +20 mV in 10mV increments with a holding potential of -50mV and with 2 seconds between successive steps. 5 μM nifedipine was added to block I_{CaL} channels and the Ca2+-sensitive I_{Cl}. $BaCl_2$ (1mM) was used to isolate I_{K1} from other background currents.

Action potentials were elicited using square wave pulses (30 – 50 pA amplitude, 10 – 30 ms duration) generated by a DS8000 digital stimulator (World Precision Instruments, Sarasota, FL) and recorded at 37°C with pipette solution containing (in mM): $MgCl_2$ (1), EGTA (1), KCl (150), HEPES (5), phosphocreatine (5), K_2ATP (4.46), b-hydroxybutyric acid (2), adjusted to pH 7.2 with KOH; and extracellular solution containing (in mM): NaCl (148), NaH_2PO_4 (0.4),

$MgCl_2$ (1), glucose (5.5), KCl (5.4), $CaCl_2$ (1), HEPES (15), EGTA (1), pH adjusted at 7.2 with NaOH.

APD rate adaptation was analyzed by steady state stimulation at progressive shorter cycle lengths (CL) starting at 1000 ms, decreasing the CL slowly by 100 ms steps down to 300 ms and then by 20 ms steps after 300 ms cycle length. Action potentials at 1000, 500 and 300 ms CL were plotted in the rate adaptation curve.

Histology: Tissue samples were sectioned longitudinally to the atrial wall plane at 4 μm, fixed in 10% buffered formalin, embedded in paraffin, and stained with picrosirius red. Patchy and interstitial fibrosis was quantified in both atria and in the PLA at 10x and 20x magnifications, respectively, using the BioQuant software (Bioquant Image Analysis Corporation, Nashville, TN). A minimum of 20 randomly selected pictures per slide were analyzed by a blinded investigator, carefully excluding endocardial, epicardial and peri-vascular regions.

Computer Simulations: We implemented modified versions of the Grandi-Pandit[4] model of the normal human atrial cell to simulate the cardiac action potential and its robust propagation in 2D cardiac tissue. The formulation for the fast sodium current in the original model was replaced with that of a mammalian ventricular myocyte model[5] to achieve propagation in 2D cardiac tissue. In addition, the maximum conductance value for the inward rectifier potassium current, I_{KI}, was increased by 30% to achieve tissue excitability and smooth propagation. The conduction velocity in the tissue was adjusted to 0.58 m/s.[6, 7]

Atria in SR (equivalent to the Sham group in our study) and at the transition stage from paroxysmal to persistent AF (equivalent to the Transition group) were simulated by modifying the magnitudes of I_{Na}, I_{CaL}, I_{to}, and I_{KI} as observed in the experiments (listed in Table S5). Paroxysmal AF was simulated by incorporating all ionic changes similar to that in transition AF, except for I_{CaL}, whose density was reduced by 30% only, such that the APD_{90} has values approximately half way in between SR and transition AF. See supplemental tables S5 and S6). The steady-state cardiac action potentials were obtained by pacing the models for 50 seconds at 1 Hz. In all cases, reentry in 2D sheets (6 cm^2) was initiated using the S1-S2 cross-field protocol.

Statistical analyses: In all measurements N and n represent the number of animal and cells for each experiment, respectively. Normally distributed data are expressed as mean ± SEM. A mixed regression model was applied to multiple group analyses and repeated measured data. APD analyses and voltage clamp experiments were compared using a two tailed unpaired Student t tests. RT-PCR and Westerns blot data were analyzed using two-way ANOVA. A $p<0.05$ was considered statistically significant.

Supplemental Results:

AF remodeling and Ca^{2+}-handling proteins. We conducted Western blot analyses in five different calcium handling proteins (ryanodine receptor type two-, RyR2; SR Ca^{2+}-ATPase, SERCA, phospholamban, PLN; Na^{+}-Ca^{2+} exchanger, NCX and Ca^{2+}/calmodulin-dependent protein kinase-II, CaMKII) in the left and right atria appendages in each of the three groups of sheep (i.e., sham, transition and persistent AF). As illustrated in Figures S9 and S10, RyR2, SERCA, PLN and CaMKII were either down-regulated or unchanged, while NCX was increased only in the LA. In addition, RyR2 phosphorylation was not affected and thus, the ratio of pRyR2/total RyR2 was unchanged. Altogether, these results suggest that in this model one

should not expect an increase in the spontaneous release of Ca^{2+} from the SR or that DADs and triggered activity would be involved in transition from paroxysmal to more stable forms of the arrhythmia.

Roles of individual ionic changes. Rotors were simulated in 2D sheets, when individual ionic currents were changed, compared to controls. When I_{KI} alone was increased by 100% compared to controls (Figure S12), the action potential shortened by 23%, the resting membrane potential hyperpolarized by -2 mV (Figure S12A) and the rotors with DF of 4.7 Hz were seen (Figure S12B). When I_{CaL} alone was decreased by 30% compared to controls (as simulated in paroxysmal AF), APD_{90} was reduced by 37%, and resulted in a meandering rotor with a frequency of 4.7 Hz (Figure S13A). When I_{CaL} was decreased by 65%, as observed in persistent AF, APD was greatly reduced (~64%), which provided sufficient substrate for a very stable rotor at 8.0 Hz (Figure S13B). Decreasing I_{to} density by 75% resulted in an unstable, meandering rotor with DF = 3.38 Hz (Figure S14), whereas decreasing I_{Na} density alone by 50% resulted in an unstable rotor with DF of 3.8 Hz (Fig. S15). These simulation results thus indicate that changes in I_{KI} and I_{CaL} are key determinants of rotor acceleration in paroxysmal and transition AF.

Fast versus slow transition. To search for determinants of the rate of AF progression, we separated slow and fast progressing animals sacrificed at transition depending on the median time to progression (<45 days: 4 animals; >45 days: 3 animals). As expected, dDF/dt was significantly larger for the animals progressing quickly to persistent AF (p=0.005 for LA), which also showed significantly shorter APDs in the LA than the slow transition animals, with a trend for shorter RA APDs in the former than the latter (Figure S16B). A trend for smaller I_{CaL} current densities suggested a mechanism for the APDs in the fast transition sheep (Figure S16C). Conversely, I_{KI} appeared to be relatively larger in slow transition animals (Figure S16D) which had significantly larger atrial dimensions (124% vs. 45% increase in LA atrial area; p=0.014, Figure S17). However, the degree of fibrosis, the cell dimensions and atrial weights were similar in both groups. Accordingly the major factor contributing to the larger dDF/dt in the fast transition animals was greater APD shortening secondary to I_{CaL} reduction. On the other hand, the slow transition animals seemed to require an additional thrust to achieve AF persistence, which was brought about by additional I_{KI} increase and greater structural remodeling (Figure S17C and D).

References

1. Filgueiras-Rama D, Price NF, Martins RP, Yamazaki M, Avula UM, Kaur K, Kalifa J, Ennis SR, Hwang E, Devabhaktuni V, Jalife J, Berenfeld O. Long-term frequency gradients during persistent atrial fibrillation in sheep are associated with stable sources in the left atrium. Circ Arrhythm Electrophysiol.5(6):1160-1167.
2. Gottdiener JS, Bednarz J, Devereux R, Gardin J, Klein A, Manning WJ, Morehead A, Kitzman D, Oh J, Quinones M, Schiller NB, Stein JH, Weissman NJ. American Society of Echocardiography recommendations for use of echocardiography in clinical trials. J Am Soc Echocardiogr. 2004;17(10):1086-1119.
3. Escande D, Coulombe A, Faivre JF, Deroubaix E, Coraboeuf E. Two types of transient outward currents in adult human atrial cells. Am J Physiol. 1987;252(1 Pt 2):H142-148.
4. Grandi E, Pandit SV, Voigt N, Workman AJ, Dobrev D, Jalife J, Bers DM. Human atrial action potential and Ca2+ model: sinus rhythm and chronic atrial fibrillation. Circ Res.109(9):1055-1066.
5. Viswanathan PC, Shaw RM, Rudy Y. Effects of IKr and IKs heterogeneity on action potential duration and its rate dependence: a simulation study. Circulation. 1999;99(18):2466-2474.

6. Gelband H, Bush HL, Rosen MR, Myerburg RJ, Hoffman BF. Electrophysiologic properties of isolated preparations of human atrial myocardium. Circ Res. 1972;30(3):293-300.
7. Workman AJ, Kane KA, Rankin AC. The contribution of ionic currents to changes in refractoriness of human atrial myocytes associated with chronic atrial fibrillation. Cardiovasc Res. 2001;52(2):226-235.

Supplemental Tables:

Table S1: Echocardiographic findings. (LVEF = left ventricular ejection fraction; LA = left atria; RA = right atria; *p<0.05 vs sham; †p<0.05 vs Transition)

	Sham	Transition AF	LS-PAF	p
LVEF (%)				
Baseline	73.7±2.4	75.3±1.7	73.7±2.2	0.82
Last follow-up	75.5±1.4	75.6±1.0	72.7±1.7	0.30
LA area (cm²)				
Baseline	7.6±0.3	7.2±0.4	7.7±0.2	0.56
Last follow-up	10.0±0.8	12.8±1.1	20.9±2.1*	0.004
RA area (cm²)				
Baseline	5.2±0.4	5.5±0.2	5.9±0.3	0.30
Last follow-up	7.3±0.7	8.6±1.0	14.3±1.0*†	0.006
Mitral regurgitation, /4				
Baseline	0.0±0.0	0.1±0.1	0.0±0.0	0.19
Last follow-up	0.1±0.1	0.8±0.3	1.2±0.2*	0.03

Table S2. Regional dry weights in the atria of sham, transition and LA-PAF animals.

Tissue Region	Sham	Transition	LA=PAF
LA	6.5 ± 0.6 g	10.6 ± 1.3 g (NS)	15.4 ± 2.1 g (p<0.02)
RA	7.4 ± 0.8 g	9.9 ± 1.2 g (NS)	17.3 ± 2.8 g (p<0.04)
PLA	9.8 ± 1.7 g	13.9 ± 1.3 g (NS)	20.1 ± 2.9 g (p<0.04)

Table S3: Structural remodeling associated with AF. (RA = right atria; LA = left atria; PLA = posterior left atria; *p<0.001 vs sham; †p=0.005 vs sham; ‡p<0.001 vs sham and Transition AF; §p<0.05 vs sham).

	Sham	Transition AF	LS-PAF	p
LA cell size				
Length, μm	153.3 ± 4.1	188 ± 4.0*	186.1 ± 4.1*	<0.001
Width, μm	16.2 ± 0.4	18.2 ± 0.4†	19.0 ± 0.4*	<0.001
RA cell size				
Length, μm	155.4 ± 3.7	161.9 ± 4.2	168.8 ±3.8	0.07
Width, μm	17.0 ± 0.9	18.3 ±0.4	21.4 ± 0.5§	<0.05
Patchy Fibrosis, %				
RA	5.4±0.4	5.4±0.4	6.3±0.6	0.30
LA	5.0±0.4	5.8±0.8	6.2±0.7	0.49
PLA	6.2±0.7	6.6±0.8	9.3±1.2	0.13
Interstitial Fibrosis, %				
RA	5.1±0.9	5.5±0.7	6.6±0.6	0.34
LA	5.5±1.2	7.0±0.6	10.7±1.5§	0.018
PLA	4.1±0.6	7.9±0.7	14.6±1.4‡	<0.001

Table S4: Primers used for RT-PCR.

Gene	Protein		Forward Primer (5'->3')	Reverse Primer (5'->3')
CACNA1C	Cav1.2	XM_004007606.1	GGAGCGGGTGGAGTATCTCT	GAGGTAAGCGTTGGGGTGAA
SCN5A	Nav1.5	XM_004018231.1	GCAACTTCACGGTGCTCAAC	TGAGGTAGAGGTCCAGCGAT
KCND2	Kv4.2	XM_004008268.1	GGAAGCTCCACTATCCTCGC	CGGCGATCCTTGTACTCCTC
KCNJ4	Kir2.3	XM_004023651.1	CTACTTCGCCAACCTGAGCA	TCATGAGCATGTAGCGCCAG
KCND3	Kv4.3	XM_004002324.1	CTCCACCATCAAGAACCACGA	CGTGTGGACGGGTAGTTCTG
KCNJ2	Kir2.1	XM_004013146.1	CCCTCACGAGCAAAGAGGAA	GCCTGGTTGTGCAGGTCTAT

Table S5: Modifications in currents of GP atrial model to implement paroxysmal and transition AF.

Current	Paroxysmal AF	Transition AF
I_{Na}	-50%	-50%
I_{CaL}	-30%	-65%
I_{K1}	+100%	+100%
I_{to}	-75%	-75%

Table S6: Action potential durations (APDs) obtained in the three models: sham, paroxysmal and transition AF.

APD	Sham (ms)	Paroxysmal AF (ms)	Transition AF (ms)
APD_{30}	5.5	15.0	8.5
APD_{50}	42.0	64.5	31.0
APD_{90}	203.0	168.5	99.5

Supplemental Figures:

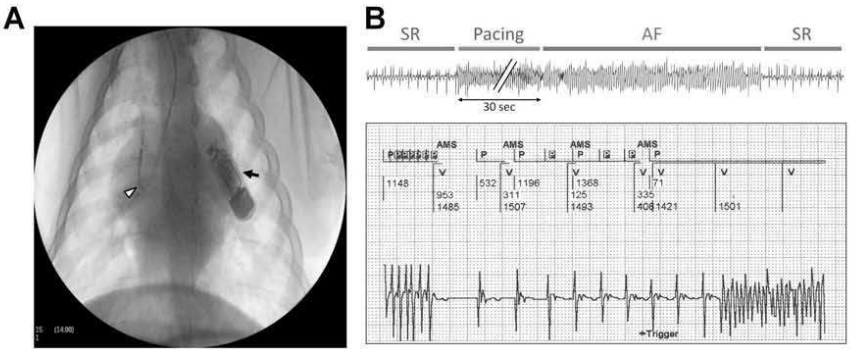

Figure S1: Experimental and pacing protocols. A: Fluoroscopy image showing the RA lead screwed to the right atrial (RA) appendage (arrowhead) and the implantable loop recorder (ILR, black arrow) fixed subcutaneously in close proximity to the left atrium (LA). B: Top: A 30-second burst of tachypacing (20 Hz) during sinus rhythm (SR) induces a short-lasting episode of AF; bottom: intracardiac electrogram recorded from the RA showing AF termination (left), detection of SR by the automatic mode switching (AMS) algorithm and automatic resumption of pacing.

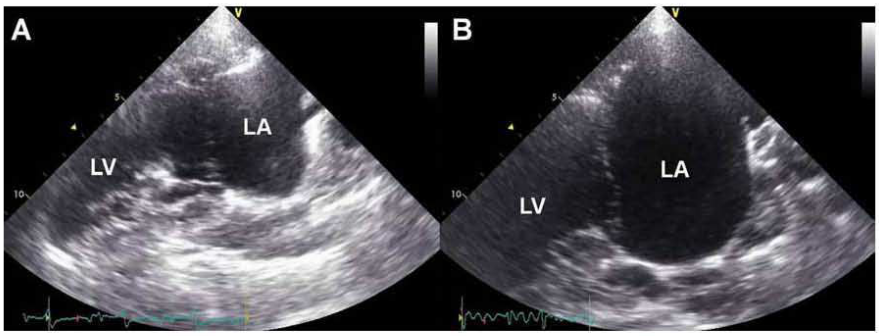

Figure S2: Echocardiographic evidence of sustained AF-induced atrial dilatation. Parasternal long-axis view of the heart of a sham-operated (A) and a long-standing persistent AF animal (B). Note substantial atrial dilatation in B (scale bar on the left of each image in cm).

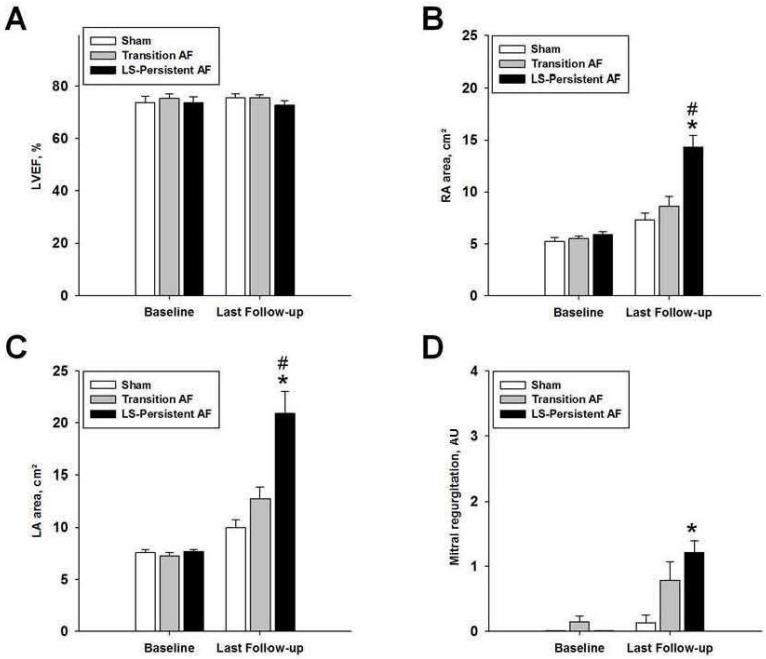

Figure S3: Quantification of echocardiographic findings. A: Left ventricular ejection fraction (LVEF) did not change over the time of the study. B and C: Both atria were significantly dilated in the LS-persistent AF animals. D: Mitral valve regurgitation, measured in arbitrary units (AU) of severity, where 1 is mild and 4 is severe, was significant in LS-persistent AF animals. *p<0.05 *vs.* sham, #p<0.05 *vs.* transition; N=6, N=7 and N=7 for the sham-operated, transition and LS-PAF groups. N = number of animals.

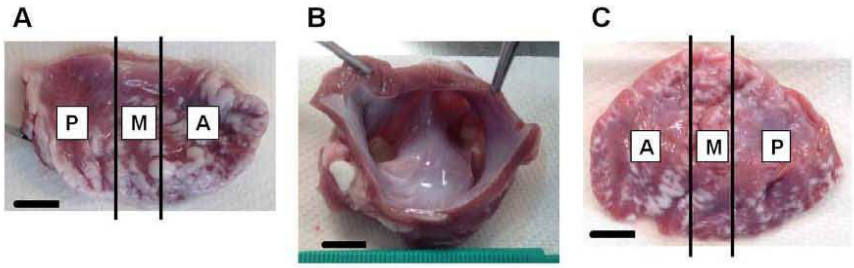

Figure S4. After the heart was explanted, the atria were removed and cut in the following three sections: RA wall (panel A), PLA (panel B) and LA wall (panel C). The posterior part of the PLA was used for histology (fibrosis analysis), whereas both RA and LA walls were cut in three pieces: anterior (A), medial (M), and posterior (P). PLA and posterior LA differ since they were separated from each other by the pulmonary veins (which can be seen in the PLA photography). Scale bar = 1 cm.

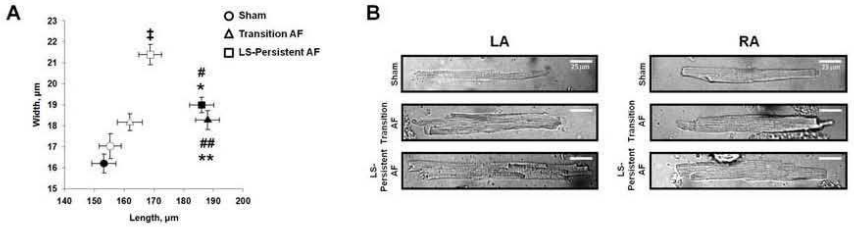

Figure S5: Sustained AF induces atrial myocyte hypertrophy. A: Average lengths and widths for cells isolated from RA (open symbols) and LA (filled symbols). N=3/n=60 (sham), N=4/n=70 (transition), and N=5/n=90 (LS-PAF). B: Representative phase contrast micrographs. For RA LS-PAF myocytes: ‡p=0.001 *vs.* sham for width. For LA Transition and LS-PAF myocytes: *p=0.01 and **p< 0.001 *vs.* sham for width and length, respectively; #p<0.001 and ##p=0.002 *vs.* RA LS-PAF myocytes for width and length, respectively.

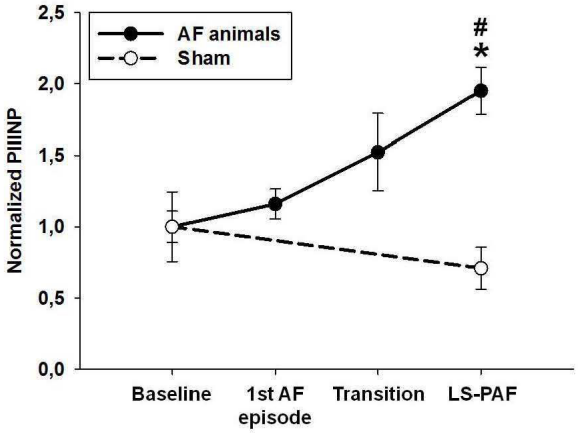

Figure S6: Sustained AF increases serum levels of Procollagen III N-Terminal Propeptide (PIIINP). *p< 0.001 *vs.* sham, #p=0.06 *vs.* baseline.

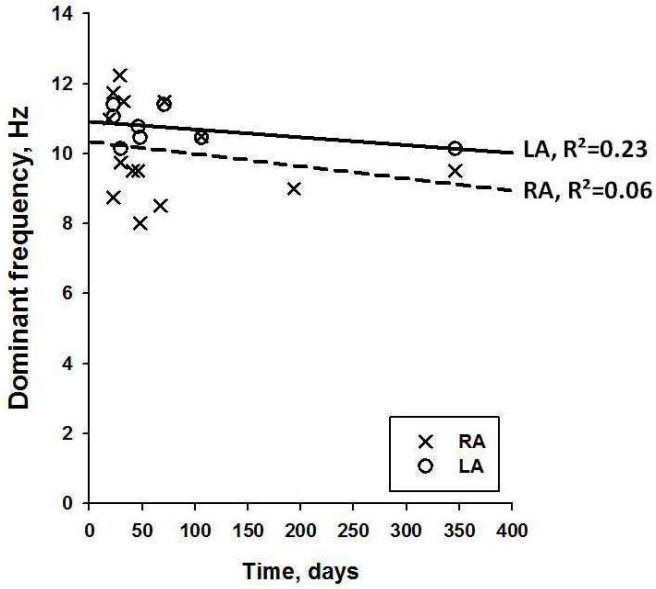

Figure S7: Relationship between DF and time to transition to persistent AF. No correlation was found between the DF at transition and the time from the first episode of AF to the transition to self-sustained persistent AF.

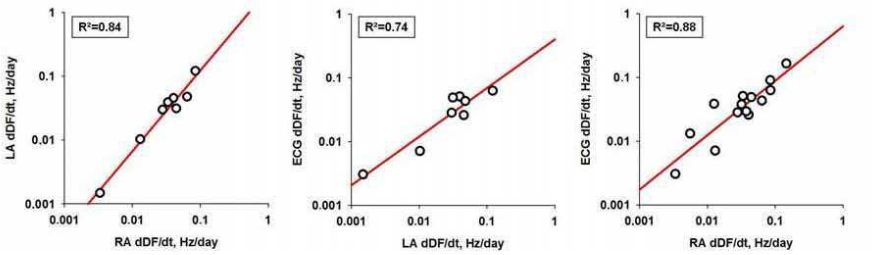

Figure S8: Correlations between dDF/dt measured from the signal obtained through the RA intracardiac lead, the ILR and the ECG (lead I). A correlation between the dDF/dt measured from LA and RA (left), ECG and LA (middle) and ECG and RA (right) was observed.

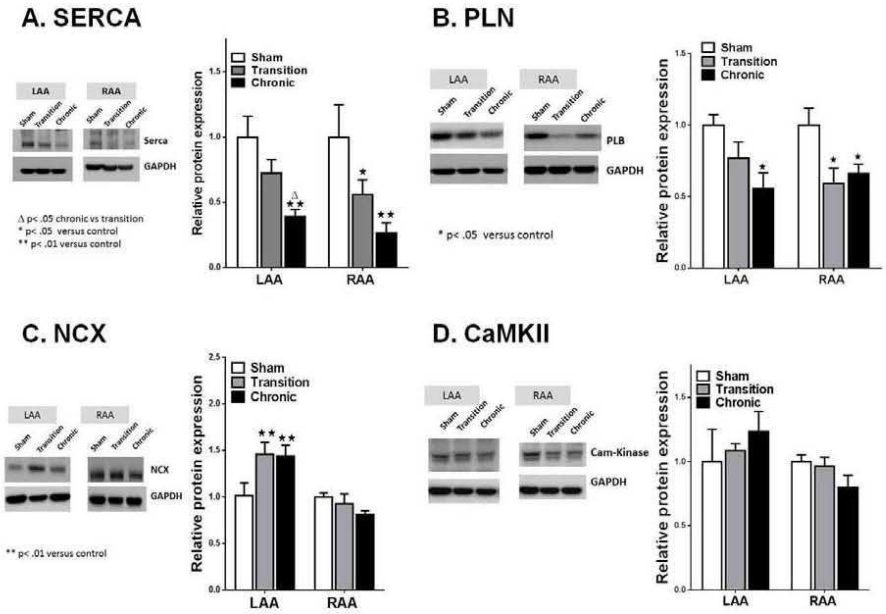

Figure S9: Calcium handling protein changes. Western blot analysis of SERCA (panel A), phospholamban (Panel B), Sodium-calcium exchanger (NCX, panel C) and CaMKII (panel D). Left: representative blots; right: quantification of protein expression relative to GAPDH. N=6 per group.

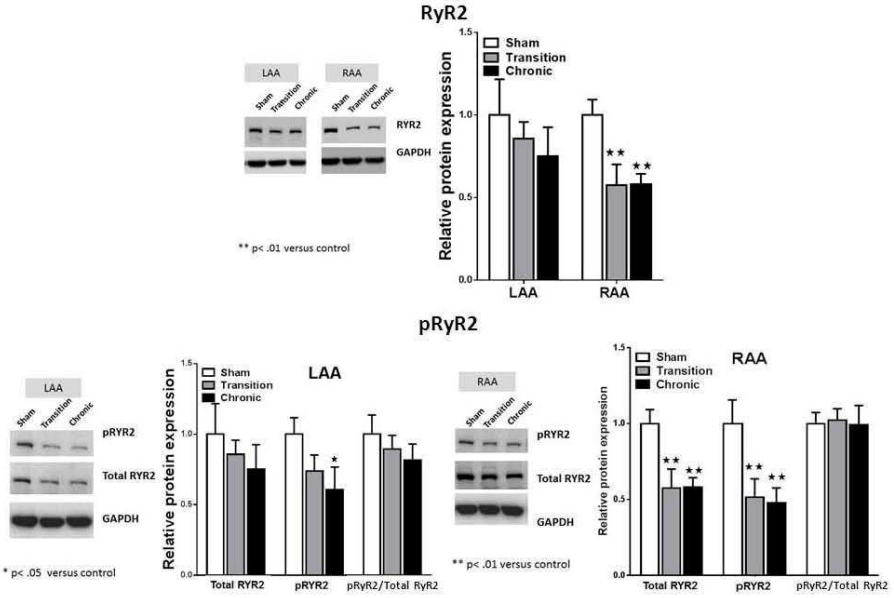

Figure S10: Ryanodine receptor (RyR2) changes. Western blot analysis of RyR2 (top), and phosphorylated RyR2 (pRyR2, bottom), Left: representative blots; right: quantification of protein expression relative to GAPDH. N= 6 per group.

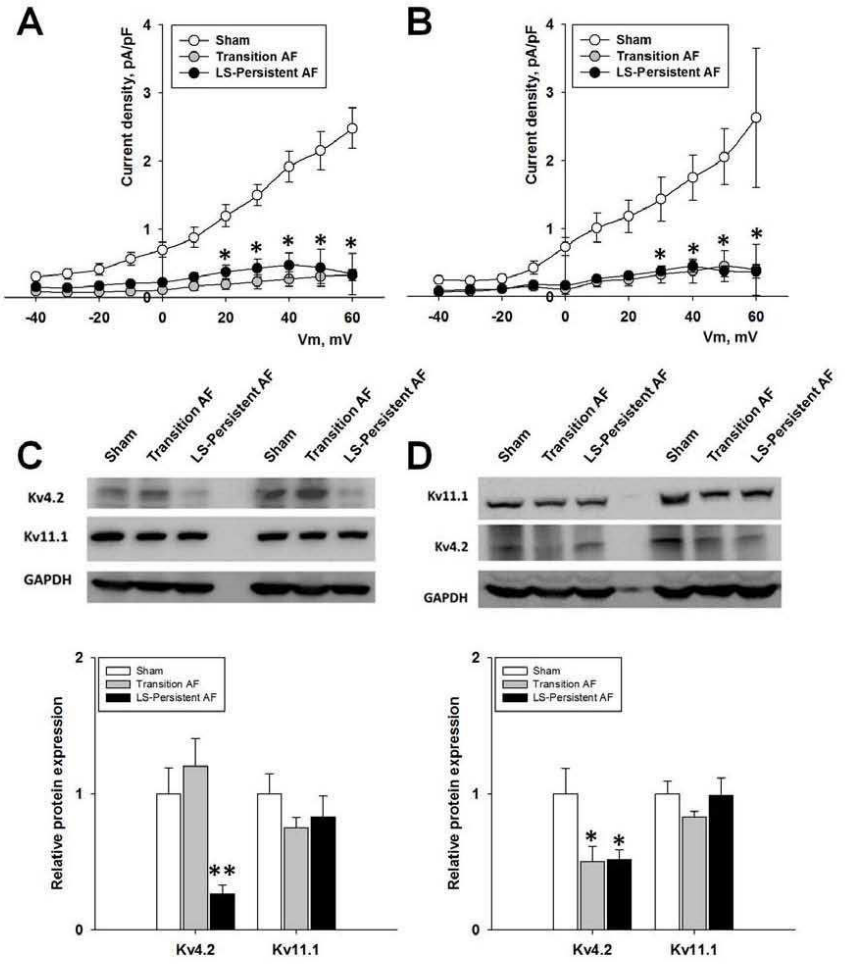

Figure S11: Sustained AF reduces functional expression of the transient outward potassium channel (I_{to}) but not hERG. A and B: Current-voltage relationships for I_{to} in cells from the LA (A) and the RA (B). For the LA: N=2/n=6 (sham), N=3/n=5 (transition), N=6/n=10 (LS-PAF); for the RA: N=2/n=6 (sham), N=3/n=5 (transition), N=3/n=5 (LS-PAF). *p<0.05 *vs.* sham for the transition and LS-PAF groups. C and D: Western blot analysis of $K_V4.2$ and $K_V11.1$ protein expression in LA (C) and RA (D) tissue homogenates. Top, Representative blots; bottom, Quantification of protein expression relative to GAPDH. N=6. Note significant reductions of $K_V4.2$, but not $K_V11.1$ (hERG) *p<0.05 *vs.* sham, **p<0.01 *vs.* sham.

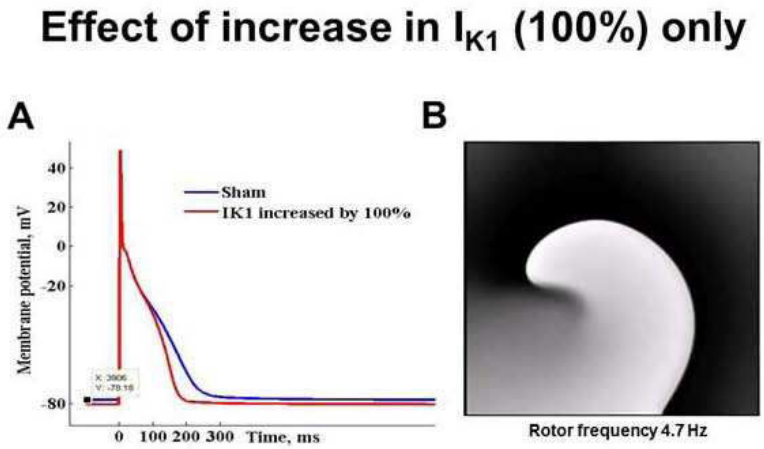

Figure S12: Effects of increasing I_{K1} alone in the Grandi-Pandit human atrial model. A: Increasing I_{K1} by 100% alone as seen in myocytes from transition sheep hyperpolarized the resting membrane potential by -2 mV and significantly shortened the APD (23%) with respect to sham. B: I_{K1} increase alone resulted in a meandering rotor at 4.7 Hz.

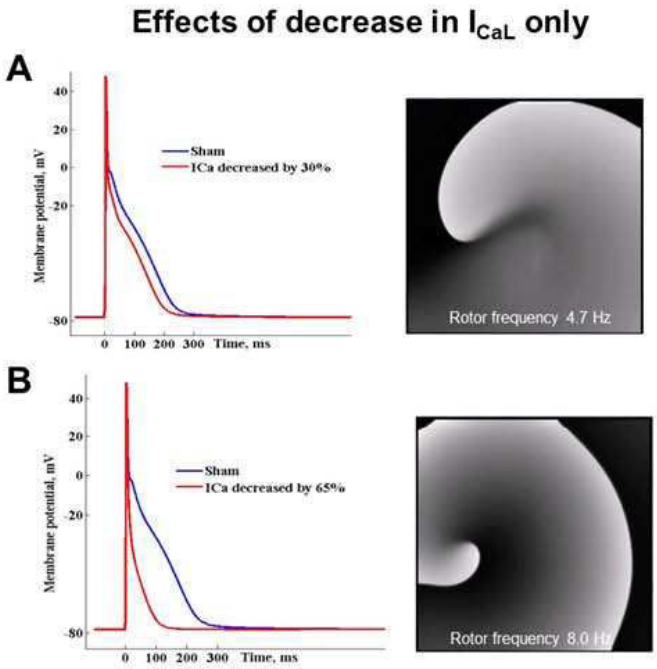

Figure S13: Effects of reducing I_{CaL} alone in the Grandi-Pandit human atrial model. A: When I_{CaL} was reduced by 30%, as simulated in paroxysmal AF, APD_{50} and APD_{90} were reduced (~37%), which resulted in a meandering rotor that eventually died out. B: When I_{CaL} was reduced by 65%, as observed in transition AF, APD_{50} and APD_{90} were greatly reduced (~64%). This reduction in APD provided sufficient substrate for a very stable rotor with DF=8.0 Hz

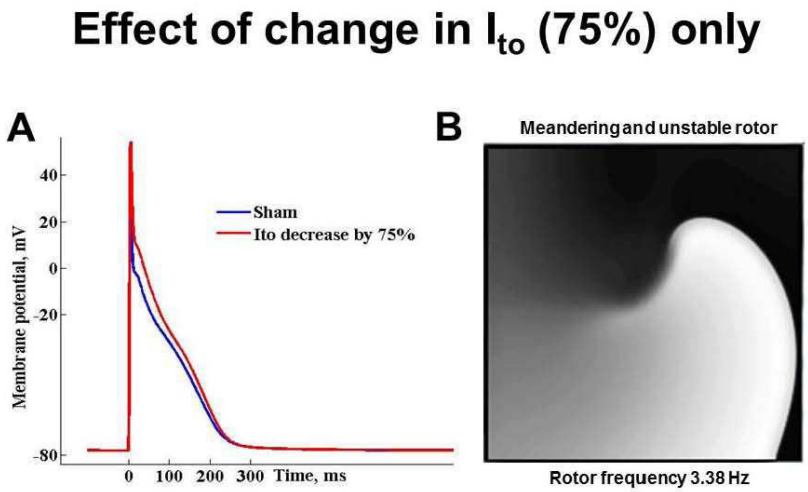

Figure S14: Effects of reducing I_{to} alone in the Grandi-Pandit human atrial model. A. reducing I_{to} by 75 % resulted in only slight increases in APD_{30} and APD_{50}. B: This condition yielded a meandering and unstable rotor whose DF was 3.38 Hz

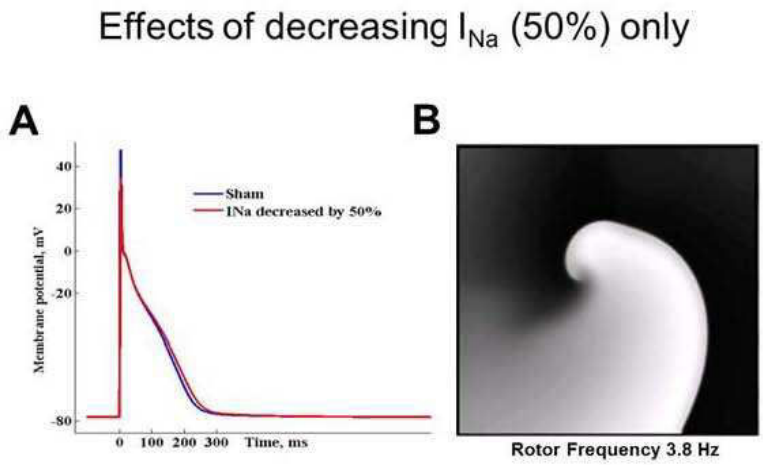

Figure S15 : Effects of reducing I_{Na} alone in the Grandi-Pandit human atrial model. A. reducing I_{Na} by 50 % negligibly changed APD_{90}. B: this condition resulted in an unstable rotor whose DF was 3.82 Hz

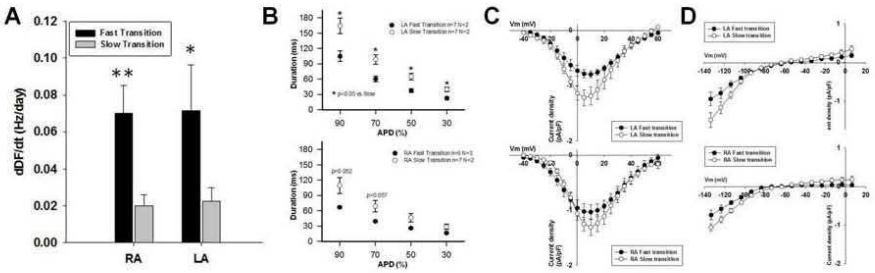

Figure S16: Electrophysiological differences between fast and slow transition animals. A. dDF/dt was significantly higher in fast transition sheep (0.07±0.02 Hz/day; N=7) than slow transition sheep (0.02±0.007 Hz/day; N=7; **p=0.007; *p=0.036). B, Mean APD at 30-90% repolarization was shorter in fast than slow transition animals. C, I_{CaL} tended to be lower in fast than slow transition animals; top, LA bottom, RA. D, I_{K1} tended to be larger in slow transition animals. N=4, fast transition; N=3 slow transition sheep.

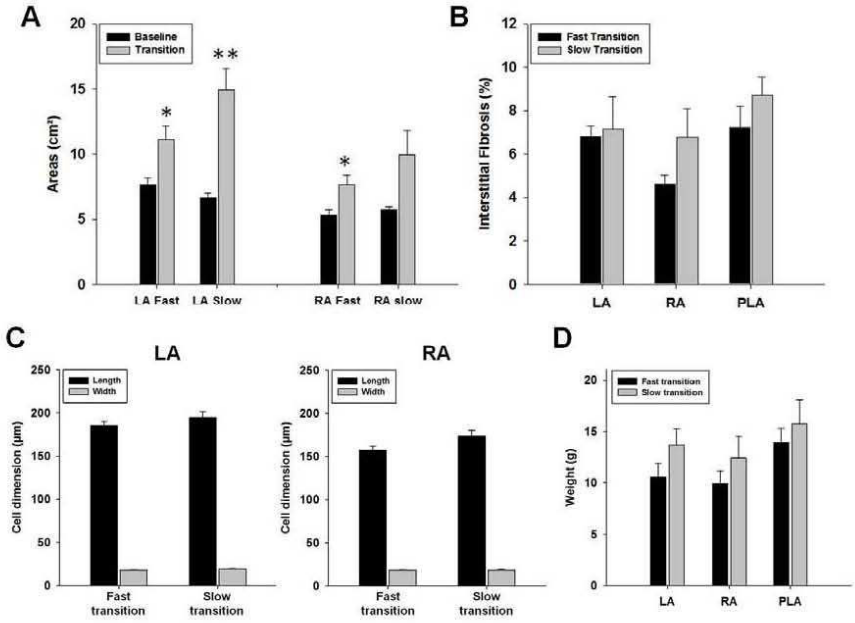

Figure S17: Structural differences between fast and slow transition animals. LA area was significantly increased in both groups (**p=0.007; *p<0.05), although a more pronounced atrial dilatation was observed in slow transition animals (124% *vs.* 45% increase in LA atrial dilatation; p=0.014, panel A). Trends for higher degree of fibrosis (panel B), longer and wider cells (panel C) and heavier atria (panel D) were observed. N=4 fast transition; N=3 slow transition sheep.

Troisième partie

Prise en charge thérapeutique

A. Généralités

La présentation clinique de la FA est variable. Parfois asymptomatique, elle peut le plus souvent se présenter comme une arythmie invalidante, altérant la qualité de vie des patients et nécessitant une cardioversion rapide. La FA paroxystique, si elle est symptomatique et que les épisodes sont récurrents, est communément traitée par anti-arythmiques (« rhythm control »), alors que la forme persistante est traitée par des médicaments ralentisseurs pour contrôler la cadence ventriculaire (« rate control »). Le traitement anti-arythmique permet d'atténuer les symptômes, de réduire la durée des épisodes et de diminuer le nombre d'hospitalisations.[177, 178] Cependant, la plupart des traitements pharmacologiques actuellement utilisés n'ont qu'une efficacité limitée pour restaurer le rythme sinusal ou prévenir la récidive de nouveaux épisodes. Par ailleurs, la majorité d'entre eux ont une activité pro-arythmique à l'étage ventriculaire et ont parfois des effets secondaires extra-cardiaques sévères. La publication il y a une dizaine d'années d'études ayant comparé les stratégies du contrôle du rythme et du contrôle de la fréquence, parmi lesquelles les études AFFIRM[164] et RACE,[179] ont mis en évidence l'absence de supériorité d'une stratégie par rapport à l'autre en termes d'accidents thrombo-emboliques ou de mortalité. Au contraire, une tendance à une mortalité plus élevée était retrouvée dans le groupe « contrôle du rythme » en rapport avec les effets secondaires des traitement anti-arythmique.[179] Ces études n'ont pas modifié la prise en charge des patients fortement symptomatiques, ayant une FA de découverte récente, ou jeunes, mais ont amené les cliniciens à proposer plus fréquemment une stratégie de contrôle de la fréquence chez les patients peu symptomatiques, ayant une cadence ventriculaire peu élevée ou plus âgés. Il est vraisemblable que la mise sur le marché de nouvelles molécules permettant de mieux assurer le maintien du rythme sinusal sans disposer d'effets secondaires graves (qu'ils soient ou non, cardiaques) mènerait à un changement de cette tendance vers une stratégie de contrôle du rythme plus fréquente. En attendant de telles molécules, l'alternative dont nous disposons aujourd'hui est l'ablation endocavitaire. Plusieurs études ont démontré la supériorité d'une stratégie ablative par rapport au traitement anti-arythmique en termes de réduction des symptômes et de maintien du rythme sinusal à moyen terme.[180-183] Initialement en seconde ligne thérapeutique après l'échec d'un traitement anti-arythmique, l'ablation est désormais passée dans les dernières recommandations au même niveau que le traitement pharmacologique, pouvant ainsi être proposée en première intention.[184] La récente étude MANTRA-PAF a cependant démontré qu'une telle stratégie n'apportait pas de bénéfice en termes de charge cumulée de FA sur un suivi de 2 ans.[185] En s'affranchissant de la sur-mortalité infligée par la prescription d'un traitement anti-arythmique, il est cependant licite d'envisager qu'en cas de succès de la procédure, l'ablation entrainerait une diminution de la mortalité à long terme. L'étude randomisée CABANA (ClinicalTrials. Gov NCT00911508), prévue pour inclure près de 3000 patients et dont les résultats seront connus en 2016, apportera sans doute la réponse à cette question.

B. Nouvelles avancées dans le traitement anti-arythmique de la FA

Les traitements anti-arythmiques sont des molécules ayant une activité sur les canaux ioniques membranaires des cardiomyocytes, modulant l'ouverture ou la fermeture des canaux, modifiant la fonction des pompes ou bloquant des récepteurs membranaires. Sur le plan électrophysiologique, ils entraînent une augmentation de la période réfractaire des cardiomyocytes, ralentissent la vitesse de conduction du myocarde ou la bloquent à certains points vulnérables, ou alors diminuent l'hyperautomaticité et les décharges focales. La majorité des molécules actuellement disponibles n'est pas atrio-spécifique, et provoque également des modifications de l'électrophysiologie cellulaire ventriculaire, expliquant ainsi leur caractère pro-arythmique.

Sur le plan théorique, le parfait anti-arythmique ne devrait cibler que les cellules atriales (évitant ainsi le risque de troubles du rythme ventriculaires), être efficace pour prévenir les récidives de FA, et le cas échéant, ralentir la cadence ventriculaire, être utilisable en cas d'insuffisance cardiaque, et par conséquent ne pas avoir d'effet inotrope négatif, être responsable de peu d'interférences médicamenteuses afin de ne pas interférer avec le traitement anticoagulant, et enfin avoir peu d'effets secondaires.[186] Bien que certains anti-arythmiques dont nous disposons possèdent quelques unes de ces caractéristiques, aucun d'entre eux ne possède une efficacité et une sécurité d'emploi suffisantes pour l'ensemble des patients en FA. L'amiodarone est actuellement l'un des anti-arythmiques les plus efficaces dont les cliniciens disposent pour prévenir les récidives de FA, et a peu d'effets sur la mortalité.[187] Ses complications extra-cardiaques sont cependant nombreuses, ce qui en limite l'intérêt, particulièrement chez le sujet jeune. La flécaïnide est fréquemment utilisée, particulièrement chez les sujets présentant un accès récent de FA, mais n'est utilisable qu'en l'absence de cardiopathie figurée. Les β-bloquants n'ont qu'une faible efficacité anti-arythmique (hormis dans les cas de FA adrénergique ou secondaire à une hyperthyroïdie).

La mise sur le marché de nouveaux anti-arythmiques est donc nécessaire afin de diminuer la charge en arythmie et d'améliorer ainsi la qualité de vie des patients en FA. De nombreuses molécules sont à l'étude, parmi lesquelles la chloroquine et la ranolazine.[188] Afin de mieux comprendre les effets anti-arythmiques de ces molécules, nous avons menés des travaux sur des cœurs de moutons perfusés via un système de Langendorff sur un modèle de FA induite par le stretch.

1. Effets anti-arythmiques de la chloroquine

a. Hypothèse de travail

Les courants potassiques à rectification entrante (I_{K1}, I_{KAch} et I_{KATP}) jouent un rôle important dans le contrôle de la dynamique des ondes de fibrillation, et principalement celle des rotors.[189, 190] Récemment, Noujaim et al ont démontré que la chloroquine, molécule antipaludique, bloquait les sous-unités Kir2.1, Kir3.1 et Kir6.2 respectivement responsables

des courants potassiques à rectification entrante (I_{K1}), sensible à l'acétylcholine (I_{KAch}) et à l'ATP (I_{KATP}). Ainsi, elle provoque une dépolarisation du potentiel transmembranaire de repos et potentiellement une hyperautomaticité.[191] Etant donné que les rotors jouent un rôle majeur dans le maintien de la FA, et qu'I_{K1} contrôle leur fréquence et leur stabilité, nous avons voulu tester l'effet anti-arythmique de la chloroquine sur des cœurs ovins explantés et perfusés, en le comparant à la flécaïnide, molécule utilisée quotidiennement en pratique clinique. Nous avons décidé de comparer l'effet de la chloroquine à la flécaïnide car, tout comme l'amiodarone[192] ou les derniers traitements anti-arythmiques introduits sur le marché tels que la dronédarone[193] et le vernakalant,[194] elle ne bloque pas I_{K1} à sa concentration thérapeutique.[195]

b. Méthodes

Afin d'étudier l'efficacité de ces deux molécules, nous avons analysé par cartographie optique leurs propriétés anti-arythmiques sur de la FA induite par le stretch sur 30 cœurs de moutons explantés.[132] Après perfusion sur un système de Langendorff, la pression intra-atriale était augmentée à 14 cmH_2O et de la FA induite par stimulation rapide à 12Hz. Après 15 minutes de FA, les effets de 4µmol/l de chloroquine (n=7) et de 2 à 4µmol/l de flécaïnide (n= 5) étaient comparés (doses basées sur les concentrations thérapeutiques observées chez l'homme[196, 197]). La perfusion de l'anti-arythmique était maintenue pendant 20 minutes, temps au bout duquel la concentration était doublée et maintenue pour une durée supplémentaire de 30 minutes en l'absence de retour en rythme sinusal. En cas de persistance de FA pendant les 50 minutes de l'expérience, une cardioversion externe était réalisée. Une tentative de réinduction par stimulation était alors effectuée avant et après une période d'élimination de 30 minutes pour la flécaïnide et de 45 minutes pour la chloroquine.

c. Résultats

Comme le montre la Figure 36, la chloroquine à 4µmol/l entraine rapidement une réduction de la DF_{max} de 10.6±0.7 à 6.3±0.2 Hz (n=7) puis un retour en rythme sinusal après 4 à 19 minutes. A l'opposé, la perfusion de 2µmol/l de flécaïnide pendant 20 minutes puis de 4µmol/l pendant 30 minutes entraine une diminution de la DF_{max} de 11.1±1.3Hz à 8.1±1.3Hz (p=0.0014) avec passage en tachycardie atriale (TA) sur 2 cœurs, mais sans retour en rythme sinusal (Figure 37, n=5). Ainsi, l'effet anti-arythmique de la chloroquine était significativement supérieur à celui de la flécaïnide (Figure 37B, 0/5 versus 7/7, p=0.0013).

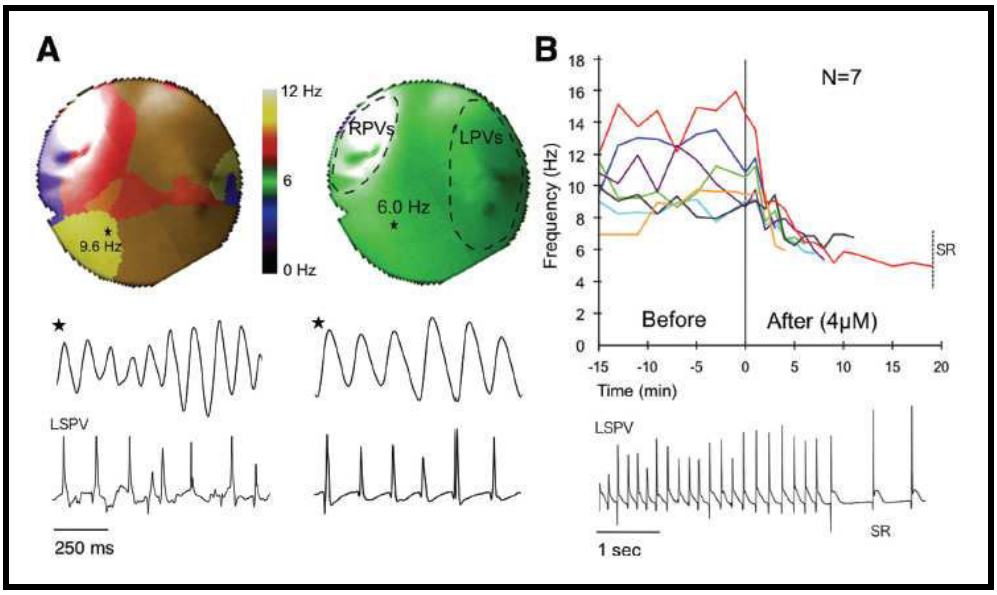

Figure 36 : Effet de la chloroquine sur la dynamique de la FA. A. Haut : Carte de DF de l'endocarde postérieur de l'OG en FA et avant retour en rythme sinusal. Milieu : EGM local enregistré par cartographie optique au niveau du point marqué *. Bas : EGM local de la veine pulmonaire supérieur gauche (VPSG) enregistré par une électrode bipolaire. B. Haut : Evolution de la DF_{max} avant et après la perfusion de la chloroquine. Bas : EGM enregistré dans la VPSG au moment du retour en rythme sinusal.

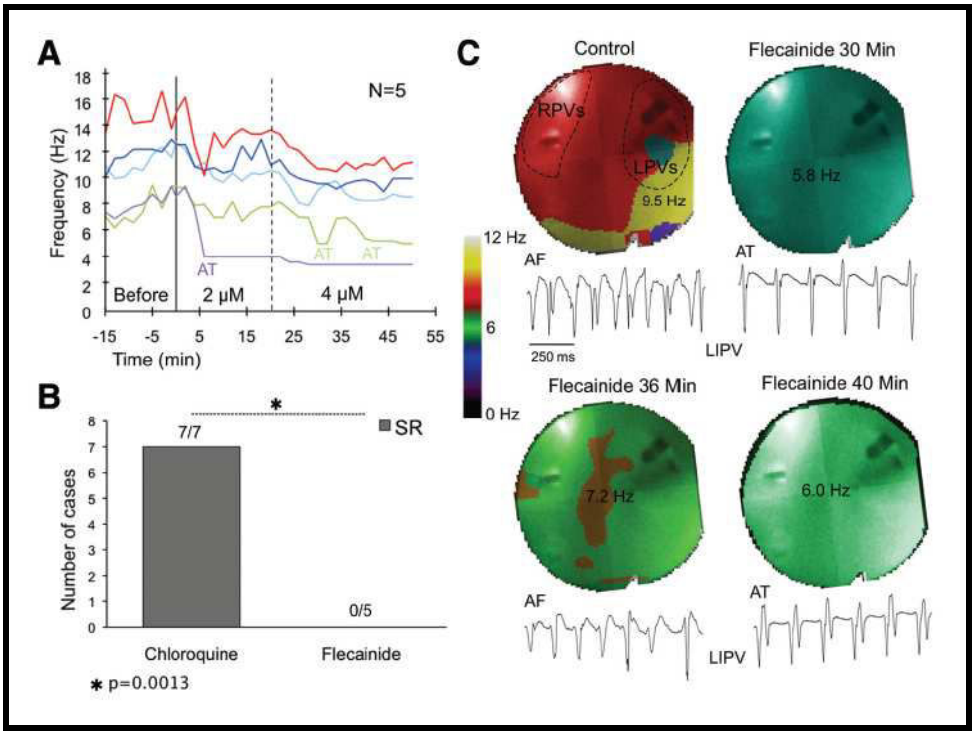

Figure 37. Effet de la flécaïnide sur la dynamique de la FA. A. Evolution de la DF_{max} avant et après perfusion de flécaïnide. B. L'efficacité de la flécaïnide est inférieure à celle de la chloroquine. C. Cartes de DF de la paroi postérieure de l'OG avec EGM local de la veine pulmonaire inférieure gauche (VPIG) à l'état basal et après perfusion de flécaïnide.

Après cardioversion, seules des arythmies non-soutenues étaient induites en présence de chloroquine (n=7) alors que des épisodes de FA (N=4) ou de TA (N=1) soutenus étaient réinduits en présence de flécaïnide (Figure 38). Après la période d'élimination de 30 minutes, des arythmies soutenues étaient déclenchables sur l'ensemble des cœurs.

Dans le sous-groupe de cœurs sur lesquels la flécaïnide n'entrainait pas de retour en rythme sinusal, nous avons testé l'effet anti-arythmique de la chloroquine après réinduction de FA. Bien que la DF_{max} en FA était supérieur à celle initialement observée (16.9±2.0 versus 11.1±1.3Hz, p=0.018, différence probablement en rapport avec la détérioration des cardiomyocytes après 3 heures de perfusion sur le système de Langendorff ou avec l'activation d'I_{KATP}), la chloroquine à 4µmol/l entrainait une diminution de la DF_{max} et une restauration du rythme sinusal (Figure 38C).

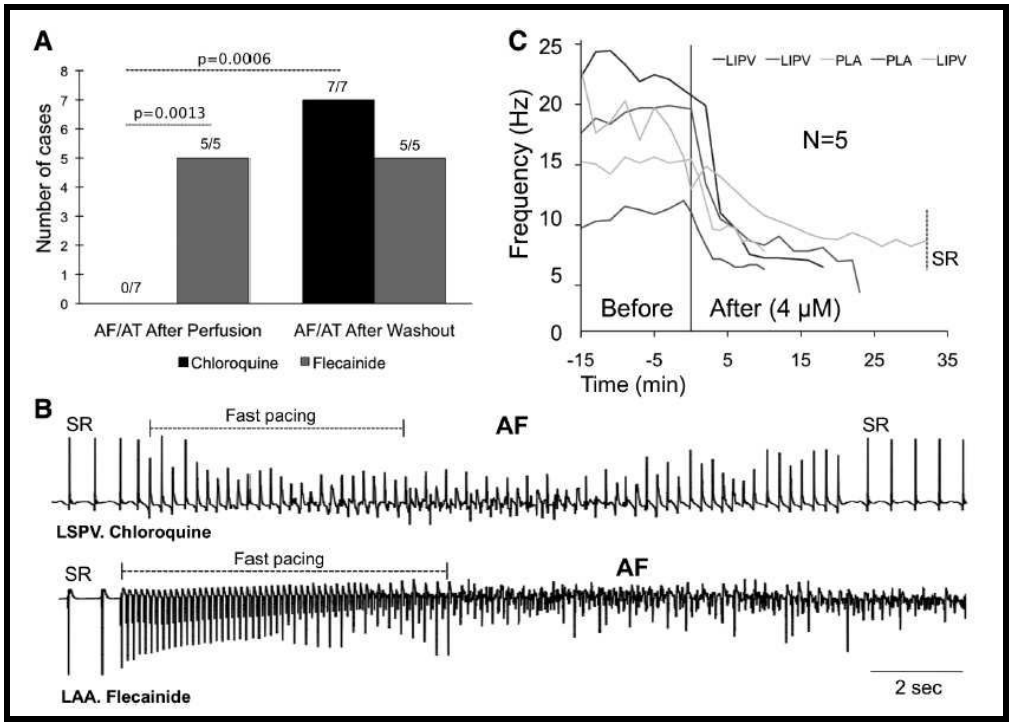

Figure 38. A. Gauche : Des arythmies atriales soutenues (FA/TA) sont réinductibles lors de la perfusion de flécaïnide mais pas en cas de perfusion de chloroquine. B. La stimulation atriale à haute fréquence (12Hz) ne capture pas l'oreillette en 1:1 et n'induit qu'un court épisode de FA lors de la perfusion de chloroquine. A la même fréquence de stimulation, une FA soutenue est induite sous flécaïnide.

Afin de comprendre le mécanisme anti-arythmique de la chloroquine, nous avons analysé la durée des PA, la vitesse de conduction et la dynamique des ondes fibrillatoires (rotors et décharges focales) avant et après perfusion de la molécule.

Tout d'abord, nous avons mis en évidence que la chloroquine entrainait un élargissement du PA (augmentation respective de la durée de l'APD_{70} de 155±3.1 à 176±6.0 ms et de 144±3.4 à 158±5.0 ms à 300 et 250 ms de cycle de stimulation, $p<0.05$, Figure 39). La flécaïnide n'avait au contraire aucun effet sur la durée du PA.

Les deux molécules diminuaient significativement la vitesse de conduction (Figure 39), la chloroquine de part une diminution de la disponibilité des canaux sodiques secondaire à l'hyperpolarisation membranaire (12% de réduction) et la flécaïnide directement par inhibition d'I_{Na} (33% de réduction).

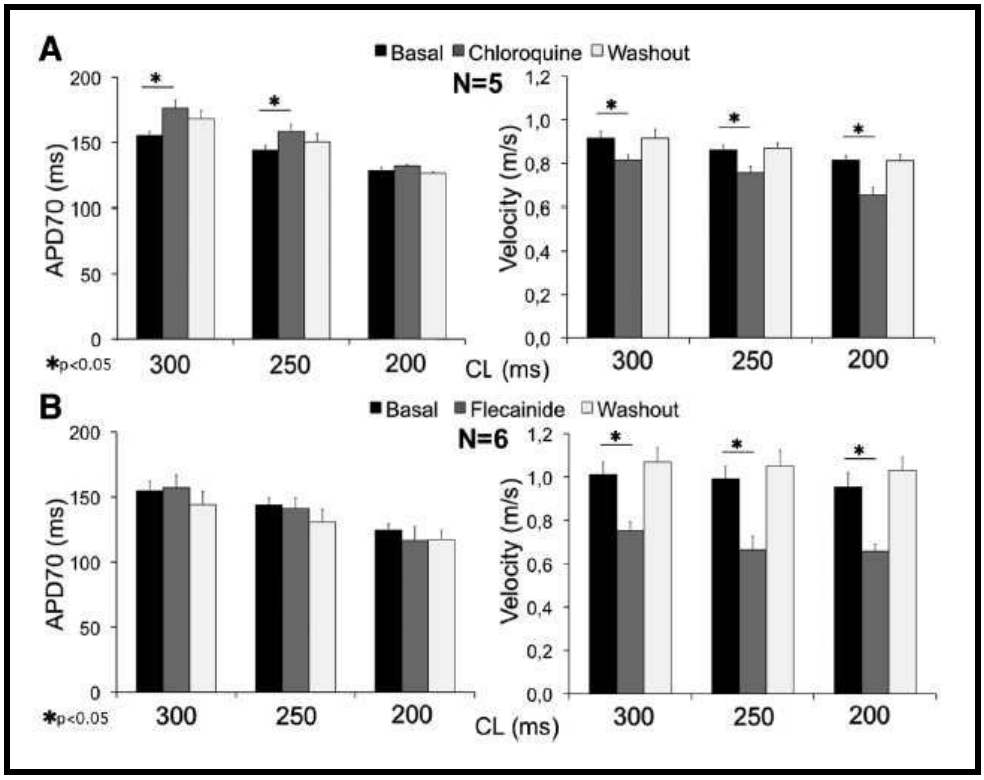

Figure 39. Durée des PA et vitesse de conduction à l'état basal et après perfusion de chloroquine (A) et de flécaïnide (B).

Nous avons ensuite étudié la dynamique des ondes de fibrillation avant et après perfusion des anti-arythmiques. Comme le montre la Figure 40A, la chloroquine induisait une diminution significative du nombre de rotors par cm² sur l'endocarde postérieur (de 3.2±0.3 à 0.7±0.3, p=0.003) et sur l'auricule gauche (de 1.6±0.1 à 0.6±0.2, p=0.0002), dont le diamètre des cores augmentait significativement (Figure 40B et C). La chloroquine entrainant une dépolarisation du potentiel transmembranaire de repos, favorisant potentiellement l'hyperautomaticité.[191] Cependant, nous avons observé une diminution du nombre de décharges focales (de 12.3±0.8 à 6.8±0.7, p=0.03, Figure 40D) évoluant parallèlement à la diminution du nombre de rotors, donnée suggérant que ces décharges sont en fait le reflet d'activités réentrantes intra-murales.

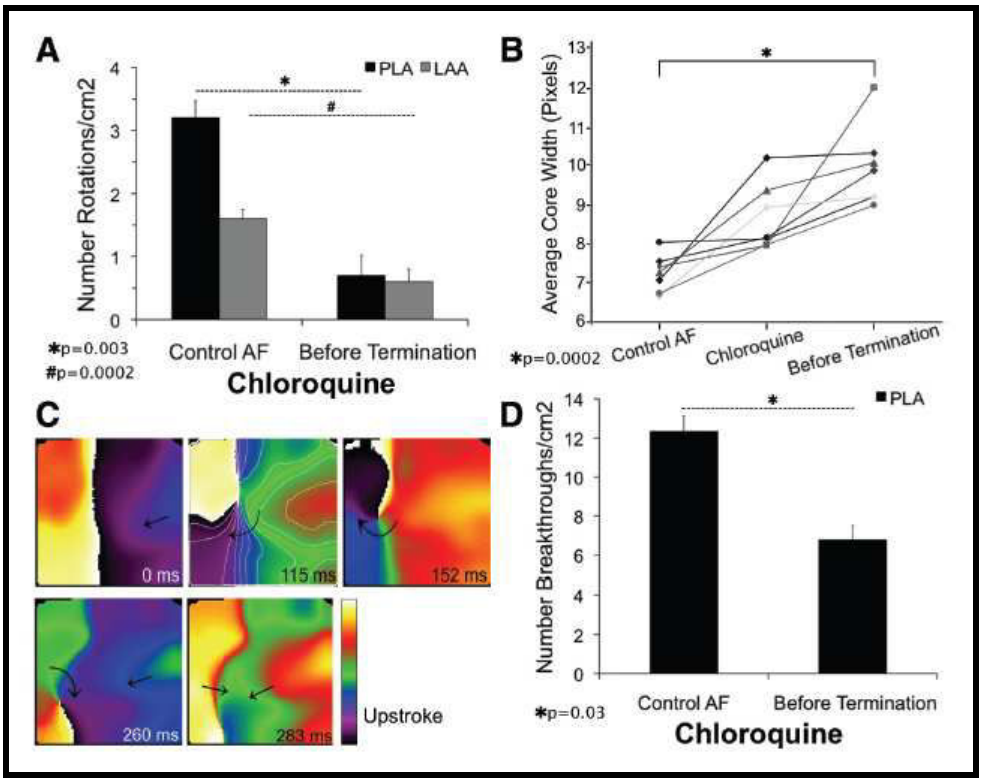

Figure 40. Effets de la chloroquine sur les rotors et les décharges focales. A. Nombre de rotations par cm² dans l'endocarde postérieur (PLA) et l'auricule gauche (LAA) en FA et avant retour en rythme sinusal. B. La taille des core augmente significativement après la perfusion de chloroquine. C. Cartes de phase montrant une collision entre un front et une queue d'activation qui donne naissance à un rotor. Celui-ci ne réalise pas une rotation complète et disparait spontanément en présence de chloroquine. D. Nombre de décharges focales par cm² en FA et avant retour en rythme sinusal.

Comme que le montre la Figure 41, le nombre de rotors par cm² après perfusion de flécaïnide diminuait sur l'endocarde postérieur (de 3.7±0.2 à 2.7±0.4, p=NS) comme sur l'auricule gauche (de 2.0±0.2 à 1.1±0.1, p<0.05). Cependant, seule la chloroquine diminuait significativement le nombre de rotors et de décharges focales sur l'endocarde postérieur (respectivement de 3.2±0.3 à 0.7±0.3 et de 12.3±0.8 à 6.8±0.7, p<0.05). Enfin, le diamètre du core n'augmentait pas après perfusion de 4µmol/l de flécaïnide.

Bien qu'étant un bloqueur préférentiel d'I_{K1}, la chloroquine peut inhiber d'autres courants, parmi lesquels I_{Kr}. Afin de séparer l'effet de l'inhibition sur I_{K1} par rapport à celui sur I_{Kr}, nous avons étudié l'effet anti-arythmique de 0.5 et 1µmol/l d'E-4031 (bloqueur spécifique d'I_{Kr}) sur ce modèle de FA sur cœur explanté. Sur 7 expériences complémentaires, nous avons observé que l'E4031 ne permettait un retour en rythme sinusal que si la DF_{max} en FA était inférieure à 8Hz, alors que l'effet anti-arythmique de la chloroquine était observé même si la DF_{max} était > 8 Hz (0/3 versus 7/7, p=0.008).

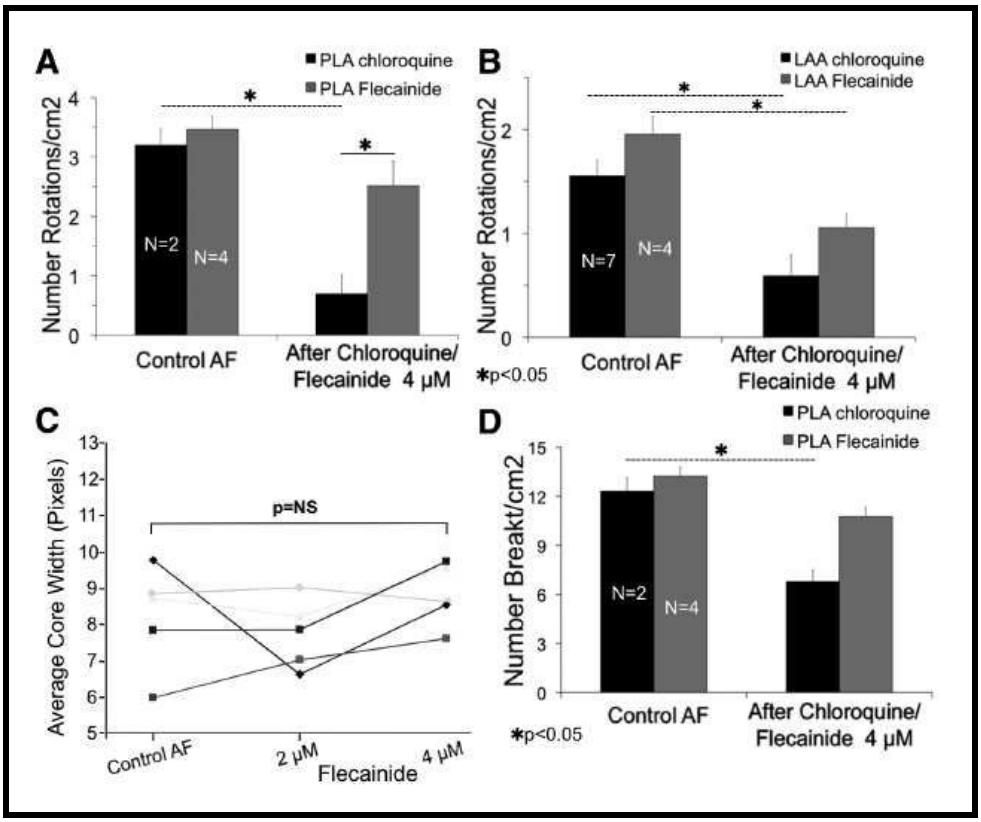

Figure 41. Comparaison de l'efficacité de la chloroquine et de la flécaïnide. A et B. Bien que la flécaïnide réduise le nombre de rotations par cm² au niveau de l'endocarde postérieur et de l'auricule gauche, seule la chloroquine entraine une diminution significative du nombre de rotations par cm² sur l'endocarde postérieur. C. Aucun changement significatif de la taille des cores des rotors n'est retrouvé après perfusion de flécaïnide. D. Seule la chloroquine induit une diminution de décharges focales par cm² au niveau de l'endocarde postérieur.

d. Discussion

La flécaïnide est plus efficace que l'amiodarone pour restaurer le rythme sinusal lors d'épisodes récent de FA[198] (<48 heures) et est recommandée chez les patients sans cardiopathie sous-jacente.[1] Cependant, nos données démontrent que la chloroquine est plus efficace que le flécaïnide pour restaurer le rythme sinusal dans ce modèle de FA induite par le stretch. Sur le plan mécanistique, nous avons observé qu'elle entraînait un ralentissement de la fréquence de rotation des rotors et un élargissement de la taille des cores, phénomènes menant au retour en rythme sinusal et liés à une inhibition préférentielle d'I_{K1} et à une moindre mesure d'I_{Kr} et d'I_{KAch} comme cela a récemment été démontré.[199] Ces observations confirment l'importance d'I_{K1} dans le maintien de la FA observées sur le plan expérimental[189] et clinique.[120]

La faible efficacité de la flécaïnide dans ce travail est probablement secondaire au modèle de FA étudié, i.e. la FA induite par le stretch. En effet, ce dernier entraine une activation des canaux activés par le stretch (« stretch activated channels ») et une dilatation atriale entraînant une perte de l'activité anti-arythmique de la flécaïnide chez l'homme.[200]

Bien qu'efficace, les inhibiteurs d'I_{K1} ne sont pour le moment pas été utilisés en clinique compte tenu de leur manque de biodisponibilté (faible efficacité anti-arythmique supposée aux concentrations thérapeutiques) et par crainte d'induire des dépolarisations diastoliques spontanées (hyperautomatisme lié à la dépolarisation membranaire induite par l'inhibition d'I_{K1}).[201] Cependant, des études expérimentales ont démontré que la chloroquine n'entraînait pas de post-dépolarisations, même à forte dose (10µmol/l),[191] et dès 1958, dans un papier publié dans le *New England Journal of Medicine*, Burrell et al ont mis en avant les propriétés anti-arythmiques.[202]

Par ailleurs, l'expression des sous-unités de Kir2.X est variable au sein des cavités cardiaques, et il a été démontré que Kir2.3 était préférentiellement exprimée dans l'oreillette.[203] Les techniques de cristallisation protéique et de modélisation moléculaire permettront probablement de synthétiser de nouvelles molécules disposant d'un effet inhibiteur préférentiel sur Kir2.3, évitant ainsi les écueils lié à l'inhibition d'I_{K1} au niveau ventriculaire.[204]

Enfin, nous avons testé l'efficacité de la chloroquine sur des cœurs « sains », supposés naïfs de toute arythmie atriale antérieure. L'effet sur des oreillettes ayant subi le remodelage électrophysiologique secondaire à la FA (qui entraîne par exemple au stade de la transition une augmentation de 100% d'I_{K1} comme nous l'avons précédemment démontré) et inconnu et nécessitera des études complémentaires.

Circulation
Arrhythmia and Electrophysiology

American Heart Association

Chloroquine Terminates Stretch-Induced Atrial Fibrillation More Effectively Than Flecainide in the Sheep Heart

David Filgueiras-Rama, Raphael P. Martins, Sergey Mironov, Masatoshi Yamazaki, Conrado J. Calvo, Steve R. Ennis, Krishna Bandaru, Sami F. Noujaim, Jérôme Kalifa, Omer Berenfeld and José Jalife

Circ Arrhythm Electrophysiol. 2012;5:561-570; originally published online March 30, 2012;
doi: 10.1161/CIRCEP.111.966820
Circulation: Arrhythmia and Electrophysiology is published by the American Heart Association, 7272 Greenville Avenue, Dallas, TX 75231

Print ISSN: 1941-3149. Online ISSN: 1941-3084

Chloroquine Terminates Stretch-Induced Atrial Fibrillation More Effectively Than Flecainide in the Sheep Heart

David Filgueiras-Rama, MD; Raphael P. Martins, MD; Sergey Mironov, PhD; Masatoshi Yamazaki, MD; Conrado J. Calvo, MSc; Steve R. Ennis, PhD; Krishna Bandaru, MD; Sami F. Noujaim, PhD; Jérôme Kalifa, MD; Omer Berenfeld, PhD; José Jalife, MD

Background—Blockade of inward-rectifier K^+ channels by chloroquine terminates reentry in cholinergic atrial fibrillation (AF). However, it is unknown whether inward-rectifier K^+ channels and reentry are also important in maintaining stretch-induced AF (SAF). We surmised that reentry underlies SAF, and that abolishing reentry with chloroquine terminates SAF more effectively than traditional Na^+-channel blockade by flecainide.

Methods and Results—Thirty Langendorff-perfused sheep hearts were exposed to acute and continuous atrial stretch, and mapped optically and electrically. AF dynamics were studied under control and during perfusion of either chloroquine (4 μmol/L, n=7) or flecainide (2–4 μmol/L, n=5). Chloroquine increased rotor core size and decreased reentry frequency from 10.6±0.7 Hz in control to 6.3±0.7 Hz ($P<0.005$) just before restoring sinus rhythm (7/7). Flecainide had lesser effects on core size and reentry frequency than chloroquine and did not restore sinus rhythm (0/5). Specific I_{Kr} blockade by E-4031 (n=7) did not terminate AF when frequency values were >8 Hz. During pacing (n=11), flecainide reversibly reduced conduction velocity (≈30% at cycle length 300, 250, and 200 ms; $P<0.05$) to a larger extent than chloroquine (11% to 19%; cycle length, 300, 250, and 200 ms; $P<0.05$). Significant action potential duration prolongation was demonstrable only for chloroquine at cycle length 300 (12%) and cycle length 250 ms (9%) ($P<0.05$).

Conclusions—Chloroquine is more effective than flecainide in terminating SAF in isolated sheep hearts by significantly increasing core size and decreasing reentry frequency. Chloroquine's effectiveness may be explained by its inward-rectifier K^+ channel blockade profile and suggest that reentry is important to maintain acute SAF. **(*Circ Arrhythm Electrophysiol*. 2012;5:561-570.)**

Key Words: arrhythmia mechanisms ■ atrial fibrillation ■ drug therapy ■ electrophysiology mapping

Atrial fibrillation (AF) is the most common sustained arrhythmia in clinical practice.[1] Although the mechanisms that sustain AF are incompletely understood, strong evidence in humans[2] and in animal models[3,4] supports the hypothesis that high-frequency reentrant sources (rotors) are essential to maintain AF. It is possible to demonstrate discrete sites of high frequency periodic activity during AF, along with frequency gradients between left and right atria.[3] Occasionally, a long-lasting rotor is identified within the area of maximum dominant frequency (DF_{max}).[5]

Clinical Perspective on p 570

In the human heart, atrial dilatation and stretch predisposes to AF with DF values directly related to left atrial (LA) pressure.[6] Similarly, in a sheep model of stretch-induced AF (SAF), the posterior left atrium (PLA) plays a major role in the maintenance of the arrhythmia.[4]

Less clear is the role of rotors in SAF, where focal discharges (FDs) and reentrant sources interact in such a way that FDs can destabilize and terminate rotors but also can give raise to new wave breaks and rotor formation.[5] The mechanism underlying FDs is uncertain with either triggered activity or reentry being possible; a more depolarized resting membrane potential (RMP) and the activation of stretch-activated nonselective cationic channels enable the generation of afterdepolarizations[7] that might explain FDs (breakthroughs) in the optically-mapped areas. However, FDs might also be the surface reflection of intramural reentrant sources.[8]

Inward-rectifier K^+ currents (I_{K1}, $I_{K\text{-}Ach}$, and $I_{K\text{-}ATP}$) play important roles in controlling rotor dynamics.[2,9,10] Recently, Noujaim et al[11] have demonstrated that chloroquine blocks the pore-forming subunits Kir2.1, Kir3.1, and Kir6.2 responsible for the inward-rectifier K^+ current (I_{K1}), the acetylcholine-sensitive K^+ current ($I_{K\text{-}Ach}$), and the ATP-sensitive K^+ current ($I_{K\text{-}ATP}$), respectively. Interestingly, chloroquine depolarizes the RMP and increases automaticity, which can be explained by its blocking

Received August 8, 2011; accepted March 19, 2012.

From the Center for Arrhythmia Research, Department of Internal Medicine, University of Michigan, Ann Arbor, MI.

The online-only Data Supplement is available at http://circep.ahajournals.org/lookup/suppl/doi:10.1161/CIRCEP.111.966820/-/DC1.

Correspondence to Omer Berenfeld, PhD, Center for Arrhythmia Research, University of Michigan, 5205 Venture Dr, Ann Arbor, MI 48108. E-mail oberen@med.umich.edu

effects on I_{K1}.[12] The latter might increase FDs underlying a triggered activity mechanism.

We hypothesized that if reentry plays a critical role sustaining SAF, then chloroquine should effectively restore sinus rhythm (SR), based on its ability to preferentially block inward-rectifier K^+ currents. We therefore compared the effects of chloroquine with those of flecainide on SAF and excitation properties using optical mapping in Langendorff-perfused sheep hearts. The rationale for such a comparison was based on the fact that, similar to amiodarone[13] and the most recently introduced drugs dronedarone[14] and vernakalant,[15] flecainide[16] does not block I_{K1} within the therapeutic range of concentrations. Flecainide is more effective than amiodarone in early reversion of recent-onset AF[17] (<48 hours), and it is highly recommended in patients with no underlying structural heart disease.[18] However, our data demonstrate that chloroquine is more effective than flecainide in restoring SR in this model. Taken together, our results support the hypothesis that rotor activity underlies SAF and that blockade of inward-rectifier K^+ currents may be a viable approach for its termination.

Methods

Experimental Setup

All procedures were approved by the University of Michigan Committee on Use and Care of Animals (UCUCA) and complied with National Institutes of Health guidelines. Thirty, 6-month-old sheep (weight, ≈35 kg) were included in the study. Anesthesia was induced with 4 to 6 mg/kg of propofol and 60 to 100 mg/kg of sodium pentobarbital. Hearts were removed via thoracotomy and connected to a Langendorff perfusion system with recirculating oxygenated (95% O_2, 5% CO_2) Tyrode solution at constant flow rate of 240 to 270 mL/min, pH 7.4 and 35.5 to 37.5°C. The Tyrode composition (in mmol/L) was: NaCl 130, KCl 4.0, MgCl2 1, CaCl2 1.8, NaHCO3 24, NaH2PO4 1.2, glucose 5.6, and albumin 0.04 g/L. Blebbistatin 10 μmol/L was used to reduce the contractile force.

After atrial transseptal puncture, the intra-atrial pressure was increased to 14 cm H_2O to induce continuous atrial stretch. Bipolar electrograms from each of the pulmonary veins (PVs), top and roof of the left atrial appendage (LAA) and right atrial appendage (RAA) were obtained (sampling rate, 1.0 kHz). All vein orifices were sealed except for the inferior vena cava, which was cannulated and used for controlling the level of the intra-atrial pressure.

Optical mapping movies (5 seconds) were obtained using a Little Joe CCD camera (80×80 pixels, 500–1000 frames per second). After a bolus injection of 5 to 10 mL Di-4-ANEPPS (10 mg/mL) (Sigma-Aldrich), voltage-sensitive fluorescence was acquired from the RAA and LAA (area, ≈14 cm^2). In 7 experiments, epicardial mapping from the LAA was complemented with endocardial mapping of the PLA (area, ≈3.7 cm^2), using a dual-channel rigid borescope (see online-only Data Supplement Methods and online-only Data Supplement Figure I).

Experimental Protocols

Baseline action potential duration at 70% repolarization (APD_{70}) was optically measured on both atrial appendages (n=5) at progressively shorter pacing cycle lengths (CLs; 300, 250, 200 ms). The pacing electrode was placed on the top of the LAA. Mean APD_{70} was obtained for RAA and LAA surfaces by averaging APD_{70} from all pixels. AF was then induced via burst pacing (12 Hz) and allowed to continue for 15 minutes of baseline control. Thereafter, the antifibrillatory effects of either 4 μmol/L chloroquine diphosphate (n=7) or 2 μmol/L flecainide (n=5) (Sigma-Aldrich) dissolved in Tyrode solution were investigated. The concentrations were based on the highest therapeutic level for flecainide[19] and chloroquine.[20] Drug perfusion was maintained for 20 minutes, after which the concentration was doubled and maintained for 30 additional minutes, as long as SR was not already restored. AF was terminated by DC shock in those hearts in which AF persisted for 50 minutes. Burst pacing was subsequently applied after AF termination to reinduce AF. Finally, AF reinduction was attempted again after a washout period of 30 and 45 minutes for flecainide and chloroquine, respectively.

To better delineate the specific roles of I_{K1} versus I_{Kr} we conducted experiments (n=7) using the same stretch-induced AF model to study the antifibrillatory effects of specific I_{Kr}-blockade. After 15 minutes of baseline AF, 0.5 to 1 μmol/L E-4031 was perfused for 20 and 30 minutes as above.[21]

An additional set of experiments was carried out to investigate the electrophysiological effects of 4 μmol/L chloroquine (n=5) and 4 μmol/L flecainide (n=6). Pacing protocols were completed under basal conditions, after 15 minutes of either chloroquine or flecainide, and after washout. No AF was induced in these hearts. Activation times were determined at 50% of action potential amplitude and conduction velocity (CV) was calculated.[22] Online-only Data Supplement Figure II, A and B, illustrates the time line of all experimental protocols.

Frequency Analysis

Dominant frequency (DF) maps were obtained for each optical movie in AF after applying a fast Fourier transform (FFT) of the fluorescence signal recorded at each pixel.[23] Bipolar electrograms recorded during AF were high-pass–filtered at 3 Hz and low-pass–filtered at 35 Hz. FFT was also applied to the 5-second bipolar signals synchronized with the optical movies.

AF Dynamics

Phase movies were constructed using the Hilbert transformation.[24] In each movie, a rotor was defined as a point of phase convergence (singularity point; SP) lasting more than 1 rotation. A breakthrough was defined as a wave appearing inside the field of view and propagating outward (online-only Data Supplement Figure III). During AF, 5-second movies were acquired and analyzed frame by frame. Rotor analysis was carried out on the PLA and LAA by measuring the total number of rotations in 5 seconds, regardless of the lifespan of individual rotors but considering their frequency of rotation. The number of breakthroughs in 5 seconds was also quantified on the PLA, since PVs represent the region where FDs are identified in some cases of AF.[25]

Reentry meandering around SPs was analyzed further to quantify the respective effects of chloroquine and flecainide on the unexcited core size. A detailed description of the method is described in Figures IV, V, and VI in the online-only Data Supplement.

Statistical Analyses

Results are reported as mean±SEM. DF data were verified (Shapiro-Wilk) and other continuous measurements were assumed to distribute normally. One-way or 2-way repeated-measures ANOVA or a mixed-model ANOVA was used for continuous measurements as appropriate. Fisher exact test was used to demonstrate significant differences on AF termination and reinducibility. Post hoc comparisons were used after Bonferroni correction. $P<0.05$ was considered statistically significant.

Results

SAF in the Control

Figure 1A (left) shows examples of simultaneously obtained single pixel recordings from the LAA (red) and RAA (black) at 300-ms CL. As summarized graphically on the right, APD_{70} was significantly shorter in LAA than RAA (n=5) at 3 different CLs (300, 149.3±9.3 versus 175.7±8.2 ms; 250, 138.7±6.0 versus 153.3±4.5 ms; 200, 123.5±5.0 versus 132.8±3.6 ms, $P<0.05$).

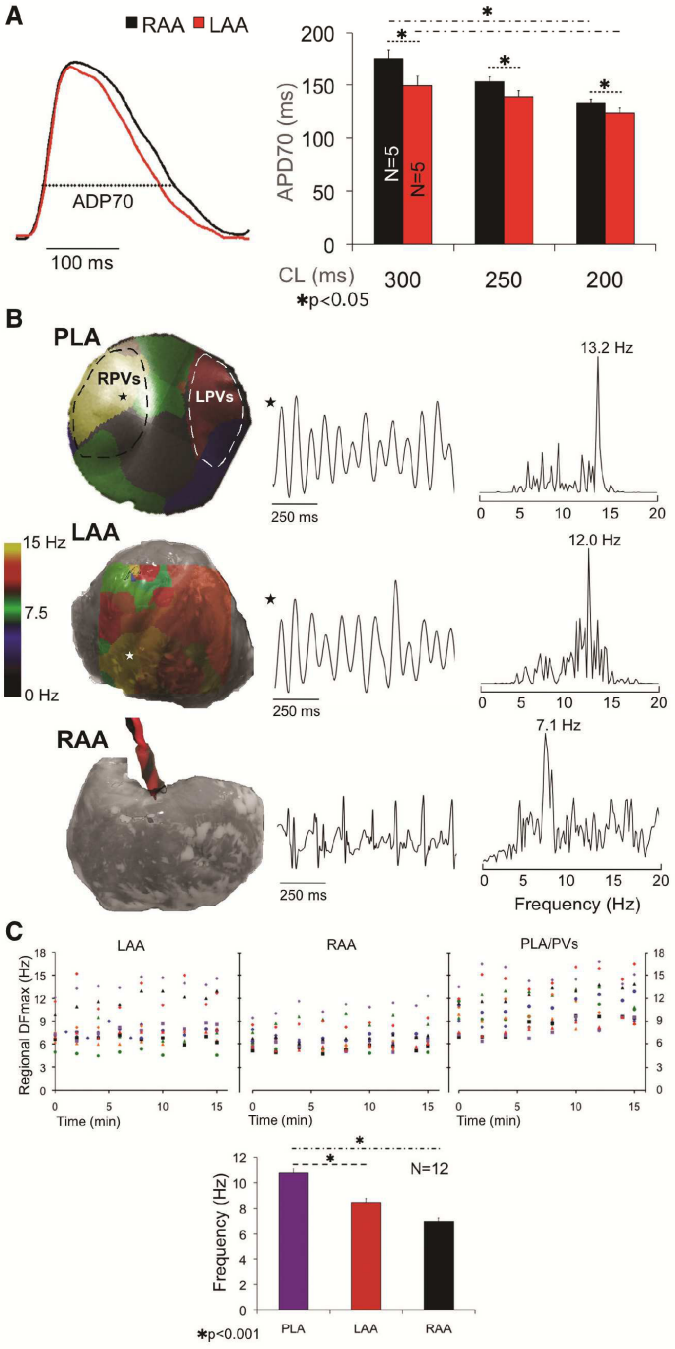

Figure 1. A, left, Single-pixel action potential (AP) from the left atrial appendage (LAA, red) and right atrial appendage (RAA, black). **Right**, Action potential duration $(APD)_{70}$ at varying pacing cycle lengths (CLs) is shorter in LAA than RAA. APD_{70} significantly shortens in both appendages from 300 to 200 ms CL. **B, left column**, Dominant frequency (DF) maps of the posterior left atrium (PLA) and LAA and electrode location on the RAA. **Center column**, Single-pixel activations (PLA, LAA) and bipolar electrograms (RAA). **Right column**, Power spectra showing DF_{max} at each location. **C, top**, LAA, RAA, and PLA/pulmonary veins (PVs) DF_{max} during 15 minutes of control AF. **Bottom**, Bar graph of mean±SEM. DF_{max} during control AF shows significant DF gradient between PLA and LAA/RAA.

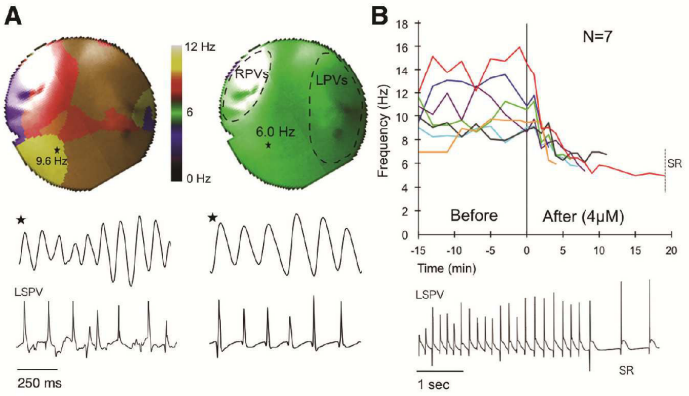

Figure 2. Chloroquine terminates atrial fibrillation (AF). **A, top,** Dominant frequency (DF) maps of the posterior left atrium during control AF and before termination; **middle** and **bottom,** single-pixel recordings and electrograms from the left superior pulmonary vein (LSPV). **B, top,** Time course of DF_{max}, before and during chloroquine; **bottom,** electrograms from LSPV at the moment of termination.

Once SAF stabilized, the DF_{max} locations were identified across the mapped regions. Figure 1B shows DF maps, sample local activations, and corresponding power spectra from the PLA, LAA, and RAA after 14 minutes of control AF in a representative heart. The DF_{max} was localized at the right PVs with a frequency gradient from PLA (13.2 Hz) to LAA (12.0 Hz), and RAA (7.1 Hz).

The regional DF_{max} was consistently localized either at one of the PVs or somewhere on the PLA (Figure 1C, top). As expected,[4] a statistically significant frequency gradient was observed from PLA to LAA and RAA (Figure 1C, bottom) (10.8±0.3 Hz, 8.5±0.2 Hz, and 7.0±0.1 Hz, respectively; n=12, $P<0.001$).

Chloroquine Terminates SAF

To test the hypothesis that reentry is essential to maintain SAF, we determined the effect of 4 μmol/L chloroquine in terminating AF, based on its ability to block the inward-rectifier K^+ currents.[11] As shown in Figure 2, 4 μmol/L chloroquine reduced AF frequency and restored SR after 4 to 19 minutes (n=7). Figure 2A shows representative PLA DF maps in control AF (DF_{max} 9.6 Hz) and just before AF termination (DF_{max} 6 Hz). Single-pixel optical activations from the DF_{max} region and electrograms from the left superior PV (LSPV) are shown below the maps. Figure 2B shows the time course of the DF_{max} location in control AF and after chloroquine. The DF_{max} sharply decreased from 10.6±0.7 Hz to 6.3±0.2 Hz (n=7) in the first few min after chloroquine onset.

Five additional experiments were conducted, using 1 to 2 μmol/L chloroquine to increase the selectivity of I_{K1} blockade.[12] At 1 μmol/L, chloroquine terminated AF in 4 of 5 AF episodes after 3.5 to 9.5 minutes. Increasing the concentration to 2 μmol/L restored SR in the fifth AF episode after 14 minutes. The DF_{max} decreased from 10.5±0.8 Hz in control to 6.7±0.2 Hz before resumption of SR (online-only Data Supplement Figure VIII).

Flecainide Does Not Terminate SAF

Na^+-channel blockade may affect reentrant activity and rotor dynamics leading to AF termination.[26] As illustrated in Figure 3A, after 15 minutes of control AF, perfusion with 2 μmol/L flecainide for 20 minutes and 4 μmol/L for 30 additional minutes significantly decreased the DF_{max} from 11.1±1.3 Hz to 8.1±1.3 Hz ($P=0.0014$) but did not restore SR (n=5). As shown in Figure 3B, flecainide was significantly inferior to chloroquine in its ability to restore SR (0/5 versus 7/7, respectively, $P=0.0013$). In 2 hearts, the initial DF_{max} was slower than in the other 3 cases (8.0±0.1 Hz versus 13.1±1.8 Hz), and AF converted to atrial tachycardia (AT). Figure 3C shows DF maps and bipolar recordings from the PLA during control AF and after 4 μmol/L flecainide. Interestingly, after 40 minutes flecainide, AF converted to AT, which was sustained by a long meandering rotor located in the roof/PLA-LAA junction (online-only Data Supplement Movie I).

Sustained AF Is Inducible in the Presence of Flecainide But Not Chloroquine

As shown in Figure 4A, only nonsustained AF or AT was induced in the presence of chloroquine (n=7). Conversely, on cardioversion, AF (n=4) or AT (n=1) was reinduced and sustained for 15 minutes in the presence of flecainide. After the washout period, AF (n=6, chloroquine; n=5, flecainide) or AT (n=1, chloroquine) was reinduced and sustained in both groups. In Figure 4B, the bipolar electrograms illustrate how initial rapid pacing in the presence of chloroquine was followed by a very brief AF episode, in contrast to sustained AF under flecainide.

Chloroquine Terminates AF Where Flecainide Does Not

We determined the effects of chloroquine in the 5 experiments in which flecainide was unable to restore SR. Thus, AF was reinduced after 30 minutes of flecainide washout. Fifteen minutes of control AF was registered and optically mapped. Figure 4C shows the evolution of the DF_{max} on the PLA. DF_{max} values were significantly higher than at the beginning of the protocol (16.9±2.0 Hz versus 11.1±1.3 Hz, $P=0.018$), which might be due to a decrease in optimal conditions of the heart after 3 hours of artificial perfusion. Higher DF_{max} may also imply a role of other inward-rectifiers K^+ currents, possibly $I_{K,ATP}$. Nevertheless, 4 μmol/L chloroquine effectively terminated AF (n=5). Time to AF termination was longer (10–29 minutes) relative to the first application of chloroquine (4–19 minutes, Figure 2B).

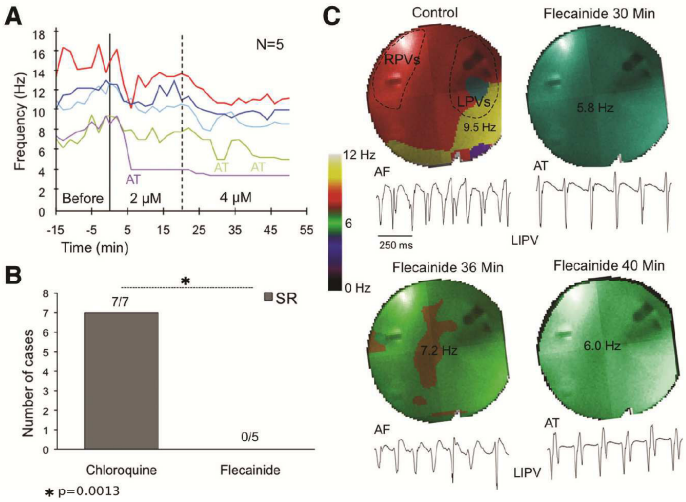

Figure 3. A, Time course of dominant frequency $(DF)_{max}$ before and during flecainide. **B**, Flecainide is significantly inferior to chloroquine in resuming sinus rhythm (SR). **C**, DF maps of the posterior left atrium (PLA) and bipolar electrograms from the left inferior PV (LIPV) show control atrial fibrillation (AF) and conversion to atrial tachycardia (AT) during flecainide.

Chloroquine Effects on Reentry and Breakthroughs

To determine the basis for chloroquine superiority, we studied the effects of each drug on AF patterns of excitation. In Figure 5A, the number of identifiable rotations was quantified on the PLA and LAA every 2 minutes in control AF and every minute after chloroquine. Data were normalized as number of rotations per centimeter squared. In control AF, the PLA (N=2; n=16; where N is the number of animals and n is the number of episodes analyzed) harbored twice as many identifiable rotations per centimeter squared compared with LAA (N=7; n=56) (3.2±0.3 versus 1.6±0.1). On

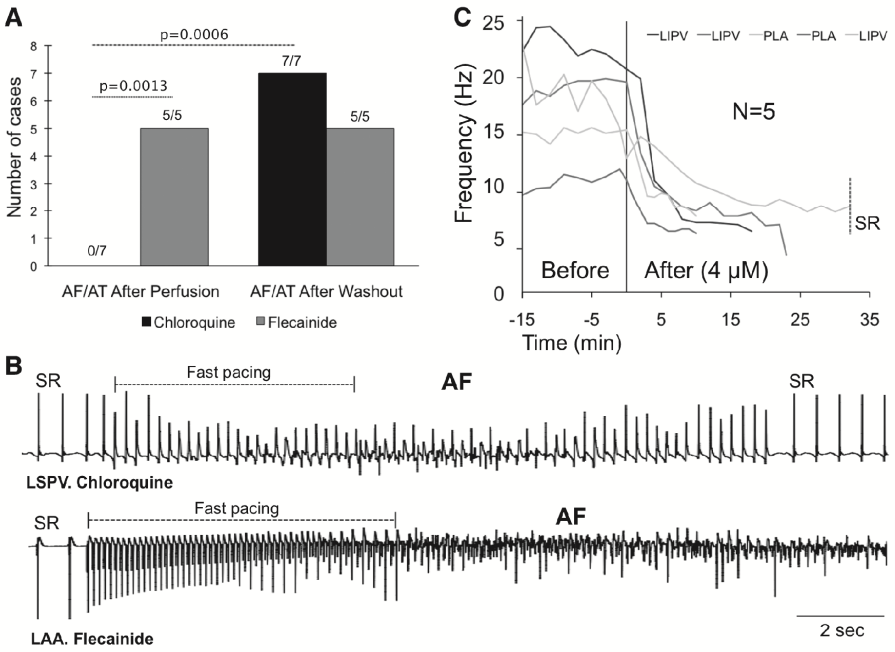

Figure 4. A, **left**, Sustained atrial fibrillation/atrial tachycardia (AF/AT) is reinducible during flecainide but not during chloroquine perfusion. **Right**, After washout, sustained AF/AT is reinducible in both groups. **B**, Representative traces; rapid pacing at 12 Hz did not capture or reinduce nonsustained AF during chloroquine (top); at the same pacing frequency, sustained AF was readily induced during flecainide (**bottom**). **C**, Time course of dominant frequency $(DF)_{max}$; sinus rhythm (SR) is restored when chloroquine was perfused after flecainide washout. LAA indicates left atrial appendage.

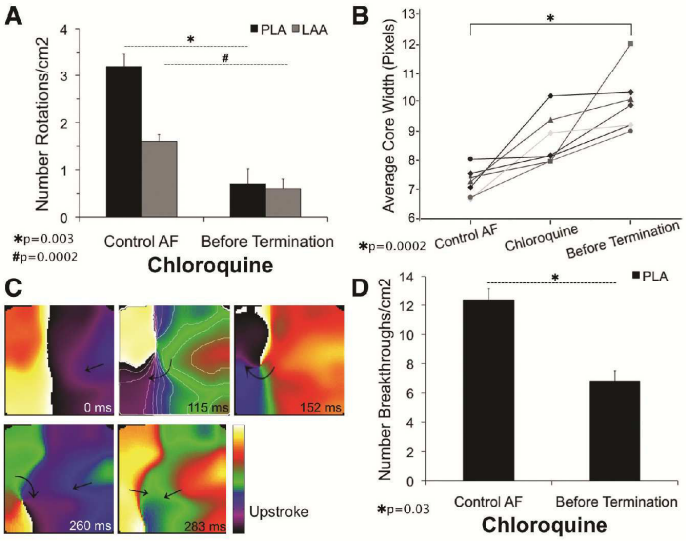

Figure 5. Chloroquine effects on reentry and breakthroughs (5-second movies). **A**, Number of rotations per centimeter squared in the posterior left atrium/left atrial appendage (PLA/LAA) in control and just before chloroquine-induced atrial fibrillation (AF) termination. **B**, Average core width significantly increases in size during chloroquine. **C**, Phase maps show a wave break and the initiation of a rotor that cannot complete an entire rotation during chloroquine. **D**, Number of breakthroughs per centimeter squared in control and during chloroquine.

chloroquine, the last 2 minutes before termination showed a drastic reduction in the number of rotations in both PLA (3.2±0.3 to 0.7±0.3, P=0.003) and LAA (1.6±0.1 to 0.6±0.2, P=0.0002) (see also online-only Data Supplement Figure VII, A). Online-only Data Supplement Movies II and III show, respectively, PLA movies of short-lasting rotors (1–2 rotations) in control AF and during a short time before termination. Quantification of the core width using the new method illustrated in online-only Data Supplement Figures IV to VI, showed a significant increase before AF termination under chloroquine (Figure 5B). A larger core due to preferential I_{K1} blockade may reduce the probability of stable rotor initiation as shown in Figure 5C, where a rotor around a SP is observed after a wave break and curling of the wave front. However, the rotating front is annihilated by a new wave front coming from the PLA.

In the stretched atrium, chloroquine's effects on I_{K1} might increase automaticity and FDs,[12] which may underlie breakthroughs in the field of view. However, the number of breakthroughs per centimeter squared decreased (12.3±0.8 to 6.8±0.7, P=0.03; Figure 5D), suggesting that such breakthroughs represented intramural reentrant activity. AF terminated despite the fact that just before termination the number of breakthroughs per centimeter squared was higher than the number of identifiable per centimeter squared in control AF (6.8±0.7 versus 3.2±0.3, respectively), which supports the essential role of reentrant activity to sustain SAF.

Reentry and Breakthroughs Under Flecainide

As shown in Figure 6A and 6B, the number of identifiable rotations decreased after 4 μmol/L flecainide (n=4), both in the PLA (3.7±0.2 to 2.7±0.4, P=NS) and the LAA (2.0±0.2 to 1.1±0.1, P<0.05) (see also online-only Data Supplement Figure VII, B, and online-only Data Supplement Movies IV and V). However, only chloroquine significantly decreased the number of rotations and breakthroughs at the PLA (3.2±0.3 to 0.7±0.3 and 12.3±0.8 to 6.8±0.7, respectively, P<0.05; Figure 6A and 6D). The core size showed no significant increase after 4 μmol/L flecainide (Figure 6C).

Electrophysiological Effects of Chloroquine and Flecainide

As summarized on the left side of Figure 7A and 7B; 4 μmol/L chloroquine significantly increased the APD_{70} at 300 and 250-ms CL (155±3.1 to 176±6.0 and 144±3.4 to 158±5.0 ms, respectively, P<0.05) compared with 4 μmol/L flecainide, which had no significant effect at any pacing CL (online-only Data Supplement Figure IX). On the right side of Figure 7A and 7B, both chloroquine and flecainide decreased the CV at all CLs. However, flecainide's effects were substantially greater than chloroquine: 33% reduction at 250-ms CL compared with 12% reduction, respectively.

Role of I_{Kr} in Acute SAF

Chloroquine, while nominally an I_{K1} blocker, also blocks other currents, including I_{Kr}. An additional series of experiments (n=7) using the same AF model showed that I_{Kr}-blockade after 0.5 to 1 μmol/L E-4031 restored SR in 4 of 7 animals (Figure 8A). When we classified those experiments based on DF_{max} values at baseline (Figure 8B, left); E-4031 restored SR in those cases in which the AF DF_{max} was <8 Hz (4/4) but not in cases with DF_{max} >8 Hz (0/3) (7.1±0.4 Hz versus 9.2±0.5 Hz, respectively, P=0.029). Unlike E-4031, chloroquine effectively terminated SAF when DF_{max} was >8 Hz (7/7 versus 0/3, P=0.008. Figure 8B, right).

Discussion

The present study demonstrates that chloroquine but not flecainide effectively converted SAF to SR in a sheep heart model that approximates AF in the human heart with pressure overload and atrial dilatation.[6] SAF termination by chloroquine

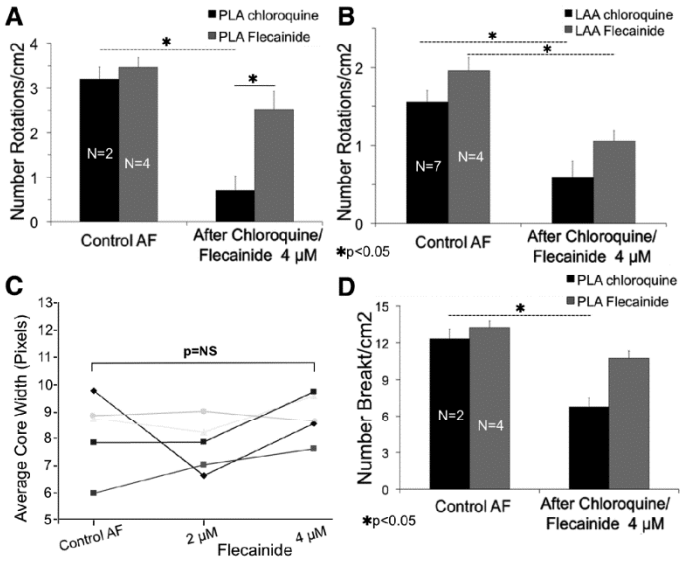

Figure 6. Comparing chloroquine with flecainide. **A** and **B**, Although flecainide reduces the number of rotations per centimeter squared at the posterior left atrium (PLA) and left atrial appendage (LAA) (5-second movies), only chloroquine significantly decrease the number of rotations per centimeter squared at the PLA. **C**, Core size does not significantly increase during flecainide. **D**, Similarly, only chloroquine significantly decreases the number breakthroughs per centimeter squared at the PLA.

is preceded by a significant increase in rotor core size, which correlates with a reduction in AF frequency and number of breakthroughs. Altogether, these data support the idea that reentry and fibrillatory conduction underlie the overall dynamics of SAF in this model. The Na^+-channel blocker flecainide converted AF to AT but did not restore SR. Preferential blockade of the inward-rectifier K^+ currents by chloroquine[11] terminated fast reentrant sources persisting after flecainide washout. In addition, unlike E-4031, chloroquine terminated AF episodes whose DF_{max} was >8 Hz. Thus, even though E-4031 terminated some of the episodes, the above results demonstrate the superiority of chloroquine over E-4031 in terminating SAF. Nevertheless, chloroquine being a "dirty drug,"[12] its antifibrillatory effect probably is not due solely to I_{K1} blockade but to some combination of I_{K1} and I_{Kr} blockade, which would vary, depending on the dose being used.

Because $I_{K\text{-}ATP}$ plays a prominent role in ischemia[27] and $I_{K,ACh}$ underlies vagally mediated AF,[11] it seems reasonable to consider the role of I_{K1} in the present SAF model. Rotor acceleration and stabilization of the reentry have been associated with I_{K1} overexpression.[9] In humans, gain of function of I_{K1} due to mutation in *KCNJ2* is also associated with familial AF.[28]

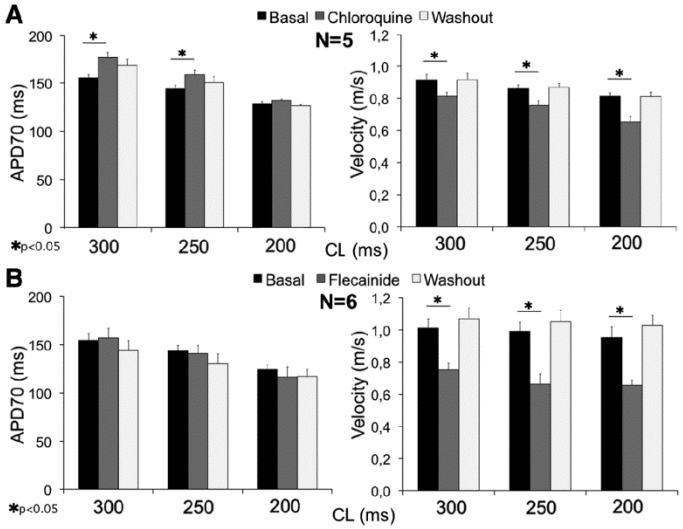

Figure 7. **A**, **left**, Mean action potential duration $(APD)_{70}$ for control, chloroquine, and washout at 300-, 250-, and 200-ms cycle length (CL); **right**, mean conduction velocity for control, chloroquine, and washout; 300-, 250-, and 200-ms CL. **B**, **left**, Flecainide does not significantly affect the APD_{70} at any CL; **right**, flecainide strongly reduces velocity in a reversible manner.

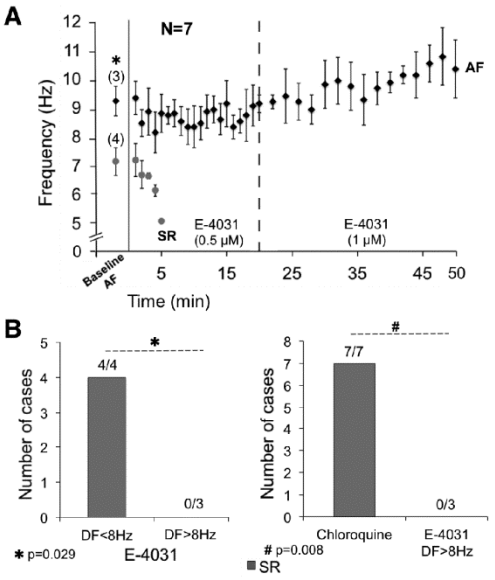

Figure 8. A, Time course of maximal dominant frequency $(DF)_{max}$ before and during 0.5 and 1 μmol/L E-4031. Animals are grouped based on baseline DF_{max} of less (gray) or more (black) than 8 Hz. **B**, **left**, E-4031 restored sinus rhythm (SR) in those cases with DF_{max} <8 Hz. **Right**, Chloroquine was more effective than E-4031 in terminating stretch-induced atrial fibrillation (SAF) with DF_{max} >8 Hz.

Why Is Chloroquine More Effective Than Flecainide in SAF?

The greater effectiveness of chloroquine over flecainide in terminating SAF in this model may be related to the fact that atrial dilatation decreases the CV and increases the degree of spatial heterogeneities in conduction.[29] Therefore, under conditions of stretch, anatomic, and functional obstacles may become prominent and facilitate initiation and maintenance of reentrant activity. Flecainide further decreases CV, which increases core size and promotes attachment to and rotation around an obstacle. It therefore results in slower rotating activity. This would explain the decrease in DF values and conversion to AT in the presence of flecainide. Under certain critical conditions, unexcitable obstacles may destabilize propagation, causing the formation of self-sustained vortices. Wave front instabilities have been demonstrated after blockade of Na^+-channel conductance leading to detachment of the wave front from the edge of the functional/anatomic barrier and initiation of reentry.[30]

Controversies in SAF

The mechanisms sustaining acute SAF are controversial. Stretch induces depolarization of the RMP and generation of afterdepolarizations.[7] Stretch promotes the occurrence of breakthroughs in the LAA,[5] which might be interpreted as being produced either by local triggered activity or intramural reentry. In the present study, a higher number of breakthroughs compared with reentrant activity were also identified at the endocardial side of the PLA. However, after either chloroquine or flecainide, the number of breakthroughs decreased concomitantly with reentry, suggesting the possibility that the breakthroughs represent intramural reentry. More interesting is the role of chloroquine, which, on preferential blockade of the inward-rectifier K^+ channels, strongly affects reentry and terminates AF. Patterns of activation on the PLA before AF termination also show that the number of breakthroughs is higher than the number of rotors in control AF but the arrhythmia terminates. The latter suggests that reentrant activity is essential to sustain SAF and that intramural reentry in the PLA was responsible for the majority of those breakthroughs.

Clinical Perspective

Atrial dilatation and stretch predispose to AF, with DF values directly related to LA pressure.[6] Similar to the human heart,[2] SAF in the sheep heart results in DF gradients, where DF at PLA>LAA>RAA. We demonstrate that a reentry-based strategy of blocking the inward-rectifier K^+ channels effectively terminates SAF. Conversely, Na^+-channel blockade by flecainide was unable to restore SR during atrial stretch, similar to the loss of antifibrillatory effect that is observed also in patients with atrial dilatation.[31]

Although attractive, I_{K1}-blockade is currently not a clinical strategy to treat AF because of the lack of antiarrhythmic drugs having this property at therapeutic concentrations, along with the fear that reducing I_{K1} would cause diastolic depolarization and might subsequently increase the propensity for triggered arrhythmias.[32] However, such a fear may be reduced by considering that heterozygous Andersen syndrome patients, who lack 1 allele of the *KCNJ2* gene with loss-of-function of Kir2.1 channels, have mild QTc prolongation and seldom undergo sudden cardiac death.[33] In addition, chloroquine does not induce early afterdepolarizations in single myocytes under current-clamp conditions, even at 10 μmol/L.[12] Finally, Noujaim et al[11] demonstrated that rather than being proarrhythmic, I_{K1} blockade is antiarrhythmic, as evidenced by chloroquine's ability to terminate reentry in cholinergic-induced AF. In the present study, we have used a well-established model,[4] in which if at all present, the proarrhythmic effect of blocking I_{K1} should be more evident.[5,7] Clinical AF cases reported in the 1950s also demonstrated high rates of AF termination after high doses of chloroquine.[34]

Based on the expression profile of the Kir2.X subfamily, Kir2.3 transcripts are more concentrated in the human atria than in the ventricles.[35] Protein crystallization, molecular modeling, and interactions with modulators (eg, PIP2)[36] might lead to new pharmacological strategies focusing on selective blockade of Kir2.3 subunits. The latter becomes especially relevant in the setting of congestive heart failure, in which I_{K1} downregulation may be associated with increased susceptibility to ventricular arrhythmias.[37]

Limitations

Although the chloroquine concentrations we have used preferentially block the inward-rectifier K^+ channels, termination of AF might also be mediated in part through its less prominent effects on I_{Kr}, I_{Na}, and I_{CaL}. Additional experiments

with 1 μmol/L chloroquine (I_{K1}-blockade, 74%; I_{Kr},38%; I_{Na},14%)[12] and E-4031 support the role of preferential I_{K1}-blockade to terminate SAF. Further experiments would be required to rule out the possibility that the effectiveness of chloroquine in terminating SAF depends at least in part on a drug action on stretch-activated nonselective cationic channels.[38] Stretch-activated K^+ channels (TREK-1) might also be involved in the absence of APD prolongation after flecainide.

The antiarrhythmic effects of chloroquine must be tested in persistent AF, in which I_{K1} upregulation might be involved. In addition, the role of the autonomic system is difficult to mimic in isolated hearts. However, in previous experiments using the same model and adrenocholinergic stimulation, reentrant activity played a major role in the sustainability of the arrhythmia after abolishing triggered activity.

Conclusions

Chloroquine effectively terminates SAF in the sheep heart and is more effective than flecainide in restoring SR, which may be explained by a preferential blockade of the inward-rectifier K^+ channels and reentry termination. The results may open novel therapeutic strategies for clinical AF.

Acknowledgments

We thank Sherry Morgenstern and Iván Filgueiras-Rama for their help in the illustration of online-only Data Supplement Figures.

Sources of Funding

This work was supported in part by National Heart, Lung, and Blood Institute Grants (P01-HL039707 and P01-HL087226 to Drs Jalife and Berenfeld and K99HL105574 to Dr Noujaim), the Leducq Foundation and CNIC (Drs Jalife and Berenfeld), a Spanish Society of Cardiology Fellowship, the Pedro Barrié de la Maza and Alfonso Martín Escudero Foundations (Dr Filgueiras-Rama), and the Fédération Française de Cardiologie (Dr Martins).

Disclosures

None.

References

1. Kannel WB, Wolf PA, Benjamin EJ, Levy D. Prevalence, incidence, prognosis, and predisposing conditions for atrial fibrillation: population-based estimates. *Am J Cardiol*. 1998;82:2N–9N.
2. Atienza F, Almendral J, Moreno J, Vaidyanathan R, Talkachou A, Kalifa J, Arenal A, Villacastin JP, Torrecilla EG, Sanchez A, Ploutz-Snyder R, Jalife J, Berenfeld O. Activation of inward rectifier potassium channels accelerates atrial fibrillation in humans: evidence for a reentrant mechanism. *Circulation*. 2006;114:2434–2442.
3. Mandapati R, Skanes A, Chen J, Berenfeld O, Jalife J. Stable microreentrant sources as a mechanism of atrial fibrillation in the isolated sheep heart. *Circulation*. 2000;101:194–199.
4. Kalifa J, Jalife J, Zaitsev AV, Bagwe S, Warren M, Moreno J, Berenfeld O, Nattel S. Intra-atrial pressure increases rate and organization of waves emanating from the superior pulmonary veins during atrial fibrillation. *Circulation*. 2003;108:668–671.
5. Yamazaki M, Vaquero LM, Hou L, Campbell K, Zlochiver S, Klos M, Mironov S, Berenfeld O, Honjo H, Kodama I, Jalife J, Kalifa J. Mechanisms of stretch-induced atrial fibrillation in the presence and the absence of adrenocholinergic stimulation: interplay between rotors and focal discharges. *Heart Rhythm*. 2009;6:1009–1017.
6. Yoshida K, Ulfarsson M, Oral H, Crawford T, Good E, Jongnarangsin K, Bogun F, Pelosi F, Jalife J, Morady F, Chugh A. Left atrial pressure and dominant frequency of atrial fibrillation in humans. *Heart Rhythm*. 2011;8:181–187.
7. Kamkin A, Kiseleva I, Wagner KD, Bohm J, Theres H, Gunther J, Scholz H. Characterization of stretch-activated ion currents in isolated atrial myocytes from human hearts. *Pflugers Arch*. 2003;446:339–346.
8. Wellner M, Berenfeld O, Jalife J, Pertsov AM. Minimal principle for rotor filaments. *Proc Natl Acad Sci USA*. 2002;99:8015–8018.
9. Noujaim SF, Pandit SV, Berenfeld O, Vikstrom K, Cerrone M, Mironov S, Zugermayr M, Lopatin AN, Jalife J. Up-regulation of the inward rectifier K+ current (I k1) in the mouse heart accelerates and stabilizes rotors. *J Physiol*. 2007;578:315–326.
10. Uchida T, Yashima M, Gotoh M, Qu Z, Garfinkel A, Weiss JN, Fishbein MC, Mandel WJ, Chen PS, Karagueuzian HS. Mechanism of acceleration of functional reentry in the ventricle: effects of ATP-sensitive potassium channel opener. *Circulation*. 1999;99:704–712.
11. Noujaim SF, Stuckey JA, Ponce-Balbuena D, Ferrer-Villada T, Lopez-Izquierdo A, Pandit S, Calvo CJ, Grzeda KR, Berenfeld O, Chapula JA, Jalife J. Specific residues of the cytoplasmic domains of cardiac inward rectifier potassium channels are effective antifibrillatory targets. *FASEB J*. 2010;24:4302–4312.
12. Sanchez-Chapula JA, Salinas-Stefanon E, Torres-Jacome J, Benavides-Haro DE, Navarro-Polanco RA. Blockade of currents by the antimalarial drug chloroquine in feline ventricular myocytes. *J Pharmacol Exp Ther*. 2001;297:437–445.
13. Sato R, Koumi S, Singer DH, Hisatome I, Jia H, Eager S, Wasserstrom JA. Amiodarone blocks the inward rectifier potassium channel in isolated guinea pig ventricular cells. *J Pharmacol Exp Ther*. 1994;269:1213–1219.
14. Patel C, Yan GX, Kowey PR. Dronedarone. *Circulation*. 2009;120:636–644.
15. Fedida D. Vernakalant (rsd1235): a novel, atrial-selective antifibrillatory agent. *Expert Opin Investig Drugs*. 2007;16:519–532.
16. Caballero R, Dolz-Gaiton P, Gomez R, Amoros I, Barana A, Gonzalez de la Fuente M, Osuna L, Duarte J, Lopez-Izquierdo A, Moraleda I, Galvez E, Sanchez-Chapula JA, Tamargo J, Delpon E. Flecainide increases kir2.1 currents by interacting with cysteine 311, decreasing the polyamine-induced rectification. *Proc Natl Acad Sci USA*. 2010;107:15631–15636.
17. Donovan KD, Power BM, Hockings BE, Dobb GJ, Lee KY. Intravenous flecainide versus amiodarone for recent-onset atrial fibrillation. *Am J Cardiol*. 1995;75:693–697.
18. Camm AJ, Kirchhof P, Lip GY, Schotten U, Savelieva I, Ernst S, Van Gelder IC, Al-Attar N, Hindricks G, Prendergast B, Heidbuchel H, Alfieri O, Angelini A, Atar D, Colonna P, De Caterina R, De Sutter J, Goette A, Gorenek B, Heldal M, Hohloser SH, Kolh P, Le Heuzey JY, Ponikowski P, Rutten FH, Vahanian A, Auricchio A, Bax J, Ceconi C, Dean V, Filippatos G, Funck-Brentano C, Hobbs R, Kearney P, McDonagh T, Popescu BA, Reiner Z, Sechtem U, Simes PA, Tendera M, Vardas PE, Widimsky P, Agladze V, Aliot E, Balabanski T, Blomstrom-Lundqvist C, Capucci A, Crijns H, Dahlof B, Folliguet T, Glikson M, Goethals M, Gulba DC, Ho SY, Klautz RJ, Kose S, McMurray J, Perrone Filardi P, Raatikainen P, Salvador MJ, Schalij MJ, Shpektor A, Sousa J, Stepinska J, Uuetoa H, Zamorano JL, Zupan I. Guidelines for the management of atrial fibrillation: the Task Force for the Management of Atrial Fibrillation of the European Society of Cardiology (ESC). *Europace*. 2010;12:1360–1420.
19. Roden DM, Woosley RL. Drug therapy. Flecainide. *N Engl J Med*. 1986;315:36–41.
20. Frisk-Holmberg M, Bergqvist Y, Englund U. Chloroquine intoxication. *Br J Clin Pharmacol*. 1983;15:502–503.
21. Spector PS, Curran ME, Keating MT, Sanguinetti MC. Class III antiarrhythmic drugs block herg, a human cardiac delayed rectifier K+ channel: open-channel block by methanesulfonanilides. *Circ Res*. 1996;78:499–503.
22. Bayly PV, KenKnight BH, Rogers JM, Hillsley RE, Ideker RE, Smith WM. Estimation of conduction velocity vector fields from epicardial mapping data. *IEEE Trans Biomed Eng*. 1998;45:563–571.
23. Samie FH, Berenfeld O, Anumonwo J, Mironov SF, Udassi S, Beaumont J, Taffet S, Pertsov AM, Jalife J. Rectification of the background potassium current: a determinant of rotor dynamics in ventricular fibrillation. *Circ Res*. 2001;89:1216–1223.
24. Warren M, Guha PK, Berenfeld O, Zaitsev A, Anumonwo JM, Dhamoon AS, Bagwe S, Taffet SM, Jalife J. Blockade of the inward rectifying potassium current terminates ventricular fibrillation in the guinea pig heart. *J Cardiovasc Electrophysiol*. 2003;14:621–631.
25. Haissaguerre M, Jais P, Shah DC, Takahashi A, Hocini M, Quiniou G, Garrigue S, Le Mouroux A, Le Metayer P, Clementy J. Spontaneous ini-

tiation of atrial fibrillation by ectopic beats originating in the pulmonary veins. *N Engl J Med*. 1998;339:659–666.
26. Kneller J, Kalifa J, Zou R, Zaitsev AV, Warren M, Berenfeld O, Vigmond EJ, Leon LJ, Nattel S, Jalife J. Mechanisms of atrial fibrillation termination by pure sodium channel blockade in an ionically-realistic mathematical model. *Circ Res*. 2005;96:e35–e47.
27. Noma A. ATP-regulated K+ channels in cardiac muscle. *Nature*. 1983;305:147–148.
28. Xia M, Jin Q, Bendahhou S, He Y, Larroque MM, Chen Y, Zhou Q, Yang Y, Liu Y, Liu B, Zhu Q, Zhou Y, Lin J, Liang B, Li L, Dong X, Pan Z, Wang R, Wan H, Qiu W, Xu W, Eurlings P, Barhanin J. A kir2.1 gain-of-function mutation underlies familial atrial fibrillation. *Biochem Biophys Res Commun*. 2005;332:1012–1019.
29. Eijsbouts SC, Houben RP, Blaauw Y, Schotten U, Allessie MA. Synergistic action of atrial dilation and sodium channel blockade on conduction in rabbit atria. *J Cardiovasc Electrophysiol*. 2004;15:1453–1461.
30. Cabo C, Pertsov AM, Davidenko JM, Baxter WT, Gray RA, Jalife J. Vortex shedding as a precursor of turbulent electrical activity in cardiac muscle. *Biophys J*. 1996;70:1105–1111.
31. Bollmann A, Binias KH, Toepffer I, Molling J, Geller C, Klein HU. Importance of left atrial diameter and atrial fibrillatory frequency for conversion of persistent atrial fibrillation with oral flecainide. *Am J Cardiol*. 2002;90:1011–1014.
32. Opthof T. Ik1 blockade is unlikely to be a useful antiarrhythmic mechanism. *Cardiovasc Res*. 1994;28:420.
33. Tristani-Firouzi M, Jensen JL, Donaldson MR, Sansone V, Meola G, Hahn A, Bendahhou S, Kwiecinski H, Fidzianska A, Plaster N, Fu YH, Ptacek LJ, Tawil R. Functional and clinical characterization of kcnj2 mutations associated with lqt7 (Andersen syndrome). *J Clin Invest*. 2002;110:381–388.
34. Burrell ZL, Jr., Martinez AC. Chloroquine and hydroxychloroquine in the treatment of cardiac arrhythmias. *N Engl J Med*. 1958;258:798–800.
35. Schram G, Pourrier M, Melnyk P, Nattel S. Differential distribution of cardiac ion channel expression as a basis for regional specialization in electrical function. *Circ Res*. 2002;90:939–950.
36. Du X, Zhang H, Lopes C, Mirshahi T, Rohacs T, Logothetis DE. Characteristic interactions with phosphatidylinositol 4,5-bisphosphate determine regulation of kir channels by diverse modulators. *J Biol Chem*. 2004;279:37271–37281.
37. Pogwizd SM, Schlotthauer K, Li L, Yuan W, Bers DM. Arrhythmogenesis and contractile dysfunction in heart failure: roles of sodium-calcium exchange, inward rectifier potassium current, and residual beta-adrenergic responsiveness. *Circ Res*. 2001;88:1159–1167.
38. Kuijpers NH, Potse M, van Dam PM, ten Eikelder HM, Verheule S, Prinzen FW, Schotten U. Mechanoelectrical coupling enhances initiation and affects perpetuation of atrial fibrillation during acute atrial dilation. *Heart Rhythm*. 2011;8:429–436.

CLINICAL PERSPECTIVE

Atrial dilatation and stretch are thought to predispose to atrial fibrillation (AF), but the mechanism is not well understood. A stretch-related mechanism has been proposed in the pathogenesis of AF in various diseases, including mitral valve disease, heart failure, and sleep apnea. We have proposed that electrical rotors are the high-frequency drivers that maintain stretch-induced AF (SAF) and that are responsible for the direct relationship that exists between the dominant frequency of AF and the left atrial pressure in both human patients and animal models. Because inward-rectifier K^+ currents (IK_1, $I_{K\text{-}Ach}$, and $I_{K\text{-}ATP}$) play important roles in enabling and controlling rotor dynamics, then blocking those channels should effectively terminate SAF. We compared the effects of chloroquine, which preferentially blocks I_{K1}, with those of flecainide, which preferentially blocks I_{Na}, on acute SAF excitation properties and termination in Langendorff-perfused sheep hearts that approximate AF in the human heart with pressure overload and atrial dilatation. The results show that both chloroquine and flecainide slow activation frequency, but chloroquine is more effective than flecainide in converting SAF to sinus rhythm. As a further confirmation for the important role of the inward-rectifier K^+ currents in SAF, we observed that chloroquine terminated all AF episodes, in contrast with the I_{Kr} blocker E-4031 that did not terminate the fastest SAF episodes. The demonstration that chloroquine treatment eliminates SAF in a clinically relevant animal model suggests that novel pharmacological strategies focusing on selective blockade of inward rectifier K^+ currents may be an effective approach to treat AF.

SUPPLEMENTAL MATERIAL

Chloroquine Terminates Stretch-Induced Atrial Fibrillation in the Sheep Heart More Effectively than Flecainide.

David Filgueiras-Rama, MD, Raphael Pedro Martins, MD, Sergey Mironov, PhD, Masatoshi Yamazaki, MD, Conrado Calvo, MSc, Steve R Ennis, PhD, Krishna Bandaru, MD, Sami F Noujaim PhD, Jérôme Kalifa, MD, Omer Berenfeld, PhD, José Jalife, MD.

Supplemental Methods.

Experimental Setup.

Stretch-induced atrial fibrillation in the Langendorff-perfused sheep heart.

The isolated, coronary perfused heart underwent an atrial trans-septal puncture to enable equalize intracavitary pressure in both atria. Tetrapolar electrode catheters (Torq®, Medtronic Inc./Minneapolis/MN/USA) were placed into each of the pulmonary veins (PVs) to record bipolar signals from the two distal electrodes (sampling rate, 1.0 kHz) using a Biopac Systems amplifier (DA100C; Biopac Systems, Inc., Goleta, CA, USA). Additional bipolar recordings were obtained from the top and roof of the left atrial appendage (LAA) and right atrial appendage (RAA). All vein orifices were then sealed, except the inferior vena cava, which was cannulated and connected to a digital sensor (Biopac Systems transducer-TSD104A; Biopac Systems, Inc., Goleta, CA, USA) and to an outflow cannula whose open-ended height above the atria controlled the intra-atrial pressure. The pressure was then

increased to 14 cm H2O, which led to an increase in atrial volume and dilatation. The pressure was maintained stable throughout the experiment.[1]

Epicardial mapping of the LAA and RAA.

A bolus injection of 5 to 10 ml Di-4-ANEPPS (10 mg/mL) (Sigma-Aldrich, St. Louis, MO, USA) and a loading period of 10 min are needed to obtained voltage-sensitive fluorescence upon laser excitation (532 nm) of the epicardial surface. The emitted fluorescence is then transmitted through a 600 nm long pass filter and projected onto LittleJoe CCD video camera (80x80 pixels, SciMeasure Analytical Systems, Inc. Decatur, GA, USA) and acquired at a rate between 500-1000 frames per second. Five-second movies were obtained at 2 min intervals during control AF. The area of the mapped epicardial surface was ~14 cm^2.

Endocardial optical mapping of the posterior left atrium (PLA) of the intact heart.

A second LittleJoe CCD camera (80x80 pixels) was synchronized with the epicardial camera. A 10 mm diameter dual-channel rigid borescope (Everest VIT, Inc. Flanders, NJ, USA) with a 90-degree field of view was introduced through the anterior wall of the left ventricle, across the mitral valve and focused on the endocardial surface of the PLA (supplemental Figure 1). The optically mapped area on the PLA was ~3.7 cm^2, which allowed visualizing the four PVs and the atrial septo-pulmonary bundle. The borescope was c-mounted to the CCD camera through a custom-made eyepiece adapter. Laser excitation (532 nm) was delivered to the endocardium through a liquid light-guide (0.2 in core).[1] In 7 experiments the endocardial surface of the PLA was optically mapped.

Experimental protocols.

As shown in Supplemental Figure 2A, the intra-atrial pressure was adjusted to 14 cm H_2O at the beginning of the protocol. Baseline pacing at 300, 250 and 200 ms was applied from the LAA. We used burst pacing at 12 Hz to induce AF, which was allowed to continue for a control period of 15 min, after which either chloroquine (N=7; 4 μM) or flecainide (N=5; 2-4 μM) was added to the Tyrode's solution. The drug concentration was doubled if AF persisted after 20 min under chloroquine or flecainide. A period of 50 min was allowed for AF termination to occur. AF was then terminated by DC shock (DFib) in those cases in which it persisted. AF re-induction was then attempted via burst pacing at 12 Hz, and was considered to be persistent when it lasted 15 min or longer after re-induction. Before washout a new DC shock (DFib) was used to restore the SR, if necessary. The washout period was 45 and 30 min for chloroquine and flecainide, respectively. Finally, after the washout, AF was re-induced by burst pacing and allowed to continue for 15 more min before the end of the protocol.

Supplemental Figure 2B illustrates the protocol of an additional set of optical mapping experiments (N=11) in which we determined the effects of chloroquine and flecainide on action potential duration and conduction velocity during pacing. Mapping and pacing were conducted on the epicardial surface of the LAA. The pacing protocol (300, 250 and 200 ms CL) was carried out at baseline, after 15 min of chloroquine (N=5) or flecainide (N=6), and after the washout. Representative electrograms are shown below the time-course of both protocols.

Atrial fibrillation dynamics.

Analysis of AF dynamics takes advantage of phase movies generated via Hilbert transformation.[2] Patterns of activation allow identifying rotors and breakthroughs.

:• A rotor was identified by the presence of all phases converging on a singularity point (SP) lasting more than one rotation. Supplemental Figure 3A shows snapshots of the PLA after generation of phase maps: a rotor pattern is identified lasting for 3 rotations; from frame 0 to frame 114.

• A breakthrough was defined as a wavefront appearing in the field of view and propagating outward in a target-like pattern. Supplemental Figure 3B shows a breakthrough pattern in the PLA after generation of phase maps.

Quantification of the core size.

During functional reentry, the perimeter of the center of rotation (the "core") is inscribed by the trajectory of the rotating SP that is formed after a wavebreak.[3] As it completes full rotations, the SP in fact becomes the rotor that organizes the overall reentrant activity. The core size and shape reflect critical parameters of the excitable medium that control the frequency and dynamics of a stationary rotor responsible for generating spiral waves (SW). Typically during AF in the sheep left atrium, the cores of identifiable stationary rotors are ellipsoidal and have an area of ~4 mm^2.[4] However, most rotors that are observed during AF are non-stationary. In addition, particularly in the area with the highest frequency, multiple drifting rotors may form locally and then become extinct after highly variable lifetimes, which

makes it difficult to accurately quantify their properties. In addition, as they drift through the atrial muscle their cores no longer appear elliptical. Instead, their fingerprint in an amplitude map (see supplemental Figure 4)) is an extended dark band (i.e., a "line of block") whose dimensions (width and length) depend on the velocity of impulse propagation, the speed of the core drift, and the lifespan of the individual rotor, and whose width provides an accurate measure of the core diameter. Here, we present a technique that allowed us to estimate the core widths of non-stationary rotors during control AF and during AF in the presence of chloroquine or flecainide (see Figure 5B and 6C in main manuscript). Our approach took advantage of the fact that during optical mapping of reentry the amplitude of the fluorescence signal at the core is appreciably lower than outside the core. Thus, as the rotor drifts into a camera pixel location, its core leaves a low fluorescence mark at that location. Supplemental Figures 4-6 illustrate this new method.

Supplemental Results

Supplemental Figure 7 shows the time-course of the DF_{max}, number of rotations/cm^2 (PLA/LAA) and number of breakthroughs/cm^2 during control AF and after the administration of either chloroquine (Panel A) or flecainide (Panel B). Two representative cases are shown; one under chloroquine and one under flecainide. In panel A, the DF_{max} sharply decreases after chloroquine, along with the number of rotations/cm^2 and breakthroughs/cm^2. Few number of identifiable rotations/cm^2 are present before AF termination under chloroquine (Figure 7A, central panel). In panel B, DF_{max} slightly decreases after flecainide. The number

of identifiable rotations/cm^2 and breakthroughs/cm^2 also decrease, however the effect is not as strong as the chloroquine effect and the AF does not terminates.

Additional experiments (N=5) were performed at 1 μM chloroquine. Such a concentration has less blocking effects on I_{Kr} (38%) and I_{Na} (14%), but I_{K1} is still highly blocked (74%).[5] Supplemental Figure 8A shows how low doses of chloroquine (1 μM) were able to terminate AF in 4 out of 5 AF episodes. In one AF episode chloroquine concentration was increased to 2 μM to terminate the arrhythmia. In panel B, representative electrograms from the left superior PV (LSPV) show the restoration of SR under 1 μM chloroquine. In panel C, control DF_{max} was similar in all chloroquine groups, with a significant decrease in DF_{max} before restoration of SR. The DF_{max} decreased from 10.6±0.7 to 6.3±0.2 Hz in the first few minutes after 4 μM chloroquine, and from 10.5±0.8 Hz to 6.7±0.2 Hz after 1-2 μM chloroquine and before the resumption of the SR.

Supplemental References.

1. Filgueiras-Rama D, Martins RP, Ennis SR, Mironov S, Jiang J, Yamazaki M, Kalifa J, me, Jalife J, Berenfeld O. High-resolution endocardial and epicardial optical mapping in a sheep model of stretch-induced atrial fibrillation. *J Vis Exp*. 2011:e3103.
2. Warren M, Guha PK, Berenfeld O, Zaitsev A, Anumonwo JM, Dhamoon AS, Bagwe S, Taffet SM, Jalife J. Blockade of the inward rectifying potassium current terminates ventricular fibrillation in the guinea pig heart. *J Cardiovasc Electrophysiol*. 2003;14:621-631.
3. Jalife J, Berenfeld O. Molecular mechanisms and global dynamics of fibrillation: An integrative approach to the underlying basis of vortex-like reentry. *J Theor Biol*. 2004;230:475-487.
4. Mandapati R, Skanes A, Chen J, Berenfeld O, Jalife J. Stable microreentrant sources as a mechanism of atrial fibrillation in the isolated sheep heart. *Circulation*. 2000;101:194-199.
5. Sanchez-Chapula JA, Salinas-Stefanon E, Torres-Jacome J, Benavides-Haro DE, Navarro-Polanco RA. Blockade of currents by the antimalarial drug chloroquine in feline ventricular myocytes. *J Pharmacol Exp Ther*. 2001;297:437-445.

Supplemental Figure legends.

Figure 1. Diagrammatic representation of the experimental setup used to map optically and electrically from the endocardial and epicardial surfaces of the left atrium. Epicardial bipolar electrograms were obtained from the PVs in all experiments.

Figure 2. Time-course of the experimental protocols. **A,** protocol to study AF termination after flecainide and chloroquine. **B,** protocol to study the effects of chloroquine and flecainide on action potential duration and conduction velocity during pacing. AF: atrial fibrillation. CL: cycle length. DFib: Defibrillation. SR: sinus rhythm.

Figure 3. A, snapshots of the PLA after generation of phase maps: a rotor pattern is identified lasting for 3 rotations; from frame 0 to frame 114. **B,** a breakthrough pattern in the PLA; Wavefront appearing in the field of view and propagating outward in a target-like pattern.

Figure 4. Panel **A** shows a single CCD camera pixel recording to illustrate the first step needed to build the amplitude maps used to measure core width. The peak fluorescence recorded by each pixel during each excitation (black) is counted as a fluorescence step (red) whose magnitude is measured from the zero fluorescence line, after correction of the baseline shift (blue). Panel **B** shows representative sequential amplitude maps obtained by the 80x80 pixel camera during propagation of a fibrillatory wavefront around a line of block. The frame time is indicated on the upper right corner of each frame. At time 0, the wavefront started from the top right corner of the field of view (red star), with the red arrows showing the wavefront location. Between frames 0 and 64, the same wavefront circumnavigated the line

of block, almost completing a full rotation before the next wave appeared at frame 95 (blue arrows).

Figure 5. The figure was taken from the same AF episode as figure 4. Panel **A** shows on the right a set of single pixel recordings for 4 sequential excitations recorded along the vertical red line on the amplitude map of panel **B**. In **A**, the upper recordings marked in red correspond to a wavefront that moved downward and from left to right during frames 150-250 in the map; the lower recordings are marked blue. On the left of panel A is the consolidated 3D amplitude profile across the dark band for the blue signals at frames 150 and the red signals at frame 200. Note that in each case the amplitude of the recordings gradually decreased toward the center of the map forming a clearly visible dark band. This dark band closely associated with singularity points (SPs). In panel **C** the red spots represent all the SPs obtained during propagation of the red wave. All the SPs were located inside the dark band, which clearly demonstrates that such a band is the fingerprint of a drifting core.

Figure 6. A and B, to measure the width of a dark band (panel **A**) we first draw an isoamplitude line (IAL) at about 30% of the maximal wave amplitude (panel **B**) to mark the dark band perimeter. Then lines are drawn perpendicular to the IAL across the width of the dark band at each relevant pixel location. The length of each perpendicular is a measure of the local core width. **C and D,** lines that do not encounter an IAL on both sides of the dark band are automatically excluded (green in panel C), as are lines whose angle was significantly different from 90 degrees (blue in panels C and expanded inset in D). In panel **E**, the obtained local core band width is plotted versus the distance along the IAL, where point 0 corresponds to the tip of the band (circle on panel B) and the shape of the plot is relatively

symmetrical at either side of point 0. Thereafter, all the obtained values for any particular band are averaged and the result is considered to be the width of that particular core.

Figure 7. Two representative cases are shown**. A, t**he DF_{max} sharply decreases after chloroquine, along with the number of rotations/cm^2 and breakthroughs/cm^2. **B,** DF_{max}, the number of identifiable rotations/cm^2 and breakthroughs/cm^2 slightly decrease after flecainide (5-sec long movies were analyzed).

Figure 8. A, low doses of chloroquine (1 μM) were able to terminate AF in 4 out of 5 AF episodes. **B,** representative electrograms from the left superior PV (LSPV) show the restoration of SR under 1 μM chloroquine. **C,** control DF_{max} was similar in all chloroquine groups, with a significant decrease in DF_{max} before restoration of SR.

Figure 9. A, B, single pixel action potential from the LAA at baseline stretch (black), after chloroquine 4μM (red) and flecainide 4 μM (blue). APD_{70} significantly prolongs after chloroquine. Conversely, non-significant changes are present after flecainide.

Supplemental Movie legends.

Movie 1. Phase movie showing a long meandering rotor anchored to the roof/PLA-LAA junction after 40 min of flecainide.

Movie 2. Phase movie of the posterior left atrium; short-lasting rotors (1-2 rotations) are present in control AF (chloroquine protocol).

Movie 3. Same AF episode as in Movie 2 after chloroquine; very few rotors are identified during the last minute before AF termination.

Movie 4. Phase movie of the posterior left atrium during control AF (flecainide protocol).

Movie 5. Same AF episode as in Movie 4; although reentrant activity decreases still persists after 50 min under flecainide.

Supplemental Figures.

Figure 1.

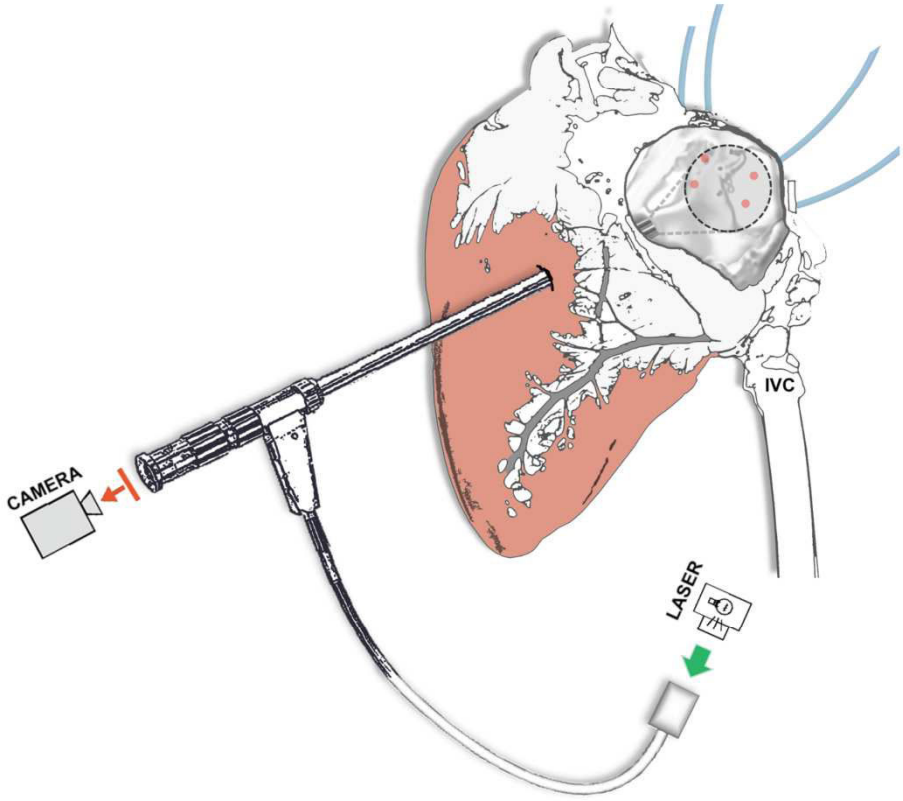

12

Figure 2.

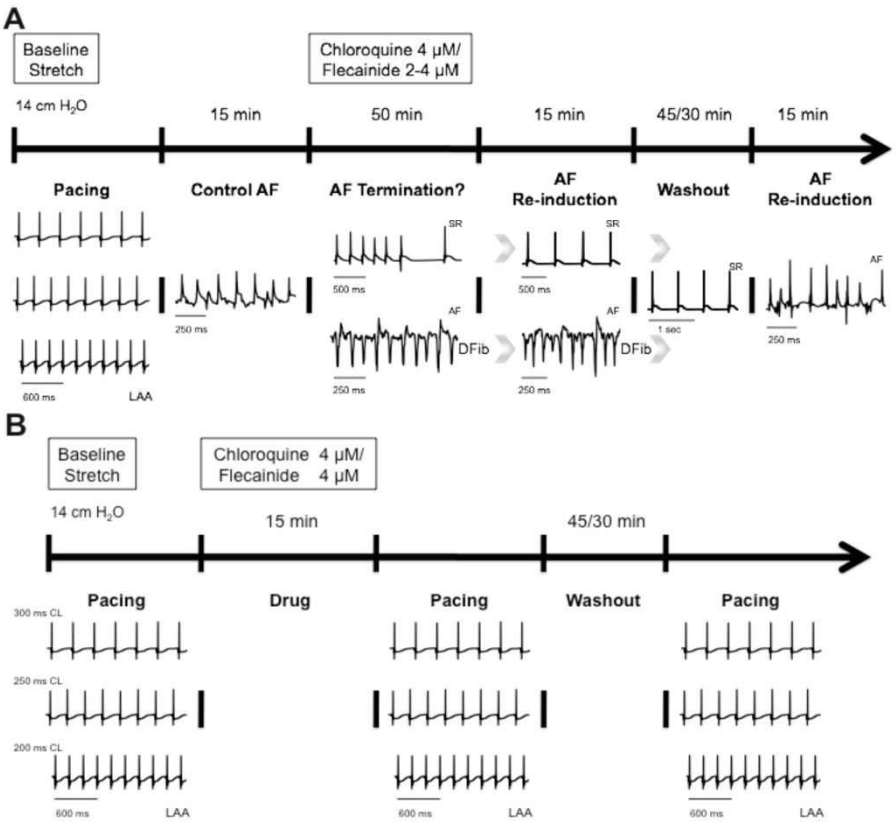
A
Baseline Stretch
14 cm H2O
Chloroquine 4 µM/ Flecainide 2-4 µM
15 min
50 min
15 min
45/30 min
15 min
Pacing
Control AF
AF Termination?
AF Re-induction
Washout
AF Re-induction
SR
AF
DFib
600 ms
LAA
250 ms
500 ms
1 sec
B
Baseline Stretch
14 cm H2O
Chloroquine 4 µM/ Flecainide 4 µM
15 min
45/30 min
Pacing
Drug
Pacing
Washout
Pacing
300 ms CL
250 ms CL
200 ms CL
600 ms
LAA

Figure 3.

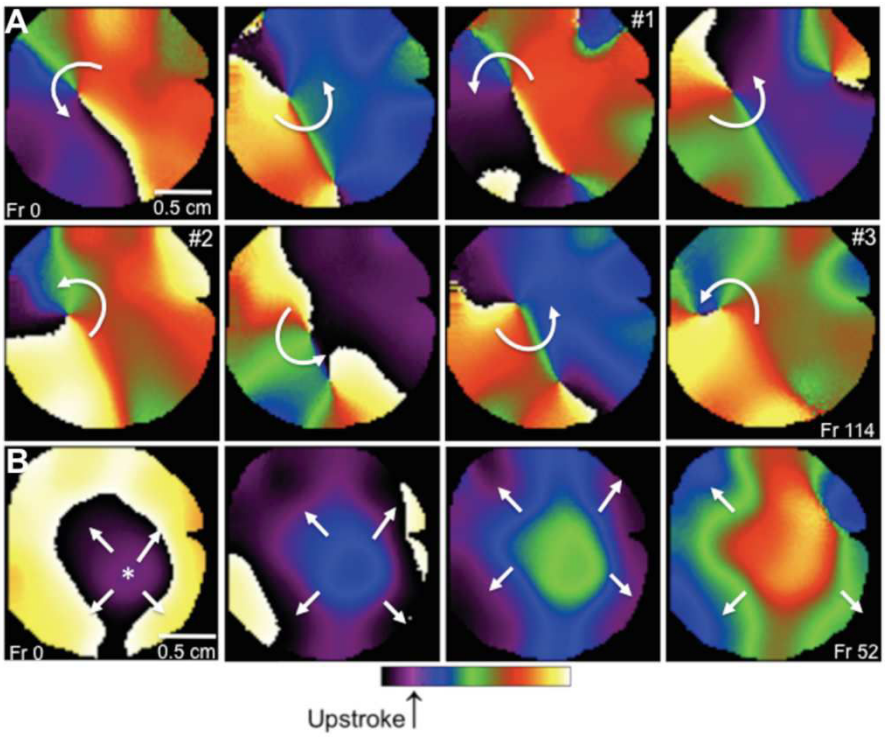

14

Figure 4.

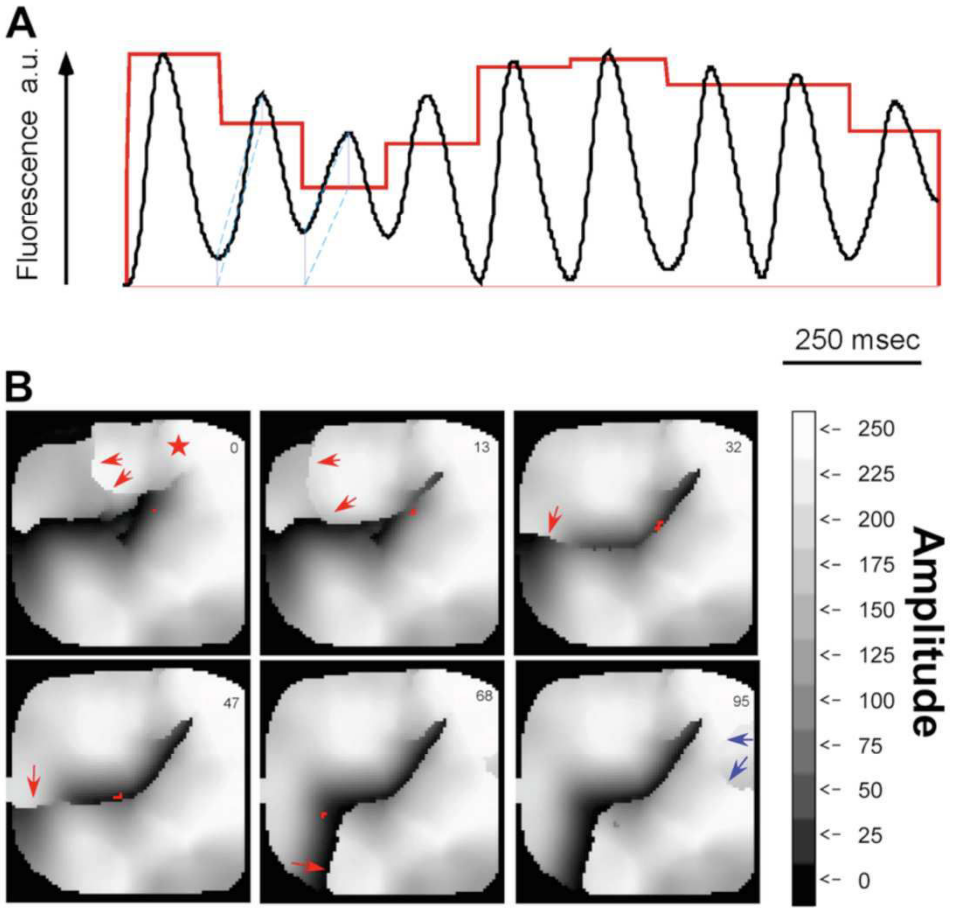
A
Fluorescence a.u.
250 msec
B
0
13
32
47
68
95
<- 250
<- 225
<- 200
<- 175
<- 150
<- 125
<- 100
<- 75
<- 50
<- 25
<- 0
Amplitude

Figure 5.

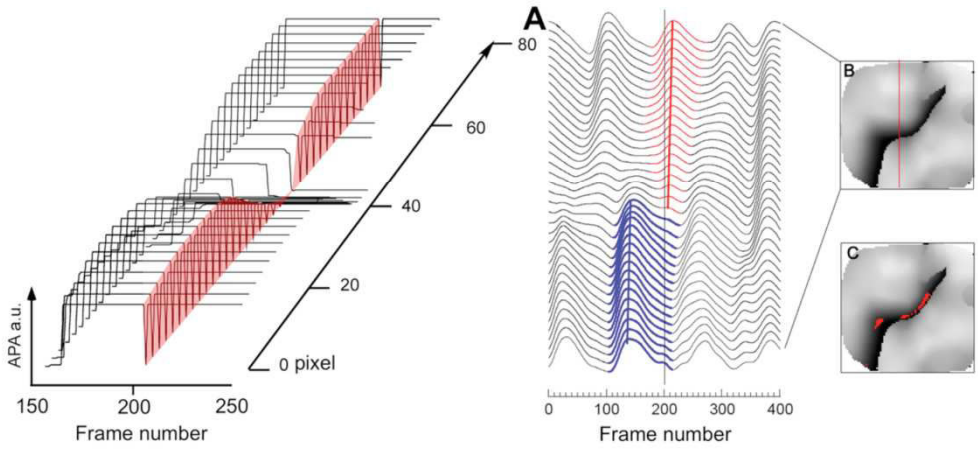
A
80
60
40
20
0 pixel
APA a.u.
150
200
250
Frame number
0
100
200
300
400
Frame number
B
C

Figure 6.

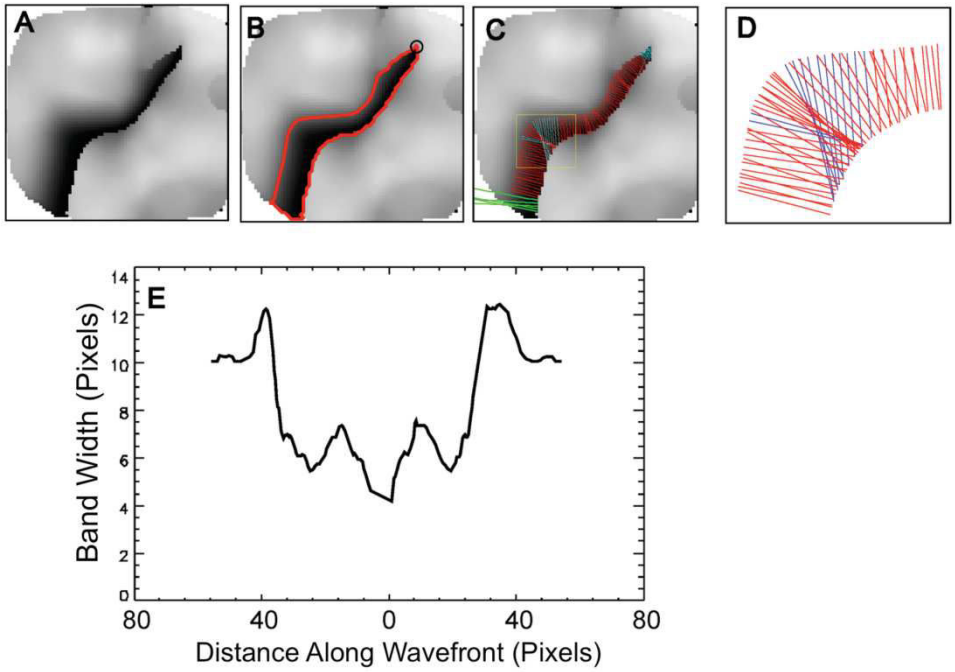
A
B
C
D
E
Band Width (Pixels)
0
2
4
6
8
10
12
14
80
40
0
40
80
Distance Along Wavefront (Pixels)

Figure 7.

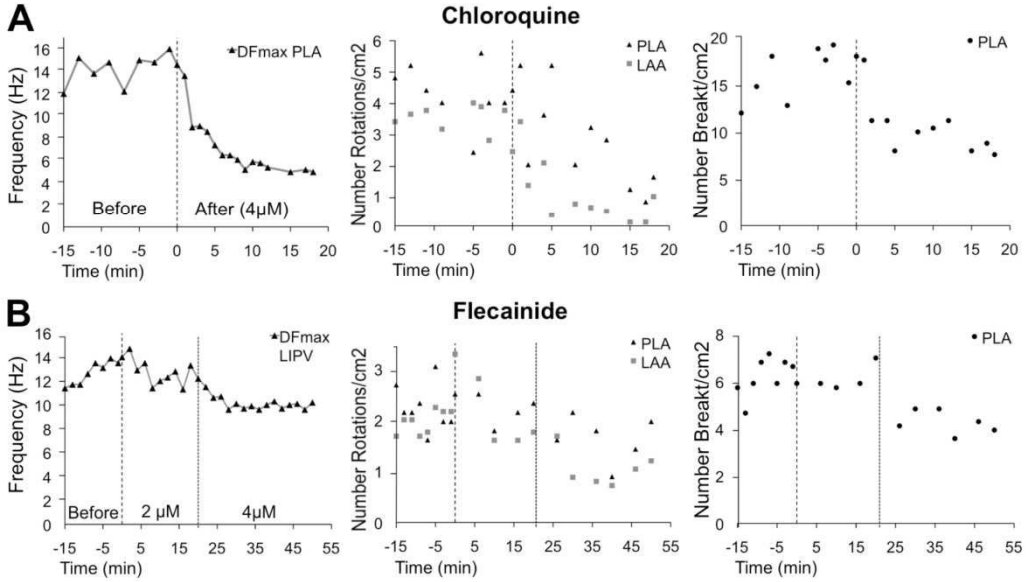
A
Chloroquine
DFmax PLA
Frequency (Hz)
Before
After (4μM)
Time (min)
Number Rotations/cm2
PLA
LAA
Number Breakt/cm2
B
Flecainide
DFmax
LIPV
2 μM
4μM

Figure 8.

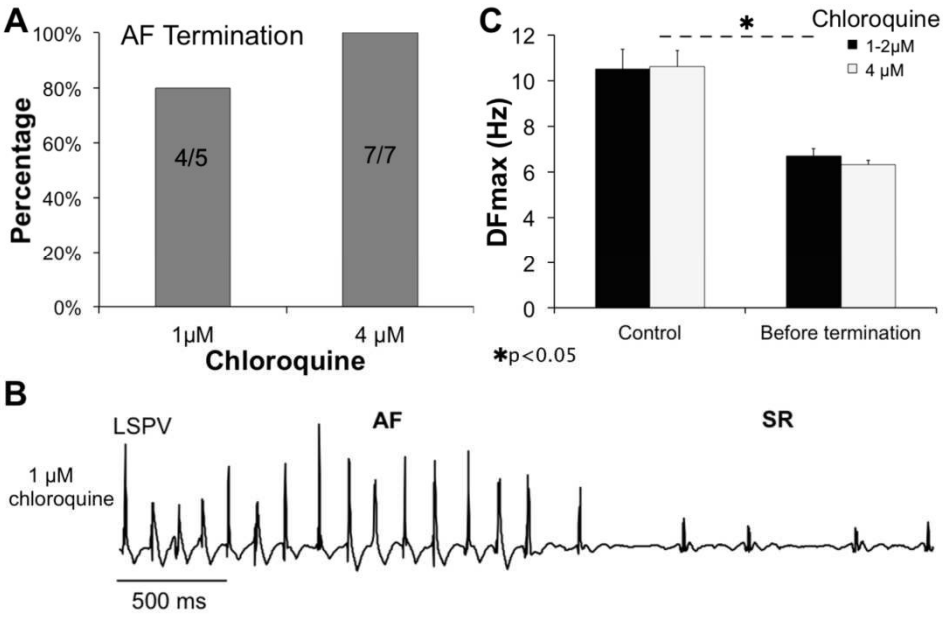
A
AF Termination
100%
80%
60%
40%
20%
0%
Percentage
4/5
7/7
1μM
4 μM
Chloroquine
C
Chloroquine
1-2μM
4 μM
12
10
8
6
4
2
0
DFmax (Hz)
Control
Before termination
*p<0.05
B
LSPV
AF
SR
1 μM
chloroquine
500 ms

20

Figure 9.

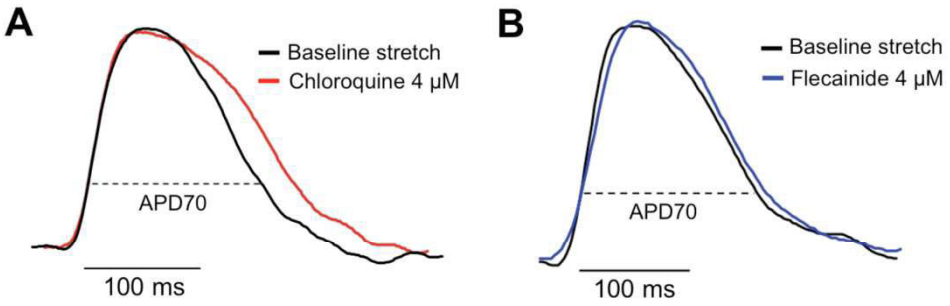

20

2. Effets anti-arythmiques de la ranolazine

a. Hypothèse de travail

La ranolazine est une molécule commercialisée initialement comme médicament adjuvant dans le traitement symptomatique de l'angor stable mal contrôlé par les anti-angineux habituels (Ranexa®, CV Therapeutics Inc, Palo Alto, CA ; AMM européenne obtenue en 2008).[205, 206] Elle est actuellement utilisée dans de nombreux pays (Etats-Unis, Allemagne, …) mais n'est pas commercialisée en France.

Différentes études ont démontré qu'elle possédait par ailleurs une activité anti-arythmiques de classe I de part son effet inhibiteur sur le courant sodique tardif (« late I_{Na} ») et principalement sur la FA.[207-210] Cependant, les mécanismes expliquant son effet anti-arythmique sur la FA sont peu connus,[207] et sa capacité à restaurer le rythme sinusal en cas de FA persistante n'ont pour le moment jamais été étudiés. Nous avons donc débuté un travail de recherche visant à étudier l'efficacité de la ranolazine et ses mécanismes d'action anti-arythmique ex-vivo sur un modèle ovin (cœur explanté et perfusé sur un système de Langendorff) de FA paroxystique et persistante.

b. Méthodes

Afin d'induire un épisode de FA paroxystique sur cœur sain, nous avons utilisé le modèle de FA induite par le stretch. L'endocarde postérieur et la paroi libre de l'OG étaient cartographiées, comme décrit dans la première partie du manuscrit (N=5). Après augmentation de la pression intra-atriale à 12.7±0.7 cmH_2O, la FA était induite par stimulation atriale et maintenue pendant une durée contrôle de 50 minutes.

Parallèlement, l'effet de la ranolazine sur la FA persistante a été étudié (N=3), induite par un protocole de stimulation chronique tel qu'utilisé dans notre travail publié dans *Circulation Arrhythmia and Electrophysiology* (alternance de 30 secondes de stimulation et de 10 secondes de blanking, maintenue pendant 20-24 semaines), avec une pression intra-atriale physiologique de 6.2±0.2 cmH_2O.[143]

Après une période de 50 minutes de FA, 10µM de ranolazine était rajoutés à la solution de perfusion, concentration doublée en cas de persistance de FA.

c. Résultats

Dès la première minute de perfusion, une important diminution de la DF_{max} était observée, passant de 10.1±1.6 à 7.2±0.9 Hz (p=0.008 *vs.* état basal, Figure 42A), suivie d'un retour en rythme sinusal après 15±4 minutes (de 12 à 20 minutes). Des cartes de DF avant et après administration de ranolazine sont représentées sur la Figure 42B. Par ailleurs, le nombre de points de singularité observés (correspondant aux « wavebreaks » initiant des rotors) diminuait significativement (Figure 42C et D, Figure 43).

Une fois le retour en rythme sinusal obtenu, une tentative de réinduction était effectuée. Sur 4 des 5 cœurs étudiés, seuls de courts épisodes non soutenus de FA (de quelques secondes à 14 minutes, durée médiane = 28 secondes) ont été initiés.

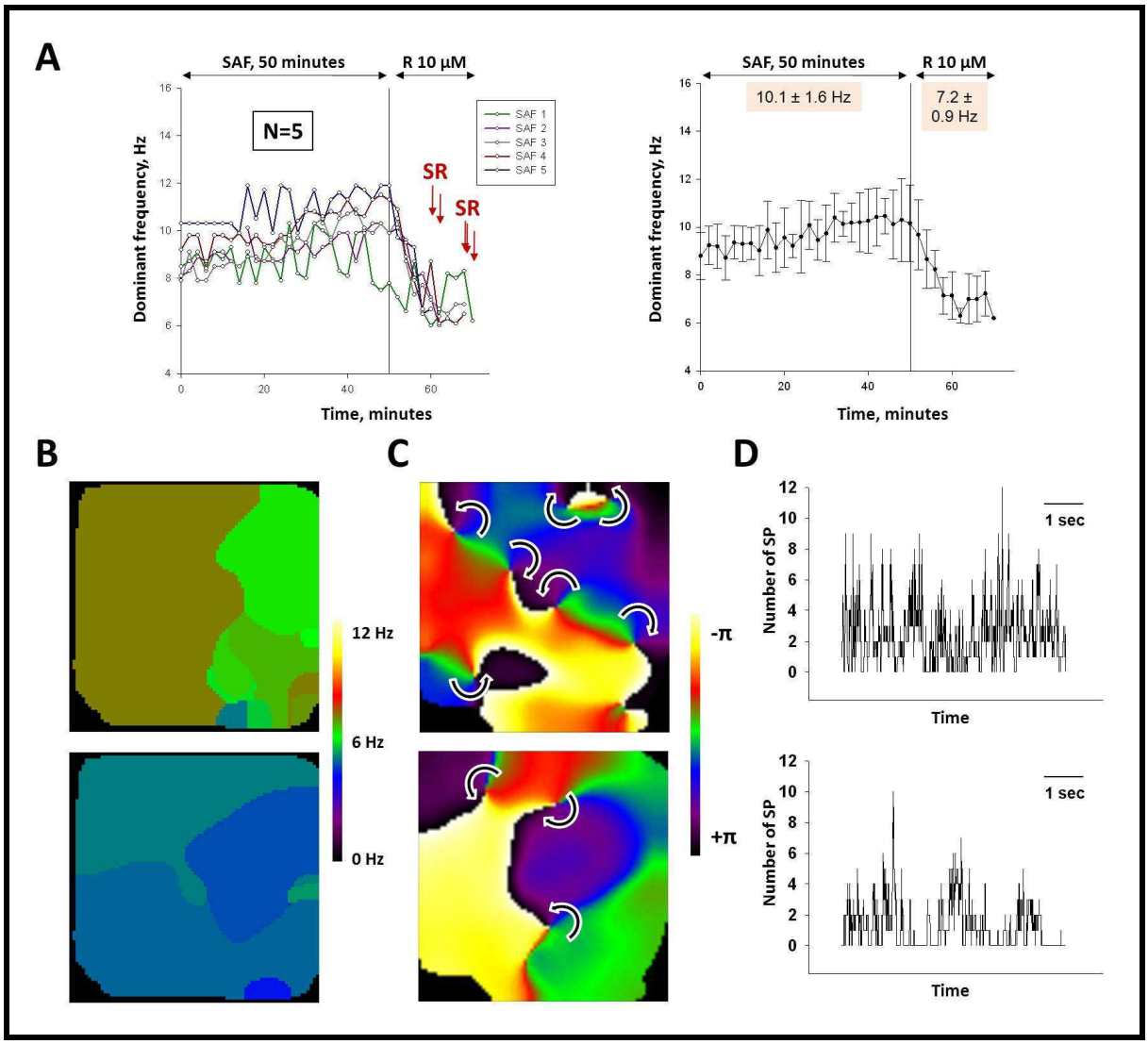

Figure 42: A. Effets de la ranolazine sur la DF_{max} sur des cœurs perfusés sur un système de Langendorff en cas de FA paroxystique (n=5). B. Cartes de DF_{max} avant (haut) et après (bas) perfusion de ranolazine. C. Carte de phase montrant les rotors avant (haut) et après (bas) perfusion de ranolazine. D. Nombre de points de singularité en fonction du temps sur des films de 5 secondes avant (haut) et après (bas) perfusion de ranolazine.

Sur les cœurs en FA persistante (stimulation à haute fréquence pendant 6 mois), et comme cela était observé sur cœur sain, la ranolazine à 10µM entrainait une diminution rapide et importante de la DF de 10.9±2.9 à 7.2±11 Hz (p=0.01, Figure 43A). Cependant, malgré une diminution similaire à celle observée en FA paroxystique, aucun retour en rythme sinusal n'était observé. Le doublement de la concentration de ranolazine (20µM) entrainait une diminution supplémentaire de la DF (5.8±0.2 Hz, p<0.05 *vs.* 10µM) sans passage en TA ni en rythme sinusal (Figure 43A). Des cartes de DF avant et après administration de ranolazine sont représentées sur la Figure 43B. Par ailleurs, le nombre de points de singularité (significativement inférieur à ce qui était observé précédemment) ne variait pas malgré l'administration de la molécule (Figure 43C et D).

Le rotor représenté au bas de la Figure 43C a ainsi été observé pendant plus de 20 minutes, stable et ne se déplaçant que de quelques millimètres à chaque rotation.

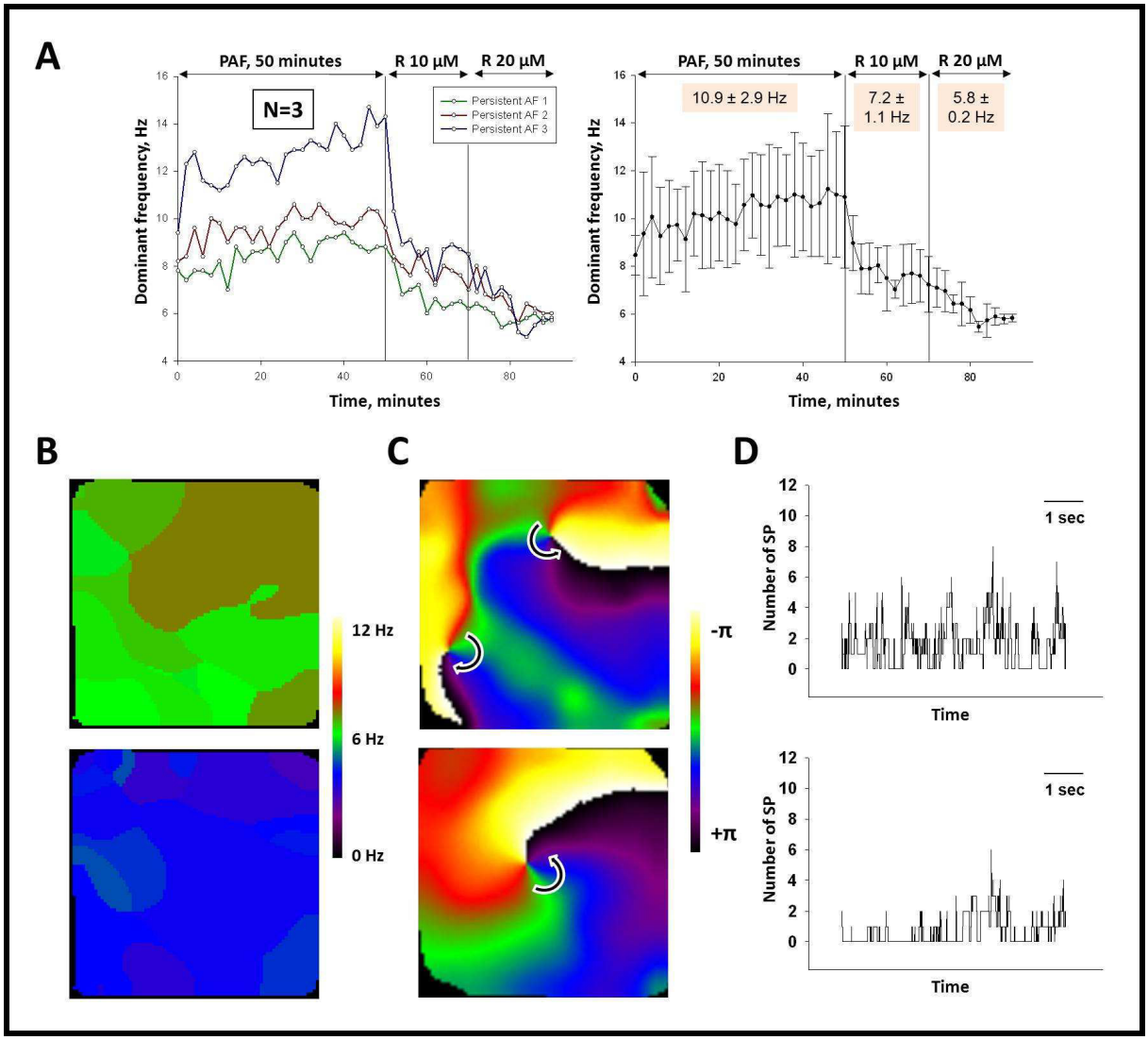

Figure 43: A. Effets de la ranolazine sur la DF_{max} sur des cœurs perfusés sur un système de Langendorff maintenus en FA persistante pour une durée de 6 mois (n=3). Malgré l'augmentation de la concentration à 20µM, aucun retour en rythme sinusal n'a été observé. B. Cartes de DF_{max} avant (haut) et après (bas) perfusion de ranolazine. C. Carte de phase montrant les rotors avant (haut) et après (bas) perfusion de ranolazine. D. Nombre de points de singularité en fonction du temps sur des films de 5 secondes avant (haut) et après (bas, 20µM) perfusion de ranolazine.

Le pourcentage de réduction de la DF_{max} induit par la ranolazine est résumé dans la Figure 44A. En cas de FA induite par le stretch, la DF_{max} diminuait respectivement de 20 et 25% dans l'endocarde postérieur et dans l'auricule gauche à une concentration de 10µM et avant retour en rythme sinusal. Une réduction d'ampleur similaire était observée sur les cœurs en FA persistante (respectivement 24 et 29% de réduction) sans retour en rythme sinusal. La FA se maintenait à 20 µM et malgré une réduction de 39 et 37% de la DF_{max}. L'effet sur le nombre de points de singularité est représenté dans la Figure 44B. Une diminution significative du nombre de points de singularité était observée parralèllement à la diminution de la DF_{max} (de 51.9±11.9/cm²/5sec à 29.5±4.6/cm²/5sec, p=0.005). A l'opposé, une

diminution moindre et non significative était observée sur les cœurs en FA persistante, même à une concentration de 20µM (de 17.3±3.6/cm²/5sec à 10.7±3.6/cm²/5sec, p=NS).

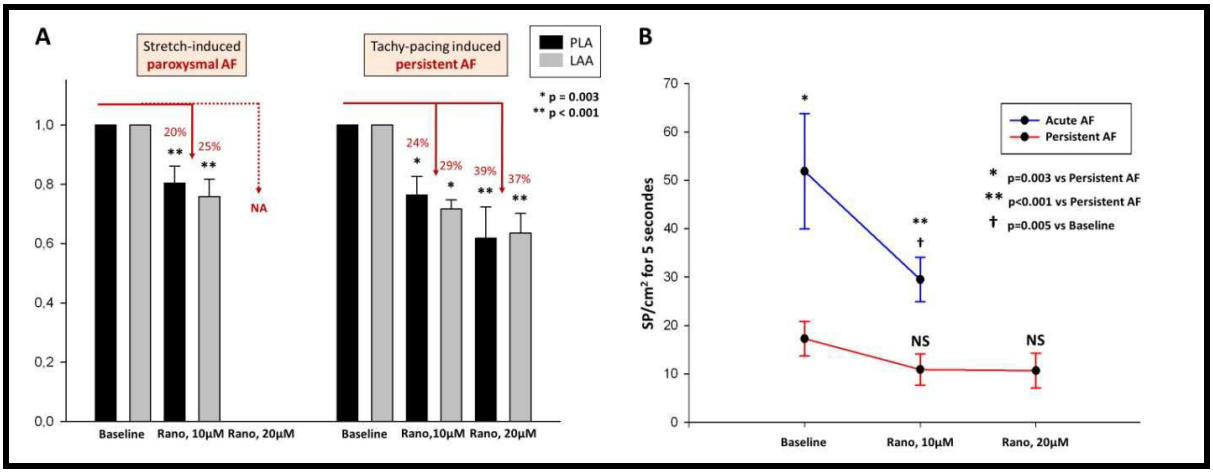

Figure 44: A. Effet de la ranolazine à 10 et 20µM sur la FA induite par le stretch et sur la FA persistante. Malgré une diminution plus importante de la DF_{max}, aucun retour en rythme sinusal n'était observé dans les 3 cas de FA persistante. B. Effets de la ranolazine sur le nombre de points de singularité. A l'état basal, le nombre de points de singularité était supérieur dans les cas de FA paroxystique, par rapport aux cœurs en FA persistante. Le remodelage structurel (fibrose) survenu en FA persistante explique probablement que les rotors soient plus stables, donc moins nombreux. La ranolazine induit une diminution significative du nombre de points de singularité en cas de FA paroxystique, mais non dans les cas de FA persistante, même à une concentration de 20µM.

d. Discussion

En résumé, la ranolazine possède une activité anti-arythmique puissante sur la FA paroxystique, de part une réduction de la DF_{max} et du nombre de points de singularité. Dans les cas de FA persistante et malgré une réduction de la DF_{max}, le retour en rythme sinusal n'est pas observé, possiblement de part l'absence de réduction du nombre de points de singularité (représentant les « wavebreaks », première étape dans la genèse des rotors). La vitesse de rotation des rotors est ainsi diminuée, mais leur nombre est inchangé. Ces derniers sont donc plus stables dans l'espace et n'entrent pas en collision avec des obstacles anatomiques (Figure 43C, bas), permettant à l'arythmie de se maintenir.

La capacité d'un traitement anti-arythmique à rétablir le rythme sinusal a été étudiée par de nombreux laboratoires. De nombreuses hypothèses ont été émises. Tout d'abord, une théorie communément admise est la capacité de la molécule à prolonger la longueur d'ondes des circuits de fibrillation.[211] L'équipe de S. Nattel avait postulé que la flécaïnide pouvait terminer la FA vagale sur les cœurs de chien lorsqu'elle était capable d'augmenter la longueur d'onde des ondes fibrillatoires.[212] Ils ont également découvert que l'effet de cet anti-arythmique était également en rapport avec sa capacité à abolir l'hétérogénéité régionale des longueurs d'ondes et des périodes réfractaires effectives des cardiomyocytes.[212] Le groupe de M. Allessie a retrouvé des résultats contradictoires, suggérant que le retour en rythme sinusal ne dépendait pas de paramètres tels que le cycle moyen d'activation, la période réfractaire effective ou la vitesse de conduction.[213, 214] Ils ont ainsi démontré que la flécaïnide pouvait

prolonger le cycle d'activation atriale, parfois même de 100%, sans que la FA ne s'interrompe, et qu'au contraire, seul l'élargissement du gap excitable pouvait expliquer le retour en rythme sinusal.[214] De récentes études ont exploré l'action des anti-arythmiques, dont celui de la ranolazine, sur un modèle de FA induite par le stretch chez le lapin.[210] Les auteurs ont mis en évidence que la capacité de la ranolazine à prolonger la période réfractaire effective atriale, le temps de conduction inter-atrial et la période réfractaire effective post-repolarisation, expliquaient son effet anti-arythmique sur le modèle de stretch. Par ailleurs, une récente étude a démontré que $Na_v1.5$ était sensible à l'étirement, et que la ranolazine inhibait ce phénomène.[215]

Le concept de longueur d'onde est difficile à interpréter dans le contexte des rotors, puisque celle-ci varie selon que l'on se situe à proximité ou non du core (conséquence de la diminution de la durée du PA et du ralentissement de la vitesse de conduction à proximité du centre de rotation). Par conséquent, nous avons préféré étudier l'effet de la ranolazine sur les propriétés et la dynamique des rotors, c'est-à-dire via la DF_{max} et le nombre de points de singularité. Nos résultats suggèrent que la capacité de la ranolazine à interagir sur le canal sodique n'était pas altérée en cas de FA persistante. De façon intéressante, nos données ont retrouvé que le nombre de points de singularité n'était réduit qu'en cas de FA paroxystique, probablement compte-tenu de la présence d'obstacles anatomiques (fibrose, conséquence du remodelage structurel induit par la FA) dans les cas de FA persistante. Ces obstacles sont autant de zones d'ancrage stabilisant les rotors, et permettant le fractionnement des fronts d'activation et la genèse de nouveaux rotors. Ceci explique leur persistance à un nombre invariable combiné à leur diminution de fréquence de rotation, malgré la perfusion de l'anti-arythmique. Des modélisations informatiques seront nécessaires afin de confirmer ces hypothèses.

C. Nouvelles avancées dans la prise en charge de la FA par l'ablation

1. Vers l'ablation ciblée des rotors

a. Généralités

La découverte en 1998 par Haissaguerre et al[5] du rôle des VP dans l'initiation des épisodes de FA a révolutionné la prise en charge de cette arythmie. Initialement, seule l'isolation de la VP supposée être l'initiatrice de la FA était effectuée. Cependant, le taux élevé de récurrences, la mise en évidence que les 4 VP pouvaient être à l'origine d'extrasystoles atriales initiatrices, les avancées technologiques et le perfectionnement technique des électrophysiologistes a modifié la procédure d'ablation, et actuellement, l'isolation des 4 VP est le « gold standard » dans la prise en charge non médicamenteuse de cette arythmie.

Par ailleurs, d'une ablation segmentaire ciblant directement les potentiels veineux pulmonaires, la procédure a évolué vers une ablation plus antrale, changement secondaire à la mise en évidence d'une complication rare mais grave, la sténose des VP. Par la suite, plusieurs travaux ont émis l'hypothèse que ce type d'ablation pouvait offrir un bénéfice supplémentaire en termes d'efficacité anti-arythmique, de part la réduction de la masse atriale active en FA, l'élimination de foyers pouvant se situer plus à distance des VP ou par la destruction des plexi ganglions environnants. L'utilisation de ces techniques combinée aux nouveaux outils actuellement à disposition des électrophysiologistes a permis d'améliorer l'efficacité de la procédure. Le dernier registre mondial sur l'ablation publié en 2010 par Cappato et al[6] reportait un taux de maintien du rythme sinusal sans et avec anti-arythmique respectivement de 74.9% et de 83.2%. Cependant, le succès de l'ablation de la FA persistante est plus faible, estimée entre 50 et 60%, et ce d'autant qu'elle est de longue durée.

Par ailleurs, le succès après une procédure unique d'ablation est faible, respectivement de 40%, 37% et 29% après un suivi d'1, 2 et 5 ans,[163] et le plus souvent, de nouvelles procédures sont nécessaires pour ré-isoler les VP, cibler de nouveaux foyers ou compartimentaliser l'oreillette (ligne d'ablation sur le toit de l'OG ou sur l'isthme mitral). Ceci a récemment valu à la FA persistante de longue durée le terme de « metastatic cancer of electrophysiology » (cancer métastatique de l'électrophysiologie) dans un éditorial de J.D. Burkhardt dans le *Journal of American College of Cardiology*.[216] Après plusieurs ablations, le taux de succès est amélioré, bien qu'imparfait (87%, 81% et 63% à 1, 2 et 5 ans).[163]

La FA est ainsi l'arythmie pour laquelle l'efficacité de l'ablation est la moins bonne, loin derrière les taux de succès de l'ablation de flutter ou de tachycardie jonctionnelle, avoisinant les 95%, et celui des tachycardies ventriculaires (TV).

Comment expliquer une telle disparité ? Il en va sans doute de la cible actuellement choisie de l'ablation de FA, à savoir les VP, qui sont le mécanisme d'initiation et non pas de maintien de l'arythmie.

Pour les arythmies citées précédemment (flutter, tachycardie jonctionnelle, TV), la technique d'ablation aujourd'hui utilisée par tous les centres consiste à cibler le mécanisme de maintien de ces arythmies réentrantes (à savoir, respectivement, l'isthme cavo-tricuspide, la

voie nodale lente ou un faisceau accessoire, et enfin l'isthme d'une TV) et non pas son mécanisme initiateur (extrasystoles atriales ou ventriculaires). Même s'il est théoriquement concevable que la suppression des extrasystoles initiatrices, quelque soient leur origine, soit suffisante à assurer l'absence de récidive de ces arythmies, on imagine aisément que le taux de maintien en rythme sinusal serait faible, compte tenu de la persistance du substrat arythmogène au sein du myocarde atrial ou ventriculaire. Seule l'ablation du circuit de réentrée permet d'assurer un taux élevé d'efficacité dans le cas précis de ces arythmies, ablation rendue aisée par le caractère fixe de ce substrat arythmogène.

A l'opposé, l'ablation de la FA telle qu'elle est réalisée de nos jours cible les VP, sources des ectopies initiant l'arythmie, et non pas son mécanisme d'entretien, tels que décrits dans la première partie du manuscrit, à savoir les ondes fibrillatoires organisées sous formes de rotors. En translatant notre expérience actuelle dans l'ablation de flutter, de tachycardie jonctionnelle ou de TV vers la FA, on peut être amenés à imaginer un taux de succès similaire sur le long terme en cas d'ablation des rotors. La difficulté d'une telle approche réside dans leur caractère mobile et leur capacité à facilement s'ancrer et se détacher d'obstacles anatomiques et de zones fonctionnellement réfractaires. La relativement bonne efficacité de l'ablation antrale au large des ostia pulmonaires s'explique probablement par le fait qu'en plus d'isoler les VP, celle-ci isole une partie de la masse atriale capable d'abriter des rotors. La probabilité de collision avec un obstacle et d'extinction est aussi plus élevée, rendant le maintien de l'arythmie dans le temps plus aléatoire, et favorisant le retour en rythme sinusal.

b. Systèmes permettant l'ablation des rotors

Le système de cartographie optique tel que nous l'avons utilisé dans nos études sur les cœurs explantés et perfusés sur un système de Langendorff[132] n'est pas réalisable chez l'homme compte tenu de la toxicité du produit fluorescent sensible au voltage injecté (Di-4-ANEPPS). Cette technique ne pourra être transposée chez l'homme qu'après la mise en évidence de molécules disposant des mêmes avantages techniques sans en posséder les effets secondaires. A défaut de disposer de telles molécules, des équipes ont essayé de nouveaux systèmes de cartographie pour mettre en évidence les rotors, parmi lesquelles celle de Michel Haissaguerre à Bordeaux et celle de Sanjiv Narayan à San Diego.

Le système utilisé par l'équipe bordelaise est dénommé le CardioInsight®. Il s'agit d'une veste composé de 252 électrodes disposée sur le patient. Un scanner thoracique est réalisé afin de détecter la position exacte de chacune de ces électrodes, les coordonnées géométriques étant définies en termes de distance par rapport aux structures cardiaques. Le signal reçu par chacune de ces électrodes lors de diastoles longues (afin d'éviter les artefacts liés à l'activation ventriculaire) est traité et analysé pour réaliser une cartographie de l'activité électrique en FA. Les rotors peuvent être visualisés et les trajectoires des cores suivies au cours de leurs rotations successives (Figure 45).

Haissaguerre et al ont défini 8 régions (VP gauches, VP droites, OG postérieure/basse, OG antérieure, toit de l'OG, isthme mitral, OD supérieure, OD inférieure) et démontré que des décharges focales et des rotors étaient retrouvés dans chacune d'entre elles, bien que plus fréquemment visualisés au niveau des VP et de l'OG postérieure. De façon très intéressante, il

a été mis en évidence que chez les patients atteints de FA persistante arrivant en rythme sinusal en salle d'électrophysiologie, seules 2 régions abritaient des rotors lorsque la FA était réinduite. Lorsque la FA était persistante depuis moins de 3 mois ou entre 4 et 6 mois, ceux-ci étaient retrouvés respectivement dans 3 et 4 régions des oreillettes. Au-delà de ce délai de 6 mois, presque toutes les régions étaient capables d'abriter des rotors.
Une fois les régions abritant le plus souvent les rotors identifiées, elles ont été ciblées par ablation. En cas de FA persistante depuis moins de 6 mois, le rythme sinusal était rétabli chez près de 86% des patients après ablation des rotors seuls (sans isolation veineuse pulmonaire). L'importance de l'ancienneté de la FA persistante dans le nombre de régions abritant des rotors était également retrouvée dans les résultats de l'ablation, puisque celle-ci ne permettait le retour en rythme sinusal respectivement que dans près de 60%, 30% et 12% des FA persistante de 7 à 9 mois, de 10 à 12 mois, et supérieures à 1 an. Seule la réalisation de lignes (toit de l'OG, isthme mitral) permettait à ce stade d'arrêter l'arythmie.

Pour le moment, seule une étude a été publiée dans le domaine de la cartographie de l'activité atriale en FA.[217] D'autres travaux seront nécessaires pour connaitre l'efficacité de l'ablation guidée par ce système.

L'inconvénient de cette technique est qu'elle n'explore principalement que l'activité épicardique des oreillettes. Or, le muscle atrial est une structure tridimensionnelle pouvant abriter des rotors également endocardique, voire même intra-muraux, qui ne seront pas détectés par le système.

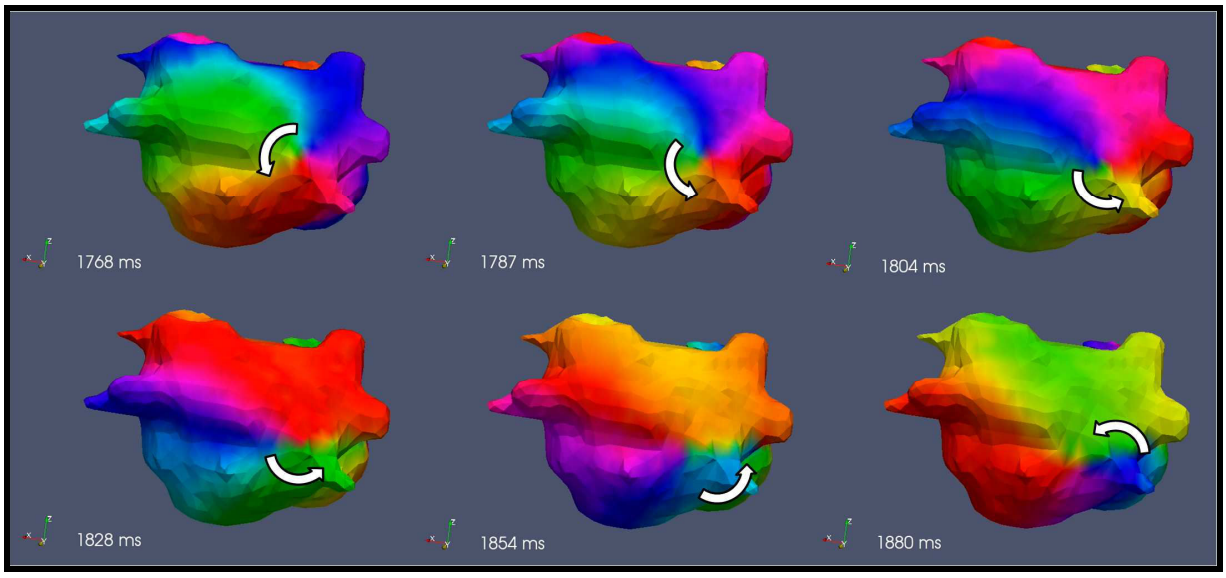

Figure 45 : Cartographie atriale épicardique en FA réalisée par le système CardioInsight®. Un rotor tournant dans le sens anti-horaire et ancré au niveau de la veine pulmonaire inférieure droite (VPID) est visible sur les clichés successifs (de gauche à droite, et de bas en haut ; vue postérieure de l'OG). Modifié d'après Haissaguerre et al.[217]

Le deuxième système actuellement disponible pour cartographier les sources maintenant la FA est le système Topera® utilisant la technique de « Focal Impulses and Rotor Modulation » (FIRM). Un cathéter sphérique (« basket cathéter ») composé de 64 électrodes est introduit par voie veineuse fémorale dans l'OD ou l'OG (par voie trans-septale) et

permettant, après traitement du signal, d'effectuer une cartographie de l'activité atriale en FA (Figure 46).

Dans l'étude CONFIRM, Narayan et al ont démontré que des sources maintenant la FA étaient détectables chez 97% des patients en FA paroxystique ou persistante.[218] L'ablation de ces sources en plus de l'isolation veineuse conventionnelle permettait le maintien du rythme sinusal chez 82.4% des patients contre 44.9% dans le groupe ne bénéficiant que de l'ablation conventionnelle. Une récente étude a par ailleurs démontré que le succès de l'ablation de la FA était supérieur lorsque l'ensemble des sources était éliminé, qu'elles le soient de façon dirigée par le FIRM ou de façon coïncidente par l'isolation veineuse pulmonaire conventionnelle ; intermédiaire si seulement certaines sources étaient ciblées ; et faible si toutes étaient « ratées » par l'ablation.[219]

L'inconvénient majeur de cette technique est qu'elle ne fournit des informations que sur l'activation endocardique des oreillettes, et qu'aucune information concernant l'activité épicardique ou intra-murale n'est disponible. Par ailleurs, une des limites de la technique réside dans le contact entre le basket cathéter et les oreillettes, celui-ci pouvant ne pas être en contact et n'enregistrant alors qu'un « far-field » de l'activité atriale.

Par ailleurs, contrairement à ce qui a été décrit sur le plan expérimental (tant sur les travaux de simulations que chez l'animal) et par l'équipe bordelaise, les rotors retrouvés par Narayan et al sont fixes ou très peu mobiles. Afin d'en réaliser l'ablation, des tirs « ponctuels » de RF étaient effectués (contrairement à la technique utilisée par l'équipe bordelaise ciblant des régions abritant préférentiellement les rotors). Ceci est en contradiction avec ce qui est connu aujourd'hui sur les rotors qui, du fait de la présence d'un gap excitable et de l'hétérogénéité du substrat, sont mobiles au sein des oreillettes.

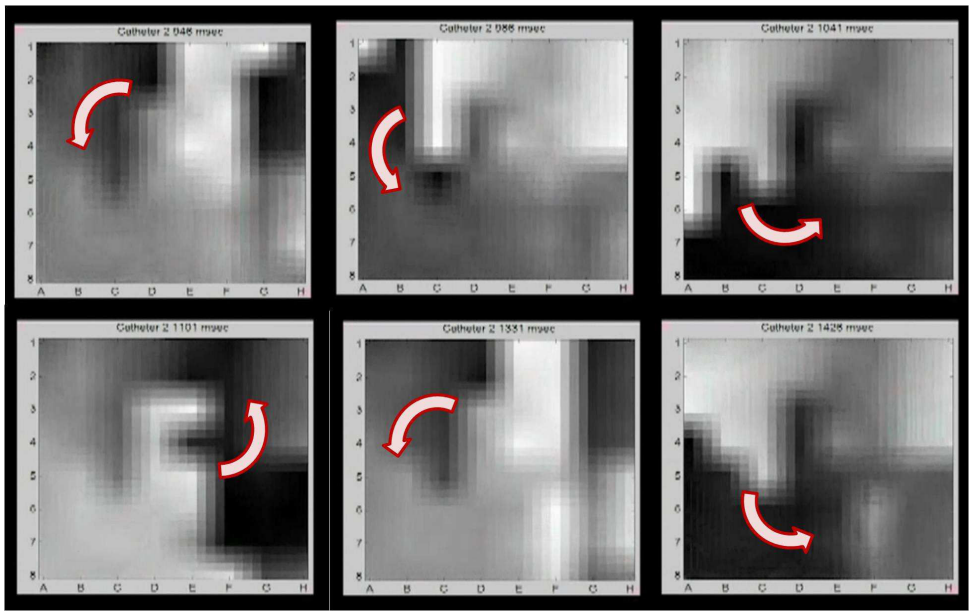

Figure 46 : Cartographie atriale endocardique en FA réalisée par le système Topera®. Un rotor tournant dans le sens anti-horaire est visible sur les clichés successifs (de gauche à droite, et de bas en haut ; vue de l'endocarde postérieure de l'OG). Modifié d'après Narayan et al.[220]

Des études à moyen et à long terme seront nécessaire afin d'évaluer l'impact de ces deux techniques ainsi que de déterminer le type de population qui en tirerait le plus le bénéfice. Les patients en FA paroxystique, chez qui la maladie est principalement dépendante des « triggers » (ectopies veineuse pulmonaire), pourraient ne bénéficier que d'une isolation veineuse pulmonaire. A l'opposé, les patients en FA persistante, qui ont en plus des « triggers » une maladie du substrat (remodelage électrophysiologique et structurel ayant favorisé l'accélération et la stabilisation des rotors) pourraient probablement bénéficier d'une stratégie mixte, associant isolation veineuse pulmonaire et ablation ciblée des rotors.

c. Etude préliminaire sur l'efficacité de l'ablation des rotors

Afin d'évaluer l'effet de l'ablation des zones abritant les rotors, nous avons menés une étude préliminaire sur 5 cœurs de moutons isolés et perfusés sur un système de Langendorff. De la FA induite par le stretch était induite comme décrit précédemment.[132]

Des EGM bipolaires des 4 VP et des auricules droit et gauche étaient enregistrés en FA. Par ailleurs, une cartographie optique de la paroi latérale de l'OG était réalisée afin d'étudier la dynamique fibrillatoire, d'effectuer et analyser en direct des cartes de phase pour repérer les zones abritant le plus souvent les points de singularité (correspondant aux « wavebreaks », première étape dans la formation des rotors), et de déterminer la DF_{max}.

Une fois ces régions déterminées, une ablation par RF était effectuée pour évaluer les changements dans la dynamique de l'activité fibrillatoire (5-15W, 30-60 sec).

Après avoir localisé les rotors et pratiqué une ablation sur les zones d'intérêt sur la paroi latérale de l'OG (Figure 47), nous n'avons pas observé de retour en rythme sinusal (0/5, ablation de 19 sites à densité élevée de points de singularité). Cependant, l'ablation de ces zones a provoqué un changement de localisation de la région abritant les rotors puisque ceux-ci se sont préférentiellement relocalisés dans les régions péri-veineuses pulmonaires (4/5). Une diminution de la DF_{max} de la paroi latérale de l'OG était observée (de 13.2±0.98 à 9.23±2.17 Hz, n=5), alors que celles de l'OD et des VP était paradoxalement augmentées (respectivement de 8.92±0.6 à 10.8±0.37 Hz et de 9.23±2.17 à 13.25±2.86 Hz, n=5, $p<0.05$). Enfin, une disparition du gradient OG-OD était mise en évidence, passant de 4.28 Hz avant l'ablation à 0.97 Hz après celle-ci ($p<0.05$).
Par ailleurs, les sites à haute densité de points de singularité et de DF_{max} ne coïncidaient pas et n'étaient adjacents que sur 2/5 cœurs.

Ces expériences préliminaires ont démontré que l'ablation des sites abritant les rotors résultait en une relocalisation de ceux-ci vers d'autres régions et provoquait une modulation importante de la DF_{max}. Des études plus détaillées, comprenant une cartographie extensive des oreillettes (notamment l'endocarde postérieur de l'OG) seront nécessaires afin d'évaluer la meilleure stratégie d'ablation des sources maintenant la FA.

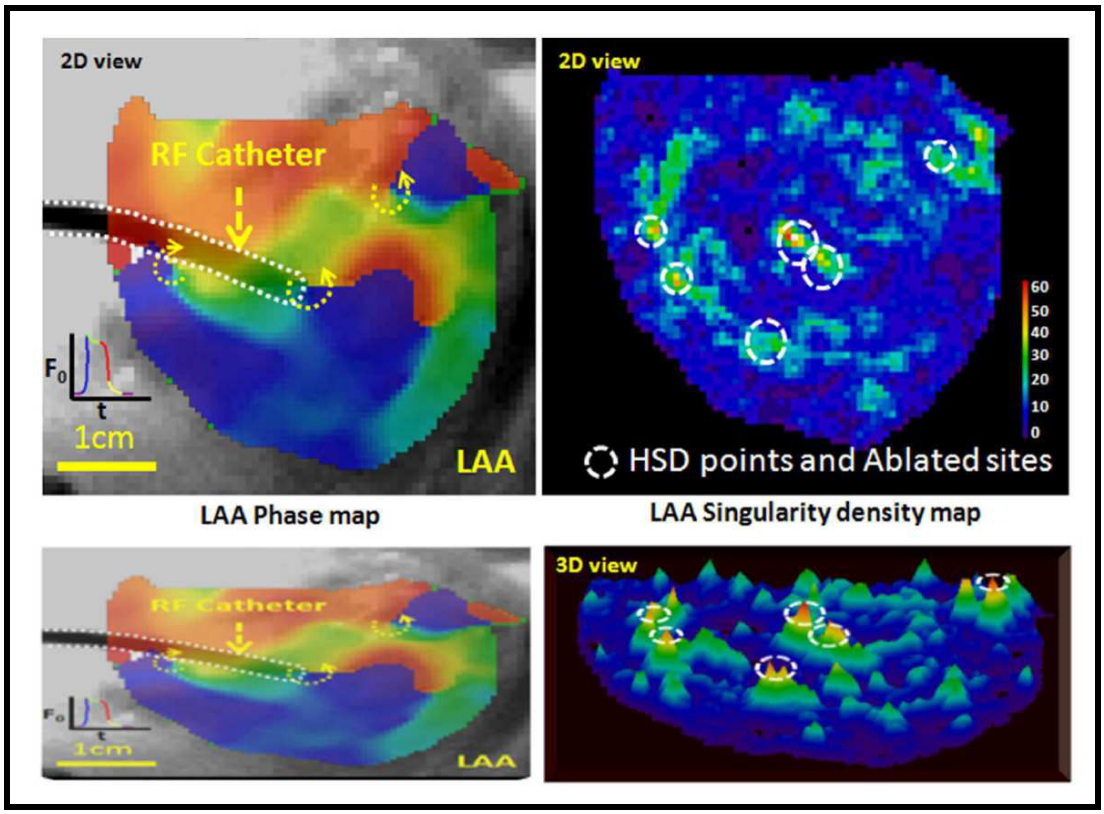

Figure 47 : Gauche : carte de phase de l'épicarde de la paroi latérale de l'OG mettant en évidence 3 rotors. L'anatomie atriale ainsi que la sonde d'ablation sont visibles par transparence. Droite : Carte montrant la densité des points de singularité sur chaque pixel analysé en FA, et correspondant aux zones ablatées lors de l'expérience.

2. Vers l'amélioration des techniques ablatives

a. Généralités

L'ablation par RF est aujourd'hui la technique la plus utilisée compte tenu de son efficacité pour réaliser une isolation veineuse pulmonaire. Cependant, cette technique est complexe (imposant une ablation point par point), chronophage et expose à des complications rares mais sévères.[6] De nouvelles énergies sont actuellement utilisées quotidiennement par de très nombreux centres, telles que la cryothérapie, et d'autres sont à l'étude (laser, ultrasons,…). Des technologies récentes, tels que la robotique ont également été testés pour faciliter le positionnement des cathéters dans l'OG.

L'ablation par ballon laser (HeartLight™, CardioFocus Inc.;LB, CardioFocus Inc., Marlborough, MA, USA) permet une ablation point par point sous contrôle de la vue via un endoscope intégré. Cette technique est disponible en Europe, mais non disponible aux USA pour le moment, et quelques études ont rapporté son efficacité et sa sécurité d'utilisation.[221, 222] Bordignon et al ont démontré que l'isolation veineuse pulmonaire était réalisable dans 98.9% des cas, avec des temps de procédure et de fluoroscopie courts (respectivement 144±33 minutes et 15±6 minutes). Une parésie du nerf phrénique (PNP) est survenue chez 4.2% des patients et après une période de 3 mois de blanking, 27% des patients ont présenté une récurrence de FA.[221] Dans ce travail, les auteurs ont comparé le ballon laser à la cryoablation et n'ont pas mis en évidence de différence enter termes d'efficacité ou de sécurité entre les deux techniques.

L'ablation par ultrasons a récemment été testée dans une population de patients atteints de FA paroxystique. Cette technique est basée sur l'utilisation d'un ballon couplé à une énergie ultrasons à haute intensité (« High intensity focused ultrasound », ProRhythm®, Ronkonkoma, NY, USA) qui, placé dans l'ostium veineux pulmonaire, permet une ablation circonférentielle en une application sans nécessité de recourir à un système de cartographie tridimensionnelle. L'avantage de cette technique est qu'elle ne nécessite pas un contact parfait avec le tissu atrial pour réaliser une lésion atriale. Dans une étude comprenant 32 patients, Metzner et al ont démontré qu'une isolation veineuse pulmonaire était possible dans 87% des cas.[223] Cependant, seuls 56% des patients ne présentaient pas de récurrence après un suivi médian de plus de 3 ans. Chez les 9 patients ayant bénéficié d'une nouvelle procédure d'ablation, 20 VP présentaient une reconnexion (55%).

L'ablation par cryoballon (CB) est actuellement utilisée dans de nombreux centres comme alternative à l'ablation par RF pour les patients en FA paroxystique. Cette technique permet une isolation simple et rapide des VP, parfois même en une seule application. [224-226] Par ailleurs, la courbe d'apprentissage est plus rapide que pour l'ablation par RF. Cependant, elle ne doit être utilisée que chez des patients ciblés, présentant une forme focale pure de la maladie, puisque la réalisation de lignes parfois nécessaires chez les patients présentant une forme persistante de FA n'est pas possible. L'efficacité immédiate et à 1 an est similaire à celle de la RF,[227-229] particulièrement en réalisant une ablation plus antrale via la technique du « single big 28-mm CB » décrite par Chun et al.[224] La complication principale de la cryoablation au ballon, la PNP, survient plus fréquemment lors de l'utilisation de ballons de petite taille (23-mm), qui permettent la réalisation de lésions plus distales dans les veines pulmonaires droites.

Le cahier des charges de l'outil d'ablation parfait allie simplicité d'utilisation, reproductibilité interindividuelle, faible coût, assurance de la réalisation d'une véritable lésion transmurale durable et sécurité avec un taux de complications majeures faible. Les nouvelles techniques actuellement à l'étude ainsi que le perfectionnement des outils aujourd'hui à notre disposition pourraient sans doute permettre un jour d'atteindre un tel niveau d'exigence.

b. Hypothèse de travail

La première génération de CB, l'Arctic Front® CB (ARC-CB, Medtronic, Inc., Minneapolis, MN), disposait d'une zone de réfrigération située à l'équateur du CB. Par conséquent, même en cas d'occlusion veineuse parfaite, le CB devait être parfaitement centré sur l'antre veineux afin de réaliser une lésion circonférentielle. De nombreuses équipes ont mis en évidence cet inconvénient,[230] amenant ainsi la société Medtronic à développer un CB de deuxième génération, l'Arctic Front Advance (ARC-Adv) CB, équipé d'un système de réfrigération avec une disposition plus homogène sur l'ensemble de la moitié distale du CB (Figure 48).[230]

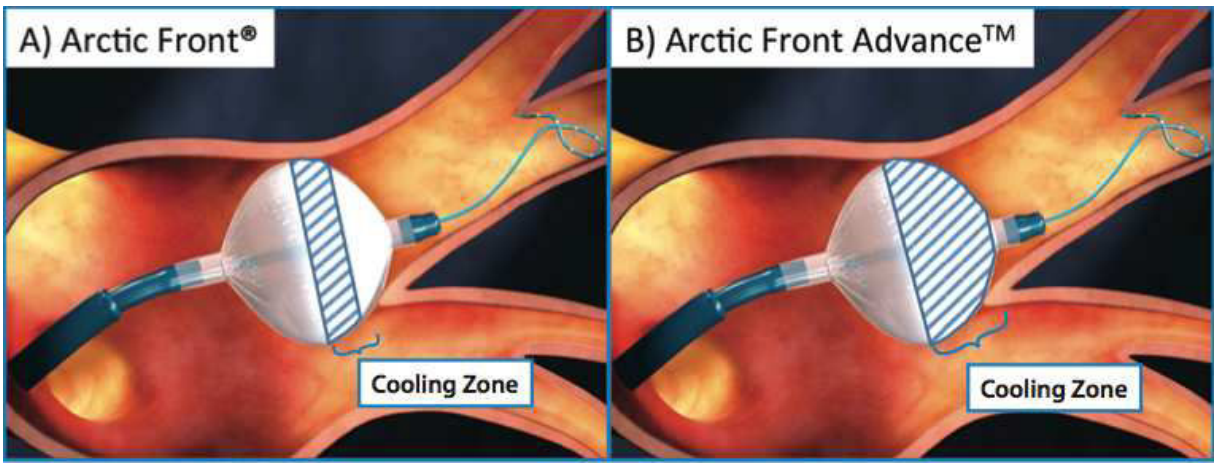

Figure 48 : Différence de localisation de la zone réfrigérante entre les deux CB. Seule la partie équatoriale de l'ARC-CB était réfrigérée (A), contrairement à l'ARC-Adv-CB qui dispose d'une réfrigération sur l'ensemble de sa moitié distale. Ceci explique pourquoi un alignement parfait entre l'ARC-CB et la veine était nécessaire pour assurer une isolation complète.
D'après *http://www.eplabdigest.com/articles/US-Multicenter-Examination-New-Cryoballoon-Early-Experience-Procedural-Enhancements-Treatme*

Ainsi l'isolation veineuse pulmonaire peut tout de même être réalisée, même en cas d'alignement imparfait ou dans les cas d'anatomie veineuse atypique, augmentant de ce fait l'efficacité globale du CB.[231, 232] Cependant, de part l'émission plus profonde de la cryoénergie et de la persistance d'un « glaçon » (ice cap) de taille plus importante après déflation du CB,[233] une augmentation du risque de PNP peut être attendue.

Afin d'évaluer l'efficacité et la sécurité d'utilisation de ce nouveau CB, nous l'avons comparé au CB d'ancienne génération. De plus, nous avons testé l'efficacité d'un prédicteur de survenue de PNP.

c. Méthodes

Entre août 2011 et juillet 2013, les patients atteints de FA paroxystique symptomatique résistante à plus d'un anti-arythmique ont été successivement inclus dans cette étude. L'ARC-Adv-CB n'étant pas disponible dès le début de l'étude, les patients inclus entre août 2011 et septembre 2012 ont bénéficié d'une ablation par l'ARC-CB, alors que ceux inclus entre août 2012 et juin 2013 ont été traités par l'ARC-Adv-CB.

Nous avons utilisé la technique du « single big 28-mm CB » telle que décrite par Chun et al pour réaliser l'isolation veineuse pulmonaire.[224] La disparition PVP était évaluée lors du tir grâce à un cathéter Achieve^{TM} avancé le long du CB jusqu'à l'orifice veineux pulmonaire. Une application de 300 sec pour l'ARC-CB et de 240 sec pour l'ARC-Adv-CB était réalisée, tel que recommandé par Medtronic. Une application supplémentaire était effectuée après l'obtention de l'isolation veineuse pulmonaire, sauf en cas de survenue d'une PNP lors d'un tir précédent.

Avant l'ablation des veines droites, un cathéter quadripolaire était positionné dans la VCS pour stimuler le nerf phrénique (NP) lors de l'application de la cryoénergie à 20mA pour un cycle de 2000ms. En cas de diminution ou d'arrêt de la contraction hémidiaphragmatique droite, l'application était immédiatement stoppée et le CB déflaté. Dans un sous-groupe de 40 patients traité par l'ARC-Adv-CB, nous avons estimé avant l'application de la cryoénergie la distance séparant a) la ligne verticale passant par l'extrémité distale du cathéter de stimulation du NP situé dans la VCS et b) le bord latéral du CB dans une vue antéro-postérieure, en utilisant la le diamètre équatorial du CB (28-mm) comme référence (Figure 49). Pour faciliter l'évaluation des rapports entre le cathéter de stimulation du NP et le CB, nous avons divisé la région entourant le CB en 4 zones (Figure 49 ; zone A : partie située à droite du CB vers les veines pulmonaires ; zone B1 : moitié distale du CB ; zone B2 : moitié proximale du CB ; zone C : partie située à gauche du CB).

Le critère d'évaluation primaire était le taux d'efficacité de la première application. Les critères secondaires étaient a) l'efficacité globale des CB, b) le temps et la température observées lors de l'isolation veineuse pulmonaire, c) la température minimale atteinte, d) la durée moyenne de procédure et de fluoroscopie et enfin e) le taux de complications, dont la survenue de PNP.

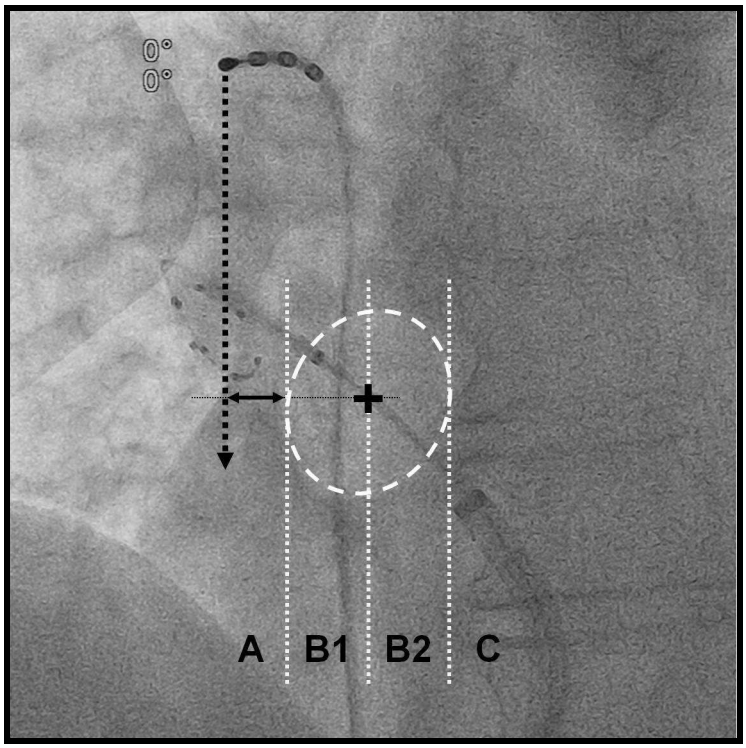

Figure 49 : Analyse de la position du cathéter de stimulation du NP par rapport au CB. En plus de la distance entre le cathéter et le CB (flèche noire), l'espace entourant le CB était séparée en 4 zones (cf texte pour la description des zones).

d. Résultats

Un total de 147 patients a été inclus dans l'étude, 66 ayant bénéficié d'une ablation par l'ARC-CB et 81 traités par l'ARC-Adv-CB. Les caractéristiques cliniques des patients étaient similaires à l'inclusion, s'agissant dans les 2 groupes de patients relativement jeunes, sans cardiopathie sous-jacente et à risque thrombo-embolique faible (Tableau 2).

Après exclusion des troncs communs gauches et droits, l'étude a respectivement porté sur un total de 252 et de 310 VP traitées par l'Arc-CB et l'ARC-Adv-CB.

Les principaux résultats des procédures d'ablation sont résumés sur le Tableau 3. L'ensemble des VP a été isolé à la fin de chaque procédure, sans nécessité d'utiliser le ballon de 23-mm ou un cathéter supplémentaire de cryoablation ou de RF.

Efficacité de l'ARC-Adv-CB

La première application de cryoablation a permis d'isoler respectivement 205/252 (81.3%) et 280/310 (90.3%) VP traitées par le ARC-CB et le ARC-Adv-CB (p=0.003). Un gain d'efficacité était retrouvé sur l'ensemble des VP, bien que n'étant significatif que pour la VPIG (85.7 versus 97.3%, p=0.03). Une moyenne de 1.3±0.7 applications (de 1 à 6) pour l'ARC-CB et de 1.1±0.3 (de 1 à 3) pour l'Arc-Adv-CB étaient nécessaires pour obtenir l'isolation veineuse (p<0.001), différence portant principalement sur les veines gauches (1.5±1.0 versus 1.2±0.5 pour la VPSG, p=0.021; et 1.2±0.6 versus 1.0±0.2 pour la VPIG; p=0.009).

La température minimale atteinte (-49.7±7.6° C pour le groupe ARC-CB versus -49.3±7.3° C pour le groupe ARC-Adv-CB; p=0.558), le grade d'occlusion veineuse (3.9±0.4 dans les 2 groups; p=0.848), le taux de visualisation de PVP lors de l'application initiale (sur 173 PV=68.6% avec l'ARC-CB sur 216 PV=69.7% avec l'ARC-Adv-CB ; p=0.712) et le

nombre de PVP visualisés (5.6±1.9 électrodes sur les 8 pôles de l'Achieve cathéter pour le groupe ARC-CB versus 5.4±2.0 électrodes pour le groupe ARC-Adv-CB ; p=0.397) étaient similaire pour les deux CB.

Enfin, le temps de procédure était raccourci en moyenne de 13 minutes (de 120.1±24.1 à 107.4±24.1 min ; p=0.002) et la durée de fluoroscopie d'environ 3 minutes (de 28.7±9.9 à 25.0±9.2 min ; p=0.02).

L'isolation veineuse pulmonaire était visualisée en direct dans 53.2% et dans 60.3% des cas pour les groupes ARC-CB et ARC-Adv-CB (p=0.106, Tableau 4).

	ARC-CB	**ARC-Adv-CB**	**P**
N	66	81	
Genre (M/F)	48/18	54/27	0.540
Age	60.9±10.3	59.4±9.5	0.35
Score CHADS-vasc	1.1±0.9	1.1±1.1	0.880
Années depuis le début de la FA	6.0±5.6	7.9±7.6	0.095
Durée des épisodes			
<24h	55 (83.3)	61 (75.3)	0.326
>24h	11 (16.7)	20 (24.7)	0.326
Nombre d'anti-arythmiques testés	2.6±1.1	2.5±1.1	0.810
FEVG (%)	65.8±5.5	64.7±7.1	0.328
Dilatation atriale			
Non dilatée	43 (65.1)	52 (64.2)	0.952
Légèrement dilatée	11 (16.7)	16 (19.7)	0.790
Modérément dilatée	8 (12.1)	8 (9.9)	0.866
Sévèrement dilatée	4 (6.1)	5 (6.2)	0.751

Tableau 2: Caractéristiques des patients à l'inclusion.

	ARC-CB	ARC-Adv-CB	P
VP (N)	252	310	
Occlusion (/4)	3.9±0.4	3.9±0.4	0.848
Visualisation de PVP (%)			
Globale	**173 (68,6)**	**216 (69,7)**	0.712
VPSG	58 (92.1)	71 (95.9)	0.548
VPIG	47 (74.6)	60 (81.1)	0.362
VPSD	51 (80.9)	61 (75.3)	0.544
VPID	17 (27.0)	24 (29.6)	0.871
Electrodes (/8)	5.6±1.9	5.4±2.0	0.397
Température minimale (°C)			
Globale	**-49.7±7.6**	**-49.3±7.3**	0.558
VPSG	-51.2±6.9	-48.4±7.1	**0.023**
VPIG	-46.8±7.3	-47.3±5.6	0.670
VPSD	-52.6±7.2	-52.0±7.5	0.590
VPID	-48.2±7.6	-49.4±7.9	0.355
Apllications necessaries à l'isolation (N)			
Globale	**1.3±0.7 (1-6)**	**1.1±0.35 (1-3)**	**<0.001**
VPSG	1.5±1.0	1.2±0.5	**0.021**
VPIG	1.2±0.6	1.0±0.2	**0.009**
VPSD	1.2±0.6	1.1±0.3	0.099
VPID	1.1±0.4	1.1±0.3	0.268
Isolations avec une seule application (%)			
Globale	**205 (81.3%)**	**280 (90.3%)**	**0.003**
VPSG	43 (68.2%)	61 (82.4%)	0.083
VPIG	54 (85.7%)	72 (97.3%)	**0.030**
VPSD	52 (82.5%)	71 (87.6%)	0.532
VPID	56 (88.9%)	76 (93.8%)	0.447

Tableau 3. Paramètres de la procedure.

	ARC-CB	ARC-Adv-CB	P
N	134	187	
Visualisation de l'isolation	53.2%	60.3%	0.106
Temps à l'isolation (sec)			
Globale	**51.7±33.8**	**40.4±25.2**	**<0,001**
VPSG (40/57)	56.9±34.6	44.0±20.1	**0.023**
VPIG (40/58)	50.0±33.9	33.9±27.3	**0.011**
VPSD (42/52)	46.3±32.1	40.7±23.3	0.326
VPID (12/20)	59.1±36.8	47.9±33.5	0.385
Temperature à l'isolation (°C)			
Globale	**-36.1±10.3**	**-32.3±10.2**	**0.001**
VPSG (40/57)	-39.4±8.1	-35.2±7.5	**0.01**
VPIG (40/58)	-33.4±10.4	-26.2±11.2	**0.002**
VPSD (42/52)	-34.7±12.3	-35.6±9.6	0.675
VPID (12/20)	-38.6±6.0	-32.6±8.2	**0.038**

Tableau 4. Temps et température à l'isolation veineuse pulmonaire.

La durée moyenne avant isolation veineuse était de 52±34 sec (de 10 à 176 sec) lors de l'utilisation de l'ARC-CB et de 40±25 sec (de 13 à 185 sec) avec l'ARC-Adv-CB (p <0.001; Figure 50). Par conséquent, la température à l'isolation était significativement moins négative avec le nouveau ballon (-32±10°C, de -53 à +17) versus -36±10°C (de -57 à +10; p=0.001). Un bénéfice pour les veines gauches et la VPID était observée, mais pas pour la VP supérieure droite (VPSD).

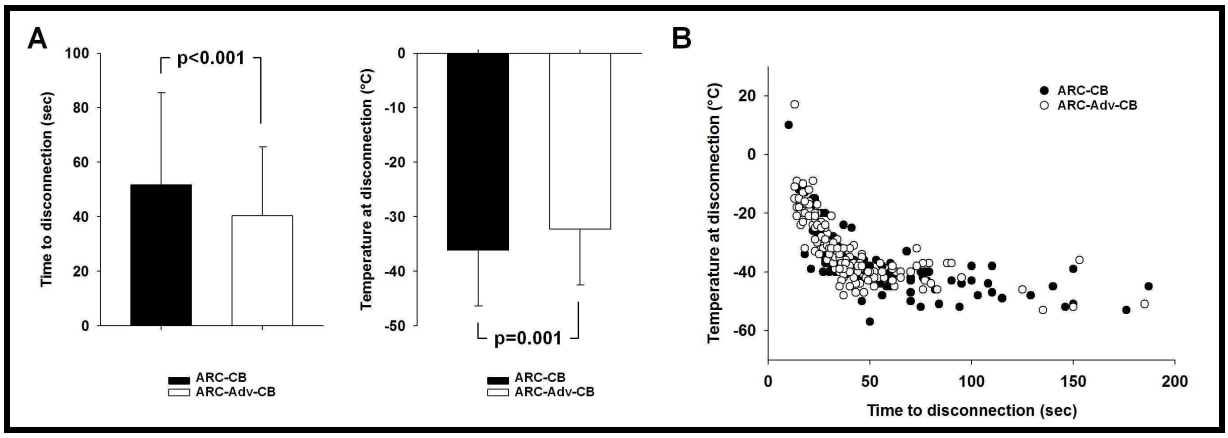

Figure 50 : Temps et température lors de l'isolation veineuse pulmonaire. A. Valeurs moyennes lors de la déconnection des VP. B. Graphique représentant l'ensemble des déconnections veineuses pulmonaires observées dans l'étude (chaque point représentant une VP) pour les deux CB.

Incidence des PNP

Sur les 288 isolations veineuses droites, 29 (10.1%) ont été compliquées d'une PNP, 7/126 (5.6%) avec l'ARC-CB et 22/162 (13.6%) avec l'ARC-Adv-CB (p=0.044), correspondant respectivement à 10.6 et 24.4% des patients (p=0.048).

La plupart des PNP sont survenues lors des applications sur la VPSD (71% avec l'ARC-CB et 77% avec l'ARC-Adv-CB). Seuls deux patients chez qui est survenue une PNP lors de l'application sur la VPSD ont eu une récidive lors de l'application sur leur VPID.

Les PNP survenaient environ 30 secondes plus tôt avec le nouveau CB, bien que cette différence ne soit pas significative (140±43 sec versus 166±66 sec, p=0.238). Toutes étaient transitoires et cédaient spontanément entre 0.5 et 20 minutes, et par conséquent, aucune PNP définitive n'est survenue au cours de l'étude.

Enfin, il est important de noter que l'isolation veineuse pulmonaire était survenue systématiquement avant l'apparition de la PNP, et que l'isolation a persisté jusqu'à la fin de la procédure malgré la réalisation d'une application plus courte.

Puisque la survenue d'une PNP mettait en jeu la sécurité de l'ablation lors de l'utilisation de l'ARC-Adv-CB, nous avons examiné dans un sous-groupe de 40 patients (80 VP droites) si la distance séparant le bord latéral du CB et l'extrémité distale du cathéter de stimulation du NP (CB-NP, figure 1) était prédictive de la survenue d'une PNP. La distance CB-NP moyenne chez les patients présentant une PNP était de -4.9±5.5 mm (médialement vers la gauche du ballon) versus 8.6±8.9 mm (latéralement vers la droite du ballon) chez ceux

n'ayant pas eu de PNP (p<0.001, Figure 51A). L'analyse de la distance par une courbe ROC (Figure 51B) a permis de démontré que les meilleures sensibilité et spécificité étaient obtenues à la valeur de 0mm (Se=92.3%, 95% CI 63.9-98.7; Spe=86.6%, 95% CI 76.0-93.7; aire sous la courbe = 0.91; 95% CI 0.82-0.96; p<0.0001).

En corrélant la survenue de PNP en fonction de la zone où se situait le cathéter de stimulation du NP (Figures 49 et 52), nous avons observé que sur 12 des 13 PNP, ce cathéter se situait en zone B1 (Figure 51A). Parmi les 67 applications non compliquées de PNP, le cathéter traversait la zone B1 pour 7 applications et une autre zones dans les 60 cas restants (Figure 51A). Ainsi, la probabilité estimée de survenue d'une PNP lorsque le cathéter de stimulation était localisé dans la zone B1 était élevée (Se=92.3%; Spe=89.9%; valeur prédictive négative=98.4 et valeur prédictive positive=63.2%).

Autres complications liées à la procédure

Une fistule artério-veineuse est survenue dans chacun des groupes, ne nécessitant pas de prise en charge chirurigcale puisque résolutives spontanément après 1 mois de suivi. Par ailleurs, un décollement péricardique asymptomatique a été retrouvé chez un patient traité par l'ARC-Adv-CB.

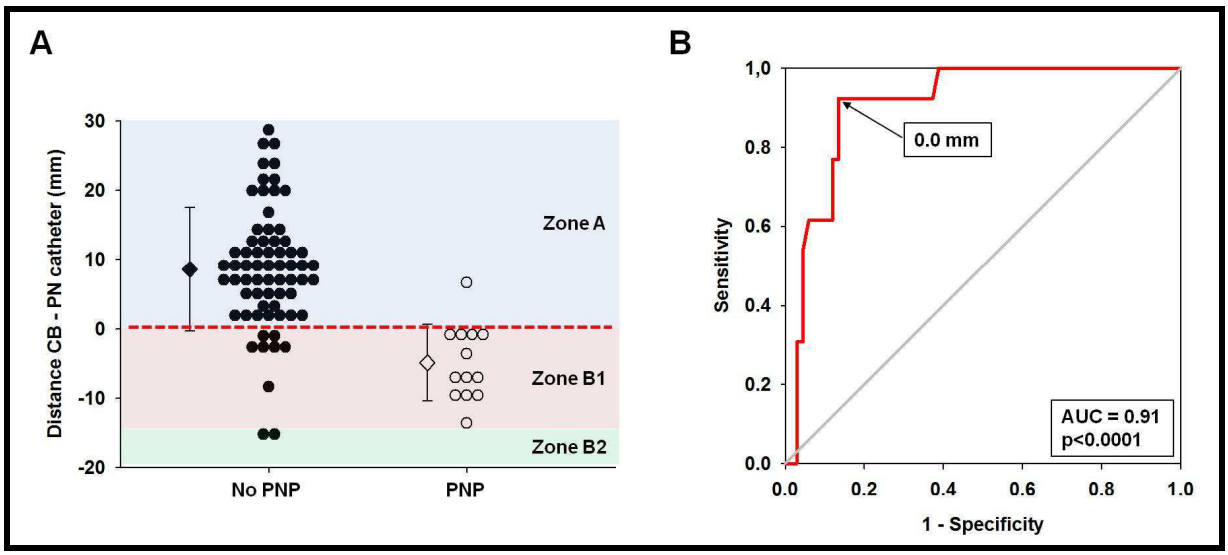

Figure 51 : Incidence de survenue d'une PNP lors de l'utilisation de l'ARC-Adv-CB. A. Distance CB-NP chez les patients ayant présenté ou non une PNP. B. Analyse ROC de la distance CB-NP montrant les sensibilité et spécificité optimales pour la valeur de 0mm.

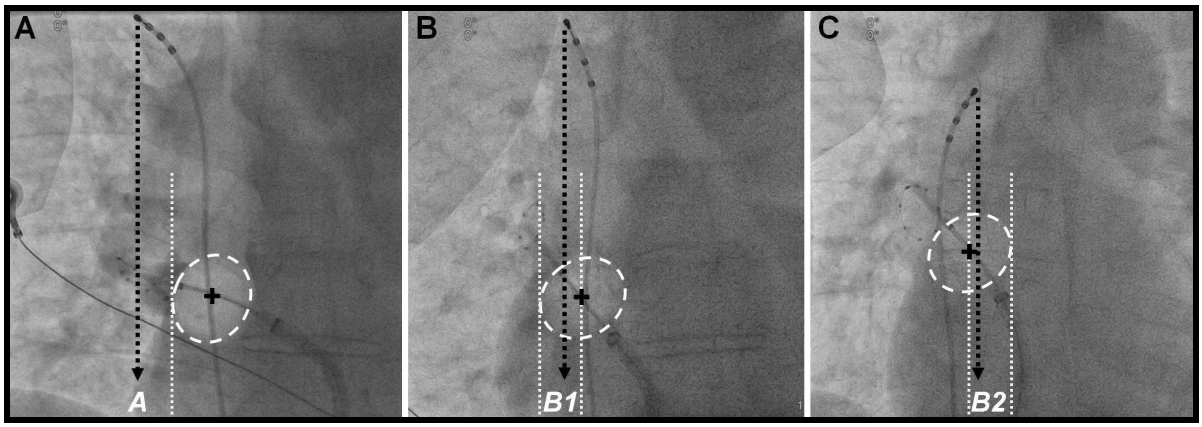

Figure 52 : Relations entre le CB et le NP en vue fluoroscopique antéro-postérieure lors d'une application sur la VPSD. A : Zone A. B : Zone B1. C : Zone B2.

e. Discussion

Cette étude a permis de démontrer que l'efficacité globale de l'ARC-Adv-CB pour isoler les VP des patients atteints de FA paroxystique était plus élevée que celle de l'ARC-CB. Un nombre significativement plus faible d'applications était nécessaire pour isoler les VP, résultant en des procédures plus courtes et à un recours moins fréquent à la fluoroscopie. Dans la plupart des cas, l'isolation veineuse pulmonaire était directement visualisée, permettant ainsi d'évaluer la durée et la tempréature de l'application à l'isolation, qui étaient alors significativement plus courte et moins négative. Cependant, une majoration du risque de PNP a été mise en évidence lors de l'utilisation de l'ARC-Adv-CB, risque dont l'incidence peut être estimée par la distance CB-NP.

Comparé avec l'ARC-CB, l'ARC-Adv-CB possède deux fois plus de points d'injection, ceux-ci étant localisés de façon à permttre une distribution homogène du gaz réfrigerant sur l'ensemble de la moitié distale du CB. Cette meilleure répartition de l'énergie augmente la zone de contact entre le CB et la VP. Ceci explique la meilleure efficacité du ballon, étant donné qu'il permet une isolation veineuse même en cas de mauvais alignement entre le CB et la veine, ou en cas d'anatomie atypique. Par ailleurs, l'ARC-Adv-CB provoque la formation d'un « glaçon » (phénomène de l'« ice cap ») de taille plus importante qui explique également l'augmentation d'efficacité du CB,[233] puisque même en cas de mauvais contact avec la VP, la formation de ce bouchon de glace empêche le réchauffement de la VP et favorise l'isolation veineuse.

Cette augmentation d'efficacité de l'ARC-Adv-CB est cependant grévée d'un risque de PNP transitoire majoré. Les précédentes études ayant analysé ce CB ont rapporté des résultats contradictoires, Casado-Arroyo et al[234] retrouvant une incidence plus élevée qu'avec l'ancien ballon, alors que Fürnkranz et al[235] ne retrouvaient aucune différence entre les 2 CB. Cette différence d'incidence peut probablement s'expliquer par la définition de la PNP utilisée par les auteurs, certains ne rapportant que les PNP persistantes alors que d'autres en rapportent les persistantes et les transitoires.

Dans cette étude, nous avons retrouvé un facteur prédictif simple et fiable de survenue de PNP. La projection du cathéter de stimulation du NP sur la zone B1 (correspondant à la

moitié distale du CB, c'est-à-dire à la zone d'injection du gaz réfrigérant) a été ainsi démontrée comme étant un excellent prédicteur de survenue de PNP. Parmi les 13 cas de PNP, seul un ne montrait pas le cathéter dans cette zone, possiblement en lien avec une variante anatomique (course oblique du NP).

Les relations entre le NP et la VPSD sont variables et difficile à prédire avant la procédure d'ablation. L'artère péricardio-phrénique droite, qui suit le NP droit le long de son trajet peut etre identifée chez près de 20% des patients par scanner.[236, 237] Une distance courte entre la VCS et la VPSD est également corrélée avec la survenue de PNP.[238] Cependant, la localisation précise du NP est variable pour chaque patient ; de plus, la force de poussée utilisée pour occlure la VPSD lors de l'application peut entrainer un changement des rapport entre les différentes structures anatomiques de la région. Par ailleurs, une chute importante de de température (température <-41°C après 30 secondes d'application) a également été démontrée comme prédisant la survenue d'une PNP.[238] Cependant, ce critère est imparfait puisqu'il n'aurait permis de prédire qu'une seule PNP des 29 survenues dans notre population.

L'utilisation de notre facteur prédictif de PNP nous a permis d'éviter la survenue d'une PNP persistante. En effet, en cas de présence du cathéter de stimulation du NP en zone B1, une attention particulière était apportée à la contraction de l'hémidiaphragmme droit. En cas de suspicion d'une diminution de la force contractile, la cryoablation était immédiatement stoppée et le ballon déflaté, expliquant probablement pourquoi l'ensemble des PNP dans notre étude n'ont été que transitoires.

Récemment, Casado-Arroyo et al ont décrit une technique servant à prévenir l'apparition d'une PNP, consistant à retirer légèrement le CB jusqu'à ce qu'une discrète fuite de produit de contraste soit observée, avant de lancer l'application.[234] Ceci permet d'appliquer l'énergie dans une zone plus proximale, diminuant ainsi le risque de PNP. A la lumière de nos résultats, l'efficacité de cette technique peut être expliquée par le passage du catheter de stimulation du PN de la zone B1 à la zone A lors du léger retrait du CB. Cependant, dans les rares cas où le cathéter se projète en zone B2 (2 cas dans notre étude), l'utilisation de cette technique peut l'ammener à se projeter en zone B1, ce qui augmente potentiellement le risque de survenue de PNP.

Enfin, il a été démontré qu'une isolation rapide des VP garantissait un faible taux de reconnections immédiates.[239, 240] Compte tenu de la meilleure efficacité de l'ARC-Adv-CB et du risque accru de PNP, il semblerait ainsi envisageable de raccouricr la durée de la cryoapplication (par exemple de 240 à 180 secondes) ou de ne pas réaliser d'application supplémentaire après obtention de l'isolation veineuse. De nouvelles études seront donc nécessaires afin d'évaluer si de telles stratégies permettent de limiter le risque de complications tout en assurant le succès de la procédure.

Elsevier Editorial System(tm) for Heart Rhythm
Manuscript Draft

Manuscript Number: HR-0131382R1

Title: Safety and efficacy of a second-generation cryoballoon in the ablation of paroxysmal atrial fibrillation

Article Type: Original-Clinical (OCL)

Keywords: Cryoablation; paroxysmal atrial fibrillation; balloon catheter ablation; pulmonary vein; pulmonary vein isolation; phrenic nerve palsy

Corresponding Author: Dr Raphaël P. Martins,

Corresponding Author's Institution: Service de Cardiologie et Maladies Vasculaires

First Author: Raphaël P. Martins

Order of Authors: Raphaël P. Martins; David Hamon; Olivier Cesari; Albin Behaghel; Nathalie Behar; Jean-Marc Sellal; Jean-Claude Daubert; Philippe Mabo; Dominique Pavin

Abstract: Background: Compared with the first-generation Arctic Front (ARC-CB), the new Arctic Front Advance (ARC-Adv-CB) cryoballoon increases efficient balloon-tissue contact surface during freezing, which may increase phrenic nerve (PN) palsy (PNP) incidence.
Objective: To evaluate the safety and efficacy of paroxysmal atrial fibrillation (AF) ablation with the ARC-Adv-CB, and the merits of a predictor of PNP.
Methods: AF ablation was performed using a "single 28-mm big CB" approach. The rate of pulmonary vein (PV) isolation with a first cryoapplication was measured. The distance between CB and a PN pacing catheter in the superior vena cava was measured to predict PNP during freezing.
Results: In 147 patients, the PV were isolated with a single cryoapplication in 205 (81.3%) of the 252 PV treated with the ARC-CB and in 280 (90.3%) of the 310 PV treated with the ARC-Adv-CB (P=0.003). Mean time to PV isolation was 40±25 versus 52±34sec (P<0.001), and temperature at time of isolation -36.1±10.3 versus -32.3±10.2°C, with ARC-CB versus ARC-Adv-CB, respectively (P=0.001). Mean procedure and fluoroscopy durations were significantly shorter with the ARC-Adv-CB. Transient PNP was observed in 10.6 and 24.4% of patients treated with the ARC-CB and ARC-Adv-CB, respectively (P=0.048). The distance between lateral edge of the balloon and a vertical line through the tip of the pacing catheter accurately predicted PNP (P<0.001).
Conclusion: The 28-mm ARC-Adv-CB enabled more efficient ablation of paroxysmal AF and shorter procedures than the ARC-CB. This higher performance was associated with a higher incidence of PNP, predicted by the distance between CB and PN.

Jean-Claude Daubert, MD
Philippe Mabo, MD
Christophe Leclercq, MD

November 26, 2013

Douglas P. Zipes, MD
Editor-in-chief
Heart Rhythm

RE: MS Number: HR-0131382

Dear Dr. Zipes,

Attached, please find our revised manuscript, titled *"Safety and efficacy of a second-generation cryoballoon in the ablation of paroxysmal atrial fibrillation"*.

We thank you for giving us this opportunity, and the Reviewers for offering constructive comments, which we have carefully considered when preparing this revised version.

We have prepared point-by-point responses to these comments as a separate file. The most important changes made to the manuscript are highlighted in **bold print**. In addition, the word count, the abstract and the number of figures and tables are now within the limits, and the reference list in the format recommended by the Journal's guidelines.

A conflict of interest statement has been added to the title page.

Finally, the manuscript has been reviewed and edited by an English-speaking medical writer.

We hope that this revised manuscript will now be acceptable for publication in *Heart Rhythm*.

We look forward to you final review

Sincerely,

Raphaël P. Martins, MD

Responses to the comments from Reviewer no 1

We thank the reviewer for offering constructive comments, which have helped us improving the quality of our manuscript.

1. *Considering the non randomized nature of the study the findings are less relevant.*
Response: The reason why our study was not randomized is explained in the "Methods" on page 5, lines 8-10. We have also acknowledged this design weakness in the *"Limitations of our study"* paragraph, on page 14, lines 22-23. When the ARC-Adv-CB became available, the general consensus was that it represented an important technological advance. Therefore, the random assignment of patients to a previous generation cryoballoon at that point was ethically problematic.

2. *However, it would be important to have clinical outcomes and to understand what was done to address the PVs associated with PNP. One would assume that those PVs were not isolated and other tools had to be used to finish the procedure. In such case the benefit of a shorter and more efficient procedure would be minimized by the increase cost. Is there a difference in cost between the two devices?*
Response: In the "Results" section of our original manuscript, we specified that PVI was completed in all patients, including when they developed PNP. PNP occurred after the delivery of energy for an average of 140±43 sec, when the veins were already isolated. Therefore, no other instrumentation was needed to complete the PVI. To clarify this point, we have added, on page 9, lines 23-25, the following explanation: *"It is noteworthy that PV isolation was observed before the development of PNP, and that all isolations persisted despite the early discontinuation of the cryoapplications."*
Furthermore, the cost of the devices is variable from one hospital to another one and depends on call for tenders.

3. *Please provide follow up data on outcomes and total number of catheters used for each procedure.*
Response: Since PVI was completed in all patients with an average of 1.1±0.35 applications (range 1-3) with the 28-mm cryoballoon, we used no other catheter or cryoballoon. In order to clarify this point, we have added the following sentence under "Results", on page 8, lines 6-8: *"The PV were completely isolated with the 28-mm CB in all patients of both groups, without requiring supplemental cryo- or radiofrequency ablation."*.

4. *Also include follow up protocol.*
This study examined the procedural safety and efficacy of the second-generation cryoballoon catheter, with a primary end-point described as "*The primary study endpoint was the rate of successful initial freezes*", on page 7, line 6. Therefore, we did not include a follow-up protocol. We have added "*Finally, since short-term isolation of the PV may not last indefinitely, whether this higher procedural success rate translates into a higher long-term rate of PV isolation and AF suppression will need to be confirmed with long-term follow-ups.*" on page 15, lines 6-9, to acknowledge this limitation of our study.

Responses to the comments from Reviewer no 2

1. *The increase in efficacy of the Arctic Front Advance cryoballoon reported in this manuscript is consistent with other recent studies.*
2. *The proposed pre-procedural indicator for cryoballoon safety where the location of the balloon relative to the phrenic nerve stimulation electrode is very promising. The reported negative predictive value, sensitivity, specificity and ROC analyses are impressive and would represent a significant improvement for cryoballoon ablation of atrial fibrillation, if confirmed.*
We thank the reviewer for these encouraging comments.

3. *Figures 1 and 4 are very helpful in illustrating the different phrenic nerve safety zones and the description of the zones is adequately described in the Methods section. However, there is essentially no explanation on how the images are captured and how the distance measurements illustrated in Figure 3A were obtained. In particular, what was the distance reference in the captured image?*
Response: We agree with this comment and have added a more detailed explanation of our measurements. The distances illustrated in figure 3A were measured, using a 28-mm reference represented by the equatorial diameter of the balloon before the cryoapplication. Based on this reference, we measured the distance between the lateral edge of the cryoballoon and the vertical line crossing the tip of the phrenic nerve pacing catheter. To clarify this point, we have added the following sentence under "Methods" on page 6, lines 12-16: *"In a subset of 40 patients, we measured, before the isolation of a right-sided PV with an ARC-Adv-CB, the distance between a) a vertical line crossing the distal SVC PN pacing catheter and b) the lateral edge of the CB in an anterior-posterior (AP) view, using the 28-mm equatorial diameter of the balloon before the initiation of freezing as reference measurement."*

4. *There are numerous grammatical errors in the manuscript text as well as the use of jargon terms like "single shot" and "bonus application" that should be changed. Terms like "distality" are also used which have no real meaning. Also, several spelling errors (per-procedural instead of pre-procedural) are seen as well. There are some sentences that have no clear meaning, in particular this sentence found near the end of the results section: "Among the 67 applications without PNP, 7 crossed zone B and 60 another one (Figure 3A)". These grammatical and terminology errors are distracting and greatly reduce the impact of the underlying safety results. Significant language editing of the manuscript is required for clarification.*
Response: We apologize for the weakness of the grammar and style of our original manuscript. This revised version has been edited by an English-speaking medical writer.

Safety and efficacy of a second-generation cryoballoon in the ablation of paroxysmal atrial fibrillation

Raphaël P. Martins, MD[1-4]*, David Hamon, MD[1-4]*, Olivier Césari, MD[5], Albin Behaghel, MD[1-4], Nathalie Behar, MD[1-4], Jean-Marc Sellal, MD[1-4], Jean-Claude Daubert, MD[1-4], Philippe Mabo, MD[1-4], Dominique Pavin, MD[1-4]

From
[1]CHU Rennes, Service de Cardiologie et Maladies Vasculaires, Rennes, F-35000, France
[2]Université de Rennes 1, LTSI, Rennes, F-35000, France
[3]INSERM, U1099, Rennes, F-35000, France
[4]INSERM, CIC-IT 804, Rennes, F-35000, France
[5]Clinique Saint Gatien, Tours, F-37000, France

*Both authors contributed equally to the manuscript

Corresponding author
Raphaël P. Martins
Service de Cardiologie et Maladies Vasculaires
CHU de Rennes, 2 rue Henri Le Guilloux
35000 Rennes, France.
Tel: + 33 299 282 527
Fax: +33 299 282 529,
e-mail: raphael.martins@chu-rennes.fr

Word count: 5000

Disclosure: OC, JCD, PM and DP have received speaker honoraria and consulting fees from Medtronic Inc.

Abstract

Background: Compared with the first-generation Arctic Front (ARC-CB), the new Arctic Front Advance (ARC-Adv-CB) cryoballoon increases efficient balloon-tissue contact surface during freezing, which may increase phrenic nerve (PN) palsy (PNP) incidence.

Objective: To evaluate the safety and efficacy of paroxysmal atrial fibrillation (AF) ablation with the ARC-Adv-CB, and the merits of a predictor of PNP.

Methods: AF ablation was performed using a "single 28-mm big CB" approach. The rate of pulmonary vein (PV) isolation with a first cryoapplication was measured. The distance between CB and a PN pacing catheter in the superior vena cava was measured to predict PNP during freezing.

Results: In 147 patients, the PV were isolated with a single cryoapplication in 205 (81.3%) of the 252 PV treated with the ARC-CB and in 280 (90.3%) of the 310 PV treated with the ARC-Adv-CB (P=0.003). Mean time to PV isolation was 40±25 versus 52±34sec (P<0.001), and temperature at time of isolation -36.1±10.3 versus -32.3±10.2°C, with ARC-CB versus ARC-Adv-CB, respectively (P=0.001). Mean procedure and fluoroscopy durations were significantly shorter with the ARC-Adv-CB. Transient PNP was observed in 10.6 and 24.4% of patients treated with the ARC-CB and ARC-Adv-CB, respectively (P=0.048). The distance between lateral edge of the balloon and a vertical line through the tip of the pacing catheter accurately predicted PNP (P<0.001).

Conclusion: The 28-mm ARC-Adv-CB enabled more efficient ablation of paroxysmal AF and shorter procedures than the ARC-CB. This higher performance was associated with a higher incidence of PNP, predicted by the distance between CB and PN.

Keywords: Cryoablation; paroxysmal atrial fibrillation; balloon catheter ablation; pulmonary vein; pulmonary vein isolation; phrenic nerve palsy

Glossary of abbreviations

AF = atrial fibrillation

ARC-Adv-CB = Arctic Front Advance cryoballoon

ARC-CB = Arctic Front cryoballoon

CB = cryoballoon

LA = left atrial

LI = left inferior

LS = left superior

PN = phrenic nerve

PNP = phrenic nerve palsy

PV = pulmonary vein

PVI = pulmonary vein isolation

RI = right inferior

RS = right superior

SVC = superior vena cava

Introduction

After the discovery of ectopic activity in the pulmonary veins (PV) as a major trigger, complete PV isolation (PVI) became first-line therapy of paroxysmal atrial fibrillation (AF).[1,2] While, because of its high success rate, radiofrequency energy remains the most frequently used technique for the ablation of paroxysmal AF, it is generally agreed that point-by-point ablation around the PV ostia is highly complex, time-consuming, and sometimes the source of major complications.[3,4] Cryothermal ablation with cryoballoons (CB) enables the PVI sometimes with a single application, is safe, straightforward and associated with a steep learning curve.[5,6] Its immediate and 1-year rates of successful PVI are similar to those of radiofrequency ablation.[7-9] Phrenic nerve (PN) palsy (PNP), the main complication of CB ablation, usually occurs with the use of 23-mm balloons, that can be advanced farther inside the right-sided PV.[10-11]

The performance of safer, more antral ablation procedures using a "single big CB technique", was described by Chun et al.[5] The first generation of Arctic Front® (ARC) CB, by Medtronic, Inc., Minneapolis, MN, was coolest at the balloon's equator. Consequently, even with a tight occlusion, the CB had to be perfectly centered inside the PV antra to create complete lesions. Liu et al. underscored this limitation and hastened the development of the second generation Arctic Front Advance (ARC-Adv) CB by Medtronic, Inc., equipped with a homogeneous refrigerant system on the distal pole of the CB.[12] Since this new design is likely to be more adaptable to atypical anatomies or imperfect CB applications, improving its overall efficacy,[13,14] one may expect an increase in the incidence of PNP, as a consequence of deeper freezing and of the ice cap that persists after deflation of the balloon.[15]

This non-randomized study was performed to compare the procedural safety and efficacy of the ARC-CB with that of the ARC-Adv-CB in the treatment of highly symptomatic paroxysmal AF. We also examined the merits of a potential predictor of PNP.

Patient enrolment and methods

This study was performed according to local institutional regulations and all patients granted their written informed consent to participate.

Between August 2011 and July 2013, consecutive patients presenting with highly symptomatic, paroxysmal AF resistant to ≥1 antiarrhythmic drug(s) were included in this study. They were excluded if they presented with a history of persistent AF, left atrial (LA) ablation or surgery, or with a prosthetic heart valve, a LA thrombus, or a ≥28-mm wide or ≥10-mm long, right or left common PV trunk. Patients enrolled between August 2011 and September 2012 were treated with the ARC-CB, while patients enrolled between August 2012 and June 2013 were treated with the ARC-Adv-CB, when it became available.

Ablation procedure

Before the ablation procedure, a transesophageal echocardiogram was performed to exclude the presence of a LA thrombus and measure the LA dimensions and left ventricular ejection fraction. LA computed tomography was performed to examine the PV anatomy. Vitamin K antagonists or other oral anticoagulants were discontinued. All procedures were performed under conscious sedation using midazolam and fentanyl as necessary. A 6F Xtrem® quadripolar catheter (Sorin SPA, Milan, Italy) was placed in the coronary sinus via the right femoral vein. A single transseptal puncture was performed under fluoroscopic and pressure guidance. Thereafter, heparin was administered intravenously to maintain an activated clotting time between 250 and 350 sec. A "single big CB" approach, using a 28-mm balloon was performed, as previously described.[5] The CB catheter was introduced into the left atrium through a steerable, 12-F in inner diameter FlexCath® sheath (Medtronic, Minneapolis, MN) constantly flushed with heparinized saline. Finally, an Achieve™ mapping catheter (Medtronic) was advanced over the CB to the PV orifice and positioned as proximally as

possible inside the vessel to record the PV potentials at baseline and monitor the isolation procedure in real time. Then the CB was inflated and advanced to the ostium of each PV. The quality of vascular occlusion was ascertained by the injection of diluted contrast material into the PV and graded from 1 to 4 as mild, medium, sub-total or total. Once the best occlusion was obtained, cryothermal energy was applied for 300 sec with the ARC-CB balloon, and for 240 sec with the new ARC-Adv-CB, as recommended by the manufacturer. An additional application of energy was systematically delivered after PVI, unless PNP was observed. Before ablation of the right-sided PV, the quadripolar catheter was relocated to the superior vena cava (SVC) to constantly pace the right PN at a 2,000 ms cycle length and 20 mA output during freezing. In case of cessation or weakening of the right hemidiaphragmatic contraction, freezing was immediately discontinued and the CB was deflated.

In a subset of 40 patients, we measured before the isolation of right-sided PV with the ARC-Adv-CB, the distance between a) a vertical line crossing the distal SVC PN pacing catheter and b) the lateral edge of the CB in an anterior-posterior (AP) view, using the 28-mm equatorial diameter of the balloon before the initiation of freezing as reference measurement. We also divided the CB and its surrounding space into 4 zones to facilitate and hasten the assessment of its relationship with the PN (figure 1; from the right to the left of the patient, respectively: zone A: right side out of CB toward right PV; zone B1: distal pole of CB from the lateral edge to its center; zone B2: proximal pole of CB from the center to its left extremity; zone C: left side, out of CB).

With each delivery of energy, the time to PVI, the temperature at the time of PVI, and the lowest balloon temperature reached during freezing were recorded. At 20 min after the end of the procedure, the persistence of PVI was ascertained, and the motion of the right hemidiaphragm was confirmed on fluoroscopy, using a "sniff test".[16]

Intravenous heparin was continued for 24 h after the procedure and oral anticoagulation begun thereafter and continued for ≥2 months. An echocardiogram was obtained before discharge of the patient from the hospital to confirm the absence of pericardial effusion.

Study endpoints

The primary study endpoint was the rate of successful initial freezes. The secondary endpoints of the study were the a) overall short-term rate of successful PVI, b) time to PVI, c) lowest balloon temperature and the temperature at the time of PVI, d) mean duration of procedure and of exposure to fluoroscopy, and e) incidence of procedure-related adverse events, including PNP.

Statistical analysis

Normally distributed variables were expressed as means±SD and compared, using Student's *t*-test or Mann-Whitney's U-test, as appropriate. Categorical variables were expressed as counts and percentages and were compared using the Chi-square test. Discrete variables were compared using Fisher's exact test. Receiver operating characteristic curves were constructed to determine the cut-off value, sensitivity (Se), specificity (Spe) and 95% confidence interval (CI) associated with each PN-CB distance. The areas under the curves measured the overall discriminating power of a model. A P value <0.05 was considered statistically significant. The analyses were performed with the SPSS statistical package, version 11.0 (SPSS Inc., Chicago, IL).

Results

We enrolled 147 patients in the study, of whom 66 underwent procedures with the ARC-CB and 81 with the ARC-Adv-CB. The characteristics of both groups were similar (table 1).

After exclusion of 3 LCPV and 3 RCPV with long common trunks, 252 PV were studied in the ARC-CB group, and after exclusion of 7 LCPV, 310 PV were studied in the ARC-Adv-CB group.

Procedural measurements

The procedural measurements are summarized in table 2. **The PV were completely isolated with the 28-mm CB in all patients of both groups, without requiring supplemental cryo- or radiofrequency ablation.** A single cryoapplication isolated 205 of the 252 PV (81.3%) treated with the ARC-CB, and 280 of the 310 PV (90.3%) treated with the ARC-Adv-CB (P=0.003). The rate of single successful applications was higher at each PV separately with the ARC-Adv-CB than with the ARC-CB, though the difference reached statistical significance (P=0.03) only at the level of the left inferior (LI) PV (85.7% versus 97.3%). The PV were isolated with a mean of 1.3±0.7 freezing applications (range 1-6) in the ARC-CB group versus 1.1±0.3 (range 1-3) in the ARC-Adv-CB (P<0.001). This difference was mainly attributable to a significantly lower mean number of freezing applications delivered in the left PV (1.5±1.0 versus 1.2±0.5 in the left superior (LS) PV; P=0.021; 1.2±0.6 versus 1.0±0.2 in the LIPV; P=0.009).

The lowest CB temperature recorded during the initial application at each PV (-49.7±7.6° C in the ARC-CB group versus -49.3±7.3° C in the ARC-Adv-CB group; P=0.558) and the PV occlusion grade (3.9±0.4 in both groups; P=0.848) were similar in both groups. PV potentials were visualized during initial freezing in 173 PV (68.6%) with the ARC-CB and in 216 PV (69.7%) with the ARC-Adv-CB (P=0.712). PV potentials were recorded on 5.6±1.9 electrodes of the 8-pole Achieve catheter in the ARC-CB group and 5.4±2.0 electrodes in the ARC-Adv-CB group (P=0.397). The procedure lasted a mean of 120.1±24.1 min in the ARC-

CB group versus 107.4±24.1 min in the ARC-Adv-CB group (P=0.002) and the duration of fluoroscopic exposure was 28.7±9.9 and 25.0±9.2 min, respectively (P=0.02).

Time to and temperature at PVI

The PVI was directly visualized in 134 PV (53.2%) in the ARC-CB group and in 187 PV (60.3%) in the ARC-Adv-CB group (P=0.106; table 3). The mean time to PVI was 52±34 sec (range 10-176 sec) with the ARC-CB and 40±25 sec (range 13-185 sec) with the ARC-Adv-CB (P <0.001; figure 2A & B). Therefore, the temperature at the time of PVI was less cold with the new ARC-Adv-CB, i.e. -32±10° C (range -53 to +17) versus -36±10° C (range -57 to +10; P=0.001; figure 2A). In separate analyses of each vein, significant temperature differences were found between the left PV and the right inferior (RI) PV, though not between the right superior (RS) PV.

Incidence and predictors of phrenic nerve palsy

Among the 288 right PVI procedures, 29 PNP (10.1%) occurred, of which 7 out of 126 (5.6%) occurred with the ARC-CB and 22 out of 162 (13.6%) with the ARC-Adv-CB (P=0.044) corresponding to 10.6 and 24.4% of patients, respectively (P=0.048). All PNP occurred during the first application and most of them (71% with the ARC-CB and 77% with the ARC-Adv-CB) during RSPV isolation. In 2 patients treated with the ARC-Adv-CB, who developed transient PNP during RSPV isolation, PNP recurred during treatment of the RIPV. PNP developed earlier with the ARC-Adv-CB (140±43 sec) than with the ARC-CB (166±66 sec), though the difference (P=0.238) was not statistically significant. All PNP were transient and resolved spontaneously within 0.5 to 20.0 min. **It is noteworthy that PVI was observed before the development of PNP, and that all isolations persisted despite the early discontinuation of the cryoapplication.**

Since PNP is a serious complication jeopardizing the overall safety of CB ablation, we examined, in a subset of 80 right-sided PVI with the ARC-Adv-CB, whether the distance between the lateral edge of the balloon and the vertical line crossing the tip of the SVC catheter stimulating the PN (CB-PN, figure 1), was a predictor of the 13 PNP that occurred in that subgroup. The mean CB-PN distance measured in patients who developed PNP was -4.9±5.5 mm leftward from the lateral edge of the CB, versus 8.6±8.9 mm rightward from the lateral edge in patients who remained free from PNP ($P<0.001$; figure 3A). By receiver operating characteristic analysis (figure 3B), the highest sensitivity and specificity were obtained at a cutoff value of 0.0 mm (Se=92.3%; 95% CI 63.9-98.7; Spe=86.6%; 95% CI 76.0-93.7; area under the curve = 0.91; 95% CI 0.82-0.96; $P<0.0001$). When we examined the position of the SVC pacing catheter relative to the 4 zones during freezing (figures 1 & 4), 12 of the 13 PNP were in zone B1 and 1 was in zone A. In the 67 uncomplicated applications, the pacing catheter crossed zone B1 in 7 and another zone in 60 (figure 3A). Thus, when the pacing catheter crossed zone B1 in the AP view, the likelihood of PN injury during right-sided PVI was high (Se=92.3%; Spe=89.9%; negative and positive predictive values=98.4 and 63.2%, respectively).

Other adverse events

A small pericardial effusion was observed in the ARC-Adv-CB group, and a single femoral arterio-venous fistula occurred in each group, which both resolved spontaneously within 1 month after the ablation procedure.

Discussion

Main findings of our study

Compared with that of the ARC-CB, the overall ability of the ARC-Adv-CB to completely isolate the PV of patients suffering from paroxysmal AF was superior. While all PV were ultimately isolated in all patients of both groups, fewer freezing applications were needed to isolate the PV and the rate of single freezes was higher when the ARC-Adv-CB was used instead of the ARC-CB, significantly shortening the mean procedural duration and exposure to fluoroscopy. In most instances, the PVI was directly visualized and the time to isolation was significantly shortened, increasing the mean temperature at the time of isolation. However, the rate of transient right-sided PNP was significantly higher with the ARC-Adv-CB, and strongly correlated with the estimates of procedural CB-PN proximity, using the SVC pacing catheter.

Contributions of the ARC-Adv-CB

Compared with the ARC-CB, the new CB has a two-fold greater number of injection spray jets that have been optimally located to more uniformly cool its tip. It is noteworthy that the higher performance of the ARC-Adv-CB was nearly entirely confined to the left PV freezing applications, while the differences in right PV were small. This observation has several putative explanations. First, in our experience with the ARC-CB, isolation of the left-sided PV was more challenging and required a greater number of freezing applications than the right-sided PV (table 2). Second, as in the case of radiofrequency ablation, the ridge between the PV ostia and the left atrial appendage represents an anatomical obstacle for CB, responsible for a high proportion of recurrent connections between the left PV and the left atrium.[17] Inferior segments are also difficult to isolate and are preferential sites of PV reconnection. Chun et al. used the crosstalk technique in >1/3 of procedures to isolate the LSPV, in contrast to a "straightforward" approach for all RSPV, highlighting the difficult access to the distal electrical connection between the left PV with the ARC-CB.[5] Third, the

higher ovality index of the left- than the right-sided PV may also be a factor, as an inverse association was found between this index and the degree of occlusion.[14]

Our results are consistent with those of a recent study, which reported a significantly greater PVI efficacy associated with the ARC-Adv-CB than with the first-generation CB.[18] The authors accurately described the technical improvements represented by the ARC-Adv-CB, consisting in an increase in the effective balloon-tissue contact area as well as the more prominent ice formation within the PV, known as the "ice cap phenomenon".[15] They hypothesized that even with a suboptimal contact, the ice cap prevents rewarming of the blood and enables PVI. In the study by Fürnkranz et al., the overall minimum balloon temperatures were lower using the ARC-Adv-CB than with the ARC-CB.[18] Some procedural characteristics may explain this difference. Indeed, the distance between the balloon surface and the proximal Achieve electrode during freezing decreased between the ARC-CB and the ARC-Adv-CB, facilitating the visualization of the PV potentials. This might have promoted the contact with the PV ostia and lower freezing temperatures.[17] Conversely, in our study, though we did not measure this distance, the rates of PV potential visualization and the low temperatures were similar. The exclusion of wide and long LCPV may also have caused these differences since they are usually associated with lower temperatures.[18]

Procedural safety

The greater efficacy of the ARC-Adv-CB was associated with a significant increase in transient PNP in our study. The previously published incidence of PNP has been variable; Casado-Arroyo et al. reported a significant increase using the ARC-Adv-CB,[19] while Fürnkranz et al. observed no difference.[18] This discrepancy might be explained by the definition of PNP, as some authors report only persistent while others report persistent and transient PNP.

The new design of the ARC-Adv-CB has considerably increased the cooling area near the tip of the CB, increasing the risk of PN injury. In this study, we found an intraprocedural, simple and reliable predictor of PNP. The vertical projection of the SVC pacing catheter to the distal segment of the CB in the AP view (zone B1, corresponding to the cooling zone) was an excellent predictor of PNP. Among the 13 cases of PNP, a single occurred while the line crossed zone A in the AP view, though it may have been caused by an ice cap, or due to an unusual oblique course of the PN.

The anatomical relationship between right PN and RSPV is variable and difficult to evaluate before the procedure. In a study using CT scans, segments of the right pericardiophrenic artery, used to locate the PN, were identified in 20% of patients,[20] while earlier studies had reported higher rates.[21] A short distance between RSPV and SVC was recently found to be correlated with PNP.[22] However, the precise course of the PN varies among patients, and the force used to occlude the PV may distort the anatomy. The same authors found that a precipitous drop in CB temperature (i.e. <-41°C at 30s) was a strong predictor of PNP.[22] However, while low temperatures are usually associated with more distal PV occlusions, in this study, among 29 transient PNP, a single would have been predicted by such a precipitous fall in temperature.

Clinical implications

The finding of a reliable predictor of PNP raises the issue of prevention when the risk of PNP is high. When the SVC pacing catheter crossed zone B1 in the AP view, and as soon as a weakening of the right hemidiaphragm contraction was suspected, we immediately discontinued freezing, deflated the CB and abstained from further treatment delivery, probably explaining the absence of persistent PNP. We believe that, when the risk of PNP during RSPV treatment is high, the RIPV should be frozen first in order to allow the

monitoring of PN during the remaining cryoapplications. Most importantly, Casado-Arroyo et al. just described a highly promising technique to prevent PNP, consisting, after tight wedging of the inflated CB inside the RSPV ostium, to withdraw it until a small leak is observed, since the CB volume increases slightly at the onset of cryoapplication.[19] This offers the advantage of a more proximal cryoapplication. In light of our observations, their lower rate of PNP might be explained by a shift of the PN projection from zone B1 to zone A. We suggest, because of the >98% negative predictive value of our PNP predictor, to use the technique of Casado-Arroyo et al., particularly when the vertical projection of the PN reaches the distal part of the CB (Zone B1). It is noteworthy that in 2 cases of PN projection in zone B2, out of 80 patients, the withdrawal of the CB might have increased the risk of PNP, since it shifted toward zone B1.

Importantly, in all instances of PNP and early cessation of the cryoapplication, the right PV were successfully isolated, without short-term reconnection. Finally, the PV were isolated more rapidly when we used the ARC-Adv-CB instead of the ARC-CB. Rapid PVI are associated with low immediate reconnection rates,[23,24] and one may hypothesize that the cryoapplication could be shortened to limit the rate of procedural complications, including PNP. However, the time to PVI has not been found to be a predictor of long-term reconnection, and further studies are needed to assess its contribution in the adjustment of the duration of applications, and need for additional cryoapplications.

Limitations of our study

Our study was not randomized as we did not have access to both CB generations simultaneously, and the patient enrolment overlapped for a period of only 2 months. We do not believe, however, that this introduced important biases, as the same trained operators participated in both phases of the study. A learning curve effect was probably not a factor

since the occlusion grade and visualization of PV potentials were identical in both groups. Moreover, whether a faster PVI is associated with a lower incidence of PV reconnection is unknown and requires further studies. The new predictor of PNP, identified on the basis of a subset of 80 isolations of right PV, will need to be confirmed with a larger number of observations. More importantly, these observations were made using a 28-mm CB, limiting the conclusions to this size of balloon. **Finally, since short-term PVI may not last indefinitely, whether this higher procedural success rate translates into a higher long-term rate of PVI and AF suppression will need to be confirmed with long-term follow-ups.**

Conclusion

Cryoablation of paroxysmal AF with the new 28-mm ARC-Adv-CB was associated with a >90% success rate with a single freezing application, and with shorter procedures than with the first generation CB. However, this higher efficacy was accompanied by a troubling increase in transient PNP. Consequently we found that the distance between CB and PN was a reliable and straightforward intraprocedural predictor of PNP.

Acknowledgments

Authors would like to thank Rodolphe Ruffy for the manuscript revision.

References

1. Haissaguerre M, Jais P, Shah DC, et al. Spontaneous initiation of atrial fibrillation by ectopic beats originating in the pulmonary veins. N Engl J Med 1998;339:659-66.

2. Natale A, Raviele A, Arentz T, et al. Venice Chart international consensus document on atrial fibrillation ablation. J Cardiovasc Electrophysiol 2007;18:560-80.

3. Cappato R, Calkins H, Chen SA, et al. Updated worldwide survey on the methods, efficacy, and safety of catheter ablation for human atrial fibrillation. Circ Arrhythm Electrophysiol 2010;3:32-8.

4. Weerasooriya R, Jais P, Hocini M, et al. Balloon cryoablation for paroxysmal atrial fibrillation. Europace 2008;10:1251-1252.

5. Chun KR, Schmidt B, Metzner A, et al. The 'single big cryoballoon' technique for acute pulmonary vein isolation in patients with paroxysmal atrial fibrillation: a prospective observational single centre study. Eur Heart J 2009;30:699-709.

6. Khairy P, Chauvet P, Lehmann J, et al. Lower incidence of thrombus formation with cryoenergy versus radiofrequency catheter ablation. Circulation 2003;107:2045-50.

7. Packer DL, Kowal RC, Wheelan KR, et al. Cryoballoon ablation of pulmonary veins for paroxysmal atrial fibrillation: first results of the North American Arctic Front (STOP AF) pivotal trial. J Am Coll Cardiol 2013;61:1713-23.

8. Van Belle Y, Janse P, Theuns D, et al. One year follow-up after cryoballoon isolation of the pulmonary veins in patients with paroxysmal atrial fibrillation. Europace 2008;10:1271-6.

9. Vogt J, Heintze J, Gutleben KJ, et al. Long-term outcomes after cryoballoon pulmonary vein isolation: results from a prospective study in 605 patients. J Am Coll Cardiol 2013;61:1707-12.

10. Van Belle Y, Janse P, Rivero-Ayerza MJ, et al. Pulmonary vein isolation using an occluding cryoballoon for circumferential ablation: feasibility, complications, and short-term outcome. Eur Heart J 2007;28:2231-7.

11. Neumann T, Vogt J, Schumacher B, et al. Circumferential pulmonary vein isolation with the cryoballoon technique results from a prospective 3-center study. J Am Coll Cardiol 2008;52:273-278.

12. Liu CF. Pulmonary vein reconnection after cryoballoon ablation: back to the drawing board. Heart Rhythm 2010;7:191-192.

13. Kubala M, Hermida JS, Nadji G, et al. Normal pulmonary veins anatomy is associated with better AF-free survival after cryoablation as compared to atypical anatomy with common left pulmonary vein. Pacing Clin Electrophysiol 2011;34:837-843.

14. Sorgente A, Chierchia GB, de Asmundis C, et al. Pulmonary vein ostium shape and orientation as possible predictors of occlusion in patients with drug-refractory paroxysmal AF undergoing cryoballoon ablation. Europace 2011;13:205-12.

15. Bordignon S, Furnkranz A, Schmidt B, Chun KR. Remaining ice cap on second-generation cryoballoon after deflation. Circ Arrhythm Electrophysiol 2012;5:e98-9.

16. Qureshi A. Diaphragm paralysis. Semin Respir Crit Care Med 2009;30:315-20.

17. Fürnkranz A, Chun KR, Nuyens D, et al. Characterization of conduction recovery after pulmonary vein isolation using the "single big cryoballoon" technique. Heart Rhythm 2010;7:184-190.

18. Fürnkranz A, Bordignon S, Schmidt B, et al. Improved procedural efficacy of pulmonary vein isolation using the novel second-generation cryoballoon. J Cardiovasc Electrophysiol 2013;24:492-497.

19. Casado-Arroyo R, Chierchia GB, Conte G, et al. Phrenic nerve paralysis during cryoballoon ablation for atrial fibrillation: a comparison between the first- and second-generation balloon. Heart Rhythm 2013;10:1318-1324.

20. Nieto-Tolosa J, Rodriguez-Sanchez D, Hurtado-Martinez JA, et al. [Phrenic nerve identification with cardiac multidetector computed tomography]. Rev Esp Cardiol 2010;64:942-944.

21. Horton R, Di Biase L, Reddy V, et al. Locating the right phrenic nerve by imaging the right pericardiophrenic artery with computerized tomographic angiography: implications for balloon-based procedures. Heart Rhythm 2010;7:937-941.

22. Kühne M, Knecht S, Altmann D, et al. Phrenic nerve palsy during ablation of AF using a 28-mm cryoballoon catheter: predictors and prevention. J Interv Card Electrophysiol 2012;36:47-54.

23. Chun KR, Fürnkranz A, Metzner A, et al. Cryoballoon pulmonary vein isolation with real-time recordings from the pulmonary veins. J Cardiovasc Electrophysiol 2009;20:1203-1210.

24. Dorwarth U, Schmidt M, Wankerl M, Krieg J, Straube F, Hoffmann E. Pulmonary vein electrophysiology during cryoballoon ablation as a predictor for procedural success. J Interv Card Electrophysiol 2011;32:205-211.

Figures legends

Figure 1: Phrenic nerve-CB relationship in the AP view

The distance between the black dotted line and the lateral edge of the CB was measured (bidirectional arrow). Four zones were defined from right to left of the patient: zone A: right side outside CB toward right PV; zone B1: distal pole of CB from lateral edge to its center; zone B2: proximal pole of CB from center to its left border; zone C: left side, outside of CB.

Figure 2:

A. Time to disconnection and temperature at time of PVI.

B. Time/temperature relationship for all PV with visible PV potentials during the cryoapplications.

Figure 3: Incidence of PNP with the ARC-Adv-CB.

A. Distance between CB and phrenic nerve (PN) in patients with versus without PNP.

B. Receiver operating characteristic analysis of CB-PN distance showing an optimal cut-off value of 0.0 cm.

Figure 4: Phrenic nerve-CB relationship in AP view during RSPV cryoapplication.

A: Zone A; B: Zone B1; C: Zone B2.

Table 1 Baseline characteristics of the study groups

	ARC-CB n=66	ARC-Adv-CB n=81	*P*
Men	48 (61)	54 (67)	0.540
Age, y	60.9±10.3	59.4±9.5	0.350
CHADS vascular score	1.1±0.9	1.1±1.1	0.880
Years with atrial fibrillation	6.0±5.6	7.9±7.6	0.095
Episodes duration			
<24 h	55 (83.3)	61 (75.3)	0.326
≥24 h	11 (16.7)	20 (24.7)	0.326
Number of unsuccessful antiarrhythmic trials	2.6±1.1	2.5±1.1	0.810
Left ventricular ejection fraction, %	65.8±5.5	64.7±7.1	0.328
Left atrial dilatation			
None (<34ml/m²)	43 (65.1)	52 (64.2)	0.952
Mild (34-44ml/m²)	11 (16.7)	16 (19.7)	0.790
Moderate (45-59ml/m²)	8 (12.1)	8 (9.9)	0.866
Severe (>60ml/m²)	4 (6.1)	5 (6.2)	0.751

Values are means±SD or numbers (%) of observations

Table 2 Procedural measurements in each study group

	ARC-CB n=252 PV	**ARC-Adv-CB n=310 PV**	*P*
Occlusion grade, 1-4	3.9±0.4	3.9±0.4	0.848
PVP visualization			
All measurements	**173 (68.6)**	**216 (69.7)**	0.712
LSPV	58 (92.1)	71 (95.9)	0.548
LIPV	47 (74.6)	60 (81.1)	0.362
RSPV	51 (80.9)	61 (75.3)	0.544
RIPV	17 (27.0)	24 (29.6)	0.871
Number of electrodes, 1-8	5.6±1.9	5.4±2.0	0.397
Lowest temperature, °C			
All measurements	**-49.7±7.6**	**-49.3±7.3**	0.558
LSPV	-51.2±6.9	-48.4±7.1	**0.023**
LIPV	-46.8±7.3	-47.3±5.6	0.670
RSPV	-52.6±7.2	-52.0±7.5	0.590
RIPV	-48.2±7.6	-49.4±7.9	0.355
Mean number of cryoapplications			
All measurements	**1.3±0.7 (1-6)**	**1.1±0.35 (1-3)**	**<0.001**
LSPV	1.5±1.0	1.2±0.5	**0.021**
LIPV	1.2±0.6	1.0±0.2	**0.009**
RSPV	1.2±0.6	1.1±0.3	0.099
RIPV	1.1±0.4	1.1±0.3	0.268
Number of single cryoapplications			
All measurements	**205 (81.3)**	**280 (90.3)**	**0.003**
LSPV	43 (68.2)	61 (82.4)	0.083
LIPV	54 (85.7)	72 (97.3)	**0.030**
RSPV	52 (82.5)	71 (87.6)	0.532
RIPV	56 (88.9)	76 (93.8)	0.447

Values are means±SD or numbers (%) of observations

Table 3 Time and temperature at time PVI

	CB-AF n=134	CB-Adv n=187	*P*
Real-time PVI visualization	53.2%	60.3%	0.106
Time to isolation, sec			
All veins	**52±34**	**40±25**	**<0.001**
Left superior (40/57)	57±35	44±20	**0.023**
Left inferior (40/58)	50±34	34±27	**0.011**
Right superior (42/52)	46±32	41±23	0.326
Right inferior (12/20)	59±37	48±33	0.385
Temperature at time of isolation, °C			
All veins	**-36±10**	**-32±10**	**0.001**
Left superior (40/57)	-39±8	-35±7	**0.01**
Left inferior (40/58)	-33±10	-26±11	**0.002**
Right superior (42/52)	-35±12	-36±10	0.675
Right inferior (12/20)	-39±6	-33±8	**0.038**

Values are means±SD or numbers (%) of observations

Figure 1
Click here to download high resolution image

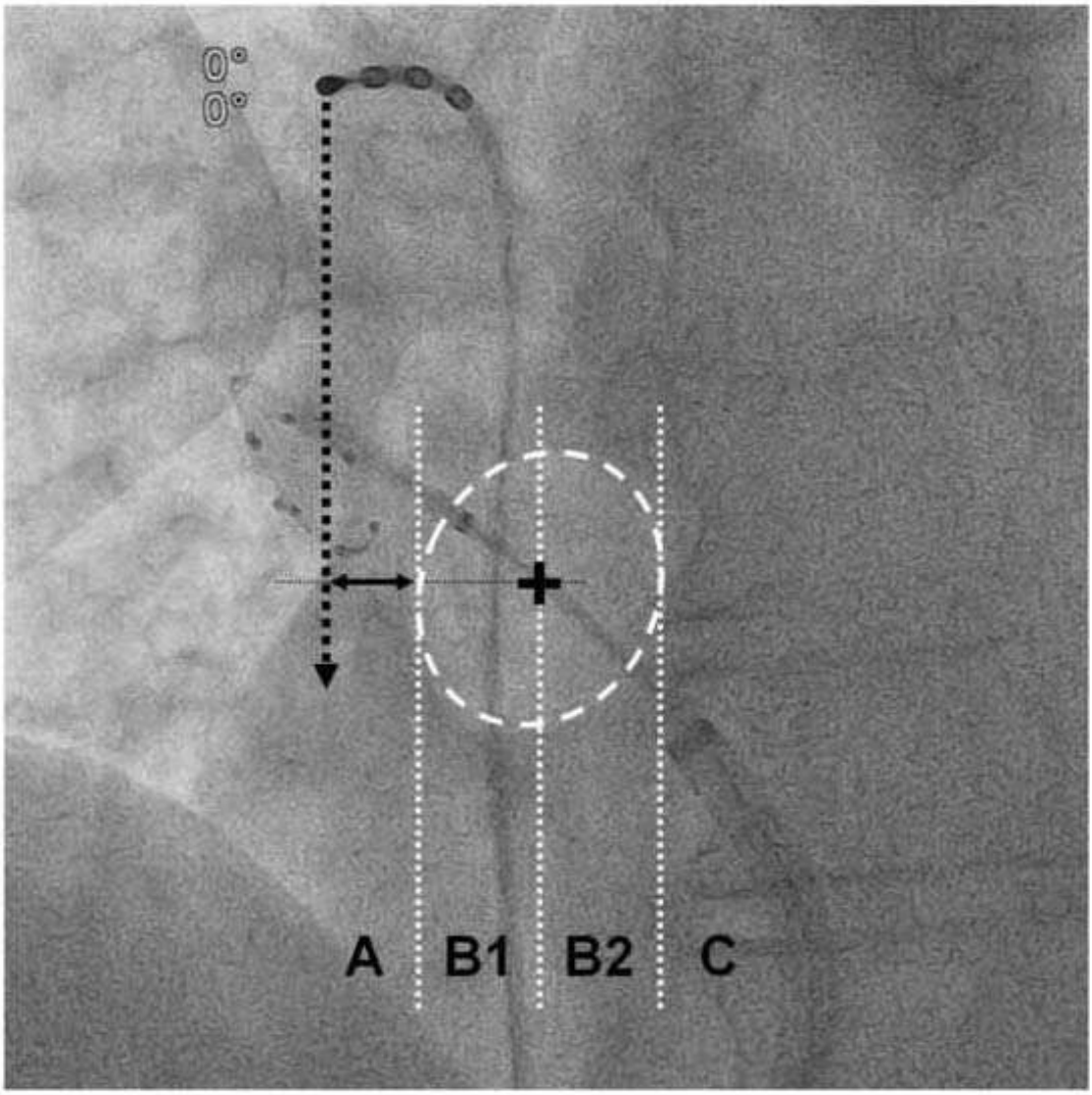

Figure 2
Click here to download high resolution image

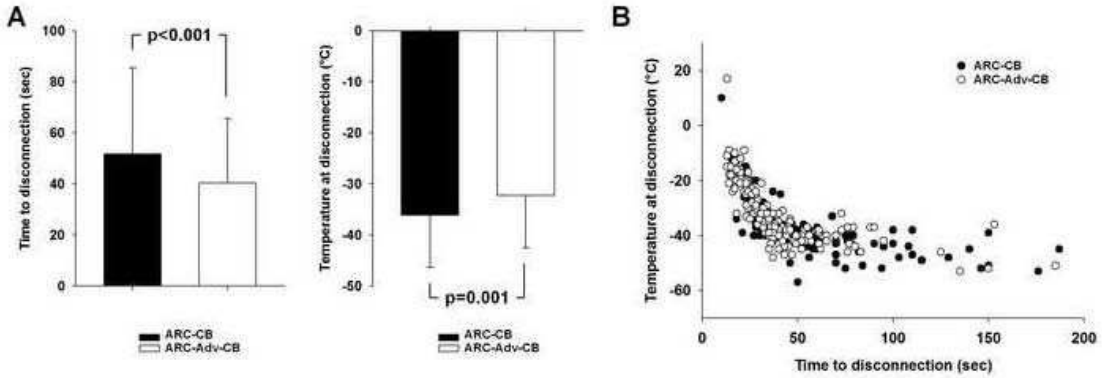

Figure 3
Click here to download high resolution image

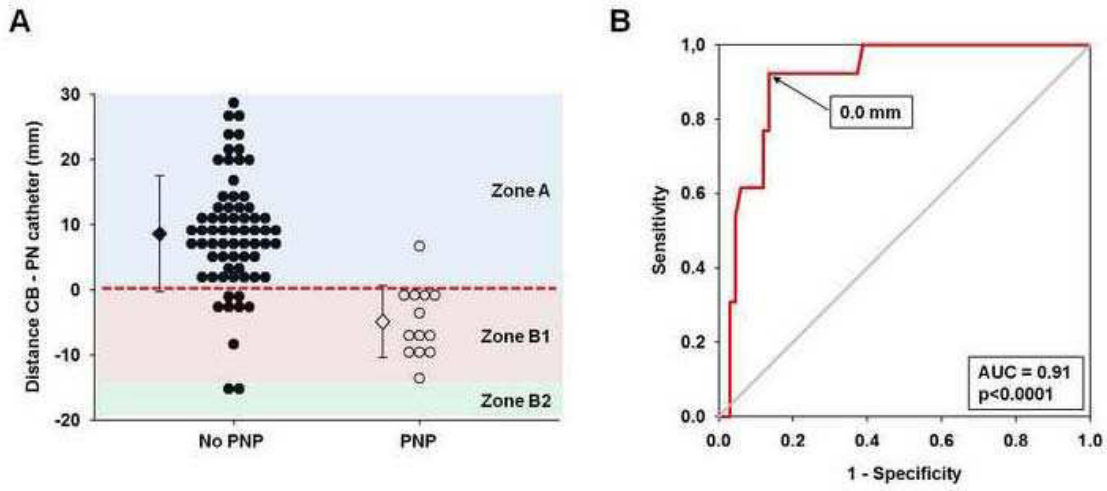

Figure 4
Click here to download high resolution image

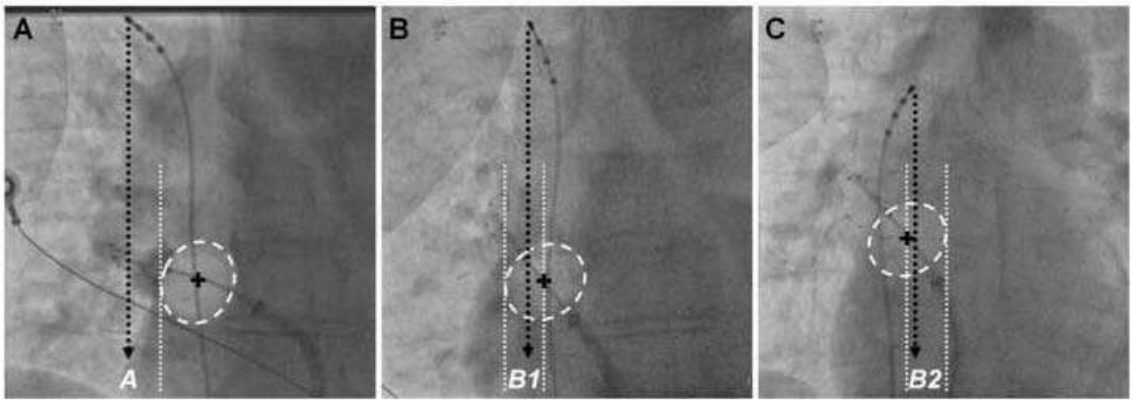

D. Conclusion

La prise en charge thérapeutique de la FA a beaucoup évolué ces dernières années, principalement à la faveur de l'essor des techniques ablatives. Quelques nouveaux anti-arythmiques ont vu le jour (vernakalant, dronédarone,…), mais certains que transitoirement compte-tenu de la mise en évidence d'effets secondaires importants, cardiaques ou non.

De nombreux progrès sont attendus dans ce domaine dans les années à venir, tant sur le versant médical qu'interventionnel, révolutionnant peut-être ainsi la qualité de vie et le devenir des patients en FA.[188]

Conclusion

"*The history of the fibrillation of the auricles will impress you with the dimness of our eyes and the opacity of the obstacles which embarrass our vision. You will know how blind we have been to things which, once seen, are so apparent."*

Sir Thomas Lewis
Conférence à l'Univeristy College Hospital of London, UK
1912

Cette phrase de Sir Thomas Lewis, un des pionniers dans la recherche des mécanismes de la FA, est plus que jamais d'actualité. Malgré plus de 100 ans de recherche fondamentale et clinique, les phénomènes exacts entrant en jeu dans la FA et expliquant son caractère récidivant restent mal compris. Comme cela a été exposé dans ce manuscrit, cette arythmie est complexe, mêlant différents mécanismes d'initiation et d'entretien. Initialement une maladie du « trigger », représentés principalement par les VP, la FA se transforme en maladie du substrat, compte tenu de la survenue d'un remodelage multiple, autant électrophysiologique, que structurel et autonomique. Par ailleurs, la prise en charge de cette arythmie n'est que sub-optimale car un grand nombre de patients ne sont pas contrôlés par les thérapeutiques aujourd'hui à notre disposition et qu'une proportion non négligeable d'entre eux progresse vers la FA persistante et permanente.

Comment progresser encore ? Dans un excellent papier de l'équipe de Stanley Nattel publié cette année et titré *« Management of atrial fibrillation in the year 2033 : new concepts, tools, and applications leading to personalized medicine »*,[241] les auteurs décrivent ce qu'ils pensent être les avancées majeures dans la prise en charge de cette arythmie dans les 20 prochaines années. Trois points majeurs sont discutés.

Tout d'abord, les auteurs imaginent une prise en charge personnalisée pour chaque malade, basée sur son génome. Il serait ainsi possible de mieux comprendre les interactions complexes entre les prédispositions génétiques des patients et l'impact des comorbidités et de l'environnement sur le tissu atrial.

Par ailleurs, les nouveaux outils décrits précédemment permettant de cartographier directement les sources maintenant la FA, les rotors, n'en sont qu'à leur balbutiement.[217, 218] Il est certains que ces systèmes, et d'autres encore moins invasifs, vont se perfectionner et se généraliser, offrant ainsi la possibilité de translater en clinique les avancées physiopathologiques des dernières années sur les mécanismes maintenant l'arythmie. Les auteurs imaginent ainsi une « Cardiac Diagnosis Suite », sorte de système d'imagerie non invasif et non irradiant, permettant d'acquérir et d'analyser facilement plusieurs cycles cardiaques, d'étudier la dynamique des ondes fibrillatoires propre au patient, et d'apprécier l'impact de la fibrose et des connections myocytaires sur la conduction atriale. Ces données, combinées aux informations apportées par le génome et par de possibles nouveaux biomarqueurs, offriraient la possibilité d'intervenir directement sur le mécanisme le plus impliqué dans le maintien de l'arythmie chez un patient donné.

Enfin, le troisième point concerne la détection de l'arythmie. Les récentes avancées technologiques permettent aujourd'hui aux patients de déterminer s'ils sont ou non en FA,

simplement via une application sur leur Smartphone.[242] La généralisation d'une telle technologie pourrait permettre aux patients eux-mêmes de monitorer leur rythme cardiaque, sans nécessiter de contact médical. Par ailleurs, de nouveaux enregistreurs d'évènements injectables vont être prochainement mis sur le marché. Les auteurs imaginent que ceux-ci pourraient être connectés à un Smartphone émettant une alerte en cas de détection de la FA. Une telle technologie offrirait la possibilité de traiter très précocement les épisodes d'arythmie, permettant ainsi d'éviter la mise en place du cercle vicieux de l'« AF begets AF » et de diminuer peut-être le taux de complications thrombo-emboliques de la maladie.

Où se situe la frontière entre utopie et réalité ? Il tarde à tous les cliniciens passionnés par la FA de le savoir. Gageons que ces auteurs auront raison…

C’est là une histoire sans fin.
Car le monde entier est encore une Amérique.
Et les mots *terra incognita* -territoire inconnu-
sont bien les plus prometteurs que l’on ait jamais
écrits sur les cartes de la connaissance humaine.

Daniel Boorstein
« Les découvreurs », 1983

Références

1. Camm AJ, Kirchhof P, Lip GY, Schotten U, Savelieva I, Ernst S, Van Gelder IC, Al-Attar N, Hindricks G, Prendergast B, Heidbuchel H, Alfieri O, Angelini A, Atar D, Colonna P, De Caterina R, De Sutter J, Goette A, Gorenek B, Heldal M, Hohloser SH, Kolh P, Le Heuzey JY, Ponikowski P, Rutten FH, Vahanian A, Auricchio A, Bax J, Ceconi C, Dean V, Filippatos G, Funck-Brentano C, Hobbs R, Kearney P, McDonagh T, Popescu BA, Reiner Z, Sechtem U, Sirnes PA, Tendera M, Vardas PE, Widimsky P, Agladze V, Aliot E, Balabanski T, Blomstrom-Lundqvist C, Capucci A, Crijns H, Dahlof B, Folliguet T, Glikson M, Goethals M, Gulba DC, Ho SY, Klautz RJ, Kose S, McMurray J, Perrone Filardi P, Raatikainen P, Salvador MJ, Schalij MJ, Shpektor A, Sousa J, Stepinska J, Uuetoa H, Zamorano JL, Zupan I. Guidelines for the management of atrial fibrillation: the Task Force for the Management of Atrial Fibrillation of the European Society of Cardiology (ESC). *Europace.*2010;12(10):1360-1420.

2. Go AS, Hylek EM, Phillips KA, Chang Y, Henault LE, Selby JV, Singer DE. Prevalence of diagnosed atrial fibrillation in adults: national implications for rhythm management and stroke prevention: the AnTicoagulation and Risk Factors in Atrial Fibrillation (ATRIA) Study. *JAMA.* 2001;285(18):2370-2375.

3. Savelieva I, Camm J. Update on atrial fibrillation: part I. *Clin Cardiol.* 2008;31(2):55-62.

4. Benjamin EJ, Wolf PA, D'Agostino RB, Silbershatz H, Kannel WB, Levy D. Impact of atrial fibrillation on the risk of death: the Framingham Heart Study. *Circulation.* 1998;98(10):946-952.

5. Haissaguerre M, Jais P, Shah DC, Takahashi A, Hocini M, Quiniou G, Garrigue S, Le Mouroux A, Le Metayer P, Clementy J. Spontaneous initiation of atrial fibrillation by ectopic beats originating in the pulmonary veins. *N Engl J Med.* 1998;339(10):659-666.

6. Cappato R, Calkins H, Chen SA, Davies W, Iesaka Y, Kalman J, Kim YH, Klein G, Natale A, Packer D, Skanes A, Ambrogi F, Biganzoli E. Updated worldwide survey on the methods, efficacy, and safety of catheter ablation for human atrial fibrillation. *Circ Arrhythm Electrophysiol.*2010;3(1):32-38.

7. Garrey WE. Auricular fibrillation. *Physiol Rev.* 1924(4):215-250.

8. Schotten U, Verheule S, Kirchhof P, Goette A. Pathophysiological mechanisms of atrial fibrillation: a translational appraisal. *Physiol Rev.*2010; 91(1):265-325.

9. Nishida K, Michael G, Dobrev D, Nattel S. Animal models for atrial fibrillation: clinical insights and scientific opportunities. *Europace.*2010; 12(2):160-172.

10. Morillo CA, Klein GJ, Jones DL, Guiraudon CM. Chronic rapid atrial pacing. Structural, functional, and electrophysiological characteristics of a new model of sustained atrial fibrillation. *Circulation.* 1995;91(5):1588-1595.

11. Wijffels MC, Kirchhof CJ, Dorland R, Allessie MA. Atrial fibrillation begets atrial fibrillation. A study in awake chronically instrumented goats. *Circulation.* 1995;92(7):1954-1968.

12. Hove-Madsen L, Llach A, Bayes-Genis A, Roura S, Rodriguez Font E, Aris A, Cinca J. Atrial fibrillation is associated with increased spontaneous calcium release from the sarcoplasmic reticulum in human atrial myocytes. *Circulation.* 2004;110(11):1358-1363.

13. Dobrev D, Voigt N, Wehrens XH. The ryanodine receptor channel as a molecular motif in atrial fibrillation: pathophysiological and therapeutic implications. *Cardiovasc Res.*2011; 89(4):734-743.

14. Voigt N, Li N, Wang Q, Wang W, Trafford AW, Abu-Taha I, Sun Q, Wieland T, Ravens U, Nattel S, Wehrens XH, Dobrev D. Enhanced Sarcoplasmic Reticulum Ca2+-leak and Increased Na+-Ca2+-Exchanger Function Underlie Delayed Afterdepolarizations in Patients with Chronic Atrial Fibrillation. *Circulation.*2012;125(17):2059-2070.

15. Ming Z, Nordin C, Aronson RS. Role of L-type calcium channel window current in generating current-induced early afterdepolarizations. *J Cardiovasc Electrophysiol.* 1994;5(4):323-334.

16. Burashnikov A, Antzelevitch C. Reinduction of atrial fibrillation immediately after termination of the arrhythmia is mediated by late phase 3 early afterdepolarization-induced triggered activity. *Circulation.* 2003;107(18):2355-2360.

17. Mines GR. On dynamic equilibrium in the heart. *J Physiol.* 1913;46(4-5):349-383.

18. Lewis T. Oliver-Sharpey Lectures ON THE NATURE OF FLUTTER AND FIBRILLATION OF THE AURICLE. *Br Med J.* 1921;1(3147):590-593.

19. Prinzmetal M, Corday E, et al. Mechanism of the auricular arrhythmias. *Circulation.* 1950;1(2):241-245.

20. Moe GK. Cardiac arrhythmias; introductory remarks. *Ann N Y Acad Sci.* 1956;64(4):540-542.

21. Moe G. On the multiple wavelet hypothesis of atrial fibrillation. *Arch Int Pharmacodyn Ther.* 1962;140:183-188.

22. Moe GK, Rheinboldt WC, Abildskov JA. A Computer Model of Atrial Fibrillation. *Am Heart J.* 1964;67:200-220.

23. Allessie MA, Lammers WJEP, Bonke FIM, Hollen J. Experimental evaluation of Moe's multiple wavelet hypothesis of atrial fibrillation. In: Zipes DP, Jalife, J, eds. *Cardiac Electrophysiology and Arrhythmias.* Orlando: Grune & Straton; 1985;p265-275.

24. Fragakis N, Pantos I, Younis J, Hadjipavlou M, Katritsis DG. Surgical ablation for atrial fibrillation. *Europace.* 2012;14(11):1545-1552.

25. Allessie MA, Bonke FI, Schopman FJ. Circus movement in rabbit atrial muscle as a mechanism of trachycardia. *Circ Res.* 1973;33(1):54-62.

26. Jalife J, Berenfeld O, Skanes A, Mandapati R. Mechanisms of atrial fibrillation: mother rotors or multiple daughter wavelets, or both? *J Cardiovasc Electrophysiol.* 1998;9(8 Suppl):S2-12.

27. Jalife J, Gray R. Drifting vortices of electrical waves underlie ventricular fibrillation in the rabbit heart. *Acta Physiol Scand.* 1996;157(2):123-131.

28. Mansour M, Mandapati R, Berenfeld O, Chen J, Samie FH, Jalife J. Left-to-right gradient of atrial frequencies during acute atrial fibrillation in the isolated sheep heart. *Circulation.* 2001;103(21):2631-2636.
29. Winfree AT. Spiral waves of chemical activity. *Science.* 1972;175(4022):634-636.
30. Berenfeld O, Pertsov AM. Dynamics of intramural scroll waves in three-dimensional continuous myocardium with rotational anisotropy. *J Theor Biol.* 1999;199(4):383-394.
31. Yamazaki M, Mironov S, Taravant C, Brec J, Vaquero LM, Bandaru K, Avula UM, Honjo H, Kodama I, Berenfeld O, Kalifa J. Heterogeneous atrial wall thickness and stretch promote scroll waves anchoring during atrial fibrillation. *Cardiovasc Res.* 2012;94(1):48-57.
32. Vaquero M, Calvo D, Jalife J. Cardiac fibrillation: from ion channels to rotors in the human heart. *Heart Rhythm.* 2008;5(6):872-879.
33. Fast VG, Kleber AG. Role of wavefront curvature in propagation of cardiac impulse. *Cardiovasc Res.* 1997;33(2):258-271.
34. Pandit SV, Berenfeld O, Anumonwo JM, Zaritski RM, Kneller J, Nattel S, Jalife J. Ionic determinants of functional reentry in a 2-D model of human atrial cells during simulated chronic atrial fibrillation. *Biophys J.* 2005;88(6):3806-3821.
35. Pandit SV, Jalife J. Rotors and the dynamics of cardiac fibrillation. *Circ Res.* 2013;112(5):849-862.
36. Cabo C, Pertsov AM, Davidenko JM, Baxter WT, Gray RA, Jalife J. Vortex shedding as a precursor of turbulent electrical activity in cardiac muscle. *Biophys J.* 1996;70(3):1105-1111.
37. Noujaim SF, Berenfeld O, Kalifa J, Cerrone M, Nanthakumar K, Atienza F, Moreno J, Mironov S, Jalife J. Universal scaling law of electrical turbulence in the mammalian heart. *Proc Natl Acad Sci U S A.* 2007;104(52):20985-20989.
38. Tanaka K, Zlochiver S, Vikstrom KL, Yamazaki M, Moreno J, Klos M, Zaitsev AV, Vaidyanathan R, Auerbach DS, Landas S, Guiraudon G, Jalife J, Berenfeld O, Kalifa J. Spatial distribution of fibrosis governs fibrillation wave dynamics in the posterior left atrium during heart failure. *Circ Res.* 2007;101(8):839-847.
39. Berenfeld O, Zaitsev AV, Mironov SF, Pertsov AM, Jalife J. Frequency-dependent breakdown of wave propagation into fibrillatory conduction across the pectinate muscle network in the isolated sheep right atrium. *Circ Res.* 2002;90(11):1173-1180.
40. Narayan S. Conventional ablation for atrial fibrillation with or without focal impulse and rotor modulation (the CONFIRM trial). *Abstract, Heart Rhythm Society Scientific Sessions.* 2011.
41. Nathan H, Eliakim M. The junction between the left atrium and the pulmonary veins. An anatomic study of human hearts. *Circulation.* 1966;34(3):412-422.
42. Hassink RJ, Aretz HT, Ruskin J, Keane D. Morphology of atrial myocardium in human pulmonary veins: a postmortem analysis in patients with and without atrial fibrillation. *J Am Coll Cardiol.* 2003;42(6):1108-1114.
43. Ho SY, Sanchez-Quintana D, Cabrera JA, Anderson RH. Anatomy of the left atrium: implications for radiofrequency ablation of atrial fibrillation. *J Cardiovasc Electrophysiol.* 1999;10(11):1525-1533.

44. Roux N, Havet E, Mertl P. The myocardial sleeves of the pulmonary veins: potential implications for atrial fibrillation. *Surg Radiol Anat.* 2004;26(4):285-289.

45. Steiner I, Hajkova P, Kvasnicka J, Kholova I. Myocardial sleeves of pulmonary veins and atrial fibrillation: a postmortem histopathological study of 100 subjects. *Virchows Arch.* 2006;449(1):88-95.

46. Hertervig E, Kongstad O, Ljungstrom E, Olsson B, Yuan S. Pulmonary vein potentials in patients with and without atrial fibrillation. *Europace.* 2008;10(6):692-697.

47. Verheule S, Wilson EE, Arora R, Engle SK, Scott LR, Olgin JE. Tissue structure and connexin expression of canine pulmonary veins. *Cardiovasc Res.* 2002;55(4):727-738.

48. Ehrlich JR, Cha TJ, Zhang L, Chartier D, Melnyk P, Hohnloser SH, Nattel S. Cellular electrophysiology of canine pulmonary vein cardiomyocytes: action potential and ionic current properties. *J Physiol.* 2003;551(Pt 3):801-813.

49. Chen YJ, Chen SA, Chen YC, Yeh HI, Chan P, Chang MS, Lin CI. Effects of rapid atrial pacing on the arrhythmogenic activity of single cardiomyocytes from pulmonary veins: implication in initiation of atrial fibrillation. *Circulation.* 2001;104(23):2849-2854.

50. Dupont E, Ko Y, Rothery S, Coppen SR, Baghai M, Haw M, Severs NJ. The gap-junctional protein connexin40 is elevated in patients susceptible to postoperative atrial fibrillation. *Circulation.* 2001;103(6):842-849.

51. de Bakker JM, Ho SY, Hocini M. Basic and clinical electrophysiology of pulmonary vein ectopy. *Cardiovasc Res.* 2002;54(2):287-294.

52. Po SS, Li Y, Tang D, Liu H, Geng N, Jackman WM, Scherlag B, Lazzara R, Patterson E. Rapid and stable re-entry within the pulmonary vein as a mechanism initiating paroxysmal atrial fibrillation. *J Am Coll Cardiol.* 2005;45(11):1871-1877.

53. Saito T, Waki K, Becker AE. Left atrial myocardial extension onto pulmonary veins in humans: anatomic observations relevant for atrial arrhythmias. *J Cardiovasc Electrophysiol.* 2000;11(8):888-894.

54. Kalifa J, Jalife J, Zaitsev AV, Bagwe S, Warren M, Moreno J, Berenfeld O, Nattel S. Intra-atrial pressure increases rate and organization of waves emanating from the superior pulmonary veins during atrial fibrillation. *Circulation.* 2003;108(6):668-671.

55. Lin WS, Tai CT, Hsieh MH, Tsai CF, Lin YK, Tsao HM, Huang JL, Yu WC, Yang SP, Ding YA, Chang MS, Chen SA. Catheter ablation of paroxysmal atrial fibrillation initiated by non-pulmonary vein ectopy. *Circulation.* 2003;107(25):3176-3183.

56. Calkins H, Kuck KH, Cappato R, Brugada J, Camm AJ, Chen SA, Crijns HJ, Damiano RJ, Jr., Davies DW, Dimarco J, Edgerton J, Ellenbogen K, Ezekowitz MD, Haines DE, Haissaguerre M, Hindricks G, Iesaka Y, Jackman W, Jalife J, Jais P, Kalman J, Keane D, Kim YH, Kirchhof P, Klein G, Kottkamp H, Kumagai K, Lindsay BD, Mansour M, Marchlinski FE, McCarthy PM, Mont JL, Morady F, Nademanee K, Nakagawa H, Natale A, Nattel S, Packer DL, Pappone C, Prystowsky E, Raviele A, Reddy V, Ruskin JN, Shemin RJ, Tsao HM, Wilber Wedge D, Prystowsky EN, Damiano R, Jr., Jackman WM, Marchlinski F, McCarthy P, Wilber D, Ad N, Cummings J, Gillinov AM, Heidbuchel H, January C, Lip G, Markowitz S, Nair M, Ovsyshcher IE, Pak HN, Tsuchiya T, Shah D, Siong TW, Vardas PE. 2012 HRS/EHRA/ECAS Expert Consensus Statement on Catheter and Surgical Ablation of

Atrial Fibrillation: Recommendations for Patient Selection, Procedural Techniques, Patient Management and Follow-up, Definitions, Endpoints, and Research Trial Design: A report of the Heart Rhythm Society (HRS) Task Force on Catheter and Surgical Ablation of Atrial Fibrillation. Developed in partnership with the European Heart Rhythm Association (EHRA), a registered branch of the European Society of Cardiology (ESC) and the European Cardiac Arrhythmia Society (ECAS); and in collaboration with the American College of Cardiology (ACC), American Heart Association (AHA), the Asia Pacific Heart Rhythm Society (APHRS), and the Society of Thoracic Surgeons (STS). Endorsed by the governing bodies of the American College of Cardiology Foundation, the American Heart Association, the European Cardiac Arrhythmia Society, the European Heart Rhythm Association, the Society of Thoracic Surgeons, the Asia Pacific Heart Rhythm Society, and the Heart Rhythm Society. *Europace.* 2012;14(4):528-606.

57. Nademanee K, McKenzie J, Kosar E, Schwab M, Sunsaneewitayakul B, Vasavakul T, Khunnawat C, Ngarmukos T. A new approach for catheter ablation of atrial fibrillation: mapping of the electrophysiologic substrate. *J Am Coll Cardiol.* 2004;43(11):2044-2053.

58. Hayward RM, Upadhyay GA, Mela T, Ellinor PT, Barrett CD, Heist EK, Verma A, Choudhry NK, Singh JP. Pulmonary vein isolation with complex fractionated atrial electrogram ablation for paroxysmal and nonparoxysmal atrial fibrillation: A meta-analysis. *Heart Rhythm.*2011;8(7):994-1000.

59. Scherr D, Dalal D, Cheema A, Nazarian S, Almasry I, Bilchick K, Cheng A, Henrikson CA, Spragg D, Marine JE, Berger RD, Calkins H, Dong J. Long- and short-term temporal stability of complex fractionated atrial electrograms in human left atrium during atrial fibrillation. *J Cardiovasc Electrophysiol.* 2009;20(1):13-21.

60. Jadidi AS, Duncan E, Miyazaki S, Lellouche N, Shah AJ, Forclaz A, Nault I, Wright M, Rivard L, Liu X, Scherr D, Wilton SB, Sacher F, Derval N, Knecht S, Kim SJ, Hocini M, Narayan S, Haissaguerre M, Jais P. Functional nature of electrogram fractionation demonstrated by left atrial high-density mapping. *Circ Arrhythm Electrophysiol.* 2012;5(1):32-42.

61. Lee G, Roberts-Thomson K, Madry A, Spence S, Teh A, Heck PM, Kumar S, Kistler PM, Morton JB, Sanders P, Kalman JM. Relationship among complex signals, short cycle length activity, and dominant frequency in patients with long-lasting persistent AF: a high-density epicardial mapping study in humans. *Heart Rhythm.* 2011;8(11):1714-1719.

62. Konings KT, Smeets JL, Penn OC, Wellens HJ, Allessie MA. Configuration of unipolar atrial electrograms during electrically induced atrial fibrillation in humans. *Circulation.* 1997;95(5):1231-1241.

63. Spach MS, King TD, Barr RC, Boaz DE, Morrow MN, Herman-Giddens S. Electrical potential distribution surrounding the atria during depolarization and repolarization in the dog. *Circ Res.* 1969;24(6):857-873.

64. Katritsis D, Giazitzoglou E, Sougiannis D, Voridis E, Po SS. Complex fractionated atrial electrograms at anatomic sites of ganglionated plexi in atrial fibrillation. *Europace.* 2009;11(3):308-315.

65. Pokushalov E, Romanov A, Katritsis DG, Artyomenko S, Shirokova N, Karaskov A, Mittal S, Steinberg JS. Ganglionated plexus ablation vs linear ablation in patients undergoing pulmonary vein isolation for persistent/long-standing persistent atrial fibrillation: a randomized comparison. *Heart Rhythm.* 2013;10(9):1280-1286.

66. Pokushalov E, Romanov A, Shugayev P, Artyomenko S, Shirokova N, Turov A, Katritsis DG. Selective ganglionated plexi ablation for paroxysmal atrial fibrillation. *Heart Rhythm.* 2009;6(9):1257-1264.

67. Zhou Q, Hou Y, Yang S. A meta-analysis of the comparative efficacy of ablation for atrial fibrillation with and without ablation of the ganglionated plexi. *Pacing Clin Electrophysiol.* 2011;34(12):1687-1694.

68. Wu J, Estner H, Luik A, Ucer E, Reents T, Pflaumer A, Zrenner B, Hessling G, Deisenhofer I. Automatic 3D mapping of complex fractionated atrial electrograms (CFAE) in patients with paroxysmal and persistent atrial fibrillation. *J Cardiovasc Electrophysiol.* 2008;19(9):897-903.

69. Qi XY, Yeh YH, Xiao L, Burstein B, Maguy A, Chartier D, Villeneuve LR, Brundel BJ, Dobrev D, Nattel S. Cellular signaling underlying atrial tachycardia remodeling of L-type calcium current. *Circ Res.* 2008;103(8):845-854.

70. Lu Y, Zhang Y, Wang N, Pan Z, Gao X, Zhang F, Shan H, Luo X, Bai Y, Sun L, Song W, Xu C, Wang Z, Yang B. MicroRNA-328 contributes to adverse electrical remodeling in atrial fibrillation. *Circulation.* 2010;122(23):2378-2387.

71. Bosch RF, Zeng X, Grammer JB, Popovic K, Mewis C, Kuhlkamp V. Ionic mechanisms of electrical remodeling in human atrial fibrillation. *Cardiovasc Res.* 1999;44(1):121-131.

72. Wang Z, Lu Y, Yang B. MicroRNAs and atrial fibrillation: new fundamentals. *Cardiovasc Res.* 2011;89(4):710-721.

73. Voigt N, Trausch A, Knaut M, Matschke K, Varro A, Van Wagoner DR, Nattel S, Ravens U, Dobrev D. Left-to-right atrial inward rectifier potassium current gradients in patients with paroxysmal versus chronic atrial fibrillation. *Circ Arrhythm Electrophysiol.* 2010;3(5):472-480.

74. Voigt N, Maguy A, Yeh YH, Qi X, Ravens U, Dobrev D, Nattel S. Changes in I K, ACh single-channel activity with atrial tachycardia remodelling in canine atrial cardiomyocytes. *Cardiovasc Res.* 2008;77(1):35-43.

75. Makary S, Voigt N, Maguy A, Wakili R, Nishida K, Harada M, Dobrev D, Nattel S. Differential protein kinase C isoform regulation and increased constitutive activity of acetylcholine-regulated potassium channels in atrial remodeling. *Circ Res.* 2011;109(9):1031-1043.

76. Sarmast F, Kolli A, Zaitsev A, Parisian K, Dhamoon AS, Guha PK, Warren M, Anumonwo JM, Taffet SM, Berenfeld O, Jalife J. Cholinergic atrial fibrillation: I(K,ACh) gradients determine unequal left/right atrial frequencies and rotor dynamics. *Cardiovasc Res.* 2003;59(4):863-873.

77. Swartz MF, Fink GW, Lutz CJ, Taffet SM, Berenfeld O, Vikstrom KL, Kasprowicz K, Bhatta L, Puskas F, Kalifa J, Jalife J. Left versus right atrial difference in dominant frequency, K(+) channel transcripts, and fibrosis in patients developing atrial fibrillation after cardiac surgery. *Heart Rhythm.* 2009;6(10):1415-1422.

78. Li D, Zhang L, Kneller J, Nattel S. Potential ionic mechanism for repolarization differences between canine right and left atrium. *Circ Res.* 2001;88(11):1168-1175.

79. Gaspo R, Bosch RF, Talajic M, Nattel S. Functional mechanisms underlying tachycardia-induced sustained atrial fibrillation in a chronic dog model. *Circulation.* 1997;96(11):4027-4035.

80. Yagi T, Pu J, Chandra P, Hara M, Danilo P, Jr., Rosen MR, Boyden PA. Density and function of inward currents in right atrial cells from chronically fibrillating canine atria. *Cardiovasc Res.* 2002;54(2):405-415.

81. Sossalla S, Kallmeyer B, Wagner S, Mazur M, Maurer U, Toischer K, Schmitto JD, Seipelt R, Schondube FA, Hasenfuss G, Belardinelli L, Maier LS. Altered Na(+) currents in atrial fibrillation effects of ranolazine on arrhythmias and contractility in human atrial myocardium. *J Am Coll Cardiol.* 2010;55(21):2330-2342.

82. Van Wagoner DR, Pond AL, McCarthy PM, Trimmer JS, Nerbonne JM. Outward K+ current densities and Kv1.5 expression are reduced in chronic human atrial fibrillation. *Circ Res.* 1997;80(6):772-781.

83. Workman AJ, Kane KA, Rankin AC. The contribution of ionic currents to changes in refractoriness of human atrial myocytes associated with chronic atrial fibrillation. *Cardiovasc Res.* 2001;52(2):226-235.

84. Cha TJ, Ehrlich JR, Zhang L, Nattel S. Atrial ionic remodeling induced by atrial tachycardia in the presence of congestive heart failure. *Circulation.* 2004;110(12):1520-1526.

85. Cha TJ, Ehrlich JR, Zhang L, Chartier D, Leung TK, Nattel S. Atrial tachycardia remodeling of pulmonary vein cardiomyocytes: comparison with left atrium and potential relation to arrhythmogenesis. *Circulation.* 2005;111(6):728-735.

86. Li D, Melnyk P, Feng J, Wang Z, Petrecca K, Shrier A, Nattel S. Effects of experimental heart failure on atrial cellular and ionic electrophysiology. *Circulation.* 2000;101(22):2631-2638.

87. Ausma J, Wijffels M, Thone F, Wouters L, Allessie M, Borgers M. Structural changes of atrial myocardium due to sustained atrial fibrillation in the goat. *Circulation.* 1997;96(9):3157-3163.

88. Frustaci A, Chimenti C, Bellocci F, Morgante E, Russo MA, Maseri A. Histological substrate of atrial biopsies in patients with lone atrial fibrillation. *Circulation.* 1997;96(4):1180-1184.

89. Vasquez C, Benamer N, Morley GE. The cardiac fibroblast: functional and electrophysiological considerations in healthy and diseased hearts. *J Cardiovasc Pharmacol.* 2011;57(4):380-388.

90. Souders CA, Bowers SL, Baudino TA. Cardiac fibroblast: the renaissance cell. *Circ Res.* 2009;105(12):1164-1176.

91. Wakili R, Voigt N, Kaab S, Dobrev D, Nattel S. Recent advances in the molecular pathophysiology of atrial fibrillation. *J Clin Invest.* 2011;121(8):2955-2968.

92. Tsai CT, Tseng CD, Hwang JJ, Wu CK, Yu CC, Wang YC, Chen WP, Lai LP, Chiang FT, Lin JL. Tachycardia of atrial myocytes induces collagen expression in atrial fibroblasts through transforming growth factor beta1. *Cardiovasc Res.* 2011;89(4):805-815.

93. Burstein B, Libby E, Calderone A, Nattel S. Differential behaviors of atrial versus ventricular fibroblasts: a potential role for platelet-derived growth factor in atrial-ventricular remodeling differences. *Circulation.* 2008;117(13):1630-1641.

94. Duisters RF, Tijsen AJ, Schroen B, Leenders JJ, Lentink V, van der Made I, Herias V, van Leeuwen RE, Schellings MW, Barenbrug P, Maessen JG, Heymans S, Pinto YM, Creemers EE. miR-133 and miR-30 regulate connective tissue growth factor: implications for a role of microRNAs in myocardial matrix remodeling. *Circ Res.* 2009;104(2):170-178, 176p following 178.

95. Maleckar MM, Greenstein JL, Giles WR, Trayanova NA. Electrotonic coupling between human atrial myocytes and fibroblasts alters myocyte excitability and repolarization. *Biophys J.* 2009;97(8):2179-2190.

96. Xie Y, Garfinkel A, Camelliti P, Kohl P, Weiss JN, Qu Z. Effects of fibroblast-myocyte coupling on cardiac conduction and vulnerability to reentry: A computational study. *Heart Rhythm.* 2009;6(11):1641-1649.

97. Ausma J, van der Velden HM, Lenders MH, van Ankeren EP, Jongsma HJ, Ramaekers FC, Borgers M, Allessie MA. Reverse structural and gap-junctional remodeling after prolonged atrial fibrillation in the goat. *Circulation.* 2003;107(15):2051-2058.

98. Gaborit N, Steenman M, Lamirault G, Le Meur N, Le Bouter S, Lande G, Leger J, Charpentier F, Christ T, Dobrev D, Escande D, Nattel S, Demolombe S. Human atrial ion channel and transporter subunit gene-expression remodeling associated with valvular heart disease and atrial fibrillation. *Circulation.* 2005;112(4):471-481.

99. van der Velden HM, Wilders R, Jongsma HJ. Atrial fibrillation-induced gap junctional remodeling. *J Am Coll Cardiol.* 2002;39(10):1709; author reply 1709-1710.

100. Gollob MH, Jones DL, Krahn AD, Danis L, Gong XQ, Shao Q, Liu X, Veinot JP, Tang AS, Stewart AF, Tesson F, Klein GJ, Yee R, Skanes AC, Guiraudon GM, Ebihara L, Bai D. Somatic mutations in the connexin 40 gene (GJA5) in atrial fibrillation. *N Engl J Med.* 2006;354(25):2677-2688.

101. Igarashi T, Finet JE, Takeuchi A, Fujino Y, Strom M, Greener ID, Rosenbaum DS, Donahue JK. Connexin gene transfer preserves conduction velocity and prevents atrial fibrillation. *Circulation.* 2012;125(2):216-225.

102. Tan AY, Li H, Wachsmann-Hogiu S, Chen LS, Chen PS, Fishbein MC. Autonomic innervation and segmental muscular disconnections at the human pulmonary vein-atrial junction: implications for catheter ablation of atrial-pulmonary vein junction. *J Am Coll Cardiol.* 2006;48(1):132-143.

103. Shen MJ, Choi EK, Tan AY, Lin SF, Fishbein MC, Chen LS, Chen PS. Neural mechanisms of atrial arrhythmias. *Nat Rev Cardiol.* 2011;9(1):30-39.

104. Kneller J, Zou R, Vigmond EJ, Wang Z, Leon LJ, Nattel S. Cholinergic atrial fibrillation in a computer model of a two-dimensional sheet of canine atrial cells with realistic ionic properties. *Circ Res.* 2002;90(9):E73-87.

105. Gould PA, Yii M, McLean C, Finch S, Marshall T, Lambert GW, Kaye DM. Evidence for increased atrial sympathetic innervation in persistent human atrial fibrillation. *Pacing Clin Electrophysiol.* 2006;29(8):821-829.

106. Machida T, Hashimoto N, Kuwahara I, Ogino Y, Matsuura J, Yamamoto W, Itano Y, Zamma A, Matsumoto R, Kamon J, Kobayashi T, Ishiwata N, Yamashita T, Ogura T, Nakaya H. Effects of a highly selective acetylcholine-activated K+ channel blocker on experimental atrial fibrillation. *Circ Arrhythm Electrophysiol.* 2011;4(1):94-102.

107. Lu Z, Scherlag BJ, Lin J, Niu G, Fung KM, Zhao L, Ghias M, Jackman WM, Lazzara R, Jiang H, Po SS. Atrial fibrillation begets atrial fibrillation: autonomic mechanism for atrial electrical remodeling induced by short-term rapid atrial pacing. *Circ Arrhythm Electrophysiol.* 2008;1(3):184-192.

108. Sheng X, Scherlag BJ, Yu L, Li S, Ali R, Zhang Y, Fu G, Nakagawa H, Jackman WM, Lazzara R, Po SS. Prevention and reversal of atrial fibrillation inducibility and autonomic remodeling by low-level vagosympathetic nerve stimulation. *J Am Coll Cardiol.* 2011;57(5):563-571.

109. Katritsis DG. Autonomic denervation for the treatment of atrial fibrillation. *Indian Pacing Electrophysiol J.* 2011;11(6):161-166.

110. Calo L, Rebecchi M, Sciarra L, De Luca L, Fagagnini A, Zuccaro LM, Pitrone P, Dottori S, Porfirio M, de Ruvo E, Lioy E. Catheter ablation of right atrial ganglionated plexi in patients with vagal paroxysmal atrial fibrillation. *Circ Arrhythm Electrophysiol.* 2012;5(1):22-31.

111. Mahida S, Lubitz SA, Rienstra M, Milan DJ, Ellinor PT. Monogenic atrial fibrillation as pathophysiological paradigms. *Cardiovasc Res.* 2011;89(4):692-700.

112. Mommersteeg MT, Christoffels VM, Anderson RH, Moorman AF. Atrial fibrillation: a developmental point of view. *Heart Rhythm.* 2009;6(12):1818-1824.

113. Fox CS, Parise H, D'Agostino RB, Sr., Lloyd-Jones DM, Vasan RS, Wang TJ, Levy D, Wolf PA, Benjamin EJ. Parental atrial fibrillation as a risk factor for atrial fibrillation in offspring. *JAMA.* 2004;291(23):2851-2855.

114. Boldt LH, Posch MG, Perrot A, Polotzki M, Rolf S, Parwani AS, Huemer M, Wutzler A, Ozcelik C, Haverkamp W. Mutational analysis of the PITX2 and NKX2-5 genes in patients with idiopathic atrial fibrillation. *Int J Cardiol.* 2010;145(2):316-317.

115. Chen YH, Xu SJ, Bendahhou S, Wang XL, Wang Y, Xu WY, Jin HW, Sun H, Su XY, Zhuang QN, Yang YQ, Li YB, Liu Y, Xu HJ, Li XF, Ma N, Mou CP, Chen Z, Barhanin J, Huang W. KCNQ1 gain-of-function mutation in familial atrial fibrillation. *Science.* 2003;299(5604):251-254.

116. Das S, Makino S, Melman YF, Shea MA, Goyal SB, Rosenzweig A, Macrae CA, Ellinor PT. Mutation in the S3 segment of KCNQ1 results in familial lone atrial fibrillation. *Heart Rhythm.* 2009;6(8):1146-1153.

117. Hong K, Piper DR, Diaz-Valdecantos A, Brugada J, Oliva A, Burashnikov E, Santos-de-Soto J, Grueso-Montero J, Diaz-Enfante E, Brugada P, Sachse F, Sanguinetti MC, Brugada R. De novo KCNQ1 mutation responsible for atrial fibrillation and short QT syndrome in utero. *Cardiovasc Res.* 2005;68(3):433-440.

118. Yang Y, Xia M, Jin Q, Bendahhou S, Shi J, Chen Y, Liang B, Lin J, Liu Y, Liu B, Zhou Q, Zhang D, Wang R, Ma N, Su X, Niu K, Pei Y, Xu W, Chen Z, Wan H, Cui J, Barhanin J. Identification of a KCNE2 gain-of-function mutation in patients with familial atrial fibrillation. *Am J Hum Genet.* 2004;75(5):899-905.

119. Ravn LS, Aizawa Y, Pollevick GD, Hofman-Bang J, Cordeiro JM, Dixen U, Jensen G, Wu Y, Burashnikov E, Haunso S, Guerchicoff A, Hu D, Svendsen JH, Christiansen M, Antzelevitch C. Gain of function in IKs secondary to a mutation in KCNE5 associated with atrial fibrillation. *Heart Rhythm.* 2008;5(3):427-435.

120. Xia M, Jin Q, Bendahhou S, He Y, Larroque MM, Chen Y, Zhou Q, Yang Y, Liu Y, Liu B, Zhu Q, Zhou Y, Lin J, Liang B, Li L, Dong X, Pan Z, Wang R, Wan H, Qiu W, Xu W, Eurlings P, Barhanin J. A Kir2.1 gain-of-function mutation underlies familial atrial fibrillation. *Biochem Biophys Res Commun.* 2005;332(4):1012-1019.

121. Jalife J, Delmar M, Anumonwo J, Berenfeld O, Kalifa J. *Basic cardiac electrophysiology for the clinician*: Blackwell Publishing; 2009.

122. Hong K, Bjerregaard P, Gussak I, Brugada R. Short QT syndrome and atrial fibrillation caused by mutation in KCNH2. *J Cardiovasc Electrophysiol.* 2005;16(4):394-396.

123. Olson TM, Alekseev AE, Liu XK, Park S, Zingman LV, Bienengraeber M, Sattiraju S, Ballew JD, Jahangir A, Terzic A. Kv1.5 channelopathy due to KCNA5 loss-of-function mutation causes human atrial fibrillation. *Hum Mol Genet.* 2006;15(14):2185-2191.

124. Yang Y, Li J, Lin X, Hong K, Wang L, Liu J, Li L, Yan D, Liang D, Xiao J, Jin H, Wu J, Zhang Y, Chen YH. Novel KCNA5 loss-of-function mutations responsible for atrial fibrillation. *J Hum Genet.* 2009;54(5):277-283.

125. Ellinor PT, Petrov-Kondratov VI, Zakharova E, Nam EG, MacRae CA. Potassium channel gene mutations rarely cause atrial fibrillation. *BMC Med Genet.* 2006;7:70.

126. Olson TM, Michels VV, Ballew JD, Reyna SP, Karst ML, Herron KJ, Horton SC, Rodeheffer RJ, Anderson JL. Sodium channel mutations and susceptibility to heart failure and atrial fibrillation. *JAMA.* 2005;293(4):447-454.

127. Makiyama T, Akao M, Shizuta S, Doi T, Nishiyama K, Oka Y, Ohno S, Nishio Y, Tsuji K, Itoh H, Kimura T, Kita T, Horie M. A novel SCN5A gain-of-function mutation M1875T associated with familial atrial fibrillation. *J Am Coll Cardiol.* 2008;52(16):1326-1334.

128. Watanabe H, Darbar D, Kaiser DW, Jiramongkolchai K, Chopra S, Donahue BS, Kannankeril PJ, Roden DM. Mutations in sodium channel beta1- and beta2-subunits associated with atrial fibrillation. *Circ Arrhythm Electrophysiol.* 2009;2(3):268-275.

129. Zhang X, Yang H, Corydon MJ, Pedersen S, Korenberg JR, Chen XN, Laporte J, Gregersen N, Niebuhr E, Liu G, Bolund L. Localization of a human nucleoporin 155 gene (NUP155) to the 5p13 region and cloning of its cDNA. *Genomics.* 1999;57(1):144-151.

130. Hodgson-Zingman DM, Karst ML, Zingman LV, Heublein DM, Darbar D, Herron KJ, Ballew JD, de Andrade M, Burnett JC, Jr., Olson TM. Atrial natriuretic peptide frameshift mutation in familial atrial fibrillation. *N Engl J Med.* 2008;359(2):158-165.

131. Magnani JW, Rienstra M, Lin H, Sinner MF, Lubitz SA, McManus DD, Dupuis J, Ellinor PT, Benjamin EJ. Atrial fibrillation: current knowledge and future directions in epidemiology and genomics. *Circulation.*124(18):1982-1993.

132. Filgueiras-Rama D, Martins RP, Ennis SR, Mironov S, Jiang J, Yamazaki M, Kalifa J, Jalife J, Berenfeld O. High-resolution endocardial and epicardial optical mapping in a sheep model of stretch-induced atrial fibrillation. *J Vis Exp.* 2011;(53).

133. Mandapati R, Skanes A, Chen J, Berenfeld O, Jalife J. Stable microreentrant sources as a mechanism of atrial fibrillation in the isolated sheep heart. *Circulation.* 2000;101(2):194-199.

134. Atienza F, Almendral J, Moreno J, Vaidyanathan R, Talkachou A, Kalifa J, Arenal A, Villacastin JP, Torrecilla EG, Sanchez A, Ploutz-Snyder R, Jalife J, Berenfeld O. Activation of inward rectifier potassium channels accelerates atrial fibrillation in humans: evidence for a reentrant mechanism. *Circulation.* 2006;114(23):2434-2442.

135. Lazar S, Dixit S, Marchlinski FE, Callans DJ, Gerstenfeld EP. Presence of left-to-right atrial frequency gradient in paroxysmal but not persistent atrial fibrillation in humans. *Circulation.* 2004;110(20):3181-3186.

136. Sanders P, Berenfeld O, Hocini M, Jais P, Vaidyanathan R, Hsu LF, Garrigue S, Takahashi Y, Rotter M, Sacher F, Scavee C, Ploutz-Snyder R, Jalife J, Haissaguerre M. Spectral analysis identifies sites of high-frequency activity maintaining atrial fibrillation in humans. *Circulation.* 2005;112(6):789-797.

137. Lin YJ, Tai CT, Kao T, Tso HW, Higa S, Tsao HM, Chang SL, Hsieh MH, Chen SA. Frequency analysis in different types of paroxysmal atrial fibrillation. *J Am Coll Cardiol.* 2006;47(7):1401-1407.

138. Elvan A, Linnenbank AC, van Bemmel MW, Misier AR, Delnoy PP, Beukema WP, de Bakker JM. Dominant frequency of atrial fibrillation correlates poorly with atrial fibrillation cycle length. *Circ Arrhythm Electrophysiol.* 2009;2(6):634-644.

139. Berenfeld O, Ennis S, Hwang E, Hooven B, Grzeda K, Mironov S, Yamazaki M, Kalifa J, Jalife J. Time- and frequency-domain analyses of atrial fibrillation activation rate: the optical mapping reference. *Heart Rhythm.* 2012;8(11):1758-1765.

140. Anne W, Willems R, Holemans P, Beckers F, Roskams T, Lenaerts I, Ector H, Heidbuchel H. Self-terminating AF depends on electrical remodeling while persistent AF depends on additional structural changes in a rapid atrially paced sheep model. *J Mol Cell Cardiol.* 2007;43(2):148-158.

141. Roka A, Toth E, Szilagyi S, Merkely B. Electrical atrial fibrillation induction affects the characteristics of induced arrhythmia. *J Electrocardiol.* 2008;41(2):131-137.

142. Yue L, Feng J, Gaspo R, Li GR, Wang Z, Nattel S. Ionic remodeling underlying action potential changes in a canine model of atrial fibrillation. *Circ Res.* 1997;81(4):512-525.

143. Filgueiras-Rama D, Price NF, Martins RP, Yamazaki M, Avula UM, Kaur K, Kalifa J, Ennis SR, Hwang E, Devabhaktuni V, Jalife J, Berenfeld O. Long-term frequency gradients during persistent atrial fibrillation in sheep are associated with stable sources in the left atrium. *Circ Arrhythm Electrophysiol.* 2012;5(6):1160-1167.

144. Atienza F, Almendral J, Jalife J, Zlochiver S, Ploutz-Snyder R, Torrecilla EG, Arenal A, Kalifa J, Fernandez-Aviles F, Berenfeld O. Real-time dominant frequency mapping and ablation of dominant frequency sites in atrial fibrillation with left-to-right frequency gradients predicts long-term maintenance of sinus rhythm. *Heart Rhythm.* 2009;6(1):33-40.

145. Hocini M, Nault I, Wright M, Veenhuyzen G, Narayan SM, Jais P, Lim KT, Knecht S, Matsuo S, Forclaz A, Miyazaki S, Jadidi A, O'Neill MD, Sacher F, Clementy J, Haissaguerre M. Disparate evolution of right and left atrial rate during ablation of long-lasting persistent atrial fibrillation. *J Am Coll Cardiol.* 2010;55(10):1007-1016.

146. Israel CW, Gronefeld G, Ehrlich JR, Li YG, Hohnloser SH. Long-term risk of recurrent atrial fibrillation as documented by an implantable monitoring device: implications for optimal patient care. *J Am Coll Cardiol.* 2004;43(1):47-52.

147. Nabauer M, Gerth A, Limbourg T, Schneider S, Oeff M, Kirchhof P, Goette A, Lewalter T, Ravens U, Meinertz T, Breithardt G, Steinbeck G. The Registry of the German Competence NETwork on Atrial Fibrillation: patient characteristics and initial management. *Europace.* 2009;11(4):423-434.

148. Nieuwlaat R, Prins MH, Le Heuzey JY, Vardas PE, Aliot E, Santini M, Cobbe SM, Widdershoven JW, Baur LH, Levy S, Crijns HJ. Prognosis, disease progression, and treatment of atrial fibrillation patients during 1 year: follow-up of the Euro Heart Survey on atrial fibrillation. *Eur Heart J.* 2008;29(9):1181-1189.

149. Barrett TW, Self WH, Wasserman BS, McNaughton CD, Darbar D. Evaluating the HATCH score for predicting progression to sustained atrial fibrillation in ED patients with new atrial fibrillation. *Am J Emerg Med.* 2013;31(5):792-797.

150. De Vos CB, Breithardt G, Camm AJ, Dorian P, Kowey PR, Le Heuzey JY, Naditch-Brule L, Prystowsky EN, Schwartz PJ, Torp-Pedersen C, Weintraub WS, Crijns HJ. Progression of atrial fibrillation in the REgistry on Cardiac rhythm disORDers assessing the control of Atrial Fibrillation cohort: clinical correlates and the effect of rhythm-control therapy. *Am Heart J.* 2012;163(5):887-893.

151. de Vos CB, Pisters R, Nieuwlaat R, Prins MH, Tieleman RG, Coelen RJ, van den Heijkant AC, Allessie MA, Crijns HJ. Progression from paroxysmal to persistent atrial fibrillation clinical correlates and prognosis. *J Am Coll Cardiol.* 2010;55(8):725-731.

152. Jahangir A, Lee V, Friedman PA, Trusty JM, Hodge DO, Kopecky SL, Packer DL, Hammill SC, Shen WK, Gersh BJ. Long-term progression and outcomes with aging in patients with lone atrial fibrillation: a 30-year follow-up study. *Circulation.* 2007;115(24):3050-3056.

153. Kerr CR, Humphries KH, Talajic M, Klein GJ, Connolly SJ, Green M, Boone J, Sheldon R, Dorian P, Newman D. Progression to chronic atrial fibrillation after the initial diagnosis of paroxysmal atrial fibrillation: results from the Canadian Registry of Atrial Fibrillation. *Am Heart J.* 2005;149(3):489-496.

154. Koide Y, Yotsukura M, Ando H, Aoki S, Suzuki T, Sakata K, Ootomo E, Yoshino H. Usefulness of P-wave dispersion in standard twelve-lead electrocardiography to predict transition from paroxysmal to persistent atrial fibrillation. *Am J Cardiol.* 2008;102(5):573-577.

155. Koide Y, Yotsukura M, Sakata K, Yoshino H, Ishikawa K. Investigation of the predictors of transition to persistent atrial fibrillation in patients with paroxysmal atrial fibrillation. *Clin Cardiol.* 2002;25(2):69-75.

156. Potpara TS, Stankovic GR, Beleslin BD, Polovina MM, Marinkovic JM, Ostojic MC, Lip GY. A 12-year follow-up study of patients with newly diagnosed lone atrial

fibrillation: implications of arrhythmia progression on prognosis: the Belgrade Atrial Fibrillation study. *Chest.* 2012;141(2):339-347.

157. Saksena S, Hettrick DA, Koehler JL, Grammatico A, Padeletti L. Progression of paroxysmal atrial fibrillation to persistent atrial fibrillation in patients with bradyarrhythmias. *Am Heart J.* 2007;154(5):884-892.

158. Zhang YY, Qiu C, Davis PJ, Jhaveri M, Prystowsky EN, Kowey P, Weintraub WS. Predictors of Progression of Recently Diagnosed Atrial Fibrillation in REgistry on Cardiac Rhythm DisORDers Assessing the Control of Atrial Fibrillation (RecordAF)-United States Cohort. *Am J Cardiol.* 2013;112(1):79-84.

159. Ruigomez A, Johansson S, Wallander MA, Garcia Rodriguez LA. Predictors and prognosis of paroxysmal atrial fibrillation in general practice in the UK. *BMC Cardiovasc Disord.* 2005;5:20.

160. Kato T, Yamashita T, Sagara K, Iinuma H, Fu LT. Progressive nature of paroxysmal atrial fibrillation. Observations from a 14-year follow-up study. *Circ J.* 2004;68(6):568-572.

161. Liu XP, Xu X, Tian Y, Tang RB, Yu RH, Long DY, Sang CH, Jiang CX, Ning M, Dong JZ, Ma CS. Morphologies of the atria and pulmonary veins in relation to lone atrial fibrillation progression: a dual-source computed tomography scan study. *J Cardiovasc Electrophysiol.* 2012;23 Suppl 1:S29-35.

162. Jongnarangsin K, Suwanagool A, Chugh A, Crawford T, Good E, Pelosi F, Jr., Bogun F, Oral H, Morady F. Effect of catheter ablation on progression of paroxysmal atrial fibrillation. *J Cardiovasc Electrophysiol.* 2012;23(1):9-14.

163. Weerasooriya R, Khairy P, Litalien J, Macle L, Hocini M, Sacher F, Lellouche N, Knecht S, Wright M, Nault I, Miyazaki S, Scavee C, Clementy J, Haissaguerre M, Jais P. Catheter ablation for atrial fibrillation: are results maintained at 5 years of follow-up? *J Am Coll Cardiol.* 2011;57(2):160-166.

164. Van Gelder IC, Hagens VE, Bosker HA, Kingma JH, Kamp O, Kingma T, Said SA, Darmanata JI, Timmermans AJ, Tijssen JG, Crijns HJ. A comparison of rate control and rhythm control in patients with recurrent persistent atrial fibrillation. *N Engl J Med.* 2002;347(23):1834-1840.

165. Pappone C, Radinovic A, Manguso F, Vicedomini G, Ciconte G, Sacchi S, Mazzone P, Paglino G, Gulletta S, Sala S, Santinelli V. Atrial fibrillation progression and management: a 5-year prospective follow-up study. *Heart Rhythm.* 2008;5(11):1501-1507.

166. Grandi E, Pandit SV, Voigt N, Workman AJ, Dobrev D, Jalife J, Bers DM. Human atrial action potential and Ca2+ model: sinus rhythm and chronic atrial fibrillation. *Circ Res.* 2011;109(9):1055-1066.

167. Bosch RF, Scherer CR, Rub N, Wohrl S, Steinmeyer K, Haase H, Busch AE, Seipel L, Kuhlkamp V. Molecular mechanisms of early electrical remodeling: transcriptional downregulation of ion channel subunits reduces I(Ca,L) and I(to) in rapid atrial pacing in rabbits. *J Am Coll Cardiol.* 2003;41(5):858-869.

168. Dobrev D, Graf E, Wettwer E, Himmel HM, Hala O, Doerfel C, Christ T, Schuler S, Ravens U. Molecular basis of downregulation of G-protein-coupled inward rectifying K(+) current (I(K,ACh) in chronic human atrial fibrillation: decrease in GIRK4

mRNA correlates with reduced I(K,ACh) and muscarinic receptor-mediated shortening of action potentials. *Circulation.* 2001;104(21):2551-2557.

169. Caballero R, de la Fuente MG, Gomez R, Barana A, Amoros I, Dolz-Gaiton P, Osuna L, Almendral J, Atienza F, Fernandez-Aviles F, Pita A, Rodriguez-Roda J, Pinto A, Tamargo J, Delpon E. In humans, chronic atrial fibrillation decreases the transient outward current and ultrarapid component of the delayed rectifier current differentially on each atria and increases the slow component of the delayed rectifier current in both. *J Am Coll Cardiol.* 2010;55(21):2346-2354.

170. Zhang H, Garratt CJ, Zhu J, Holden AV. Role of up-regulation of IK1 in action potential shortening associated with atrial fibrillation in humans. *Cardiovasc Res.* 2005;66(3):493-502.

171. Frangogiannis NG, Michael LH, Entman ML. Myofibroblasts in reperfused myocardial infarcts express the embryonic form of smooth muscle myosin heavy chain (SMemb). *Cardiovasc Res.* 2000;48(1):89-100.

172. Dobaczewski M, Gonzalez-Quesada C, Frangogiannis NG. The extracellular matrix as a modulator of the inflammatory and reparative response following myocardial infarction. *J Mol Cell Cardiol.* 2010;48(3):504-511.

173. Musa H, Kaur K, O'Connell R, Klos M, Guerrero-Serna G, Avula UM, Herron TJ, Kalifa J, Anumonwo JM, Jalife J. Inhibition of platelet-derived growth factor-AB signaling prevents electromechanical remodeling of adult atrial myocytes that contact myofibroblasts. *Heart Rhythm.* 2013;10(7):1044-1051.

174. Harada M, Luo X, Qi XY, Tadevosyan A, Maguy A, Ordog B, Ledoux J, Kato T, Naud P, Voigt N, Shi Y, Kamiya K, Murohara T, Kodama I, Tardif JC, Schotten U, Van Wagoner DR, Dobrev D, Nattel S. Transient receptor potential canonical-3 channel-dependent fibroblast regulation in atrial fibrillation. *Circulation.* 2012;126(17):2051-2064.

175. Dobrev D, Friedrich A, Voigt N, Jost N, Wettwer E, Christ T, Knaut M, Ravens U. The G protein-gated potassium current I(K,ACh) is constitutively active in patients with chronic atrial fibrillation. *Circulation.* 2005;112(24):3697-3706.

176. Roten L, Derval N, Pascale P, Scherr D, Komatsu Y, Shah A, Ramoul K, Denis A, Sacher F, Hocini M, Haissaguerre M, Jais P. Current hot potatoes in atrial fibrillation ablation. *Curr Cardiol Rev.* 2012;8(4):327-346.

177. Alboni P, Botto GL, Baldi N, Luzi M, Russo V, Gianfranchi L, Marchi P, Calzolari M, Solano A, Baroffio R, Gaggioli G. Outpatient treatment of recent-onset atrial fibrillation with the "pill-in-the-pocket" approach. *N Engl J Med.* 2004;351(23):2384-2391.

178. Reisinger J, Gatterer E, Heinze G, Wiesinger K, Zeindlhofer E, Gattermeier M, Poelzl G, Kratzer H, Ebner A, Hohenwallner W, Lenz K, Slany J, Kuhn P. Prospective comparison of flecainide versus sotalol for immediate cardioversion of atrial fibrillation. *Am J Cardiol.* 1998;81(12):1450-1454.

179. Wyse DG, Waldo AL, DiMarco JP, Domanski MJ, Rosenberg Y, Schron EB, Kellen JC, Greene HL, Mickel MC, Dalquist JE, Corley SD. A comparison of rate control and rhythm control in patients with atrial fibrillation. *N Engl J Med.* 2002;347(23):1825-1833.

180. Jais P, Cauchemez B, Macle L, Daoud E, Khairy P, Subbiah R, Hocini M, Extramiana F, Sacher F, Bordachar P, Klein G, Weerasooriya R, Clementy J, Haissaguerre M. Catheter ablation versus antiarrhythmic drugs for atrial fibrillation: the A4 study. *Circulation.* 2008;118(24):2498-2505.

181. Pappone C, Augello G, Sala S, Gugliotta F, Vicedomini G, Gulletta S, Paglino G, Mazzone P, Sora N, Greiss I, Santagostino A, LiVolsi L, Pappone N, Radinovic A, Manguso F, Santinelli V. A randomized trial of circumferential pulmonary vein ablation versus antiarrhythmic drug therapy in paroxysmal atrial fibrillation: the APAF Study. *J Am Coll Cardiol.* 2006;48(11):2340-2347.

182. Stabile G, Bertaglia E, Senatore G, De Simone A, Zoppo F, Donnici G, Turco P, Pascotto P, Fazzari M, Vitale DF. Catheter ablation treatment in patients with drug-refractory atrial fibrillation: a prospective, multi-centre, randomized, controlled study (Catheter Ablation For The Cure Of Atrial Fibrillation Study). *Eur Heart J.* 2006;27(2):216-221.

183. Wilber DJ, Pappone C, Neuzil P, De Paola A, Marchlinski F, Natale A, Macle L, Daoud EG, Calkins H, Hall B, Reddy V, Augello G, Reynolds MR, Vinekar C, Liu CY, Berry SM, Berry DA. Comparison of antiarrhythmic drug therapy and radiofrequency catheter ablation in patients with paroxysmal atrial fibrillation: a randomized controlled trial. *JAMA.* 2010;303(4):333-340.

184. Camm AJ, Lip GY, De Caterina R, Savelieva I, Atar D, Hohnloser SH, Hindricks G, Kirchhof P, Bax JJ, Baumgartner H, Ceconi C, Dean V, Deaton C, Fagard R, Funck-Brentano C, Hasdai D, Hoes A, Knuuti J, Kolh P, McDonagh T, Moulin C, Popescu BA, Reiner Z, Sechtem U, Sirnes PA, Tendera M, Torbicki A, Vahanian A, Windecker S, Vardas P, Al-Attar N, Alfieri O, Angelini A, Blomstrom-Lundqvist C, Colonna P, De Sutter J, Ernst S, Goette A, Gorenek B, Hatala R, Heidbuchel H, Heldal M, Kristensen SD, Le Heuzey JY, Mavrakis H, Mont L, Filardi PP, Ponikowski P, Prendergast B, Rutten FH, Schotten U, Van Gelder IC, Verheugt FW. 2012 focused update of the ESC Guidelines for the management of atrial fibrillation: an update of the 2010 ESC Guidelines for the management of atrial fibrillation. Developed with the special contribution of the European Heart Rhythm Association. *Eur Heart J.* 2012;33(21):2719-2747.

185. Cosedis Nielsen J, Johannessen A, Raatikainen P, Hindricks G, Walfridsson H, Kongstad O, Pehrson S, Englund A, Hartikainen J, Mortensen LS, Hansen PS. Radiofrequency ablation as initial therapy in paroxysmal atrial fibrillation. *N Engl J Med.* 2012;367(17):1587-1595.

186. Savelieva I, Camm J. Anti-arrhythmic drug therapy for atrial fibrillation: current anti-arrhythmic drugs, investigational agents, and innovative approaches. *Europace.* 2008;10(6):647-665.

187. Lafuente-Lafuente C, Mouly S, Longas-Tejero MA, Mahe I, Bergmann JF. Antiarrhythmic drugs for maintaining sinus rhythm after cardioversion of atrial fibrillation: a systematic review of randomized controlled trials. *Arch Intern Med.* 2006;166(7):719-728.

188. Dobrev D, Carlsson L, Nattel S. Novel molecular targets for atrial fibrillation therapy. *Nat Rev Drug Discov.* 2012;11(4):275-291.

189. Noujaim SF, Pandit SV, Berenfeld O, Vikstrom K, Cerrone M, Mironov S, Zugermayr M, Lopatin AN, Jalife J. Up-regulation of the inward rectifier K+ current (I K1) in the mouse heart accelerates and stabilizes rotors. *J Physiol.* 2007;578(Pt 1):315-326.

190. Wellner M, Berenfeld O, Jalife J, Pertsov AM. Minimal principle for rotor filaments. *Proc Natl Acad Sci U S A.* 2002;99(12):8015-8018.

191. Sanchez-Chapula JA, Salinas-Stefanon E, Torres-Jacome J, Benavides-Haro DE, Navarro-Polanco RA. Blockade of currents by the antimalarial drug chloroquine in feline ventricular myocytes. *J Pharmacol Exp Ther.* 2001;297(1):437-445.

192. Sato R, Koumi S, Singer DH, Hisatome I, Jia H, Eager S, Wasserstrom JA. Amiodarone blocks the inward rectifier potassium channel in isolated guinea pig ventricular cells. *J Pharmacol Exp Ther.* 1994;269(3):1213-1219.

193. Patel C, Yan GX, Kowey PR. Dronedarone. *Circulation.* 2009;120(7):636-644.

194. Fedida D. Vernakalant (RSD1235): a novel, atrial-selective antifibrillatory agent. *Expert Opin Investig Drugs.* 2007;16(4):519-532.

195. Caballero R, Dolz-Gaiton P, Gomez R, Amoros I, Barana A, Gonzalez de la Fuente M, Osuna L, Duarte J, Lopez-Izquierdo A, Moraleda I, Galvez E, Sanchez-Chapula JA, Tamargo J, Delpon E. Flecainide increases Kir2.1 currents by interacting with cysteine 311, decreasing the polyamine-induced rectification. *Proc Natl Acad Sci U S A.* 2010;107(35):15631-15636.

196. Frisk-Holmberg M, Bergqvist Y, Englund U. Chloroquine intoxication. *Br J Clin Pharmacol.* 1983;15(4):502-503.

197. Roden DM, Woosley RL. Drug therapy. Flecainide. *N Engl J Med.* 1986;315(1):36-41.

198. Donovan KD, Power BM, Hockings BE, Dobb GJ, Lee KY. Intravenous flecainide versus amiodarone for recent-onset atrial fibrillation. *Am J Cardiol.* 1995;75(10):693-697.

199. Haburcak M, Nepali P, Bassil G, Zhang P, Wang B, Baur W, Noujaim SF. Chloroquine Reduces IKACh via Both Direct Channel Blockade and Decreased Surface Expression of Kir3.1/3.4. *Heart Rhythm.* 2013;10(11):1748.

200. Bollmann A, Binias KH, Toepffer I, Molling J, Geller C, Klein HU. Importance of left atrial diameter and atrial fibrillatory frequency for conversion of persistent atrial fibrillation with oral flecainide. *Am J Cardiol.* 2002;90(9):1011-1014.

201. Opthof T. IK1 blockade is unlikely to be a useful antiarrhythmic mechanism. *Cardiovasc Res.* 1994;28(3):420.

202. Burrell ZL, Jr., Martinez AC. Chloroquine and hydroxychloroquine in the treatment of cardiac arrhythmias. *N Engl J Med.* 1958;258(16):798-800.

203. Schram G, Pourrier M, Melnyk P, Nattel S. Differential distribution of cardiac ion channel expression as a basis for regional specialization in electrical function. *Circ Res.* 2002;90(9):939-950.

204. Tristani-Firouzi M, Jensen JL, Donaldson MR, Sansone V, Meola G, Hahn A, Bendahhou S, Kwiecinski H, Fidzianska A, Plaster N, Fu YH, Ptacek LJ, Tawil R. Functional and clinical characterization of KCNJ2 mutations associated with LQT7 (Andersen syndrome). *J Clin Invest.* 2002;110(3):381-388.

205. Chaitman BR, Pepine CJ, Parker JO, Skopal J, Chumakova G, Kuch J, Wang W, Skettino SL, Wolff AA. Effects of ranolazine with atenolol, amlodipine, or diltiazem on exercise tolerance and angina frequency in patients with severe chronic angina: a randomized controlled trial. *JAMA.* 2004;291(3):309-316.

206. Stone PH, Gratsiansky NA, Blokhin A, Huang IZ, Meng L. Antianginal efficacy of ranolazine when added to treatment with amlodipine: the ERICA (Efficacy of Ranolazine in Chronic Angina) trial. *J Am Coll Cardiol.* 2006;48(3):566-575.

207. Antzelevitch C, Burashnikov A, Sicouri S, Belardinelli L. Electrophysiologic basis for the antiarrhythmic actions of ranolazine. *Heart Rhythm.* 2011;8(8):1281-1290.

208. Burashnikov A, Belardinelli L, Antzelevitch C. Atrial-selective sodium channel block strategy to suppress atrial fibrillation: ranolazine versus propafenone. *J Pharmacol Exp Ther.* 2012;340(1):161-168.

209. Kumar K, Nearing BD, Carvas M, Nascimento BC, Acar M, Belardinelli L, Verrier RL. Ranolazine exerts potent effects on atrial electrical properties and abbreviates atrial fibrillation duration in the intact porcine heart. *J Cardiovasc Electrophysiol.* 2009;20(7):796-802.

210. Milberg P, Frommeyer G, Ghezelbash S, Rajamani S, Osada N, Razvan R, Belardinelli L, Breithardt G, Eckardt L. Sodium channel block by ranolazine in an experimental model of stretch-related atrial fibrillation: prolongation of interatrial conduction time and increase in post-repolarization refractoriness. *Europace.* 2013;15(5):761-769.

211. Nattel S, Bourne G, Talajic M. Insights into mechanisms of antiarrhythmic drug action from experimental models of atrial fibrillation. *J Cardiovasc Electrophysiol.* 1997;8(4):469-480.

212. Wang Z, Page P, Nattel S. Mechanism of flecainide's antiarrhythmic action in experimental atrial fibrillation. *Circ Res.* 1992;71(2):271-287.

213. Wijffels MC, Dorland R, Allessie MA. Pharmacologic cardioversion of chronic atrial fibrillation in the goat by class IA, IC, and III drugs: a comparison between hydroquinidine, cibenzoline, flecainide, and d-sotalol. *J Cardiovasc Electrophysiol.* 1999;10(2):178-193.

214. Wijffels MC, Dorland R, Mast F, Allessie MA. Widening of the excitable gap during pharmacological cardioversion of atrial fibrillation in the goat: effects of cibenzoline, hydroquinidine, flecainide, and d-sotalol. *Circulation.* 2000;102(2):260-267.

215. Beyder A, Strege PR, Reyes S, Bernard CE, Terzic A, Makielski J, Ackerman MJ, Farrugia G. Ranolazine decreases mechanosensitivity of the voltage-gated sodium ion channel Na(v)1.5: a novel mechanism of drug action. *Circulation.* 2012;125(22):2698-2706.

216. Burkhardt JD, Di Biase L, Natale A. Long-standing persistent atrial fibrillation: the metastatic cancer of electrophysiology. *J Am Coll Cardiol.* 2012;60(19):1930-1932.

217. Haissaguerre M, Hocini M, Shah AJ, Derval N, Sacher F, Jais P, Dubois R. Noninvasive panoramic mapping of human atrial fibrillation mechanisms: a feasibility report. *J Cardiovasc Electrophysiol.* 2013;24(6):711-717.

218. Narayan SM, Krummen DE, Shivkumar K, Clopton P, Rappel WJ, Miller JM. Treatment of atrial fibrillation by the ablation of localized sources: CONFIRM

(Conventional Ablation for Atrial Fibrillation With or Without Focal Impulse and Rotor Modulation) trial. *J Am Coll Cardiol.* 2012;60(7):628-636.

219. Narayan SM, Krummen DE, Clopton P, Shivkumar K, Miller JM. Direct or coincidental elimination of stable rotors or focal sources may explain successful atrial fibrillation ablation: on-treatment analysis of the CONFIRM trial (Conventional ablation for AF with or without focal impulse and rotor modulation). *J Am Coll Cardiol.* 2013;62(2):138-147.

220. Narayan SM, Patel J, Mulpuru S, Krummen DE. Focal impulse and rotor modulation ablation of sustaining rotors abruptly terminates persistent atrial fibrillation to sinus rhythm with elimination on follow-up: a video case study. *Heart Rhythm.* 2012;9(9):1436-1439.

221. Bordignon S, Chun KR, Gunawardene M, Fuernkranz A, Urban V, Schulte-Hahn B, Nowak B, Schmidt B. Comparison of balloon catheter ablation technologies for pulmonary vein isolation: the laser versus cryo study. *J Cardiovasc Electrophysiol.* 2013;24(9):987-994.

222. Schmidt B, Metzner A, Chun KR, Leftheriotis D, Yoshiga Y, Fuernkranz A, Neven K, Tilz RR, Wissner E, Ouyang F, Kuck KH. Feasibility of circumferential pulmonary vein isolation using a novel endoscopic ablation system. *Circ Arrhythm Electrophysiol.* 2010;3(5):481-488.

223. Metzner A, Chun KR, Neven K, Fuernkranz A, Ouyang F, Antz M, Tilz R, Zerm T, Koektuerk B, Wissner E, Koester I, Ernst S, Boczor S, Kuck KH, Schmidt B. Long-term clinical outcome following pulmonary vein isolation with high-intensity focused ultrasound balloon catheters in patients with paroxysmal atrial fibrillation. *Europace.* 2010;12(2):188-193.

224. Chun KR, Schmidt B, Metzner A, Tilz R, Zerm T, Koster I, Furnkranz A, Koektuerk B, Konstantinidou M, Antz M, Ouyang F, Kuck KH. The 'single big cryoballoon' technique for acute pulmonary vein isolation in patients with paroxysmal atrial fibrillation: a prospective observational single centre study. *Eur Heart J.* 2009;30(6):699-709.

225. Khairy P, Chauvet P, Lehmann J, Lambert J, Macle L, Tanguay JF, Sirois MG, Santoianni D, Dubuc M. Lower incidence of thrombus formation with cryoenergy versus radiofrequency catheter ablation. *Circulation.* 2003;107(15):2045-2050.

226. Weerasooriya R, Jais P, Hocini M, Sacher F, Haissaguerre M. Balloon cryoablation for paroxysmal atrial fibrillation. *Europace.* 2008;10(11):1251-1252.

227. Packer DL, Kowal RC, Wheelan KR, Irwin JM, Champagne J, Guerra PG, Dubuc M, Reddy V, Nelson L, Holcomb RG, Lehmann JW, Ruskin JN. Cryoballoon ablation of pulmonary veins for paroxysmal atrial fibrillation: first results of the North American Arctic Front (STOP AF) pivotal trial. *J Am Coll Cardiol.* 2013;61(16):1713-1723.

228. Van Belle Y, Janse P, Theuns D, Szili-Torok T, Jordaens L. One year follow-up after cryoballoon isolation of the pulmonary veins in patients with paroxysmal atrial fibrillation. *Europace.* 2008;10(11):1271-1276.

229. Vogt J, Heintze J, Gutleben KJ, Muntean B, Horstkotte D, Nolker G. Long-term outcomes after cryoballoon pulmonary vein isolation: results from a prospective study in 605 patients. *J Am Coll Cardiol.* 2013;61(16):1707-1712.

230. Liu CF. Pulmonary vein reconnection after cryoballoon ablation: back to the drawing board. *Heart Rhythm.* 2010;7(2):191-192.

231. Kubala M, Hermida JS, Nadji G, Quenum S, Traulle S, Jarry G. Normal pulmonary veins anatomy is associated with better AF-free survival after cryoablation as compared to atypical anatomy with common left pulmonary vein. *Pacing Clin Electrophysiol.* 2011;34(7):837-843.

232. Sorgente A, Chierchia GB, de Asmundis C, Sarkozy A, Namdar M, Capulzini L, Yazaki Y, Muller-Burri SA, Bayrak F, Brugada P. Pulmonary vein ostium shape and orientation as possible predictors of occlusion in patients with drug-refractory paroxysmal atrial fibrillation undergoing cryoballoon ablation. *Europace.* 2011;13(2):205-212.

233. Bordignon S, Furnkranz A, Schmidt B, Chun KR. Remaining ice cap on second-generation cryoballoon after deflation. *Circ Arrhythm Electrophysiol.* 2012;5(5):e98-99.

234. Casado-Arroyo R, Chierchia GB, Conte G, Levinstein M, Sieira J, Rodriguez-Manero M, di Giovanni G, Baltogiannis Y, Wauters K, de Asmundis C, Sarkozy A, Brugada P. Phrenic nerve paralysis during cryoballoon ablation for atrial fibrillation: A comparison between the first- and second-generation balloon. *Heart Rhythm.* 2013;10(9):1318-1324.

235. Furnkranz A, Bordignon S, Schmidt B, Gunawardene M, Schulte-Hahn B, Urban V, Bode F, Nowak B, Chun JK. Improved procedural efficacy of pulmonary vein isolation using the novel second-generation cryoballoon. *J Cardiovasc Electrophysiol.* 2013;24(5):492-497.

236. Horton R, Di Biase L, Reddy V, Neuzil P, Mohanty P, Sanchez J, Nguyen T, Mohanty S, Gallinghouse GJ, Bailey SM, Zagrodzky JD, Burkhardt JD, Natale A. Locating the right phrenic nerve by imaging the right pericardiophrenic artery with computerized tomographic angiography: implications for balloon-based procedures. *Heart Rhythm.* 2010;7(7):937-941.

237. Nieto-Tolosa J, Rodriguez-Sanchez D, Hurtado-Martinez JA, Pinar-Bermudez E, Penafiel-Verdu P, Sanchez-Munoz JJ, Valdes-Chavarri M, Garcia-Alberola A. [Phrenic nerve identification with cardiac multidetector computed tomography]. *Rev Esp Cardiol.* 2011;64(10):942-944.

238. Kuhne M, Knecht S, Altmann D, Kawel N, Ammann P, Schaer B, Osswald S, Sticherling C. Phrenic nerve palsy during ablation of atrial fibrillation using a 28-mm cryoballoon catheter: predictors and prevention. *J Interv Card Electrophysiol.* 2013;36(1):47-54; discussion 54.

239. Chun KR, Furnkranz A, Metzner A, Schmidt B, Tilz R, Zerm T, Koster I, Nuyens D, Wissner E, Ouyang F, Kuck KH. Cryoballoon pulmonary vein isolation with real-time recordings from the pulmonary veins. *J Cardiovasc Electrophysiol.* 2009;20(11):1203-1210.

240. Dorwarth U, Schmidt M, Wankerl M, Krieg J, Straube F, Hoffmann E. Pulmonary vein electrophysiology during cryoballoon ablation as a predictor for procedural success. *J Interv Card Electrophysiol.* 2011;32(3):205-211.

241. Gillis AM, Krahn AD, Skanes AC, Nattel S. Management of atrial fibrillation in the year 2033: new concepts, tools, and applications leading to personalized medicine. *Can J Cardiol.* 2013;29(10):1141-1146.

242. McManus DD, Lee J, Maitas O, Esa N, Pidikiti R, Carlucci A, Harrington J, Mick E, Chon KH. A novel application for the detection of an irregular pulse using an iPhone 4S in patients with atrial fibrillation. *Heart Rhythm.* 2013;10(3):315-319.

Résumé

La fibrillation atriale (FA) est l'arythmie soutenue la plus fréquente ; elle entraine une majoration significative de la morbidité et de la mortalité. Les mécanismes qui en sont responsables sont encore incomplètement connus, et sa prise en charge n'est pas optimale.

Afin de mieux comprendre la physiopathologie de la FA, nous avons mené différents travaux sur des cœurs de moutons isolés et perfusés par un système de Langendorff mais également en créant un modèle chronique de FA persistante de longue durée.

Dans un modèle ovin de FA persistante, nous avons ainsi démontré que la fréquence dominante (DF) de la FA augmentait progressivement pendant les premières semaines de l'arythmie, alors que les épisodes étaient paroxystiques, phénomène en rapport avec le raccourcissement de la durée du potentiel d'action secondaire au remodelage électrophysiologique. La DF se stabilisait dès lors que la FA devenait persistante, une fois le remodelage électrophysiologique maximal. L'accélération de la DF (dDF/dt) était significativement corrélée au temps nécessaire à la transition vers la FA persistante. Le remodelage structurel n'apparaissait que secondairement, une fois l'arythmie devenue persistante.

Sur le plan thérapeutique, nous avons étudié les mécanismes anti-arythmiques de la chloroquine (bloqueur d'I_{K1}) et de la ranolazine (bloqueur d'I_{Na}), molécules entrainant un ralentissement de la fréquence de rotation des rotors, une diminution de la DF et un retour en rythme sinusal. Ces travaux nous ont permis de mieux appréhender le rôle des ces courants ioniques dans le maintien de la FA.

Enfin, nous avons démontré l'efficacité de l'ablation de la FA en utilisant le cryoballon (CB) de deuxième génération, efficacité grevée d'un taux de parésie du nerf phrénique élevé, dont nous avons pu prédire la survenue à l'aide d'un prédicteur simple, la distance entre le bord du CB et la cathéter permettant de stimuler le nerf phrénique pendant l'application.

Une meilleure compréhension des mécanismes à l'origine de l'initiation et du maintien de cette arythmie, ainsi qu'une meilleure prise en charge thérapeutique permettraient d'améliorer la qualité de vie des patients et d'en diminuer le taux de complications.

Abstract

Atrial fibrillation (AF) is the most common sustained arrhythmia, significantly increasing patients' morbidity and mortality. The mechanisms explaining the initiation and maintenance of the arrhythmia are incompletely understood, and the current treatment strategy is suboptimal.

To better understand the pathophysiology of AF, we conducted various projects using Langendorff-perfused sheep hearts and a chronic model of long-standing persistent AF.

In the model of persistent AF, we demonstrated that dominant frequency (DF) progressively increases during the first weeks of the arrhythmia, during its paroxysmal stage, due to the electrophysiological remodeling resulting in atrial action potential shortening. DF stabilizes once the electrophysiological remodeling is maximal, and the arrhythmia becomes persitent. The rate of DF increase (dDF/dt) was strongly correlated with the time to persistent AF. Structural remodeling appears secondarily, once transition has occured.

We also studied the anti-arrhythmic mechanisms of chloroquine (I_{K1} blocker) and ranolazine (I_{Na} blocker), which slow the frequency of rotation of rotors, decrease the DF and favor reversal to sinus rhythm. These projects helped us to better understand the importance of these currents in AF dynamics.

Lastly, we demonstrated the increased efficacy of AF ablation when using the second generation cryoballoon (CB), which regrettably increases the occurrence of phrenic nerve palsy. A simple, reliable predictor of this complication was found, the distance between the lateral edge of the CB and the phrenic nerve stimulating catheter.

A better understanding of the mechanisms underlying the initiation and maintenance of AF, in conjunction with better therapeutic strategies will help to improve patients' quality of life and decrease the complications of the arrhythmia.

ANNEXE

VU :
Le Directeur de Thèse
(Nom et Prénom)

VU :
Le Responsable de l'École Doctorale

VU pour autorisation de soutenance

Rennes, le

Le Président de l'Université de Rennes 1

Guy CATHELINEAU

VU après soutenance pour autorisation de publication :

Le Président de Jury,
(Nom et Prénom)